

N 70 37826  
DEC 4 1970  
JAN 18 1971  
FEB 23 1971  
MAR 3 1971  
AUG 4 1971

**NASA TECHNICAL  
MEMORANDUM**

**NASA TM X-52876  
Volume I**

**NASA TM X-52876  
Volume I**

PROPERTY OF U S AIR FORCE  
AEDC LIBRARY  
F40600-71-C-0002

**SPACE TRANSPORTATION SYSTEM TECHNOLOGY SYMPOSIUM**

**I - Aerothermodynamics and Configurations**

**NASA Lewis Research Center  
Cleveland, Ohio  
July 15-17, 1970**

*Copy 1*  
PROPERTY OF U S AIR FORCE  
AEDC LIBRARY  
F40600-71-C-0002

1. Report No. <b>TM X-52876 - Volume I</b>		2. Government Accession No.		3. Recipient's Catalog No.	
4. Title and Subtitle <b>SPACE TRANSPORTATION SYSTEM TECHNOLOGY SYMPOSIUM I - Aerothermodynamics and Configurations</b>				5. Report Date <b>July 1970</b>	
				6. Performing Organization Code	
7. Author(s)				8. Performing Organization Report No. <b>E-5866</b>	
9. Performing Organization Name and Address				10. Work Unit No.	
				11. Contract or Grant No.	
				12. Sponsoring Agency Name and Address <b>National Aeronautics and Space Administration Washington, D. C. 20546</b>	
12. Sponsoring Agency Name and Address				13. Type of Report and Period Covered <b>Technical Memorandum</b>	
14. Sponsoring Agency Code					
15. Supplementary Notes  <b>Held at the NASA-Lewis Research Center, July 15-17, 1970</b>					
16. Abstract The Symposium encompassed seven technical areas, each published in a separate volume of NASA Technical Memorandum X-52876: <b>Volume I - Aerothermodynamics and Configurations</b> (includes aerodynamics; atmospheric operations; and aerodynamic heating) <b>II - Dynamics and Aeroelasticity</b> (includes dynamic loads and response; aeroelasticity; and flight dynamics and environment) <b>III - Structures and Materials</b> (includes structural design technology; thermal protection systems; and materials technology) <b>IV - Propulsion</b> (includes main propulsion; auxiliary propulsion; and airbreathing propulsion) <b>V - Operations, Maintenance, and Safety (Including Cryogenic Systems)</b> (includes general and cryogenics) <b>VI - Integrated Electronics (Including Electric Power)</b> (includes system integration; data management, systems monitoring, and checkout; navigation, guidance, and control; communication, instrumentation, and display; and power subsystems) <b>VII - Biotechnology</b>					
17. Key Words (Suggested by Author(s))			18. Distribution Statement <b>Unclassified - unlimited</b>		
19. Security Classif. (of this report) <b>Unclassified</b>		20. Security Classif. (of this page) <b>Unclassified</b>		21. No. of Pages <b>546</b>	
				22. Price* <b>\$ 3.00</b>	

\*For sale by the Clearinghouse for Federal Scientific and Technical Information  
Springfield, Virginia 22151; also as microfiche  
at \$.65 per copy



## FOREWORD

The prospect of undertaking a reusable launch vehicle development led the NASA Office of Manned Space Flight (OMSF) to request the Office of Advanced Research and Technology (OART) to organize and direct a program to develop the technology that would aid in selecting the best system alternatives and that would support the ultimate development of an earth-to-orbit shuttle. Such a Space Transportation System Technology Program has been initiated. OART, OMSF, and NASA Flight and Research Centers with the considerable inputs of Department of Defense personnel have generated the program through the efforts of several Technology Working Groups and a Technology Steering Group. Funding and management of the recommended efforts is being accomplished through the normal OART and OMSF line management channels. The work is being done in government laboratories and under contract with industry and universities. Foreign nations have been invited to participate in this work as well. Substantial funding, from both OART and OMSF, was applied during the second half of fiscal year 1970.

The Space Transportation System Technology Symposium held at the NASA Lewis Research Center, Cleveland, Ohio, July 15-17, 1970, was the first public report on that program. The Symposium goals were to consider the technology problems, their status, and the prospective program outlook for the benefit of the industry, government, university, and foreign participants considered to be contributors to the program. In addition, it offered an opportunity to identify the responsible individuals already engaged in the program. The Symposium sessions were intended to confront each presenter with his technical peers as listeners, and this, I believe, was substantially accomplished.

Because of the high interest in the material presented, and also because the people who could edit the output are already deeply involved in other important tasks, we have elected to publish the material essentially as it was presented, utilizing mainly the illustrations used by the presenters along with brief words of explanation. Those who heard the presentations, and those who are technically astute in specialty areas, can probably put this story together again. We hope that more will be gained by compiling the information in this form now than by spending the time and effort to publish a more finished compendium later.

A. O. Tischler  
Chairman,  
Space Transportation System  
Technology Steering Group





# CONTENTS

	Page
<b>FOREWORD . . . . .</b>	<b>iii</b>
 <b>SPACE TRANSPORTATION SYSTEM TECHNOLOGY PROGRAM - Introduction</b>	
A. O. Tischler, NASA Headquarters . . . . .	xx
 <b>SPACE TRANSPORTATION SYSTEM OVERVIEW AND PROGRAM PLANS</b>	
Dale Myers, NASA Headquarters . . . . .	xx
 <b><u>AERODYNAMICS</u></b>	
<b>SPACE SHUTTLE BOOSTER AERODYNAMICS</b>	
Heinz G. Struck, NASA-Marshall Space Flight Center . . . . .	1
<b>SPACE SHUTTLE AIRBREATHING ENGINE EXHAUST EFFECTS</b>	
C. F. Ehrlich, Jr., Lockheed Missiles & Space Company . . . . .	24
<b>TO WHAT EXTENT SHOULD SPACE SHUTTLE STABILITY AND CONTROL BE PROVIDED THROUGH STABILITY AUGMENTATION?</b>	
M. E. Wawrzyniak, McDonnell Douglas Astronautics Company . . . . .	47
<b>ABORT SEPARATION INCLUDING AERODYNAMIC, DYNAMIC, AND TRAJECTORY INFLUENCES</b>	
John P. Decker, Robert J. McGhee, and P. Kenneth Pierpont, NASA Langley Research Center . . . . .	67
<b>POSSIBLE USE OF HALF-MODEL OSCILLATORY TECHNIQUES FOR THE STUDY OF SHUTTLE ABORT SEPARATION DYNAMICS</b>	
K. J. Orlik-Rückemann, National Aeronautical Establishment, Canada . . . . .	99
<b>THE ONERA HOT SPOT WIND TUNNELS CAPABILITIES IN THE SPACE SHUTTLE STUDIES</b>	
Jean-Pierre Chevallier, Office National d'Etudes et de Recherches Aérospatiales, France . . . . .	119
<b>THE APPLICATION OF MIL-F-8785B (ASG) TO THE EVALUATION OF LANDING-APPROACH FLYING QUALITIES OF A LIFTING-BODY-TYPE SHUTTLE VEHICLE</b>	
J. Chin, Grumman Aerospace Corporation . . . . .	127
<b>STATIC AERODYNAMICS, FLOW FIELDS AND AERODYNAMIC HEATING OF SPACE SHUTTLE ORBITERS</b>	
E. D. Katzen, J. G. Marvin, H. L. Seegmiller, J. A. Axelson, J. J. Brownson, J. W. Cleary, W. K. Lockman, and G. E. Kaattari, NASA Ames Research Center . . . . .	142

## ATMOSPHERIC OPERATIONS

### INTEGRATED LAUNCH REENTRY VEHICLE CONFIGURATION STUDY

J. Stalony-Dobrzanski, Northrop Corporation . . . . . 195

### SPACE SHUTTLE ASCENT PHASE ABORT CONSIDERATIONS

Christopher J. Cohan, General Dynamics/Convair . . . . . 221

### SUBSONIC CRUISE MODE - AN INTACT ABORT CONCEPT

A. Blanciak, O. Kramer, and J. K. Yakura, Aerospace Corporation . . . . . 256

### SPACE SHUTTLE BOOSTER RETURN PERFORMANCE

R. A. Bithell and W. A. Pence, Jr., General Dynamics/Convair . . . . . 290

### PROVIDING SAFE LANDING AT HIGH APPROACH SPEEDS FOR SPACE SHUTTLE

Robert J. Pruin, The Boeing Company . . . . . 323

## AERODYNAMIC HEATING

### SHOCK INTERFERENCE HEATING AND THE SPACE SHUTTLE

Barry E. Edney, Bell Aerospace Company . . . . . 338

### INTERFERENCE AND RADIATION BLOCKAGE EFFECTS ON SURFACE TEMPERATURES OF COMPOSITE FLIGHT VEHICLES

Alfred C. Thomas, The Boeing Company . . . . . 390

### TRANSITIONAL AND TURBULENT HEAT TRANSFER CORRELATIONS FOR A LIFTING ENTRY VEHICLE AT MACH 10

C. H. Young, D. C. Reda, and A. M. Roberge, General Dynamics/Convair . . 418

### BOUNDARY LAYER TRANSITION ON LIFTING ENTRY VEHICLE CONFIGURATIONS AT HIGH ANGLE-OF-ATTACK

R. V. Masek, McDonnell Douglas Corporation . . . . . 445

### TURBULENT HEATING ON SPACE SHUTTLE ORBITERS DURING REENTRY

H. Harris Hamilton, NASA Langley Research Center . . . . . 463

### A COMPARISON OF SIMPLE TURBULENT HEATING ESTIMATES AND BOUNDARY LAYER TRANSITION CRITERIA WITH APPLICATION TO LARGE, LIFTING ENTRY VEHICLES

Blaine E. Pearce, The Aerospace Corporation . . . . . 485

### ENTRY MANEUVER/AEROTHERMODYNAMIC INTERACTIONS FOR HIGH CROSS-RANGE CANDIDATE ORBITERS

James P. Arrington, NASA Langley Research Center . . . . . 509

### A MINIMUM HEATING FLIGHT MODE FOR HIGH LATERAL RANGE SPACE SHUTTLE ENTRIES INCLUDING THE EFFECTS OF TRANSITION

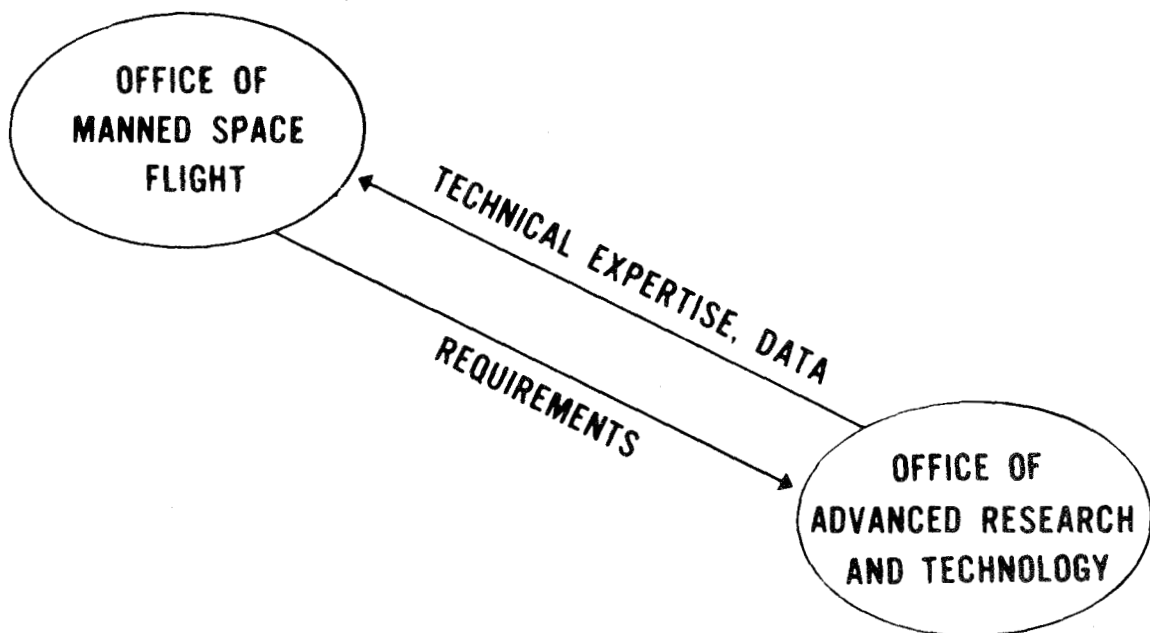
Jack D. Moote, North American Rockwell . . . . . 531

# SPACE TRANSPORTATION SYSTEM TECHNOLOGY PROGRAM

## Introduction

A. O. Tischler

National Aeronautics and Space Administration  
Washington, D.C.



## Objectives

DEVELOP BODY OF TECHNICAL INFORMATION TO SERVE AS BASIS FOR:

Design Definition  
Configuration Selection  
Materials Choices  
Fabrication Methodology etc.

PROVIDE TECHNICAL BASIS FOR ASSESSING ALTERNATIVES

ESTABLISH CADRE OF CONSULTING EXPERTS TO GUIDE DEVELOPMENT EFFORTS

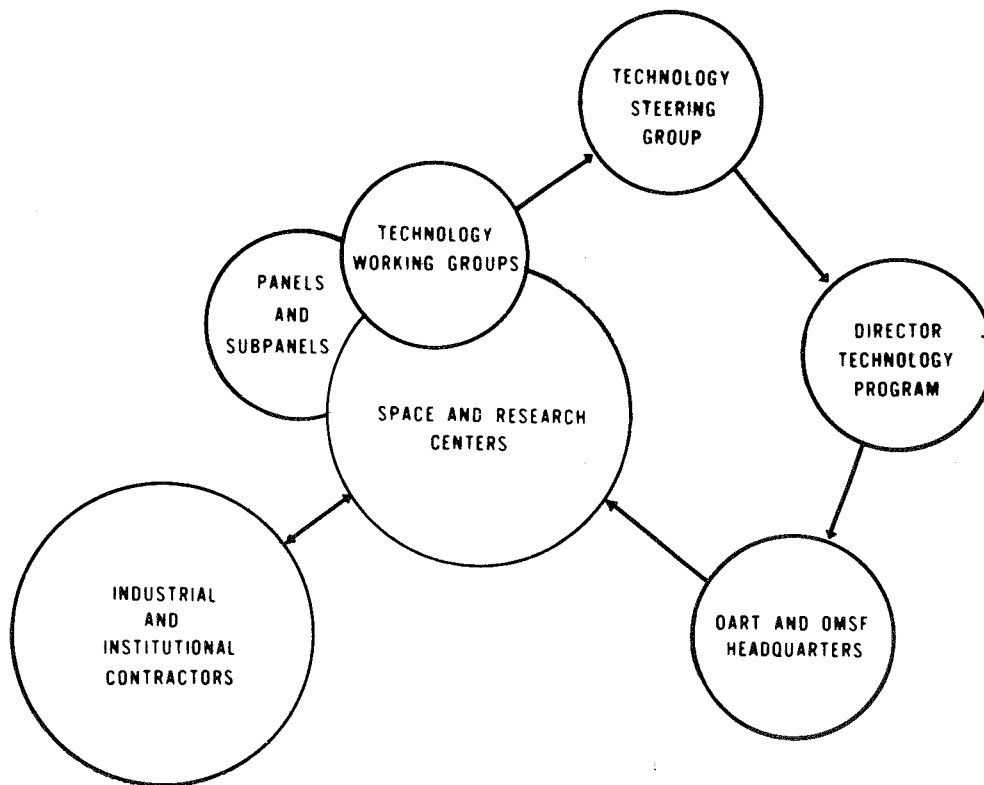
## Considerations

- SHUTTLE IS FUNDAMENTALLY BOTH SPACE VEHICLE AND AIRCRAFT
- ADVANCEMENT OF TECHNOLOGY IS CRITICAL TO PERFORMANCE OF SHUTTLE

Therefore draw together expert people from research centers (strong aeronautics background) and expert people from space flight centers (strong space background) to exploit technical progress

## Organization Plan

- KEY RESPONSIBILITIES REST WITH CENTERS WHO BOTH GENERATE AND ACCOMPLISH WORK IN-HOUSE AND WITH AEROSPACE INDUSTRY.
- COMPOSITION AND FUNCTIONS OF EACH GROUP ARE SHOWN IN THE FOLLOWING SLIDES.



## Working Groups

### COMPRISE:

- DISCIPLINARY EXPERTS FROM ALL CENTERS WORKING IN PARTICULAR AREAS
- OTHER GOVERNMENT LABORATORY REPRESENTATIVES
- HEADQUARTERS REPRESENTATIVES

### FUNCTIONS:

- RECOMMEND APPROPRIATE TECHNICAL PROGRAMS AND DETERMINE REQUIREMENTS IN EACH DISCIPLINE INVOLVED
- CARRY OUT RESEARCH AND TECHNOLOGY PROGRAMS IN-HOUSE AND ON CONTRACT
- MONITOR AND REPORT PROGRESS OF WORK
- DISSEMINATE RESULTS AND CONCLUSIONS THROUGH REPORTS CONFERENCES AND CONSULTATION

## Technical Steering Group

### COMPRISES:

CHAIRMAN OF WORKING GROUPS  
KEY MANAGERS OF CENTERS AND HEADQUARTERS STS TECHNOLOGY PROGRAM  
DIRECTOR OF STS TECHNOLOGY PROGRAM. WHO ACTS AS CHAIRMAN

### ACTS AS SENIOR BODY TO:

BALANCE W/G RECOMMENDED PROGRAMS WITHIN AVAILABLE FUNDS  
RECOMMEND CENTER ASSIGNMENTS  
DETECT "BETWEEN-THE-CRACKS" DEFICIENCIES

## Director, STS Technology Program

AS CHAIRMAN, TECHNOLOGY STEERING GROUP

Budgets available funds to best fulfill 'balanced' technology program

Develops future program plan

WITH CONSIDERABLE AID OF LINE ORGANIZATION

Justifies and defends present and future budget

Seeks out sources of necessary funds

Solicits center responses to program requirements for manpower

Reviews work progress

Coordinates technology work with study and planning report

ALSO

Develops procedures and guidelines

Resolves jurisdictional disputes

Explains it all to top management

## Line Organization

COMPRISE:

DISCIPLINARY DIVISIONS OF OART (HQ)

ADVANCED DEVELOPMENT ORGANIZATION OF OMSF (HQ)

ANY OTHER GROUPS (With Money) WHO CAN BE PERSUADED TO HELP

FUNCTIONS:

REPRESENTATIVES MEET AS PART OF WORKING GROUPS

SOLICIT CENTER RESPONSES

NEGOTIATE AGREEMENTS WITH CENTERS ON MANPOWER ALLOCATIONS ETC.

PROVIDE OVERALL MANAGEMENT OF PROJECT ASSIGNMENTS

WITH WORKING GROUPS MONITOR AND EVALUATE PROGRESS

IN SHORT, ACT AS ARMS FOR DIRECTOR, STS T/P



## Centers

- RESPOND TO RECOMMENDED PROGRAM PLAN BY ASSIGNING MANPOWER
- EXECUTE PROJECT AND TASK ASSIGNMENTS, BOTH IN-HOUSE AND CONTRACTED
- REPORT WORK STATUS AND PROGRESS TO WORKING GROUPS AND TO HQ
- ARE PRIMARILY RESPONSIBLE FOR BUILDING COMPETENCE IN SHUTTLE-RELATED TECHNOLOGY

## Working Groups

NAME	CHAIRMAN	(CENTER)
AEROTHERMODYNAMICS & CONFIGURATIONS	ARTHUR HENDERSON	(LANGLEY)
STRUCTURES & MATERIALS	ROGER ANDERSON	(LANGLEY)
DYNAMICS & AEROELASTICITY	HARRY RUNYAN	(LANGLEY)
PROPULSION	JERRY THOMSON	(MARSHALL)
INTEGRATED ELECTRONIC SYSTEMS	CLINE FRASIER	(MANNED SPACECRAFT)
BIOTECHNOLOGY	JOSEPH PECORARO	(HEADQUARTERS)
OPERATIONS MAINTENANCE & SAFETY	SAM BEDDINGFIELD	(KENNEDY)

## **Aerodynamics, Configuration Selection**

### **GOALS:**

- TO RESOLVE THE INTEGRATED AERODYNAMIC PROBLEMS RELATING TO PERFORMANCE STABILITY AND CONTROL, IMPROVE HANDLING QUALITIES, AND ASSURE ABORT SEPARATION
- TO DETERMINE SURFACE TEMPERATURES, HEAT LOADS, AND HEAT DISTRIBUTIONS, ALSO STUDY TRANSITIONAL AND TURBULENT FLOW
- TO PROVIDE ATMOSPHERIC OPERATIONAL DATA FOR ASCENT, ENTRY, AND ABORT, TRAJECTORY SHAPING, AND APPROACH AND LANDING
- TO RESOLVE INTERFACES WITH STRUCTURES AND MATERIALS THERMAL PROTECTION SYSTEMS DYNAMICS AND AEROELASTICITY

## **Dynamics & Aeroelasticity**

### **GOALS:**

- DEVELOP DYNAMICS AND AEROELASTICITY TECHNOLOGY REQUIRED BY NEW CONFIGURATIONS AND OPERATING MODES OF SPACE SHUTTLE VEHICLES SUCH AS:
  - a. Parallel Staging
  - b. Asymmetry
  - c. Lifting Surfaces During Launch
  - d. Lifting Surfaces During Entry
  - e. Severe Thermal Environment
- APPLY DYNAMICS AND AEROELASTIC TECHNOLOGY WHERE APPROPRIATE TO REDUCE STRUCTURAL WEIGHT OF SPACE SHUTTLE VEHICLES
- INCREASE THE RELIABILITY AND EFFECTIVENESS OF DYNAMICS AND AEROELASTICITY METHODOLOGIES FOR APPLICATION TO SPACE SHUTTLE VEHICLES

## **Structures & Materials**

### **GOALS:**

- IDENTIFY MINIMUM WEIGHT DESIGN OPTIONS APPROPRIATE TO SHUTTLE MISSION
- DEVELOP CRITERIA MATERIALS ANALYTICAL METHODS AND ADVANCED STRUCTURAL COMPONENTS
- VERIFY PERFORMANCE OF THERMAL PROTECTIONS AND STRUCTURAL COMPONENTS IN SIMULATED MISSION ENVIRONMENTS

## **Propulsion Technology**

### **GOALS:**

- TO IDENTIFY THE CRITICAL TECHNOLOGY AREAS IN THE SPACE SHUTTLE MAIN, AUXILIARY AND AIR BREATHING PROPULSION SYSTEMS THAT NEED TECHNOLOGICAL ADVANCEMENTS.
- TO INITIATE THE EFFORT REQUIRED TO BRING THIS TECHNOLOGY TO A STATUS THAT WILL PERMIT THE HARD DEVELOPMENT TO EMBARK FROM A FIRM TECHNICAL BASE.

## **Integrated Electronics**

### **GOALS:**

- PROVIDE TECHNOLOGICAL BASE FOR INTEGRATED MAINTAINABLE ELECTRONIC GUIDANCE, FLIGHT CONTROL, COMMUNICATIONS, POWER AND POWER DISTRIBUTION.
- FOCUS ELECTRONIC TECHNOLOGY IMPROVEMENT PROJECTS ON FULFILLMENT OF SHUTTLE REQUIREMENTS.

## **Biotechnology Program Objectives**

### **GOALS:**

- DETERMINE TOLERANCE OF SUBJECTS TO ORBITER REENTRY ACCELERATIONS UNDER VARYING DEGREES OF "ORBITAL DECONDITIONING"
- PROVIDE BASELINE CONCEPTUAL ENVIRONMENTAL CONTROL/ LIFE SUPPORT SYSTEM DESIGN
- STUDY AND TEST CONTROL AND DISPLAY FORMATS FOR MANUAL APPROACH AND LANDINGS
- EVALUATE CREW/PASSENGER PROTECTIVE SYSTEMS

## **Operations, Maintenance, and Safety**

### **GOALS:**

- TO DEVELOP LOW-COST FLIGHT OPERATIONS METHODOLOGY FOR THE SPACE SHUTTLE SYSTEM.
- TO REDUCE LOGISTICS AND MAINTENANCE PROCEDURES TO MINIMUM CONSISTENT WITH RELIABLE OPERATION.
- TO ASSURE EFFICIENT AND SAFE OPERATION OF SYSTEM, FOR LAUNCH, SPACE OPERATIONS, INCLUDING RESUPPLY OF OTHER VEHICLES, AND LANDING.

## FY 1970 Funds

- THE TECHNOLOGY PROGRAM THUS FAR COVERS ONLY THOSE ITEMS WHICH ARE PERFORMANCE OR SCHEDULE CRITICAL
- THE MAGNITUDE OF THE FY 70 TECHNOLOGY PROGRAM IS INDICATED.
- THE FIGURES REPRESENT THE NASA CONTRACTED EFFORT INCLUDING PURCHASES OF POWER, MATERIALS AND SUPPLIES USED IN-HOUSE. THE FIGURES DO NOT INCLUDE SALARIES OF NASA PERSONNEL
- FY 70 FIGURES REPRESENT ROUGHLY A PROGRAM INITIATED IN MID-YEAR.

	<u>\$ IN MILLIONS</u>
AEROTHERMODYNAMICS AND CONFIGURATIONS	3.8
STRUCTURES AND MATERIALS	10.4
DYNAMICS AND AEROELASTICITY	1.2
PROPULSION	5.0
INTEGRATED ELECTRONICS	7.4
BIOTECHNOLOGY	1.2
OPERATIONS, MAINTENANCE AND SAFETY	0.5
	<u>29.5 M</u>

## FY 1971 Fund Estimates

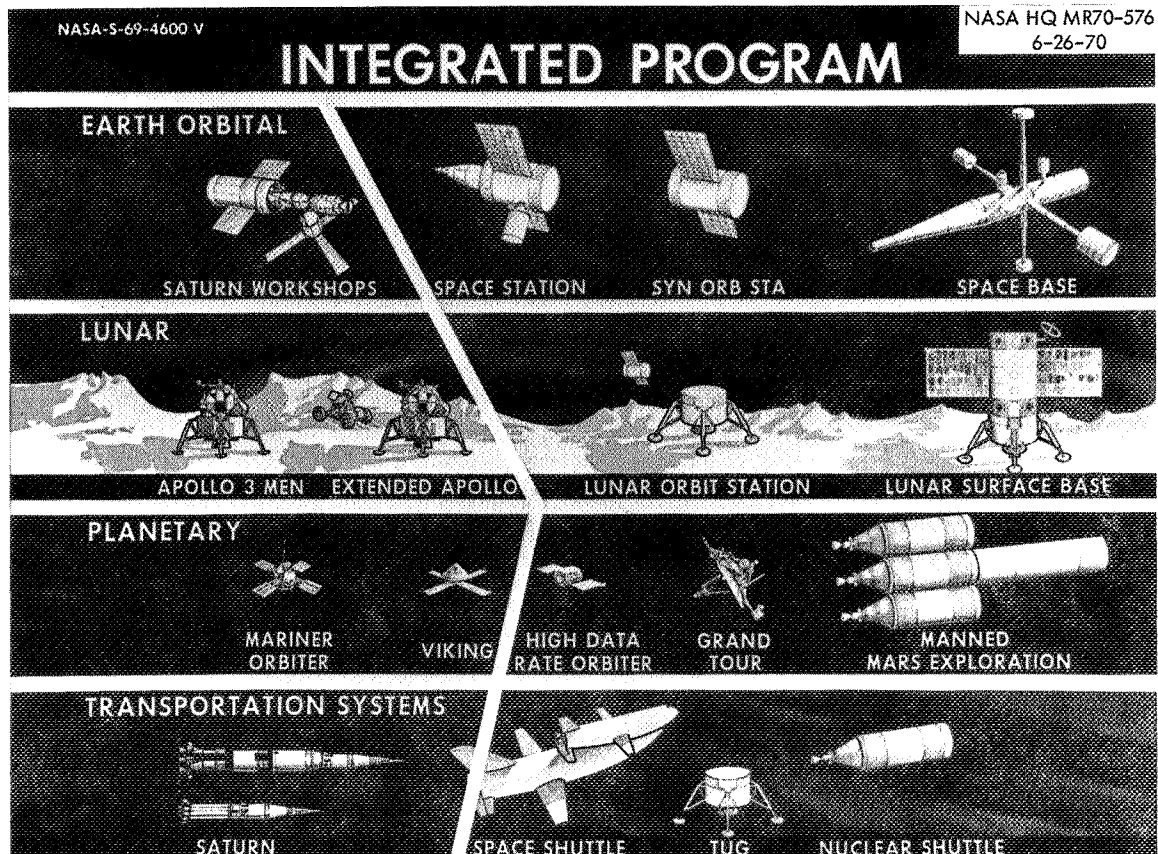
- FY 71 REPRESENTS A CONTINUATION OF FY 70 ACTIVITY AT ABOUT THE SAME LEVEL
- PROPULSION FUNDS DO NOT INCLUDE MAIN ENGINE DEVELOPMENT.

	<u>\$ IN MILLIONS</u>
AEROTHERMODYNAMICS & CONFIGURATIONS	5.9
STRUCTURES AND MATERIALS	23.4
DYNAMICS AND AEROELASTICITY	4.4
PROPULSION	11.5
INTEGRATED ELECTRONICS	8.6
BIOTECHNOLOGY	4.6
OPERATIONS. MAINTENANCE AND SAFETY	8.3
	<u>66.7</u>

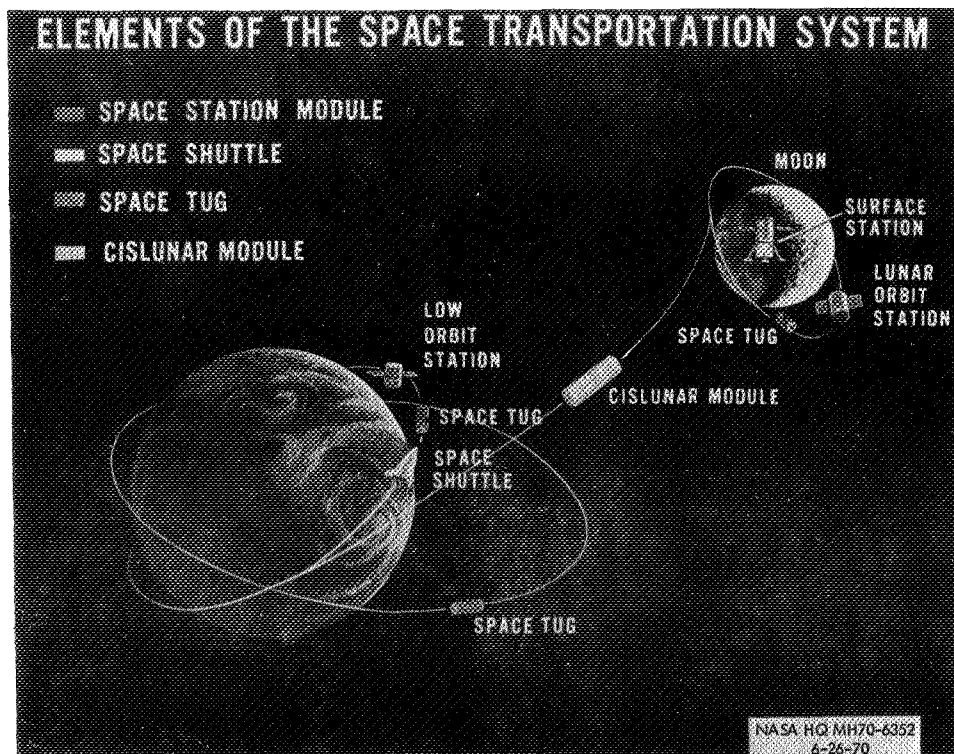
# SPACE TRANSPORTATION SYSTEM OVERVIEW AND PROGRAM PLANS

Dale D. Myers

National Aeronautics and Space Administration  
Washington, D.C.







## THE NEED FOR A SPACE TRANSPORTATION SYSTEM

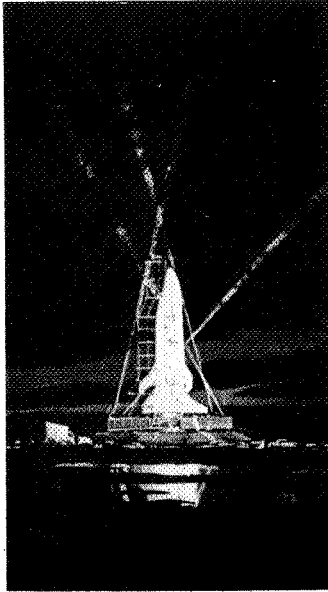
CONTINUED PROGRESS IN SPACE RESEARCH AND USE  
DEMANDS LOWER COST TO CARRY OUT VARIED  
MISSIONS REQUIRED

THE SPACE TRANSPORTATION SYSTEM REPRESENTS A  
LOGICAL STEP TOWARD EFFICIENT EXPANSION OF  
SPACE ACTIVITY BY

- REVOLUTIONARY CHANGE IN TRANSPORTATION
- GREAT FLEXIBILITY
- ECONOMICAL USE OF MAN

NASA HQ MH70-6344  
6-26-70

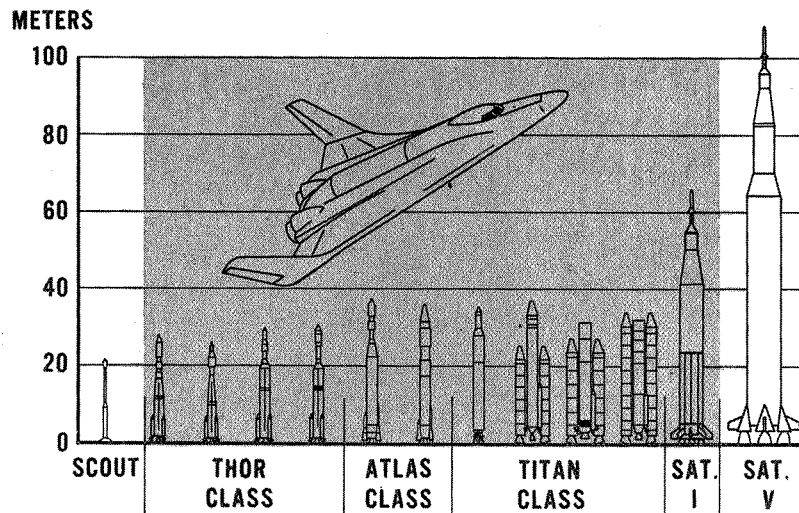
# SPACE SHUTTLE



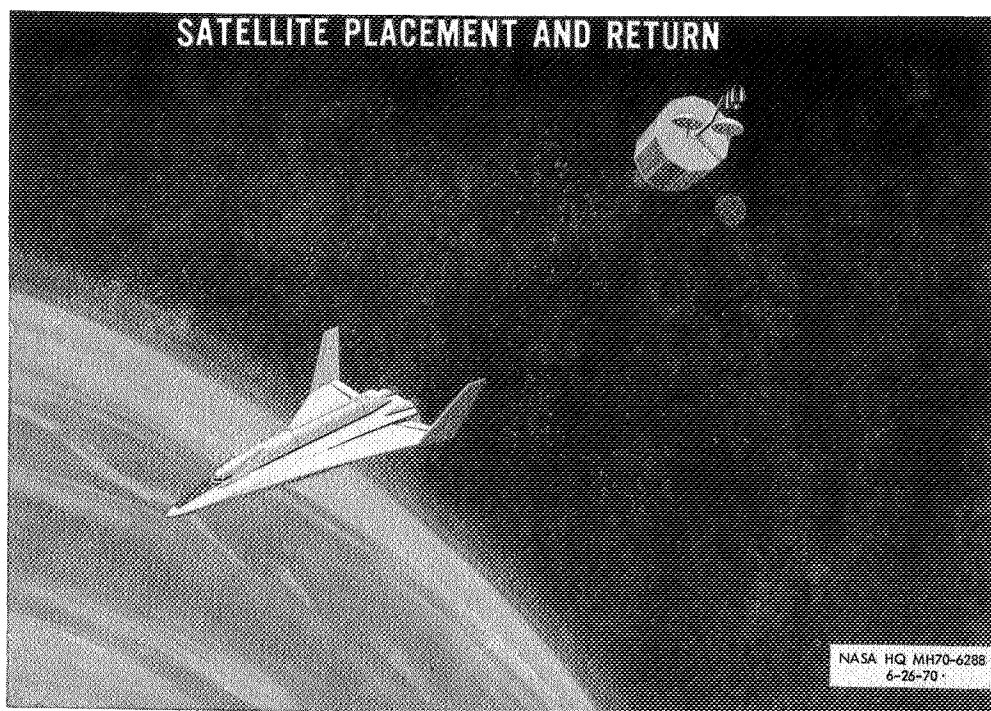
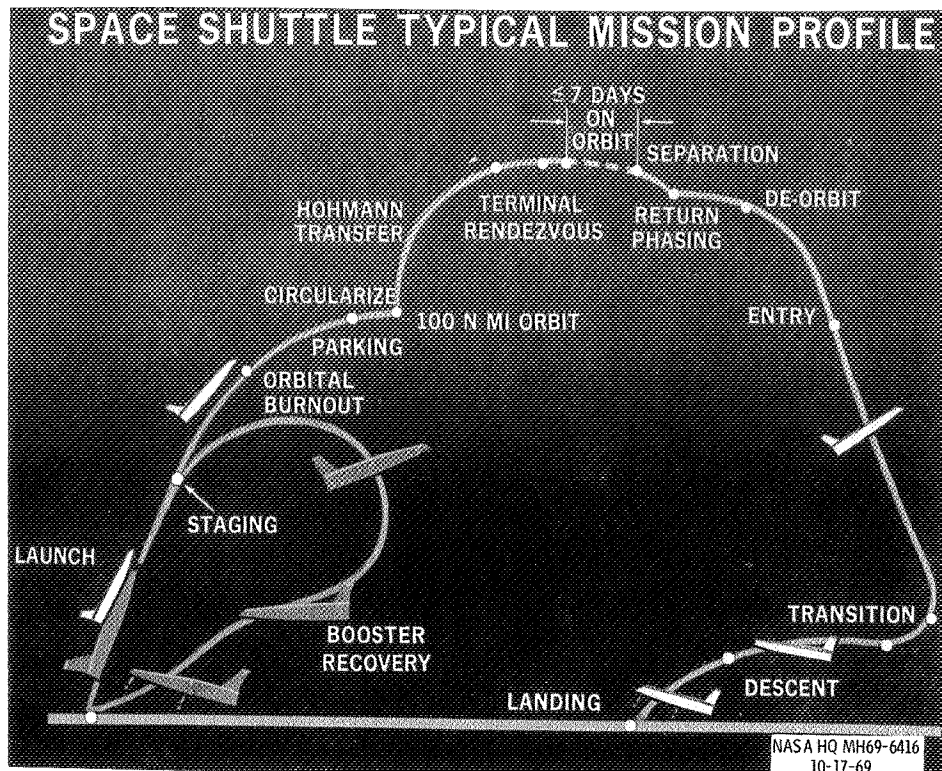
- 2 STAGES - BOOSTER AND ORBITER
- FULLY REUSABLE
- VERTICAL TAKEOFF / HORIZONTAL LANDING
- LARGE CARGO CAPABILITY
- SHIRT SLEEVE ENVIRONMENT FOR CREW AND PASSENGERS
- ACCEPTABLE G LOADS FOR NON-ASTRONAUTS
- 7 DAYS SELF-SUSTAINING
- APPROACH TO AIRLINE - TYPE OPERATIONS
- LOW COST

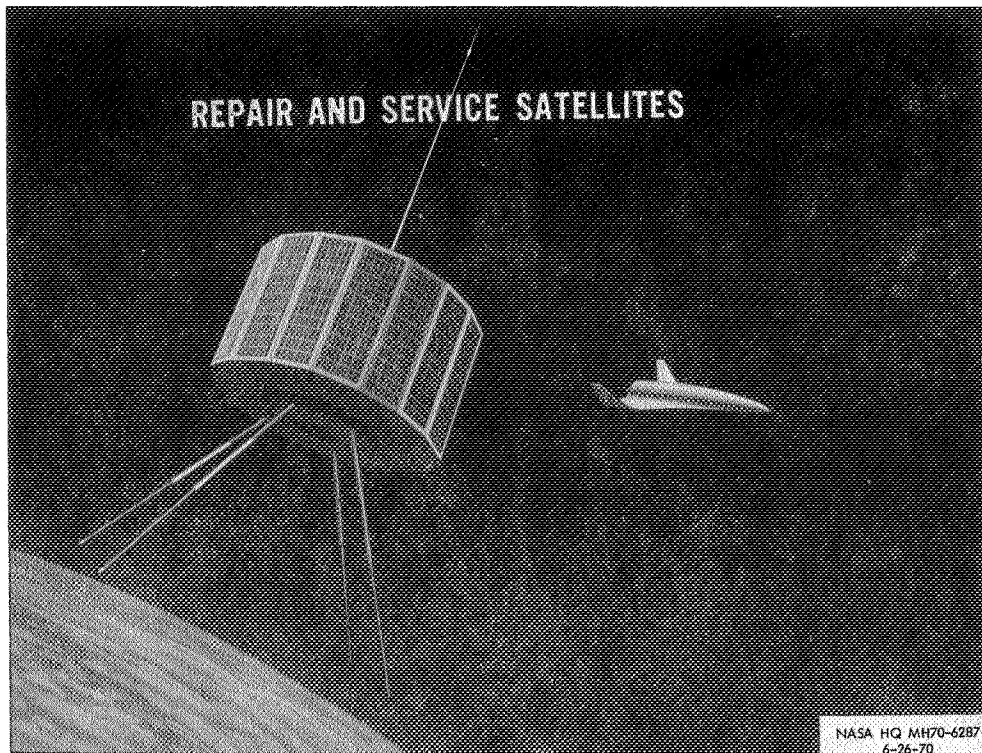
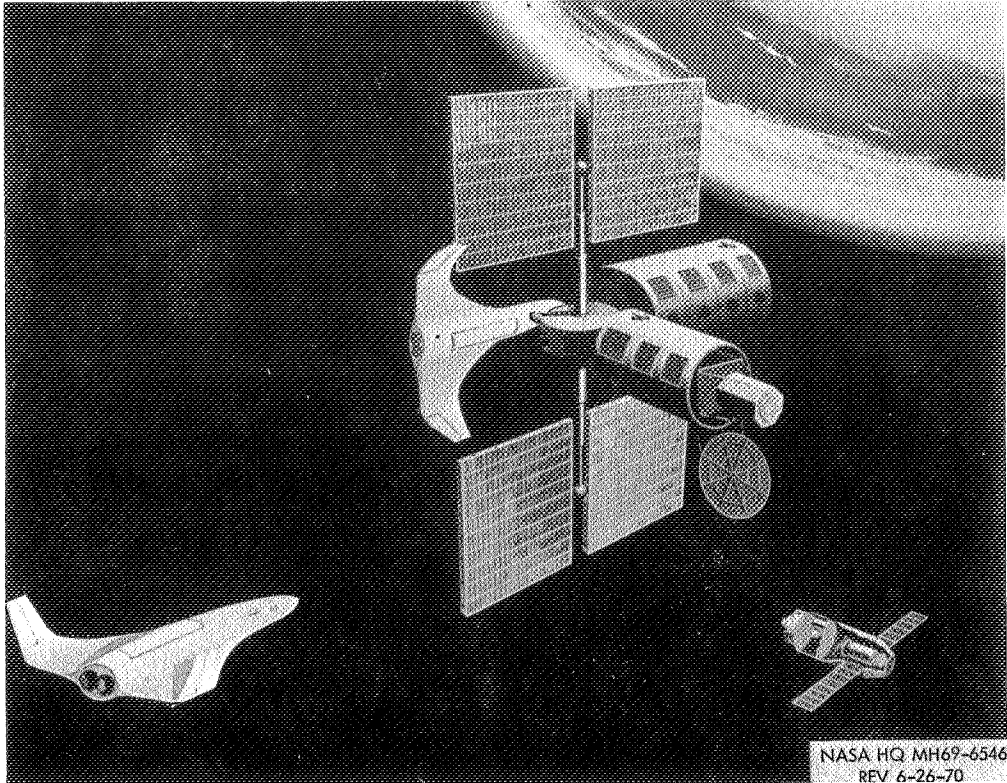
NASA HQ MH70-6345  
6-26-70

## LAUNCH VEHICLE REPLACEMENT

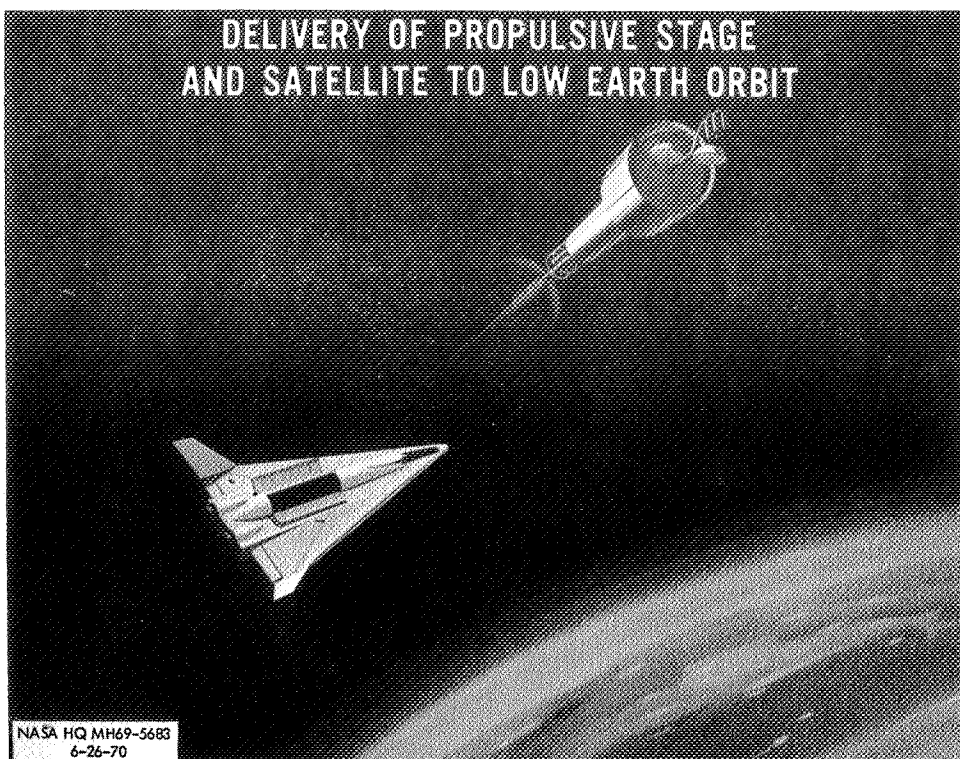


NASA HQ MH70-6353  
6-26-70

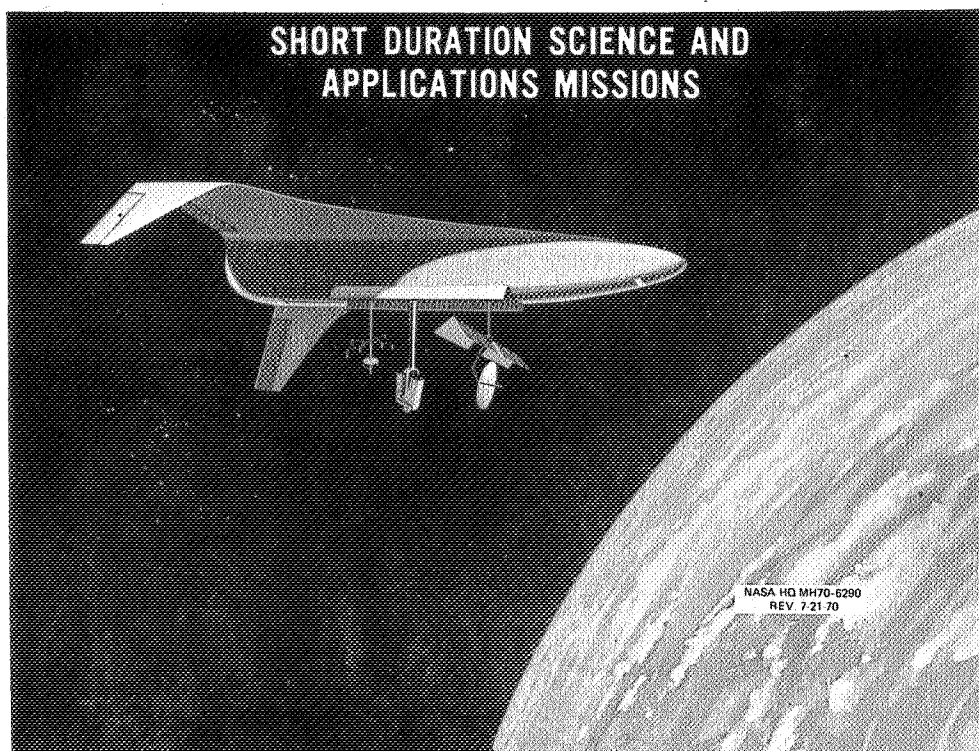




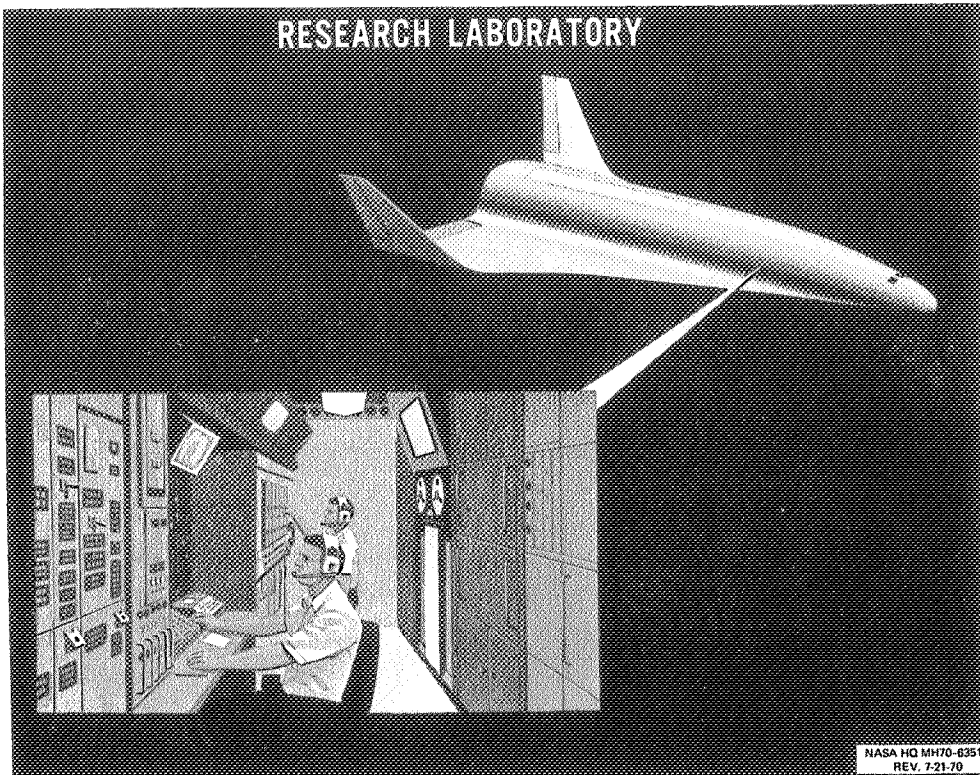
## DELIVERY OF PROPULSIVE STAGE AND SATELLITE TO LOW EARTH ORBIT



## SHORT DURATION SCIENCE AND APPLICATIONS MISSIONS

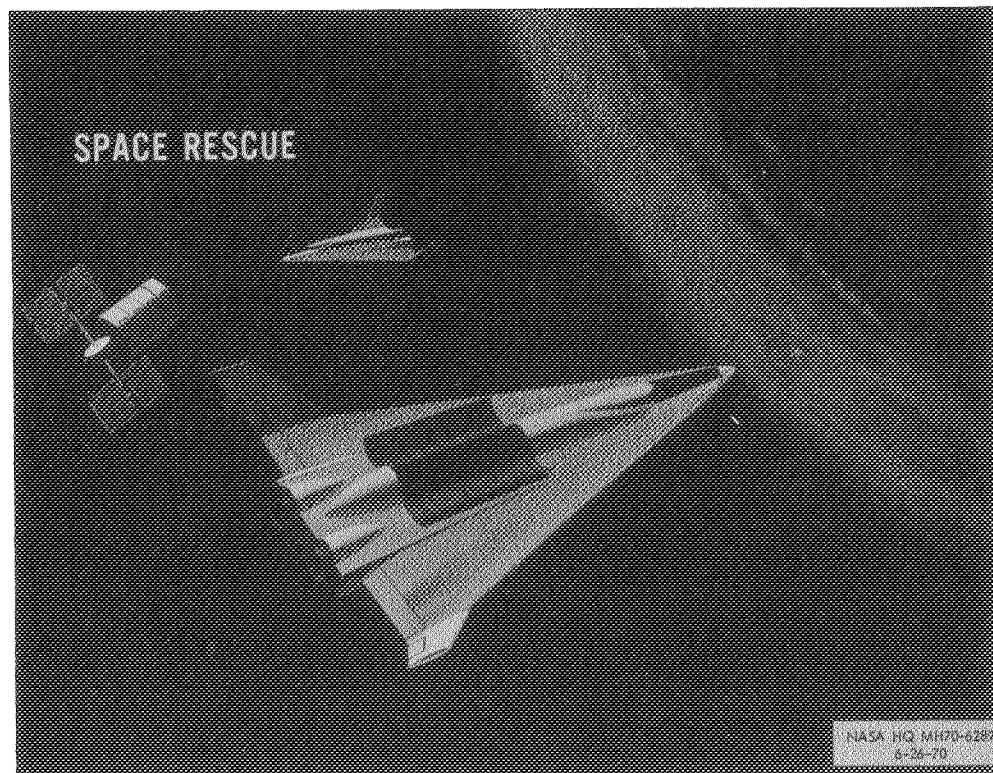


## RESEARCH LABORATORY



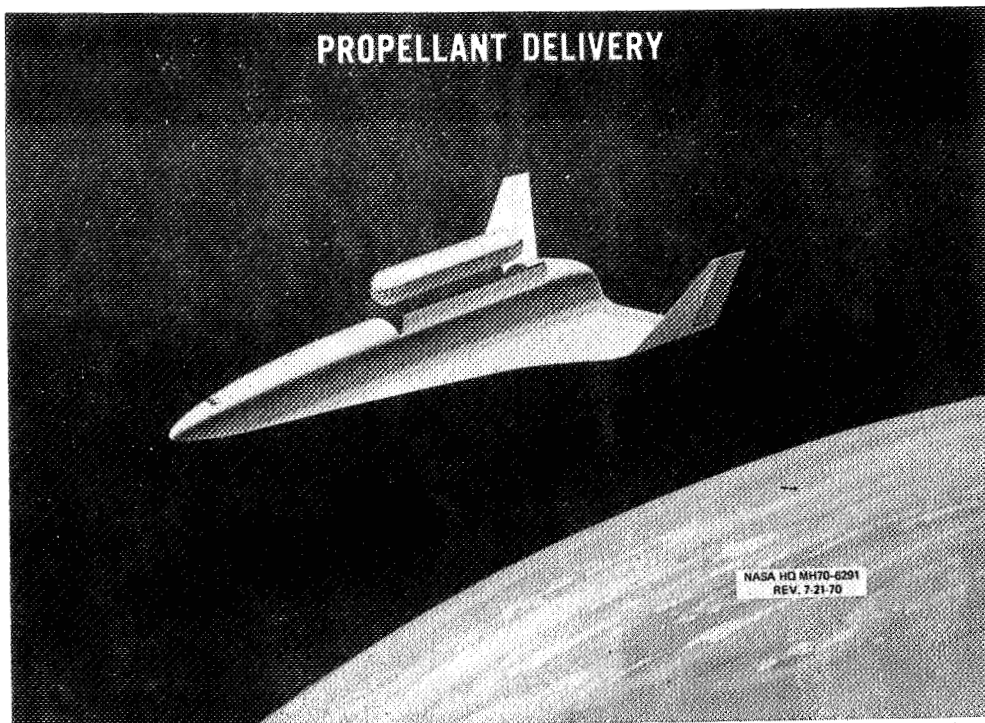
NASA HQ MH70-6351  
REV. 7-21-70

## SPACE RESCUE



NASA HQ MH70-6289  
6-26-70





## **SPACE SHUTTLE**

### **DEFINITION PHASE OBJECTIVES - VEHICLES**

- **DEFINE THE SPACE SHUTTLE SYSTEM**
- **ACCOMPLISH PRELIMINARY DESIGN**
  - **TWO POINT DESIGNS, HIGH & LOW CROSS RANGE**
  - **CONFIGURATION VERIFICATION**
- **PREDICT SCOPE, TIMING AND COST OF PROGRAM**
- **IDENTIFY TECHNOLOGY REQUIREMENTS**

NASA HQ MH70-6347  
6-26-70

## **SPACE SHUTTLE DESIGN REFERENCE CHARACTERISTICS ESTABLISHED FOR DEFINITION PHASE**

- TWO STAGE FULLY REUSABLE
- VERTICAL TAKE OFF/HORIZONTAL LANDING
- 1.5 MILLION KGS GROSS LIFT-OFF WEIGHT
- 4.6M DIAMETER X 18.3M LENGTH CARGO BAY SIZE
- TWO MAN CREW
- ORBITER SELF SUSTAINING FOR 7 DAYS
- NOMINAL 270 N. MI. ORBIT AT 55° INCLINATION
- SHIRTSLEEVE ENVIRONMENT FOR CREW AND PASSENGERS
- FLIGHT CREW CONTROLLED ABORTS
- "G" MAXIMUM ASCENT AND RE-ENTRY ACCELERATION
- BENIGN PAYLOAD ENVIRONMENT

NASA HQ MH70-6348  
6-26-70

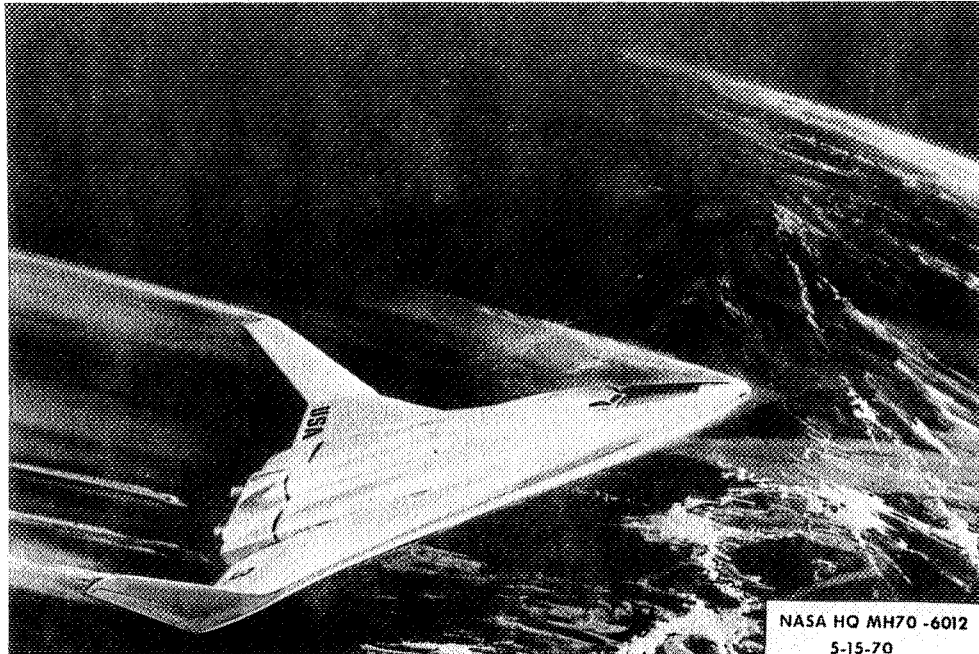
## **MAJOR SPACE SHUTTLE DEFINITION PHASE TECHNICAL TRADEOFFS**

- PAYLOAD CAPABILITY (WEIGHT AND VOLUME)
- CROSS RANGE
- UNMANNED VS. MANNED BOOSTER
- LIQUID HYDROGEN VS. JP FUEL FOR AIR BREATHING ENGINES
- POWERED VS. UNPOWERED LANDING
- INTERACTION WITH OTHER SPACE TRANSPORTATION SYSTEM  
ELEMENTS, i.e. SPACE TUG, ORBIT TO ORBIT SHUTTLE,  
NUCLEAR SHUTTLE

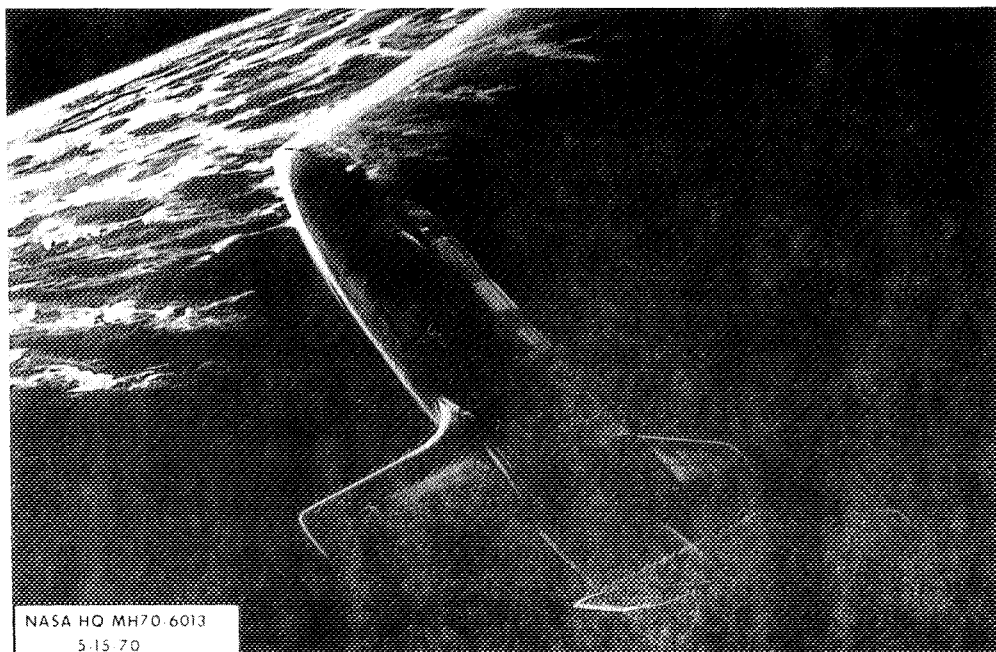
NASA HQ MH70-6346  
6-26-70



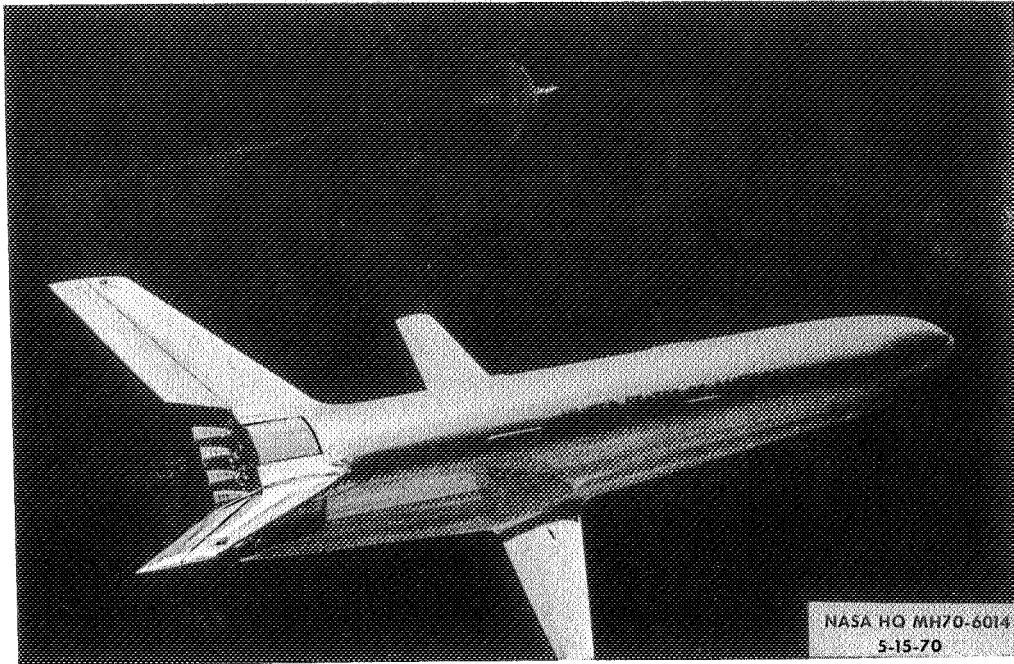
## NORTH AMERICAN ROCKWELL HIGH CROSSRANGE ORBITER



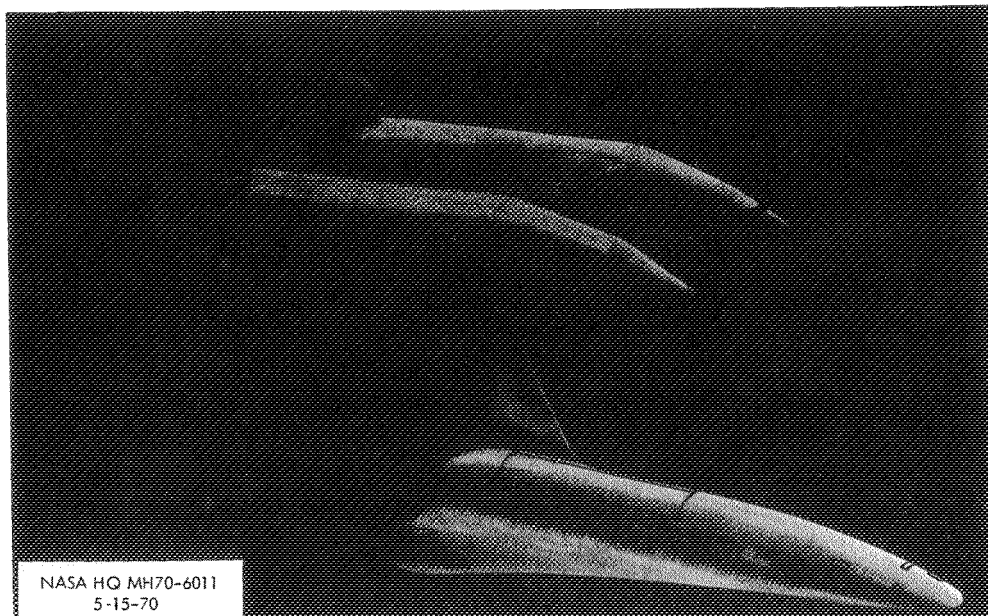
## NORTH AMERICAN ROCKWELL LOW CROSSRANGE ORBITER



**NORTH AMERICAN ROCKWELL  
COMMON BOOSTER**



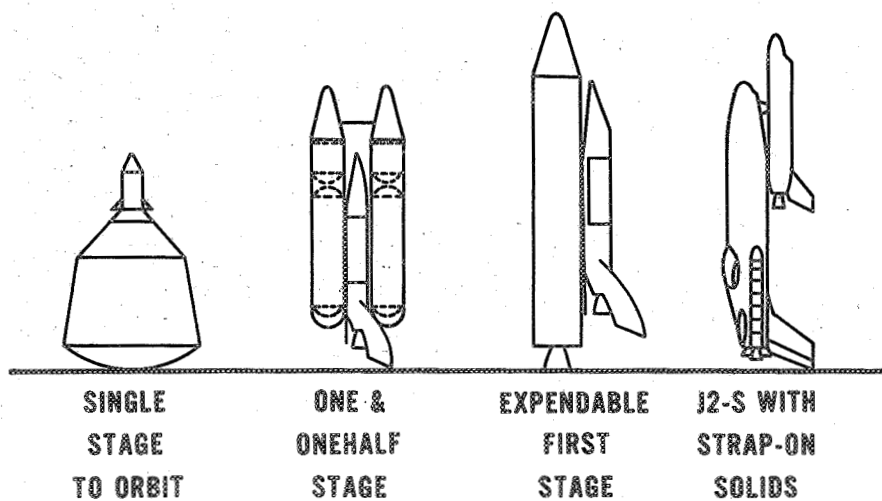
**MCDONNELL DOUGLAS  
HIGH CROSSRANGE SHUTTLE**



## MCDONNELL DOUGLAS LOW CROSSRANGE SHUTTLE

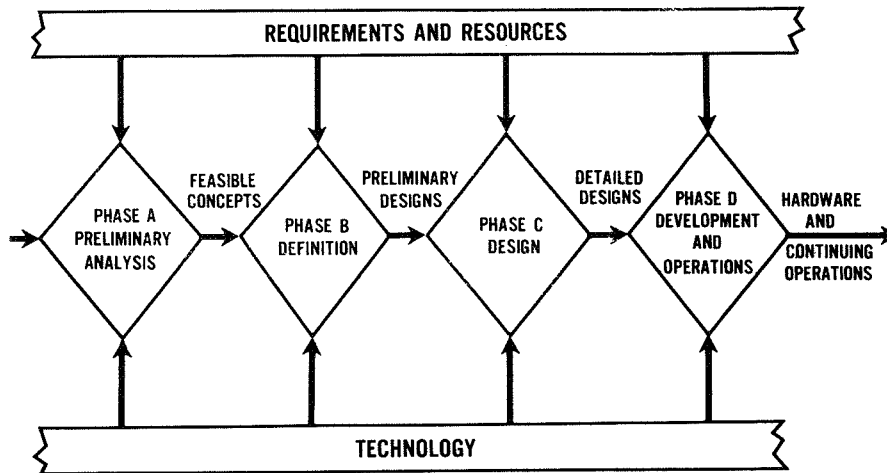


## OTHER CANDIDATE CONCEPTS



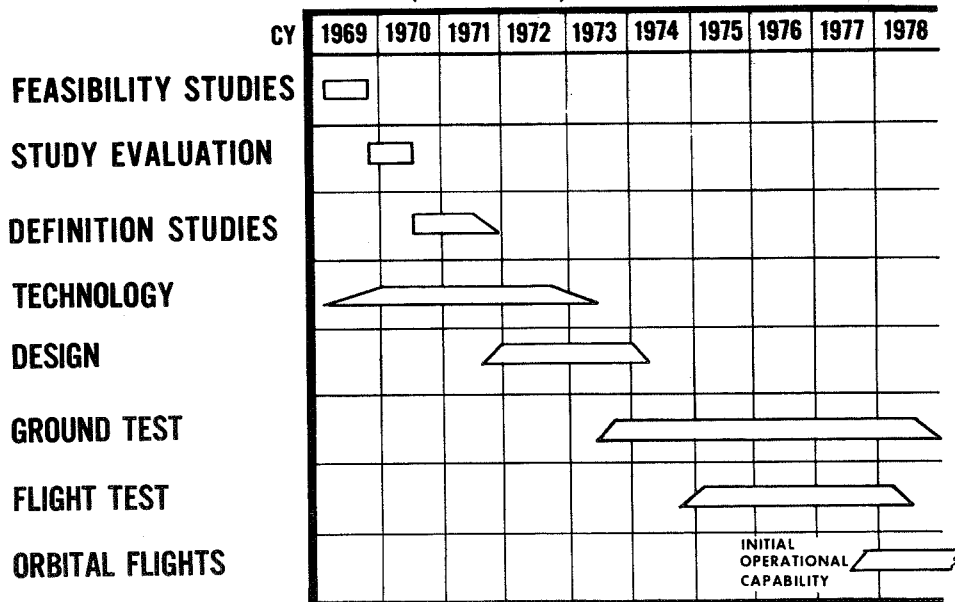
NASA HQ MH70-6274  
6-26-70

## PHASE PROJECT PLANNING



NASA HQ M470.6378  
6-26-70

## SHUTTLE PLANNING SCHEDULE (PRELIMINARY)



NASA HQ MH70-6404  
6-26-70

## SPACE SHUTTLE BOOSTER AERODYNAMICS

### Canards, a Solution to the Booster C. G. Problem

Heinz G. Struck

NASA-Marshall Space Flight Center  
Huntsville, Alabama

#### Introduction

The Space Shuttle, booster and orbiter, is primarily a space transportation system. Weight which does not serve any useful purpose toward the primary function should be considered "dead weight" and consequently be held at a minimum. From this point of view all recovery systems fall into this category. The recovery system, as aerodynamic surfaces, fly-back and landing system, should be involved in an optimization study, resulting finally in a low weight and low cost configuration. The high drag of the Space Shuttle is responsible for obtaining a moderate  $(L/D)_{max}$  despite of the relatively high aspect ratio of the wing. A reduction in drag and especially in base drag would result in quite a payload increase.

As far as the lifting device of the Space Shuttle vehicle is concerned, a delta wing or delta wing derivative of moderate aspect ratio seems to be structurally the lightest. It is usually sized for landing or cruise flight yielding exposed wing areas on the order of 6,000 to 8,000 ft<sup>2</sup> if trailing edge elevons are used for trim purposes. The excessive wing area, however, can be drastically reduced, if separate trim surfaces are employed. The location of the center of gravity (C.G.) decides then which of the two possibilities are to be used: For C.G. locations around 50 to 60 per cent of the body length the wing-fuselage-tail configuration has an undisputable advantage. For far aft C.G. locations a canard configuration is the only rational approach to this problem. Certain interference problems which are connected with canards, however, seem to reduce and cloud the clear advantage of this approach.

My intention is not to sell the canard concept, but to show that this version offers some weight advantage as a solution to the booster C.G. problem which the flying wing for instance cannot match.

## Fly-Back System Sizing Study

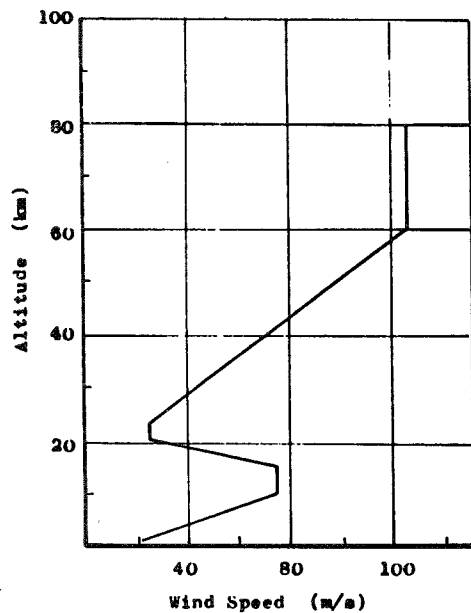
The left-hand side of the graph shows the 95 percentile design scalar wind speed profile envelope for the Eastern Test Range<sup>\*</sup>). Only 5 per cent of the time stronger winds as those shown are encountered. This wind profile was used for the fly-back system sizing study. To obtain the most unfavorable condition, this wind speed profile was used as head wind. The total fuel consumed as a consequence of this was considerably more than without head wind.

The right-hand side of the graph represents the trimmed lift to drag ratios of a family of boosters of one design philosophy. All have a wing of aspect ratio 4, however, their exposed wing area is decreasing at constant fuselage volume, diameter, length and base area. Thus the efficient lift producing element is decreasing and the inefficient mostly drag producing fuselage increasing proportionally. The result is a decrease in maximum lift to drag ratio.

---

\* Daniels, Glenn E., Editor "Terrestrial Environment (Climatic) Criteria Guidelines for use in Space Vehicle Development, 1969 Revision", NASA TM Report No. 53872  
Second Printing: March 15, 1970.

Design Scalar Wind Speed Profile Envelopes  
for ETN (95 Percentile)



Geometric Altitude		Wind Speed 95 Percentile	
km	ft	m/s	kts
1	3281	21	40.8
10	32808	75	143.8
14	45932	75	143.8
20	65617	25	48.6
23	75459	25	48.6

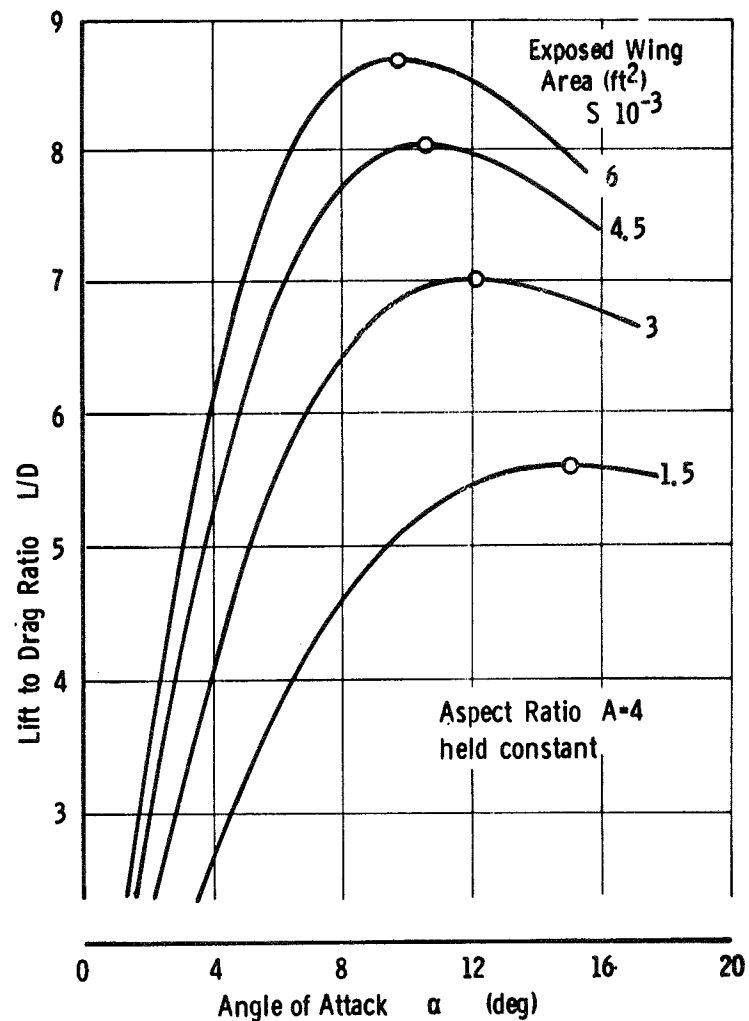


Figure 1

### Fly-Back System Sizing Study (Engine Parameters)

The ratio of the maximum cruise thrust to the sea level maximum cruise thrust of a family of hypothetical jet engines with the bypass ratios of 0, 1.3 and 5 for two altitudes, sea level and  $H = 36,100$  feet is shown in the upper left side of the graph. It was assumed that the sea level maximum cruise thrust per engine is 20,000 lb. The compressor pressure ratio of the engine is held constant and assumed to be of the order of 20 to 25. Thrust per pound of airflow and the specific fuel consumption does not change markedly over a wide range at these high compressor pressure or fan pressure ratios<sup>\*)</sup>. Therefore, no variation of this parameter was attempted. Intermediate values of thrust were extrapolated.

Standard thrust to weight ratios were assumed. The thrust to weight ratio remained constant for bypass ratios from 0 to 2. For higher bypass ratios the thrust to weight ratio decreased.

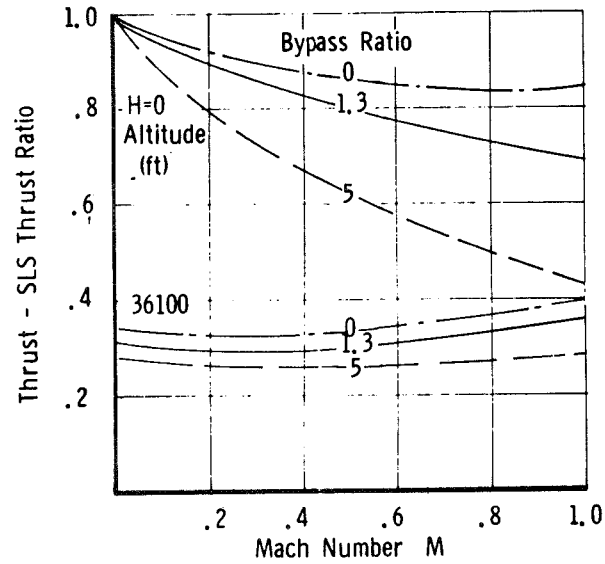
The specific fuel consumption, shown for JP-fuel, decreases with increasing bypass ratio. For a constant bypass ratio the specific fuel consumption increases with flight Mach number and decreases with increasing altitude. Above  $H = 35,000$ ft. the specific fuel consumption remains constant. The trade-off study was conducted with the assumption that the jet engines are burning  $H_2$ -fuel. To obtain, therefore, the  $H_2$ -fuel amount necessary to fly the 400 miles back to the launch complex the JP-fuel amount was multiplied with the ratio of the calorific values of JP-fuel to  $H_2$ -fuel. Thus only 37 per cent of the JP-fuel weight is taken up by the  $H_2$ -fuel.

---

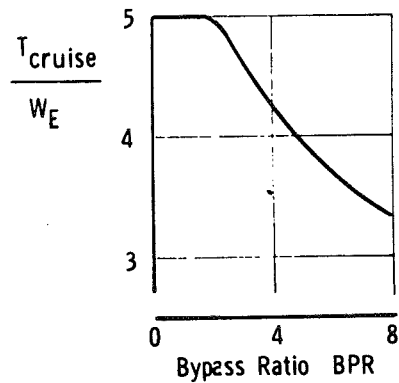
<sup>\*)</sup> Mallett, W. E. and F. W. Milke, "Turbofan Engine Thermodynamic Cycle Analysis", LTV Report No. 2-53900/2R36P, Feb. 1962.



Maximum Cruise Thrust for Jet Engines of Different Bypass Ratios (SLS Thrust = 20 000 lb)



Assumed Thrust to Weight Ratio



$$\frac{h(JP)}{h(H_2)} = 0.37$$

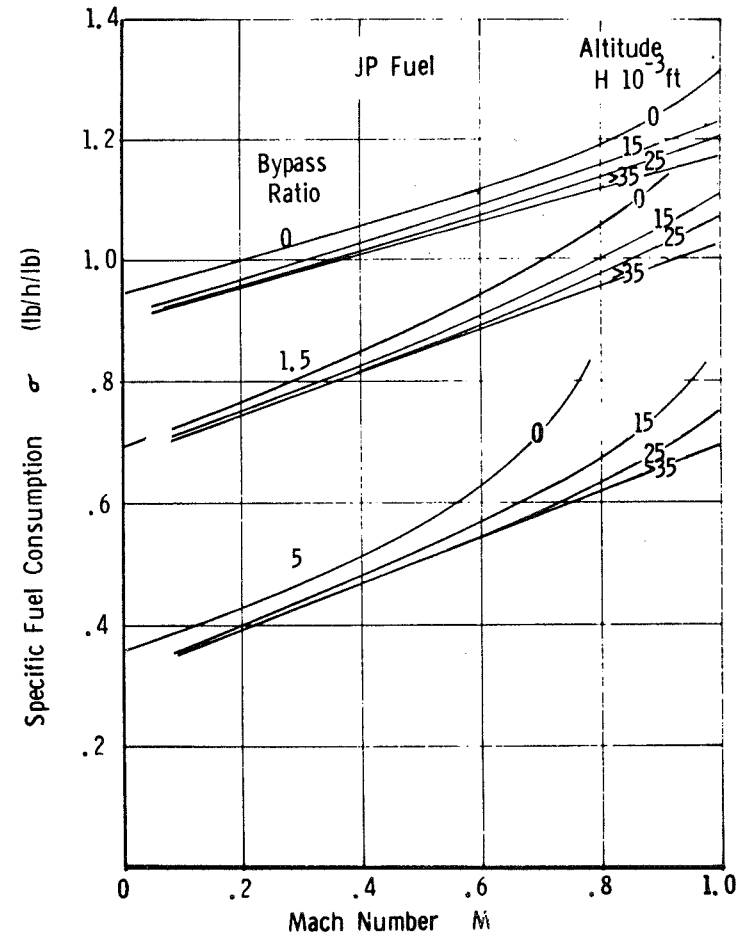


Figure 2

### Fly-Back System Sizing Study (Results)

The total fly-back system weight consists of  $W_T = W_W + W_E + W_I + W_F$  where  $W_W$  is the exposed wing weight plus the carry through structure and the thermal protection system (TPS) weight. We assume for the structural weight of the wing 7 lb/ft<sup>2</sup> and for the TPS system about 3 lb/ft<sup>2</sup>. Thus we obtain  $W_W = 10 \times S_W(\text{exp})$  (lb).

$W_E$  is the engine weight and it is a function of the number of engines, bypass ratio and thrust.

$W_I$  represents the installation weight of the jet engines. We assume this weight to be equal to 10 per cent of the engine weight and 5 per cent of the sea level static thrust.

$W_F$  designates the H<sub>2</sub>-fuel weight plus the fuel system weight (proportional to the fuel weight and taken as 10 per cent) and 10 per cent of the fuel weight as reserve.

$H = 0$  ft. The results clearly show that with decreasing wing area the fly-back system weight decreases due to wing weight. At about 2,000 ft<sup>2</sup> exposed wing area the minimum value of the fly-back system weight is obtained. From then on the engine and fuel weight increases excessively. The higher bypass ratios have a definite advantage. The minimum fly-back system weight is approximately 90,000 lb (plus approximately 17,000 lb of landing gear weight) and about 6 engines of 20,000-lb thrust each are necessary to propel the booster.

$H = 10,000$  ft. This altitude was selected as a more appropriate cruise altitude. In general, we obtain the same trend, however, at a higher weight level of about 10,000 lb more than at an altitude of  $H = 0$  ft. The number of engines increased to about eight.

L

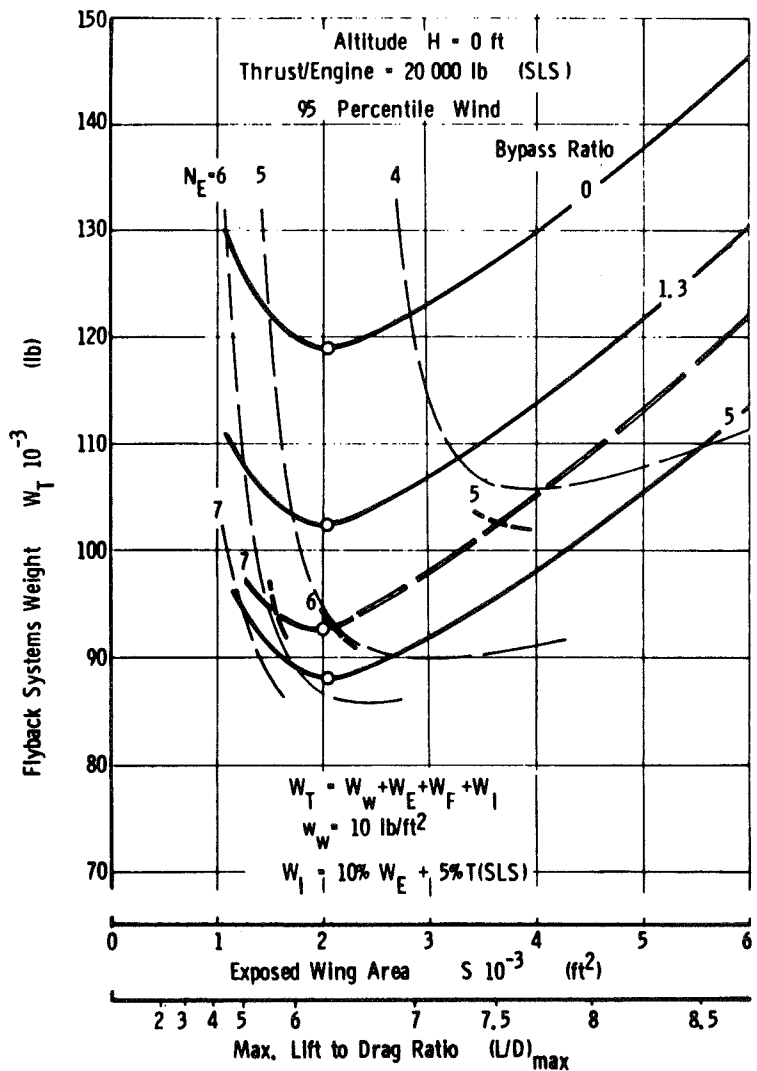
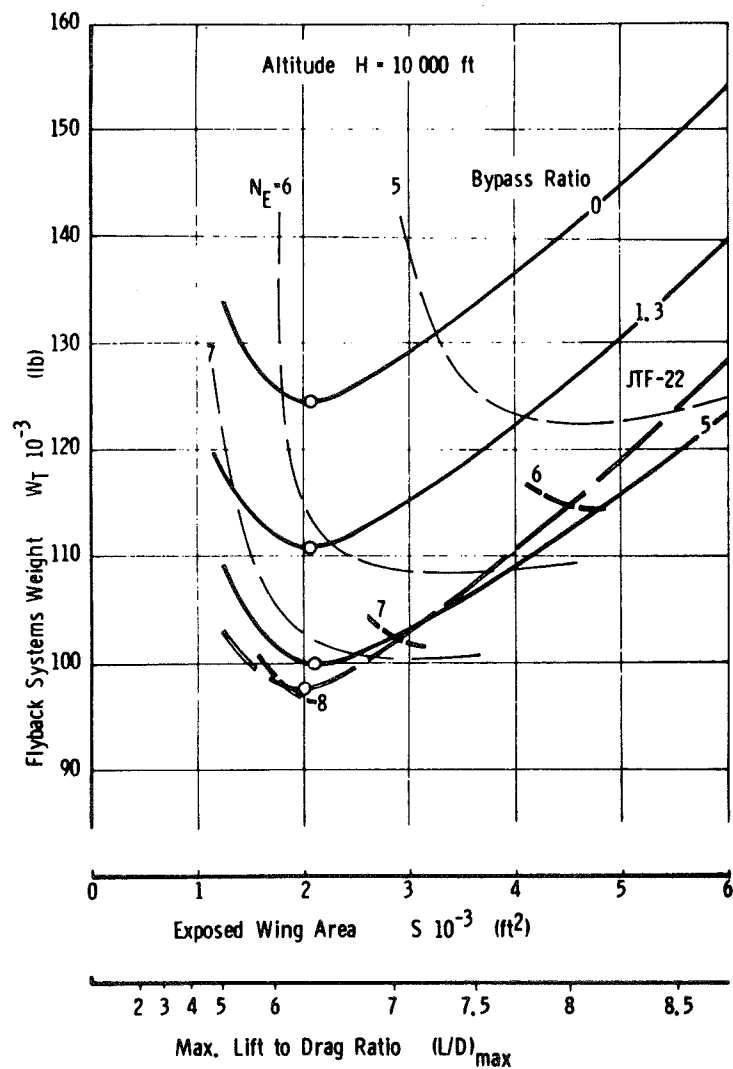


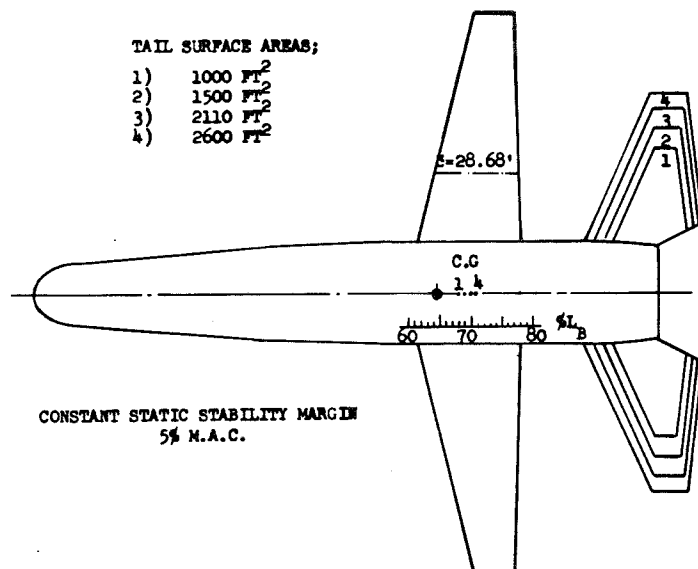
Figure 3

In addition to the hypothetical engine optimization results the results obtained with an engine presently under development are superimposed in both altitude plots. This engine has a higher thrust to weight ratio, a smaller bypass ratio and a higher thrust per frontal area. At an altitude of 10,000 feet this engine yields the lowest fly-back system weight. The cruising Mach number of the booster at 10,000 feet altitude is  $M = 0.35$  for an exposed wing area of  $4,500 \text{ ft}^2$  and  $M = 0.411$  for an exposed wing area of  $2,000 \text{ ft}^2$ .

- Conclusion:
- (A) Small wing areas are preferable (high wing loading)
  - (B) Trim devices (flaps, elevons) should not be attached to the wing trailing edge.

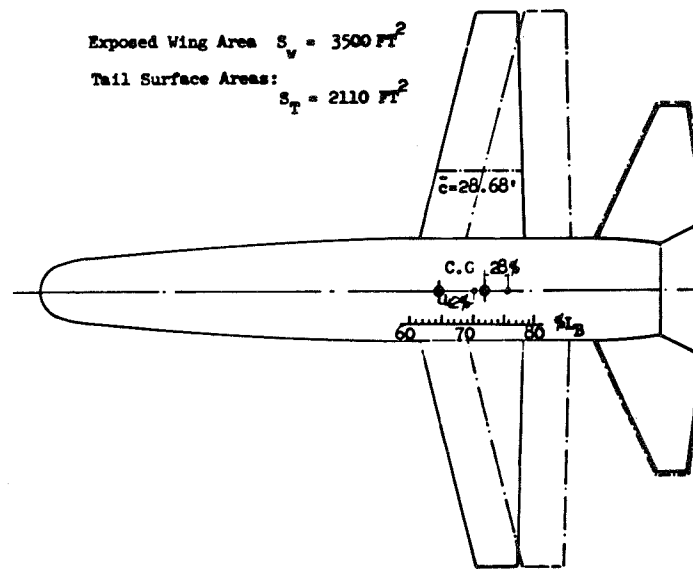
#### The Booster C.G. Problem (Wing-Fuselage-Tail-Concept)

This concept has a definite advantage over all other concepts. Should the booster C.G. fall further back, however, say to the 70 to 75 per cent point of the fuselage length and one has set his mind on keeping the concept of the straight wing, then two ways are possible though not advisable. (A) With a rearward movement of the C.G. and a fixed wing position the tail surface must increase rapidly to assure a stable airplane for the subsonic cruise. For hypersonic stability reasons these tail surfaces have to be partially unloaded. The other possibility (B) is a rearward shift of the wing with the C.G. position at roughly constant tail surface area. For a similar stability margin the wing and tail surface would blend into one another. In both cases enormous tail surfaces are necessary, which reduce the weight advantage considerably, since the total area of the exposed aerodynamic surfaces surpasses  $5,500 \text{ ft}^2$ . We do not think that placing a ballast of 40,000 to 50,000 lb into the nose of the fuselage is a wise idea. This amount of ballast would bring the C.G. forward to a tolerable location.



CONSTANT STATIC STABILITY MARGIN  
5% M.A.C.

Tail Surface Variation with C.G. Travel  
(Wing Position fixed)



Wing Variation with C.G. Travel  
(Tail Surface Area approx. constant)

Figure 4

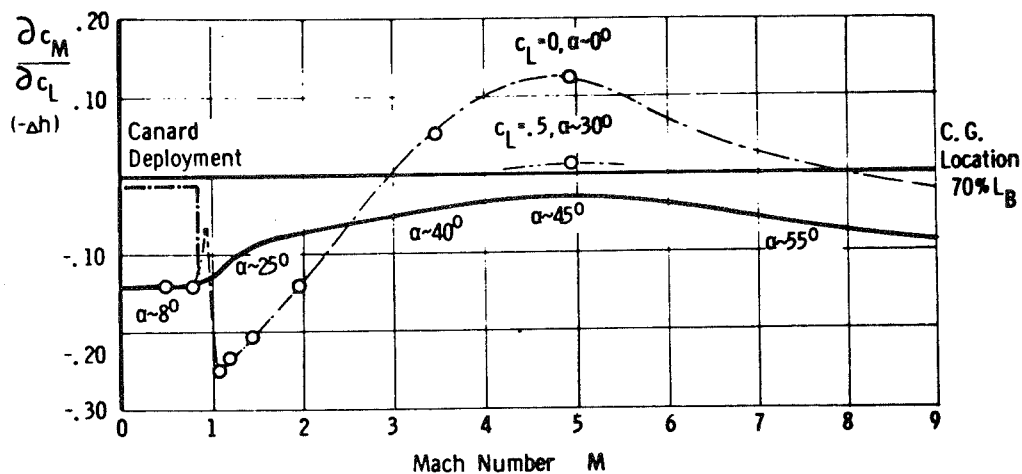
The Booster C.G. Problem (Delta-wing-fuselage versus folding canard-fuselage-wing concept)

To avoid an excessive rearward sweep of the wing for hypersonic static stability a folding canard is advantageous. During the re-entry phase of the booster trajectory the canard surfaces are folded back to the sides of the forward fuselage; it is thus shielded from excessive heating and does not need a TPS. The canard surface is hinged to the fuselage. The hinge line incidence is oriented such that the canard trims the cruise flight. To trim the higher angles of attack at landing the canard is provided with a flap (trim-tap) that can be deflected to some 15 to 20°.

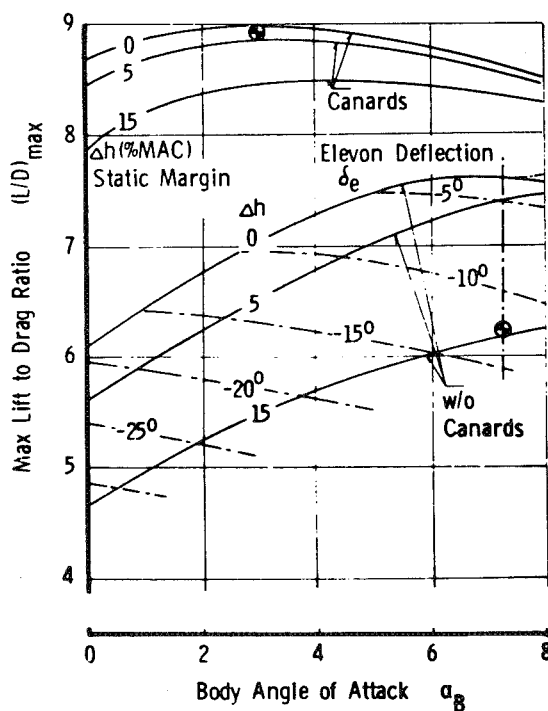
The upper graph shows an advantage of the folding canard. For a certain booster concept the aerodynamic center (A.C.) shift over the Mach number and angle-of-attack range might have the shape as shown in the graph. Wind tunnel measurements were extrapolated to higher angles of attack and combined with hypersonic theory in the Mach number range from  $M = 5$  to 10. We notice that in comparison to the low angle of attack A.C. shift the high angle of attack A.C. shift is much smoother over the Mach number range. Providing a 3 per cent stability margin at  $M = 5$  leaves us with a stability margin of  $\Delta h = 14$  per cent at the subsonic cruise condition. To reduce this large margin the canard surfaces are deployed and the A.C. moves about 12 per cent forward.

Let us now compare a booster with canard surfaces to a delta wing booster with trailing edge trim flaps. Both boosters have an aspect ratio  $A = 4$  wing of similar geometry. The trimmed maximum lift to drag ratio  $(L/D)_{\max}$  is plotted versus the body angle of attack  $\alpha_B$ . Thus the fuselage lift capability is used to aid in trimming the booster. This effect can clearly be seen in the curves representing the delta wing booster (without canards). With decreasing body angle of attack  $\alpha_B$  the elevon deflection becomes more and more negative (up-deflection). Since a static margin of 14 per cent has to be trimmed with an elevon deflection of  $\delta_e = 13$  per cent we choose a body angle of attack of  $\alpha_B = 7.25^\circ$  to

# Possible A.C. Travel within the Booster Flight Regime



## L/D Comparison for both Booster Concepts at Cruise Condition



### Booster w/o Canards

$\alpha_B = 7.25^\circ$   
 $\alpha_e = 13^\circ$   
 $L/D = 6.2$   
 $\Delta h = 14\% \bar{c}$

### Booster with Canards

$\alpha_B = 3^\circ$   
 $\alpha_e = 0^\circ$   
 $L/D = 8.9$   
 $\Delta h = 2\% \bar{c}$

Figure 5

obtain a favorable  $(L/D)$  maximum. For the booster with canards the body angle of attack has only a small influence, we choose an optimum body angle of attack of  $\alpha_B = 3^\circ$ , the flap deflection is  $\delta_e = 0^\circ$  and since the canard surfaces are deployed a small static margin has to be trimmed. (A static margin of  $\Delta h = 2$  per cent might be too small to sufficiently damp the longitudinal short period mode which will effect the handling qualities.)

### The Booster C.G. Problem (Delta-wing-fuselage versus folding canard-fuselage-wing concept)

The resulting booster concepts are shown in this graph. The booster with canards has a canard angle of attack of  $\alpha_c = 13^\circ$  to trim the cruise flight. This angle prescribes therefore the canard hinge line incidence angle with the booster centerline. This incidence angle is of the order of  $i_c = 10^\circ$ . Instead of moving the canard to a higher angle of attack to trim the landing case, we leave the hinge line at  $i_c = 10^\circ$  and deflect the canard trailing edge flap with an effectiveness of  $(\partial\alpha/\partial\delta_e)_c = -0.5$  to  $(\delta_e)_c = 14^\circ$ . We notice that the wing trailing edge flap is deflected by  $\delta_e = 13.5^\circ$  to obtain a higher usable maximum lift coefficient and thus reduce the landing speed.

The booster without canards on the other side has a high cruising attitude and even a much higher landing attitude of  $\alpha_B = 14^\circ$ . We also notice the tremendous length of the landing gear of almost 15 feet to obtain a wing tip clearance of 6 feet. The front landing gear has to accomodate much higher landing shocks as compared to those of the booster with canards.



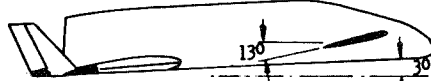
### BOOSTER WITH CANARDS

#### A) Cruise Condition

Exp. Wing Area  $S_W = 4\,000\text{ ft}^2$

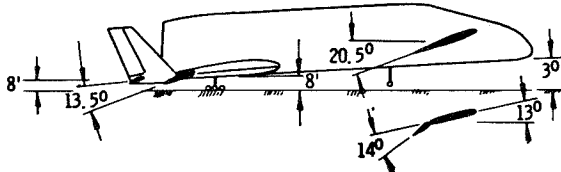
Refer. Area  $S_{ref} = 6\,700\text{ ft}^2$

$\alpha_{cr} = 7.4^\circ$	Angle of Attack
$q_{cr} = 162\text{ lb/ft}^2$	Dyn. Pressure
$\alpha_B = 30^\circ$	Body Angle of Attack
$\delta_e = 0^\circ$	Elevon Deflection
$c_L = 0.46$	Lift Coefficient
$\Delta h = 2\% \bar{c}$	Stability Margin
$\alpha_c = 13^\circ$	Canard Angle of Attack



#### B) Landing

$\alpha_L = 11^\circ$	Angle of Attack
$q_L = 110\text{ lb/ft}^2$	Dyn. Pressure
$\alpha_B = 30^\circ$	Body Angle of Attack
$\delta_e = 13.5^\circ$	Elevon Deflection
$c_L = 0.678$	Lift Coefficient
$\Delta h = 2\% \bar{c}$	Stability Margin
$\alpha_c = 20.5^\circ$	Canard Angle of Attack



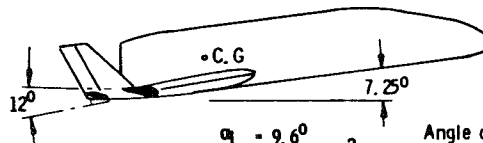
### BOOSTER WITHOUT CANARDS

#### A) Cruise Condition

Exp. Wing Area  $S_W = 5\,350\text{ ft}^2$

Refer. Area  $S_{ref} = 8\,300\text{ ft}^2$

$\alpha_{cr} = 6^\circ$	Angle of Attack
$q_{cr} = 200\text{ lb/ft}^2$	Dyn. Pressure
$\alpha_B = 7.25^\circ$	Body Angle of Attack
$\delta_e = -12^\circ$	Elevon Deflection
$c_L = 0.3$	Lift Coefficient
$\Delta h = 14\% \bar{c}$	Stability Margin



#### B) Landing

$\alpha_L = 9.6^\circ$	Angle of Attack
$q_L = 110\text{ lb/ft}^2$	Dyn. Pressure
$\alpha_B = 14^\circ$	Body Angle of Attack
$\delta_e = -18.6^\circ$	Elevon Deflection
$c_L = 0.55$	Lift Coefficient
$\Delta h = 14\% \bar{c}$	Stability Margin

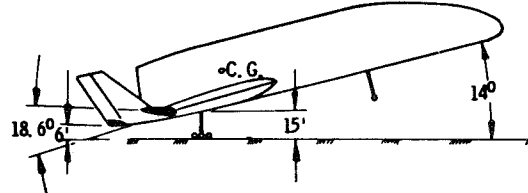


Figure 6

The Booster C.G. Problem (Delta-wing-fuselage versus folding  
canard-fuselage-wing concept)

The final weight trade-off results are shown in this table.

Explanations to:

1.) For the structural weight  $7 \text{ lb/ft}^2$  for the exposed wing area and  $3 \text{ lb/ft}^2$  for the thermal protection system was assumed. The delta wing booster with  $5,350 \text{ ft}^2$  exposed wing area and a fly-back weight of about 500,000 lb represents about the minimum wing area possible to maintain a landing speed of about 180 to 200 knots.

2.) The folding mechanism for the canard can be very simple and light if the canard is supported by a strut.

3.) The assumptions here are rather arbitrary. However, the assumption that approximately 10 per cent of the total landing gear weight is saved seems justified if we consider the shorter length (by 7 ft) and some saving in fuselage structure due to the less severe landing shock for the canard version.

4.) The full weight for both concepts was calculated for a cruise range of 500 miles without head wind.

5.) The thrust to weight ratio of  $T/W_E = 10$  is rather conservative and an increase in weight saving can be expected.

## WEIGHT TRADE-OFF RESULTS FOR CANARD AND DELTA WING BOOSTER

	DELTA WING BOOSTER	BOOSTER WITH CANARDS	LB
1) WING SIZE (EXPOSED) (10 LB/FT <sup>2</sup> STRUCT. + TPS)	$S_W = 5\,350\text{ FT}^2$	$S_W = 4\,000\text{ FT}^2$	-13 000
2) CANARD SIZE (7 LB/FT <sup>2</sup> + 1 000 LB FUSEL. STRUCT.)		$S_C = 700\text{ FT}^2$	+5 900
3) FUSELAGE-RUNWAY ANGLE	$i_L = 14^\circ$ EXCESSIVE GEAR LENGTH	$i_L = 3^\circ$ ASSUMED 10% SAVINGS	-1 600
4) PERFORMANCE DIFFER. FLY-PACK FUEL FOR 500 MILES, 300 M/H	$L/D = 6.2$ $h = 14\%$ MARGIN $W_{FUEL} = 21\,000\text{ LB}$	$L/D = 8.9$ $h = 2\%$ MARGIN $W_{FUEL} = 14\,000\text{ LB}$	-7 000
5) ADDITIONAL JET ENG. WEIGHT+INSTALLAT. (10% ENG. WEIGHT + 5% THRUST, T/W= 10).	$W_E = 12\,900\text{ LB}$	$W_E = 8\,900\text{ LB}$	-4 000
		WEIGHT SAVING FOR BOOSTER WITH CANARD	19 700

OTHER POINTS TO BE CONSIDERED:

- A) CANARDS CAUSE FLOW FIELD DISTORTIONS AT THE INTAKE OF THE JET ENGINES (WING MOUNTED).
- B) COMPLEXITY OF THE FOLDING MECHANISM AND THE TWO-POSITION DRIVE FOR THE CANARD SURFACES AND CANARD TRAILING EDGE FLAPS.

Figure 7

### Canard Characteristics

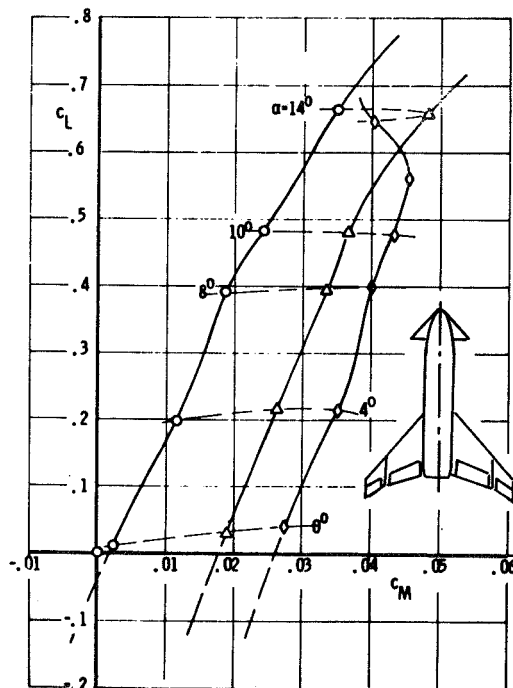
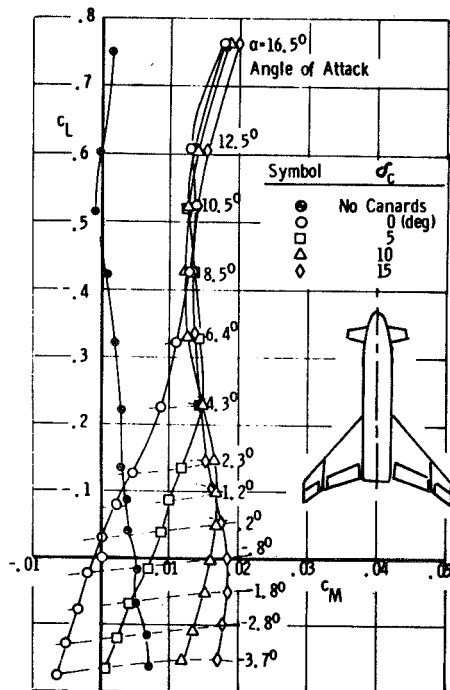
The configuration without canards was marginally stable up to an angle of attack of about  $\alpha = 10.5^\circ$  corresponding to  $c_L = 0.51$ . For higher angles of attack the configuration was unstable. The installation of canards shifted the A.C. further forward and made the configuration unstable. The A.C. location for this booster was approximately 74.2 per cent of the fuselage length. We see that the canards are totally insufficient. The flow separates from the upper surface at canard angles of attack of approximately  $\alpha_c \sim 10^\circ$ .

To remedy this inefficiency we select a delta canard of an aspect ratio (exposed)  $A_c = 2$  and keep the canard volume  $V_c = (l_c [\partial c_L / \partial \alpha] E) / (c F)$  the same. This canard configuration is much more efficient, since it has not the same stall characteristics the straight canard has. The stall angles of attack for the delta canard occur at  $\alpha_c = 25^\circ$  to  $30^\circ$ .

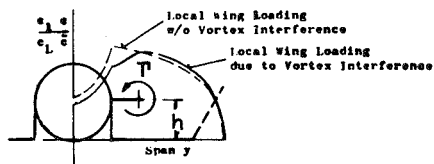
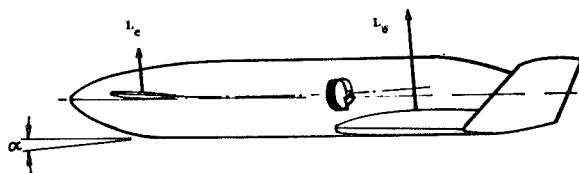
In general the canard disturbs the flow field in front of the rearward wing. The degree of disturbance is very much a function of the position of the canard and the vortex shed from it relative to the wing. The vortex strength  $\Gamma$  is proportional to the canard lift  $L_c$ . Slender body theory predicts the loss of one canard lift on the main wing if the vortex is located in the same plane as the wing. The sketch illustrates this case and shows the change of the wing loading in the vicinity of the body due to the canard vortex. With increasing vortex distance  $h$  from the plane of the wing the interference becomes smaller.

We compare now the lift curve of the booster without canard with the lift curve of the booster with canard, and find that indeed the slope is almost identical. (In this case the negative angles are plotted since the vortex passed through the plane of the wing.)

# CANARD EFFECTIVENESS



$S_{ref} = 10250 \text{ ft}^2$ ,  $\bar{c} = 74.7 \text{ ft}$ ,  $M = 0.35$   
 $x_{C.G.} = 155.8 \text{ ft}$  from Nose  
 $l_{ref} = 210 \text{ ft}$ ,  $(\partial C_M / \partial \delta_c)_{C_L=0} = 0.09$



COMPARISON OF THE TOTAL LIFT CURVE SLOPE OF A BOOSTER WITH AND WITHOUT CANARDS.

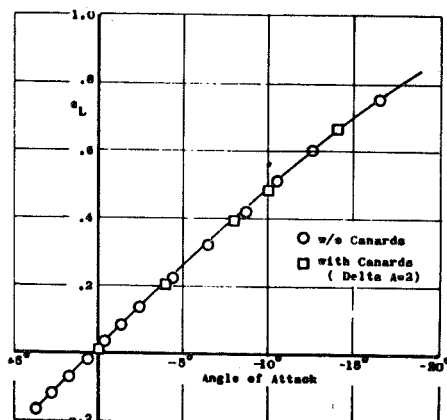


Figure 8

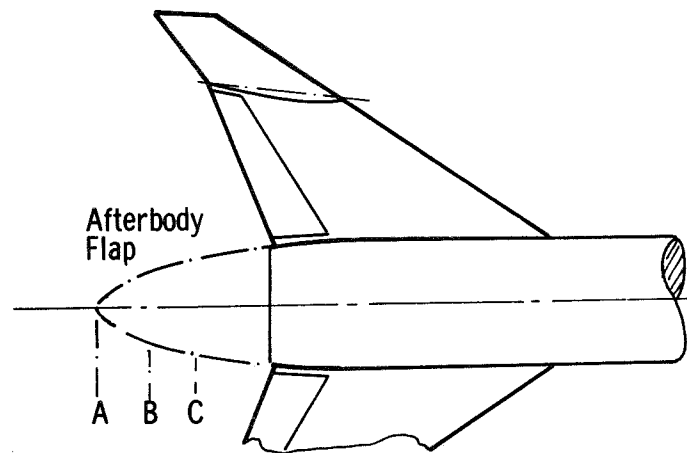
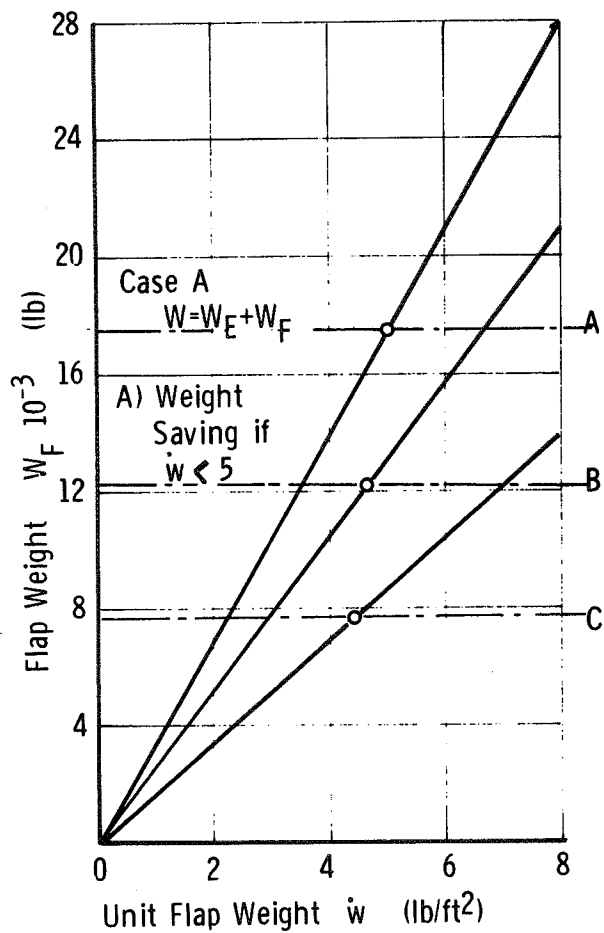
## The Base Pressure Problem

The base drag contribution to the zero drag coefficient  $c_{D0}$  is on the order of 50 per cent and more. Therefore an elimination of this portion, if one is fortunate enough to achieve it, would increase the  $(L/D)$  max ratio by more than 40 per cent. We investigated an afterbody flap which completely enclosed the base as shown in the graph and which was long enough to eliminate flow separation.

The flap weight  $W_F$  as a function of the unit flap weight was compared to the propulsion system weight which was saved due to an increase in  $(L/D)_{max}$ . We obtain a break-even point of  $\dot{w} = 5 \text{ lb/ft}^2$ . This unit weight consists of the flap weight plus the hinge and actuator weight plus any additional weight of the fuselage structure necessary to support the flap, hinge and actuator. As an alternative partial afterbody flap extensions were investigated. The base pressure was held constant for these cases and boat-tail effects were not considered. The break-even unit weight decreased to a small extent.

The break-even point depends to some extent on the level of  $(L/D)_{maximum}$ . At relatively low  $(L/D)_{max}$  the propulsion system weight saving might be higher and thus the break-even point.

To obtain a substantial weight saving the structure has to be build with a unit weight of much less than  $5 \text{ lb/ft}^2$ . It is rather doubtful that this can be achieved with conventional rigid structures.



Assumptions:

Case A	100 % Flap Area	$A = 3500 \text{ ft}^2$
B	75 %	$2600 \text{ ft}^2$
C	50 %	$1750 \text{ ft}^2$

Figure 9

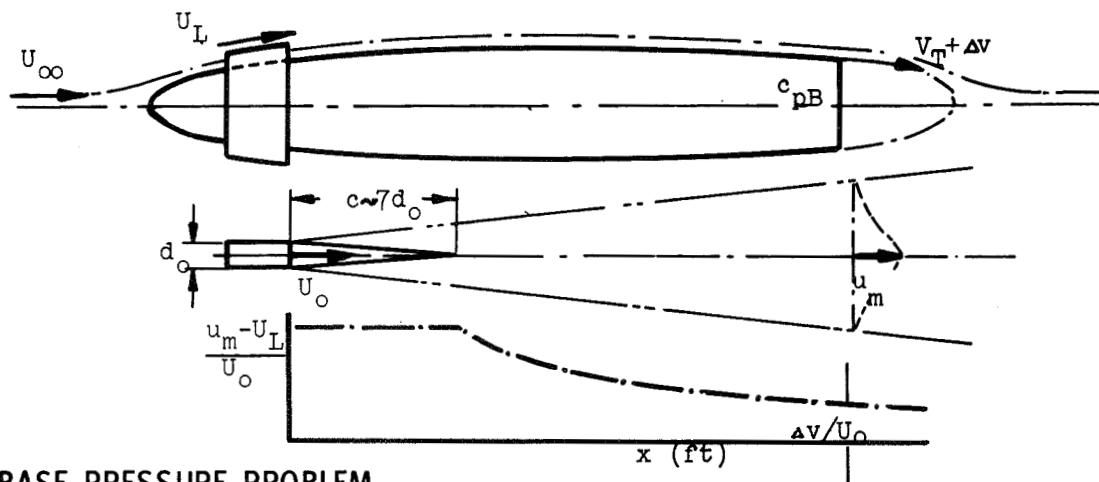
## The Base Pressure Problem

In the sketch a quite different base pressure problem is touched upon. Any fuselage-mounted jet engine increases the velocity along the body and consequently along the free streamline which we assume as an idealization of the free shear layer of the wake. Furthermore, we make the simplifying assumption that the jet engine completely surrounds the axisymmetric fuselage. We see that the base pressure increase is approximately twice the velocity increment due to the expanding jet.

A simple calculation shows the influence of the jet engine on the maximum lift to drag ratio. If we assume the base drag to be 50 per cent of the total zero drag coefficient and the jet engines increase the base pressure by 100 per cent, then we can expect a probable 20 per cent drop in  $(L/D)_{\text{maximum}}$ .

To solve this problem in future tests certain appropriate scaling laws should be established to make the experiments meaningful. Besides the Reynolds number and the geometry of the body, the pressure ratio across the jet engine exit, the Mach number and the temperature of the jet plays a role. In one of the follow-on papers we will hear about one of the early experiments which were conducted with orbiter models.





### THE BASE PRESSURE PROBLEM

ASSUMPTIONS:

- THE JET ENGINES FORM A RING AROUND THE FRONT PART OF THE FUSELAGE.
- THE JET CENTERLINE VELOCITY DECREASES AS  $(u_m - U_{\infty})/U_0 \sim (c/d_0)/(x/d_0)^{1/n} (n=1,2)$ .
- THE WAKE FREE SHEAR LAYER IS APPROXIMATED BY A FREE STREAMLINE. THE TANGENTIAL VELOCITY ALONG THE FREE STREAMLINE IS  $(V_T + \Delta v)/U_{\infty}$ .

THE BASE PRESSURE WITHOUT JET INTERFERENCE

WITH JET INTERFERENCE

THE BASE PRESSURE INCREASE IS THEREFORE

$$c_{pB} = 1 - (V_T/U_{\infty})^2$$

$$c_{pB}^* = 1 - ((V_T + \Delta v)/U_{\infty})^2$$

$$-\Delta c_{pB} \sim 2(\Delta v/U_{\infty})$$

INFLUENCE ON  $(L/D)_{\max}$

DRAG POLAR REPRESENTATION

$$c_D = c_{D0} + k(c_L)^2$$

$$\frac{(L/D)_{\max}^*}{(L/D)_{\max}} = (c_{D0}/c_{D0}^*)^{\frac{1}{2}}$$

(\* DESIGNATES JET INTERFERENCE. ASSUMPTION: THE JET VELOCITY INFLUENCES ONLY THE ZERO DRAG COEFFICIENT)

Figure 10

## Conclusion

Many more aerodynamic problems can be identified and which must be solved in the end to make the Shuttle vehicle a sufficient flying machine. Other problems which come to my mind are for instance the elevon effectiveness as a function of the Mach number. Since the flap effectiveness decreases rapidly with the Mach number due to the rather blunt flap trailing edge angle a split flap which can be adjusted to a better supersonic effectiveness is probably the answer if the weight can be kept within tolerable bounds. One other problem I want to mention is the shaping of the forward fuselage. From the point of view of the volumetric efficiency a blunt nose has the advantage. Excessive bluntness, if properly shaped, does not necessarily impede the subsonic flying qualities, however, from the composite vehicle ascent performance point of view a high slenderness ratio would definitely be preferable to reduce the wave drag and increase thus the payload capability.

In conclusion I would again like to emphasize that I do not intend to sell the idea of a canard booster version, I just want to point out that there are other avenues to reach the goal of designing an efficient Space Shuttle booster.



# SPACE SHUTTLE AIRBREATHING ENGINE EXHAUST EFFECTS

C. F. Ehrlich, Jr.

Lockheed Missiles & Space Company  
Sunnyvale, California

## PROGRAM OBJECTIVE

Airbreathing engines are required on space shuttle orbiters and boosters to permit airport go-around capability and postboost flyback. On a majority of the proposed vehicles, and particularly the orbiters, these engines have been located in the nose of the aircraft to meet aerodynamic balance and center-of-gravity requirements. On a few concepts, it has been possible to locate the engines amidships, on the wing, or (in the case of one notable example) in the body with exhaust into the base region.

With such installations, some interference of the exhaust flow on the vehicle aerodynamic characteristics, particularly in the case of the nose-mounted systems, may rightfully be expected. It appears imperative, then, to obtain test data which simulates these flow fields for preliminary evaluation. This paper presents the results of one such investigation. The particular test program was based on the Lockheed Delta-Body Orbiter and was sponsored by the NASA Marshall Space Flight Center.

## PROGRAM OBJECTIVE

---

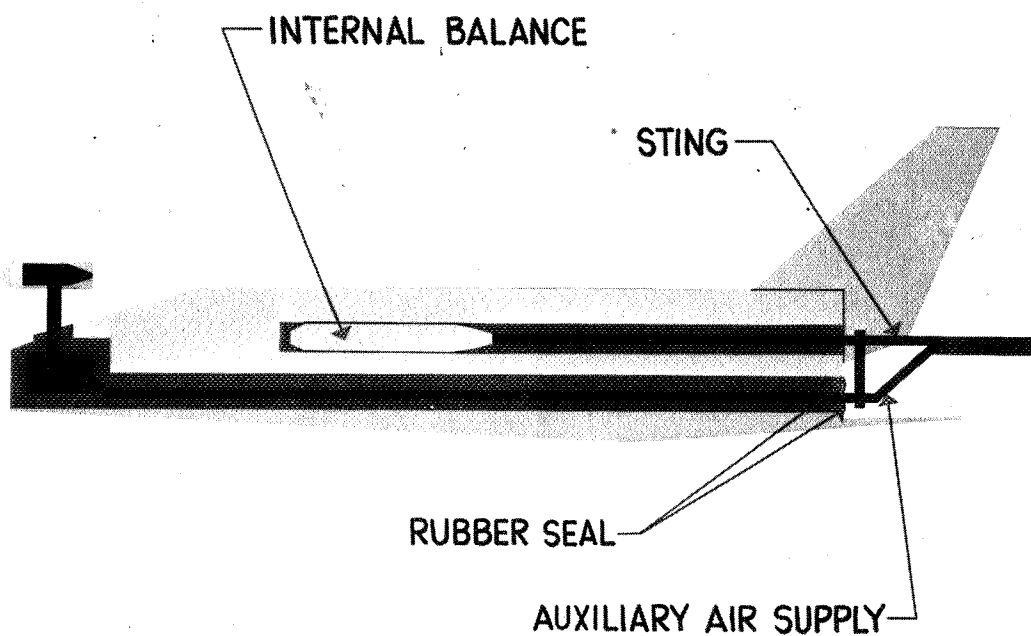
TO MAKE A PRELIMINARY EVALUATION  
OF CHANGES IN VEHICLE AERODYNAMIC  
CHARACTERISTICS INDUCED BY THE  
EXHAUST FLOW FROM NOSE-MOUNTED  
AIRBREATHING ENGINES.

## MODEL ARRANGEMENT

An existing model, which had previously been tested in a large subsonic wind tunnel, was modified for this test program. The desired data included the incremental aerodynamic effect due to the exhaust flow and the total loads exclusive of the thrust component. The model arrangement is shown schematically in this figure. Testing was performed with the nacelles off (stowed), nacelles on (power-off), and power-on in the presence of the spacecraft. The air supply and nacelle system were mounted so as to bypass the balance system and thus provide isolated air-on increments; grounding strips ensured that redundant loads were not measured. Each exit total and static pressure was monitored in order to calculate actual mass flow rates (exit mach numbers were near sonic). Because of the limitations of the existing air supply system, the achieved mass flow rate was about one-third of that required for full-scale simulation.

# MODEL ARRANGEMENT

---



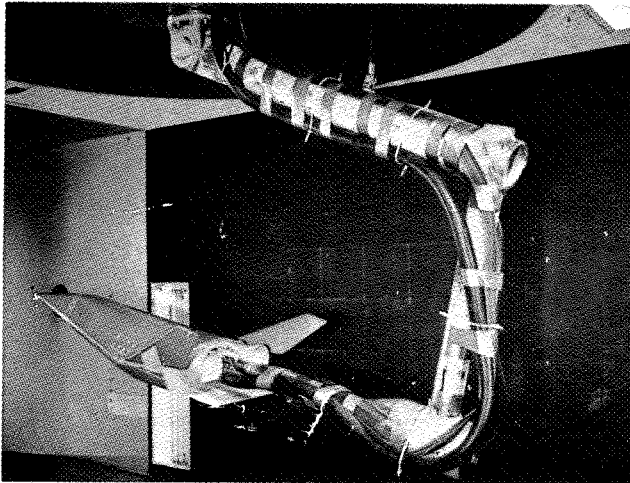
## TEST PROGRAM

The model installation employed during the present series was identical to that used during the earlier Lockheed tests. The only exceptions were that the model was rotated 180 degrees relative to the yoke support and the air supply system installed. The yoke system pivoted about the upper knuckle for pitch, and the entire system yawed for sideslip data. Maximum trim flap deflections were limited to -10 degrees as compared to the -20 degrees required for trim at landing attitudes.



## TEST PROGRAM

---



### NAVAL SHIP RESEARCH & DEVELOPMENT CENTER

- 8 FT X 10 FT SUBSONIC WIND TUNNEL

- TEST CONDITIONS

MACH NUMBER = 0.2

ANGLE OF ATTACK  $0^{\circ} \leq \alpha \leq 20^{\circ}$

SIDESLIP ANGLE  $-5^{\circ} \leq \beta \leq +5^{\circ}$

- PARAMETERS

NACELLE LOCATION

MASS FLOW RATE  $0 \leq \dot{m} \leq 2.5$  LBS/SEC

ELEVON DEFLECTION  $0^{\circ} \leq \delta_e \leq -10^{\circ}$

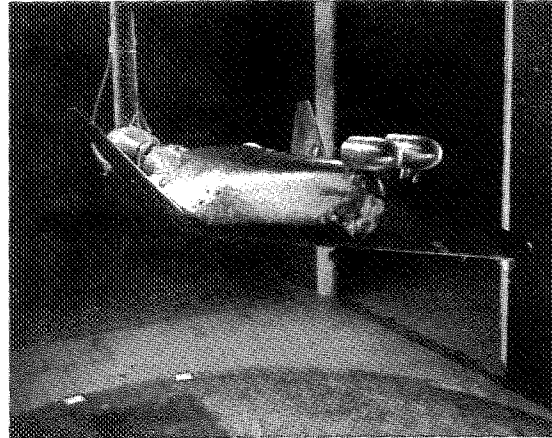
## NACELLE INSTALLATION

Each model nacelle was configured to simulate a frontal area of a two-engine nacelle deployed from a stowed position inside the body. Four nominal positions were selected for testing representing candidate installations: top, high and low sides, and lower surface. The low side position was not tested because of mechanical problems.

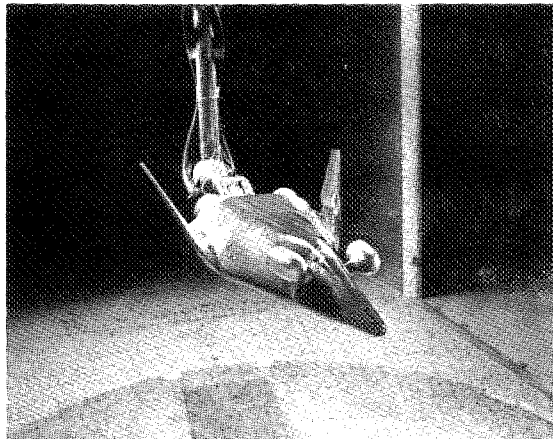
# NACELLE INSTALLATION

---

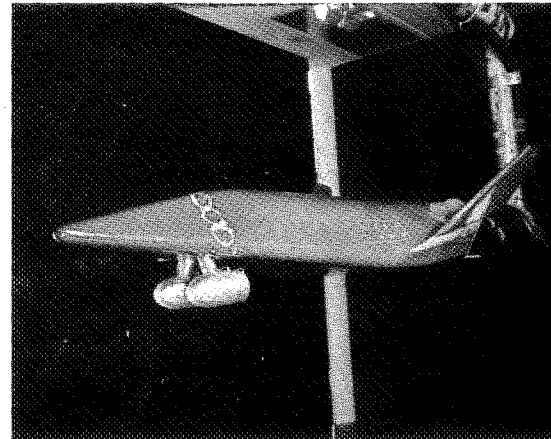
POSITION A



POSITION B



POSITION D



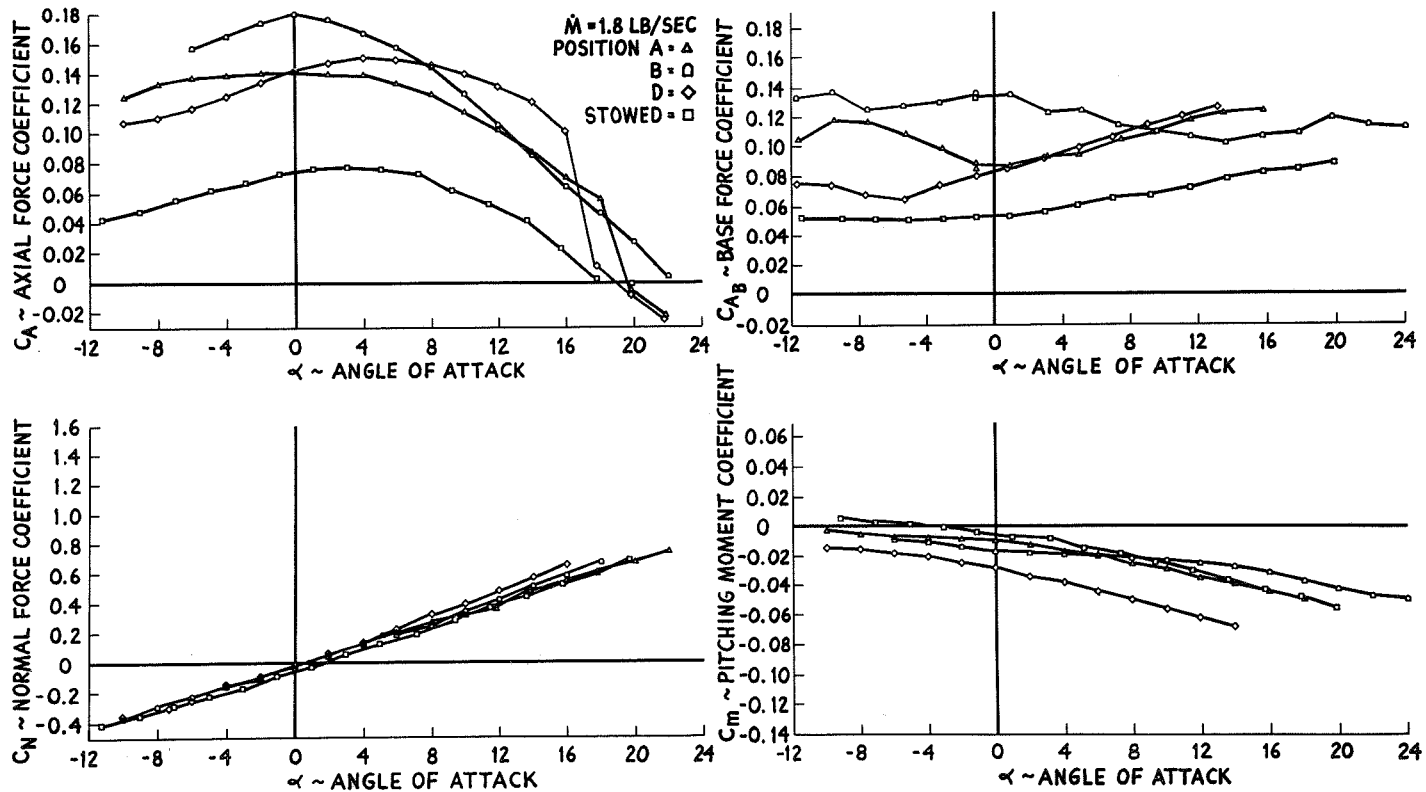
## AERODYNAMIC CHARACTERISTICS: TOTAL CONFIGURATION

Aerodynamic force and moment coefficients were reduced and are presented in two ways. First, the incremental loads induced by the exhaust were calculated from the air-on and air-off data from the isolated nacelle system. Finally, total aerodynamic loads were calculated by adding data for the dummy nacelle configuration to these incremental data, thus eliminating the thrust increment.

The data presented in this chart illustrate the relative magnitude of the exhaust-induced flow field on the total vehicle aerodynamics for zero trim flap deflection. Three nacelle positions at the maximum blowing rates are shown along with the "clean" vehicle (engines stowed). In each case, the dummy nacelles had only a relatively small effect on total vehicle characteristics. The large increments in axial force are due primarily to substantial base drag increases most likely resulting from aspiration of the base region by the higher energy flow. As noted, these increments vary considerably with angle-of-attack and nacelle position; however, in any case, significant increases in required engine thrust levels may be incurred. Pitching moment increments also vary considerably: no effect on top, a "canard" effect on the sides, and a near constant increment on the lower surface. The latter case is approximately balanced by engine thrust moments; it produces the largest increment in normal force of the three tested positions, though less dramatic than in the case of axial force. The lift-to-drag ratio increments, of course, reflect both the axial and normal force increases. As we will see later, the decrease in  $L/D$  may be reduced for this particular configuration with trim elevon deflections at flight attitudes.

# AERODYNAMIC CHARACTERISTICS

## TOTAL CONFIGURATION

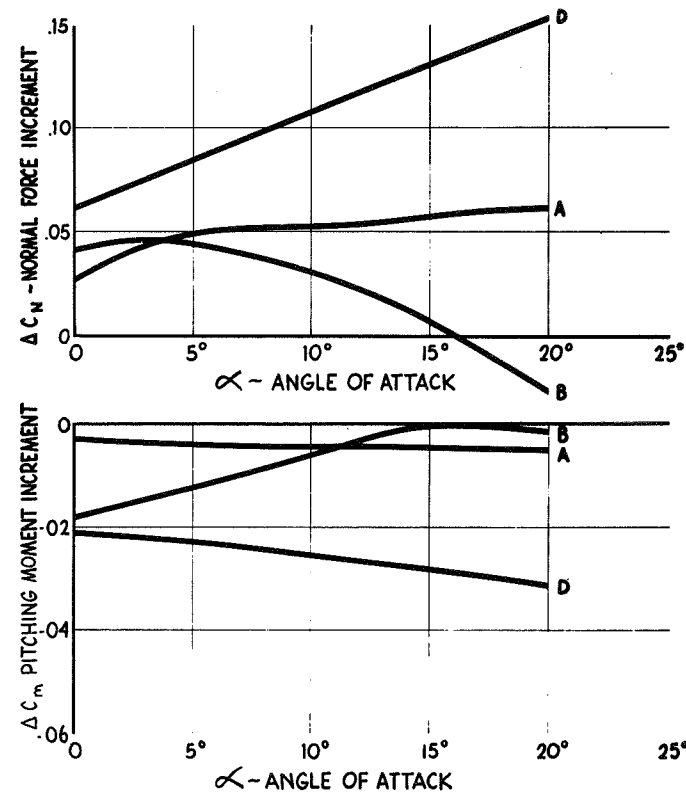
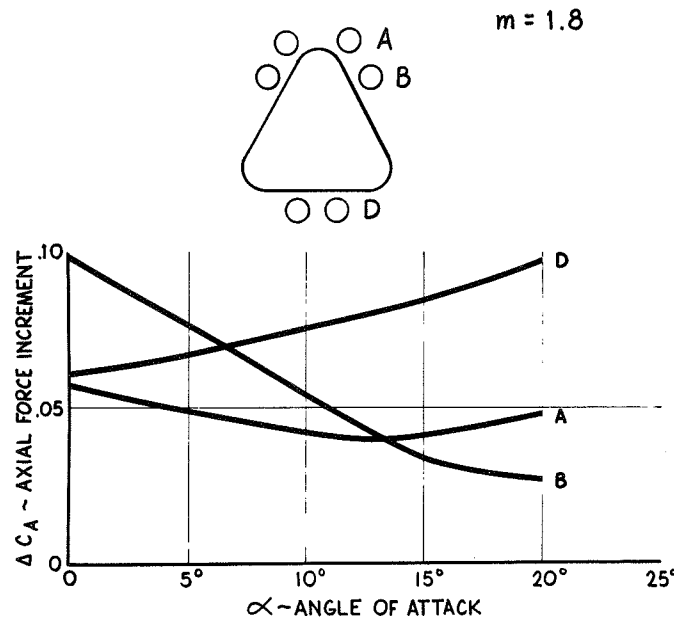


## LONGITUDINAL EFFECTS: NACELLE POSITION

The data in this and the next few charts are presented as simulated exhaust flow increments so as to illustrate the aerodynamic effects. This chart shows the incremental data of the previous chart and, as a result, emphasizes the nacelle position and angle-of-attack variations. Perhaps the most striking effects are those of nacelle Position B, where the exhaust flow interacts directly with the delta-body flow field and, to some extent, with the fins. For the other two positions, A and D, the normal and axial force increments tend to compensate each other, to some extent, for  $L/D$ . The pitching moments require additional elevon deflection for trim, although thrust moments, as noted before, tend to be compensating for Position D.

# LONGITUDINAL EFFECTS: NACELLE POSITION

35



## LONGITUDINAL EFFECTS: MASS FLOW RATE

Variations of the aerodynamic effects tended to be proportional to the mass flow rates tested; representative data from Position B are shown here. No apparent "leveling out" was noted for the present test range, so it is a matter of conjecture as to the maximum effect. It may also be possible that exit velocity may be a more realistic simulation parameter than mass flow rate. It is interesting to note the reversal in the normal force increment at low flow rates: this reversal is not seen in data for the other tested nacelle positions and is, again, likely to be related to an interaction with the delta-body flow field.



**Page intentionally left blank**

## LONGITUDINAL EFFECTS: TRIP FLAP DEFLECTION

Trim flap deflection tended to reduce the large axial force increments noted earlier at zero deflection. The tested deflections were less than those required for trim at landing attitudes, but extrapolation of the moment data implies an increased deflection requirement for trim. In the case of the present configuration, the trim flaps deflect into the base region and normally provide a boattailing effect; a similar reduction is apparent in the axial force data. Linear extrapolation of these increments, then, appears to result in a small  $L/D$  reduction for this configuration.

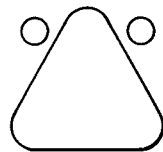
**Page intentionally left blank**

## LATERAL/DIRECTIONAL EFFECTS: MASS FLOW RATE

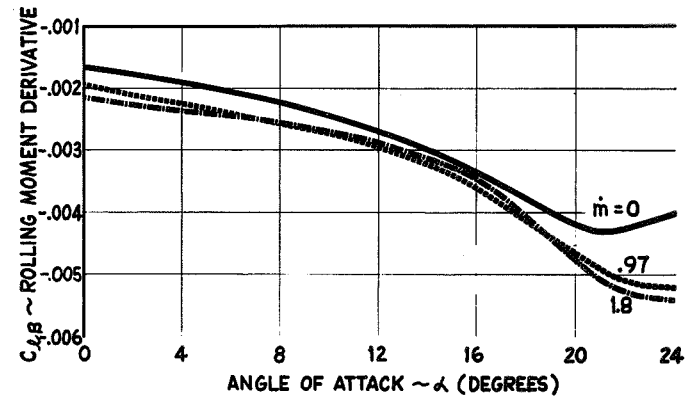
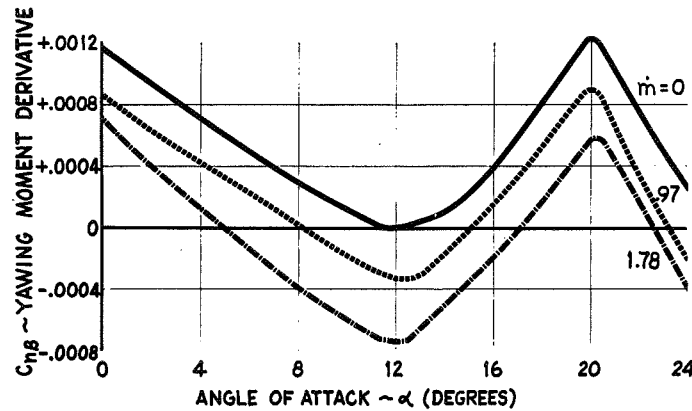
Variations in mass flow rate for the Position B installation produce a nearly linear change in the directional stability derivative; the change is essentially constant with angle-of-attack. Only small and inconclusive effects were noted for the side force derivatives and dihedral effect. These results are probably very closely related to the particular geometry inasmuch as the vertical tails may have been influenced by the exhaust flow in addition to the forebody. The "saddle" shape of the left-hand curve is typical for this configuration and is believed to be related to the body flow field interaction with the fins.

# LATERAL/DIRECTIONAL EFFECTS

## MASS FLOW RATE



POSITION B

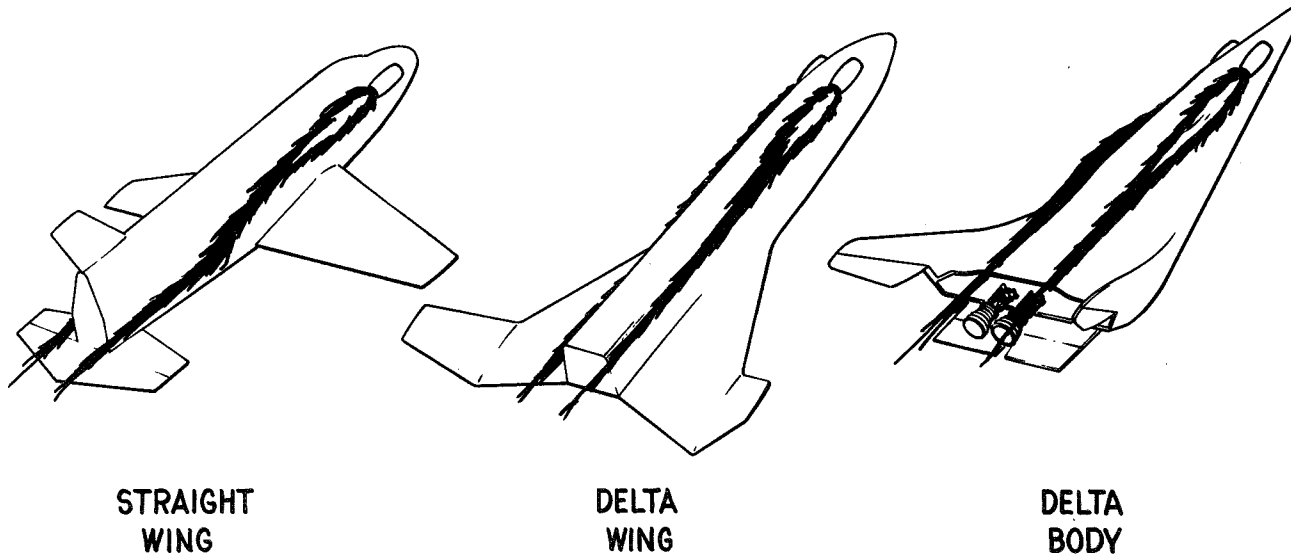


## POTENTIAL EFFECTS ON OTHER ORBITER CONCEPTS

While the present study has been limited to the delta-body concept, some speculation can be made regarding other concepts. In each case, high-velocity exhaust flow can produce an aspirating effect on the large base areas typical of orbiter and booster vehicles; it may be possible to reduce this penalty by effective reduction of base area by control deflection or by boattailing. Like the delta-body, the delta-wing configuration can expect to experience normal force increases and corresponding negative pitching moment increments. Straight-wing concepts should experience smaller changes in normal force since less of their lifting surfaces will be affected. However, significant changes in both horizontal tail and pitch control effectiveness could develop through interaction of the exhaust flow and downwash. Directional stability may be affected to some degree in all cases, depending mainly on the relative location of the vertical surfaces.

## POTENTIAL EFFECTS ON ORBITER CONCEPTS

---



## CONCLUSIONS

This brief test program has revealed that the engine installation arrangement can have a significant effect on vehicle aerodynamic performance. Because of conflicting requirements, it will be difficult in many cases to locate the air-breathing propulsion system in a noninterference position; thus there will remain a strong geometry influence on exhaust interaction. Further simulation is definitely required and perhaps expanded to include other performance aspects, simulation techniques, and technologies. Future testing should include, as a minimum, configuration build-up, surface and flow field visualization, and ultimately, surface pressure surveys.



# CONCLUSIONS

---

INFLUENCE IS GEOMETRY-ORIENTED

- MOUNTING ARRANGEMENT
- MASS FLOW RATE
- VEHICLE CONFIGURATION

SIMULATION OF SPECIFIC VEHICLES REQUIRED

- GEOMETRY INTERFERENCE
- INLET PERFORMANCE
- VELOCITY SCALING ?
- THERMAL / ACOUSTIC EVALUATION ?



TO WHAT EXTENT SHOULD SPACE SHUTTLE STABILITY AND CONTROL  
BE PROVIDED THROUGH STABILITY AUGMENTATION?

M. E. Wawrzyniak

McDonnell Douglas Astronautics Company  
St. Louis, Missouri

Introduction

It is evident that attempts to achieve "good" reentry vehicle basic airframe stability and control characteristics result in significant penalties in terms of weight, heat protection and aerodynamic performance. These penalties are ultimately reflected in smaller payloads to orbit and higher costs. Thus, there is merit in optimizing the basic airframe stability to obtain the required safety, control performance, and operational considerations for the least penalty.

The space shuttle vehicle stability problems are especially severe because of the far aft center-of-gravity which is due, to a large extent, to the large weight of the boost engines. This is especially true of the booster vehicle. The problem is further compounded because this same mass concentration, near the rear of the vehicle, results in very large pitch and yaw moments of inertia. With these greater than usual inertias (for the vehicle size), greater static margins are required to obtain the desired natural frequencies or "stiffness".

Past studies on reentry vehicle flight control and stabilization problems have led to the conclusion that lifting reentry vehicles, designed "customarily", generally require stability augmentation over most of their flight regime. Two questions then arise. What are the consequences of smaller static margins on controllability? The advent of fly-by-wire, redundancy and fail operational techniques are expected to allow reductions in basic airframe stability from a safety point of view. There remains, however, the question of what vehicle deficiencies can be practically augmented to provide the required handling qualities and automatic control system performance.

Results from a strictly theoretical analysis would not provide an adequate basis for answering these questions. Given a set of stability and control derivatives, it is theoretically possible to achieve almost any augmented stability and control characteristics. The problem is that the stability augmentation system may not be practical. For example, it may be critically dependent on poorly known data or require excessive control surface deflections. There are many other considerations such as structural resonance effects, control surface rate limits and limit cycle oscillation tendencies. Thus, there is no explicit solution, and much must be based on past simulation results, experience and engineering judgment. It is the purpose of this paper to provide an insight to the above questions.

### Typical Unaugmented Lifting Reentry Vehicle Short Period Stability Characteristics

Typical lifting vehicle basic airframe stability characteristics are expected to fall within the envelope illustrated in Figure 1. Superimposed on the plot is a commonly used handling qualities criterion referred to as the Cornell "Thumbprint" which defines combinations of frequency and damping for good piloted handling qualities.

Normally the approach is to design the vehicle such that it will exhibit a static stability margin over the flight regime. At high hypersonic speeds, however, the frequency and damping requirements are not met because of low dynamic pressures. As the vehicle flies down the entry corridor into the supersonic region, dynamic pressure increases and the vehicle natural frequencies become quite good, but the nature of the flight regime (high speed) and vehicle shape are such that short period damping is inadequate. It is not until the vehicle reaches subsonic speeds that it exhibits acceptable unaugmented handling qualities.

# UNAUGMENTED LIFTING REENTRY VEHICLE SHORT PERIOD STABILITY

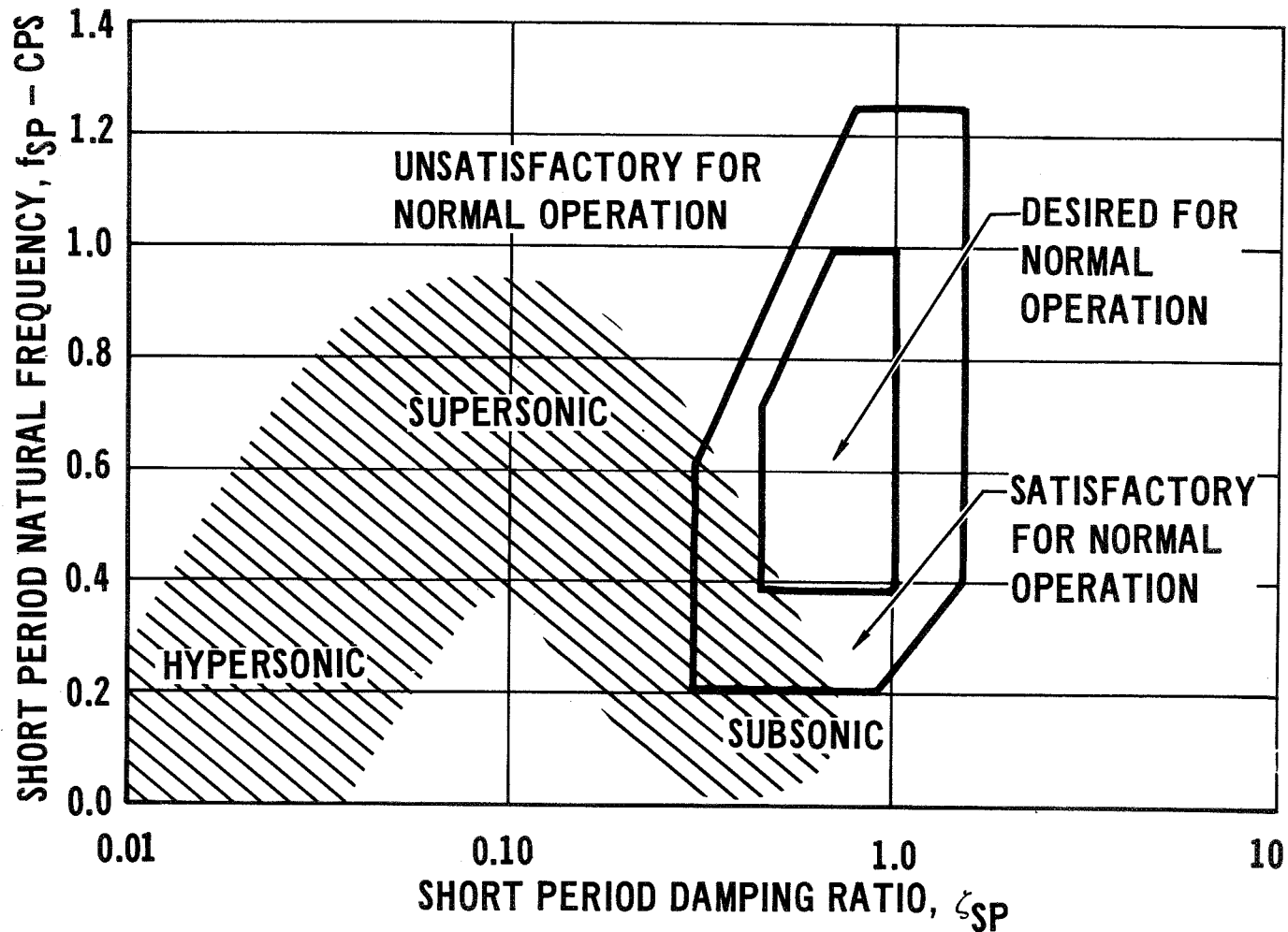


FIGURE 1

### Pitch Axis Stabilization Requirements

Pitch axis stabilization requirements are summarized in Figure 2. Increased short period damping is required throughout the flight regime except possibly some subsonic conditions. At hypersonic speeds and high altitudes there is a requirement to "stiffen" the aerodynamic spring, i.e., to increase the short period frequency. High altitude (greater than 200,000 feet) conditions that fall in the "hypersonic" region of the previous figure will generally require reaction control for damping. Often the control surfaces are sufficiently effective to trim the vehicle, but help from reaction controls is required for damping.

Control augmentation, where a vehicle motion is commanded rather than control surface position, is often required to obtain the necessary transient response characteristics to manual and/or automatic maneuver commands.

# **PITCH AXIS STABILIZATION REQUIREMENTS**

- **INCREASED SHORT PERIOD DAMPING**
- **INCREASED SHORT PERIOD NATURAL FREQUENCY  
AT HYPERSONIC SPEEDS**
- **REACTION CONTROLS DURING INITIAL ENTRY AT  
DYNAMIC PRESSURES LESS THAN 50–75 PSF**
- **CONTROL AUGMENTATION**

**FIGURE 2**

### Unaugmented Lifting Reentry Vehicle Dutch Roll Characteristics

Typical lifting vehicle lateral oscillatory characteristics are illustrated and compared with a handling qualities criteria in Figure 3. As in the longitudinal case, this criteria indicates that the vehicles would be flyable manually without augmentation at the lower speeds, but artificial damping and increased directional stiffness will be required at the higher speeds.

Although the hypersonic region indicates that the vehicles possess an aerodynamic spring (i.e., a Dutch roll frequency) it does not mean that they exhibit a positive value of  $C_{n\beta}$ . The reason for this is discussed in the next figure.



# UNAUGMENTED LIFTING REENTRY VEHICLE DUTCH-ROLL CHARACTERISTICS

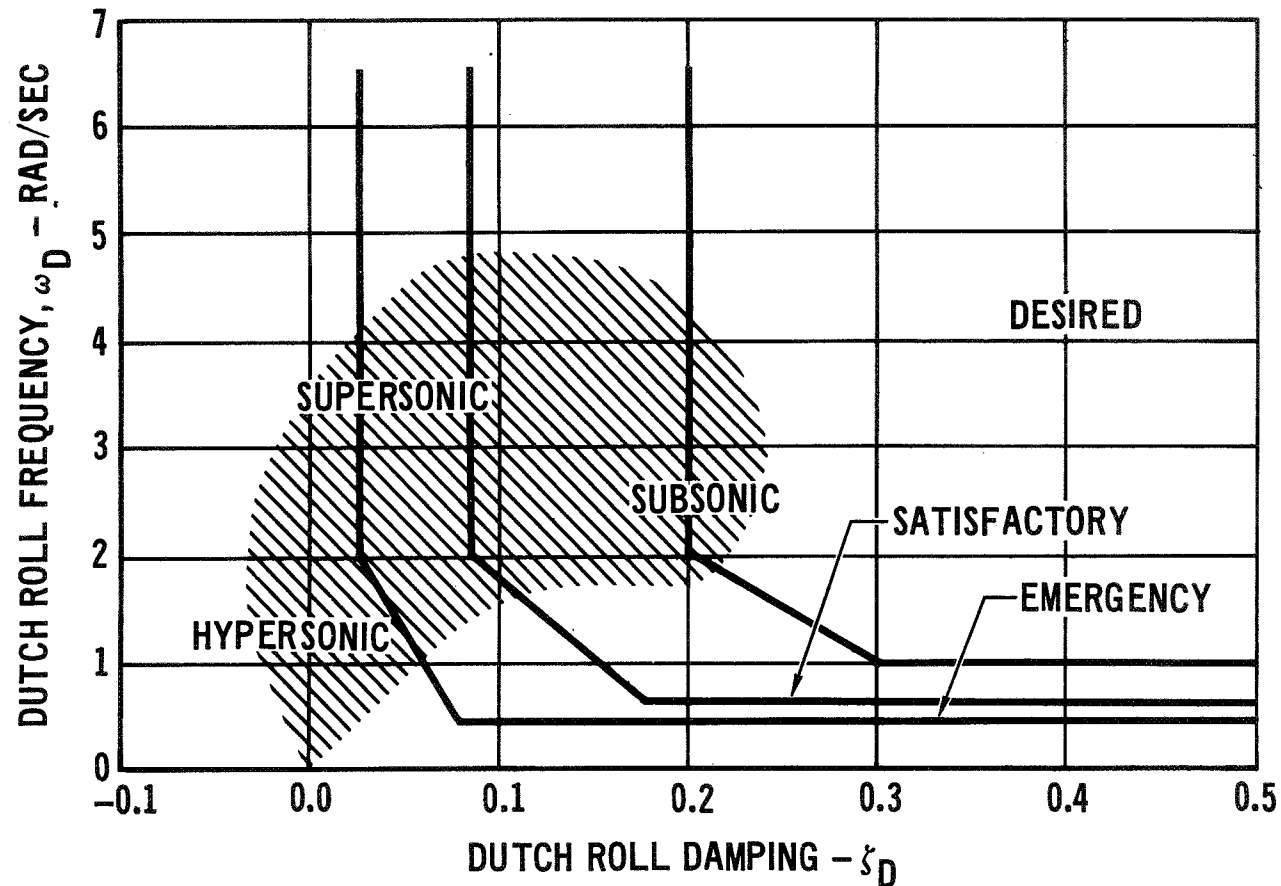


FIGURE 3

### Dynamic Stability Due to Positive Dihedral Effect

The Dutch roll frequency depends on a combination of  $C_{n\beta}$  and  $C_{l\beta}$  as defined by the expression in Figure 4. The effect of positive effective dihedral is to compensate for negative directional stability. However, the vehicle roll attitude must not be constrained to realize the stabilizing effect.

For a configuration flying at a very high angle of attack, a roll damper can be used, and vehicle bank angle maintained using a yaw attitude control system. At angles of attack below approximately 45 degrees, roll attitude control is required, and a negative directional stability requires a sideslip angle feedback.

# DYNAMIC STABILITY DUE TO POSITIVE DIHEDRAL EFFECT

$$\omega_D^2 = \frac{q S b}{I_z} C_{n\beta \text{ DYN}}$$

$$C_{n\beta \text{ DYN}} = C_{n\beta} \cos \alpha - \frac{I_z}{I_x} C_{l\beta} \sin \alpha$$

Figure 4

### Unaugmented Lifting Reentry Vehicle Lateral Control Characteristics

Typical lifting body lateral control performance is illustrated in terms of roll acceleration and roll mode time constant in Figure 5. Superimposed on the plot is an aircraft handling qualities criterion for comparative purposes. In general, the control response performance degenerates in the higher speed regimes, and control coupling effects would result in additional reductions in roll acceleration. Note that when  $N_\beta$  in the numerator of the expression for the rolling effectiveness parameter is small, the configuration is highly susceptible to adverse aileron yaw (negative  $N_{\delta a}$ ) and sluggish roll or reversal will occur. Reversal also occurs when  $N_\beta$  is negative and dominant in the numerator making  $(\omega_\phi/\omega_D)^2$  negative. A discussion of how augmentation affects the rolling effectiveness parameter is discussed on the following figure.

# UNAugmented LIFTING REENTRY VEHICLE LATERAL CONTROL CHARACTERISTICS

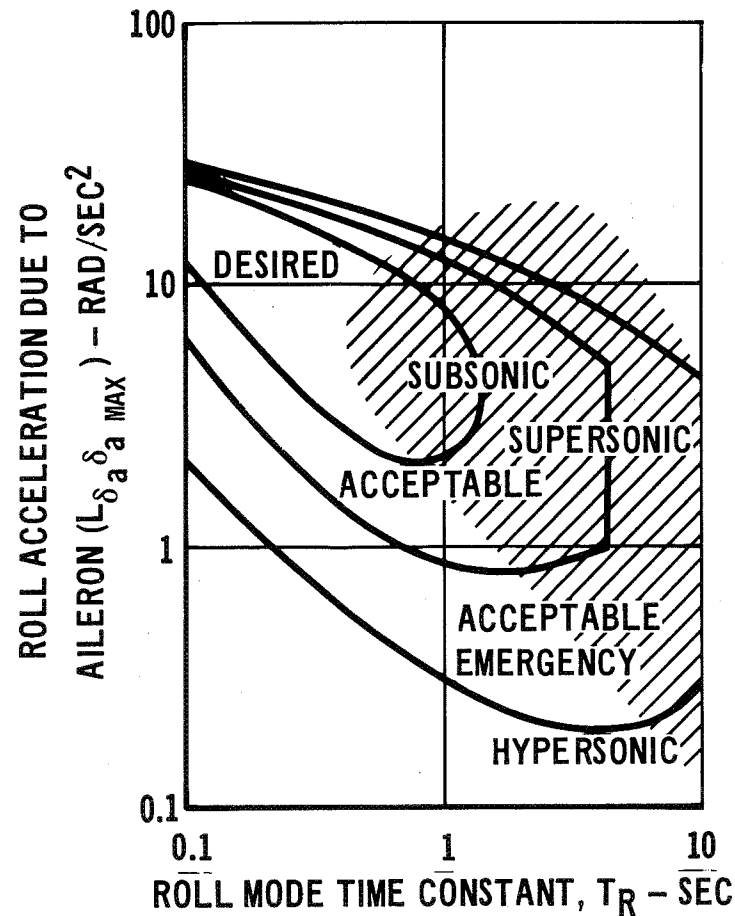


FIGURE 5

ROLLING EFFECTIVENESS  
(AILERON ALONE)

$$P_{\text{MAX}} = L_{\delta_a} \delta_{a \text{ MAX}} T_R \left( \frac{\omega_\phi}{\omega_D} \right)^2$$

$$\left( \frac{\omega_\phi}{\omega_D} \right)^2 = \frac{N_\beta - \frac{N_{\delta_a}}{L_{\delta_a}} L_\beta}{N_\beta - L_\beta \tan \alpha}$$

### Rolling Effectiveness

The derivative  $C_{n\beta}$  plays an important role on a reentry vehicle's lateral control characteristics when bank angle must be controlled through aileron or roll jets.

Handling qualities criteria, that employ the rolling effectiveness parameter, generally specify that the value of  $(\omega_\phi/\omega_D)^2$  must be between 0.5 and 1.1 for good lateral control and a minimum of sideslip excitation. A typical vehicle with moderate directional stability and typical yaw due to aileron characteristics (i.e.  $C_{n\delta_a}/C_{l\delta_a} \approx -0.5$ ) will exhibit the rolling effectiveness parameter trends shown in Figure 6. The decreasing value of  $(\omega_\phi/\omega_D)^2$  with increasing angle of attack is due to a combination of a large yaw to roll moment of inertia ratio, strong positive dihedral effect and high angle of attack.

Lateral acceleration or sideslip angle feedback will effectively increase the vehicle's directional stability, and raises the curve as shown in the figure. An aileron-to-rudder interconnect can also be employed to increase rolling effectiveness. A curve is shown which shows the effect of a fixed ratio interconnect; and also one where the ratio is varied in an optimum fashion as a function of angle of attack. It can be seen that theoretically, with optimum ratio scheduling, the rolling effectiveness parameter can be made to be ideally 1.0. This indicates no induced sideslip. However, to obtain a rolling effectiveness of 1.0 at an angle of attack of 45.0 degrees, the ratio (degrees of rudder per degree of aileron) must be roughly an order of magnitude greater than that required at zero angle of attack. For example, if a ratio of 1.0 is satisfactory at  $\alpha = 0$ , a ratio of 10.0 may be required at  $\alpha = 45$  degrees. In the hypersonic flight regime, the high crossrange vehicle will normally be flown on the back-side of the L/D curve which includes this angle of attack range.

It must be remembered that control surfaces have finite deflection limits, and that the cross-control derivatives can cancel some of the benefits gained from the primary derivatives. In addition, deflection may be limited due to reentry heating. Thus, a negative hypersonic  $C_{n\beta}$  cannot be justified for the high crossrange vehicle unless detailed control analyses (and simulation studies) confirm satisfactory operation.

# ROLLING EFFECTIVENESS

## Typical Lifting Vehicle

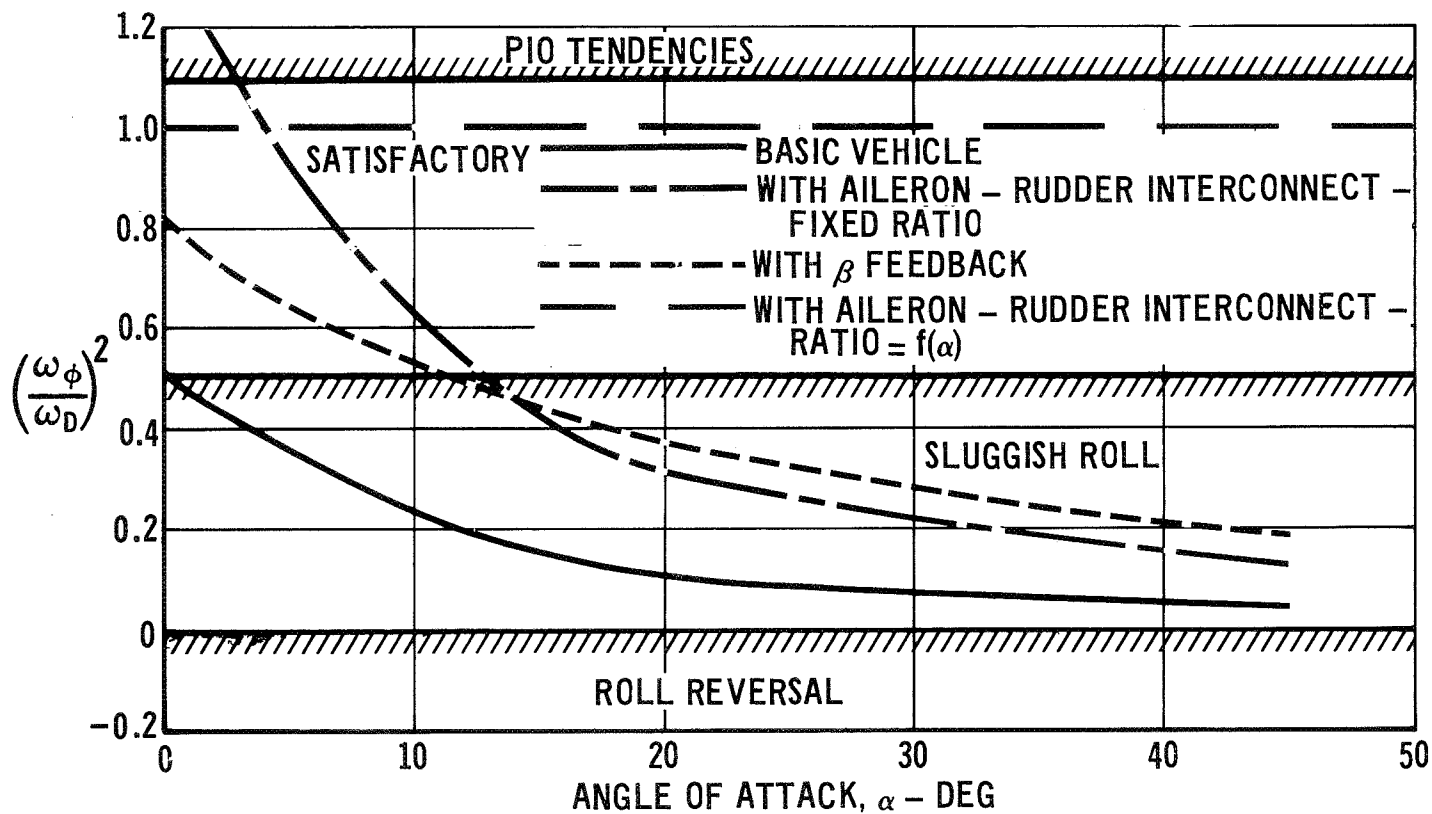


FIGURE 6

### Effect of Control Coupling on Rolling Effectiveness

Figure 7 shows the effect of control coupling on the rolling effectiveness parameter. It can be seen that if the control surfaces are to be used to provide the desired effect, the cross-control derivatives must be known accurately; the consequence of incorrect crossfeed gains can be catastrophic, especially for roll reversal conditions. In addition the moment vectors resulting from rudders and ailerons must not be nearly parallel at any flight condition or else large opposing deflections will be required for small net desired control moment.



# EFFECT OF CONTROL COUPLING ON ROLLING EFFECTIVENESS

AILERON PLUS RUDDER PROPORTIONAL TO AILERON

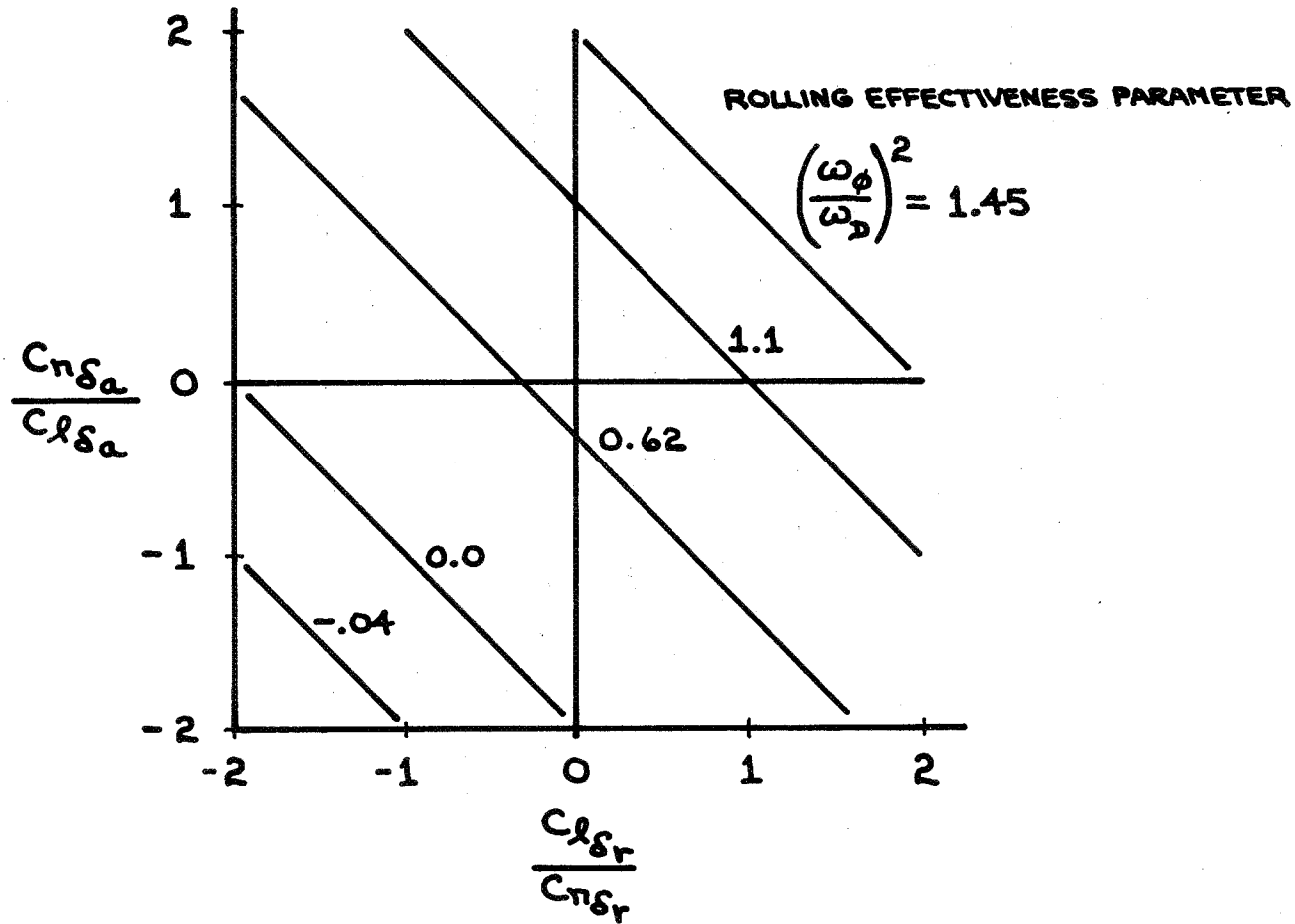


Figure 7

## Artificial Stabilization and Control Criteria

Criteria which determine the extent to which artificial stabilization and control techniques should be relied on are rather subjective and judgment dependent. Figure 8 lists the main problem areas and solutions roughly in the order of difficulty or uncertainty. The essential points of this table and the reasoning behind it are as follows:

1. Artificial damping is easy and can be relied on extensively. Careful analysis can determine the required gains with acceptable accuracy, and control deflection requirements are modest.
2. Artificial stiffening is harder. Neutral basic static stability is a reasonable limit because:
  - (a) Control deflection or impulse limits restrict gains for reasonable  $\alpha$  and  $\beta$ .
  - (b) Good reliable  $\alpha$  and  $\beta$  signals are difficult to obtain.
  - (c) Control lag is critical.
3. Roll response speed-up is no great problem provided cross control derivatives are in acceptable ranges.
4. Any control coupling can theoretically be corrected, but practical considerations should rule out configurations with basic roll reversal, because:
  - (a) Large control deflections are likely to be required, especially if  $\beta$  feedback is used.
  - (b) Complicated interconnect schedules which are critically dependent on poorly known cross derivatives would be required.
  - (c) Consequences of incorrect compensation are catastrophic.
5. Roll-spiral mode coupling is an uncertain area.

# ARTIFICIAL STABILIZATION AND CONTROL CRITERIA

PROBLEM	ARTIFICIAL SOLUTION	PRACTICAL RESTRICTIONS	REMARKS
LOW DAMPING	ANGULAR RATE FEED-BACK	FEW $\longrightarrow$ NONE	STATE-OF-ART; CAN RELY ON ARTIFICIAL DAMPING IN ALL AXES.
LOW STIFFNESS PITCH	INTEGRATED RATE / NORMAL ACCEL FEED-BACK	NONE IF BASIC VEHICLE IS NEUTRAL OR STABLE	ACCEPTABILITY OF STATIC INSTABILITY IS QUESTIONABLE. DEPENDS ON CONTROL EFFECTIVENESS AND NEED FOR $\alpha$ SENSOR.
LAT-DIRECTIONAL	LAT ACCEL FEEDBACK AT HIGH Q; SIDESLIP FEEDBACK AT LOW Q	NONE IF $C_{n\beta} > 0$ DEPENDS ON $\alpha$	USED ON SOME FIGHTERS. CROSS CONTROL DERIVATIVES IMPORTANT. NEGATIVE $C_{n\beta}$ (OR $C_{n\beta DYN}$ ) PROBABLY NOT PRACTICAL.
ROLL RESPONSE	ROLL DAMPER ROLL/YAW CROSSFEED	AVOID ROLL REVERSAL	NEED GOOD DEFINITION OF CROSS CONTROL DERIVATIVES AND ADEQUATE CONTROL EFFECTIVENESS.
LATERAL-DIRECTIONAL CONTROL COUPLING	COMBINATION CROSS-FEEDS	AVOID NEARLY PARALLEL MOMENT VECTORS	DEFINITION OF CROSS CONTROL DERIVATIVES AND COMPLEXITY OF CROSSFEED PROGRAM ARE LIMITATIONS.
ROLL-SPIRAL MODE COUPLING	COMBINATION OF ROLL AND YAW DAMPERS AND SIDESLIP FEEDBACK	NOT WELL DEFINED	COMPLEX PROBLEM; NO EXTENSIVE EXPERIENCE; INTERACTION WITH DUTCH ROLL MODE MAY REQUIRE COMPLEX COMPENSATION.

Figure 8

### Proposed Basic Airframe Stability Requirements

The stabilization and control criteria of Figure 8 were translated into a set of basic airframe stability requirements for the straight wing and high crossrange orbiter configuration concepts. The results are tabulated in Figure 9.

Neutral longitudinal static stability, i.e., zero basic short period frequency is considered a reasonable practical limit. Hypersonic lateral-directional requirements differ with configuration concept. For the straight wing concept (which remains at an angle of attack of 60 degrees until subsonic),  $C_{n\beta}$  can be negative so long as  $C_{n\beta DYN}$  is positive. This is allowable because the vehicle can be only rate stabilized in roll, and bank angle can be controlled through a yaw attitude control system. Under these conditions, the roll and yaw jets provide only damping and maneuver accelerations; they are not required to hold against an unstable moment. The high crossrange vehicle will fly at somewhat lower angles of attack, and require roll control to maintain the desired bank angle. Therefore, negative values of  $C_{n\beta}$  are not acceptable. There is also the further requirement that the basic airframe not exhibit roll reversal. The reversal criterion is satisfied by meeting the hypersonic requirements specified in Figure 9 for the high crossrange vehicle.

# PROPOSED BASIC AIRFRAME STABILITY REQUIREMENTS

SUBSONIC	HYPERSONIC
<b>LONGITUDINAL:</b> $\omega_{nSP} > 0$	<b>LONGITUDINAL:</b> $\omega_{nSP} > 0$
<b>LATERAL-DIRECTIONAL:</b> $C_{n\beta} > 0$ $C_{l\beta} < 0$	<b>LATERAL-DIRECTIONAL:</b> $C_{n\beta} \cos \alpha - \frac{I_z}{I_x} C_{l\beta} \sin \alpha > 0$ $C_{l\beta} < 0$ $\left( C_{n\beta} - \frac{C_{n\delta a}}{C_{l\delta a}} C_{l\beta} \right) > 0$ $C_{l\beta} < 0 ; C_{n\beta} > 0$
	$\left. \begin{array}{l} \text{STRAIGHT WING} \\ \alpha = 60^\circ \text{ ENTRY} \end{array} \right\}$ $\left. \begin{array}{l} \text{HIGH CROSS} \\ \text{RANGE OR} \\ \alpha < 45^\circ \text{ ENTRY} \end{array} \right\}$

FIGURE 9

## Conclusions

It is concluded that there are practical limits on the degree of instability that can be allowed in the basic airframe. The longitudinal basic airframe minimum stability requirement is a short period natural frequency equal to or greater than zero.

The low crossrange orbiter hypersonic  $C_{n\beta}$  may be negative as long as a Dutch roll oscillatory mode is maintained, and bank angle control is accomplished through yaw attitude control. A roll damper may be employed, but vehicle roll attitude must not be tightly constrained if "dynamic" lateral directional stability is to be maintained.

The lateral control considerations strongly influence the directional stability required for the high crossrange configurations, and a negative  $C_{n\beta}$  cannot be justified without a detailed control analysis.

These requirements do not necessarily represent the worst that can be augmented, but rather represent a realistic preliminary goal at this time. There will undoubtedly be a continuing evolvement and development in this area.

# ABORT SEPARATION INCLUDING AERODYNAMIC, DYNAMIC, PROPULSIVE, AND TRAJECTORY INFLUENCES

John P. Decker, Robert J. McGhee and P. Kenneth Pierpont

NASA Langley Research Center

Hampton, Virginia

## INTRODUCTION

In the last six months, a considerable amount of attention has been focused on the abort separation problem. The abort separation of the space shuttle vehicle is not a new problem. In fact, plans for separation studies of two parallel lifting stages were initiated during the 1959-1960 Air Force reusable booster studies. At the Langley Research Center, the abort separation problem has been looked at in some depth since about 1962. The work at the Langley Research Center was initiated to explore the problem of separating parallel arranged stages of a reusable launch vehicle system and this work ranged all the way from wind-tunnel investigations at subsonic speeds to hypersonic speeds and it also included such things as the horizontal lift off of a winged rocket booster from a ground accelerator. Initially, only static aerodynamic interference data were obtained for representative vehicle systems. However, it became quite apparent in this early work that in order to provide meaningful information on the magnitude and character of the separation problem, it was necessary to determine the behavior of the vehicles during the staging maneuver. Consequently, a two-body trajectory simulation computer program was developed which utilized the static aerodynamic results. The results of this early work indicated that staging should occur outside of the sensible atmosphere. All of today's space shuttle vehicle design staging conditions occur outside of the sensible atmosphere. However, it is possible that the mission may have to be aborted if the design staging conditions are not achievable. Consequently, the stages may have to perform an intact abort separation maneuver where the two stages are physically separated to bring them safely back to a ground base. Emphasis should be placed on the word safety as an abort requirement.

Needless to say, the abort separation problem is tremendously different than any other abort separation problem for a space vehicle designed up to the present. In fact, the ability to have the space shuttle safely perform an abort separation maneuver is a very important operational aspect of the space shuttle.

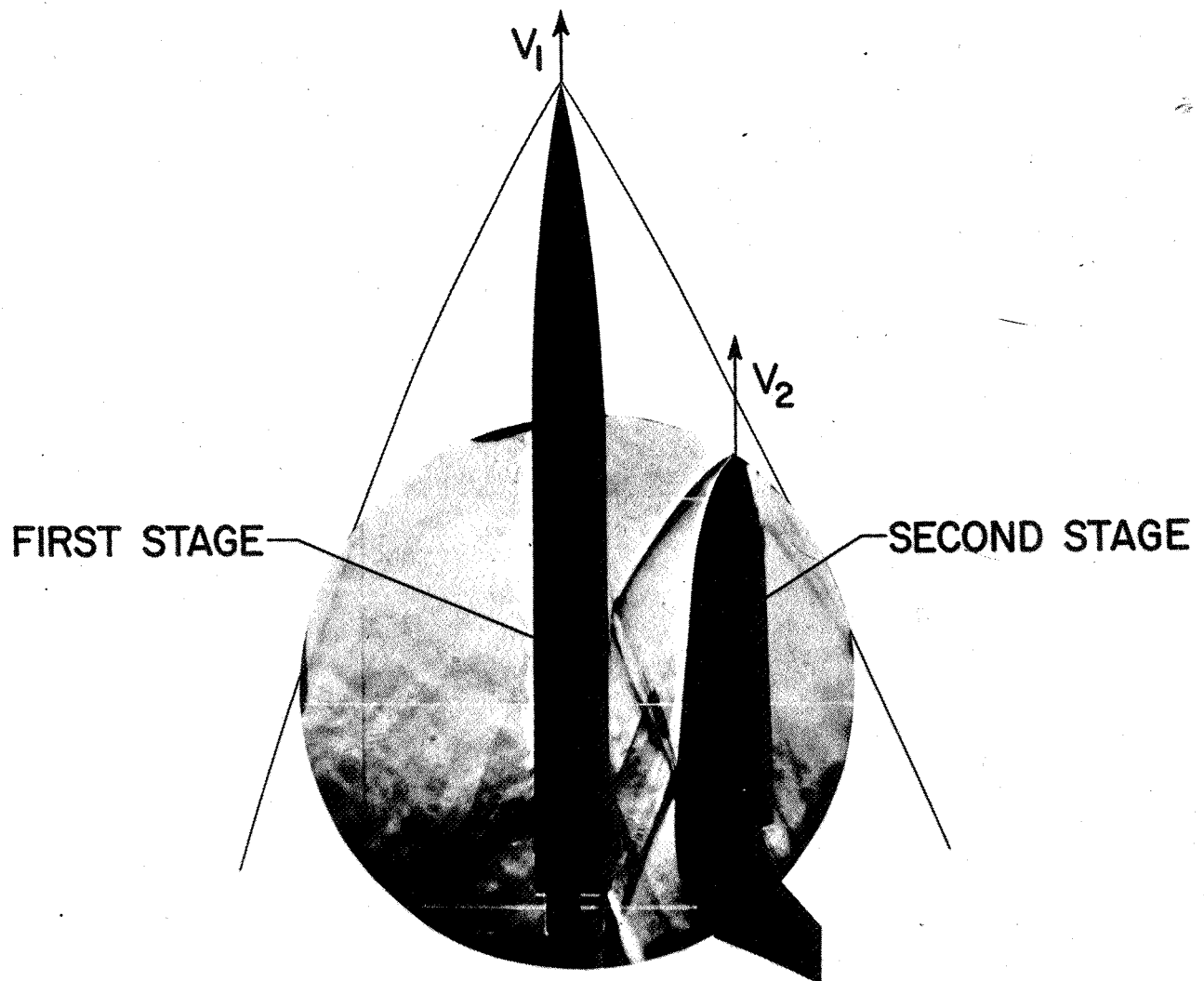
Some of the necessary considerations for safe abort separation and also the subjects that will be discussed in this paper consist of the following:

1. The aerodynamic interference effects of two stages of a space shuttle vehicle when in close proximity,
2. The propulsive effects with emphasis on plume interference effects as well as using separation thrust to separate the two vehicles,
3. The dynamic damping derivatives and how they influence the abort separation maneuver, and
4. The trajectory influences and the importance of what Mach number and altitude an abort separation maneuver takes place.

Figure 1 shows a space shuttle vehicle just as the second stage separates during the early phase of an abort separation maneuver occurring at supersonic or hypersonic speeds and illustrates some of the types of interferences that can be anticipated to result. Some of the static stability and control problems caused by this type of interference will be discussed in this paper.

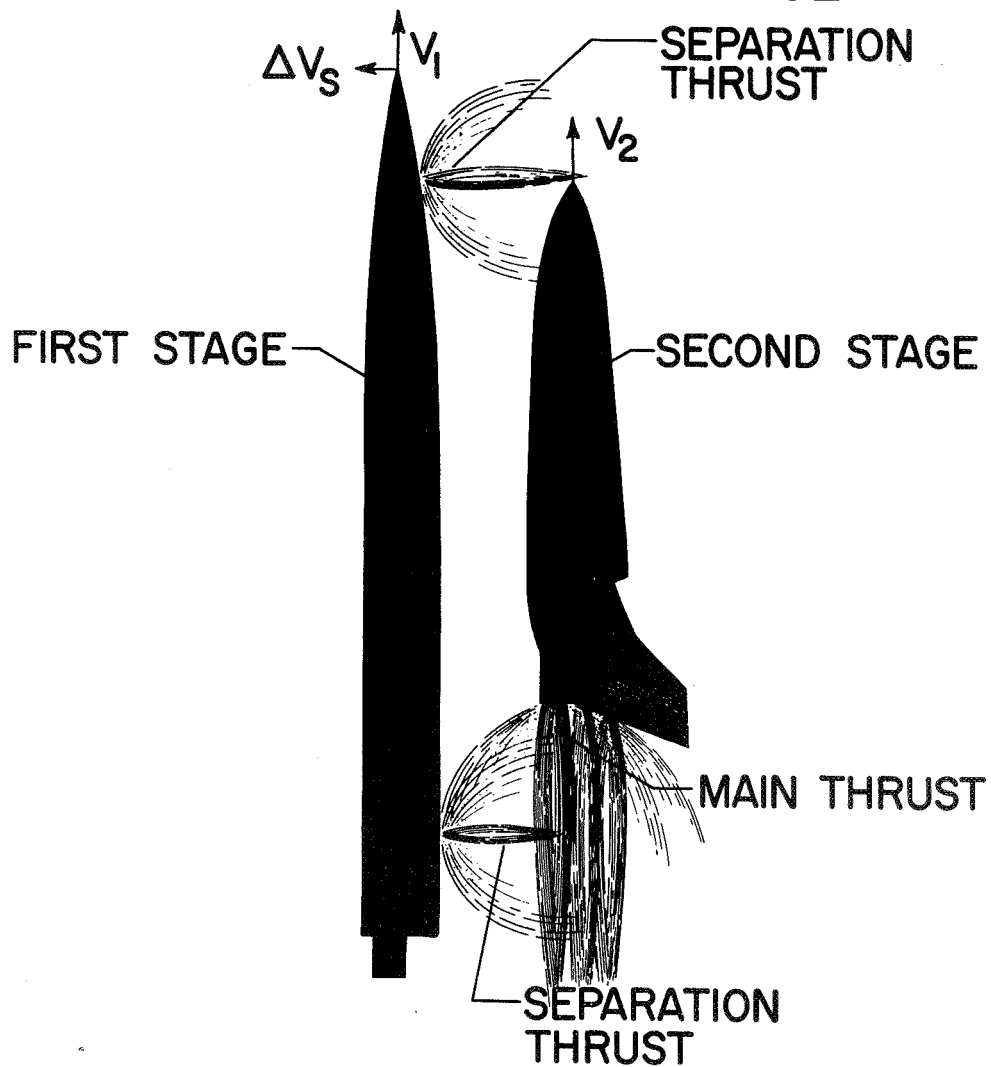


# AERODYNAMIC INTERFERENCE



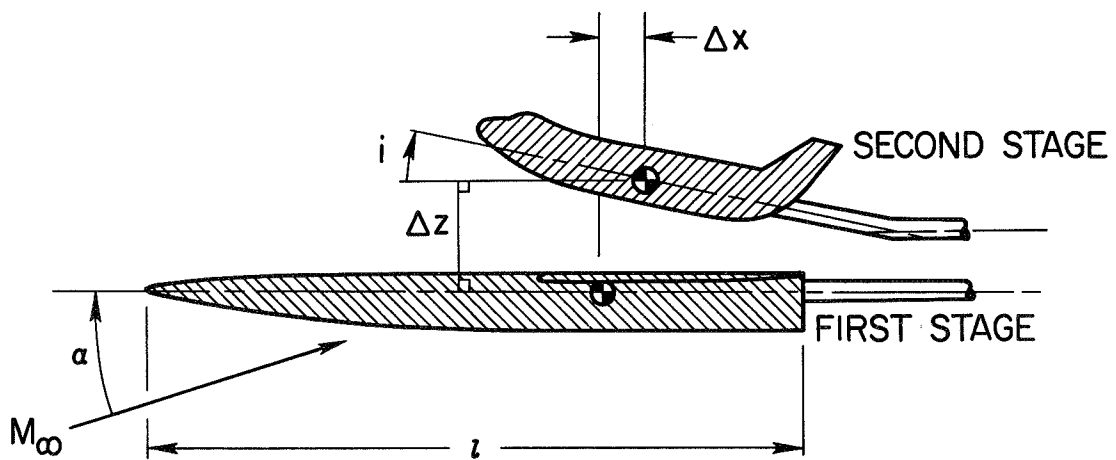
If the second stage rocket engine is ignited prior to unlatch as presently envisioned on at least one space shuttle concept and if separation rockets are used to try and separate the two vehicles, figure 2 illustrates the additional interferences that can be expected to occur. The plume from the second stage rockets as well as the plume from the separation rockets could separate the entire flow field between the two vehicles and present a very complicated flow field. Some plume interference experimental work will be discussed later.

## PROPULSIVE INTERFERENCE



The method that has been used to obtain the static aerodynamic interference data is illustrated in figure 3. Static aerodynamic data were obtained for each stage with strain gage balances mounted on separate stings. Position variables  $\Delta x$  and  $\Delta z$ , as well as the relative incidence angle,  $i$ , were varied for a range of angle of attack and Mach number. These variables were systematically varied in the wind tunnel to obtain the aerodynamic data needed for the trajectory computations. Wind-tunnel data which will be illustrated in this paper were obtained for a delta wing body first stage and a lifting body second stage as well as for a wing body second stage.

## STAGING VARIABLES

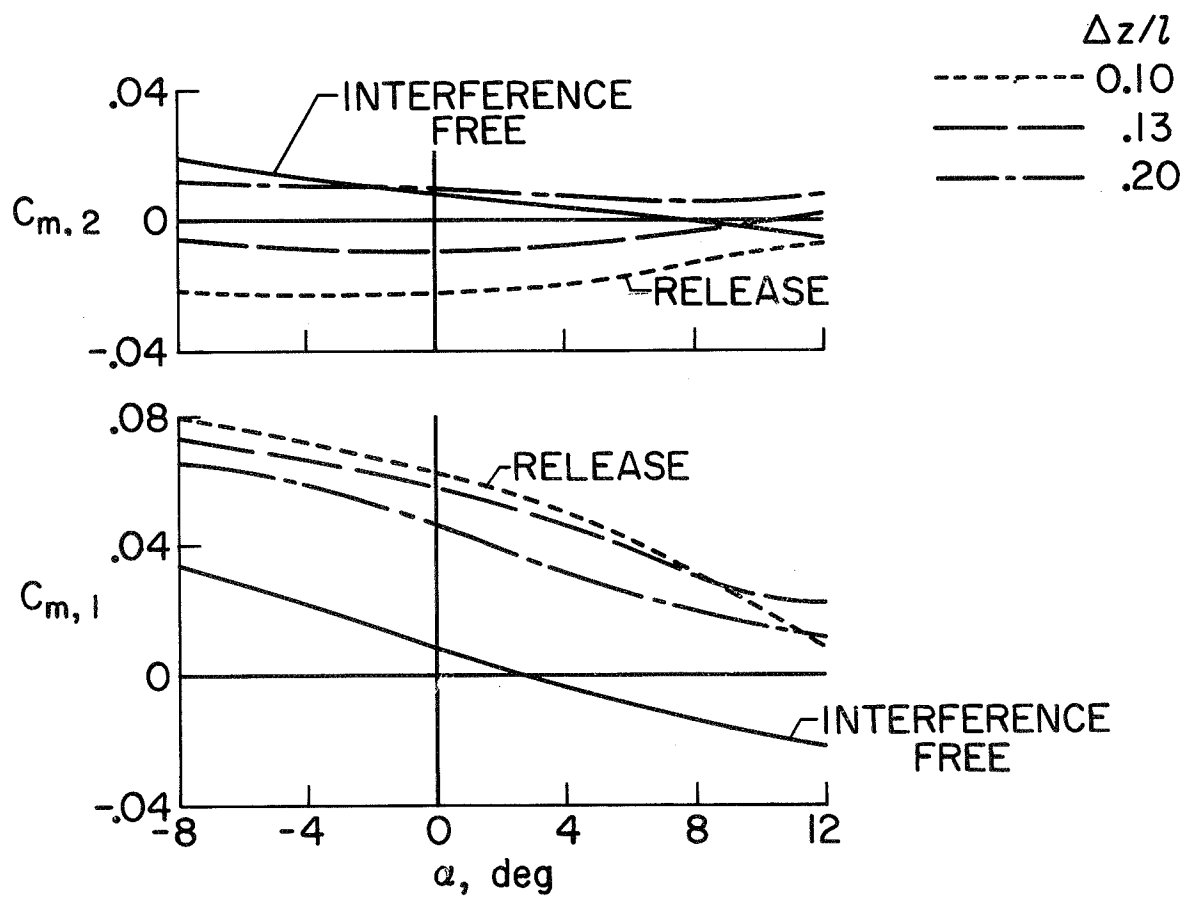


An example of the data obtained from this method of testing is illustrated in figure 4. Here the effect of spacing is shown for a Mach number of 3.0 and an incidence angle of  $0^\circ$  or where the vehicles are parallel to each other. Pitching-moment coefficients for the first and second stage have been plotted against angle of attack. For reference, the interference free curve or the pitching moment curve at very large separation distance is shown for both the first and second stage. The other data corresponds to various non-dimensional spacings from a value of 0.10 to 0.20.

For the second stage, it is seen that the stability level changed and the magnitude of the pitching moment varied with spacing. For the first stage vehicle, the stability did not change appreciably; however, there is a large positive increment in the magnitude of the pitching moment due to the interference. Also, for the maximum spacing tested, large interference is still present because the curve has not yet approached the interference free curve. Data that has been obtained at other Mach numbers has indicated large changes in the stability level for both stages. Also, from control effectiveness data not shown here, there appears to be no reasonably sized aerodynamic control surface which could overcome such large pitching-moment increments.

# EFFECT OF SPACING

$M_\infty = 3; i = 0^\circ$



To illustrate the effects of configuration, the next two figures compare just the pitching moment curves for two different second stage configurations. Figure 5 is data just presented for the lifting body second stage where pitching-moment coefficients are plotted against angle of attack. Again the interference free curve as well as curves for various non-dimensional spacings are illustrated. The data shown in this figure combined with figure 6 illustrates the effect of configuration.



# EFFECT OF SPACING ON LIFTING BODY $M_\infty = 3; i = 0^\circ$

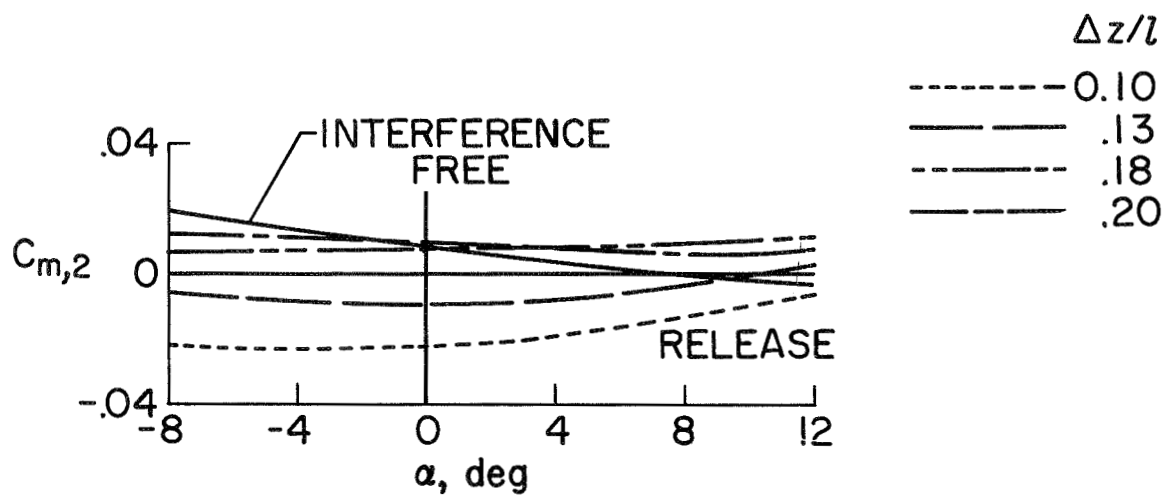
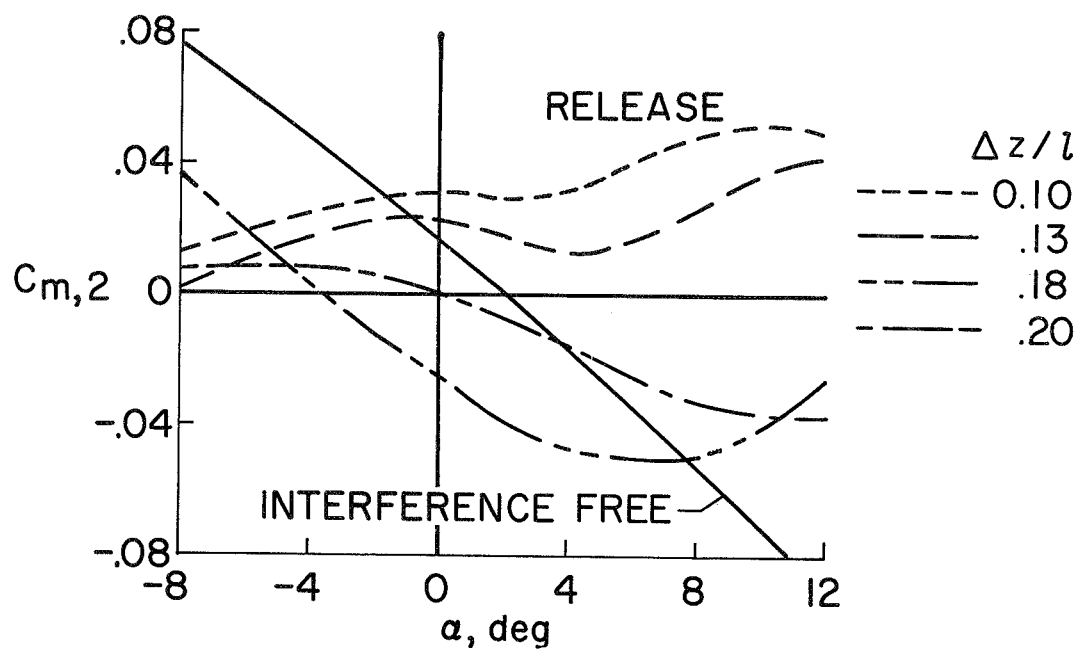


Figure 6 shows the same type of data illustrated in figure 5 but for a wing body second stage. Comparing figure 5 and figure 6 indicates that the pitching-moment curves for these two vehicle shapes are markedly different. Also, for the wing body second stage, figure 6, not only is the stability during separation changing rapidly, that is, the curves are not parallel to each other, but also the curves are not in sequential order.

# EFFECT OF SPACING ON WING BODY

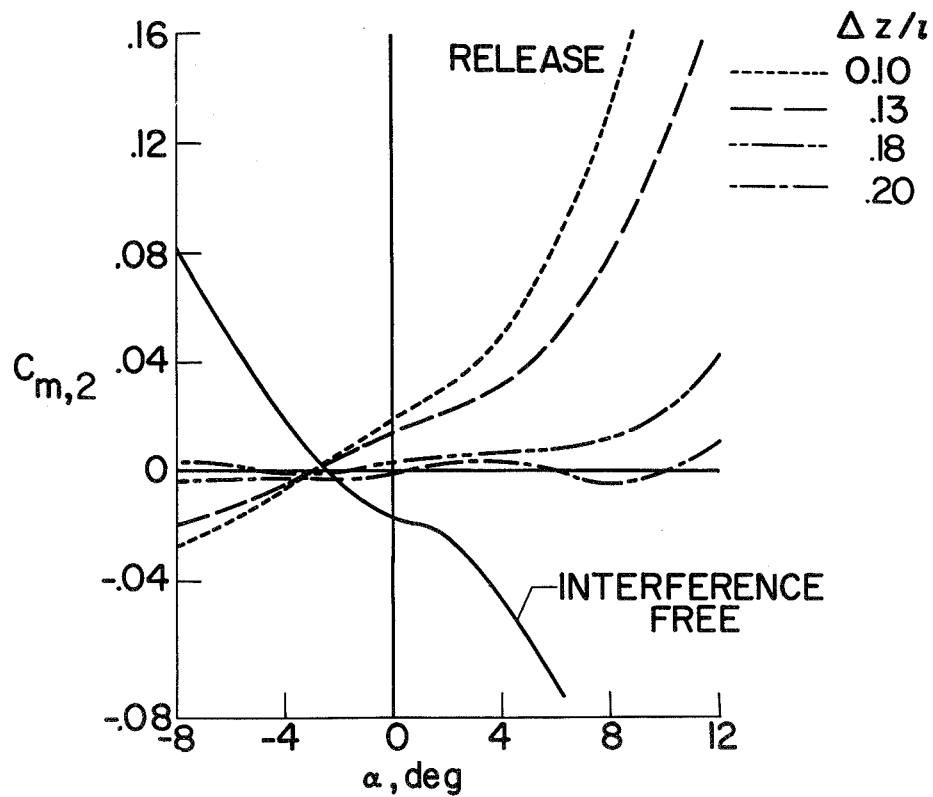
$$M_\infty = 3; i = 0^\circ$$



One final aerodynamic effect can be illustrated from figure 7 again for just the wing body second stage where pitching-moment coefficient is plotted against angle of attack for the same non-dimensional spacings. Remember, that the data in figure 6 are at a Mach number of 3. The data in figure 7 are at a subsonic Mach number of 0.60 and not only are the curves very different from those at supersonic speeds, but the interference is so large that at angles of attack above about  $4^\circ$ , the vehicle is highly unstable at the lower non-dimensional spacings. Similar type data at transonic speeds is once again different in character and the impact on abort separation would be quite unlike that which will be shown subsequently.

# EFFECT OF SPACING ON WING BODY

$M_\infty = 0.60; i = 0^\circ$



The real complexity of the aerodynamic interference problem is better illustrated in figure 8. Here a series of schlieren photographs are shown at a Mach number of 3 and 6 for an angle of attack range from  $-9^\circ$  to  $12^\circ$ . Needless to say, the flow field is extremely complex and the flow field is seen to vary with changes in angle of attack. Compare for example, the flow field at  $M = 3$  and  $\alpha = -9^\circ$  with the flow field at  $\alpha = 12^\circ$  and note the changes in the shock system between the vehicles.

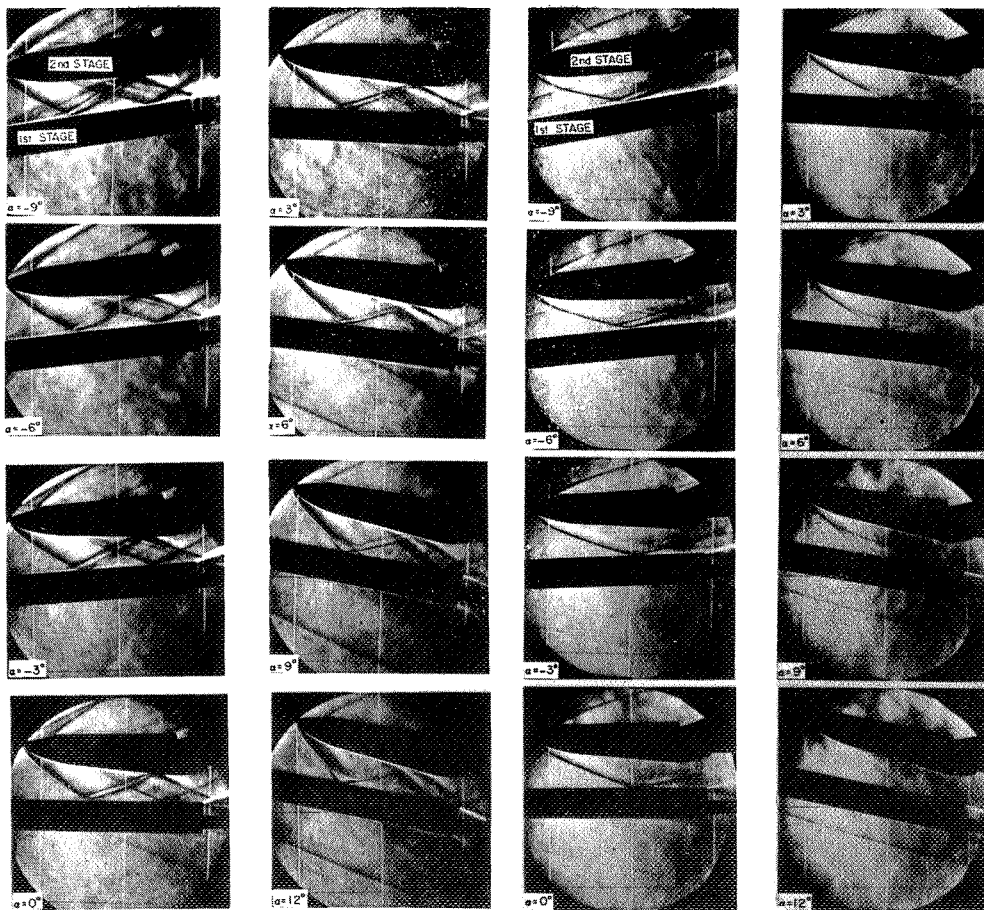
One additional interference phenomenon is illustrated at a Mach number of 6. The flow field at the lower angles of attack is similar to the data shown at the left. Notice the bow shock from the second stage at low angles and compare this data with the schlieren photographs at high angles. Here it is seen that the bow shock from the second stage is completely disgorged, a phenomenon which normally occurs at supersonic speeds when an air inlet unstarts. A complete explanation of this flow phenomenon illustrated here is not presently known. However, it is possible that the flow between the configurations at this condition is subsonic and that a single strong bow wave lies ahead of the two vehicles. Attempts have been made to actually predict some of these interference effects but so far little success has been obtained. One also wonders what happens to the flow between the two vehicles when the second stage rocket engine is ignited.

# SHOCK-WAVE INTERFERENCE

$$i = 0 ; \Delta z / l_1 = 0.20$$

$M_\infty = 3$

$M_\infty = 6$

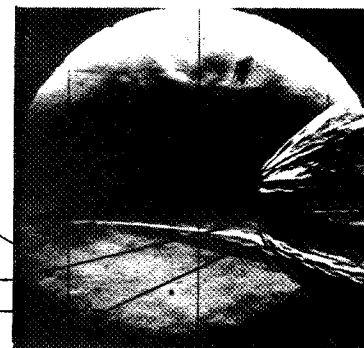
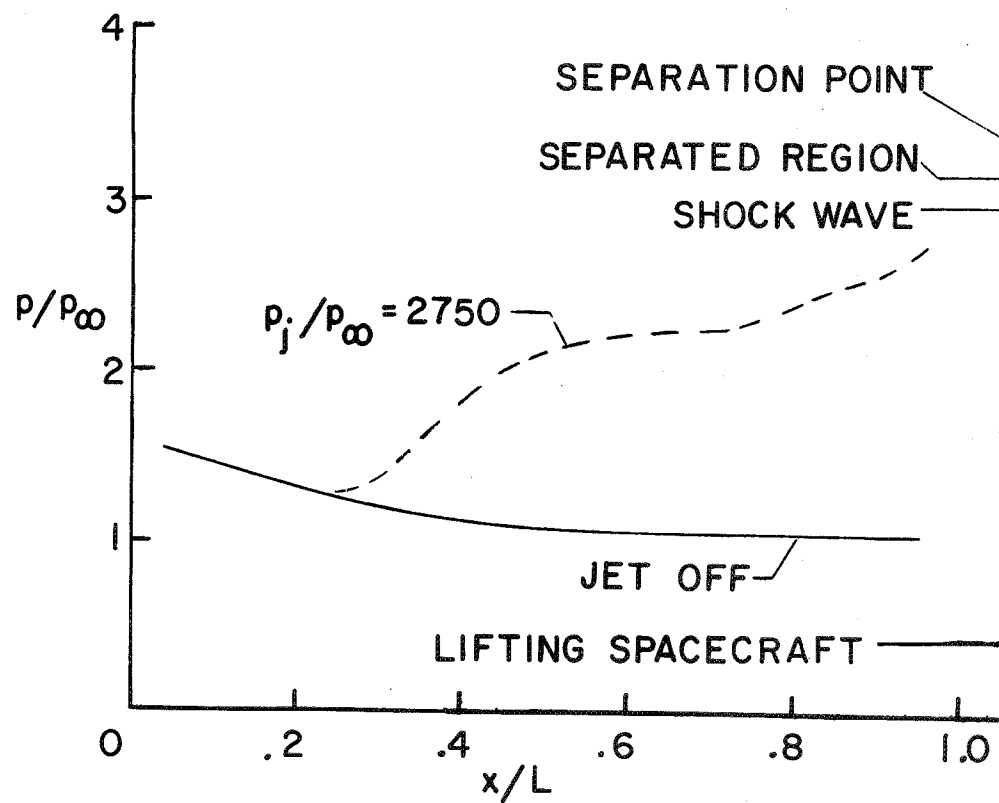


To illustrate some of the potential effects that the plume might have on the abort separation problem, figure 9 shows some plume interference data on a simplified lifting spacecraft vehicle at a Mach number of 6 and an angle of attack of  $0^\circ$ . Here the centerline pressure distribution on the spacecraft is plotted against distance from the nose. Two curves are illustrated, one is for a jet off condition, and the other for a jet on condition corresponding to a pressure ratio of 2750. The plume induces a separated region on the lower surface of the spacecraft and causes a sharp rise in the centerline pressure distribution. The impact of the plume on the abort separation problem has not been ascertained up to the present. However, investigations to determine the effect of the plume on two vehicles in proximity are presently underway at Langley Research Center.

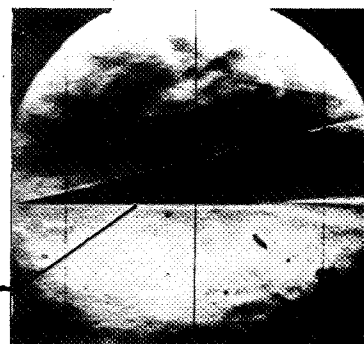


# PLUME INTERFERENCE

$$M_{\infty} = 6 ; \alpha = 0^{\circ}$$



$$p_j/p_{\infty} = 2750$$



JET OFF

Using the wind-tunnel data of the type illustrated in previous figures, the implication of the interference can be obtained using a Langley developed two-body trajectory simulation computer program. The computer program integrates the longitudinal equations of motion for each of the vehicle stages and calculates their relative position and attitude. The inputs for this program are shown in figure 10. They consist of the static aerodynamic data for both stages, the dynamic derivatives for both stages, the vehicle characteristics such as mass and moments of inertia, the launch vehicle trajectory quantities at separation, and the initial attitude and position of the second stage. The important quantities in this list are the static aerodynamic data which have a tremendous influence on the abort separation trajectories and as to whether the vehicles collide or separate. This data as previously shown can be obtained in the wind tunnel but is Mach number as well as configuration sensitive and to date no data is available which includes effects of rocket plumes, whether propulsive, separation, or just attitude control systems are employed during the separation maneuver. Equipment and facility limitations may impose restrictions on the usefulness of some data of this general type. For example, whether or not sufficiently high Reynolds numbers and exhaust plume static pressure ratios can be simultaneously obtained is an interesting if not vitally significant question. The least accurately known quantities in this list are the dynamic derivatives, not only at interference free conditions but more importantly when the vehicles are in proximity to each other. The data that will be illustrated in the following figures pertains to the launch vehicle system having a delta wing body first stage and a lifting body second stage.

## INPUTS FOR TRAJECTORY PROGRAM

STATIC AERODYNAMIC DATA :  $C_N$  ;  $C_m$  ;  $C_A$

DYNAMIC DERIVATIVES :  $C_{m_q}$  ;  $C_{m_{\dot{\alpha}}}$  ;  $C_{N_q}$  ;  $C_{N_{\dot{\alpha}}}$

VEHICLE CHARACTERISTICS :  $m$  ;  $I_{yy}$

LAUNCH VEHICLE TRAJECTORY

QUANTITIES AT SEPARATION :  $h$  ;  $q$  ;  $\gamma$  ;  $V_c$

INITIAL ATTITUDE AND POSITION

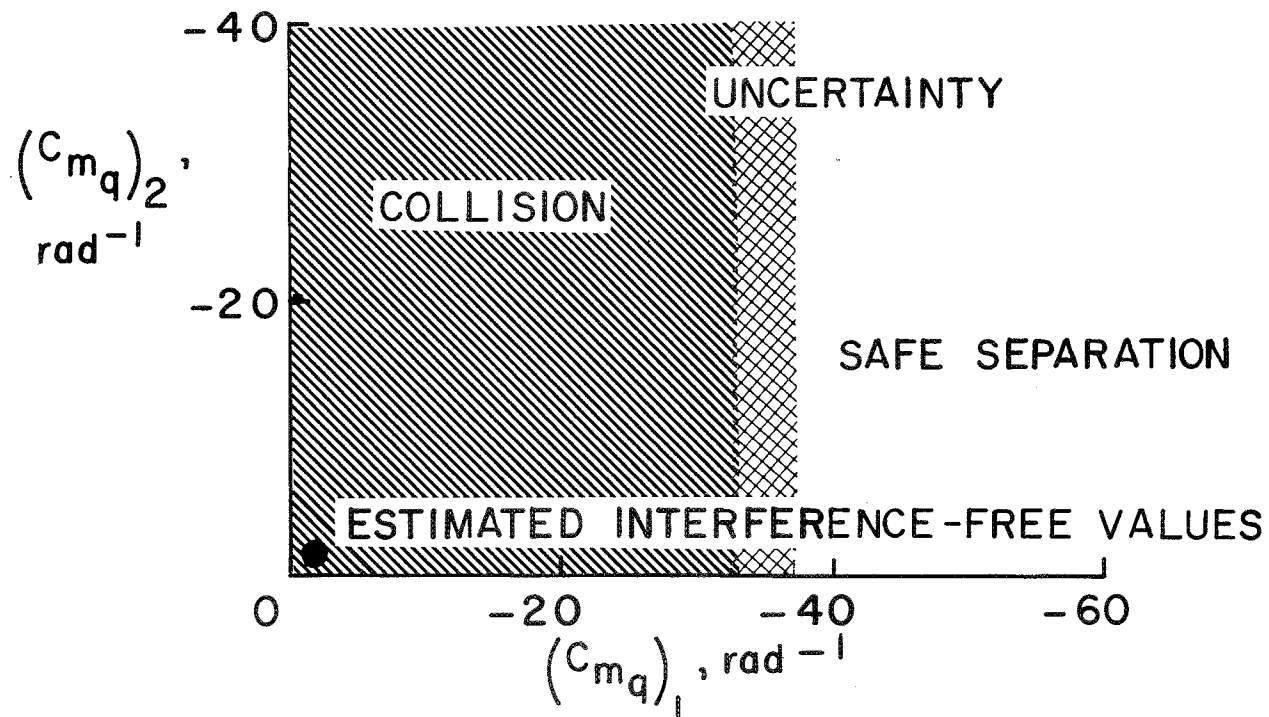
OF SECOND STAGE :  $\Delta x$  ;  $\Delta z$  ;  $i$

The effect of some of the dynamic derivatives is better illustrated in figure 11. Here the effect of the dynamic derivatives are illustrated for an abort separation maneuver occurring at a Mach number of 3 and a dynamic pressure of 670 psf.  $C_{mq}$ , the pitching moment due to pitch rate for the second stage, is plotted against  $C_{mq}$  for the first stage. Indicated on this figure are the regions where the two vehicles collided, an approximate region where they safely separated, and a region of uncertainty as to whether the two vehicles would collide or separate. Way down here in the corner you can see the best current estimates of the interference free values of  $C_{mq}$  for both the first and second stage which were obtained from data for similar type configurations such as the XB-70 for the first stage and the HL-10 for the second stage. These values for this particular vehicle concept are one (1) or more orders of magnitude smaller than the values needed to achieve safe operation at these conditions. Methods to increase the magnitude of  $C_{mq}$  would be by using stability augmentation assuming you have adequate control effectiveness and other auxiliary devices as well as changing the configuration so that conventional horizontal tails could be utilized. However, we still do not know how  $C_{mq}$  varies when the two vehicles are in proximity to each other and Mr. Orlik-Rückemann, in a succeeding paper, will discuss how some of this type data may be obtained. Although the magnitude of the other dynamic derivatives have not been perturbed in this analysis, it can be expected that similar figures could be generated for these quantities.

# EFFECT OF DYNAMIC DERIVATIVES

$$M_{\infty} = 3$$

ALTITUDE = 70 000 ft ; DYNAMIC PRESSURE = 670 psf

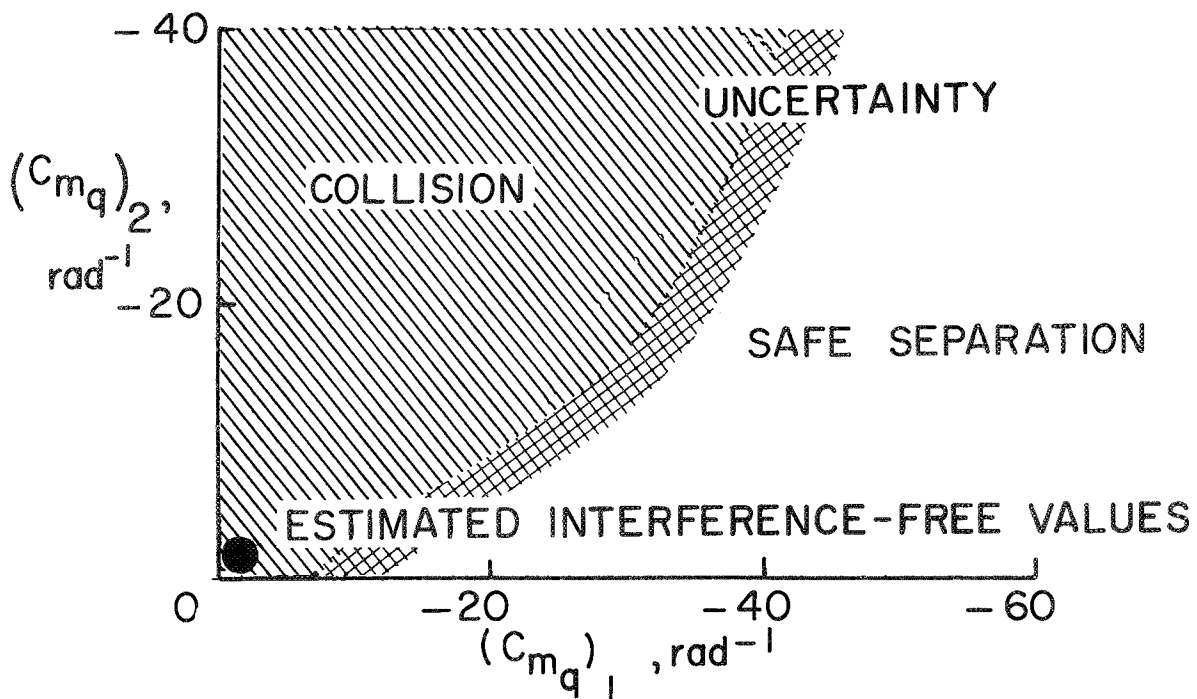


To illustrate the effect of the initial conditions on the dynamic derivatives, figure 12 shows the same type of data illustrated in figure 11 but for a Mach number of 6 and a dynamic pressure of 380 psf. Again  $C_{mq}$  for the second stage is plotted against  $C_{mq}$  for the first stage and the regions of collision and safe separation are again shown as well as the interference free values of  $C_{mq}$  for the first and second stage. The Mach number and dynamic pressure at which the abort maneuver takes place has a tremendous impact as to whether the vehicles collide or separate.

# EFFECT OF DYNAMIC DERIVATIVES

$$M_{\infty} = 6$$

ALTITUDE = 110 000 ft ; DYNAMIC PRESSURE = 380 psf

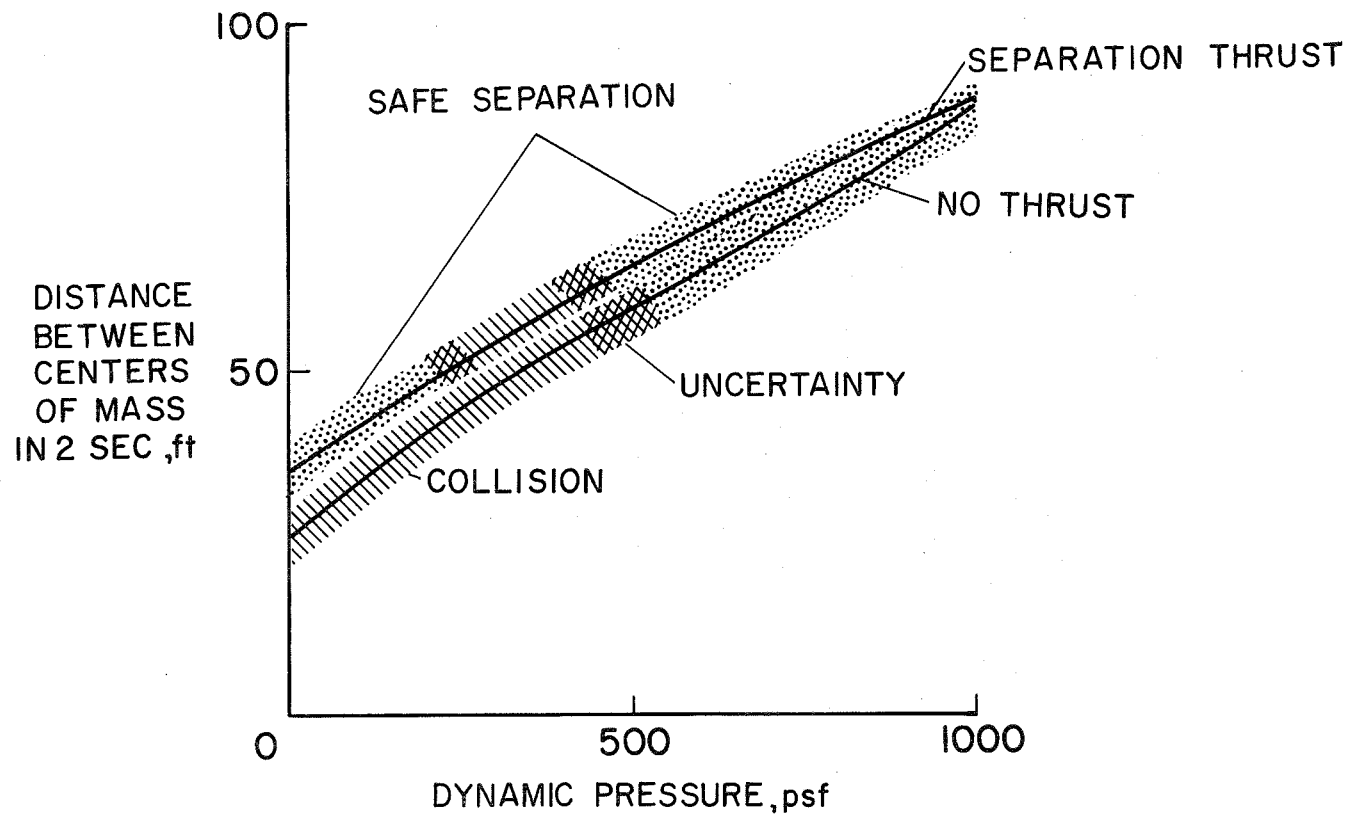


To illustrate further the effect of dynamic pressure, figure 13 presents results for an abort separation maneuver occurring at a Mach number of 3. Here the separation distance or the distance between the center of gravities of the two stages in 2 seconds after release has been plotted against dynamic pressure. Two curves are presented; one is for a condition in which no propulsive or separation thrust was used in the calculations and the other is for the conditions in which a constant separation thrust corresponding to a thrust to weight ratio of 0.1 has been applied to the first stage. However, plume effects have not been accounted for. For the no thrust condition, at zero dynamic pressure, the position and attitude of the vehicles do not change and separation does not occur, and consequently some  $\Delta V$  must be applied to separate the vehicles. For this case, safe separation can be expected only at relatively high dynamic pressures. For the vertical thrust case, safe separation is achieved at low dynamic pressures but as the dynamic pressure increases, there is a region of collision. At the higher dynamic pressures, safe separation could also be expected. It is important to note in this figure that at the higher dynamic pressures, the vehicles could experience large normal load factors and consequently from a pilot and structural viewpoint, the high dynamic pressure abort may be impracticable.



## EFFECT OF DYNAMIC PRESSURE

$$M_{\infty} = 3$$



The ability of two stages of a space shuttle vehicle to perform a safe abort separation maneuver has been found to depend on the aerodynamic interference data which in turn was found to be dependent on configuration, Mach number, angle of attack, and relative position and attitude of the two stages. In this paper the aerodynamic data was obtained for rigid models so consequently scale effects and aeroelastic effects are not included. Their importance is not yet known.

The abort maneuver analysis has indicated a strong dependency of dynamic derivatives and as mentioned previously are least known. The manner in which dynamic data can be obtained when two vehicles are in close proximity is the topic of Mr. Orlick-Rückemann's paper. Definitely, dynamic derivative data of this type is urgently needed.

Safe abort will also depend on propulsive considerations such as the main thrust from the second stage and its associated plume interference. Other interferences generated by the separation rockets and attitude control rockets must be considered.

The trajectory results have also indicated that safe abort separation to be strongly dependent on both the Mach number and dynamic pressure.

Investigations are planned in the very near future to determine the effect of the plume from the second stage main engine on the separation trajectories. The data will be obtained in a similar fashion as illustrated in this paper. Both jet on and jet off data will be obtained and the effect of this aerodynamic interference data on the separation trajectories will be ascertained.

What has been shown in this paper suggests that whatever abort requirements are decided upon for the space shuttle, the abort problem may actually overpower the design concept.

## CONCLUDING REMARKS

SAFE ABORT DEPENDS ON :

AERODYNAMIC —

CONFIGURATION

MACH NUMBER

ANGLE OF ATTACK

INCIDENCE ANGLE

RELATIVE POSITION OF STAGES

DYNAMIC DERIVATIVES

PROPULSIVE —

MAIN THRUST

SEPARATION THRUST

ATTITUDE CONTROL

TRAJECTORY —

MACH NUMBER

DYNAMIC PRESSURE

## BIBLIOGRAPHY

1. Donaldson, J. C.: Aerodynamic Interference Effects of Parallel Delta Wings and Cone-Cylinder Bodies in Close Proximity: Force Tests at Mach Numbers 2, 5, and 10. AEDC-TDR-64-135, 1964 (Confidential).
2. Sayano, S.; Erickson, C. R.; and Murphy, J. S.: Aerodynamic Interference Associated With Two Parallel Bodies in Close Proximity in Hypersonic Flow. AFFDL-TR-64-158, 1964 (Confidential).
3. Donaldson, J. C.: Aerodynamic Interference Effects of Parallel Delta Wings and Cone-Cylinder Bodies in Close Proximity: Pressure Tests at Mach Numbers 5 and 10, Heat-Transfer Tests at Mach Number 10. AEDC-TDR-64-172, 1964 (Confidential).
4. Spurlin, C. J.: Aerodynamic Interference Effects of Delta Wings in Close Proximity: Pressure Tests at Mach 8. AEDC-TR-66-215, 1964 (Confidential).
5. Decker, John P.; and Pierpont, P. Kenneth: Aerodynamic Separation Characteristics of Conceptual Parallel-Staged Reusable Launch Vehicles at Mach 3 to 6. NASA TM X-1051, 1965 (Confidential).
6. Decker, John P.: Aerodynamic Abort-Separation Characteristics of a Parallel-Staged Reusable Launch Vehicle From Mach 0.60 to 1.20. NASA TM X-1174, 1965 (Confidential).
7. McGhee, Robert J.: Some Effects of Jet Pluming on the Static Stability of Ballistic Bodies at a Mach Number of 6.00. NASA TN D-3698, 1966.
8. Decker, John P.: Experimental Aerodynamic and Analysis of the Stage Separation of Reusable Launch Vehicles. Paper presented at Conference on Hypersonic Aircraft Technology held at Ames Research Center, May 16-18, 1967. NASA SP-148 (Confidential).
9. Jones, Jerry H.: Force Tests on the Two Stages of an Aerospace Plane Configuration as the Stages Separated at Mach 3. AEDC-TR-67-45, 1967 (Confidential).
10. Decker, John P.; and Gera, Joseph: An Exploratory Study of Parallel Stage Separation of Reusable Launch Vehicles. NASA TN D-4765, 1968.
11. Jenson, Richard; Dahlem, Valentine; and Schnabel, Charles: Hypersonic Aerodynamic Interference Analysis of Parallel Staged Blunt Delta Wings. AFFDL-TR-68-116, 1968.

12. Decker, John P.: An Exploratory Experimental and Analytical Study of Separating Two Parallel Lifting Stages of a Reusable Launch Vehicle at Mach Numbers of 3 and 6. A Thesis presented to the Faculty of the School of Engineering and Applied Science, University of Virginia, Master of Aerospace Engineer, May 1968.
13. Decker, John P.: Aerodynamic Interference Effects Caused by Parallel-Staged Simple Aerodynamic Configurations at Mach Numbers of 3 and 6. NASA TN D-5379, 1969.
14. Fong, M. C.; and Ehrlich, C. F.: Propulsion Effects on Aerodynamic Characteristics of Lifting Reentry Vehicles. AFFDL-TR-70-12, 1970.
15. Flaherty, Jack I.; and Dahlem, Valentine: A Prediction Technique for Estimating Interference Effects During a Parallel Staged Separation Maneuver at Supersonic Speeds. AFFDL-TR-70-21, 1970.
16. Lanfranco, M. J.: Wind-Tunnel Investigation of the Separation Maneuver of Equal-Size Bodies. AIAA Paper No. 70-260, 1970.
17. McGhee, Robert J.: Jet Plume Induced Flow Separation on a Lifting Entry Body at Mach Numbers From 4.00 to 6.00. NASA TM X-1997, 1970.



# POSSIBLE USE OF HALF-MODEL OSCILLATORY TECHNIQUES FOR THE STUDY OF SHUTTLE ABORT SEPARATION DYNAMICS

K. J. Orlik-Rückemann

National Aeronautical Establishment, Ottawa, Canada

## INTRODUCTION

As indicated by other investigators (see for example Ref. 1) the prediction of the abort separation maneuver may strongly depend on the value of dynamic stability derivatives - and particularly on the value of the damping-in-pitch derivative - of both the orbiter and the booster. Since an abort maneuver may have to take place at speeds anywhere between practically zero and the speed for normal separation (say 10,000 fps), the derivatives are needed for speeds up to and including the lower hypersonic range. Immediately after the separation, when the two vehicles are in close proximity to each other, large aerodynamic interference effects can be expected, especially at supersonic and hypersonic speeds, which may seriously affect the aerodynamic characteristics of the two vehicles. For a realistic motion analysis, the aerodynamic data are therefore required for a large number of possible relative positions of the booster and the orbiter, as well as for a range of the initial attitudes of the two vehicles immediately before separation. Even if we introduce the simplifying assumption that the initial separation maneuver is entirely symmetrical, the number of relative positions of the two vehicles with respect to each other and with respect to the flow direction remains very large. Under these circumstances, a wind tunnel determination of the damping-in-pitch using standard sting-supported models not only could be rather difficult but also would require a prohibitive number of sting arrangements. In addition, serious sting interference effects could be expected for a combination of two sting-supported models at incidence. An attractive alternative appears to be the adaptation for this purpose of the seldom-used technique of half-models, which would permit a relatively simple variation of the relative position and attitude of the two models, at the same time eliminating all sting interference problems. In this paper the use of half models for oscillatory experiments is discussed, based on an evaluation of selected previous half-model results for various configurations, and examples of possible experimental arrangements for the determination of the damping-in-pitch derivative during the shuttle separation maneuver are indicated.

### HALF MODEL TECHNIQUE

When studying symmetrical wind tunnel models in symmetrical flow conditions it is possible to obtain the aerodynamic reactions on a complete configuration by measuring them on one half of the configuration and using the tunnel wall or a suitable reflection plate as the model longitudinal plane of symmetry. Such an approach has many advantages:

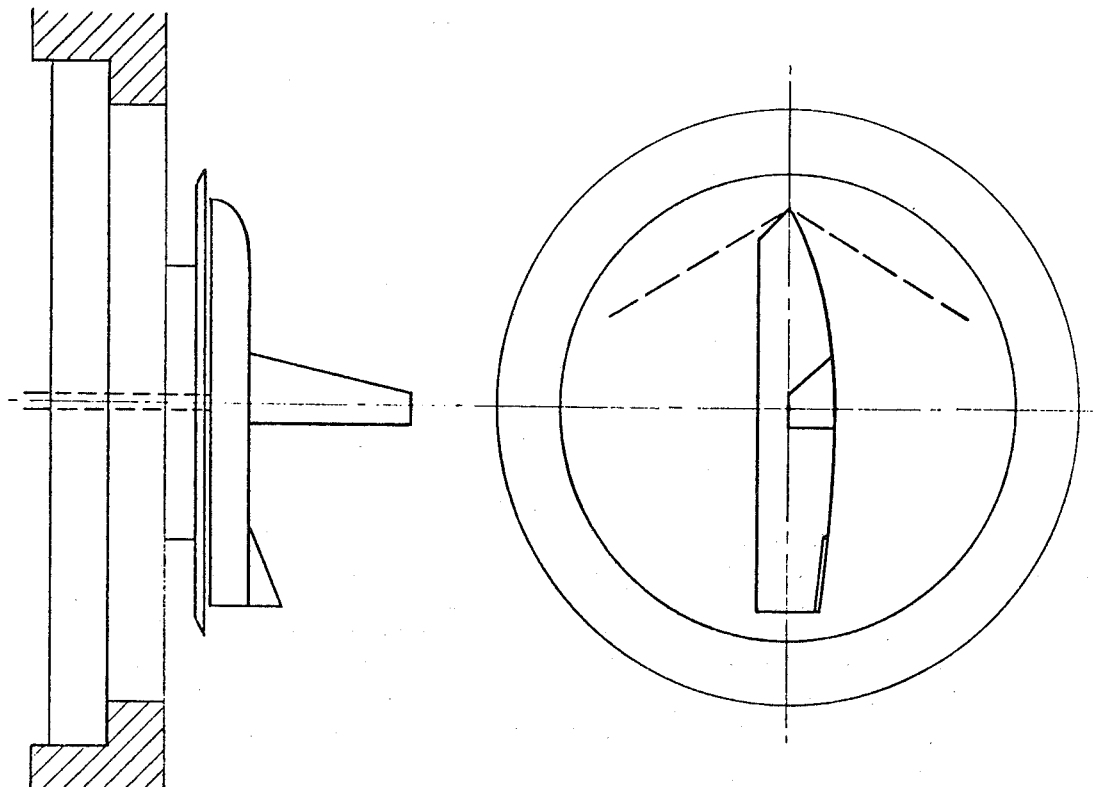
1. It permits location of the test equipment such as balances, dynamic test rigs, etc., outside of the wind tunnel, where there are no serious space limitations;
2. It permits a very simple change of model incidence, by rotating the mounting plate in the wind tunnel wall;
3. It permits the use of larger models than otherwise possible, improving the test accuracy and resulting in a higher Reynolds number;
4. It obviates the need for using a sting and sting-support, thereby eliminating possible sting-and-strut interference problems;
5. It provides a relatively rigid model suspension; eliminating, for example, the problem of sting oscillation;
6. It can be used on models where no base area is available for sting support, such as wings without bodies or bodies with boattail.

For supersonic experiments, the disadvantages are as follows:

1. The effect of the gap between model and reflection plate. This effect may be kept small by making the gap as small as possible and by introducing a root fence on the model to reduce pressure equalization through the gap.
2. The effect of interaction of shock waves from the model and the boundary layer on the reflection plate. This can be kept small by extending the reflection plate only very little in front of the model. It should be noted that the presence of the reflection plate eliminates interactions with the tunnel wall boundary layer.
3. The limitation to symmetrical flow conditions.



# HALF MODEL TECHNIQUE



## ADVANTAGES

1. EXPERIMENTAL APPARATUS OUTSIDE WIND TUNNEL
2. SIMPLE CHANGE OF MODEL INCIDENCE
3. NO AERODYNAMIC STING OR STRUT INTERFERENCE
4. NO MECHANICAL STING INTERFERENCE
5. USE OF RELATIVELY LARGE MODELS AND MODELS WITH NO BASE AVAILABLE FOR SUPPORT

## DISADVANTAGES

1. GAP EFFECTS
2. SHOCK / BOUNDARY LAYER INTERACTION
3. LIMITED TO SYMMETRICAL FLOW CONDITIONS

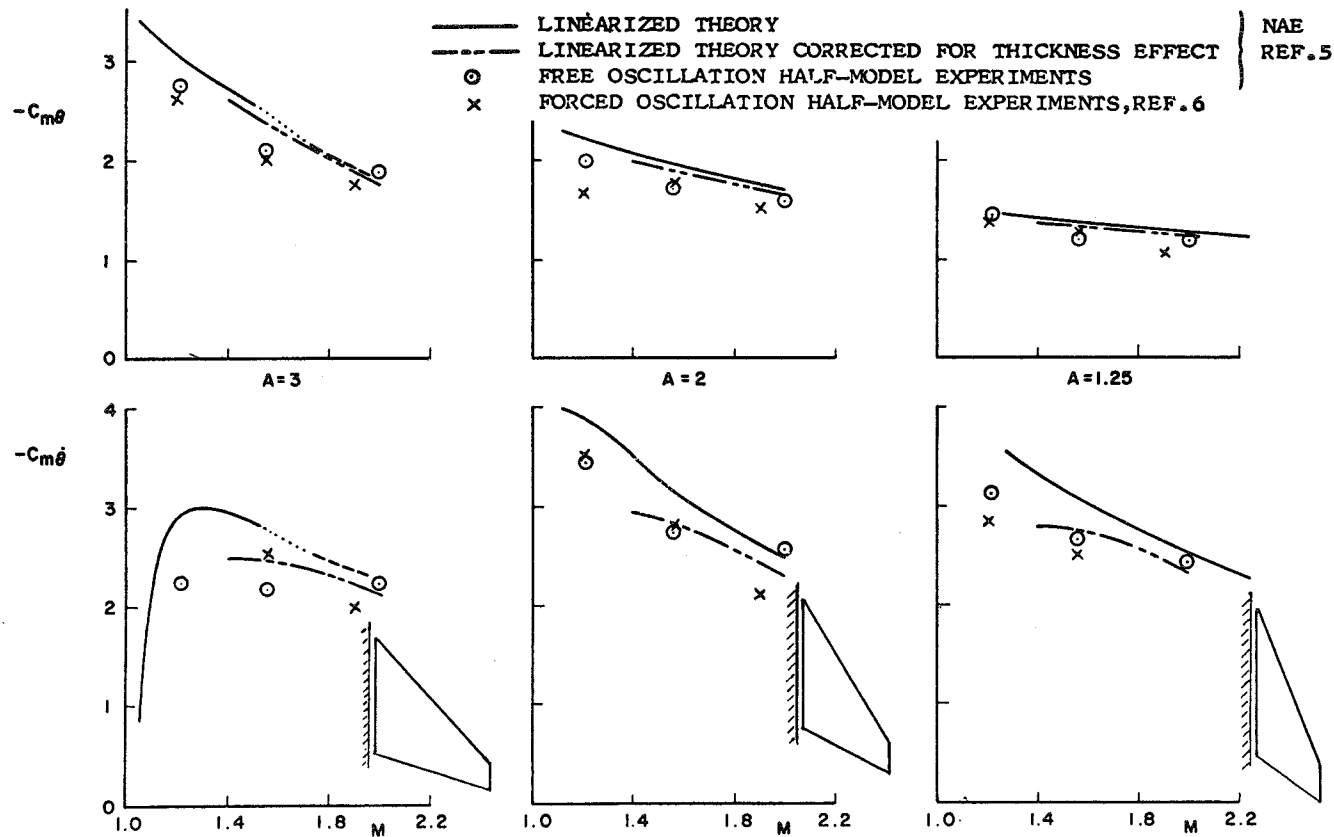
## COMPARISON OF HALF-MODEL DATA WITH THEORY

The best way to assess the reliability of the half-model technique is to compare its results with the corresponding full-model results or, if these are not available, with the theory. Such comparisons are very scarce in the literature and so far have been available almost exclusively for static aerodynamic data (Ref. 2). In this paper comparisons are presented for oscillatory aerodynamic results on representative types of configurations such as wings alone, bodies alone, and finally a wing-body configuration.

Static and dynamic pitching moment derivatives for a series of tapered sweptback wings are presented as functions of Mach number. All derivatives are referred to the apex of the wings. The symbol  $C_{m\dot{\theta}}$  refers to the damping-in-pitch

around a fixed axis, i.e. it is equivalent to the more commonly known ( $C_{m_q} + C_{m_{\dot{\alpha}}}$ ). Two sets of half-model results are presented:

our own (Ref. 5), obtained with a free oscillation technique and those of Hawker-Siddeley Dynamics in England (Refs. 6 and 7), obtained with a forced oscillation technique. The results compare favourably with each other and with the theoretical results based on the linearized supersonic-flow theory and corrected for thickness effect by means of a second order strip theory. In the NAE results, the static pitching moment derivatives around the experimental axes were corrected for the loss of lift through the gap, prior to using them in the axis transfer equations. No such correction was applied to the dynamic derivatives.

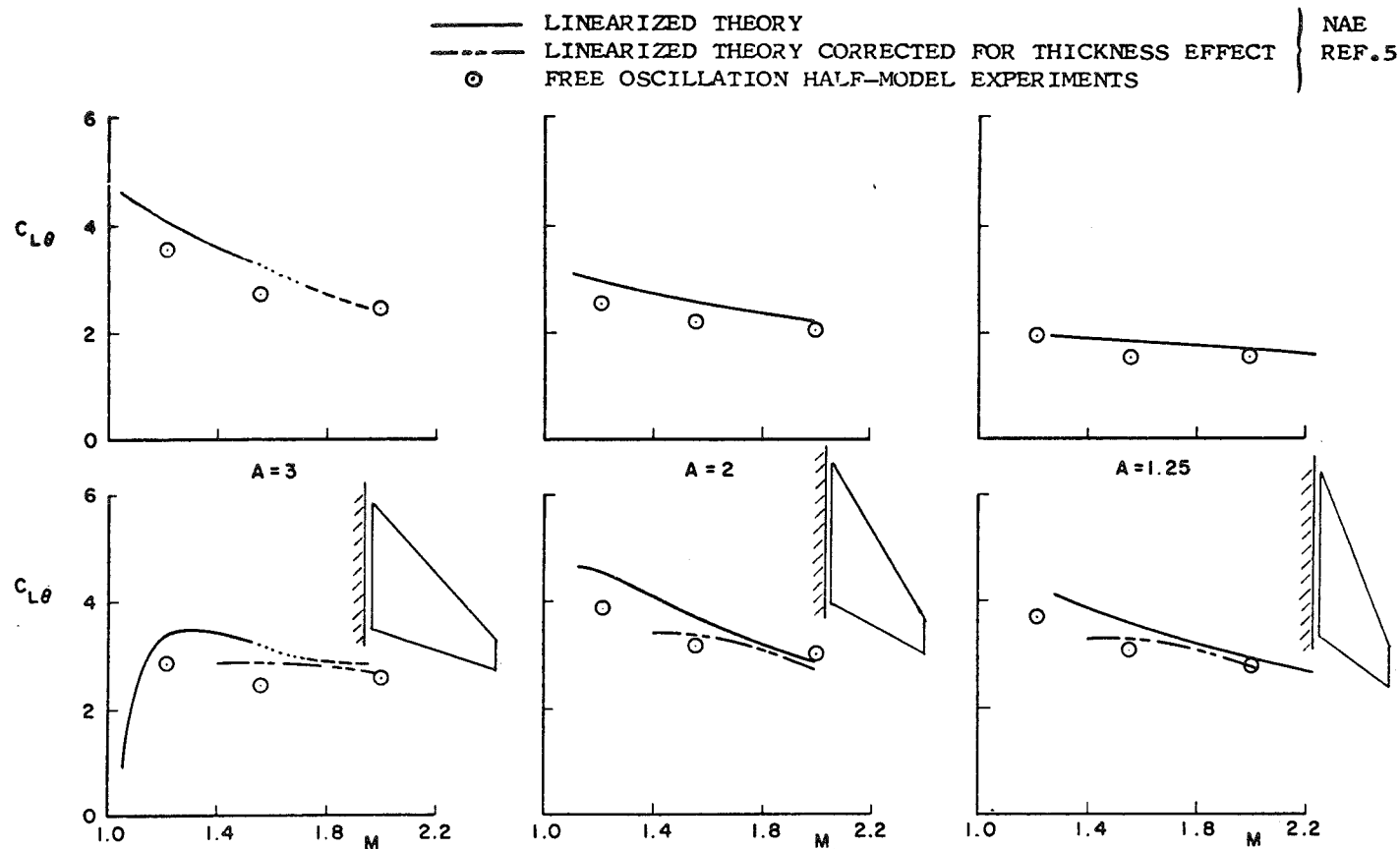


### COMPARISON OF HALF-MODEL DATA WITH THEORY

FIRST-ORDER PITCHING MOMENT DERIVATIVES ABOUT APEX FOR TAPERED SWEEPBACK WINGS

## COMPARISON OF HALF-MODEL DATA WITH THEORY

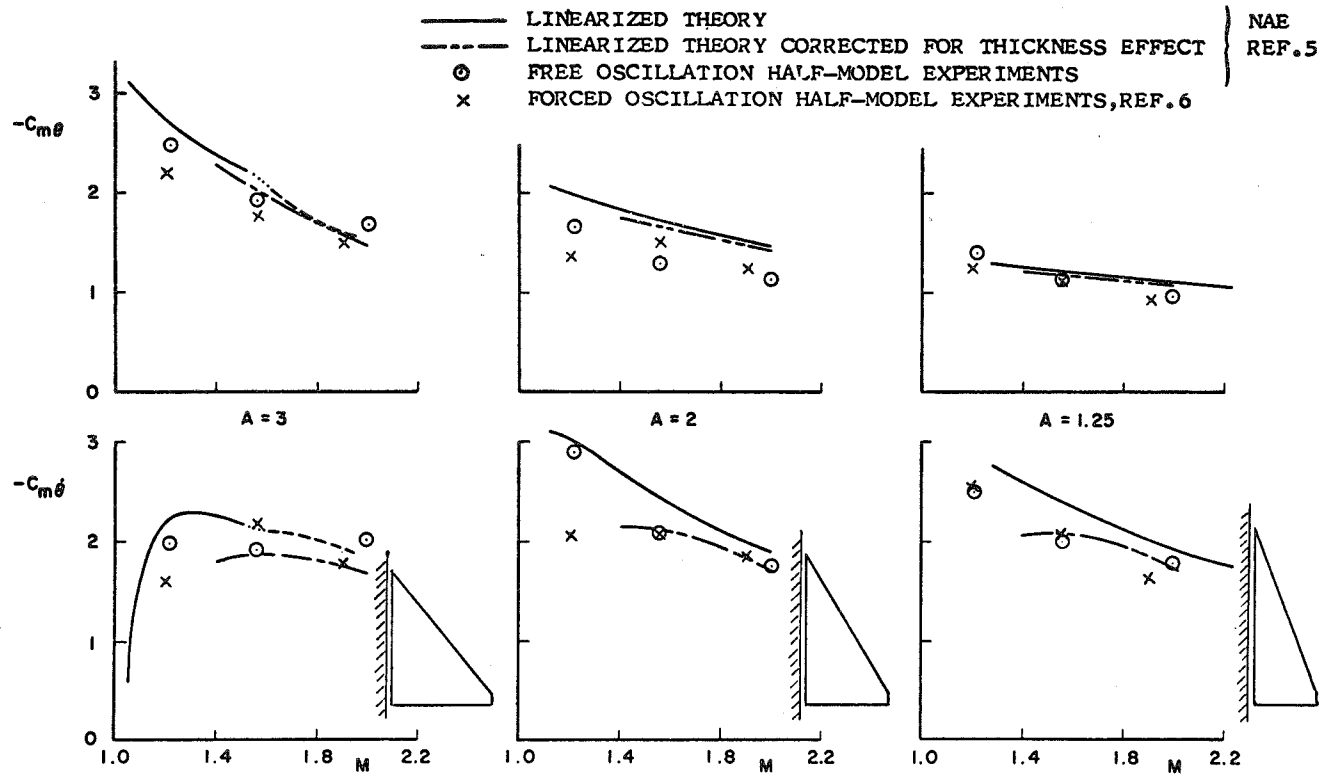
If free oscillation experiments are conducted about two longitudinally displaced axes of oscillation, the static and dynamic lift force derivatives may be calculated from the primary pitching moment data. A comparison of the so-obtained half-model results with the theory for the same series of tapered sweptback wings as in Fig. 2 is again very favourable. All derivatives were obtained at two values of reduced frequency ranging from 0.05 to 0.19, but were reduced to very low reduced frequency before comparison with the theory. The Reynolds number of the experiments was in the range of 3 - 4 million, based on the wing root chord. The results are valid for the amplitude range 0.8 - 1.6 degrees; all models were equipped with a small wing root fence and were mounted on a reflection plate outside the main portion of the wind tunnel boundary layer.



COMPARISON OF HALF-MODEL DATA WITH THEORY  
FIRST-ORDER LIFT DERIVATIVES ABOUT APEX FOR TAPERED SWEEPBACK WINGS

### COMPARISON OF HALF-MODEL DATA WITH THEORY

Similar comparisons of the static and dynamic pitching moment derivatives but for a series of slender cropped delta wings show again a good agreement between the two sets of half-model results and the theory. All comments from Figs. 2 and 3 apply here as well.



### COMPARISON OF HALF-MODEL DATA WITH THEORY

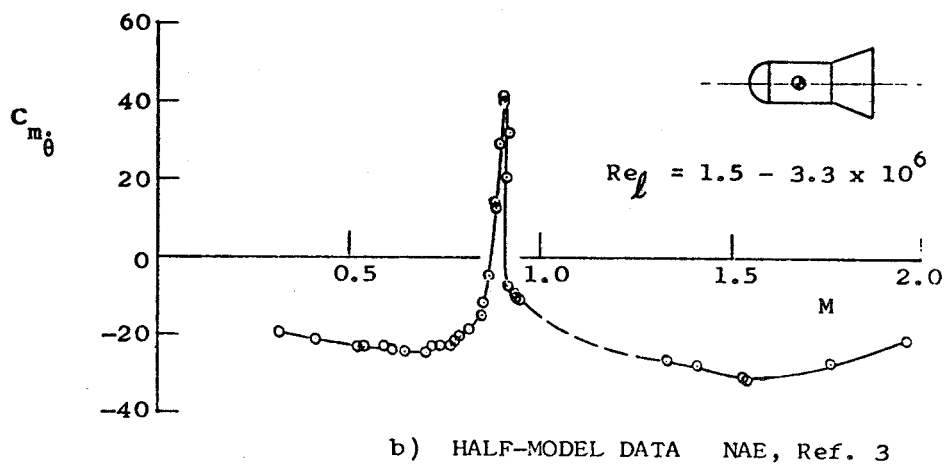
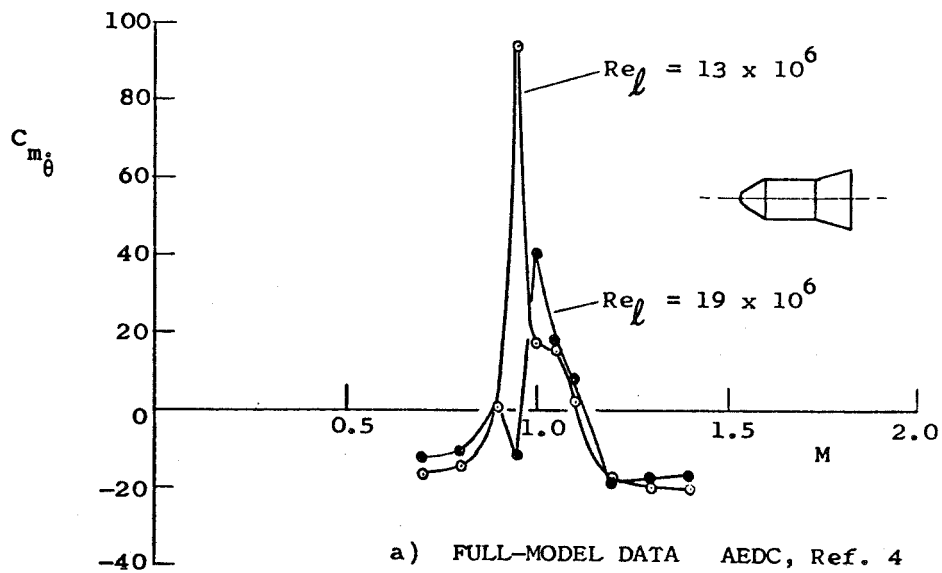
FIRST-ORDER PITCHING MOMENT DERIVATIVES

ABOUT APEX FOR CROPPED DELTA WINGS

### DAMPING-IN-PITCH FOR TWO BLUNT BODIES

The only comparison which can be made here for bodies alone is between half-model data on a hemisphere cylinder-flare configuration obtained with free-oscillation technique at NAE (Ref. 3) and full-model data on a blunted cone-cylinder-flare configuration obtained with forced oscillation technique at AEDC (Ref. 4). Since also the Reynolds number of the two sets of data was rather different, the only conclusion possible is that the general trend of the variation of damping-in-pitch with Mach number is quite similar, both sets displaying a large transonic instability peak and about the same value of the negative (stable) damping derivative at both the subsonic and supersonic Mach numbers. The NAE results were obtained with the model mounted on a reflection plate, as before.





DAMPING-IN-PITCH FOR TWO BLUNT BODIES

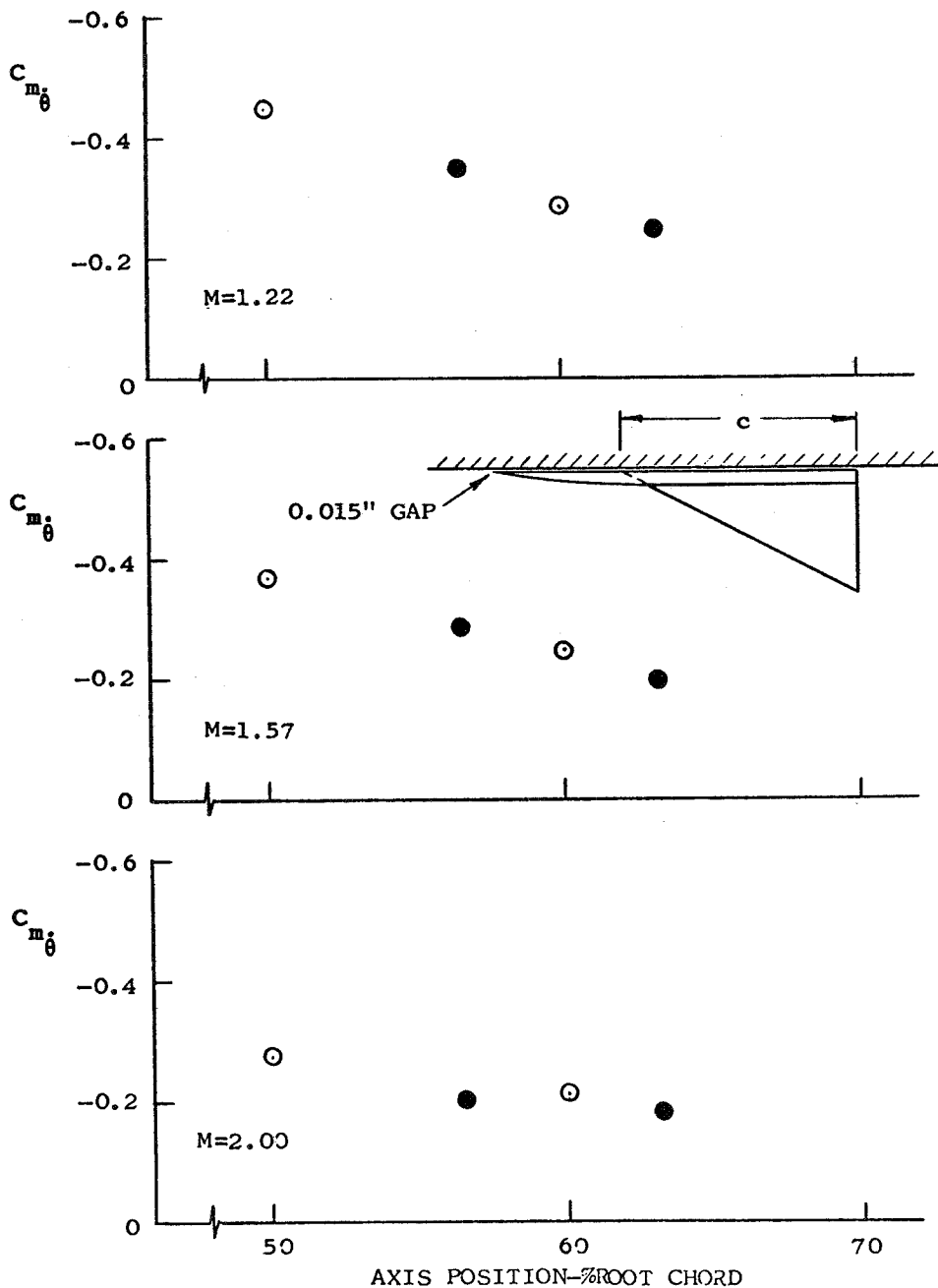
COMPARISON OF HALF-MODEL AND FULL-MODEL DAMPING RESULTS  
FOR A WING-BODY COMBINATION

In Fig. 6 a direct comparison is presented of the damping-in-pitch results for a slender delta-wing and body configuration. The half-model data were obtained from an unpublished NAE memorandum quoted in Ref. 5, and the full-model data at NACA (Ref. 8); both sets were obtained in the same range of Reynolds number. The results are shown as functions of the axis position for three Mach numbers. The agreement for Mach numbers 1.22 and 1.57 is excellent and at Mach number 2.00 still very good. It should be noted that although the  $C_{m\dot{\theta}}$  derivative usually displays a parabolic variation with axis position, the scale of Fig. 6 is such that this parabolic variation would be rather flat; consequently a straight-line fit through the experimental points may be considered as fairly good approximation. No reflection plate was used for the half-model results and it appears that on a wing-body configuration this may be permissible since the wing, which contributes most of the damping, is displaced by the body radius from the tunnel wall and hence is well outside the tunnel wall boundary layer. In addition, the presence of the body also reduces the gap effect on the flow over the wing.

Figures 2 to 6 indicate that half-model oscillatory experiments may lead to highly acceptable supersonic damping-in-pitch results for several different configurations and especially so for wing-body configurations. This technique appears therefore directly applicable to those shuttle configurations which are based on a wing-body geometry. In addition the dynamic half-model experiments on wings alone appear to give fairly acceptable damping-in-pitch results, but care has to be taken on wings alone to properly correct for the static loss of lift through the gap. Thus even for a more wing-like shuttle geometry (such as represented by some concepts of the lifting-body) the half model technique offers some promises.

All the data shown were obtained with oscillation in pitch about zero mean incidence. No direct comparison can be made at the present time for oscillation about non-zero incidence. However it is felt that for the relatively low mean incidence, say not higher than 5 to 7 degrees, which may be expected for the shuttle separation maneuver, the comparisons presented here and the conclusions reached may still apply.

- HALF-MODEL  $k \approx 0.10$ ,  $Re = 3 \times 10^6$ , NAE REF.5  
 ● FULL-MODEL  $k \approx 0.03$ ,  $Re = 3 \times 10^6$ , NACA REF.8



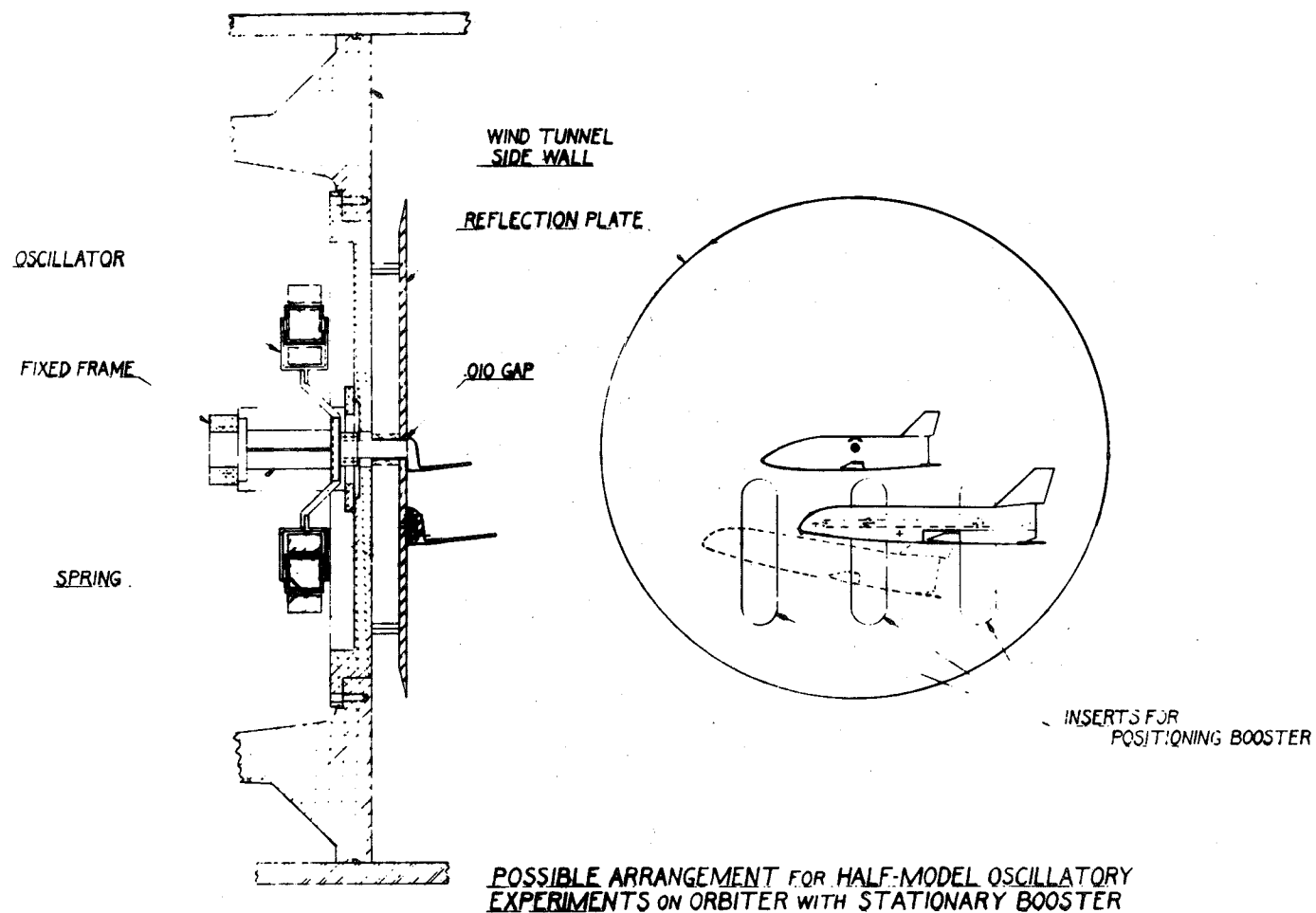
COMPARISON OF HALF-MODEL AND FULL-MODEL DAMPING RESULTS FOR WING-BODY COMBINATION AT ZERO MEAN INCIDENCE

POSSIBLE ARRANGEMENT FOR HALF-MODEL OSCILLATORY EXPERIMENTS  
ON ORBITER WITH STATIONARY BOOSTER

A possible arrangement for oscillatory experiments on the orbiter in the presence of the booster is shown schematically in Fig. 7. Half-models of both vehicles are mounted close to a reflection plate which in turn is mounted on a rotatable plate in the wind tunnel wall. The orbiter model is mounted on a shaft which goes through both plates and is firmly attached to a dynamic-test apparatus outside the wind tunnel, while the booster model is mounted to the reflection plate by a system of easily interchangeable plate inserts and a longitudinal slot inside the model. This mounting permits an easy stepwise variation of the vertical spacing and the relative incidence between the two vehicles and a continuous variation of the longitudinal spacing. In addition, the incidence of the two-vehicle combination can be varied in a continuous fashion by simply rotating the wind tunnel plate.

This arrangement would permit the measurement of the static and dynamic pitching moment derivatives on the orbiter for an arbitrary number of booster locations. Conversely, by interchanging the two models, the oscillatory characteristics of the booster could be measured for an arbitrary number of orbiter locations. As a result, the static and dynamic pitching moment derivatives could be obtained as functions of the relative position of the two vehicles and of the incidence of the two-vehicle combination. By performing the measurements around two axes of oscillation also the normal force derivatives could be obtained.

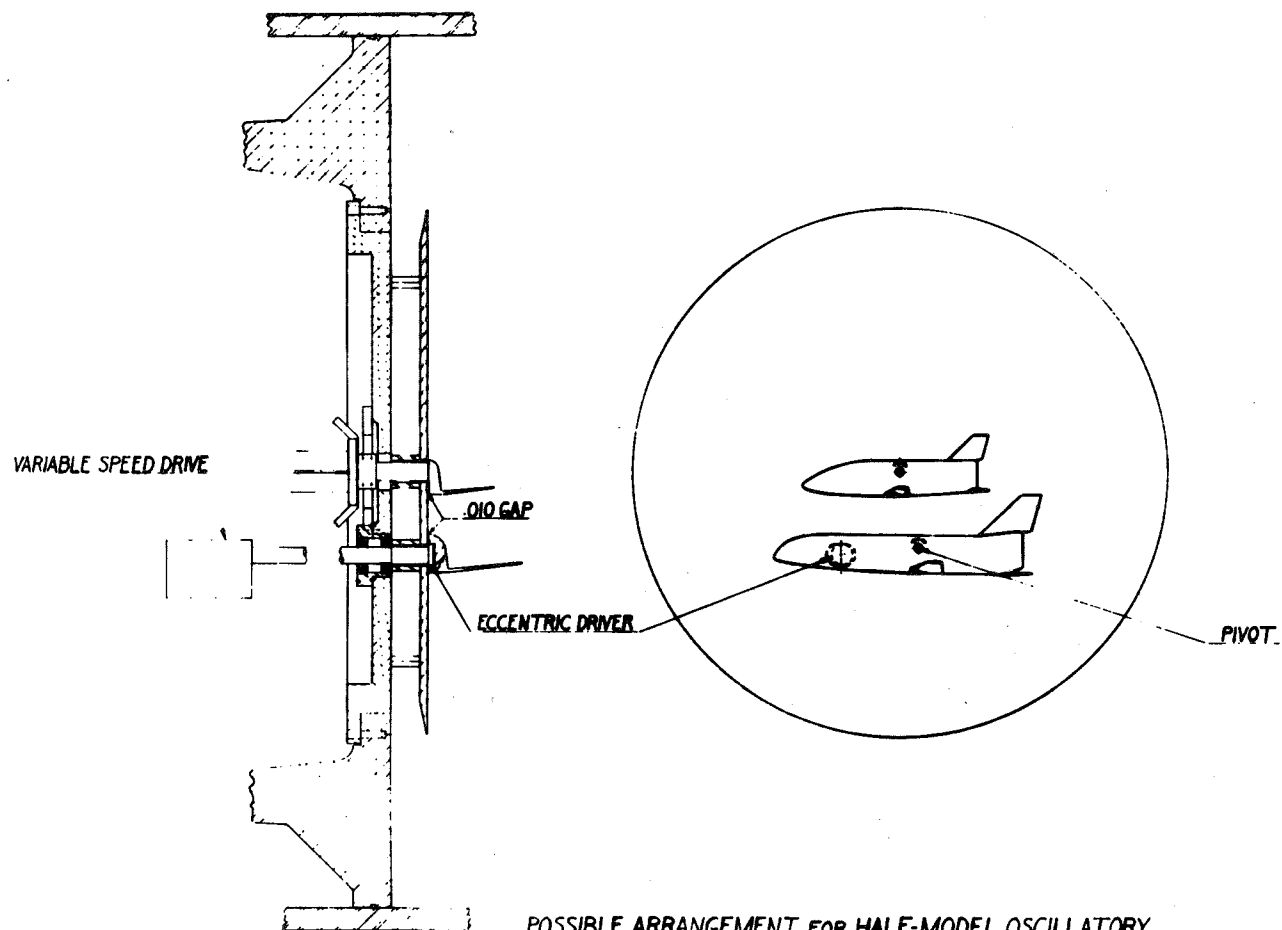
All measurements could be performed using the standard NAE technique of free oscillation with automatically recycled feedback excitation. Both this technique and the dynamic-test apparatus have been described before (see for example Refs. 3 and 5).



POSSIBLE ARRANGEMENT FOR HALF-MODEL OSCILLATORY EXPERIMENTS  
ON ORBITER WITH OSCILLATING BOOSTER

In an actual separation maneuver both vehicles will be moving at the same time. It may therefore be important to determine not only the static interaction effect caused by the stationary presence of the other vehicle but also the dynamic interaction effect associated with the fact that the other vehicle is moving. Of the various possible modes of motion, the one which is likely to cause the largest dynamic interaction on the oscillatory characteristics to be measured is the rotation of the other vehicle. By modifying the experimental arrangement shown before, the other vehicle (in this case the booster) could be driven in a sinusoidal pitching oscillation by means of a variable speed motor, a rotating shaft and an eccentric disc. This would permit obtaining the oscillatory characteristics of the orbiter as a function of not only the relative position of the two vehicles but also as a function of the amplitude and frequency of the booster.

The experimental investigations indicated in this paper would yield oscillatory characteristics of the two vehicles in the presence of both the static and dynamic interaction effects and could be used for a much more realistic (than it is now possible) estimate of the aerodynamic functions required to formulate the equations of motion for the separation maneuver. The validity of such equations of motion could then be evaluated by computing a separation-maneuver time-history for the wind tunnel conditions and comparing the results with an experimental release and separation of the two vehicles in the wind tunnel.



POSSIBLE ARRANGEMENT FOR HALF-MODEL OSCILLATORY  
EXPERIMENTS ON ORBITER WITH OSCILLATING BOOSTER

## SUMMARY AND CONCLUSIONS

Since the initial phases of the shuttle stage separation can be considered as a symmetrical maneuver, the technique of half-models may be used for the required dynamic wind tunnel experiments. The reliability of such a technique as applied to oscillatory experiments was reviewed in this paper and some possible arrangements for half-model oscillatory experiments on the individual stages in the presence of the other stage were discussed. It is concluded that

1. Half-model oscillatory experiments may be expected to yield acceptable supersonic results on the damping-in-pitch derivative for wing-body configurations;

2. The half-model technique appears very attractive for dynamic experiments during which the relative positions of the two stages and their overall incidence have to be varied in a large number of steps.

3. The techniques and experimental arrangements described in this paper could easily be used to determine the dynamic characteristics in pitch for one of the stages not only as function of the relative position of the two stages and their incidence but also as function of the amplitude and frequency of the other stage. Such information could then be used to obtain a more realistic set of equations of motion for the separation maneuver.



## References

1. Decker, J. P. An exploratory experimental and analytical study of separating two parallel lifting stages of a reusable launch vehicle at Mach numbers of 3 and 6. M.A.E. Thesis, University of Virginia, 1968.
2. Van der Blik, J.A. Notes on half model testing in wind tunnels. National Research Council of Canada NAE LR-235, 1959.
3. LaBerge, J.G. Effect of flare on the dynamic and static moment characteristics of a hemisphere-cylinder oscillating in pitch at Mach numbers from 0.3 to 2.0. National Research Council of Canada NAE LR-295, 1961.
4. Dubose, H.C. Static and dynamic stability of blunt bodies. AGARD Report 347, 1961.
5. Orlik-Rückemann, K.J.  
LaBerge, J.G. Static and dynamic longitudinal stability characteristics of a series of delta and sweptback wings at supersonic speeds. National Research Council of Canada NAE LR-396, 1966.
6. Hall, G.Q.  
Osborne, L.A. Transonic and supersonic derivative measurements on the planforms of the Ministry of Aviation Flutter and Vibration Committee's first research programme. Hawker-Siddeley Dynamics Ltd., ARL 64/9, A.R.C. 26016, 1964.
7. Woodcock, D.L. Co-ordinated experimental and theoretical research on the oscillatory airforces for selected planforms at subsonic and supersonic speeds. RAE TR 68033, 1968.

8. Tobak, M.

Damping in pitch of low-aspect-  
ratio wings at subsonic and  
supersonic speeds.  
NACA RM A52L04a, 1953.

THE ONERA HOT SHOT WIND TUNNELS CAPABILITIES  
IN THE SPACE SHUTTLE STUDIES

by Jean-Pierre CHEVALLIER

Office National d'Etudes et de Recherches Aéronautiques (ONERA)

92 - Châtillon, France

INTRODUCTION

The ONERA wind tunnels ARC1 and ARC2, by their design and equipments, offer exceptional capabilities for the hypersonic studies in the Mach number range from 15 to 20 with large variations of the Reynolds number.

A clean flow, with a useful run larger than 50 msec at reduced enthalpies up to 150 ( $h_o/RT_a \leq 150$ ) is specially convenient for black-out studies.

A short description of these facilities, a table with their main features, their simulation range, the list of their equipment for measures with some result samples about electromagnetic waves transmission in the plasma are given below to point out the work these facilities can do in the space shuttle study.

DESCRIPTION OF THE FACILITIES

The ONERA hot shot wind tunnels ARC1 and ARC2 are installed at Fontenay (4 miles from Paris) in the research and development center of "Electricité de France" and directly supplied by the National Grid (available power  $10^9$  VA during 0.1 sec). Thanks to this high power a large arc chamber is used [1], giving a quasi steady flow with a mean run duration of about 100 msec. The available energy and power are sufficient to obtain high enthalpies ( $h_o/RT_a = 150$ ,  $T_o = 8000^\circ K$ ) even with 50 amagat. The electric supply (Fig. 1) of the arc chamber includes the breaker and some coils in the high voltage circuit for adjusting the corresponding intensity in the secondary circuit up to 80 000 A. The arc duration control is obtained by the lag between the two fast acting switches.

To initiate the arc between the wall and the insulated electrode a small silver paint trace is used. A silastene coating of the arc chamber prevents the surface from melting, so that the metallic pollution of the gas is reduced to a very low level [2].

The two tunnels are shown in figure 2, and their salient characteristics are listed in Table I.

The aerodynamic range of operation when the hot shots are used as conventional hypersonic wind tunnels is described in the Mach-Reynolds number plane (Fig. 3), in which a hypothetical space shuttle trajectory is also indicated.

For the non-equilibrium real gas effects the speed of the flow and the product of density and length (or the corresponding altitude, taking into account the scale model) are the significant parameters. The restitution range for these parameters is given figure 4.

T A B L E I

## ONERA HOT-SHOT WIND TUNNELS

TUNNEL	ARC1	ARC2
Arc chamber volume	2.5 dm <sup>3</sup>	8 dm <sup>3</sup>
Nozzle	Conical, metallic	Contoured, plastic
Length	3 m	4 m
Throat diameter	4.5 mm	5.2 mm
Exit diameter	500 mm	670 mm
Test section	Open jet or solid walls	Open jet in a fiber glass tank
Length	1 m	1.2 m
Vacuum tank		
Volume	15 m <sup>3</sup>	47 m <sup>3</sup>
Electric supply	≤ 40 000 A	≤ 80 000 A
Reservoir		
Temperature	2000 to 5000°K	2000 to 8000°K
Pressure	20 to 2000 atm.	20 to 1500 atm.
Reynolds number	6 · 10 <sup>6</sup> /meter	5 · 10 <sup>6</sup> /meter
Typical model length	0.25 m	0.5 m
Mach number	15 to 20	15 to 20
Useful run duration	0.1 sec	0.05 to 0.15 sec

MEASURING DEVICES

The same Faraday cage is used for the two wind tunnel measuring equipments, which are as follows :

- 4 piezoelectric channels for the reservoir pressure measurements;
- 50 20kHz channels for pressure transducers;
- 10 heat flux channels (direct current amplifiers and derivators) used with thermocouples;
- 6 channels for three-component balance with compensation for inertial effects (piezoelectric dynamometer and accelerometer)
- 12 channels : direct current amplifiers and analog computer used with a six-component balance with inertial effects compensation;
- Analog recorder P.M. 40 channels, on magnetic tape;
- Analog-digital converter, magnetic recorder and tape puncher for data scanning and reduction;
- Analog recorder for the display of the data after the run (42 cathodic oscilloscopes);

- Special devices for Langmuir probes, and electromagnetic wave measurements.

The ARC1 wind tunnel is used especially in conventional measurements : pressures, aerodynamic forces, heat fluxes. It is equipped with devices giving a motion to the model during the run. The variation of angle of attack ( $10^\circ$  in 50 ms) or the rotation of the model (half a turn around its axis) [3] combined with the use of inertial compensated balances [4] and short response time transducers (Fig. 5) enable us to obtain during a single run all the aerodynamic coefficients or a full distribution of pressure, or heat fluxes on an axisymmetric body at incidence.

The ARC2 wind tunnel, specially designed for electromagnetic wave transmission studies [5], is built without metal in the test section (Fig. 6). Three antennas for emission can be seen on the model. The antennas for reception, in two planes out of the test section, are protected against reflection by the walls of a cubic room (4 x 4 x 4 m). The anechoic coating can be seen on the left side and through the windows behind the model.

An example of the results currently obtained is given figure 7. The power received at about the same time (within one msec.) from the three antennas in different directions is shown on these radiations diagrams. The heavy lines correspond to the case of an electronic density just a little higher than the critical one for antennas 2 and 3. The dashed lines are obtained with lower densities. These curves may be compared to the theoretical results obtained assuming a multilayer, plane or cylindrical plasma. This method is very accurate when the frequency corresponds to the critical electronic density. By using waves in the range from 1 to 100 GHz, the electronic density between  $10^8$  and  $10^{14}$  electrons/cm<sup>3</sup> can be measured.

The other means used to obtain a local plasma diagnostic is the electric probe (Langmuir probe) which gives the electron density and temperature [6], [7]. The upper limit due to the probe heating is of the order of  $10^{13}$  electrons/cm<sup>3</sup>, the lower about  $10^6$  e/cm<sup>3</sup>. To avoid the errors due to induced potentials we use the triple probe [7] which implies only differential voltage and current measurements, and avoids the periodic voltage sweeping. The probe can be displaced during the run in order to obtain density profile.

For the wake study the interferometric method with emission and reception antennas surrounding the transparent material tube following the test section may be used.

#### REFERENCES

- [1] P. CARRIERE and J.P. CHEVALLIER : Recent progress in the ONERA hot shot wind tunnels. 5th Hypervelocity Techniques Symp. Denver, March 16-17, 1967 - T.P. ONERA No 447.
- [2] J.P. CHEVALLIER : Recent improvements in the ONERA ARC2 wind tunnel. 33rd Supersonic Tunnel Association Meeting, Los Angeles, May 7-8, 1970. - T.P. ONERA No 827.
- [3] A. LHULLIER : Continuous pressure measurements in a rotating model during a hot shot run. 23rd S.T.A. Meeting, Long Island, May 3-4, 1965 - T.P. ONERA No 234.
- [4] J. BERRY and R. HOARAU : Mesure des efforts dans une soufflerie à arc par une balance piézoélectrique à trois composantes compensée en inertie. IEEE/AES Transactions, vol. 1, No 1, 1965.

- [5] C. POUIT : Reflectométrie hyperfréquence sur un plasma aérodynamique. Jour. de Physique, Suppl. No 4, 29, 1968, C 3, pp. 235 à 237.
- [6] D. COMPARD and J. DOREY : Caractérisation des plasmas de rentrée dans les souffleries hypersoniques à arc. VIIIème Conf. Int. sur les phénomènes dans les gaz ionisés, Vienne, 27.8.1967, p. 476.
- [7] J. DOREY and D. COMPARD : Experimental studies of plasma sheath surrounding models in hot shot wind tunnels. IEEE/AES Transactions, vol. 3, No 2, 1967.

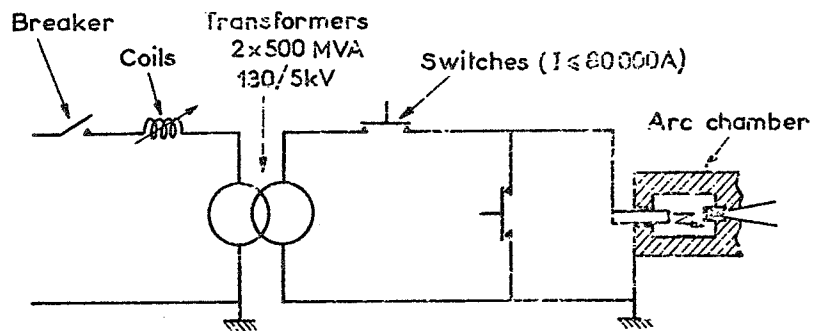
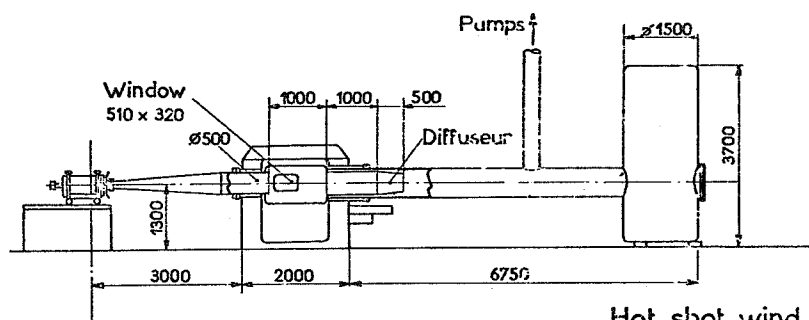
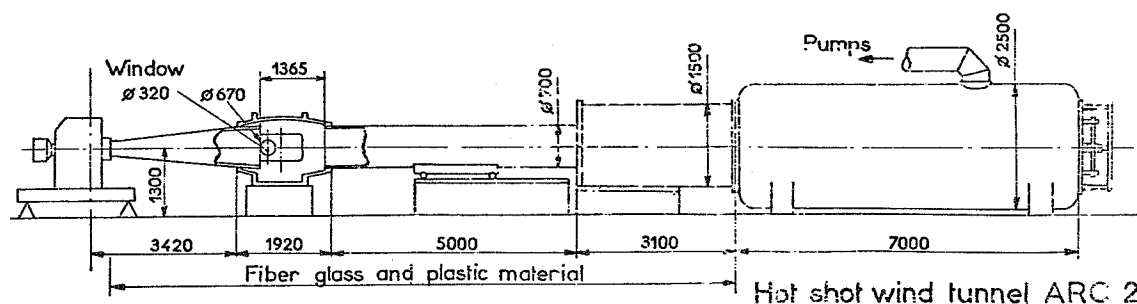


Figure 1 : Electric supply of the ARC chamber.



Hot shot wind tunnel ARC 1



Hot shot wind tunnel ARC 2

Figure 2 : Hot shot wind tunnels ARC1 and ARC2.

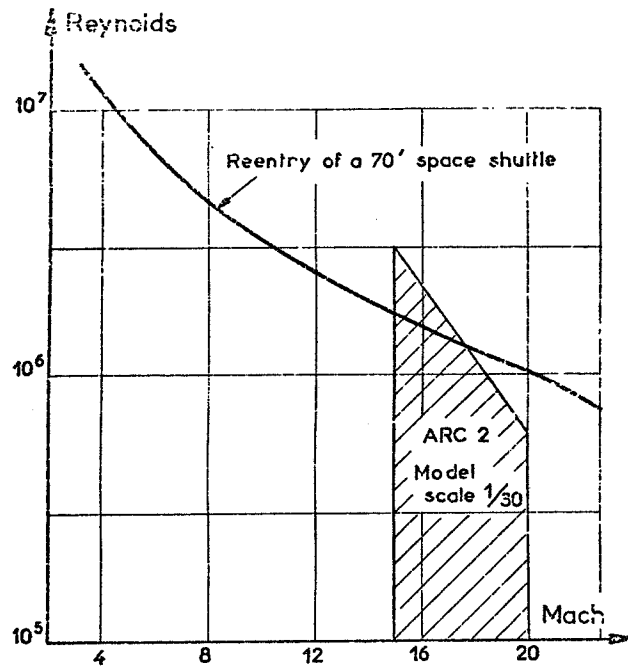


Figure 3 : Simulation range in the Mach-Reynolds number plane.

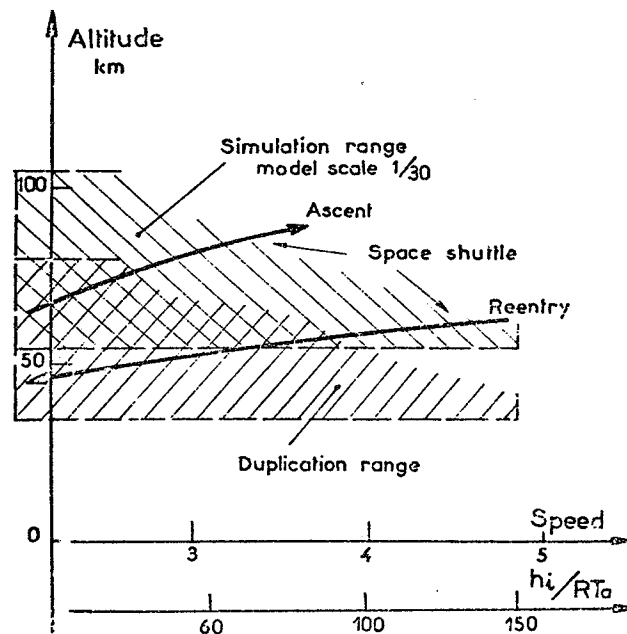


Figure 4 : Duplication range in speed-altitude plane.



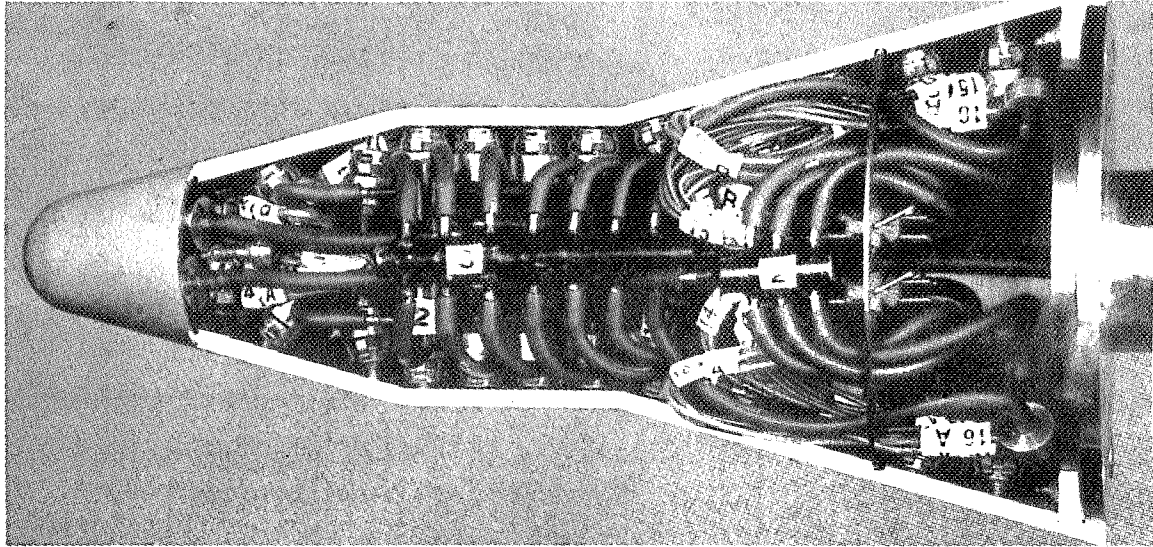


Figure 5 : 8" length model equipped with 25 pressure transducers.

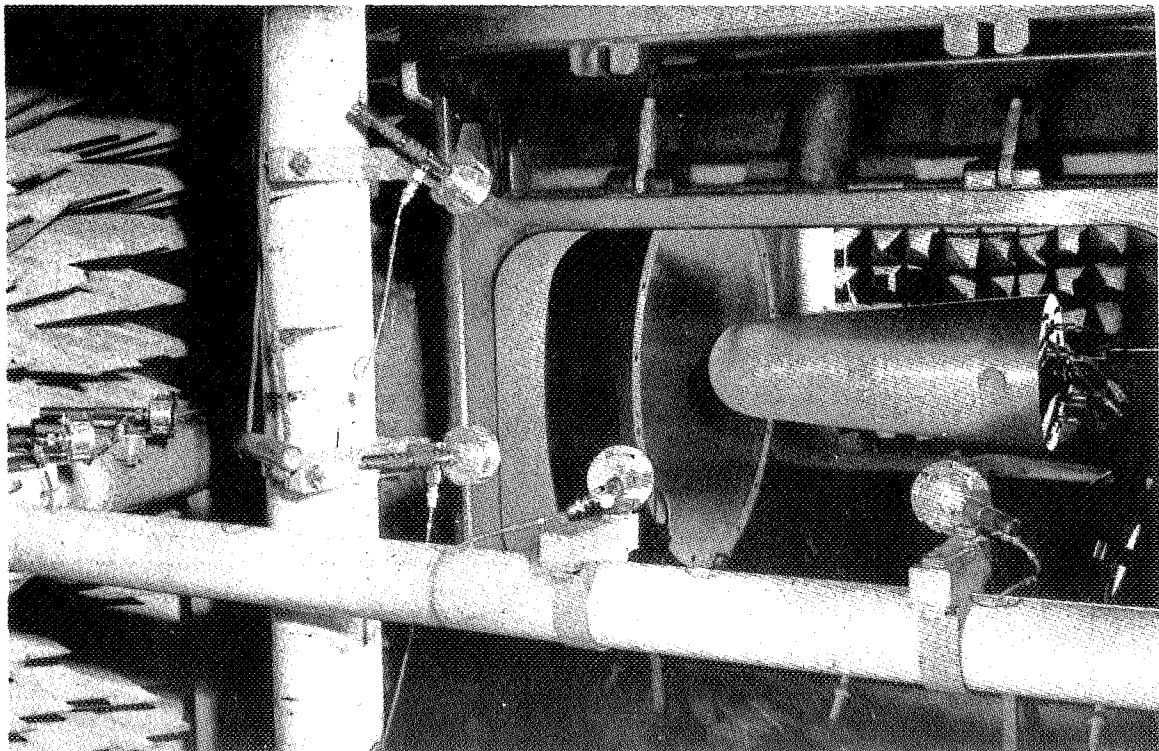


Figure 6 : ARC2 test section. Model with 3 transmitting antennas. Vertical and horizontal beams supporting the reception antennas and anti echo material on the walls.

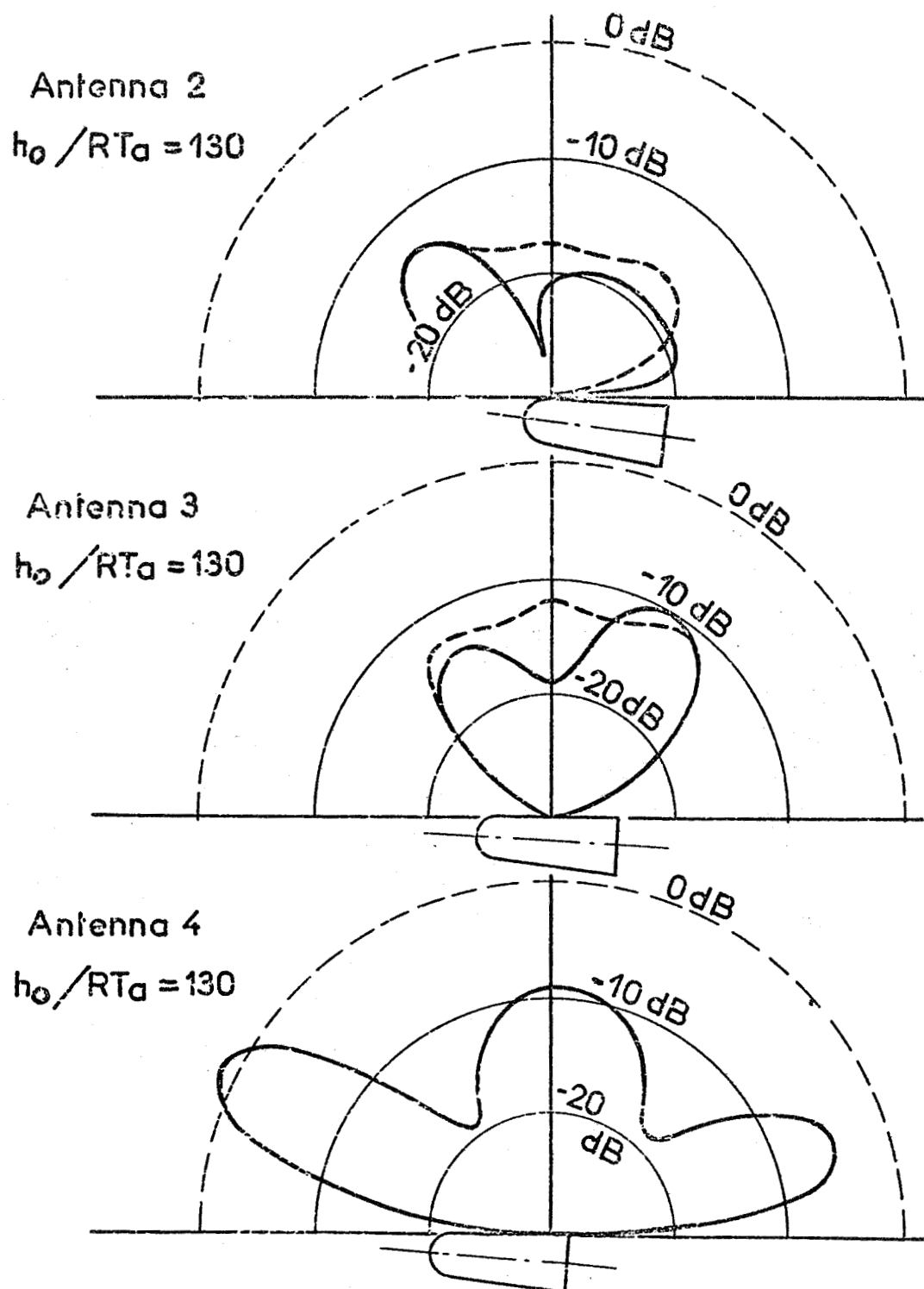


Figure 7 : Antennas emission diagram through the plasma.

THE APPLICATION OF MIL-F-8785B (ASG) TO  
THE EVALUATION OF LANDING-APPROACH  
FLYING QUALITIES OF A LIFTING-BODY-TYPE SHUTTLE VEHICLE

J. Chin

Grumman Aerospace Corporation  
Bethpage, New York

Abstract

The estimated flying-quality parameters of a lifting-body-type shuttle vehicle in the landing-approach mode is compared with requirements from the new Military Flying Qualities Specification, MIL-F-8785B (ASG). Based on these comparisons, a level of pilot rating is estimated. This is compared with pilot ratings from an inflight simulation of the shuttle vehicle using a B-26 variable-stability aircraft. The conclusion, within these comparisons, is that the Mil Spec is applicable for evaluating the landing-approach flying qualities of a lifting-body-type vehicle.

Introduction

During Grumman's design study of the space shuttle concept, MIL-F-8785B was used as a guide for evaluating the landing-approach flying qualities of a lifting-body-type reentry vehicle. An inflight simulation study of this configuration was made with Cornell Aeronautical Laboratory's B-26 variable-stability aircraft. The objectives of this study were to provide added insight into the basic, unaugmented vehicle's flying qualities, to confirm the predictions made, and to assess the applicability of the Mil Spec to this type of vehicle.

### Grumman Design 518

A three-view of the lifting-body design is shown in Fig. 1. Outboard tails, canted 45 deg, are carefully tailored to provide hypersonic longitudinal and directional stability, as well as low-speed longitudinal stability. A center vertical tail provides additional directional stability in the conventional flight mode. Aerodynamic control in landing approach is provided by a rudder on the center vertical tail and by elevons on the outboard tails. The elevons are deflected symmetrically for pitch and asymmetrically for roll.

Roll reversal, induced by the adverse yaw of the elevons during asymmetric deflections and the high dihedral effect of the vehicle, is effectively eliminated via a stick-to-rudder interconnect. This is shown in Fig. 2, where the roll-rate reversal has been eliminated and the sideslip history significantly reduced. A rudder-to-elevon interconnect is also found desirable since the rudder-induced rolling moment was found to be disconcerting in the presence of an apparently lightly damped vehicle in roll.

# GRUMMAN DESIGN 518

$$WT = 199,870 \text{ LB}$$

$$I_{yy} = 10.7 \times 10^6 \text{ SLUG FT}^2$$

$$I_{zz} = 10.9 \times 10^6 \text{ SLUG FT}^2$$

$$I_{xx} = .649 \times 10^6 \text{ SLUG FT}^2$$

$$S_{REF} = 6100 \text{ SQ FT}$$

PA FLT COND:

$$V_{PA} = 180 \text{ KT}$$

$$\alpha_{PA} = 10 \text{ DEG}$$

$$\gamma = -2.5 \text{ DEG}$$

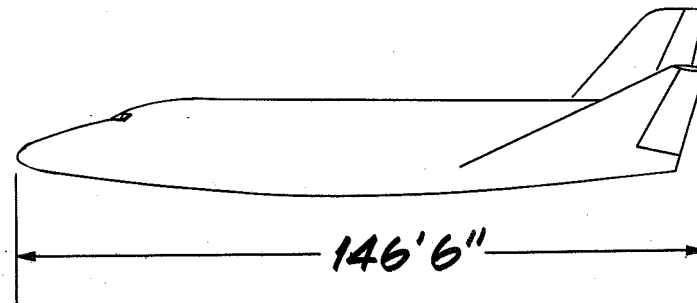
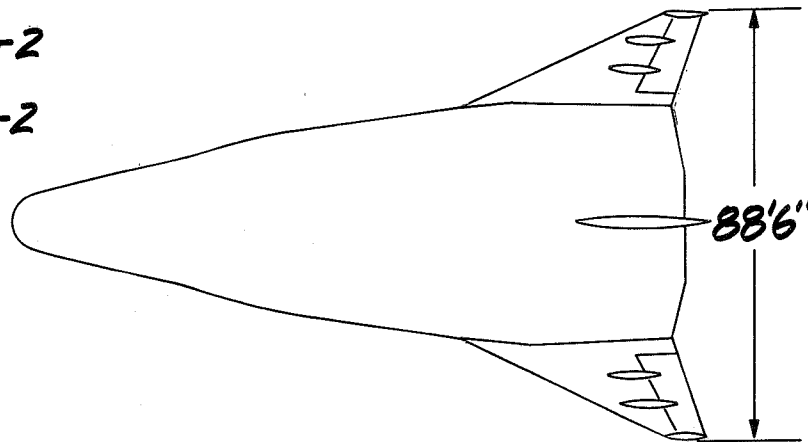
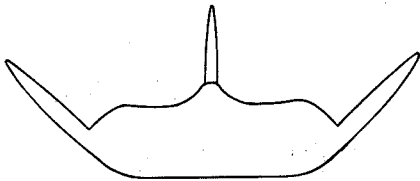


Fig. 1

# EFFECTIVENESS OF AILERON-RUDDER INTERCONNECT

(DESIGN S1B ORBITER LANDING APPROACH)

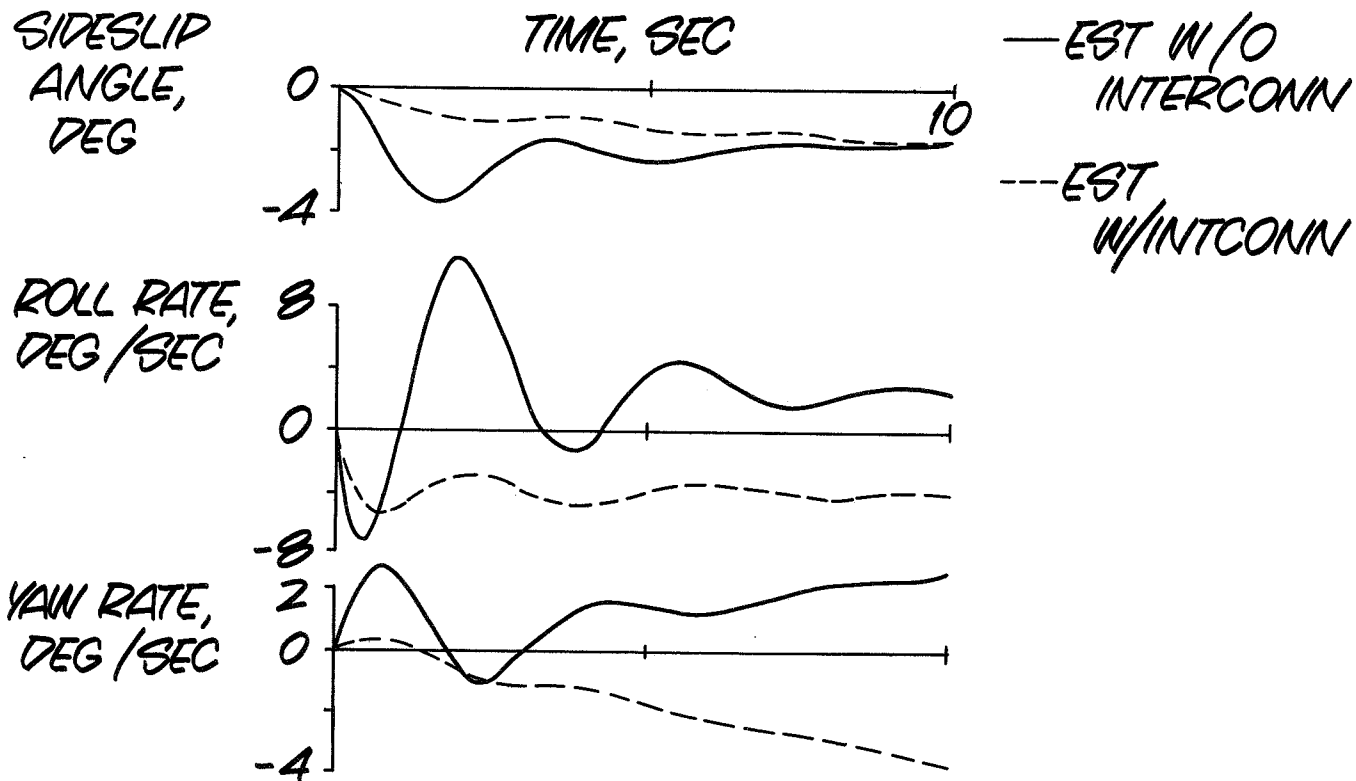


Fig. 2

### Relation Between Quantitative Values of Flying Qualities Parameters & Pilot Ratings

MIL-F-8785B specifies a relation between the quantitative values of numerous flying-quality parameters and levels of acceptability. These levels of acceptability are directly related to pilot ratings. In particular, the relation between the levels and the Cooper-Harper pilot rating scale is shown in Fig. 3. An example of how these levels of acceptability are related to the flying-quality parameters is given in Fig. 4. Because of the relations, one can gain insight into the degree of acceptability of the vehicle being studied.

## FLYING QUALITY ACCEPTABILITY LEVELS

MIL SPEC 8785B	PILOT RATING	PILOT OPINION
LEVEL 1	1	SATISFACTORY & ACCEPTABLE
	2	
	3.5	
LEVEL 2	3.5	UNSATISFACTORY BUT ACCEPTABLE
	5	
	6.5	
LEVEL 3	6.5	UNACCEPTABLE
	8	
	9+	

Fig. 3



# SHORT-PERIOD FREQUENCY REQUIREMENTS

## LANDING APPROACH - LARGE TRANSPORTS

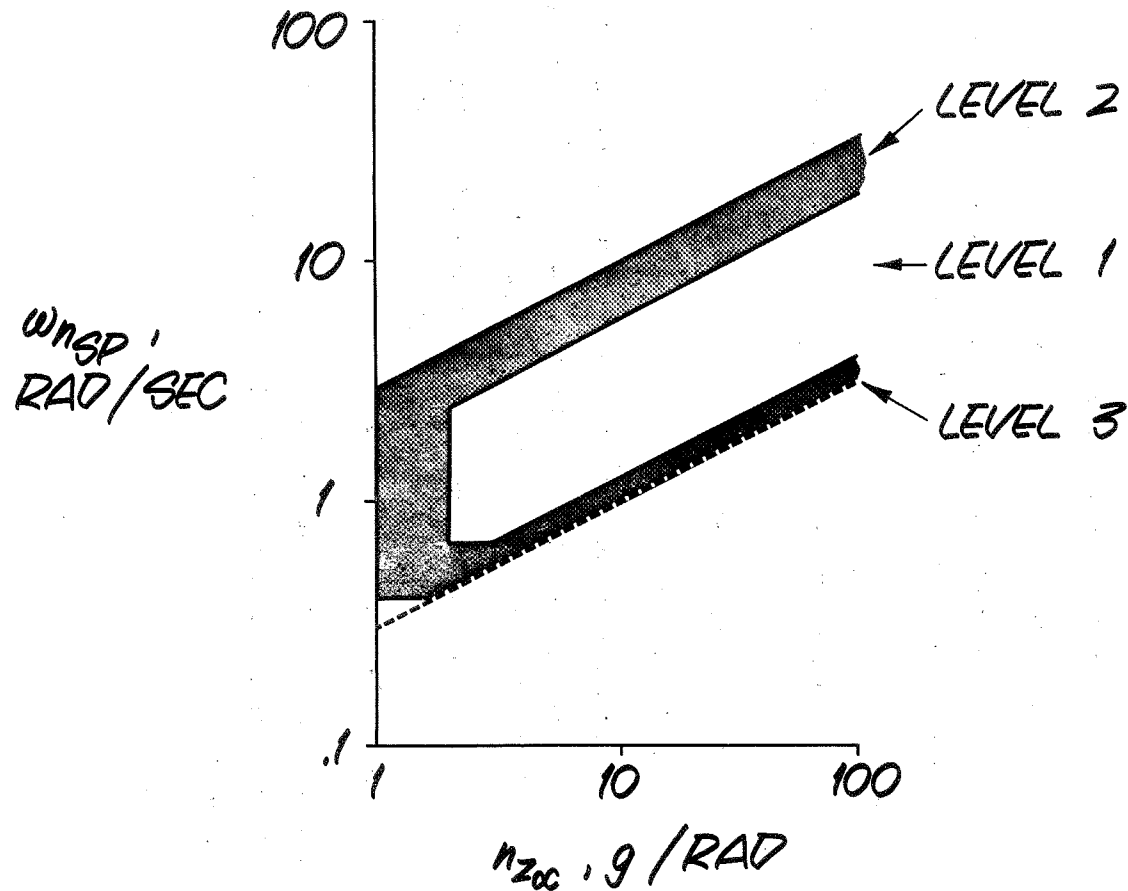


Fig. 4

### Flying-Qualities Evaluation

The flying-qualities evaluation of Design 518, based on MIL-F-8785B, is shown in Fig. 5, with the estimated level of acceptability. These results are for the basic unaugmented vehicle with simple stick-to-rudder and rudder-to-elevon interconnects. Briefly, the vehicle flying qualities can be summarized as follows:

- Longitudinal
  - Pitch response tends to be sluggish
  - Phugoid mode is satisfactorily damped
  - Vehicle flies on the backside of the power curve, but the degree of back-sidedness should cause no difficulty
- Lateral
  - Dutch-roll dynamics appear satisfactorily damped and frequency is adequate
  - Roll-mode time constant is low
  - Spiral mode is stable
  - With the interconnects that were simulated, the roll response is acceptable, but requires pilot's compensation. This is due partly to the residual adverse yaw which still appears (Fig. 2)
  - $\phi/\beta$  , not a requirement per se, but is indicative of the vehicle's responsiveness to lateral gust, is fairly high due to the high dihedral effect of the vehicle

In summary, the vehicle is expected to be somewhat sluggish in pitch, quite responsive to lateral gust, and some coordination must be provided by the pilot during bank maneuvers.

# THEORETICAL FLYING QUALITIES EVALUATION

MIL 8785B REQMT	DES 518	EST LEVEL
(SHORT PD FREQ) <sup>2</sup> VS $\eta_{200}$ $.16 < \frac{\omega_{HSP}^2}{\eta_{200}} < 3.6$	.135	2
SHORT PD DAMPING $.35 < \zeta_{SP}$	.85	1
LONG'L PLUG DAMP $\zeta_{PH} > .04$	.088	1
FLT PATH STAB $\frac{d\gamma}{dV} < .06 \text{ DEG/KT}$	.03	1
DUTCH ROLL FREQ $\omega_{nd} > .4 \text{ RAD/SEC}$	1.8	1
DUTCH ROLL DAMPING $\zeta_d > .08$	.21	1
ROLL TIME CONST $\tau_r < 1.4 \text{ SEC}$	.56	1
SPIRAL TIME CONST $t_2 > 20 \text{ SEC}$	$t_{1/2} = 42$	1
$\phi/\beta$ (NOT SPECIF REQMT)	3.9	-
INIT(MIN/MAX) ROLL RATE (%)	47	2
OBC/AVG ROLL RATE VS $\psi_B$	.355 @ -206 DEG	2

Fig. 5

## Fidelity of Inflight Simulation

Comparison of the Orbiter's estimated dynamic characteristics with the corresponding simulated values in Fig. 6 shows the following interesting points:

- Approach velocity restricted to 160 kt due to B-26 landing gear structural limitations. Differences in the velocity should not significantly affect pilot rating
- Flight path stability is well simulated
- The objective was to maintain the same level of  $\omega_n^2/n_z\alpha$  to obtain equivalent pilot ratings. Since Design 518's  $n_z\alpha$  level cannot be simulated by the B-26 at 160 kt, the short-period frequency was simulated to give the same level of  $\omega_n^2/n_z\alpha$
- Short-period damping, phugoid dynamics, and lateral-directional characteristics roots are well simulated
- Bank-to-sideslip ratio and roll response are well simulated
- No attempts were made to duplicate the Orbiter's cockpit environment due to the preliminary nature of simulation. Thus, controls used were essentially a center wheel type of the B-26
- Control forces and gearing were empirically determined to give proper control harmony

A comparison of time histories in the lateral directional channel verifies that the simulation accurately simulated the pertinent character of the Design 518 dynamics (Fig. 7).

## COMPARISON OF EST/SIMUL CHARACTERISTICS

FLYING QUALITY PARAMETER	ORBITER	SIMULATION
LANDING APPROACH KT	180	160
FLT PATH STAB, $\frac{dx}{dv}$ DEG/KT	.03	.03
LONG'L HDLG QUAL, $\omega_n^2/n_{200}$	.135	.142
SHORT PD DAMP'G RATIO, $\xi_{SP}$	.85	.75
PHUGOID FREQ, $\omega_{ph}$ RPS	.114	.167
PHUGOID DAMP'G RATIO, $\xi_{ph}$	.088	.100
DUTCH ROLL NAT FREQ, $\omega_{nd}$ RPS	1.84	1.8
DUTCH ROLL DAMP'G RATIO, $\xi_d$	.21	.21
ROLL TIME K, $T_r$ SEC	.56	.54
SPIRAL TIME K, $T_s$ SEC	61	61
INIT(MIN/MAX) ROLL RATE %	47	47

Fig. 6

# LANDING APPROACH COMPARISON-SIMUL VS EST

(TIME HISTORY RESPONSES TO 10°AILERON STEP INPUTS)

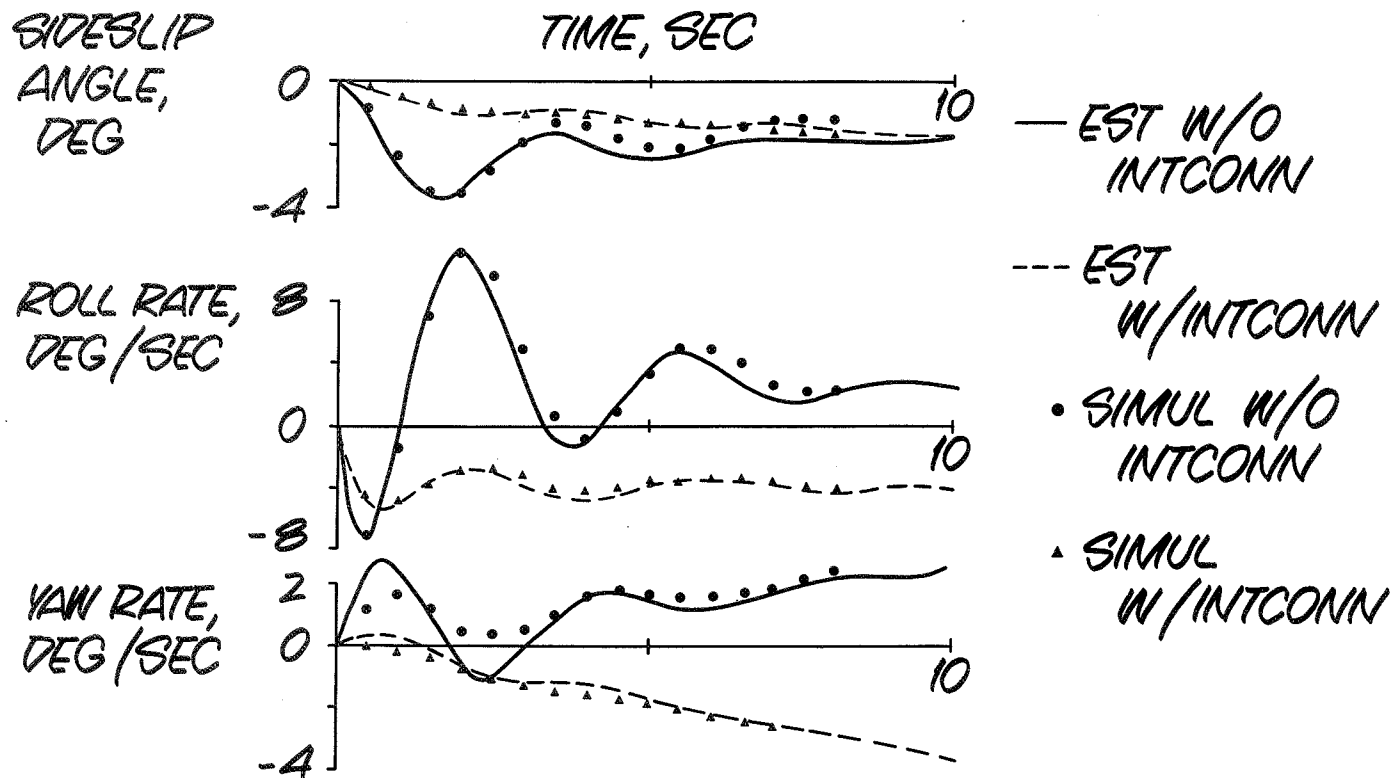


Fig. 7

## SYNOPSIS OF INFLIGHT SIMULATION RESULTS & PILOT COMMENTS

Evaluation flights of the simulated Design 518 were flown by three Grumman pilots, two CAL pilots, and an Eastern Airlines captain. The pilot task during the evaluation flight can be divided into two categories: (1) a mild control task involving heading and attitude changes, and (2) a more precise tracking task of acquiring and flying down a localizer beam in an ILS approach.

### Longitudinal Dynamic Characteristics

The vehicle tends to be sluggish in pitch, as expected. Pilot comments, such as: "vehicle is heavily damped... flies like a transport... flies like a DC-8," seem to verify this point. Generally, pilots find this sluggishness to be no real problem until the more precise tracking task. There, the pilot's comments seem to indicate that the sluggishness tends to accentuate any difficulties that may occur during the precise maneuvering task.

The vehicle flying on the backside of the power curve was also commented on as no real problem in itself, but tends to aggravate the lateral-directional handling qualities during the precise tracking pilot task. Pilot comments such as: "yo-yo'ed up and down glide slope", or "had to concentrate on speed control more than wanted", tend to confirm this conclusion.

### Lateral-Directional Dynamic Characteristics

The lateral-directional mode was given an average Cooper-Harper rating of 5-6 in moderate turbulence. A review of pilot comments indicates that the high  $\phi/\beta$ , or the vehicle's responsiveness to lateral gust coupled with its marginal roll control power, posed the prime problem. Some pilot comments which tend to confirm this conclusion are: "gust response disturbing, have to work in instrument approach, especially in turbulence..," or, "had a couple of gusts which caused wing drop," or, "when a gust hits you, it wakes you up." Comments on vehicle roll response were apparent: "desirable aircraft requires half ailerons.....didn't respond briskly enough.. must use rudder throw, definite need for interconnect," or, "somewhat difficult to make precise changes in the tracking of the localizer," or, "roll attitude control required greatest amount of attention."

## Conclusions

A review of pilot comments seems to agree with the flying qualities evaluation based on Mil-F-8785B. The vehicle appears longitudinally sluggish, high  $\phi/\beta$  is disturbing in the lateral directional channel, and interconnects are a must to alleviate most of the adverse yaw from the controls. The roll channel is apparently the most disturbing since this came in for the most comments. Generally the Cooper rating was a 5-6 for flight in moderate turbulence and for a precise tracking task. This rating can improve to 3-4 for smooth air and without the precise tracking task. The Mil Spec level analysis does indicate level two rating (Cooper-Harper pilot rating from 4 through 6) in these regimes, and appears consistent with the results. The additional insight from the simulation study not specifically indicated by the theoretical analysis is that a rudder-to-eleven interconnect significantly improves vehicle flying qualities. Also, vehicle sluggishness and backsidedness were not bad in themselves, as estimated, but aggravated the lateral directional handling qualities instead.



## References

1. Chalk, C.R., Neal, T.P., Harris, T.M., Pritchard, F.E., and Woodcock, R.J. Background Information and User Guide for MIL-F-8785B(ASG), "Military Specification, Flying Qualities of Piloted Airplanes," AFFDL, TR 69-72, August, 1969.
2. Farley, H.C., Rowley, F.F., and Smyth, R.K., Pilot Evaluation of Predicted Low Subsonic Handling Qualities of Orbiter Design 518 in a Variable Stability Aircraft, GAC IM B31-53MO-7, May, 1970.
3. Klafin, J.F., Results of EOS Longitudinal Axis Approach Simulation, GAC Memo B31-172-11, 11 May 1970.
4. Bull, G., Harris, T.M., and Ledder, H.J., In Flight Landing Approach Simulation of the Grumman Orbiter with the CAL Variable Stability B-26. CAL Report VI-2953-F, 1 May 1970.

STATIC AERODYNAMICS, FLOW FIELDS AND AERODYNAMIC  
HEATING OF SPACE SHUTTLE ORBITERS

E. D. Katzen, J. G. Marvin, H. L. Seegmiller, J. A.  
Axelson, J. J. Brownson, J. W. Cleary, W. K. Lockman  
and G. E. Kaattari

NASA, Ames Research Center  
Moffett Field, California

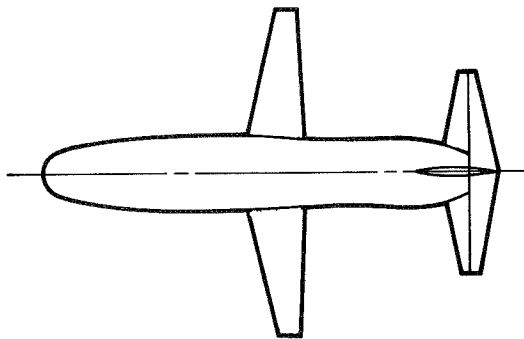
As part of the effort on the space shuttle at the Ames Research Center, we are reviewing technology developments by evaluating, as indicated on figure 1, aerodynamic performance, aerodynamic stability and control, and aerodynamic heating for low and high cross-range orbiters. In our evaluation, we are attempting to pinpoint and find solutions to problems; as a corollary, we also expect to find areas where we have confidence that the technology is in good shape. Extensive pre phase-B wind tunnel testing has been conducted and the results have been published, with limited distribution, in 12 preliminary data reports (refs. 1 to 12). This paper highlights the results obtained in the pre phase-B efforts and it describes our intended emphasis during phase B.

## OBJECTIVES

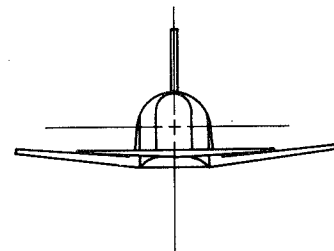
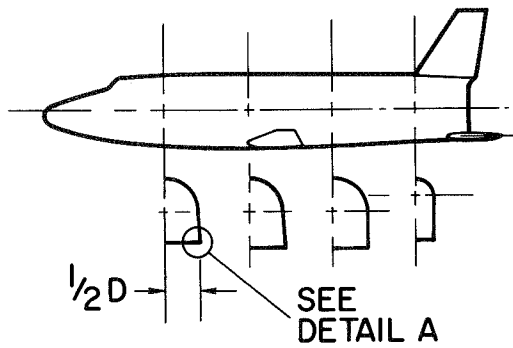
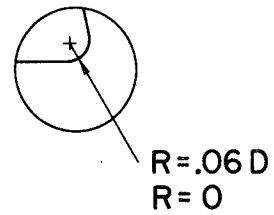
- EVALUATE (FOR LOW AND HIGH CROSS RANGE ORBITERS)
  - AERODYNAMIC PERFORMANCE
  - AERODYNAMIC STABILITY AND CONTROL
  - AERODYNAMIC HEATING
- PINPOINT AND FIND SOLUTIONS TO AEROTHERMODYNAMIC PROBLEMS

Pre phase-B efforts at Ames started with tests of the low cross-range orbiter shown in figure 2. This is the straight-wing design proposed by the Manned Spacecraft Center (described in reference 13). One of the geometric variations on the models studied at Ames is the effect on the aerodynamic characteristics of rounding of the corner between the bottom and sides of the body (see inset A); more will be said about this later in the paper.

## LOW CROSS RANGE ORBITER



DETAIL A



More recently, the orbiter proposed for high cross-range by the North American Rockwell Corporation (fig. 3) has been tested. This is a blended delta model.

## HIGH CROSS RANGE ORBITER

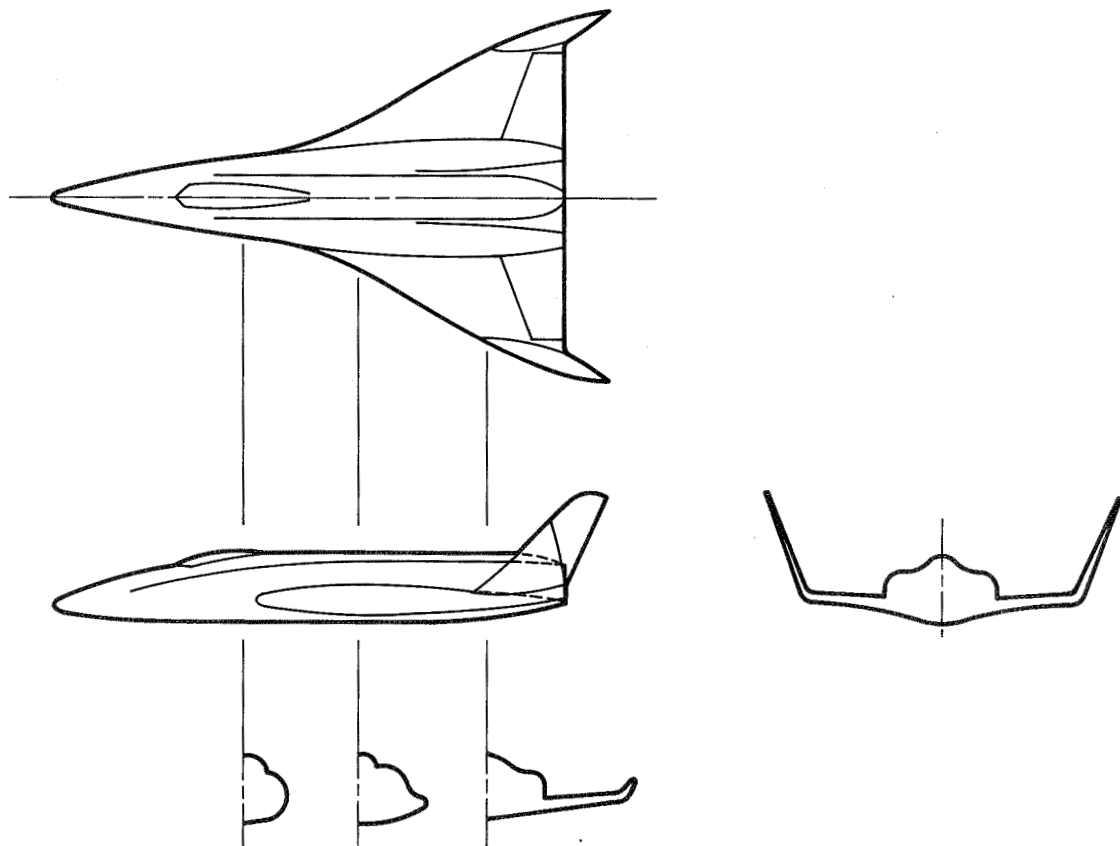


Figure 4 shows a comparison of the hypersonic performance, that is, the hypersonic lift-drag ratio, for the high cross-range and the low cross-range orbiters. Lift-drag ratio is shown as a function of angle of attack. The data are represented as bands because there are many geometric variables included, such as control deflections from plus 40 to minus 40 degrees, with and without fillets between the wing and the body, and in some cases, without the wing. Trimmed lift-drag ratios are included and they are close to the upper part of the band for each of the orbiters. The main point of this slide is that at hypersonic speeds, the lift-drag ratio is mainly sensitive to the fineness ratio of the body; the body of the low cross-range orbiter is much blunter than the body of the high cross-range orbiter.



## HYPERSONIC LIFT-DRAG RATIO

$$M_{\infty} = 7.4$$

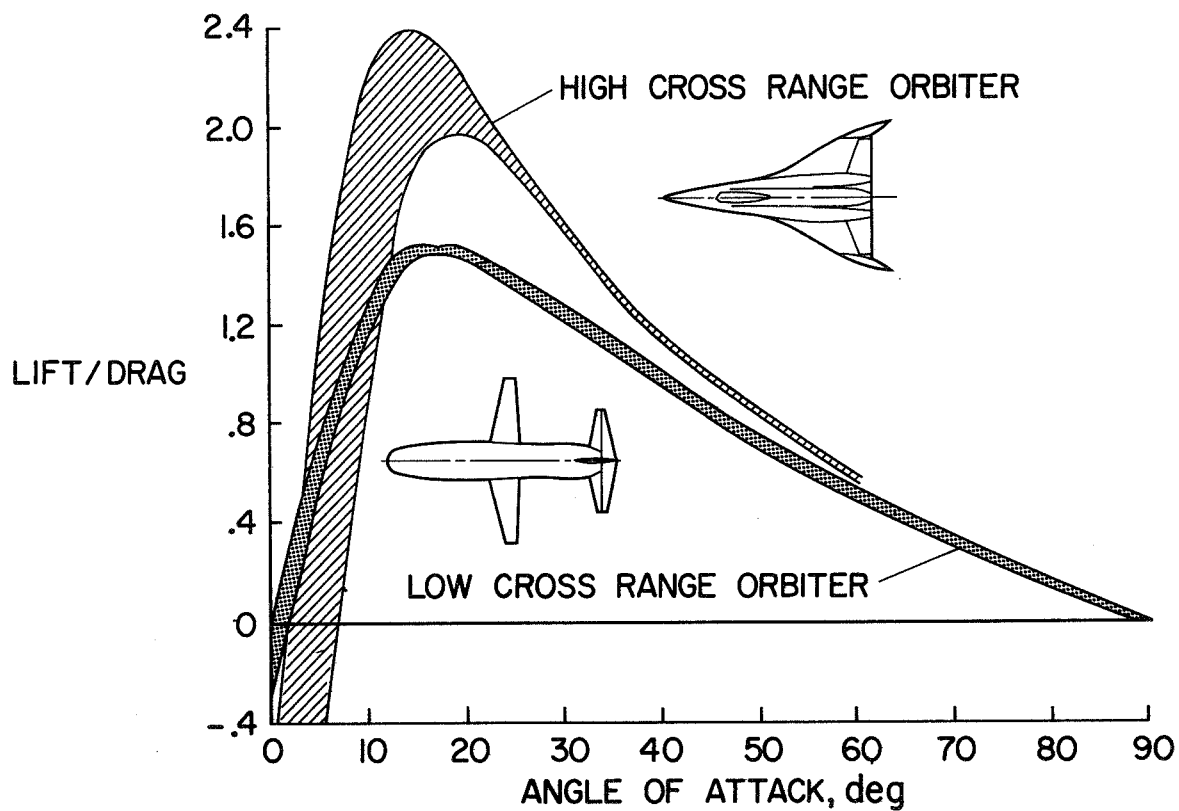


Figure 5 compares predictions and experiments for the high cross-range orbiter at hypersonic speeds; lift coefficient, pitching moment and lift-drag ratio are shown as functions of angle of attack. Lift coefficient and lift-drag ratio are shown for the elevon undeflected; pitching moment coefficients for two control deflections,  $0^\circ$  and  $-20^\circ$  (trailing edge up), are shown. Newtonian theory was used for the predictions. Agreement between predictions and experiments are considered satisfactory for Phase-B studies.

# COMPARISONS OF PREDICTIONS AND MEASUREMENTS HIGH CROSS RANGE ORBITER-HYPERSONIC SPEED $M_\infty = 7.4$

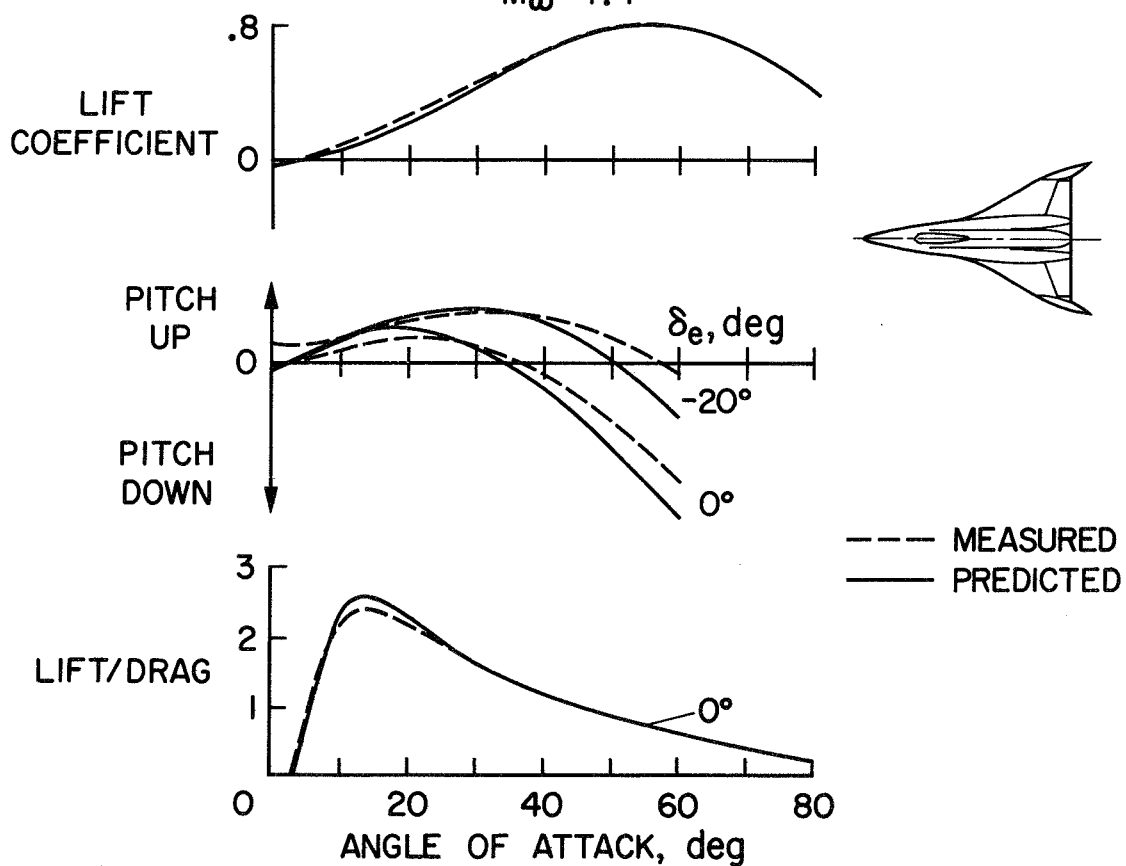
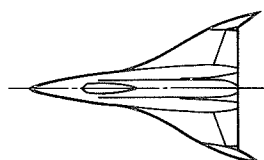
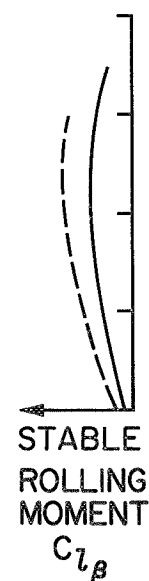
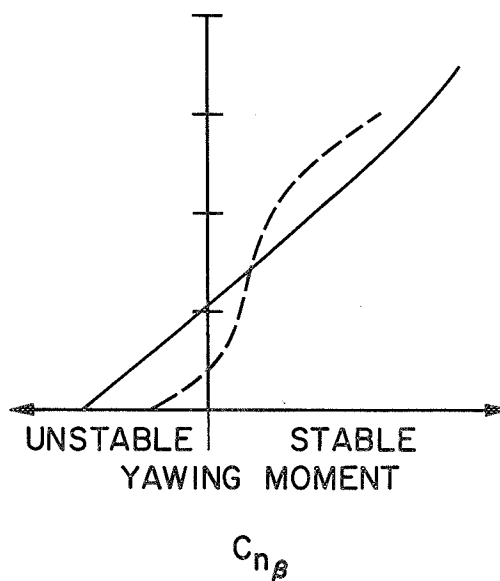
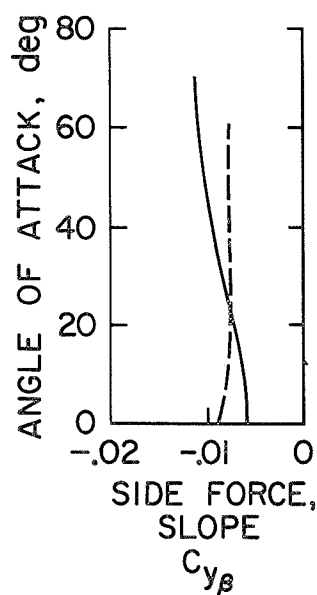


Figure 6 compares predictions and experiments for the lateral-directional characteristics of the high cross-range orbiter at hypersonic speeds; side-force, yawing-moment and rolling-moment slopes ( $C_{Y_\beta}$ ,  $C_{n_\beta}$  and  $C_{l_\beta}$ ) are shown. Again, agreement between measurements and predictions is considered satisfactory. The orbiter is stable in the operating angle-of-attack range. The data are not shown but agreement between measurements and predictions for the low cross-range orbiter is about the same as that for the high cross-range orbiter.

COMPARISONS OF PREDICTIONS AND MEASUREMENTS  
 HIGH CROSS RANGE ORBITER-HYPERSONIC SPEED  
 $M_\infty = 7.4$



— PREDICTED  
 - - - MEASURED



Figures 7 through 10 are photographs of oil-flow studies of the high cross-range orbiter. The angle of attack is that for maximum lift-drag ratio,  $15^{\circ}$ . The elevon is deflected 15 degrees, (trailing edge down), the deflection required for trim. Figure 7 shows the lower surface of the complete model. Figures 8, 9 and 10 are blowups showing details of the flow in the elevon region for three different Reynolds numbers, all of which occur in the hypersonic portion of the flight trajectory.

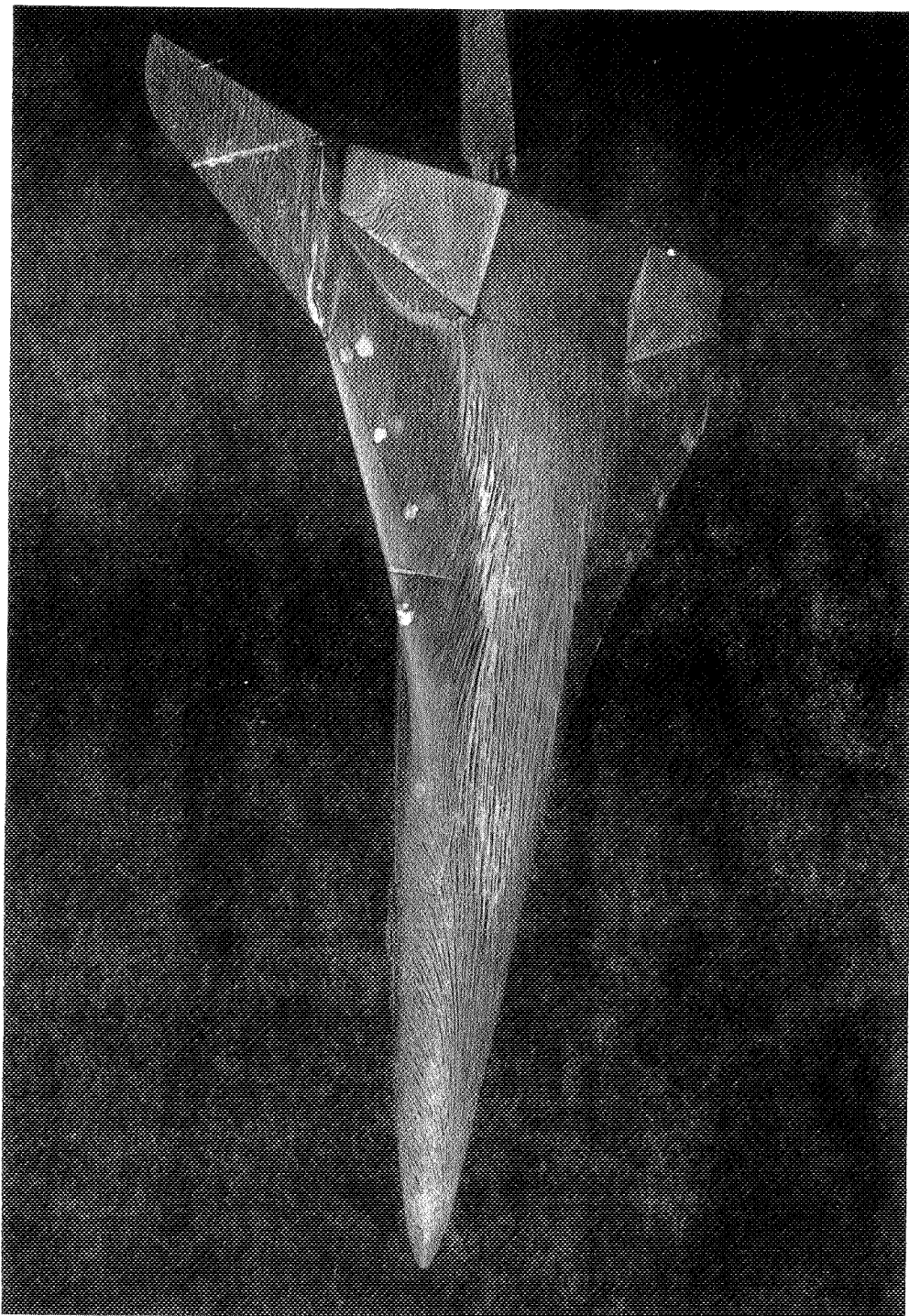
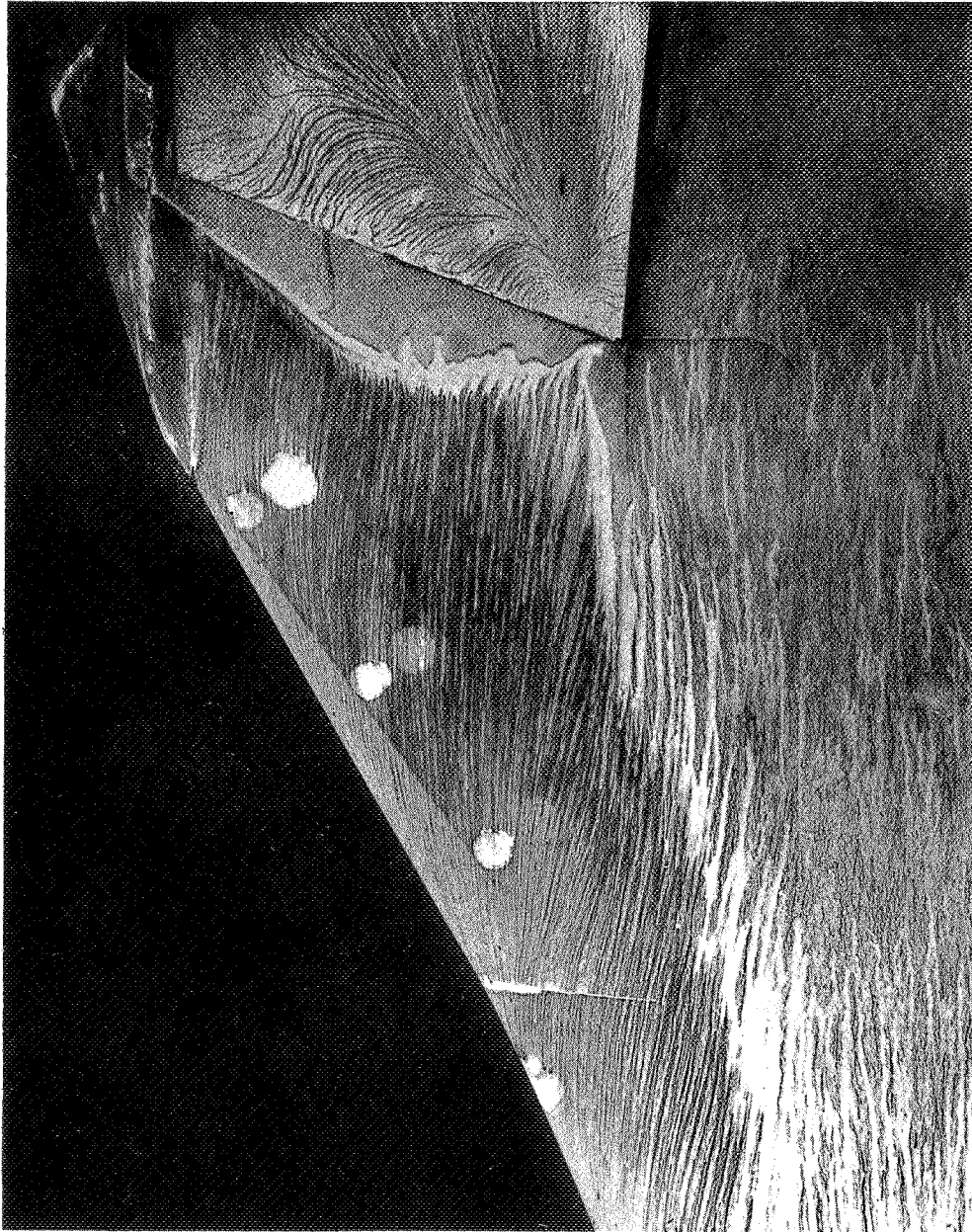
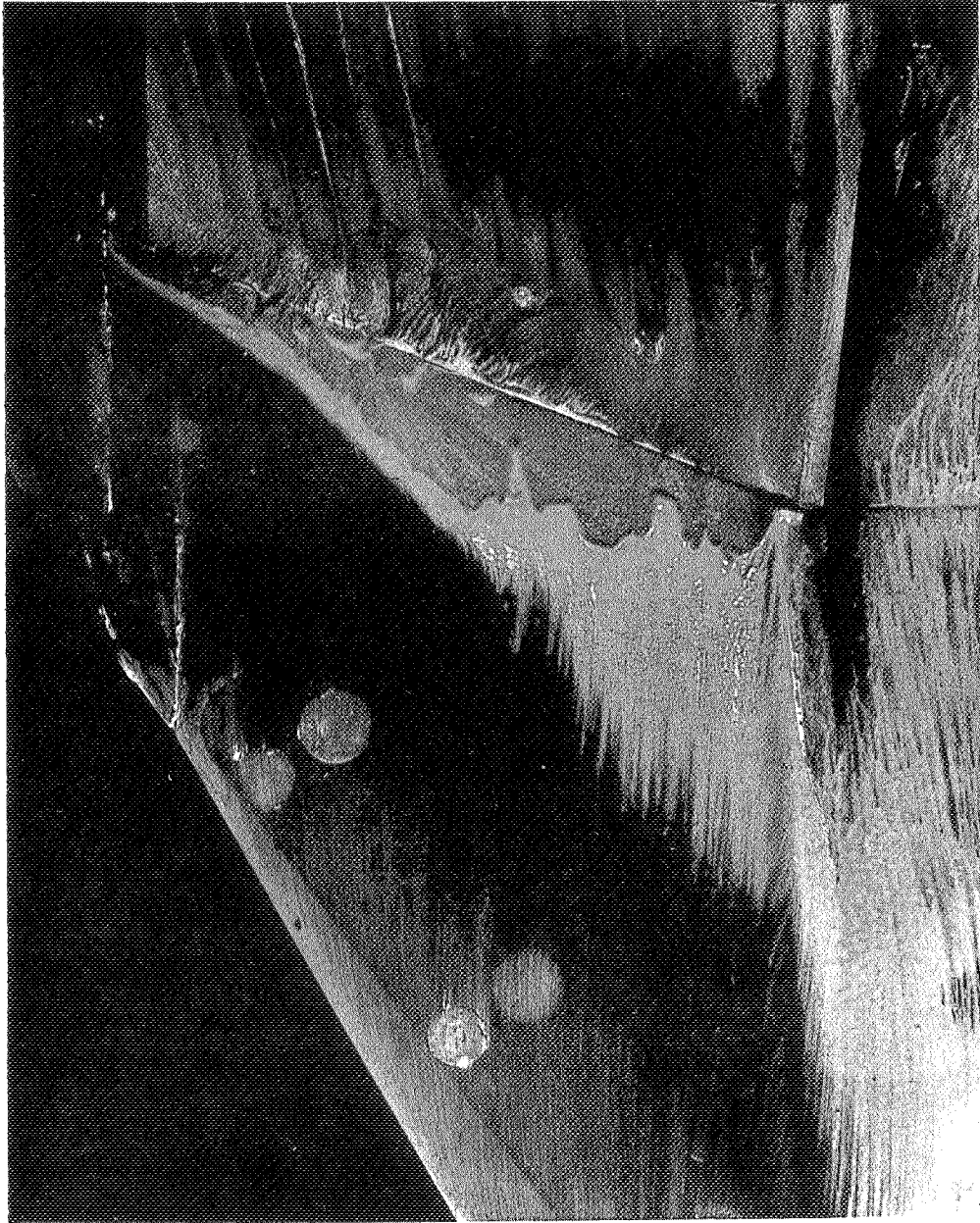


Figure 8 is for a Reynolds number of  $1.4 \times 10^6$ , which occurs at a point in the flight trajectory after peak heating. The boundary layer is separated ahead of the elevon and reattaches on the elevon; ahead of reattachment the flow is in the upstream direction.





As the Reynolds number is increased to  $2.8 \times 10^6$  (figure 9) a complex vortex pattern appears at reattachment.



At a Reynolds number of  $5.7 \times 10^6$  (figure 10), the boundary-layer flow appears to be attached to the elevon. Three main points can be drawn from the oil-flow studies: (1) the flow on the high cross-range orbiter (as well as that on the low cross-range orbiter) can be quite complex, (2) the elevon effectiveness should be checked through a range of Reynolds numbers and (3) since boundary-layer separation is sensitive to wall temperatures and Mach number, care must be exercised in applying wind-tunnel data to the flight vehicle.

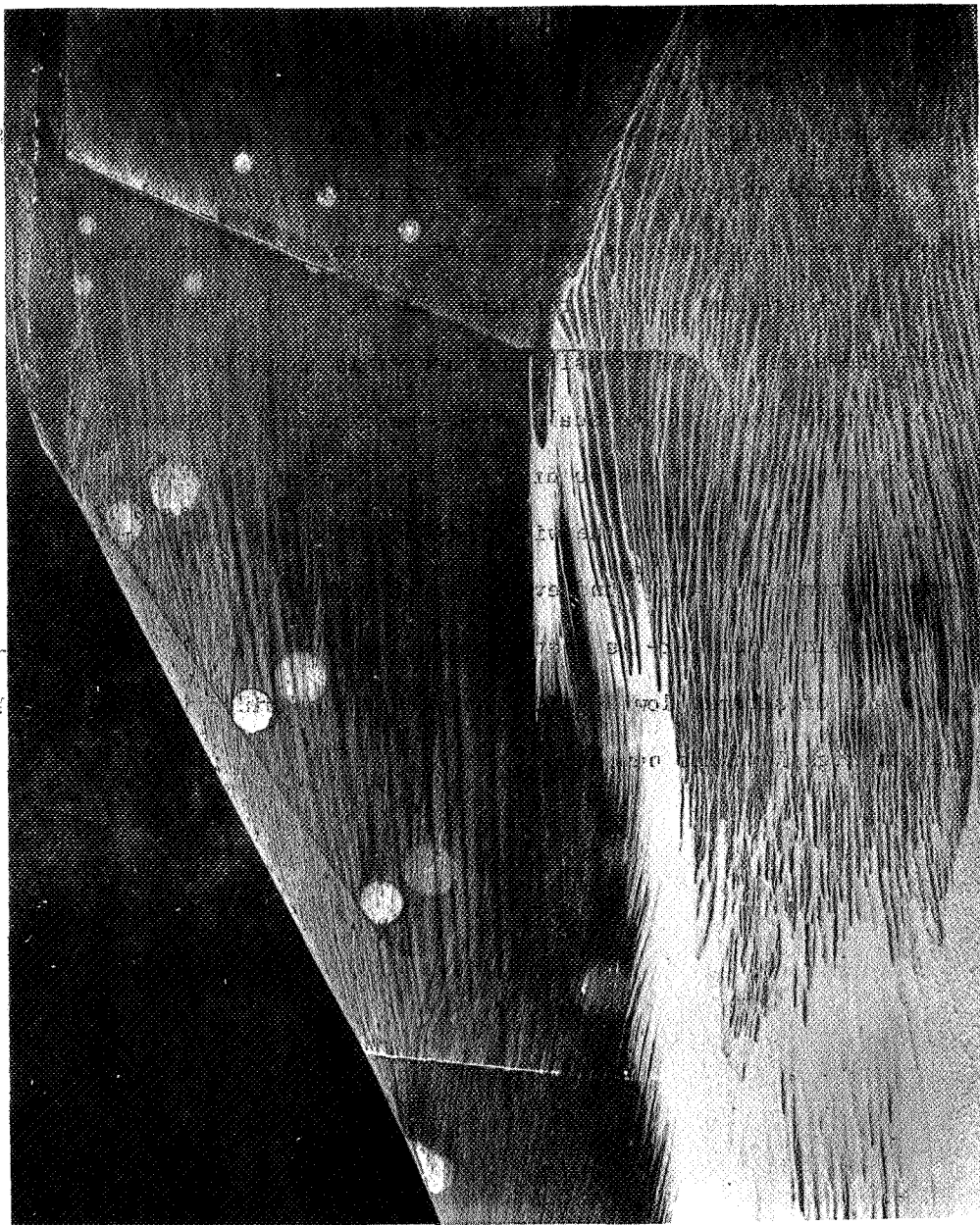


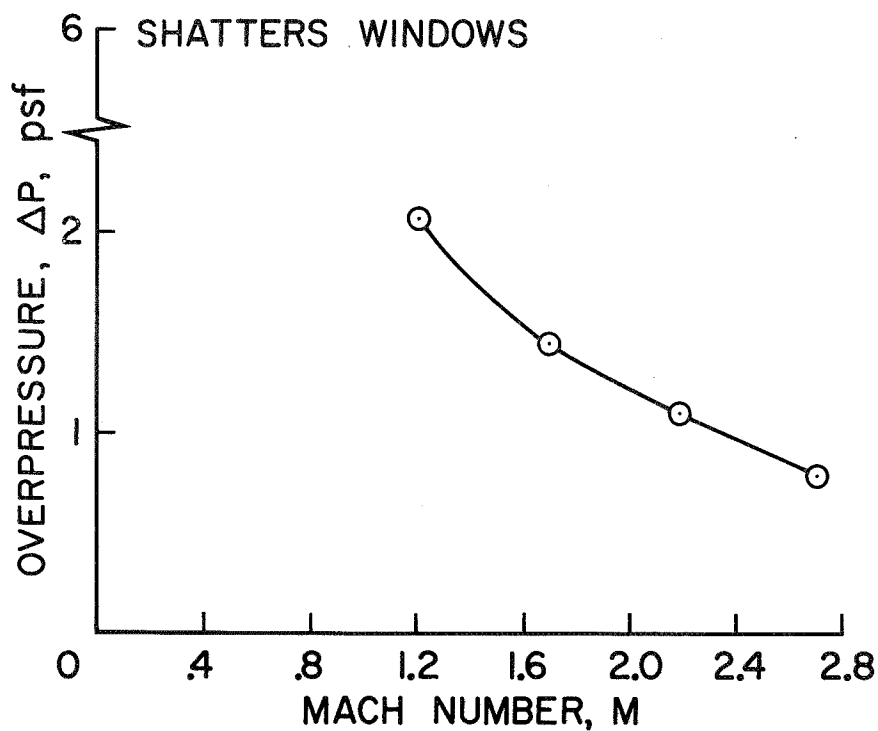
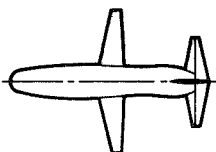
Figure 11 shows the effect of corner rounding (at the juncture of the bottom and sides of the body) and Reynolds number on the pitching moment of the low cross range orbiter. The elevon is deflected  $-30^{\circ}$  (trailing edge up). The data are for  $M = .25$ , the Mach number for starting the transition from high to low angles of attack. For the sharp cornered model increasing the Reynolds number from 4 to  $17 \times 10^6$  had no effect; it is probable that both Reynolds numbers were below the critical Reynolds number (the cross flow is separated and the wake is not closing in either case, thus there is high cross-flow drag of the nose and pitch-up). Flight Reynolds number for the start of the transition maneuver is about  $60 \times 10^6$ . Large effects of corner rounding and scale are to be expected from the early work by Polhamus (ref. 14) on the drag of two-dimensional cylinders. Corner rounding (6-percent of the width) reduced the pitch-up somewhat at a Reynolds number of  $4 \times 10^6$  and even more at a Reynolds number of  $17 \times 10^6$ . The main point here is that one must be very careful about applying high angle of attack, low Reynolds number data obtained in wind tunnels, to flight at high Reynolds numbers.

EFFECTS OF CORNER ROUNDING AND SCALE ON  
PITCHING MOMENT-LOW CROSS RANGE ORBITER

Figure 12 shows the results of an estimate of the overpressures on the ground, resulting from sonic boom, for the low cross-range orbiter. The estimate is made by combining theory and wind-tunnel pressure measurements. The overpressures are sufficiently high that further study is warranted - the results might influence whether or not one would want to land the orbiter at large airports in built-up areas.



ESTIMATED SONIC BOOM  
LOW CROSS RANGE ORBITER  
 $\alpha = 60^\circ$



In the following portion of the paper the flow field and heating studies performed at the Ames Research Center on models of the MSC low cross-range orbiter will be discussed. Our early work was concerned with obtaining an extensive set of oil-flow photographs which have been used to pinpoint complex flow regions and to aid in locating positions for instrumentation such as thermocouples and pressure orifices. We have also used these photographs to evaluate boundary-layer prediction methods as will be discussed in this paper. More recently, we have obtained and analyzed the first set of thermocouple laminar heat-transfer data on the low cross-range orbiter. Although we discuss herein the results for  $\alpha = 60^\circ$ , it should be mentioned that similar data are now available at  $\alpha = 40^\circ$ ,  $50^\circ$  and  $70^\circ$ .

A photograph taken during the heating tests on a thermocouple model of the MSC orbiter is shown. The tests were performed in the Ames 42" shock tunnel at a free-stream velocity about 14,000 ft/sec. The shock layer is made luminous by the shock heated air passing over the model.

The photograph illustrates the complex inviscid flow over this vehicle. The presence of wing-body shock interference region near the wing mid-span location can be seen and the horizontal tail appears inside the body shock. Presently, there are no exact methods for predicting the flow within the shock layer, but since heating prediction methods depend on a knowledge of the inviscid flow, approximate descriptions of the inviscid flow have been investigated. In the following slides comparisons of predictions and test data will serve to evaluate these approximate techniques.

## MODEL OF M.S.C. ORBITER

$\alpha = 60^\circ$     $M_\infty = 15$     $Re_{\infty L} = 3 \times 10^4$     $H_0 = 4000$  Btu/lb



The laminar heating rates and surface flow directions on the windward surface of the MSC orbiter fuselage and wing outboard of the body shock have been predicted by two-dimensional cross-flow theory. At any axial cross section the free-stream velocity vector is divided into its normal and tangential components. The inviscid flow at the boundary layer edge is obtained by superposition of the local normal flow and the tangential flow which is constant and not affected by the presence of the bow shock wave. The local normal flow is obtained from two-dimensional inviscid flow calculations. For the fuselage this calculation was obtained from a computer program described in ref. 15 and for the wing by a semi-empirical method developed by George Kaattari of the Ames Research Center.

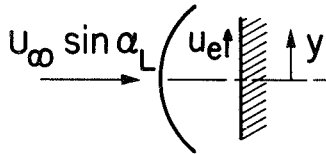
Using the inviscid flow description above, the heating rates and surface shear directions were obtained from local similarity solutions to the laminar boundary-layer equations given in reference 16. The first equation, taken from reference 16, is the expression used to obtain the cold wall lateral heating rate, normalized with respect to the 2-D stagnation line heating rate. (See ref. 16 for the nomenclature.) The second equation gives the ratio of stagnation line heating to that for a sphere for the same free-stream condition. A value of 1.1 was used for the exponent (a) on the sine term.

As a test of this approach comparisons of viscous streamline directions and heating rates have been made on the following slides.

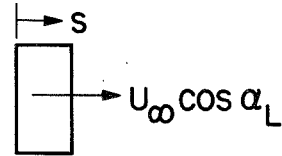
## TWO DIMENSIONAL CROSS FLOW THEORY

- AT ANY CROSS SECTION...

NORMAL FLOW FROM  
TWO DIMENSIONAL  
INVISCID CALCULATIONS



TANGENTIAL FLOW FROM  
LOCAL SURFACE ANGLE  
OF ATTACK



- HEATING RATE AND SHEAR FROM LOCAL SIMILARITY...

$$\frac{\dot{q}(y)}{\dot{q}_{SL}} = \left\{ \frac{p_e}{p_{e_{SL}}} \frac{t_{e_{SL}}}{t_e} \frac{du_e/ds}{(du_e/ds)_{SL}} \frac{1}{\beta} \right\}^{1/2} \frac{g'(0)}{(g'(0))_{SL}} \left\{ \frac{t_{aw} - t_w}{(t_{aw})_{SL} - t_w} \right\}$$

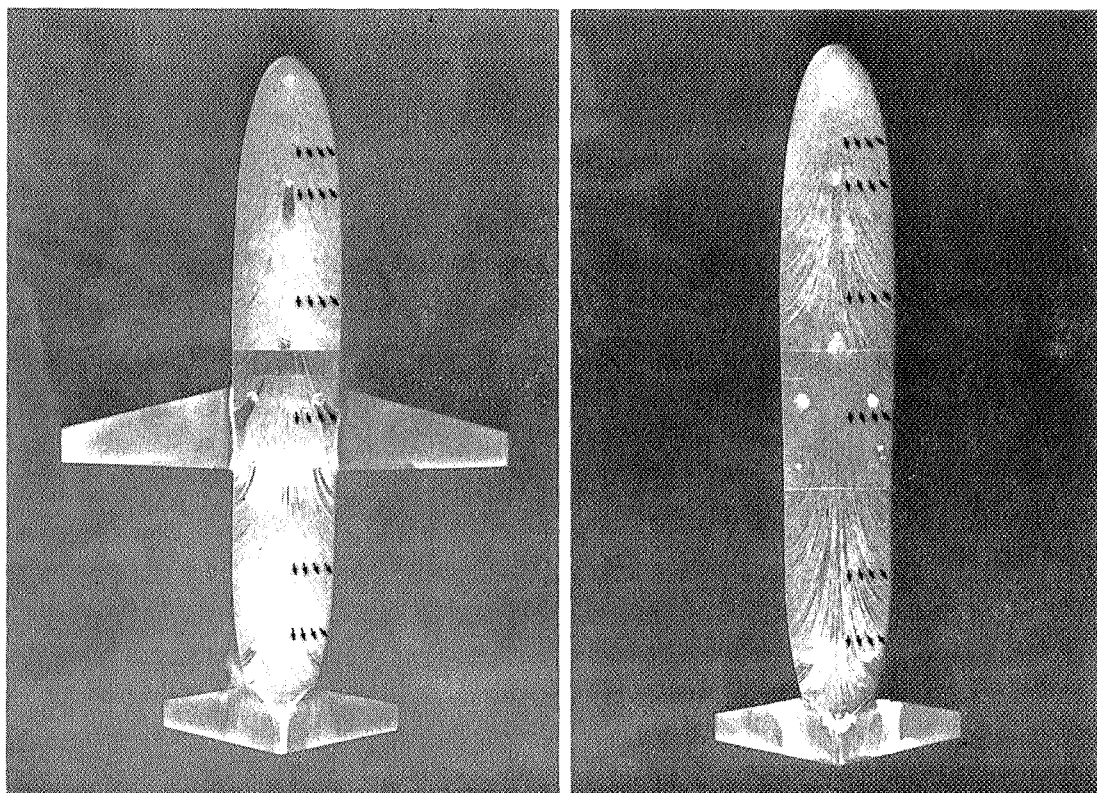
$$\frac{\dot{q}_{SL}}{\dot{q}_{SPHERE}} = \frac{\sin^2 \alpha_L}{1.4} \left\{ \frac{(du_e/ds)_{SL}}{(du_e/ds)_{SPHERE}} \right\}^{1/2} \frac{t_{aw} - t_w}{1 - t_w}$$

Oil flow photographs taken in the Ames 3.5 foot wind tunnel of the MSC orbiter at  $\alpha = 60^\circ$  are shown. The oil flow patterns resulting from the local laminar boundary-layer shearing action describe the direction of the boundary-layer flow at the wall. Stagnation regions and complex flow patterns over the wing inside the body shock and over the tail can be easily recognized using this technique (see refs. 3 and 6).

The arrows on the fuselage superimposed on the photographs represent viscous surface streamline directions ( $\tan^{-1} \tau_Y/\tau_S$ ) obtained using the 2D cross-flow theory applied locally at the various cross sections. The agreement between predicted and observed directions is good, except near the vicinity of the wing-fuselage junction. Without the wing, agreement is good over all cross sections. It can be concluded that the simple cross-flow theory can be used with confidence to predict the shear over most of the orbiter fuselage.

Obvious complex flow regions on the wing and tail within the influence of the body shock wave preclude the application of this theory and other methods must be developed.

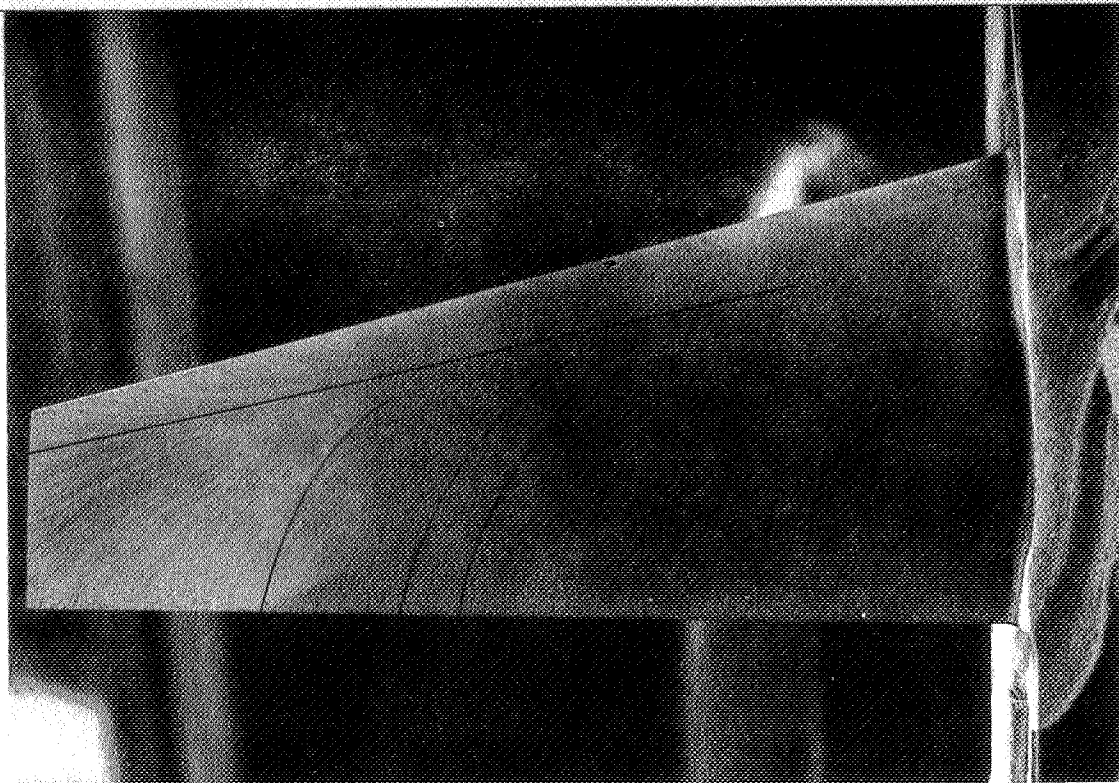
COMPARISON OF PREDICTED AND OBSERVED SURFACE STREAMLINES  
 $M_\infty = 10.4 \quad \alpha = 60^\circ$



An enlargement of the oil-flow pattern over the wing is shown along with predicted surface streamlines using 2D cross-flow theory. The predictions are made without regard to the presence of the body shock wave and as such should be compared with the patterns outboard of the body shock (beyond the 50% span location). The patterns near the 50% span region including the stagnation line agree reasonably well with the predictions, but the wing tip influences the surface flow and agreement with theory becomes poorer near the tip. Thus, two-dimensional approximations must be used with a certain degree of caution on the wing, and further studies of this flow are warranted. Inside the region of the body shock, the stagnation line moves closer to the leading edge and the flow becomes even more difficult to predict because the wing is in a low Mach number regime. As we will see later, the heating in this region is somewhat higher due to the presence of the body shock wave.



COMPARISON OF PREDICTED AND OBSERVED  
SURFACE STREAMLINES  
 $M_\infty = 7.4$   $\alpha = 60^\circ$

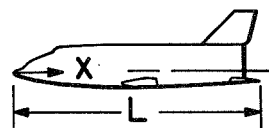
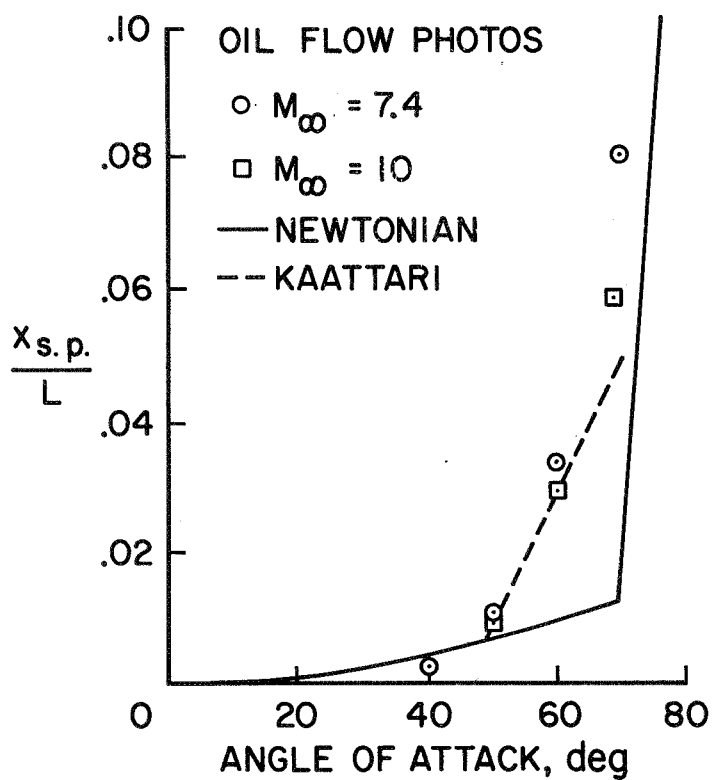


An additional problem under study is the prediction of the fuselage stagnation-region flow since its location and the magnitude of the heating is expected to be affected by the actual flight conditions which cannot be duplicated by wind-tunnel tests.

The stagnation point locations on the fuselage obtained from oil flow photographs taken from reference 3 are shown for various angles of attack. The measured locations are compared with predictions using Newtonian theory and an adaptation of the method described by Kaattari in reference 17. Above  $\alpha = 45^\circ$  the stagnation-point location moves from the rounded nose onto the flat portion of the fuselage and Newtonian theory fails to predict the location. Kaattari's method does predict the proper movement, but underpredicts the location at  $\alpha = 70^\circ$ .

For the actual flight conditions the stagnation location will be between the Newtonian prediction ( $\rho_2/\rho_\infty = \infty$ ) and the observed location from these wind-tunnel tests ( $\rho_2/\rho_\infty \approx 5.4$ ). The magnitude of the heating during flight will probably be higher in this region because the body geometry directly affects the magnitude of the velocity gradients.

## LOWER SURFACE FUSELAGE STAGNATION POINT LOCATION



The fuselage centerline heating rates measured on a thermocouple model of the MSC orbiter are plotted against the normalized distance along the model centerline. These measurements were obtained in air at  $M_\infty = 15$ ,  $Re_{\infty L} = 30,000$  and  $H_o = 4000$  Btu/lb. The heating rates have been normalized by the measured heating rate on a sphere, appropriately scaled to an equivalent 1-foot hemisphere and a vehicle 150 ft. long. The bars represent the lateral variation across the fuselage. The ordinate on the right-hand side gives the radiation equilibrium surface temperatures in degrees Rankine corresponding to the maximum heating point along a typical trajectory for this vehicle. The temperatures along the centerline range from 2400 °R to 2000 °R and agree with the predicted values from the 2D cross-flow theory. A single data point from the Langley phase change paint results of R. A. Jones at  $M_\infty = 10$  is given for comparison and it shows a higher heating rate than the thermocouple data. Nevertheless, equilibrium surface temperatures based on the data of the two test techniques are in reasonable agreement.

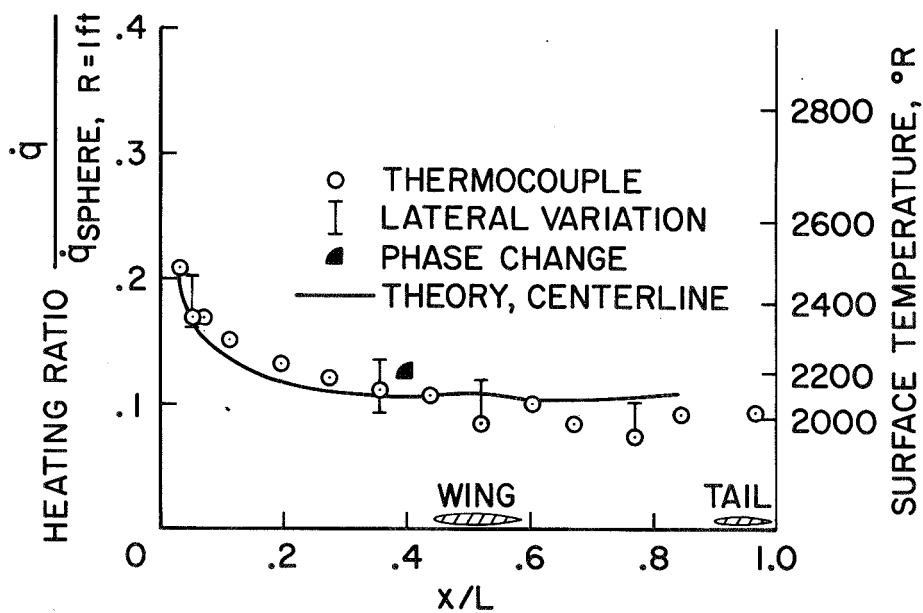
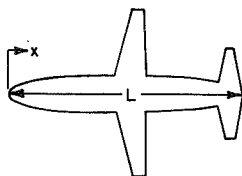
# LOWER SURFACE FUSELAGE CENTERLINE HEATING

$$\alpha = 60^\circ$$

$$\dot{q}_{\text{SPHERE}, R=1 \text{ ft}} = 70 \frac{\text{Btu}}{\text{ft}^2 \text{ sec}}$$

$$\epsilon = .8$$

$$L = 150 \text{ ft}$$

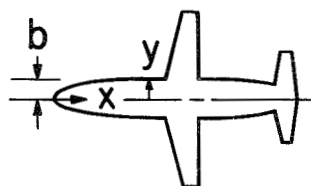


The fuselage lateral heating between  $X/L = .3$  and  $.8$  on the thermocouple model is shown. The heating rates have been normalized by their respective centerline values to show the variation across the fuselage. For comparative purposes phase-change data obtained by R. A. Jones at Langley are also shown along with a prediction using 2D cross-flow theory. The radiation equilibrium surface temperatures shown are based on a single predicted centerline heating rate.

The heating rates and corresponding surface temperatures increase toward the edge of the fuselage and in general lie above the prediction. The magnitude of the temperature rise indicated by the data could present a structural design problem and further investigation of the magnitude of the lateral surface temperature variation is warranted. One way to alleviate the temperature variation would be to provide corner rounding, but the resulting change in aerodynamic characteristics would have to be assessed.

# LOWER SURFACE FUSELAGE LATERAL HEATING

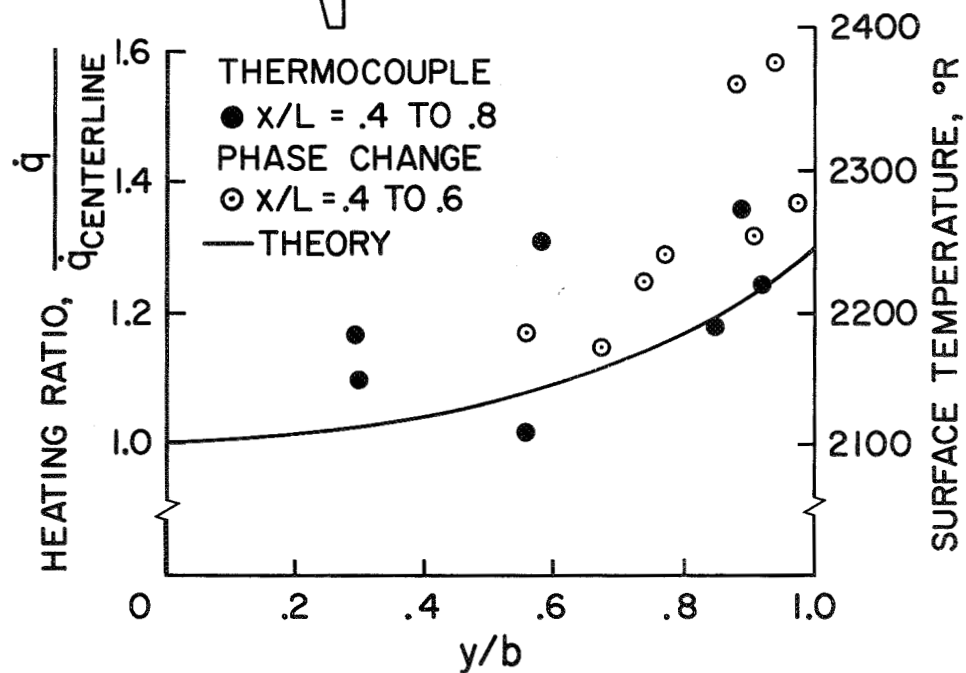
$$\alpha = 60^\circ$$



$$q_{\text{SPHERE}, R = 1 \text{ ft}} = \frac{\text{Btu}}{\text{ft}^2 \text{ sec}}$$

$$\epsilon = .8$$

$$L = 150$$

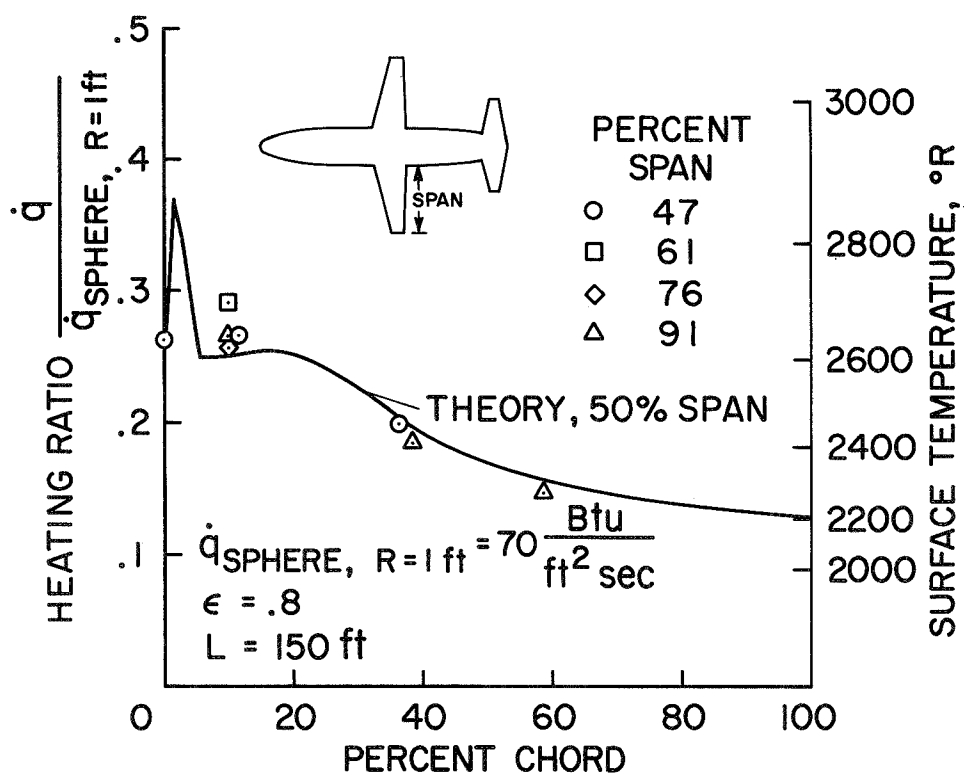


The measured heating rates and corresponding equilibrium surface temperatures on the windward surface of the wing at  $\alpha = 60^\circ$  outboard of the body shock is shown as a function of percent chord for the span locations indicated. The data are compared with a 2D cross-flow prediction for the 50% span location. The surface temperatures are in general higher than those on the fuselage except near the wing trailing edge. The peak temperature will probably occur at a location near the leading edge of the wing as predicted rather than along the stagnation line (i.e., 18% chord) due to the acceleration of the flow over the leading edge. More measurements will be needed to fix the precise magnitude of this peak temperature because the selection of the thermal protection material depends on this temperature.



# WINDWARD SURFACE WING HEATING OUTBOARD OF BODY SHOCK

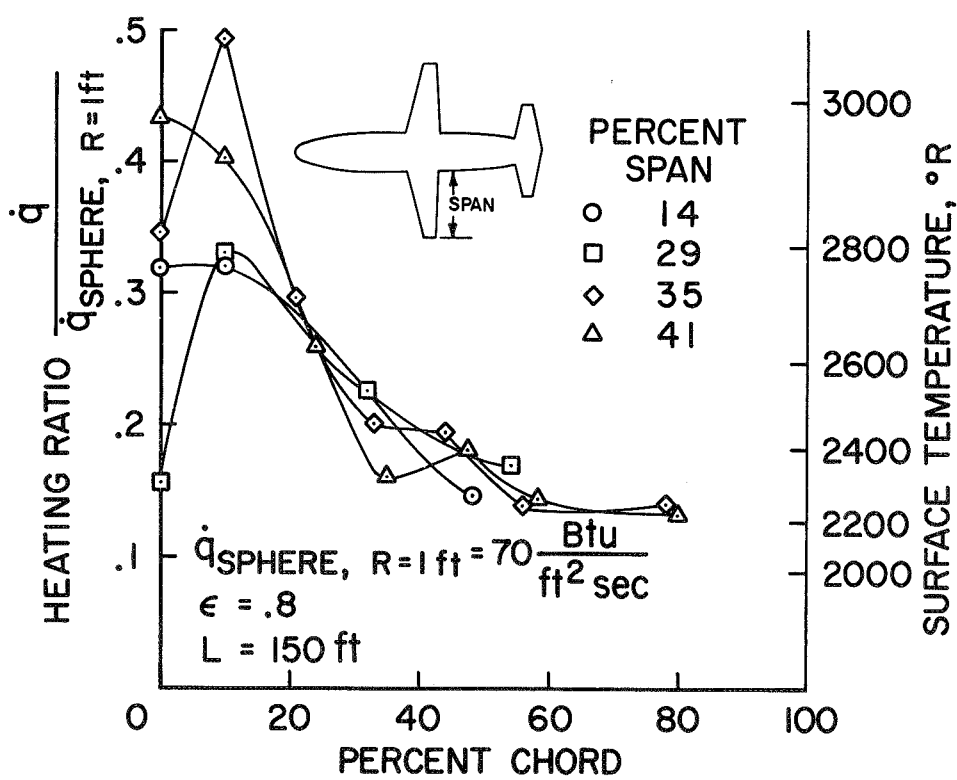
$\alpha = 60^\circ$



The measured heating rates and corresponding surface temperatures on the windward surface of the wing at  $\alpha = 60^\circ$  inboard of the body shock are shown as a function of percent chord for the span locations indicated. For percent chord locations less than 25%, the complexity of the heating distribution is obvious. The corresponding radiation equilibrium temperatures vary considerably within this region, having a peak value over 3000  $^\circ\text{R}$ . Therefore the thermal protection materials choice will depend on an accurate understanding of the heating within this region. Beyond the 25% chord location the temperature at the different span locations are not widely different and a comparison with the data from the previous slide shows that the spanwise surface temperatures beyond the 25% chord location are essentially uniform.

# WINDWARD SURFACE WING HEATING INBOARD OF BODY SHOCK

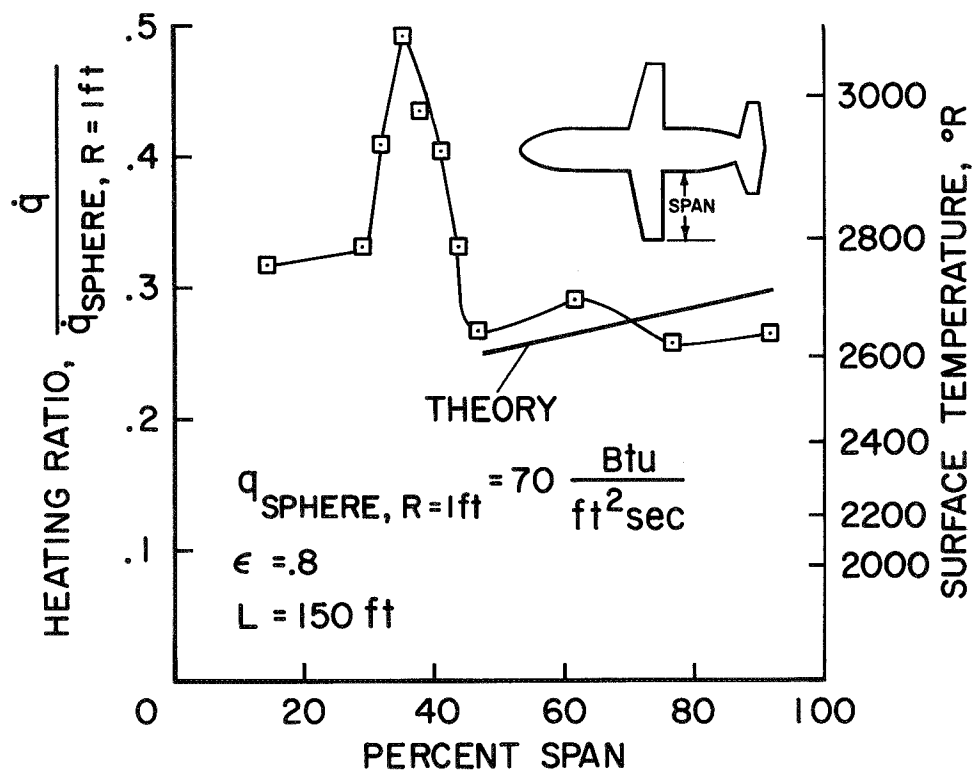
$$\alpha = 60^\circ$$



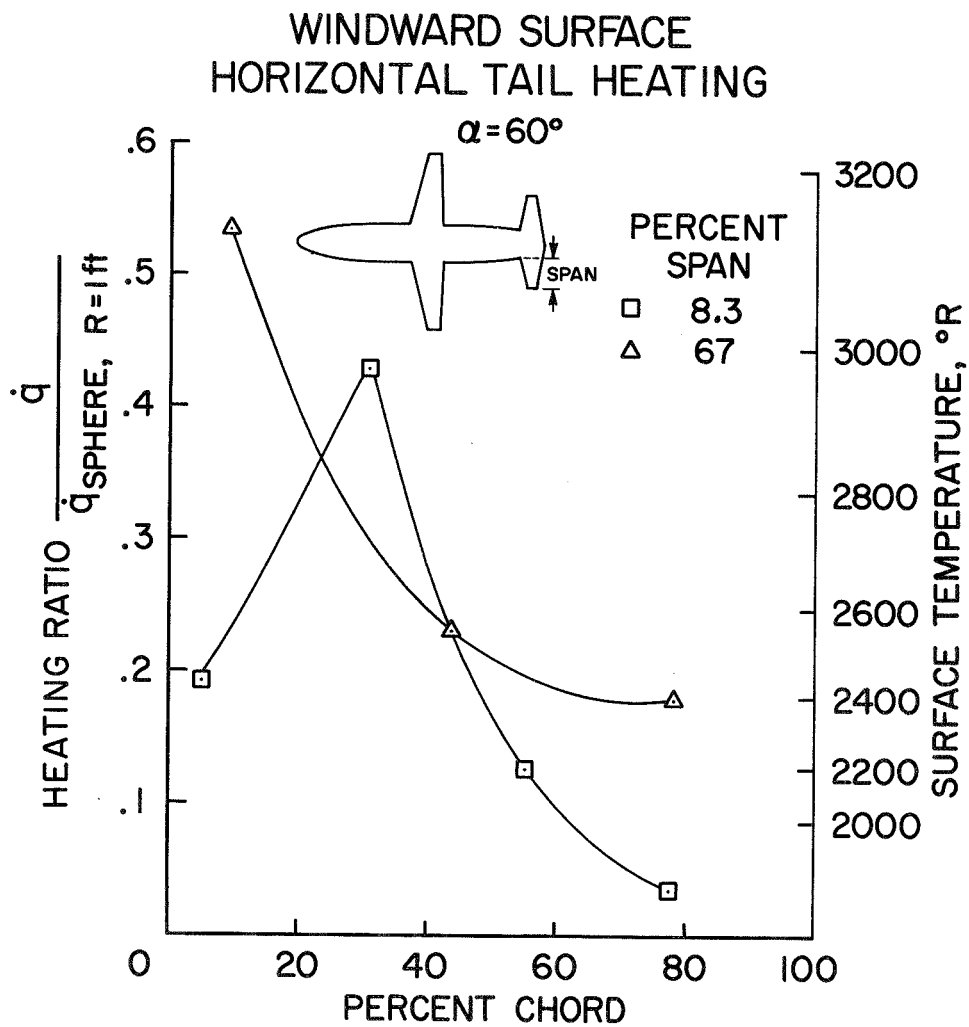
The spanwise heating distribution at the 10-percent chord location is shown to further illustrate the complexity of the wing heating in the vicinity of the wing-body shock interaction region. Outboard of the body shock the heating rates are in reasonable agreement with predicted levels using 2D cross-flow theory. The heating rises abruptly between the 35% and 45% span locations, then decreases as the fuselage is approached. Recall that the body temperatures were around 2100 °R and here the wing is operating at temperatures between 2600 °R and over 3000 °R.

The body and wing shock interaction may well account for the complex heating variation within the 50 percent span locations. Since the interaction depends on the density ratios across the shock waves the magnitude of the surface temperature will probably depend on the vehicle flight conditions and direct extrapolation of wind-tunnel data to this condition must be exercised with caution. A study of the body-shock interaction problem is certainly necessary to resolve the complex nature of this flow.

WINDWARD SURFACE SPANWISE  
HEATING ALONG 10 PERCENT CHORD LINE  
 $\alpha = 60^\circ$



Limited measured heating data and corresponding surface temperatures on the windward surface of the tail are shown as a function of percent chord for two span locations. These data serve to illustrate the complexity of the heating to the tail surface. There are extreme temperature variations in both the chordwise and spanwise directions. A maximum surface temperature slightly over 3100 °R could be realized on the full-scale vehicle, but it is not known whether this is the hottest spot, because the thermocouple instrumentation was sparse. More tests must be performed to better define the heating on the tail, but the magnitude of the temperatures indicated on this slide indicate that ablative protection may be necessary over part of the tail.



The possibility of transition from laminar to turbulent flow on the shuttle vehicles at high angle of attack is also being considered in our in-house program. The importance of such knowledge is emphasized by way of example in this slide. A typical result from a study made recently in the Ames 3.5 foot tunnel is shown, see ref. 9. The configuration is a pyramid model having an  $85^{\circ}$  sweep angle. Although this is not a shuttle configuration, if the results were strictly applicable to an orbiter 150 ft long, transition would not occur until an altitude of 160,000 ft and well beyond the peak heating location in the trajectory. Furthermore, if transition occurs, factors of 2 or higher in heating rate will have to be taken into account.

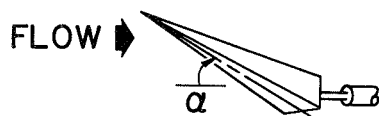
Tests are planned for the near future to obtain similar transition data on the MSC low cross range orbiter and the NAR high cross-range orbiter.



# HEATING ON FLAT-BOTTOMED BODY

$$\alpha = 50^\circ$$

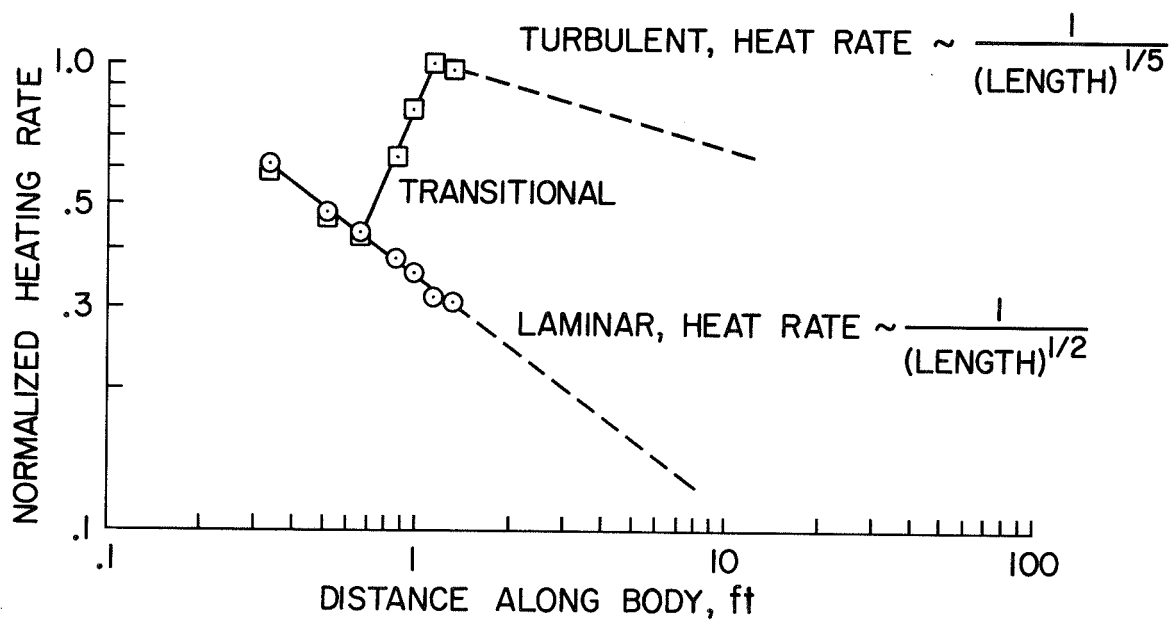
$$M_\infty = 7.4$$



$$Re_l$$

$$\circ 2 \times 10^6$$

$$\square 6 \times 10^6$$



## SUMMARY

Extensive wind-tunnel tests will be conducted at the Ames Research Center on orbiters, boosters and launch configurations in direct support of the Phase B contracts. In addition, Ames initiated wind-tunnel tests and analyses will emphasize the technology areas listed in figure 25 for orbiters: Static stability and control will be evaluated for subsonic and transonic speeds. Boundary-layer transition will be measured. Heat transfer will be measured for laminar, transitional and turbulent boundary layers; the results will be compared with predicted results to provide confidence for using predictions to extrapolate wind-tunnel results to flight conditions. Heat transfer will be measured and analyzed in regions of interfering flow fields. Although the heat transfer is relatively low in shielded regions, large surfaces are involved such that pinpointing the heating rate levels accurately is necessary for realistic predictions of weight.

## EMPHASIS

- STABILITY AND CONTROL AT SUBSONIC AND TRANSONIC SPEEDS
- BOUNDARY LAYER TRANSITION AT HIGH ANGLES OF ATTACK
- TRANSITIONAL AND TURBULENT HEATING
- INTERFERENCE HEATING
- HEATING IN SHIELDED REGIONS

## REFERENCES

1. Brownson, Jack J.: Static Stability Characteristics of MSC Orbiter Preliminary Tests at Mach No. 0.25-2.0. SSPD-1
2. Brownson, Jack J.: Static Stability Characteristics of MSC Orbiter: Effect of Reynolds Number and Body Corner Radius at  $M \leq 0.5$ . SSPD-2.
3. Seegmiller, H. Lee: Shadowgraphs and Surface-Flow Visualization Photographs of the MSC Orbiter at Mach No. 7.4. SSPD-3.
4. Axelson, John A.: Static Stability Characteristics of MSC Orbiter: Tests at Mach No. 7.4. SSPD-4.
5. Brownson, Jack J.: Static Stability Characteristics of MSC Orbiter: Tests of Revised Configuration at Mach No. 0.25-2.0. SSPD-5.
6. Seegmiller, H. Lee: Surface-Flow Visualization Photographs of MSC Orbiter and a 55° Swept Delta Wing Modification for Several Reynolds Numbers at Mach No. 10.4. SSPD-6.
7. Cleary, Joseph W.: Hypersonic Stability and Control Characteristics of High Cross-Range Orbital Vehicle. SSPD-7.
8. Seegmiller, H. Lee: Surface-Flow Visualization Investigation of a High-Cross Range Shuttle Configuration at a Mach No. of 7.4 and Several Reynolds Numbers. SSPD-8.
9. Lockman, William K.: Transition Reynolds Number, Convective Heating Distributions, and Surface-Flow Patterns for a Flat-Surfaced Pyramid Model at Angle of Attack. SSPD-9.
10. Levy, Lionel L., Jr., Hicks, Raymond M., Mendoza, Joel P.: Investigation of Sonic Boom for the Space Shuttle: Low Cross-Range Orbiter. SSPD-10.
11. Brownson, Jack J.: Static Stability Characteristics of MSC Orbiter: Effect of Reynolds Number and Body Corner Radius at Mach No. 0.6-1.35. SSPD-11.
12. Hicks, Raymond M., Mednoza, Joel P., and Levy, Lionel L., Jr.: Investigation of Sonic Boom for the Space Shuttle: High Cross-Range Orbiter. SSPD-12.

13. Faget, Maxime A.: New Configuration Concept for Space Shuttle That Provides Suitable Characteristics for Launch, Entry, and Landing. Paper presented at AIAA 6th Annual Meeting and Technical Display, Anaheim, California, October 20-24, 1969.
14. Polhamus, Edward C.: Effect of Flow Incidence and Reynolds Number on Low-Speed Aerodynamic Characteristics of Several Noncircular Cylinders with Applications to Directional Stability and Spinning. NASA TR R-29, 1959.
15. Inouye, M, Marvin J. G., and Sinclair, A. R.: Comparison of Experimental and Theoretical Shock Shapes and Pressure Distributions on Flat-Faced Cylinders at Mach 10.5. NASA TN D-4397, Feb. 1968.
16. Beckwith, I. E., Cohen, N. B.: Application of Similar Solutions to Calculation of Laminar Heat Transfer on Bodies with Yaw and Large Pressure Gradient in High Speed Flow. NASA TN D-625, 1961.
17. Kaattari, G. E.: Predicted Gas Properties in the Shock Layer Ahead of Capsule-Type Vehicles at Angles of Attack. NASA TN D-1423, Oct. 1962.



# INTEGRATED LAUNCH REENTRY VEHICLE CONFIGURATION STUDY

by J. Stalony-Dobrzanski

Northrop Corporation  
Hawthorne, California

## INTRODUCTION

The objective of this study is to examine critically the "tip tank" configuration concept.

The basic feature of the tip tank configuration is the location of all the engines on the shuttle vehicle which thus are recovered and reused. This design feature stems from the assumption that such engine reuse lowers the cost of the overall system in comparison to the orthodox multi-stage boost vehicles in which the engines are expended with the lower stages. The validity of this assumption is examined in this study. Two very different aerodynamic configurations were chosen for this purpose to make sure that the conclusions are valid for a wide range of shuttle vehicle configurations. The configurations are Northrop modified M2 with a moderate L/D ranging with modifications from 1.3 to 1.7, and FDL-5 with a high L/D of about 2.7. For each aerodynamic configuration, a range of propulsive configurations were generated with distribution of thrust between the shuttle vehicle and tip tanks being varied. At one end of the range, all the engines are on the tip tanks, and the configuration is, in this case, a single stage to orbit. At the other end, all the engines are on the shuttle vehicle, and this configuration is the original tip tank concept. Design layouts were performed over the parametric range of engine distribution to investigate the feasibility of engine installations.

The configurations are designed to common ground rules and mission payload. They are evaluated with respect to the overall lift-off weight and total space transportation system cost over a 10-year program, using a total number of flights as a parameter.

### CONFIGURATIONS

The configurations used in the design optimization cycle are Modified M2 and FDL-5.

The Modified M2 refers to Northrop modifications of the M2-F3 lifting body vehicle presently used in low speed flight test research program at NASA Edwards Flight Research Center. The modifications involve primarily the nose area, and are intended to improve the hypersonic L/D. Hypersonic aerodynamic computations performed on these modified shapes show that the L/D can be increased from the current vehicle L/D of 1.3 to about 1.7.

The Low Cost Launch Vehicle (LCLV) plus Modified M2 and the Intermediate 20-Modified M2 are used only for cost comparisons with the tip tank configurations.



# *CONFIGURATIONS*

---

- INTEGRATED LAUNCH REENTRY VEHICLE (ILRV)
  - MODIFIED M2
  - FDL-5A
- LOW COST LAUNCH VEHICLE (LCLV)
  - MODIFIED M2
- INTERMEDIATE 20 - MODIFIED M2

#### DESIGN GROUND RULES

All configurations were designed to the same ground rules.

The subsystems and provisions needed for the operation of the crew of two pilots for the mission time are provided outside of payload. For longer times in orbit, the shuttle vehicle is locked to the space station and any necessary support during that period is provided from the space station.

## *DESIGN GROUND RULES*

---

PAYLOAD	20,000 LBS
RETURN PAYLOAD	4,000 LBS
CREW	2
MISSION TIME	24 HOURS
PROPELLANT	LOX/LH <sub>2</sub>
PROPELLANT BOIL OFF	5%
ENGINE TYPE	AEROSPIKE

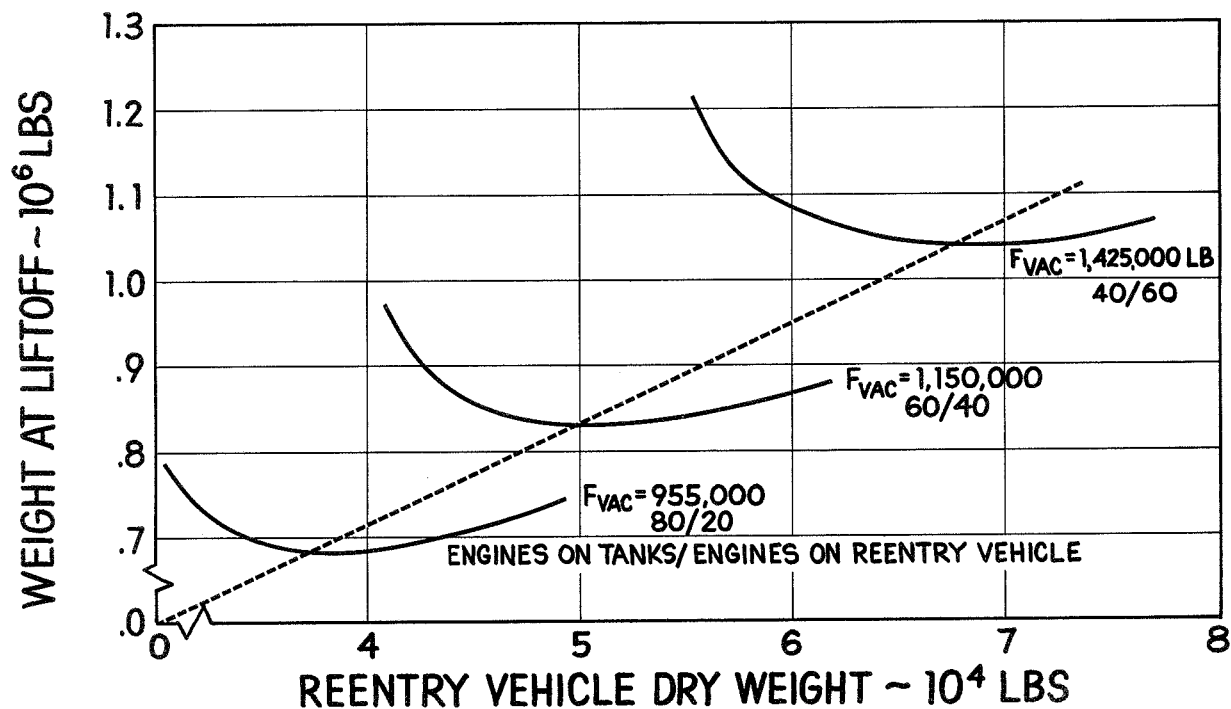
### ILRV CONFIGURATION SIZING

The configurations were sized by a computer program. For any initially assumed thrust level, the program designs a range of configurations to determine the minimum weight configuration. The thrust-to-weight ratio at S.L. is then checked for required design ratio and, if necessary, the procedure is iterated until the required T/W at minimum weight is obtained. The minimum lift-off weight system has the optimum distribution of propellants between the shuttle vehicle and the tip tanks.

Typical results for several ratios of engine distribution between tanks and the vehicle are shown on Figure 3. The length of the shuttle vehicle for the optimum tip tank configuration, that is, with 20% of thrust on the vehicle, is 52 ft., and the wing loading at landing is 46 lbs./ft.<sup>2</sup>. The overall length of the configuration with tip tanks is 110 ft.

# ILRV CONFIGURATION SIZING

## MODIFIED M2 REENTRY VEHICLE



### ILRV CONFIGURATION OPTIMIZATION

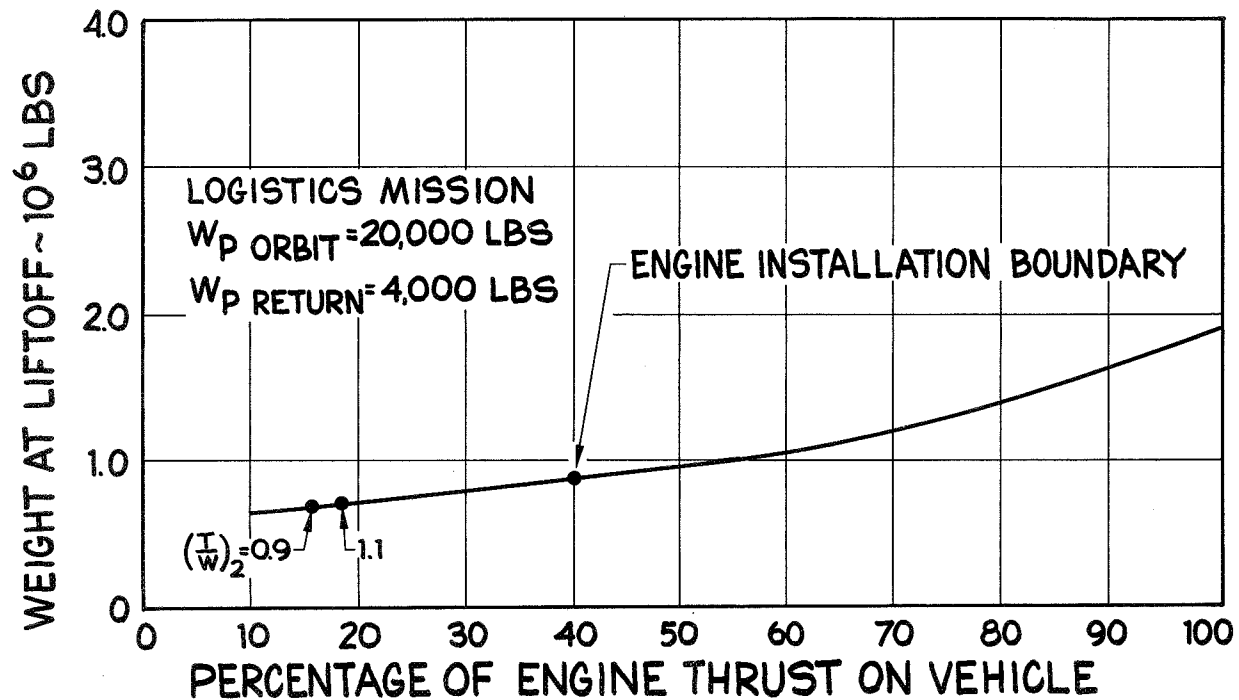
The minimum weight points from the configuration sizing presented on Figure 3 are plotted versus percentage of engine thrust on the vehicle.

These optimum designs were then checked for physical installation of the engines. For the Modified M2 design, no more than 40% of the engines can be accommodated on the vehicle because of base size limitations. Therefore, the curve beyond this value is of theoretical interest only, and the true stage-and-a-half (100% engines on the vehicle) is not feasible with this configuration. On the low end, the percentage of thrust on the vehicle is restricted to some minimum value by the required T/W ratio after staging of the tanks. A minimum value of T/W in this study was taken as 1.1.

The important conclusion from this plot is that as more engines are put on the vehicle, the overall system weight at lift-off increases.

# ILRV CONFIGURATION OPTIMIZATION

## MODIFIED M2 REENTRY VEHICLE

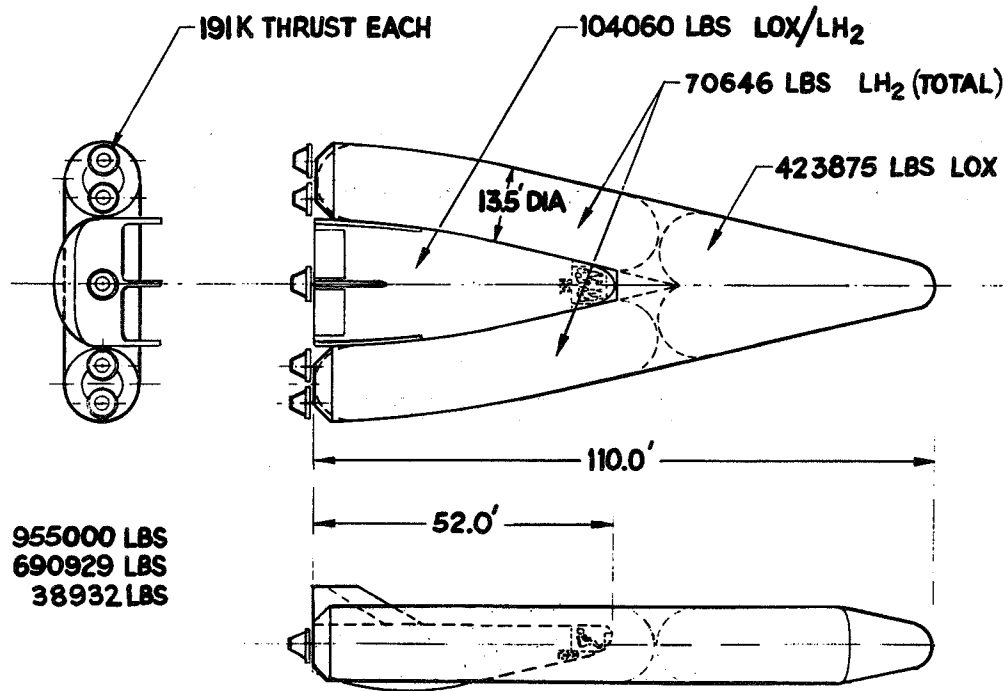


ILRV (M2 TYPE) WITH "V" TANKS

Typical design with tanks arranged in "V" shape is shown in Figure 5 for the case of 20% of engine thrust on the shuttle vehicle, and 80% on the drop tanks.



# ILRV (M2 TYPE) WITH "V" TANKS

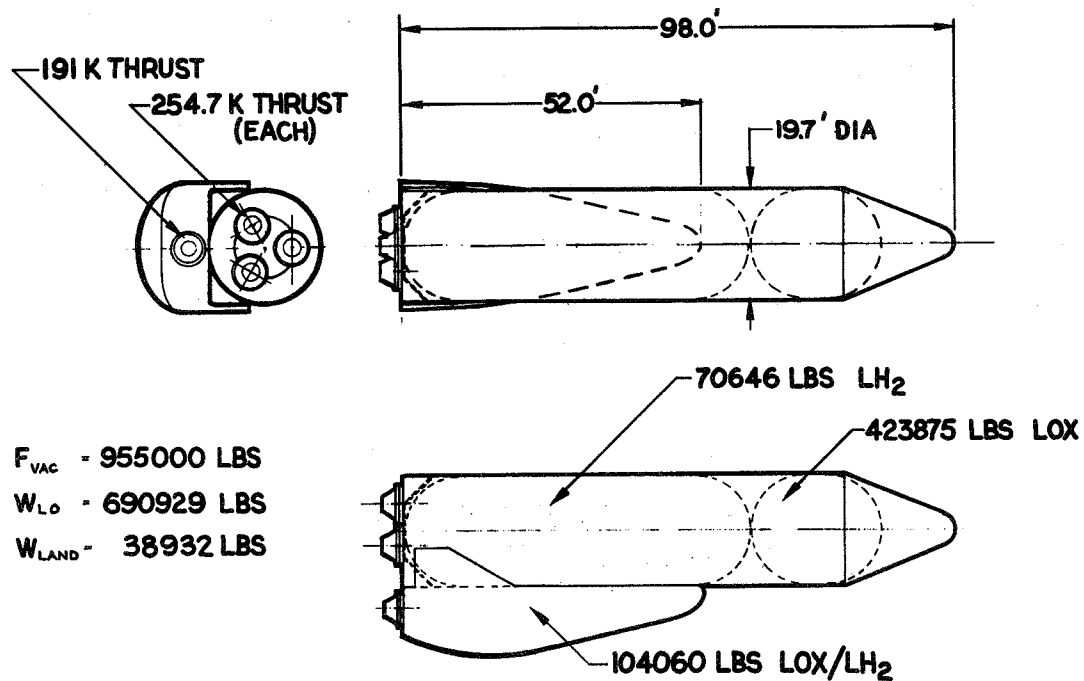


ILRV (M2 TYPE) WITH SINGLE TANK

An alternate design arrangement is shown on Figure 6 for the same design point as that for Figure 5.

In this case, a single tank is used and the concept is very similar to an ordinary two stage vehicle.

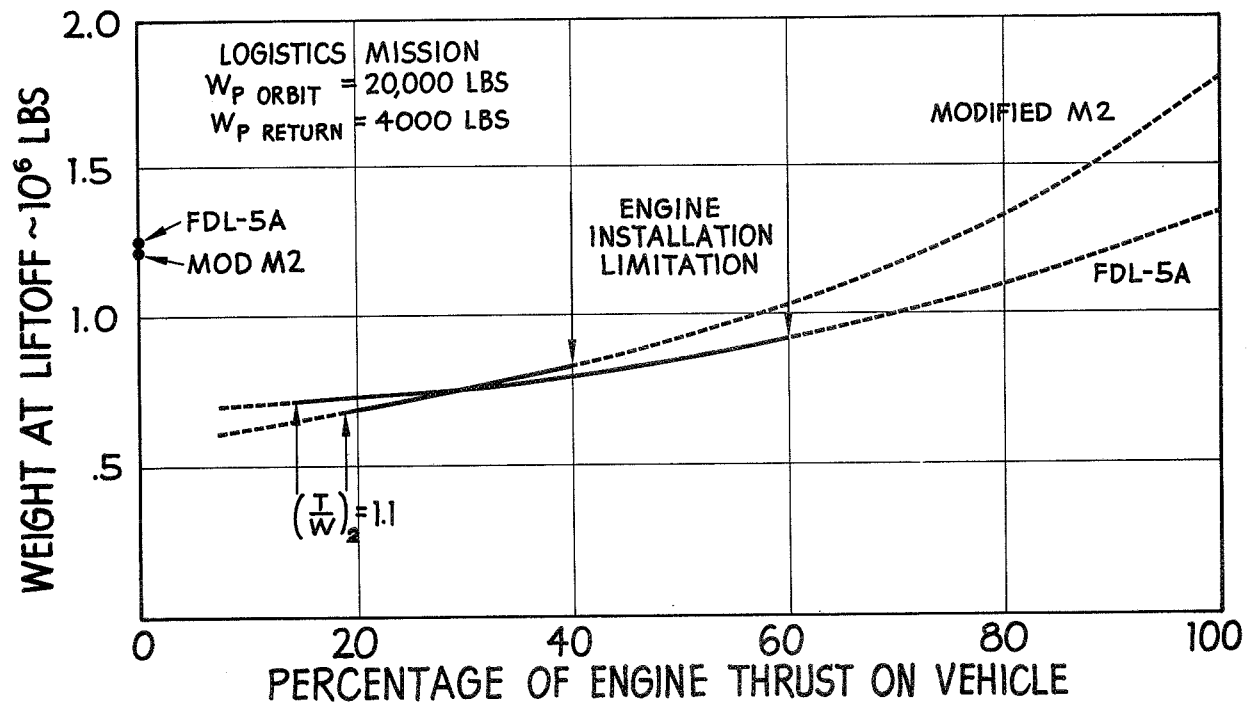
# ILRV (M2 TYPE) WITH SINGLE TANK



COMPARISON OF LIFT-OFF WEIGHTS  
FOR ILRV MODIFIED M2 AND FDL-5

In a manner similar to that described for the Modified M2, the optimum configurations were generated for the FDL-5 for varying proportion of the thrust on the vehicle. A similar trend can be observed of increasing system lift-off weight with increased proportion of engines on the shuttle vehicle. In the case of the FDL-5, up to 60% of engines can be accommodated on the vehicle base. For comparison, single stage designs of the Modified M2 and FDL-5 are also shown. In single stage designs, all engines are on the tanks and are propelling the core vehicle to orbital conditions. The tanks are then left in orbit. The tip tank configuration with FDL-5 as shuttle vehicle is shown on Figure 10.

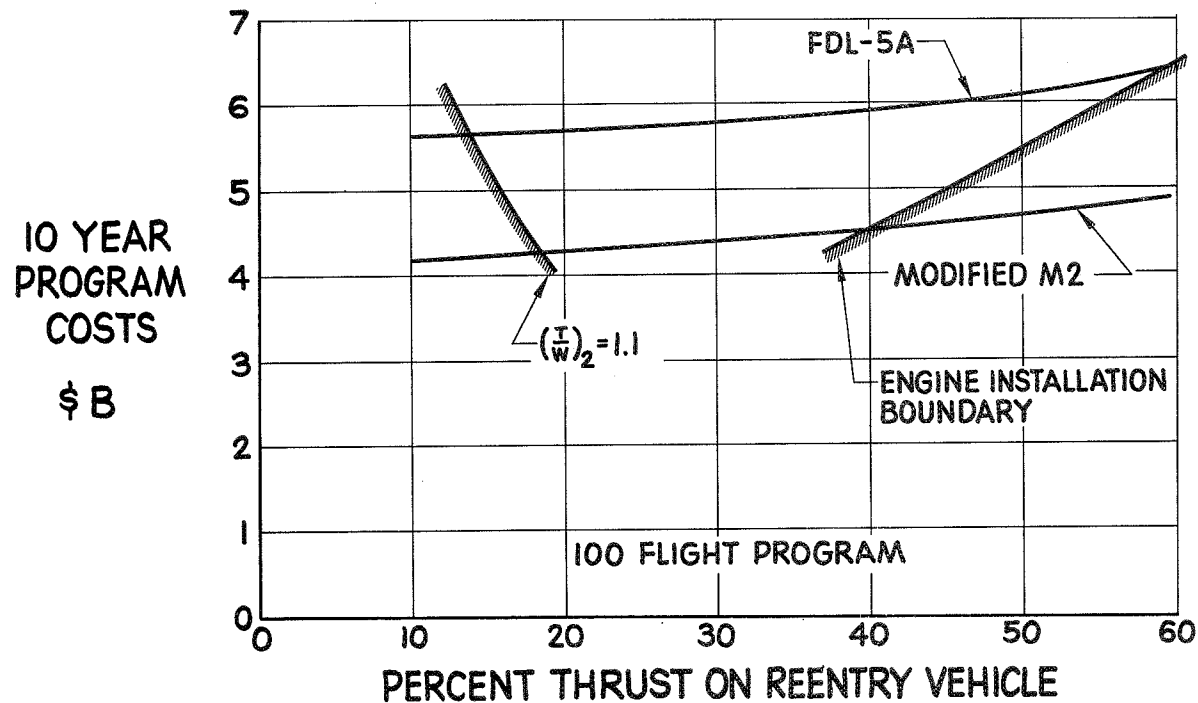
# COMPARISON OF LIFTOFF WEIGHTS FOR ILRV MODIFIED M2 AND FDL-5



EFFECT OF THRUST DISTRIBUTION ON PROGRAM COSTS  
FOR M2 AND FDL-5 ILRV

The cheapest system for both Modified M2 and FDL-5 configurations is the system with the minimum of engines, consistent with required T/W at tanks staging, on the shuttle vehicle. The true stage-and-a-half with all engines on the vehicle (were it possible to overcome base installation problem) would be considerably more expensive.

## *EFFECT OF THRUST DISTRIBUTION ON PROGRAM COSTS FOR M2 AND FDL-5A 1LRV*



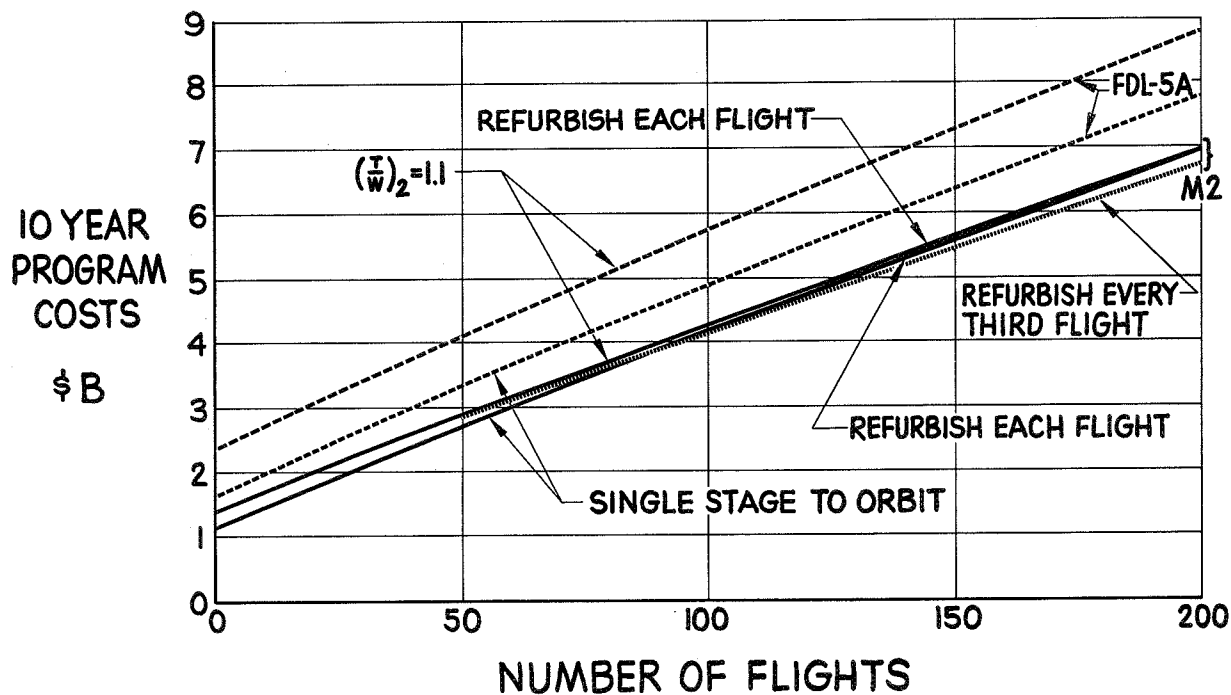
SPACE TRANSPORTATION PROGRAM COSTS  
MODIFIED M2 AND FDL-5 ILRV

The total system costs for a 10-year program are shown as a function of the total number of flights in the program. The FDL-5 system costs are significantly higher than the M2 system costs.

It is worth noting that the costs of single stage to orbit system for both configurations are lower than the optimum tip tank configuration, although the single stage to orbit has approximately twice as heavy lift-off weight than the tip tank configuration, as was shown on Figure 7.



# SPACE TRANSPORTATION PROGRAM COSTS MODIFIED M2 AND FDL-5A ILRV

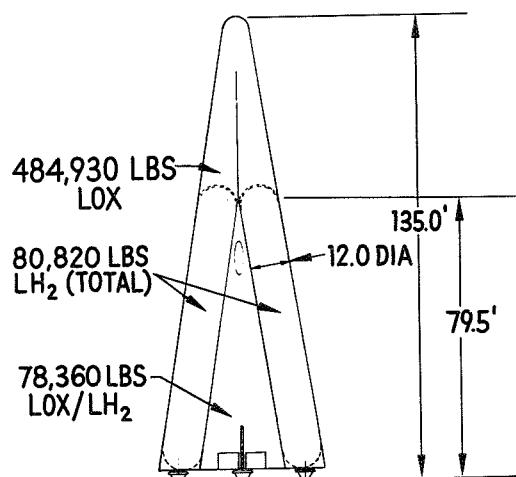


FDL-5 AND M2 ILRV CONFIGURATIONS  
FOR EQUAL CROSSRANGE PERFORMANCE

The designs, system costs of which were compared in Figure 9, are carrying the same payload, but due to unequal hypersonic L/D, the FDL-5 configuration has considerably more crossrange performance. To eliminate this bias, a series of M2 tip tank designs were generated which not only carry the same payload for the same mission, but also have crossrange performance of 3100 n.mi. equal to FDL-5 glide performance. This was achieved in the case of the M2 by carrying fuel in an external tank strapped on to the upper surface of the vehicle, and employing rocket propulsion during reentry just after the first pullout. After completion of this propulsive maneuver, the tank is jettisoned at about 24,000 fps so that it does not impair vehicle flight characteristics at lower speeds.

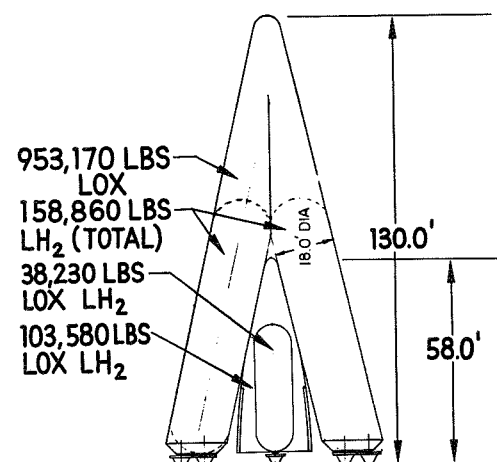
The lift-off weight of FDL-5 design for equal crossrange performance is approximately half the weight of the M2 design. However, this weight increase in M2 design is primarily due to increased propellants and does not reflect similar cost effect. In fact, as shown in the next slide, the relative cost of the two designs shows a reverse trend.

# FDL-5 AND M2 ILRV CONFIGURATIONS FOR EQUAL CROSSRANGE PERFORMANCE



204.7K LBS THRUST  
FDL-5  $L/D_{MAX} = 2.7$

$F_{VAC} = 1,023,500$  LBS  
 $W_{LO} = 741,360$  LBS  
 $W_{LAND} = 39,410$  LBS



$F_{VAC} = 1,927,000$  LBS  
 $W_{LO} = 1,395,380$  LBS  
 $W_{LAND} = 42,560$  LBS

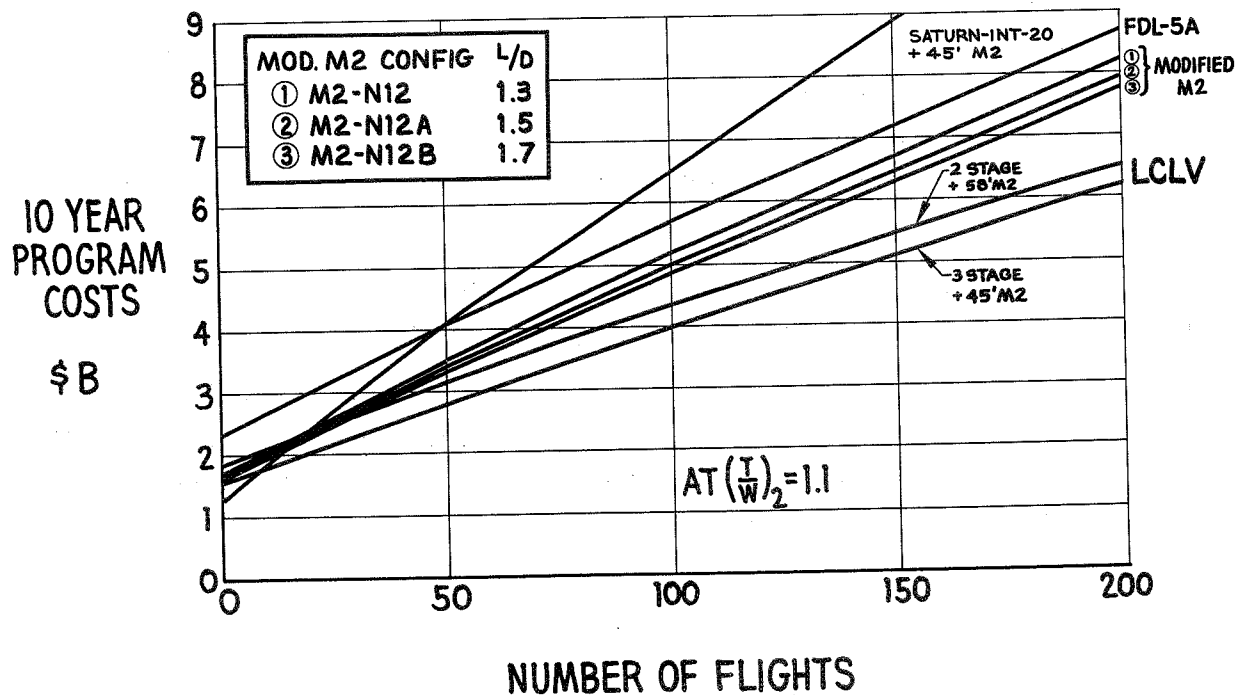
285 K LBS THRUST EACH  
217 K LBS THRUST  
M2  $L/D_{MAX} = 1.5$

PROGRAM COSTS FOR SYSTEMS WITH REENTRY CROSSRANGE OF 3100 N.MI.

All the configurations shown on Figure 11 are designed for the same payload, same mission, and have same maximum crossrange performance of 3100 n.mi. The crossrange augmentation feature for the M2 configurations, by use of rocket propulsion during reentry, was discussed in connection with Figure 10.

The cost of M2 configurations is significantly lower than FDL-5 configuration in spite of the M2 configurations having higher lift-off weights. This is due primarily to more complex and expensive technology required for the radiatively cooled FDL-5 shuttle vehicles versus M2 vehicles provided with ablative heat shields. However, the most impressive cost reduction is obtained by using orthodox Low Cost Launch Vehicle (LCLV), for boost to orbit, employing storable propellants. It is of interest to note that a system using a 2-stage LCLV, in which the shuttle vehicle acts as a third stage, is more expensive than a system using a 3-stage LCLV. This again emphasizes the point that the shuttle vehicle itself should not be used as a propulsive stage to orbit. The Saturn-Intermediate 20 booster with M2 shuttle is not competitive costwise with either a tip tank or LCLV system.

# PROGRAM COSTS FOR SYSTEMS WITH REENTRY CROSSRANGE OF 3,100 N MI



## CONCLUSIONS

The parametric study of optimum designs shows that the fewer engines there are on the shuttle vehicle, the less is the system lift-off weight and the more economical is the 10-year space transportation program. The minimum of thrust needed on the shuttle vehicle is determined by the minimum required T/W after staging the tip tanks to avoid excessive gravity losses.

Single stage to orbit, that is, a configuration with all the engines on the tip tanks, is more economical than optimum stage-and-a-half configuration. This trend is more pronounced on the FDL-5 configuration than on the M2 configuration.

For the configurations studied, the true stage-and-a-half with all the engines on the vehicle is impractical because of limited base area available for engine installation. In fact, this limitation is reached with FDL-5 at approximately 60% of total thrust on the shuttle vehicle, and with M2 at approximately 40% of total thrust on the vehicle.

The lowest transportation program cost with shuttle vehicle capable of 3100 n.mi. reentry crossrange is obtained using a 3-stage Low Cost Launch Vehicle (LCLV) for boosting to orbit Modified M2 shuttle. The M2 shuttle carries fuel to augment its gliding crossrange to 3100 n.mi. by application of thrust after the first pullout at near orbital velocity.

# CONCLUSIONS

---

- FEWER ENGINES ON SHUTTLE VEHICLE -
  - LESS WEIGHT, MORE ECONOMY
- SINGLE STAGE TO ORBIT
  - LESS EXPENSIVE THAN OPTIMUM  $1\frac{1}{2}$ -STAGE CONFIGURATION
- BASE LIMITATIONS FOR CONFIG'S EXAMINED -
  - MAKE TRUE  $1\frac{1}{2}$ -STAGE IMPRACTICAL
- LEAST EXPENSIVE OF ALL SYSTEMS -
  - LCLV + MODIFIED M2 SHUTTLE VEHICLE





## SPACE SHUTTLE ASCENT PHASE ABORT CONSIDERATIONS

by Christopher J. Cohan

General Dynamics/Convair  
San Diego, California

The subject of abort, although it is necessary for all flight vehicles, is never a popular subject since it generally involves a penalty with respect to the performance of the design mission. To some extent it is a more involved area than merely designing for a nominal mission since it must consider all sorts of possible situations and develop corresponding procedures to use.

This paper addresses the subject of Space Shuttle abort during the boost phase of the mission, i.e., liftoff through orbiter injection. The material is directed primarily at the problems, potential solutions and necessary considerations involved rather than quantitatively describing a particular abort procedure. The reason for this is that it is felt that many studies remain to be accomplished before an optimum abort procedure can be definitely established for the shuttle. It is hoped that the information in this paper will assist those who are performing the quantitative studies in terms of making them aware of the factors which must be considered to obtain meaningful answers.

This paper will present and explain the definitions related to abort which are being applied to the Space Shuttle program. The rationale for the current shuttle abort philosophy of intact abort will be explained. The types of abort situations and the procedures used in establishing these situations will be discussed. The main emphasis in the paper however will be on abort procedures. Since this meeting is directed towards Space Shuttle technology the conclusions will include a summary of the abort related technology problems.

The abort definitions shown in the figure are those currently being used in the Space Shuttle program. Intact abort is a baseline requirement for the Phase B shuttle studies. In the definition of intact abort the words "safe landing" are interpreted to mean a landing such that the vehicle is reusable with only minor additional refurbishment necessary as a result of the abort. This intact abort requirement differs from earlier manned space vehicles which employed escape systems over all or part of the boost phase. As will be indicated later this requirement can impose severe requirements on the vehicle design.

# **ABORT DEFINITIONS**

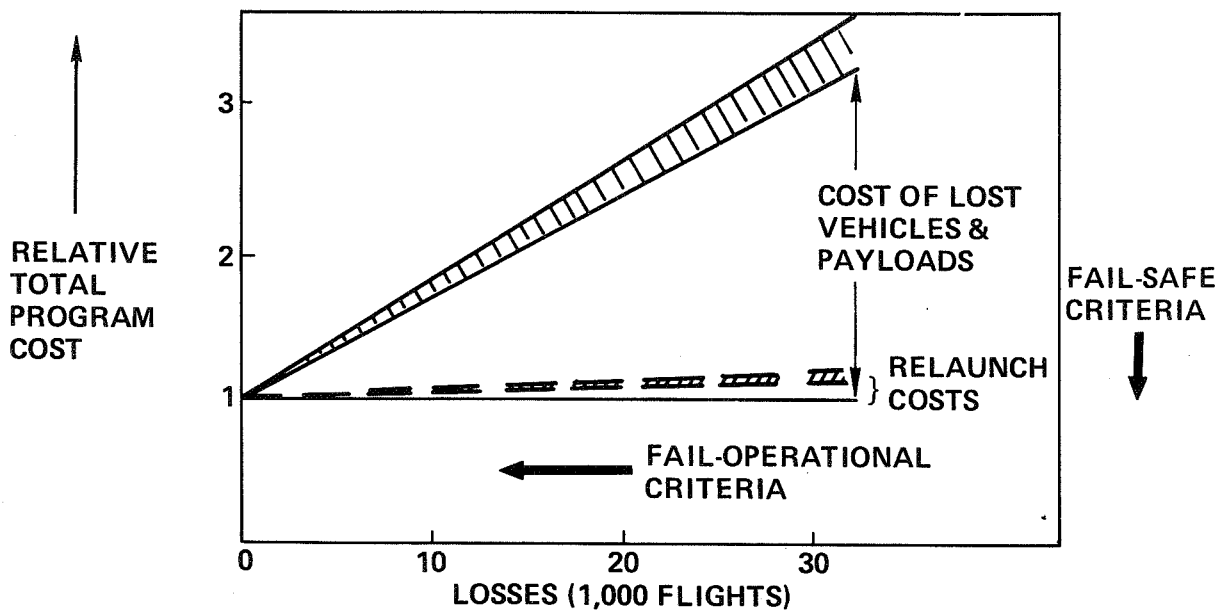
**ABORT — PREMATURE OR ABNORMAL MISSION TERMINATION**

**INTACT ABORT — CAPABILITY OF BOOSTER & ORBITER TO  
SEPARATE & CONTINUE FLIGHT TO A  
SAFE LANDING. THE ORBITER TO LAND  
WITH A FULL PAYLOAD**

This figure presents the rationale behind the baseline requirement for intact abort capability, i.e., return of the vehicles. This discussion will center on the vehicle aspects since it is assumed that safety is a basic requirement in any case. The intact abort philosophy arises from the Space Shuttle program goals established by NASA. The program goal of airline type operations implies an intact abort approach since this is the abort approach used by commercial transports. The primary driver for intact abort is the program goal of a low cost space transportation system. The figure indicates how intact abort is related to cost. The figure specifically relates cost to losses. If the vehicle does not have intact abort capability aborts represent vehicle losses (not personnel losses since it is assumed that under these conditions safety is provided in some other way) and the cost curve is the upper curve in the figure which represents the cost of replacing vehicles and payloads and relaunching the system. With intact abort capability as previously defined the losses represent mission losses and the cost curve is essentially the relaunch costs which are relatively low. This is the reason why the goal of low program cost leads to an intact abort philosophy. The fail safe criteria on subsystems as applied to safe return of the vehicle is necessary to have intact abort capability. The fail operational criteria where operational refers to operation of the mission merely reduces the number of mission losses. Since relaunch costs are relatively low there is a potential tradeoff between the cost of providing fail operational capability and the relaunch costs. In order to avoid confusion with the criteria of personnel safety it must be emphasized that the above discussion is directed at the vehicle where safe means vehicle return essentially reusable and operational means mission completion. It is noted that if the vehicle is "safe" then the personnel are safe and an intact abort philosophy provides personnel safety.

## RATIONALE FOR INTACT ABORT

- PROGRAM GOAL OF AIRLINE TYPE OPERATIONS
- PROGRAM GOAL OF LOW-COST ECONOMICAL SPACE TRANSPORTATION SYSTEM

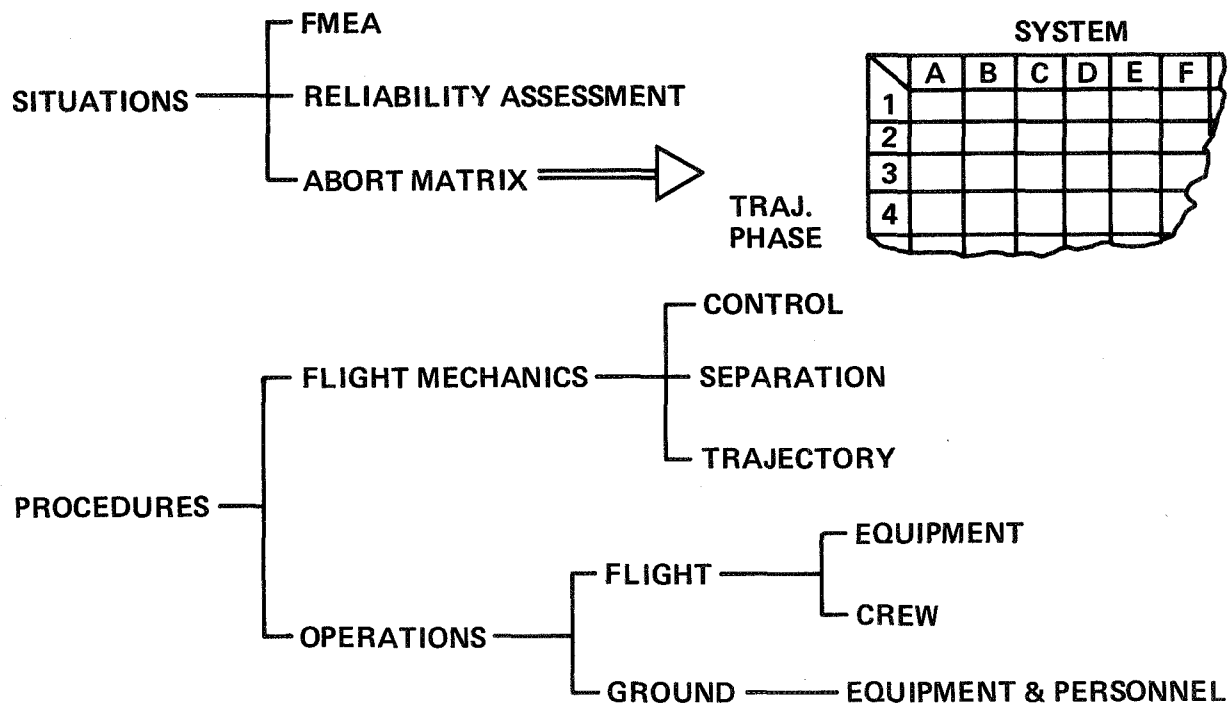


**GENERAL DYNAMICS**  
Convair Division

Abort analyses encompass most all of the disciplines and analyses required in analyzing the basic mission. This figure indicates the major tasks involved in abort analyses. There are two categories of tasks, those involving situation analyses, i.e., the nature of the problem causing an abort situation and procedure analysis, i.e., what is done about the problem. A key element of the situation analyses is the failure modes and effects analyses. Related to this and essential to evolving an abort philosophy is a reliability assessment or the determination of the probability of occurrence of abort situations. The situation data is generally presented in the form of an abort matrix which is a matrix of mission phases and subsystems. The matrix is filled out with data on the effects of failures and recommended corrective action.

The abort procedure analyses encompass flight mechanics analyses and operations analyses. The flight mechanics analyses include such things as control, separation and trajectory analyses. The operations analyses involve the operational requirements imposed on personnel and equipment both in the flight vehicles and at ground facilities. Included in this area would be such things as the requirements for an automatic abort warning system and the ground based guidance and navigation computer equipment, if any, required to affect a successful abort maneuver.

# ABORT ANALYSES

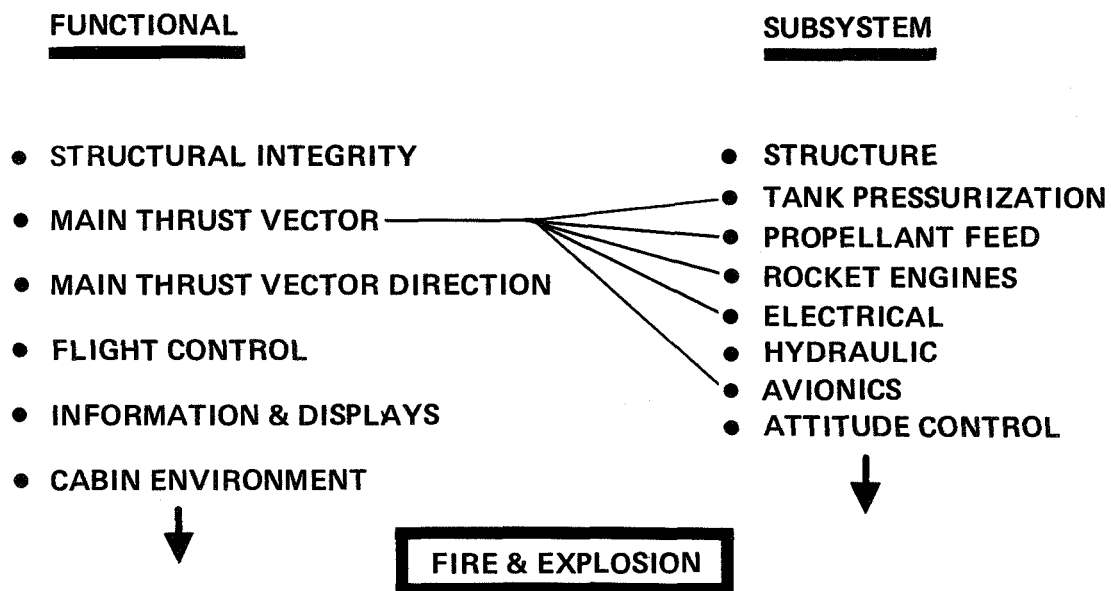


A necessary element in developing an abort approach is information on the nature of the abort situation. As indicated on the figure there are two basic approaches to situation analyses; a functional approach and a subsystem approach. The functional approach is based on the fact that the shuttle vehicle system must perform certain functions and that it is loss of functional capability which creates the problem. The functional list on the figure is only a partial list and merely indicates the nature of functions. The functional approach to situation analyses investigates the consequences of loss of functional capability. The subsystem analyses investigates the effects of failures in individual subsystems. The list on the figure is only a partial list and a complete analyses must consider all subsystems. Initial abort analyses generally employ the functional approach and as the design as defined in more detail the subsystem approach is used.

There is one other category of hazardous situations which is important from an abort standpoint and that is fire and explosion. This is of great concern to the Space Shuttle system since both the booster and orbiter contain large quantities of  $\text{LO}_2$  and  $\text{LH}_2$ . Since hydrogen can present a hazardous situation over an extremely wide mixture ratio range the consequences of leaks can be very severe. With the large amount of propellant plumbing on the Space Shuttle vehicles the problem of leaks and therefore a fire and/or explosion hazard is probably the most significant potential abort situation especially since subsystems have a design requirement of fail-operational/fail-safe. In addition to the hazard during the launch phase where there are large quantities of propellant there is also a hazard associated with the residual propellants during return.



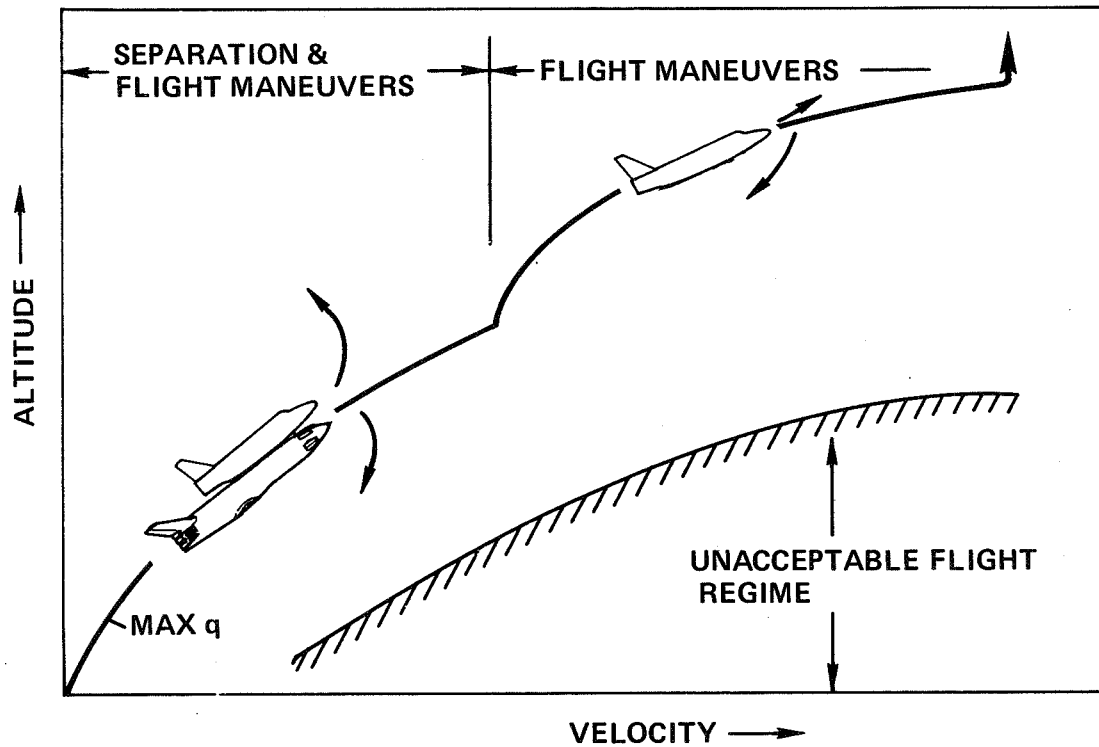
## APPROACHES TO SITUATION ANALYSES



The primary objective of any abort procedure is to terminate the mission in the safest manner possible. This includes providing for a safe landing as specified in the definition of intact abort. The figure illustrates a typical ascent trajectory and indicates the two basic procedures that may be involved in accomplishing an abort. During mated flight from liftoff through staging the abort procedure consists of two areas, separation and post-separation flight maneuvers. After nominal staging an abort procedure involves flight maneuvers only. Because of heating and load factor considerations there is a region of the altitude-velocity spectrum in which flight is unacceptable. Abort maneuvers must preclude flight into this region. In addition to this high velocity-low altitude flight region which must be avoided there is the problem of landing the vehicle which sets upper limits on the vehicle weight. Since the conditions, e.g., vehicle weight and environmental conditions vary along the trajectory, the problems and considerations involved with evaluating abort procedures also vary along the trajectory.

# ABORT PROCEDURES

OBJECTIVE: TERMINATE MISSION IN SAFEST MANNER POSSIBLE



The information in this figure indicates some of the basic factors which must be considered in analyzing and evaluating abort procedures. Most of the items will be covered in more detail later so they will only be touched on briefly at this point. With respect to separation there is the basic problem of maintaining control of both vehicles during any separation maneuver. The control problem is complicated by the possibility of propellant slosh and resultant center of gravity variations. The separation procedure itself must consider the problems of interference aerodynamics and orbiter engine plume effects if the orbiter engines are ignited while in the vicinity of the booster. If an early separation capability is a requirement for abort then there are requirements composed on the orbiter main propulsion system to provide engine start capability at off nominal conditions.

The post-separation abort maneuvers must consider the problem of depleting at least most of any remaining propellants since the vehicles can neither enter or land under high weight conditions. The propellant can only be depleted through burning or dumping. If dumping is required, the dump rates are a function of time from liftoff since the propellant weight decreases with time. The propellants must be dumped at a rate which presents excessive load factors or temperatures occurring during entry. In burning or dumping propellants consideration must be given to vehicle center of gravity variations and control requirements. Since an abort is not successful until the vehicle lands safely there is the problem of landing site availability and the related guidance and navigation problems.

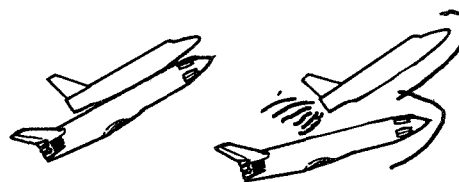
# ABORT PROCEDURE CONSIDERATIONS

## SEPARATION PHASE

CONTROL, SLOSH, CG

INT. AERO, PLUME

AIRLOADS, ENGINE START



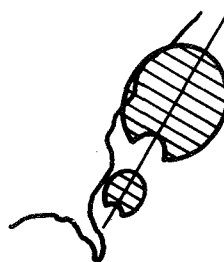
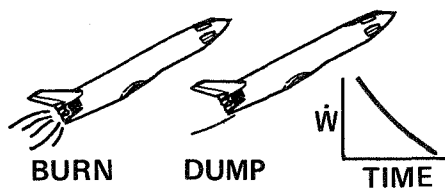
## POST-SEPARATION MANEUVERS

PROPELLANT DEPLETION

STAB. & CONTROL, CG

LOADS & TEMPERATURES

LANDING SITES, G&N



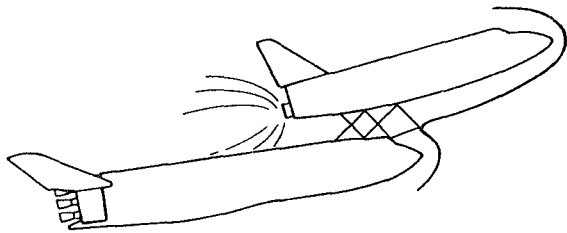
The previously discussed definition of intact abort contains the phrase, "capability of booster and orbiter to separate". Separation particularly early separation for abort can be a major problem area. The basic requirement on any shuttle separation system is that it provide separation without collision and that both vehicles can be safely recovered from the separation. This latter requirement differs from the requirements on previous launch vehicle separation systems in which there was no concern for the flight of the lower stage as long as it did not present a collision hazard to the upper stage. This allowed separation systems which sent the lower stage tumbling away. Obviously with two reusable stages such separation procedures cannot be tolerated.

As listed on the figure there are many separation schemes currently being considered for the Space Shuttle. They fall into two broad categories, those which use the orbiter thrust to provide the separation force and those which use another technique such as a piston to impart the basic separation force with orbiter engine start occurring further away from the booster. There are certain general problem areas which all of these schemes must deal with. Since these problems are affected by vehicle characteristics and flight environment their magnitude is a function of the point along the trajectory where separation is desired. The first problem any system must overcome are any compressive aerodynamic forces tending to hold the vehicles together. These would become particularly significant in the region of maximum dynamic pressure and would also be affected by wind characteristics. There is the problem of interference aerodynamics. NASA and contractor wind tunnel investigations have shown that these are very non-linear with respect to relative position and can be such as to tend to pitch the vehicles back together.

For those schemes which use orbiter thrust as the separation force or ignite the orbiter engines in the vicinity of the booster there is the problem of rocket plume effects. There is not only the problem of direct plume impingement on the booster with resulting force and heating effects but the problems associated with the plume changing the external flow field and hence affecting the aerodynamic characteristics. Finally there is the problem of maintaining control of both vehicles in a complex time variant situation. Several other papers at this meeting have dealt with the subject of separation in much more detail. Although the Phase B studies will yield the final results it is quite possible that the penalties involved with providing "immediate" separation capability from any point along the trajectory will be prohibitive and in certain regions such as maximum dynamic pressure separation will have to be delayed until conditions become more favorable.

# SEPARATION

**REQUIREMENT: NO COLLISION & RECOVER BOTH VEHICLES**



## SCHEMES

- ORBITER THRUST PLUS LINKAGE
- PISTON
- SOLID ROCKETS
- AERO SEPARATION (LINKAGE)
- ORBITER THRUST PLUS RAILS
- RETRO ON BOOSTER
- ?

## PROBLEMS

- OVERCOMING ANY COMPRESSIVE AERO FORCES
- INTERFERENCE AERO & PLUME EFFECTS
- MAINTAINING CONTROL OF BOTH VEHICLES

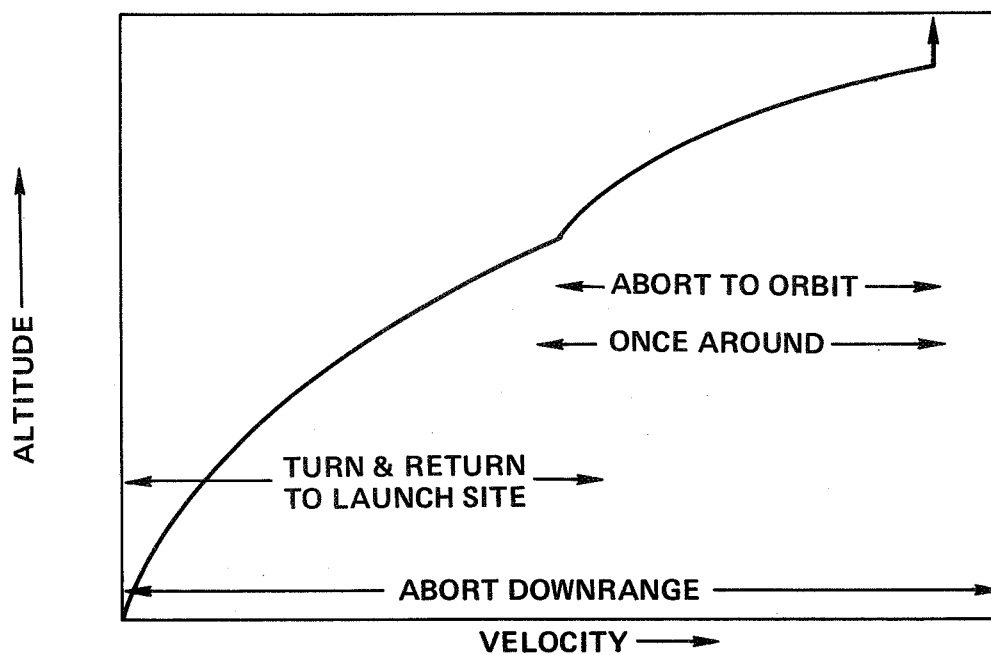
There are various types of post-separation abort procedures that can feasibly be employed to return the vehicles safely. The possibility for these maneuvers is based on the assumptions that the booster has a nominal flyback capability and the orbiter has thrust capability and a large  $\Delta V$  capability. Both the booster and orbiter have the potential for flying downrange from any point in the launch trajectory. For velocities at least up through nominal staging there is the possibility of a turn maneuver with return to the launch site. For higher velocities the orbiter has the potential for a once around maneuver or an abort to orbit. The next several figures will explain these maneuvers in more detail.

The type of maneuver to be employed in any abort situation is dependent on the nature of the failure and the time in the ascent at which the failure occurs. The most significant failures from the standpoint of abort are those which result in reduction or loss of thrust and those which present a fire or explosion situation. The reason for this is that these situations can have an immediate impact on the flight trajectory characteristics and requirements, e.g., requirement for immediate separation.



# POSSIBLE POST-SEPARATION ABORT PROCEDURES

- ASSUMPTIONS
- BOOSTER HAS NOMINAL FLYBACK CAPABILITY
  - ORBITER HAS THRUST & LARGE  $\Delta V$

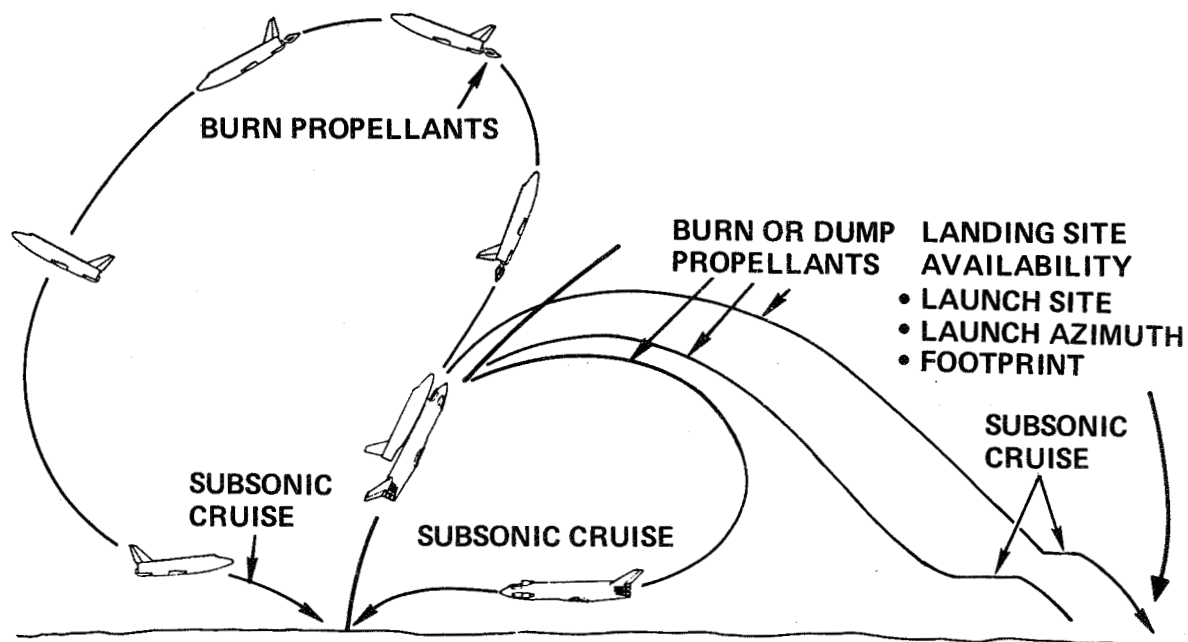


This figure shows the post-separation abort maneuvers which can be considered for abort during mated flight. Both the booster and orbiter can abort downrange. In accomplishing this maneuver at least most of any remaining propellant must be depleted prior to any entry pullout maneuver in order to prevent excessive load factors or heating. The propellants can be depleted through burning in the rocket engines or, if the engines are inoperable, through dumping. As mentioned previously, required dumping rates are a function of time from liftoff. The glide phase can be followed by a subsonic cruise phase. With a booster having flyback capability a subsonic cruise capability is built in. With an orbiter which does not have cruise propellant for the design mission, a subsonic cruise can only be accomplished by utilizing some of the ascent hydrogen. This would involve additional plumbing but is a possibility. One of the most important factors to be considered with this abort procedure is the availability of a landing site. In addition to being a function of the time at which abort occurs, landing site availability also depends on launch site and azimuth and glide capability of the vehicles, i.e., footprint.

The booster with a flyback capability for the design mission has a potential for returning to the launch site in the event of an abort. As with all abort procedures most of any remaining propellants must be depleted.

For the orbiter to return to the launch site it is necessary to burn off the propellants in a useful fashion to assist in performing the return maneuver. After propellant depletion the vehicle performs a glide. If fuel were provided in the manner discussed above for downrange abort than the orbiter could have a subsonic cruise phase prior to landing. The next figure presents more data on this orbiter return maneuver.

## MATED FLIGHT - POST-SEPARATION ABORT MANEUVERS

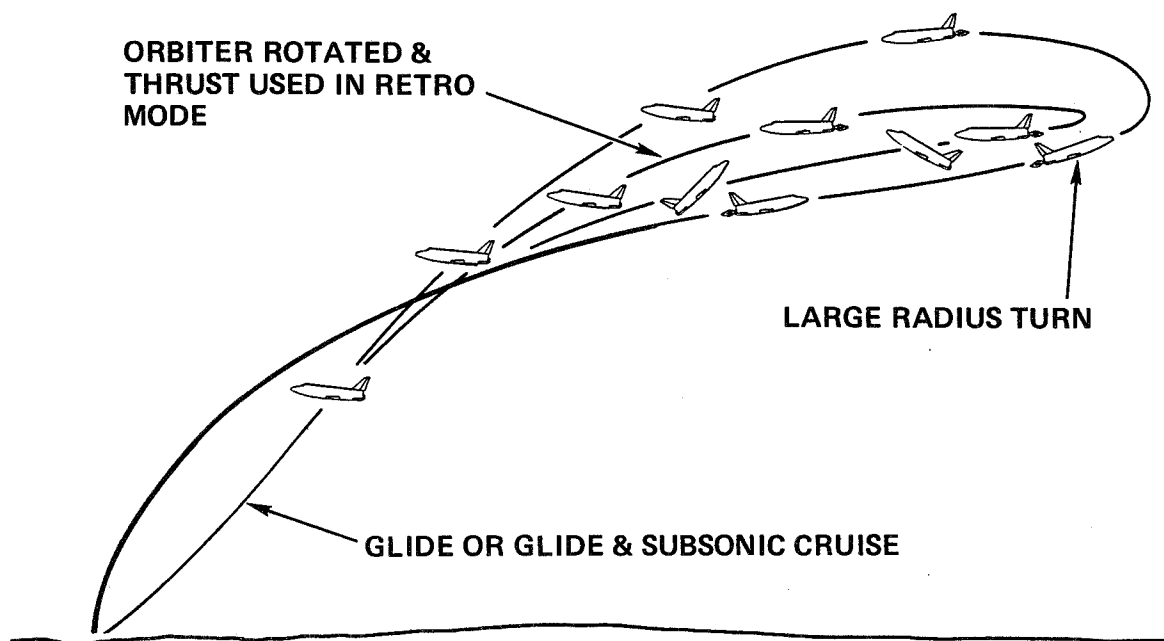


This figure illustrates in more detail the maneuvers involved with orbiter return to the launch site. These maneuvers are based on the fact that the orbiter has a large  $\Delta V$  available. Although this  $\Delta V$  is in the vehicle for acceleration purposes on the baseline mission it can also be used to change the direction of the orbiter velocity vector. In performing those maneuvers the thrust must also be employed to provide some vertical force to prevent the vehicle from getting into an unacceptable low altitude - high velocity condition.

There are two possible maneuvers. In one, the orbiter is rotated and uses the rocket thrust in a retrograde fashion to eliminate the downrange velocity and provide a velocity component towards the launch site. When the propellants are depleted the vehicle performs a glide or a glide plus subsonic cruise back to the launch site. The other type of maneuver is one in which thrust is continuous and the orbiter performs a large radius turn to get headed towards the launch site. The procedures after propellant depletion are the same as with the other maneuver. In performing this maneuver the engine thrust be controlled in a manner to prevent excessive velocity increase.

# ORBITER RETURN TO LAUNCH SITE

BASIS: ORBITER HAS  $14,000 \text{ FPS} \leq \Delta V \leq 18,000 \text{ FPS}$  AVAILABLE



This figure illustrates the orbiter maneuvers that can be used for a high velocity abort situation, i.e., abort during orbiter burn or the late stages of mated ascent. These maneuvers are abort downrange, abort once around and abort to orbit. The latter two maneuvers require all or partial orbiter thrust. The downrange abort procedure was discussed earlier. The advantage of this maneuver is that it has a minimum effect on nominal mission performance. The biggest disadvantage of this maneuver is the problem of landing site availability which could limit mission flexibility.

The once around abort maneuver is accomplished by injecting the orbiter into an elliptical orbit such that entry occurs during the first orbit followed by a glide to a landing site. This maneuver reduces the landing site problem compared with downrange abort for a small additional  $\Delta V$  requirement under conditions of one orbiter engine failure. For launch from ETR all low earth orbits could have a single abort landing site in Southern Texas with very little cross-range capability required. Launches from WTR into the higher inclination orbits have a landing site problem since the first orbit comes back well out in the Pacific Ocean which would require a large cross-range capability to reach the West coast. There is a potential disadvantage associated with this maneuver in that the entry maneuvers may be off nominal with respect to heating and make the abort situation the design point for the vehicle. The maneuver may also be subject to significant dispersions.

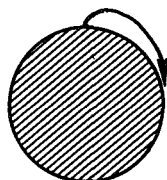
The abort to orbit procedure has the advantage of allowing the entry and landing site to be nominal which minimizes the effect of launch site and azimuth. The disadvantage of this maneuver is that it requires a significant  $\Delta V$  which may affect baseline performance capability as shown in the next figure.

# **HIGH VELOCITY ABORT**

## **ABORT DURING ORBITER BURN OR LATE STAGE OF MATED ASCENT**

**ASSUMPTION: ALL OR PARTIAL ORBITER THRUST AVAILABLE**

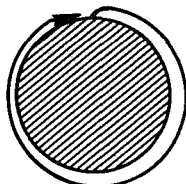
**ABORT  
DOWNRANGE**



**ADV. — MINIMUM EFFECT ON PERFORMANCE**

**DISADV. — LANDING SITE AVAILABILITY**

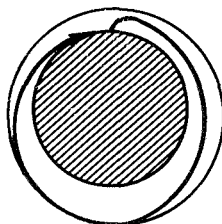
**ABORT  
ONCE AROUND**



**ADV. — REDUCES LANDING SITE PROBLEM**

**DISADV. — ENTRY PERF. OFF NOMINAL**

**ABORT  
TO  
ORBIT**



**ADV. — ABORT ENTRY NOMINAL**

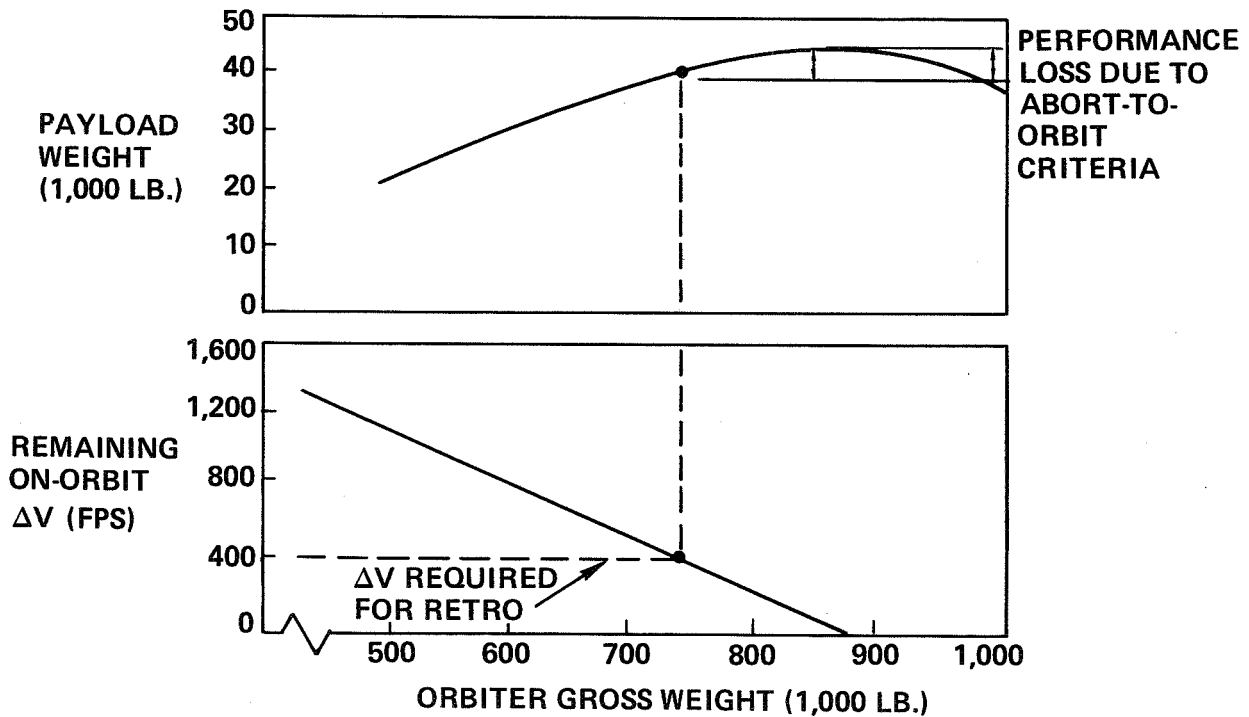
**DISADV. — REQUIRES SIGNIFICANT  $\Delta V$**

When either the once around abort or abort to orbit procedures are used in the event of an orbiter engine failure there is an additional  $\Delta V$  requirement to overcome the increased losses due to the lower thrust. If the additional  $\Delta V$  is within the 1500 fps on orbit  $\Delta V$  capability of the orbiter there is no penalty associated with the maneuver. When the additional  $\Delta V$  required exceeds the 1500 fps the maneuver imposes a penalty on the vehicle. The nature of this penalty is shown by the example presented in the figure. The curves show the effect of orbiter gross weight on payload and  $\Delta V$  remaining in a 100 n.mi. orbit assuming one engine out at staging. The payload curve represents the effect of staging velocity on performance and is a function of the inert fractions of each stage. The  $\Delta V$  curve merely provides a graphical presentation of the fact that for a fixed thrust system the losses increase as the weight increases due to the lower thrust to weight ratio. As indicated on the figure the orbiter gross weight is limited by the requirement that there be sufficient  $\Delta V$  remaining in the 100 n.mi. orbit to accomplish the retro maneuver. In the example shown, this yields an orbiter weight which is less than the optimum weight for payload performance and hence there is a performance penalty due to abort. Whether or not there is a penalty for abort to orbit on any given shuttle system is a function of the specific characteristics of the system.



## ABORT TO ORBIT-100N.MI.

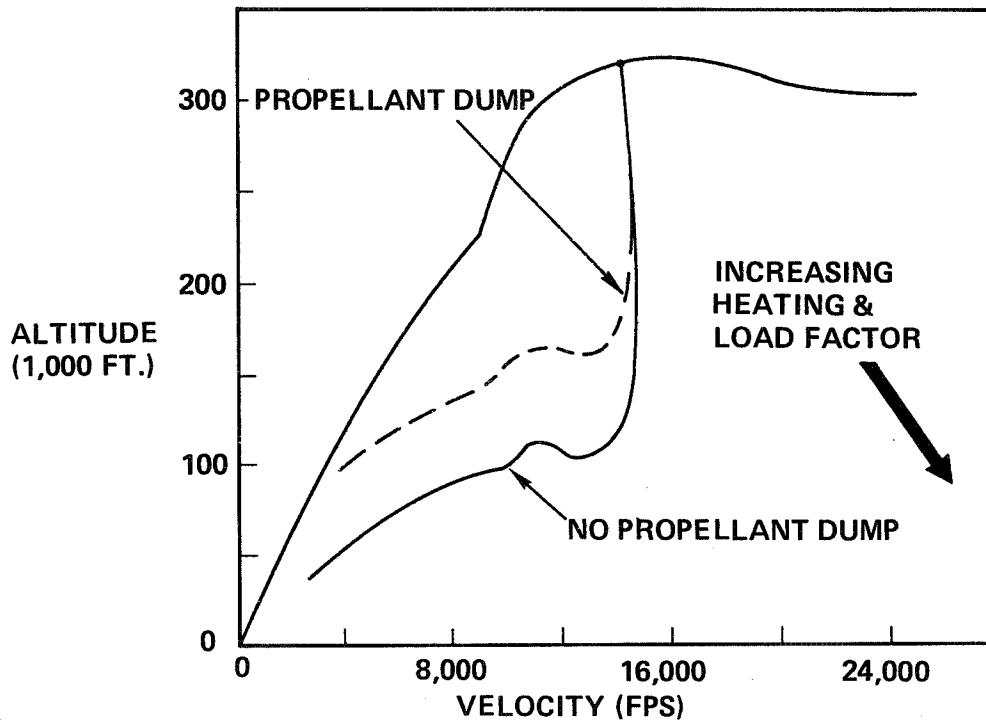
ASSUMPTIONS: GLOW = 3.5M LB. — THRUST = 400K LB. — ON-ORBIT  $\Delta V$  = 1500 FPS  
2 ENGINE ORBITER — 1 ENGINE OUT AT STAGING



The situation of complete loss of orbiter thrust either through failure to ignite at staging or premature termination presents a very severe abort situation. The orbiter becomes a glide vehicle and performs an entry such as shown in the figure. The first problem associated with this abort situation is the problem of propellant depletion since without propellant depletion the vehicle would experience excessive load factors and heating as well as having too high a landing weight. Since the orbiter engines are inoperative the propellant depletion must be accomplished with a propellant dump system. The dumping must be accomplished quickly in order to yield a higher altitude pullout condition. For aborts at or near the staging point, when there are large quantities of propellant on board, the required dump rates can exceed the nominal flow rates required for the engines.

A second problem associated with this abort situation is the problem of landing site availability. With no rocket thrust available the landing footprint is limited to the glide footprint plus any additional range from a subsonic cruise. As noted earlier a subsonic cruise for the orbiter under current design requirements would require provisions for using some of the ascent hydrogen. This landing site problem could lead to launch azimuth restrictions or a design requirement for water landing capability such as required on commercial aircraft operating over the ocean. For aircraft the requirement is that the vehicle be capable of landing in the water without disintegrating and that it float for some period of time.

## TOTAL ORBITER THRUST LOSS

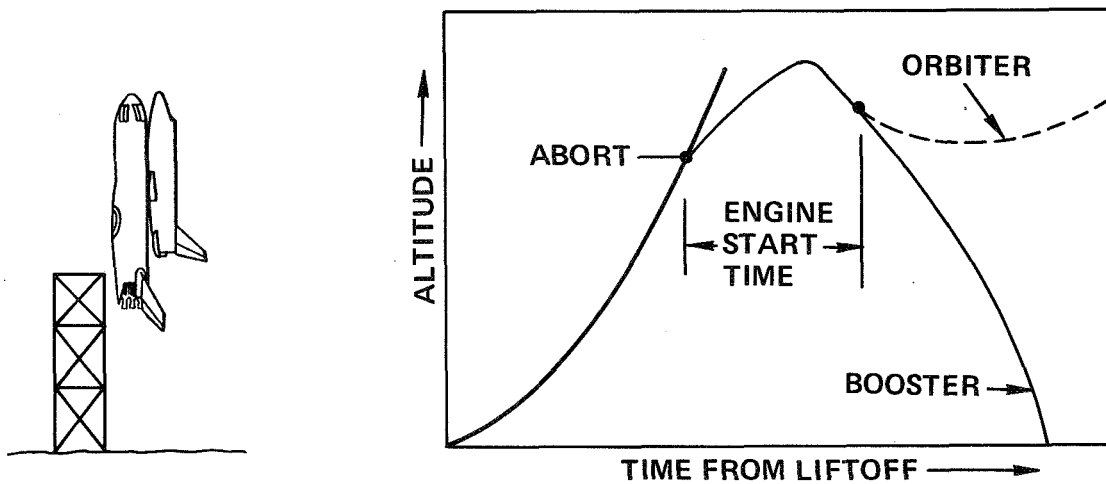


PROBLEMS: DUMP RATES GREATER THAN NOMINAL FLOW RATES  
LANDING SITE AVAILABILITY/WATER LANDING?

The abort situation of total booster thrust loss at or near liftoff presents certain unique problems. The situation is time critical because of the problem of booster fall back to the pad. A schematic time history of this situation is shown in the figure. Thrust is assumed to be lost at the point labeled abort on the figure. The booster having a vertical velocity component will continue to rise until the vertical velocity reaches zero and then fall back under gravity impacting the ground. With a separation system which uses orbiter thrust as part of the separation procedure the orbiter will remain with the booster during the finite engine start time. The engines currently being considered for the Space Shuttle have a start time of about 5 seconds. Depending on the time of abort the mated configuration can be falling back towards the ground before separation occurs as indicated by the situation presented in the figure. In this situation the orbiter continues downward until the acceleration due to thrust can produce an upward velocity. The minimum requirement in this situation is that the low point of the orbiter separation trajectory clear the tower. For any given system this requirement establishes a time from liftoff below which tower clearance cannot be assured. With an engine start time of about 5 seconds this requirement can only be met for aborts after about 8 seconds from liftoff. If it is assumed that the booster explodes on impact the requirement becomes one of avoiding some level of explosion overpressure. Assuming a maximum allowable overpressure of 1 psi a safe abort could not be obtained during approximately the first 17 seconds after liftoff. Although the exact numbers are a function of specific design characteristics the basic problem of a period of time near liftoff where safe intact abort cannot be accomplished will continue to exist.

## ABORT-NEAR LIFTOFF

### TOTAL BOOSTER THRUST LOSS



APPROX. 8 SEC. DEADBAND FOR TOWER CLEARANCE  
APPROX. 17 SEC. DEADBAND FOR 1 PSI EXPLOSION OVERPRESSURE

This paper has indicated many problems associated with abort. Although many of the problems are design problems there are several that can be classed as technology problems. Potentially the most critical and the area where there is the least amount of data is the area of separation considering all factors. For example, the work that has been accomplished to date has not included rocket plume effects. Another technology area is in the area of fire and explosion hazards. There is a need for additional work in the area of hydrogen fire detection and suppression and related to this is the detection of impending explosions. Since explosions are a time critical phenomena anything that can increase the available warning time will either decrease the requirements on the system and/or lessen the chance for a catastrophic failure. With the many possible post-separation abort maneuvers there is the problem of the guidance and navigation and related software necessary to accomplish these maneuvers.

# **ABORT-RELATED TECHNOLOGY PROBLEMS**

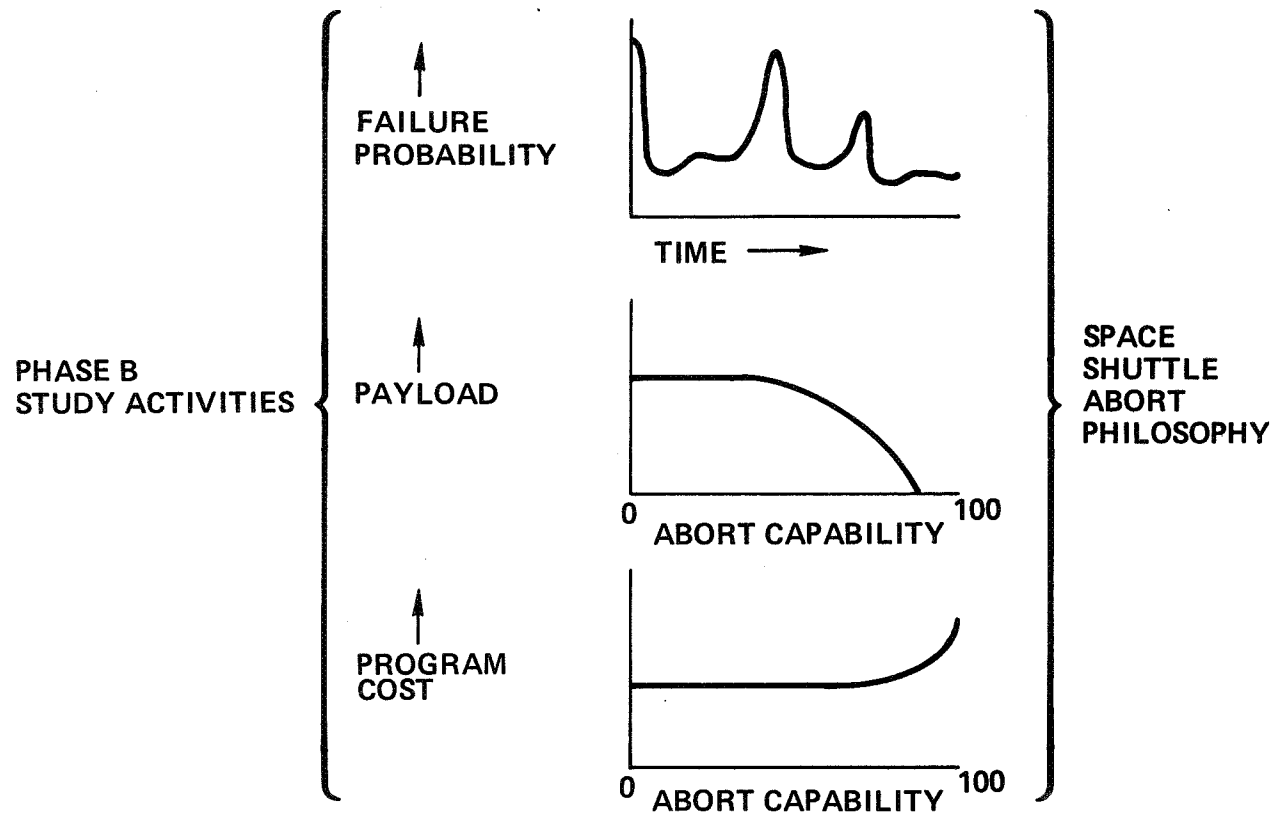
- **EARLY SEPARATION**
  - INTERFERENCE AERODYNAMICS**
  - PLUME EFFECTS**
  - VEHICLE DYNAMICS & CONTROL**
- **FIRE DETECTION & SUPPRESSION**
- **DETECTION OF IMPENDING EXPLOSIONS**
- **GUIDANCE & NAVIGATION & RELATED SOFTWARE  
FOR POST-SEPARATION ABORT MANEUVERS**

As indicated at the beginning this paper has been devoted primarily to abort considerations and possible abort procedures rather than quantitatively presenting a recommended abort procedure for the Space Shuttle. The reason for this is that it is felt that the Space Shuttle abort philosophy is still in the development phase. The studies currently underway will provide the information required to select a philosophy. The reason for this is illustrated in the figure and is related to the fact that abort capability must be related to the probability of abort situations in order to develop a philosophy which is realistic and yields an adequate performance capability for the design missions. It must be recognized that any system will have some finite probability of a catastrophic failure.

The Phase B studies will yield information on the probability of failures throughout the mission. Undoubtedly, certain regions will be more critical than others. The studies will also yield data of the effect of providing abort capability on such parameters as payload and program cost. As shown schematically some abort capability is inherent in any vehicle design and does not affect payload or cost. Providing additional capability is only accomplished with some penalty in payload and/or program cost. This effect of abort capability on payload and cost is of course related to the distribution of failure situations throughout the mission. If there is no abort situation or the probability is very low in some region of the mission there is no point in providing abort capability for that region. These data must be obtained and then evaluated to yield a final Space Shuttle abort philosophy. The final selected approach will be between the extremes which are a system with a high amount of abort capability and no payload and a system with high payload and little abort capability.



# SPACE SHUTTLE ABORT PHILOSOPHY DEVELOPMENT



This figure summarizes the principal conclusions developed in this paper. It has been shown that the requirement for intact abort arises not only from safety considerations but considerations of program cost. With a fail-operational, fail-safe design philosophy on subsystems the most severe failures during the boost phase are thrust loss or reduction and fires and explosions. The problems and considerations involved with several post-separation abort procedures have been discussed. It has been shown that the applicability of these maneuvers is a function of launch site and azimuth, and vehicle footprint capability since an intact abort is not successful until the vehicles have landed safely. Performing early separation in the event of an abort is a potential severe problem area due to various interference effects and the associated control problems. Since fire is a potential severe hazard with the large quantities of propellant on board the vehicles the prevention and suppression of fires is very significant. Finally, it is anticipated that the analyses to be conducted during Phase B will lead to the development of a final shuttle abort philosophy.

## **SUMMARY**

- **INTACT ABORT REQUIRED DUE TO COST & SAFETY CONSIDERATIONS**
- **MOST SEVERE BOOST FAILURES – THRUST LOSS, FIRE, EXPLOSION**
- **SEVERAL POST-SEPARATION ABORT FLIGHT MANEUVERS – ABORT DOWNRANGE, TURN & RETURN, ONCE AROUND, ABORT TO ORBIT**
- **ABORT MANEUVERS = f (LAUNCH SITE & AZIMUTH, FOOTPRINT)**
- **EARLY SEPARATION IS POTENTIALLY SEVERE PROBLEM**
- **LH<sub>2</sub> FIRE PREVENTION/SUPPRESSION VERY IMPORTANT**
- **PROPELLANT DUMP SYSTEM MAY BE REQUIRED**
- **PHASE B ABORT STUDIES WILL DEVELOP SHUTTLE ABORT PHILOSOPHY**

## SUBSONIC CRUISE MODE - AN INTACT ABORT CONCEPT

by A. Blanciak, O. Kramer, and J. K. Yakura

Aerospace Corporation  
El Segundo, California

Intact abort is a concept essential to the economic success of a fully reusable two stage earth-to-orbit shuttle (EOS) system. Operationally, this concept involves the ability to safely terminate a mission and to execute a safe return of the crew and the recovery of the cargo and spacecraft. Of key importance to the EOS design is the formulation of abort options and the definition of feasible abort envelopes. In the present study, these key questions were addressed by assessing the feasibility of an abort option referred to as the subsonic cruise mode. Subsonic cruise is an abort mode considered for the orbiter which utilizes the "go-around" hydrogen airbreather propulsion system and residual boost fuel to cruise back to the launch or emergency landing site.

The basic approach taken in the conduct of this study was to assess the capability of an existing vehicle design (Phase A) to perform the abort mission. Vehicle modifications were held to a minimum in order that maximum advantage of existing EOS design effort with attendant design depth could be utilized. Assumptions inherent in the above approaches include the following: (1) a vehicle basically designed to perform the baseline STS mission; (2) a normal ascent trajectory performance unperturbed for abort; (3) a return to the launch site launch site as the basic success goal. In reference to the latter assumption, landing at downrange emergency sites is a valid possibility; however, this contingency was left for future studies because of the added scope.

## OBJECTIVES AND APPROACH

### ● OBJECTIVES

- / ESTABLISH FEASIBILITY OF HYDROGEN-FUELED AERO-PROPULSION POWERED INTACT ABORT MODE
- / ASSESS IMPACT ON ORBITER DESIGN AND SYSTEM CHARACTERISTICS

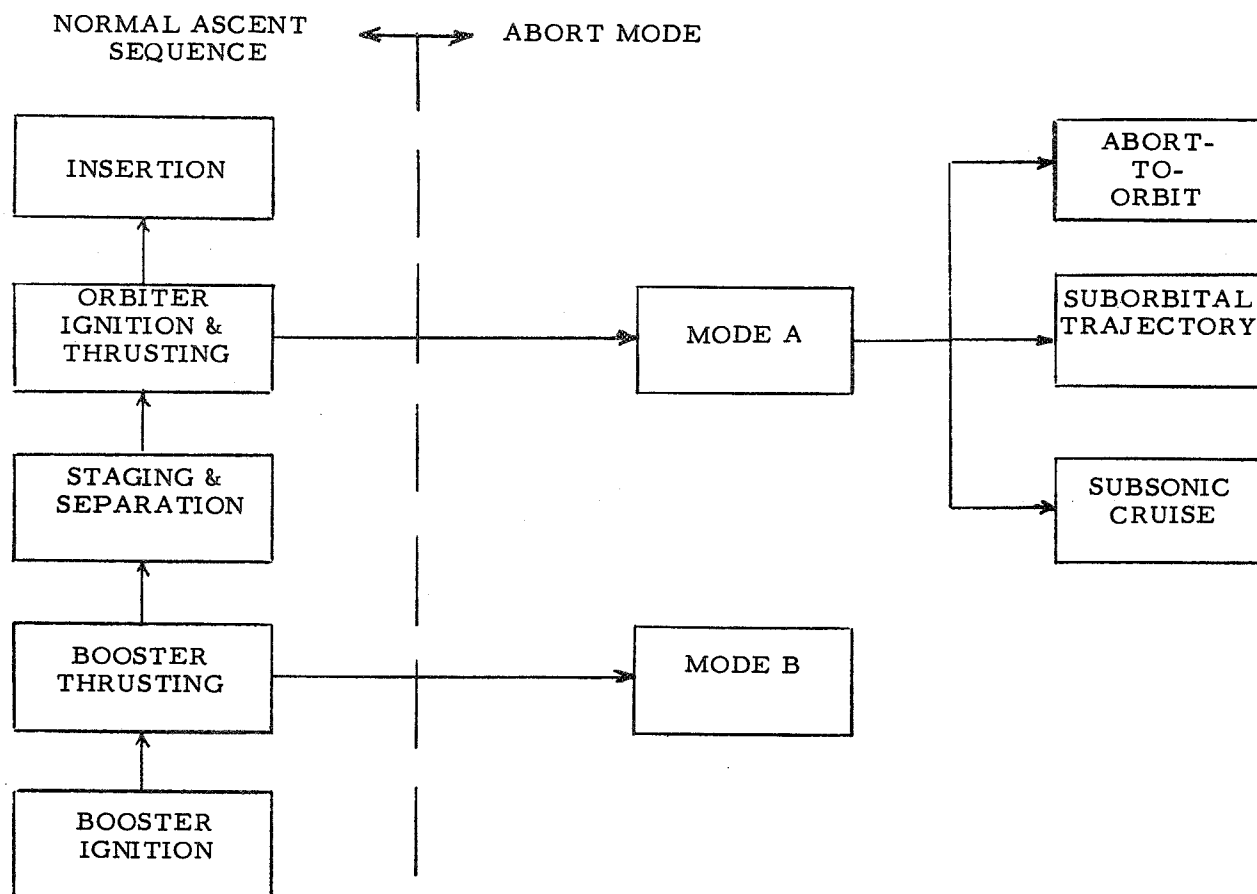
### ● APPROACH

- / SELECTED LMSC ILRV ORBITER
- / ESTABLISHED DESIGN ASSUMPTIONS
  - NORMAL ASCENT TRAJECTORY - UNPERTURBED
  - AERO-PROPULSION ENGINES - 100,000 LB THRUST, H<sub>2</sub> CONVERSION
  - NORMAL LOAD FACTOR LIMIT - 2.5 G
  - LOWER SURFACE TEMPERATURE LIMIT - 2200<sup>0</sup>F
- / DEFINED ABORT MODE ASSUMPTIONS - ORBITER PHASE ONLY
- / DEFINED CRITICAL AREAS FOR ESTABLISHING FEASIBILITY

## ASCENT ABORT MODES

Subsonic cruise mode is available during the critical ascent phase of flight and is but one option in the total abort spectrum. Basically, two classes of abort modes for the orbiter exist during the ascent flight. The first class, designated as Mode A, involves an abort dictated by a major failure during the orbiter vehicle engine ignition and thrusting mode. The second abort class, designated as Mode B, involves an orbiter abort owing to a booster malfunction. This study is mainly concerned with Mode A type abort sequences and in particular with the relative feasibility of the subsonic cruise option. The preferred mode of the three indicated options are functions of the failure mode, abort performance capability and the operational features.

## ASCENT ABORT MODES



## FINDINGS - I

An orbiter vehicle abort by the subsonic cruise mode involves the performance of two basic flight phases following thrust termination; emergency reentry and subsonic cruise. The system feasibility analysis is separated into these two major sections. The reentry phase involves the ability to decelerate safely and reduce altitude without exceeding the environmental limits imposed by the vehicle design. The second phase concerns the acquisition of range by subsonic cruise in order to land at the launch site, preferably, or at an alternate downrange landing site. Within the above two flight phases, eight specific areas were investigated for system criticality.



## FINDINGS - I

- CRITICAL FEASIBILITY AREAS

- / REENTRY

- MASS PROPERTIES ANALYSIS
    - EXCESS FUEL DISPOSAL
    - AERODYNAMIC STABILITY AND CONTROL
    - TRAJECTORY ANALYSIS
    - HEATING CONSTRAINTS

- / SUBSONIC CRUISE

- AERODYNAMIC STABILITY AND CONTROL
    - CRUISE PERFORMANCE
    - HYDROGEN ENGINE PERFORMANCE

## FINDINGS - II

Study findings in each of the critical areas indicate feasibility of conducting the subsonic cruise mode. Previewed here are the major results peculiar to the vehicle configuration utilized in this study. In the assessment of feasibility, conservative criteria were utilized in critical areas such as propellant disposal and TPS temperature predictions. In other areas showing marginal performance, less stringent criteria were used because performance improvement options were readily available. Overall, the system penalties for accommodating this mode are considered to be nominal and occur in the areas of propellant disposal and airbreather modifications. Abort performance is shown to be possible over portions of the abort spectrum with major constraints being the TPS temperature limit and cruiseback range limit.

## FINDINGS - II

### ● PROPELLANT DISPOSAL FEASIBLE

- / EXTENDED REENTRY FLIGHT TIMES > 400 SEC
- / 35 PSIA PRESSURIZATION OF TANKS ADEQUATE FOR DUMPING
- / DUMP RATE REQUIREMENTS FUNCTION OF HAZARDS CRITERIA
- / SERIES DUMP OF LH<sub>2</sub> AND LOX APPEARS NON CRITICAL

### ● REENTRY FLIGHT FEASIBLE

- / MAX C.G. VARIATION FROM  $.687 \leq X/L \leq .759$
- / ADEQUATE HYPERSONIC STABILITY AND CONTROL
- / MAX NORMAL LOAD FACTOR MAINTAINED AT 2.5 G
- / HEAT SHIELD TEMPERATURE LIMIT PRIMARY CONSTRAINT

### ● CRUISE BACK FLIGHT FEASIBLE

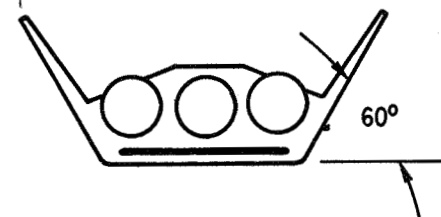
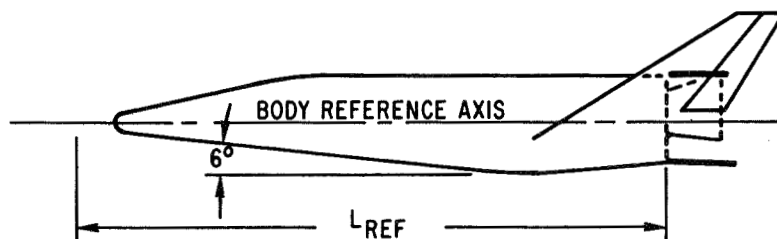
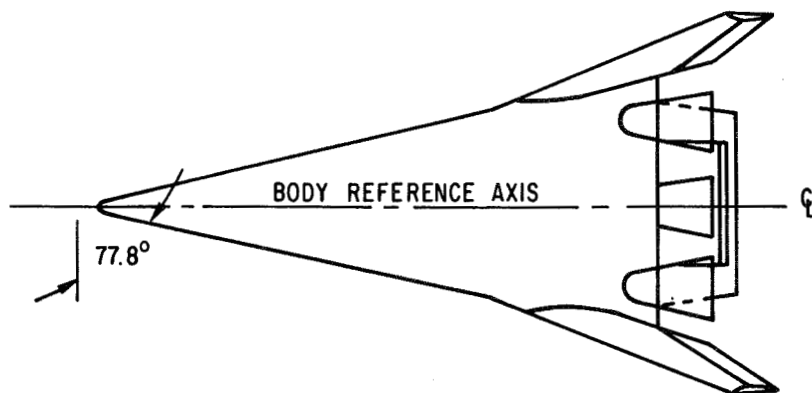
- / SUBSONIC AERO STABILITY AND CONTROL ADEQUATE
- / ADEQUATE CRUISE THRUST WITH "GO-AROUND" SYSTEM
- / PLANFORM LOADING RESTRICTED TO  $W/S \leq 56$  PSF
- / MAX ABORT CRUISE BACK RANGE - 900 N MI

## SPACECRAFT CONFIGURATION - LMSC ILRV

The configuration selected for analysis was an ILRV orbiter vehicle designed by Lockheed Missile and Space Company (LMSC). Configuration design and aerodynamic characteristics of this delta planform vehicle were investigated in the Shuttle Phase A studies. The vehicle choice was based upon configuration maturity and performance validation provided by extensive wind tunnel testing. A subsonic lift-to-drag ratio of 4.7 provides a conservative cruise performance which assures that the study results are not biased toward achieving feasibility. A basic design characteristic unique to the LMSC vehicle which enhanced the study was the multiple cryogenic tankage arrangement. This design, as well as the three rocket engines, were retained in the study vehicle. The primary vehicle modification was the substitution of hydrogen aero-propulsion engines for four JP-fueled airbreathers. This substitution was conducted with a minimum of changes to the vehicle performance.

# SPACECRAFT CONFIGURATION

## LMSC ILRV



## PROFILE OF ABORT TRAJECTORIES

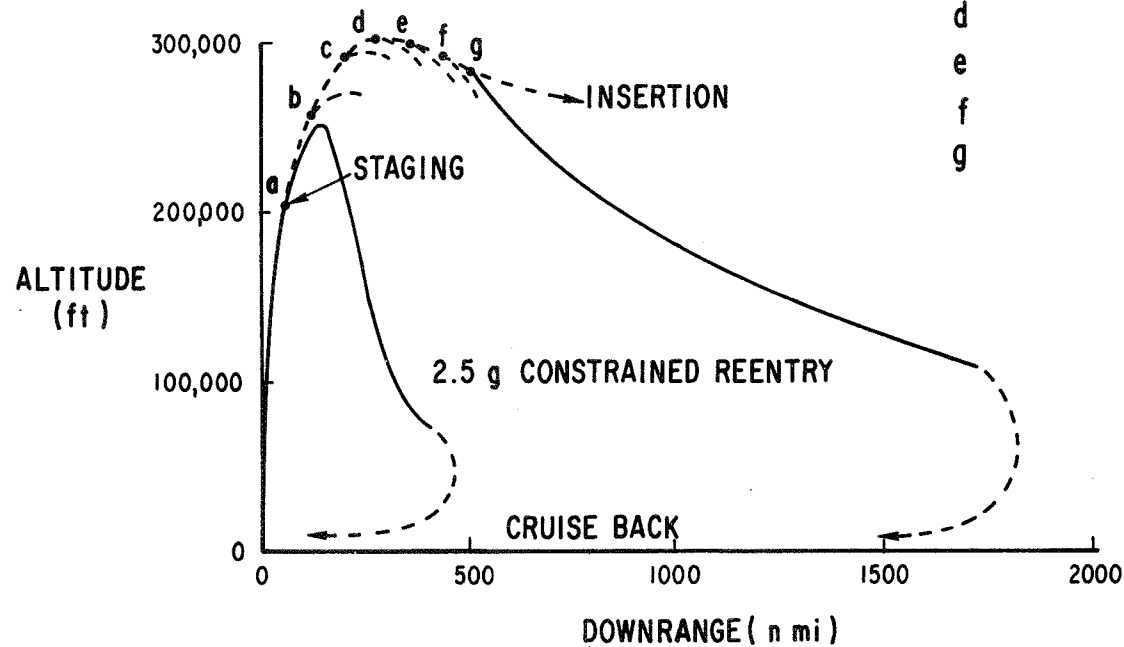
The reentry trajectory environments define the system requirements and characteristics necessary to satisfy the concept of intact abort. The primary considerations in the generation of the abort reentry trajectories were to avoid exceeding the 2.5 g limit on normal load factor, maximize the flight time available for the disposal of excess propellants and minimize the downrange flight distance for which cruiseback range capability is required. An analysis of the resulting environments was performed to assess the effects of propellant disposal rate and velocity at abort initiation on the downrange distance and on the peak heating on the vehicle lower surface centerline.

The normal ascent trajectory profile consists of booster operation to staging at an altitude of 206,000 feet and a velocity of 8844 feet per second, and then orbiter operation to orbit insertion. Points of malfunction were considered during the orbiter portion of the ascent trajectory, beginning at the staging point, and at velocities with increments of approximately 2000 feet per second from this point to 20,032 feet per second.

# 

### 

POINTS	ABORT VELOCITY fps
a	8,844
b	10,131
c	12,096
d	14,141
e	16,170
f	18,085
g	20,032



### CRUISE RANGE REQUIREMENTS

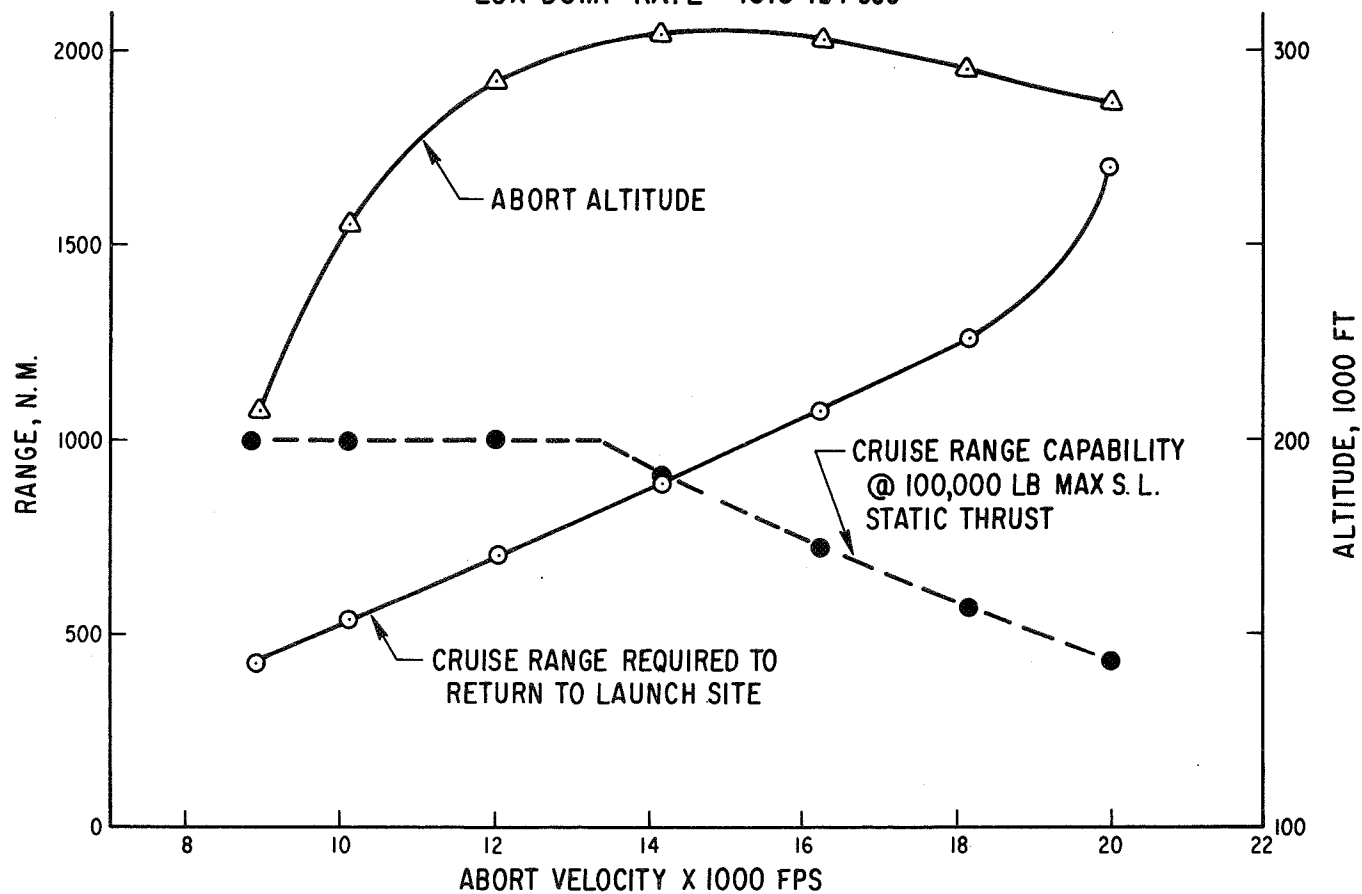
Cruise range requirements and capabilities were found to be related to flight conditions at initiation of the abort maneuver. With increasing abort velocity, the required cruiseback range increases; however, the capability for cruiseback decreases because less boost fuel is available for cruise. The range capability is constant at low abort velocities because the fuel load was restricted by a planform loading limit ( $W/S = 56$  psf), corresponding to the maximum cruise weight.

Maximum cruise performance is attained for an abort initiated at a velocity of 14,000 fps, where the cruise range required for return to launch site and the cruise range capability are both 900 n mi. For abort sequences with an initial velocity above 14,000 fps, the cruise range capability is insufficient for return to the launch site and a landing at a downrange site is necessary.



# CRUISE RANGE REQUIREMENTS

$N_K = 2.5 \text{ G's}$   
 LOX DUMP RATE = 1513 lb/sec



## PROPELLANT DISPOSAL REQUIREMENT

A high capacity propellant disposal system is critical to the subsonic cruise abort mode because of the planform loading limitations for subsonic flight and the potential hazards associated with fuel disposal. In order to assess the first level feasibility of such a system, the weight and hazards for a system to accomplish excess propellant disposal were evaluated. The propellant disposal system is sized by an abort at staging because of the full propellant load and corresponding minimum reentry time for propellant disposal. For this particular abort sequence, all of the LOX (617,000 lb) and 33,000 lb of the 88,000 lb of LH<sub>2</sub> are required to be jettisoned in 400 seconds as determined by the reentry analysis.

Disposal requirements are dependent upon the hazards criteria considered for operational use. Three were considered here with various dump sequences and altitudes for completing LH<sub>2</sub> dump. For the most liberal and conservative criteria, I and II respectively, the pressurization system weights were found to be nominal. Weight of dump valves and accessories must be added to obtain the total disposal system weight.

## PROPELLANT DISPOSAL REQUIREMENT\*

HAZARDS CRITERIA			DISPOSAL REQUIREMENTS		
CATEGORY	PROPELLANT DUMP SEQUENCE	ALTITUDE FOR COMPLETION OF LH <sub>2</sub> DUMP, KFT.	LH <sub>2</sub> RATE LB/SEC	LO <sub>2</sub> RATE LB/SEC	EST. SYSTEM** WT LB
I	SIMULTANEOUS	80	100	1513	200
II	SIMULTANEOUS	150	>223	1513	-
III	SERIES WITH LH <sub>2</sub> FIRST	150	>223	>2470	200

\* REQUIREMENTS FOR ABORT AT STAGING

/ 617,000 LB OF LO<sub>2</sub>

/ A MINIMUM OF 33,500 LB OF LH<sub>2</sub>

\*\*PRESSURIZATION SYSTEM WEIGHT ONLY; DOES NOT INCLUDE DUMP VALVE WEIGHTS

## EXCESS FUEL DISPOSAL - CANDIDATE PRESSURIZATION SYSTEMS

The propellant disposal system operates in the absence of engine operation to pressurize the main propellant tanks and dispose of propellant through large dump valves. Four candidate pressurization systems were examined for the conditions of hazards criteria category I.

For the evaluation of candidate excess propellant disposal systems, the following conditions were assumed:

1. After separation, orbiter vehicle acceleration is sufficient to provide propellant settling.
2. The propellant tanks are pressurized to 35 psia.
3. One oxidizer feed line valve, with an eight-inch diameter opening, is opened for LOX disposal and one fuel feed line valve, with a four-inch diameter opening, is opened for LH<sub>2</sub> disposal. The corresponding LOX and LH<sub>2</sub> feed lines to the engine are 11 and 5 inches in diameter, respectively.
4. The propellant line pressure drops are 3 psi and 5 psi, respectively, for LOX and LH<sub>2</sub> flow.
5. Engines are not used for excess propellant disposal.

# EXCESS FUEL DISPOSAL - CANDIDATE PRESSURIZATION SYSTEMS\*

SYSTEM	PRESSURANT	TEMPERATURE	STORAGE TANKS	SPECIAL REQUIREMENTS	EST. SYSTEM** WEIGHT, LB
A	COLD He @ 4000 PSIA	170 <sup>0</sup> R	ALUM., 8.1' DIA INSIDE LOX TANK @ 170 <sup>0</sup> R	LARGE VOLUME	7000
B	HEATED He @ 3000 PSIA	100 <sup>0</sup> F	TIT., 4.2' DIA INSIDE LH <sub>2</sub> TANK @ 38 <sup>0</sup> R	HEATED TO 100 <sup>0</sup> F BY GAS GENERATOR RUN BY GOX & GH <sub>2</sub> FROM RCS ACCUMULATOR	870
C	GOX & GH <sub>2</sub>	GOX @ 300 <sup>0</sup> F GH <sub>2</sub> @ 200 <sup>0</sup> F	RCS ACCUMULATOR	RCS SYSTEM CAPABILITY DOUBLED TO PROVIDE HIGH FLOW RATES	100
D	GOX & GH <sub>2</sub>	GOX @ 300 <sup>0</sup> F GH <sub>2</sub> @ 200 <sup>0</sup> F	MAIN LH <sub>2</sub> AND LOX	TURBOPUMP AND HEAT EXCHANGER POWERED BY RCS FED GAS GENERATOR	200

\* LOX RATE OF 1513 LB/ SEC

LH<sub>2</sub> RATE OF 100 LB/ SC

\*\* DOES NOT INCLUDE DUMP VALVE WEIGHTS

## HAZARDS OF FUEL DUMP

The hazards of disposing  $\text{LH}_2$  into the flow field and wake of a reentry vehicle are difficult to assess owing to processes which are complex and highly probabilistic. Because of these difficulties, only a cursory analysis was attempted in this study to establish a non-critical case for assessing feasibility.

The conditions (Category III) chosen for investigation of a non-critical case was the dumping of  $\text{LH}_2$  alone into the vehicle wake. Worst case trajectory conditions representative of an abort initiated at staging were utilized. With the  $\text{LH}_2$  dump sequence initiated above 200 K ft and completed before descending to 150 K ft, it was determined that the mass flow of atmospheric oxygen intercepted by the orbiter flow field is only sufficient to react (if possible) with a few percent of the jettisoned  $\text{LH}_2$ . The possibility of immediate ignition is suppressed because of the cooling effect of the expanding cryogenic fuel, lag time to achieve a mixture, and a restriction on reaction rates because of the low pressure environment at these high altitudes. Another inhibitor would be the possible formation of solid particles rather than  $\text{GH}_2$  with the expansion of cryogenic fuel. Under this type of an environment, it is postulated that even with ignition burning will probably be limited to the periphery of the vehicle wake. The effect on the vehicle will be radiative heating rather than convective heating that would result from large-scale base burning. The magnitude of this radiative heating is expected to be negligible.

Assessment of hazards criteria I and II is recommended for follow-on studies in order to reduce the disposal requirements.

## HAZARDS OF FUEL DUMP

- CATEGORY III CRITERIA CONSIDERED NONCRITICAL
  - / CONSERVATIVE REQUIREMENTS - HIGH ALTITUDE LH<sub>2</sub> DUMP ALONE
  - / FACTORS WHICH CAN SUPPRESS IGNITION AND BURNING
    - COOLING FROM EXPANSION OF LH<sub>2</sub>
    - FINITE MIXING TIME
    - LOW AMBIENT OXYGEN DENSITY AND PRESSURE
    - LACK OF IGNITER SOURCE (HIGH TEMPERATURE FLOW FIELD OR TPS?)
  - / NEGLIGIBLE HEATING EVEN IF BURNING OCCURS
    - BURNING LIMITED TO ONLY A FEW PERCENT OF AVAILABLE H<sub>2</sub>
    - RADIATION FROM PERIPHERY OF WAKE FLOW FIELD
- ASSESSMENT OF CATEGORY I AND II SHOULD BE FOLLOW-ON EFFORT
  - / SUFFICIENT OXYGEN AVAILABLE BUT IGNITION NOT CERTAIN
  - / CONVECTIVE BASE BURNING POSSIBLE

## MASS PROPERTIES ANALYSIS

The effects of abnormal depletion of the propellants on the center of gravity of the vehicle were investigated for the following two conditions:

### Case I

Abort is initiated at staging with full propellant loads. LOX and LH<sub>2</sub> are dumped until 21,500 lb of LH<sub>2</sub> remain onboard to meet the cruiseback requirement.

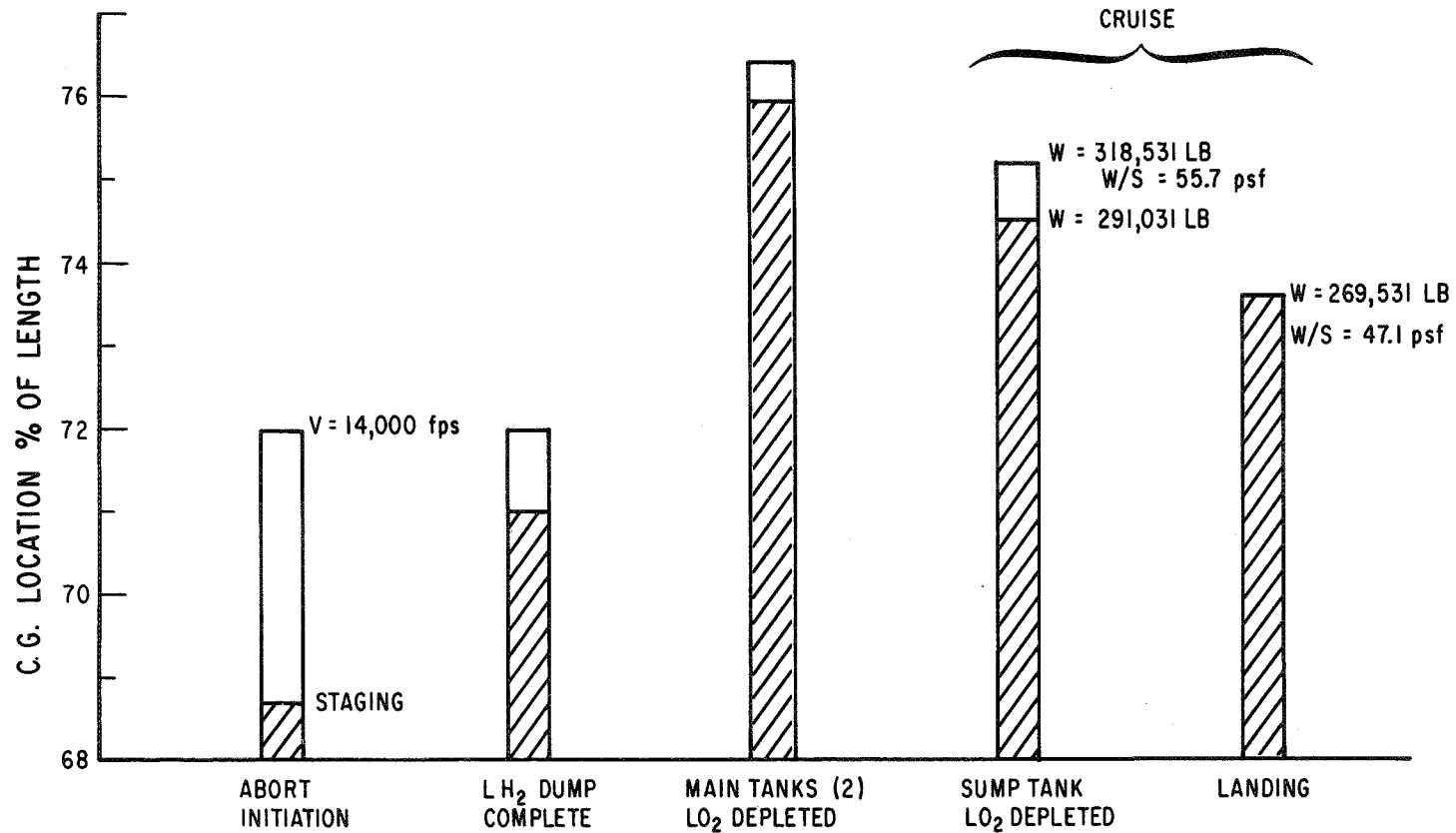
### Case II

Abort is initiated at approximately 14,000 fps where all of the remaining LH<sub>2</sub> is required for cruiseback and only LOX is dumped. LH<sub>2</sub> available for cruiseback = 49,000 lb.

Center of gravity excursions were examined for a given disposal sequence of propellants. The most forward c.g. location is 68.7 percent of the vehicle length and occurs at separation, while the most aft is at 76 percent of the length and occurs after the main LOX tanks are depleted.



# MASS PROPERTIES ANALYSIS



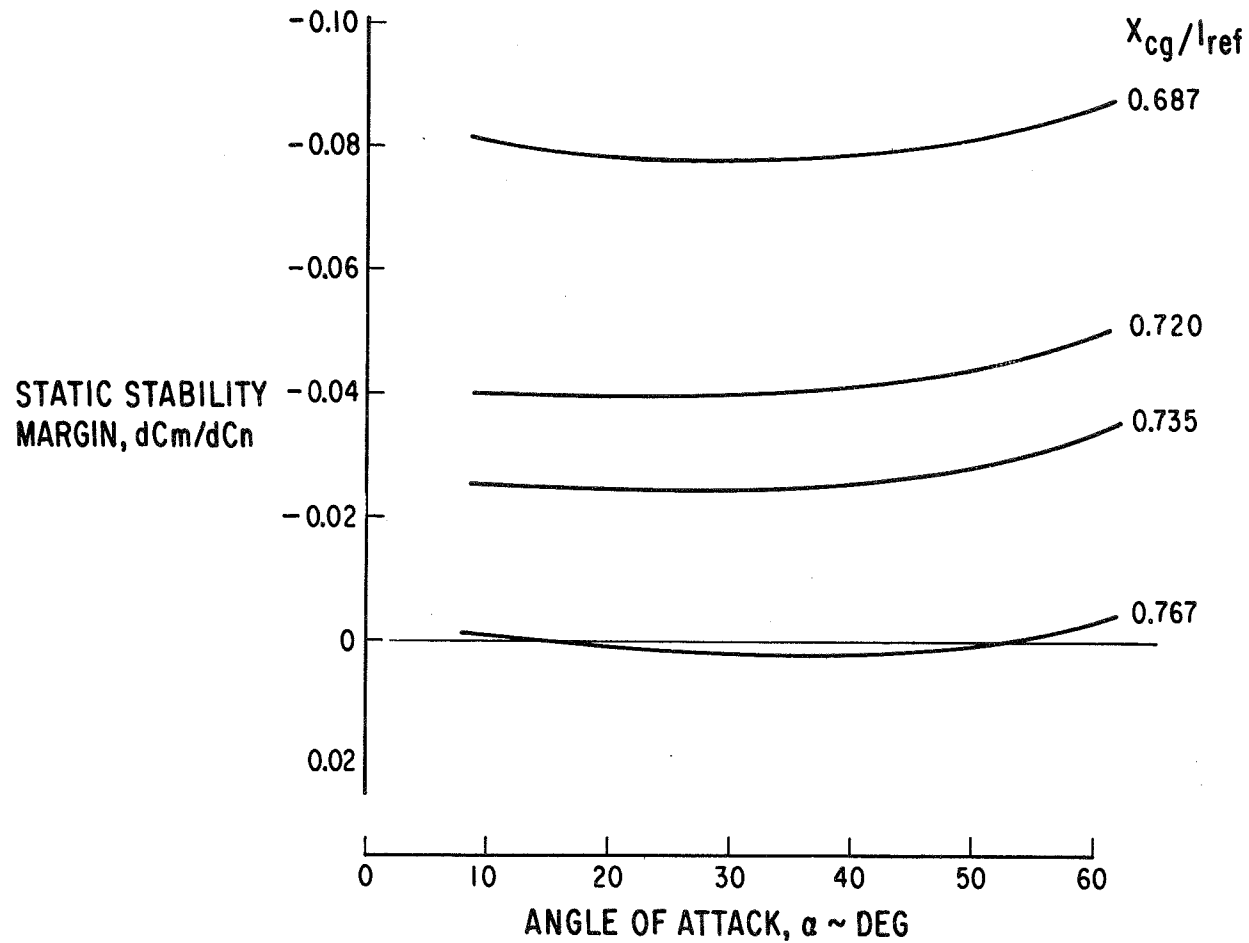
### HYPERSONIC STATIC STABILITY MARGIN

The availability of adequate stability and control during the reentry trajectories was examined for the range of c. g. locations resulting from excess propellant disposal. Static stability was utilized in the analysis for indicating feasibility. This assessment should have a high degree of validity because the aerodynamic characteristics for the study vehicle are based on data obtained from an extensive wind tunnel test program conducted for the Phase A configuration.

For hypersonic flight, the configuration was found statically stable for all c. g. positions except the aft-most position where it is neutrally stable. The vehicle is also capable of trimming to any angle of attack from  $(L/D)_{\max}$  to  $C_{L_{\max}}$  over the operational c. g. range.

In the subsonic flight regime, the configuration is statically stable at all c. g. positions except for the aft-most location at an angle of attack of 30 degrees where neutral stability is displayed. Control capability exists for trimming at the angle of attack for the critical cruise parameter for all design c. g. positions.

## HYPERSONIC STATIC STABILITY MARGIN

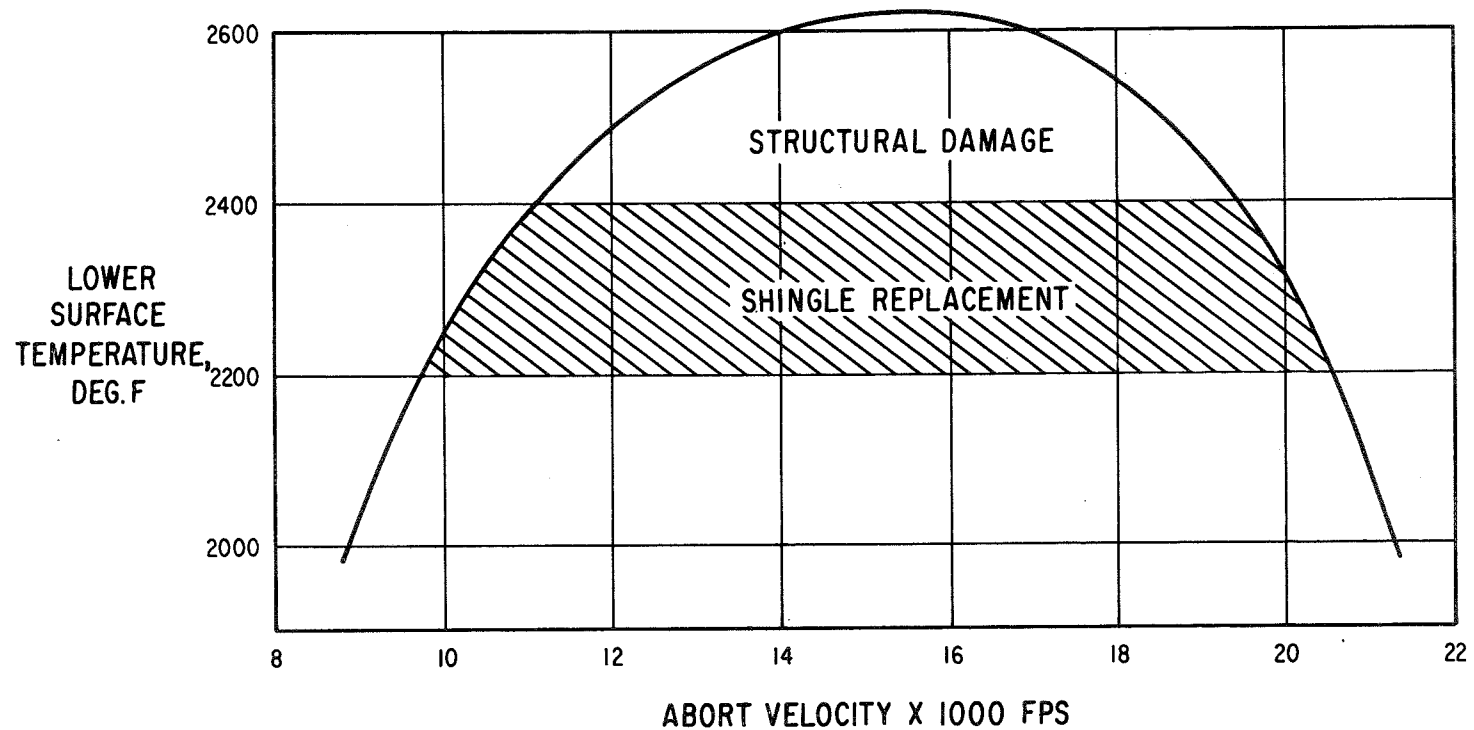


## TEMPERATURE/VELOCITY ABORT CONSTRAINTS

The peak temperature of the TPS panels on the lower surface of the orbiter vehicle was selected as the governing aerodynamic heating constraint for the abort sequence atmospheric reentry thermal analyses. The primary TPS material for this area is TD-NiCr and the alternate material is coated columbium. The parameters whose effects were investigated in the thermal analyses were planform loading - as influenced by the LOX disposal rate - and the altitude and velocity at the point on the ascent trajectory where the abort sequence was initiated. The minimum LOX dump rate of 1513 pounds per second was used as a baseline condition.

The peak lower surface temperature encountered during abort reentry was found to be a function of the relative velocity at abort initiation. Temperatures are the peak temperatures along the vehicle lower surface centerline. Reuse thermal limits for TD NiCr panels constrain the abort performance to reentries with peak temperatures below 2200°F. Major refurbishment would be required for higher temperatures up to 2400°F. Above this limit TPS failure and basic structures damage are most likely. With the alternate TPS material, coated columbium, abort performance is expanded significantly. Temperature limits of 2400°F for reuse and 2700°F for replacement after an abort could eliminate the performance constraint.

# TEMPERATURE / VELOCITY ABORT CONSTRAINTS (TD Ni Cr PANELS)

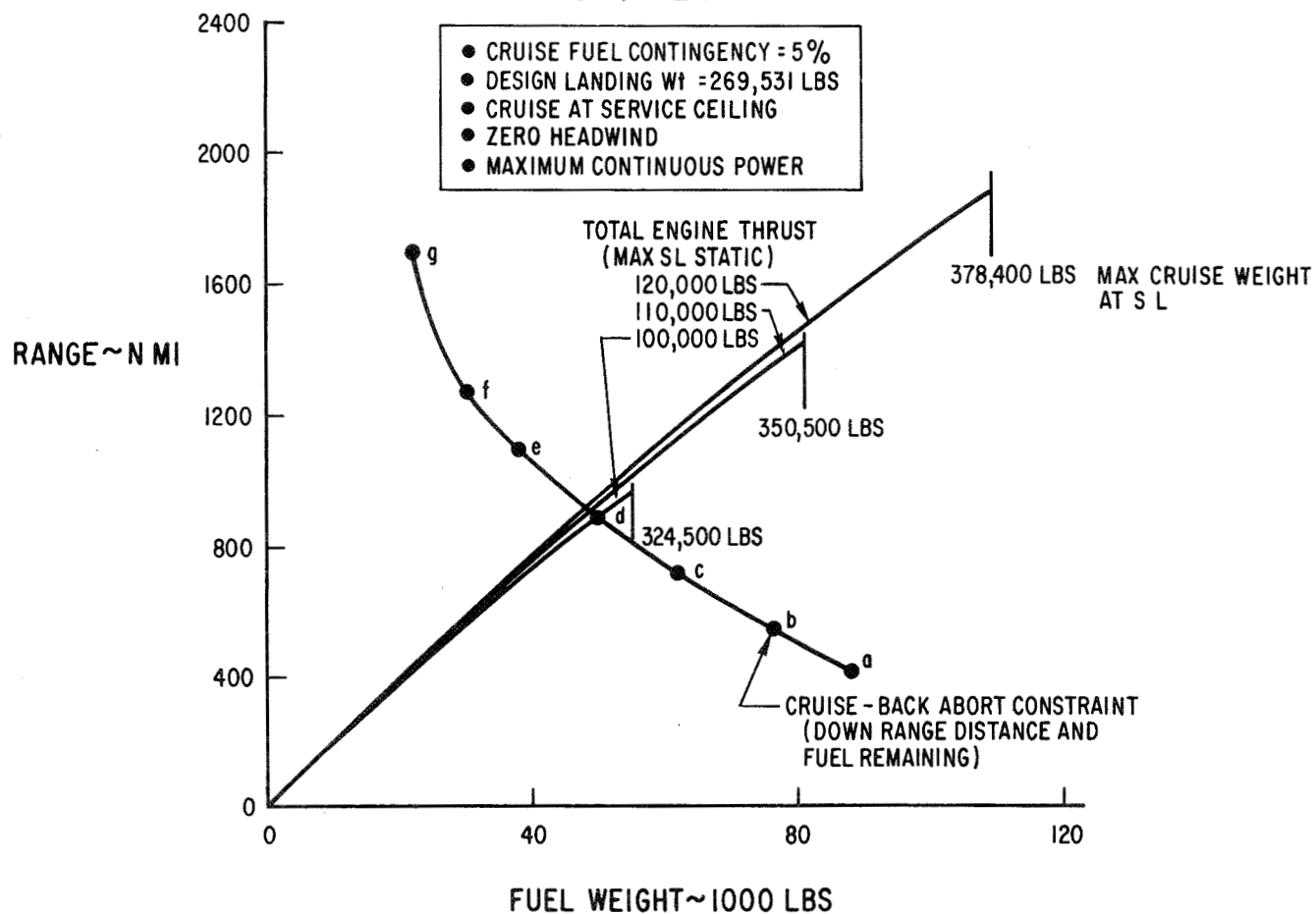


## CRUISE PERFORMANCE - BASIC VEHICLE

The cruise capability of the LMSC orbiter vehicle with c. g. at  $0.72l_{ref}$  and powered by hydrogen burning turbojet engines was evaluated using estimated engine characteristics. The cruise was performed at the  $C_{LTrim}$  corresponding to the maximum value of nautical miles per pound of fuel,  $(n \text{ mi/lb})_{max}$ , and at the altitude corresponding to the service ceiling of the vehicle.

The basic vehicle range performance with a total engine thrust of 100,000 lb (max S. L. static) is limited only by the maximum fuel load at maximum cruise weight. Determination of the maximum downrange distance from which the orbiter vehicle can return to the launch site using subsonic cruise, however, requires a simultaneous solution of the fuel on-board at abort initiation and the fuel required for the return to the launch site. This solution indicates a maximum downrange recovery and cruiseback distance of 900 n mi utilizing the 49,000 lbs of fuel remaining at abort. This abort, reentry and transition is the governing constraint to subsonic cruiseback range capability improvement, i. e., the 20 percent thrust increase provides a return cruise of only 920 n mi.

# CRUISE PERFORMANCE - BASIC VEHICLE LMSC ORBITER

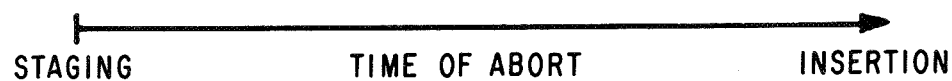


## ORBITER ABORT CAPABILITY ZONES

A comparison of abort performances for two options within mode A is indicated in terms of capability zones. Abort-to-orbit is an option capable of recovery with reuse for aborts initiated at any time during the burn phase. Thus, this should be the preferred mode for failures involving partial loss of thrust resulting from a single engine-out (with a 2 or 3 engine orbiter). Capabilities of the subsonic cruise mode show that an abort is possible with vehicle reuse for the initial 10 percent of the baseline orbiter burn phase. Aborts requiring major refurbishment can increase performance to 20 percent of the orbiter burn phase. The required cruiseback range (to the launch site) for these cases are well within the maximum capability indicated. An upgrading of the lower TPS panel temperature limit to 2400°F by the use of coated columbium (Cb) permits a significant expansion of abort performance. With this material, maximum cruiseback range of 900 n mi (limited by available fuel) becomes the performance constraint when major refurbishment of the TPS is permitted. The range constraint occurs after 44 percent of the orbiter burn phase has been completed. In this study cruiseback to the launch site was considered as the only assured return mode independent of launch site and azimuth. Downrange landing sites do exist; however, their utilization was not examined because of operational complexity.



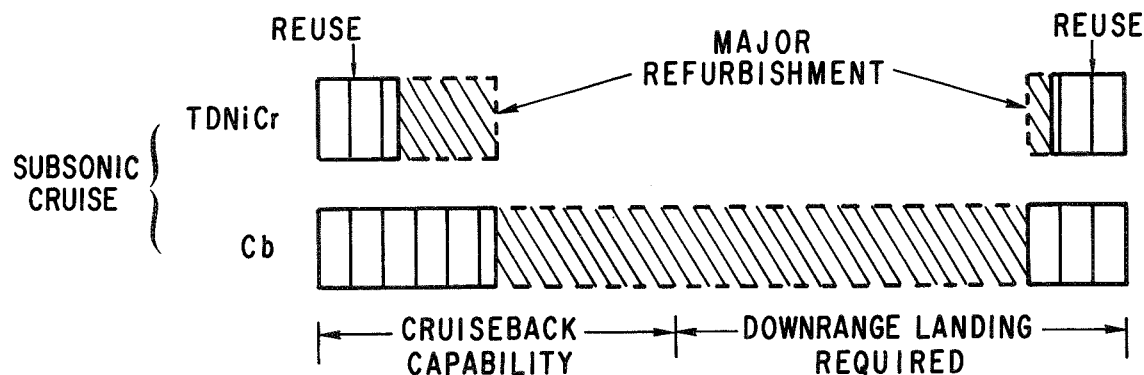
# ORBITER ABORT CAPABILITY ZONES



## ABORT OPTIONS

ABORT-TO-ORBIT

## ABORT CAPABILITIES



## CONCLUSIONS

The findings of this study, compiled from limited investigations conducted in several critical areas, indicate that subsonic cruise is a feasible option for intact abort of an EOS orbiter. A basic requirement is that the vehicle be designed for go-around capability. Performance of critical abort functions, although marginal in some cases, was determined to be possible with nominal system penalties and minor modifications to the configuration selected for study. The over-all intact abort performance of this mode, however, is restricted to a portion of the orbiter ascent trajectory. Significant improvements, however, can be made to the abort performance by a number of additional design and performance modifications. Within its region of performance capability, the subsonic cruise mode is an abort option applicable for a variety of failure modes. It serves as a primary abort mode for the case of total thrust loss and as an alternative to the abort-to-orbit mode for partial loss of thrust. Attractive operational features of immediate reentry, zero crossrange requirement, assured access to the launch site, and compatibility with ferry operations places this abort mode on the list of credible candidates for the EOS.

## CONCLUSIONS

- FEASIBLE OPTIONS EXIST FOR INTACT ABORT OF ORBITER
  - / OPTION AVAILABILITY FUNCTION OF FAILURE MODE AND VELOCITY
  - / SUBSONIC CRUISE (W/O MODS) CONSTRAINED TO LOWER VELOCITIES
- SUBSONIC CRUISE MODE APPLICATION
  - / ALTERNATE OPTION FOR PARTIAL LOSS OF THRUST
  - / PRIMARY MODE FOR FULL LOSS OF THRUST
  - / PROVIDES UNIQUE OPERATIONAL FEATURES FOR OTHER CRITICAL FAILURES
    - IMMEDIATE REENTRY
    - RETURN TO LANDING SITE W/O CROSSRANGE MANEUVER
- POTENTIAL PERFORMANCE IMPROVEMENTS
  - / HIGHER TEMPERATURE HEAT SHIELD
  - / DOWNRANGE LANDING SITE UTILIZATION
  - / ASCENT TRAJECTORY SHAPED TO ABORT CORRIDOR LIMITS
  - / AND OTHERS

## RECOMMENDATIONS

Development of a total intact abort concept is the basic recommendation of this study. One facet of this concept was presented herein, however, many other areas of equal importance remain to be examined. Based upon the understanding acquired in this study and the limitations placed on both the study scope and results, specific endorsements are made for studies arranged in two basic groups. The first group deals with further studies of the subsonic cruise mode in order to assess the impact on EOS design and operations characteristics. The integration of abort modes and causative factors into an overall abort philosophy will require studies of the second group which establish feasibility of other abort options and their priorities.

## RECOMMENDATIONS

- DEVELOP A TOTAL ABORT CONCEPT
- SUBSONIC CRUISE MODE FOLLOW ON STUDIES
  - / PROBLEM AREAS
    - HAZARDS OF SIMULTANEOUS LOX/LH<sub>2</sub> DUMP
    - TRANSONIC STABILITY AND CONTROL
    - CRUISE TERRAIN RESTRICTIONS
  - / POTENTIAL PERFORMANCE IMPROVEMENTS
- SEPARATE INTACT ABORT STUDIES
  - / EXAMINATION OF MODE B ABORTS
  - / FAILURE MODE PROBABILITY ANALYSIS

# SPACE SHUTTLE BOOSTER RETURN PERFORMANCE

by R. A. Bithell and W. A. Pence, Jr.

General Dynamics/Convair

San Diego, California

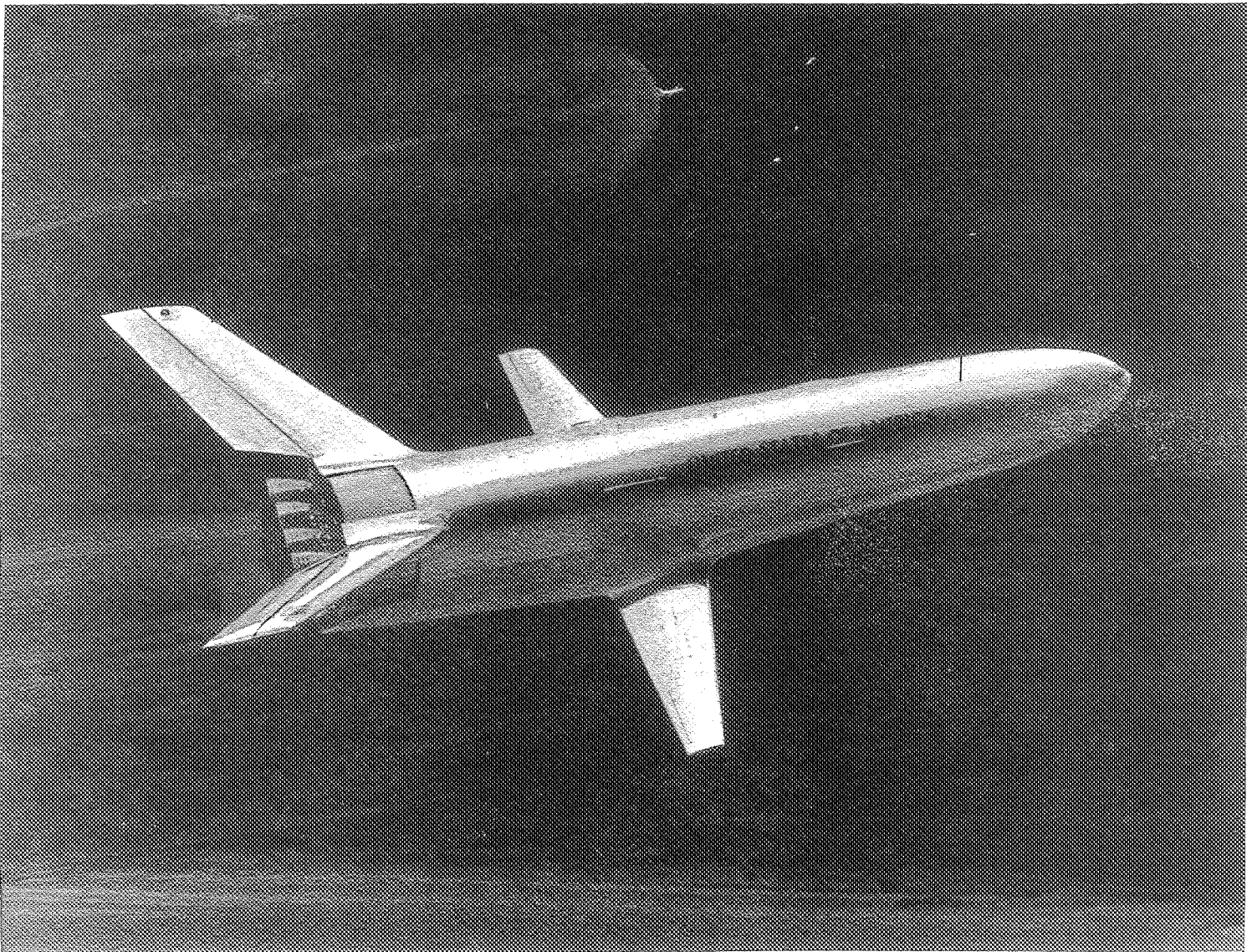
## INTRODUCTION

A design requirement placed on the current shuttle booster is that it must return to the launch site after completing its launch mission. If one considers that the wing, the cruise engines, and the cruise fuel are chargeable to the return function, this represents about 20% of the booster entry weight, or 100,000 lb. If this weight could be reduced by 10%, a 2000 lb increase in the payload could be realized. Thus with these results in mind it is obviously advantageous to minimize the weight associated with the flyback function. To do this, one must understand the booster return performance.

Booster return performance may be divided into two phases, i.e., the booster entry phase and the subsonic phase. In the booster entry phase, the vehicle functions as an unpowered glider and decelerates from hypersonic Mach numbers to subsonic Mach numbers. Performance analysis of this phase is directed primarily towards developing entry maneuvers that minimize flyback range within loading constraints. In the subsonic phase, the booster operates as a large subsonic jet-powered airplane. Performance analysis of this phase includes cruise performance, landing and take-off performance, go-around performance, and ferry performance. This analysis is directed towards defining the best aerodynamic configuration and propulsion system that will meet the various performance goals, including establishing flyback fuel requirements.

## BOOSTER CONFIGURATION

Configuration geometry for a representative Space Shuttle Booster vehicle is presented. Details of the Booster performance in the entry and subsonic phases are based on this configuration.



## BOOSTER RETURN MISSION PROFILE

The booster return mission begins after separation of the booster and the orbiter and terminates after a successful landing at the launch site. A typical booster mission profile is presented. Significant phases and events along this profile are discussed.

The initial conditions are defined by booster performance in the ascent phase and by the separation maneuver. The impulse required for separation imparts a nose down motion to the booster which is overcome by the attitude control system as the booster and orbiter separate. The nose down motion is stopped by the time an angle of attack of  $\alpha = -20^\circ$  is reached. This is assumed to be the point at which booster entry begins.

The nominal initial entry attitude is a sixty degree angle of attack and a roll angle adjusted to minimize flyback range within load factor limitations. Attainment of this attitude is assumed to occur over a time span representative of the control capability of the booster.

Since staging occurs with a positive flight path angle, the booster continues to gain altitude for about one minute until it reaches apogee. Subsequent to this, the booster begins descending into the denser atmosphere, passes the maximum load factor point and initiates the turn back to the launch site at a maximum bank angle of  $75^\circ$ .

By the time the vehicle reaches subsonic velocities, the required heading has been attained, and a subsonic glide at  $(L/D)_{\max}$  is established; this continues until the desired altitude for subsonic cruise is reached. The total time to reach this point is about 10 minutes from the staging point. For the nominal case, the booster is 311 nautical miles from the launch site at this time. The subsonic cruise is conducted at the best cruise conditions taking into account headwinds and the failure of one engine. The required cruise fuel is fixed by 3 engine performance against headwinds. The cruise phase of the mission is by far the longest, requiring approximately 1.75 hours.

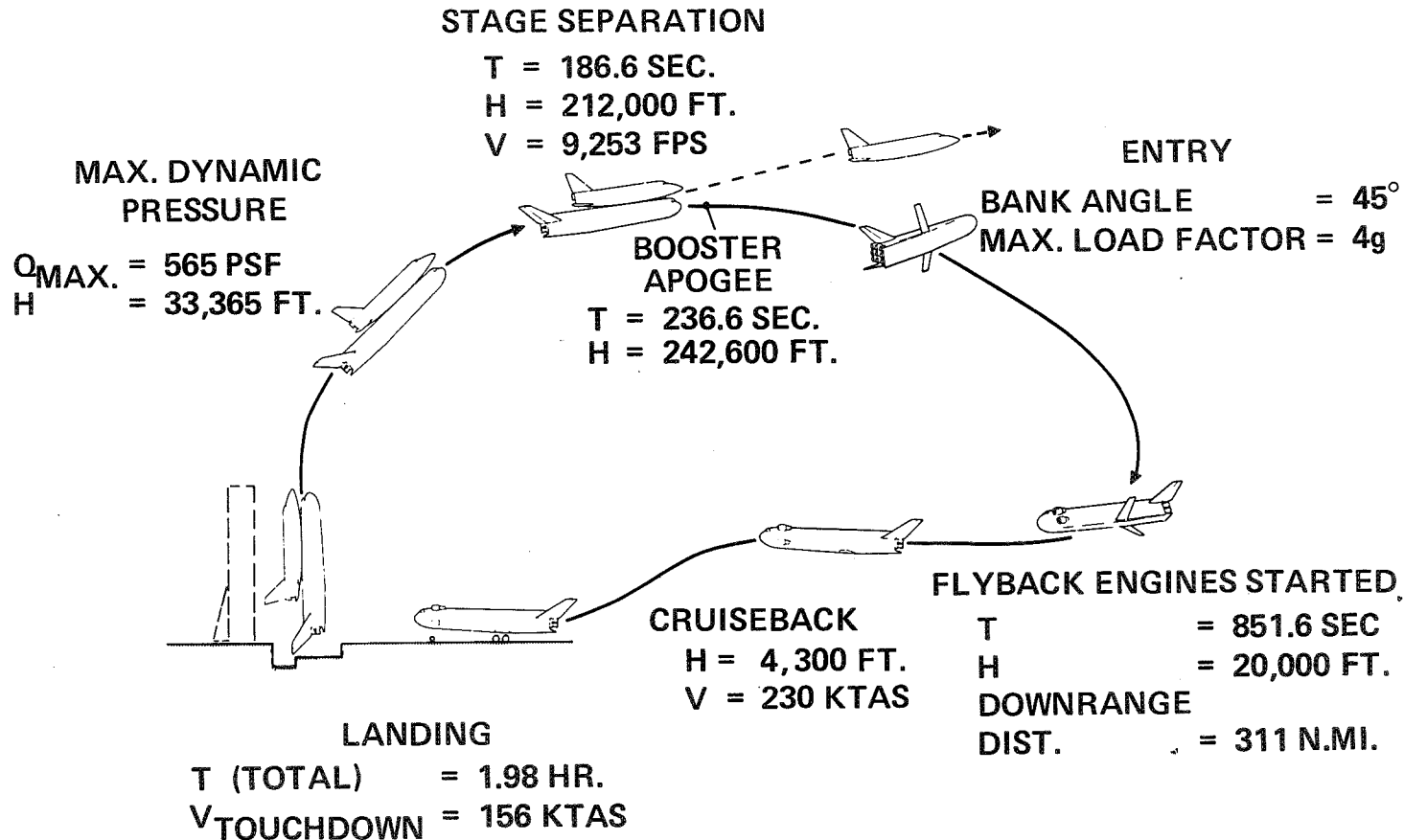
For approach and landing, flaps are deployed at  $45^\circ$ . The vehicle touchdown speed is assumed to be  $1.1 V_{\text{stall}}$  of the unpowered, flapped configuration. For the baseline booster, touchdown is at 156 knots and total landing distance is 8400 ft.

In the event of a waveoff during approach, a go-around maneuver is initiated. The booster must achieve a positive rate of climb to pattern altitude, turn, fly a downwind leg, turn again, and re-intercept the glide path.

As an additional mission, the Space Shuttle Booster must be capable of ferry. The booster performs a conventional take-off, climbs to a suitable cruise altitude, cruises, descends, and lands.



# BOOSTER FLIGHT PROFILE



## BOOSTER ENTRY PERFORMANCE

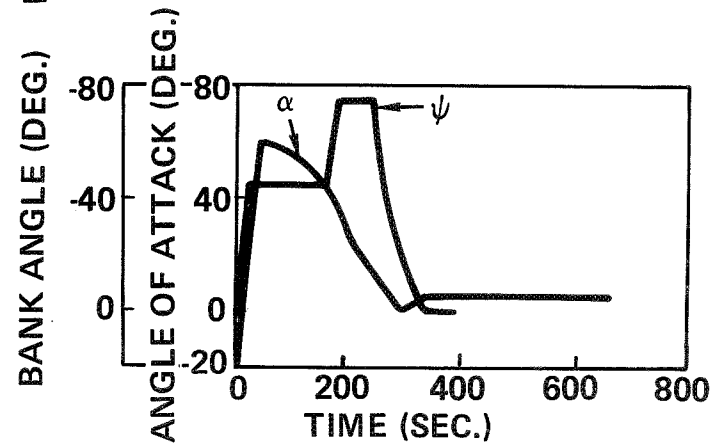
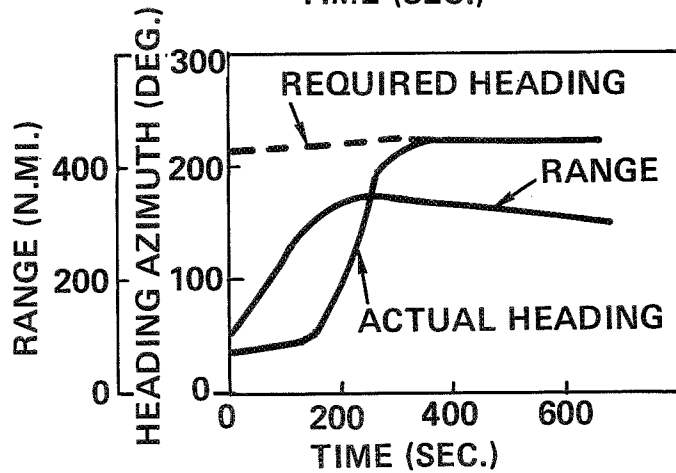
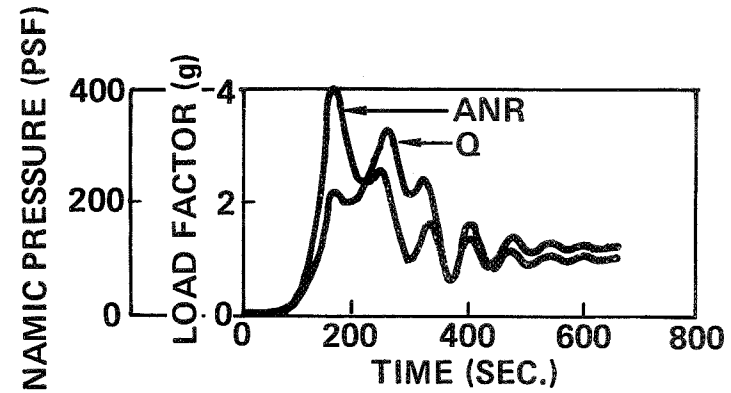
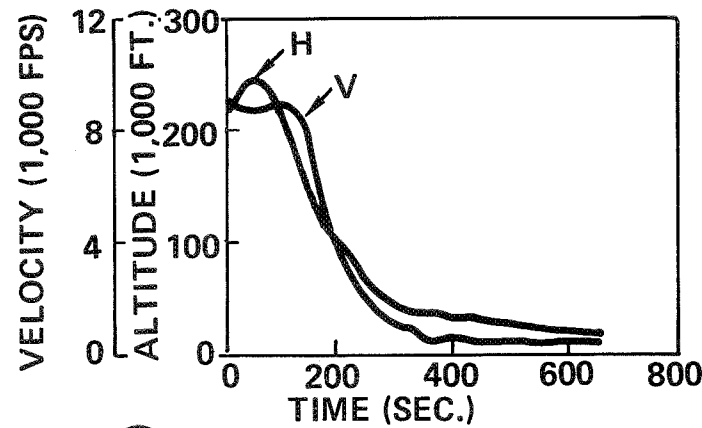
The booster entry phase of the return mission profile spans the time from the end of separation until the cruise engines are started. This phase covers a time span of only 10 minutes, but the booster flyback range is determined in this phase, and the maximum loads are encountered.

Factors influencing booster flyback performance include initial conditions, flyback mode, design constraints, and environmental factors. The important initial conditions are the altitude, velocity, and flight path angle, the plan loading parameter  $W/C_{LS}$ , and the  $L/D$  at the entry attitude. The flyback mode, i.e., the pitch and roll attitude schedule, must be tailored to minimize flyback range within design constraints. The constraints considered herein are a maximum resultant load factor of 4.0 g's, and a dynamic pressure less than that encountered in the boost phase. Environmental factors considered include the atmosphere model and the effect of winds during booster entry.

A nominal booster entry trajectory is presented as a time history of important parameters. This nominal trajectory employs the "gradual pitch transition" mode of entry, which is based on the fact that for a fixed control setting the trim angle of attack of the booster decreases with Mach number.

In the first 40 seconds, the booster attains its entry attitude of  $\alpha = 60^\circ$  and  $\psi = -45^\circ$ . The entry bank angle,  $\psi = -45^\circ$ , is selected so that the maximum entry load factor will not exceed 4.0 g's. The booster continues to gain altitude until its apogee is reached at a time of 50 seconds. After apogee, the booster descends and the dynamic pressure and resultant load factor increase until a maximum of 4 g's is reached at  $t = 160$  seconds. The bank angle is increased at this point to  $75^\circ$  to accelerate the turning. As the vehicle heading azimuth approaches the required heading angle for direct flight to the launch site, the bank angle is reduced to zero. After passing through the transonic region at low angle of attack, a subsonic glide at  $(L/D)_{\max}$  is established. This subsonic glide continues until the cruise altitude is reached and the cruise engines are deployed and started. This ends the booster entry phase at a time of 665 seconds after separation. The distance from the launch site or flyback range at this time is 311 nautical miles, defined as the great circle distance between the end point of the ground trace and the launch site.

# NOMINAL BOOSTER ENTRY TRAJECTORY

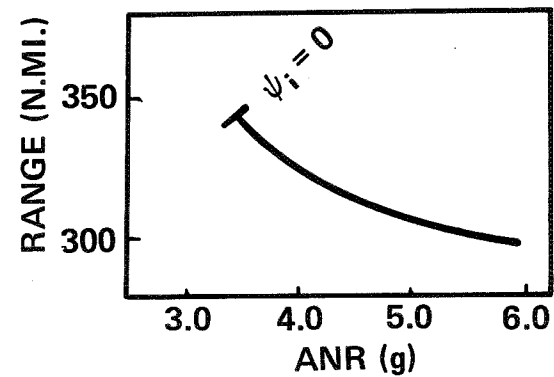
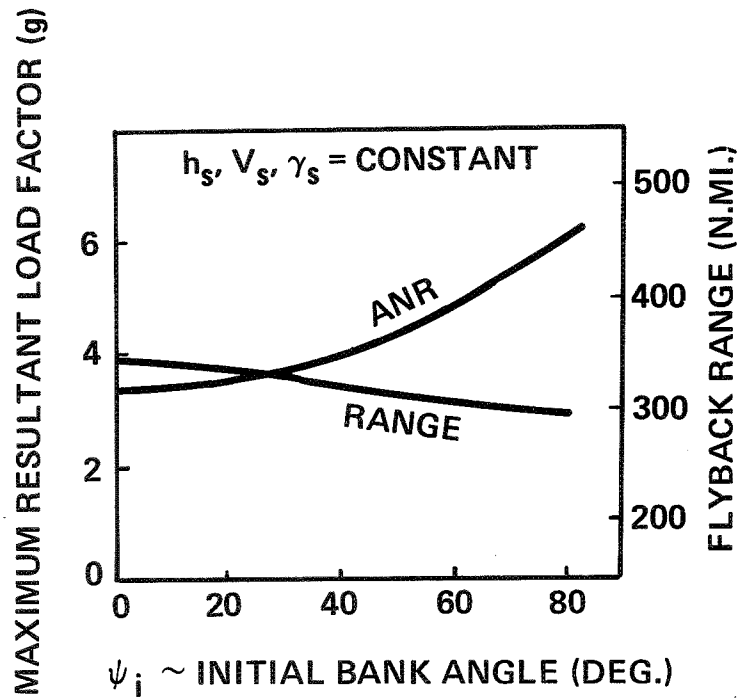


## EFFECT OF LOAD FACTOR ON ENTRY PERFORMANCE

Booster entry trajectories are calculated utilizing a digital computer program that numerically integrates the equations of motion of a point mass flying about a rotating spherical earth. This program utilizes 1962 Standard Atmospheric properties; however, other atmosphere models are available.

Utilizing the digital computer program described, the effect of the resultant load factor on entry performance was determined. This was done by varying the initial bank angle over a range from  $0^\circ$  to  $75^\circ$  for fixed staging conditions. The resulting maximum load factor and flyback range are presented as a function of the initial bank angle. The flyback range for the nominal staging point is also shown as a function of resultant load factor. The minimum load factor occurs for  $\psi_i = 0^\circ$ . The level of this minimum is a direct function of the staging conditions.

# EFFECT OF LOAD FACTOR ON ENTRY PERFORMANCE

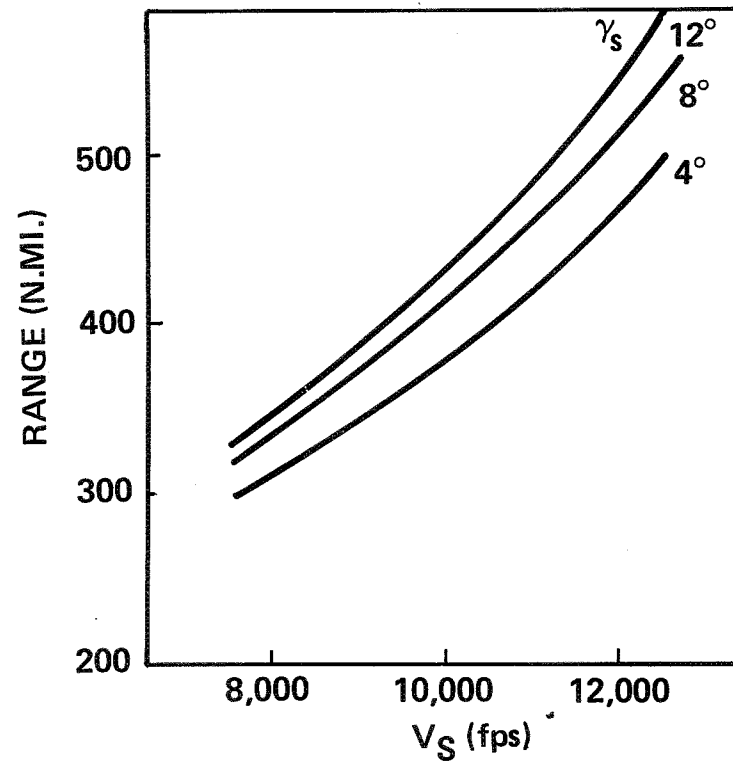
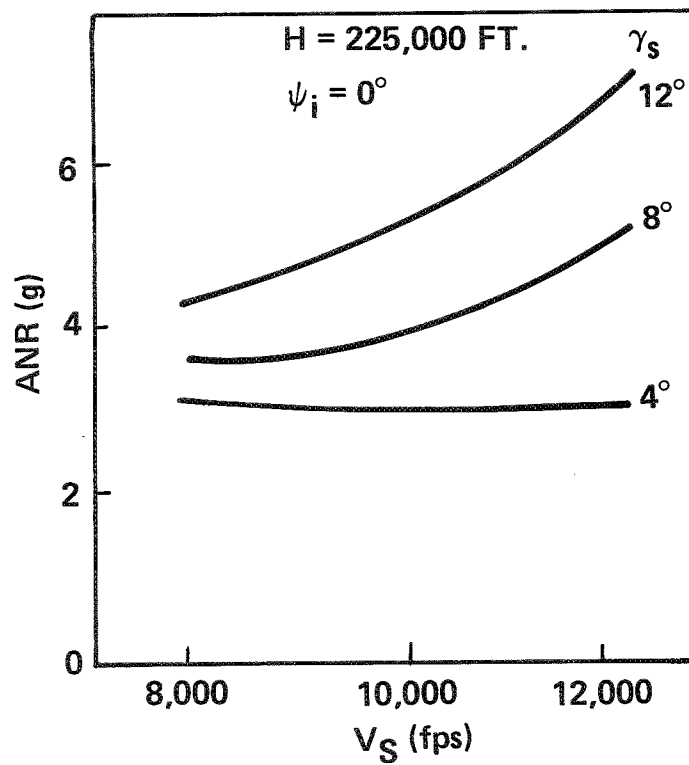


T34-1  
T34-5  
T34-4

## EFFECT OF STAGING CONDITIONS ON ENTRY PERFORMANCE

The effect of staging conditions on entry load factor and flyback range was determined for a range of staging conditions. Typical results are presented for varying staging velocities and flight path angles, at a staging altitude of 225,000 feet. The trajectories calculated from these staging points are similar to the nominal booster entry trajectory, except that they utilize an initial bank angle of zero degrees. These represent minimum load factor trajectories, and from these results load factor constraint on staging conditions can be determined.

## EFFECT OF STAGING CONDITIONS ON ENTRY PERFORMANCE

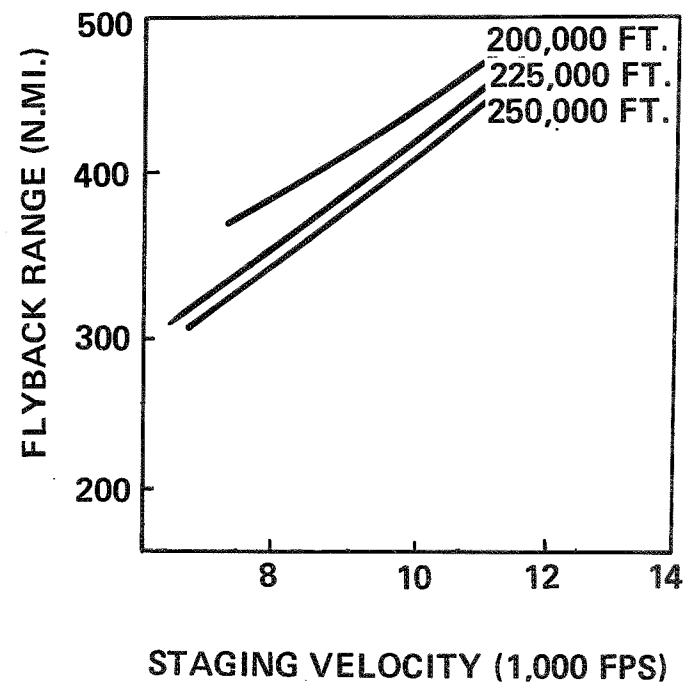
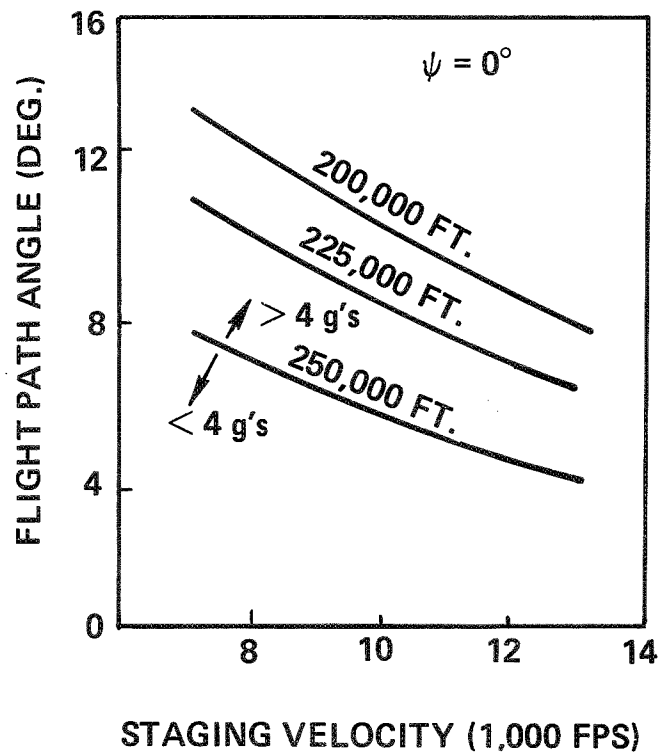


#### 4G LOAD FACTOR CONSTRAINT ON STAGING CONDITIONS

The design constraint on the entry trajectory is a maximum resultant load factor of 4.0 g's. Presented are staging conditions which produce the maximum load factor with no banking. At the altitudes shown, increases in staging flight path angle or velocity will produce load factors in excess of 4 g's. The effect of the 4g constraint on flyback range is also shown.



# 4G LOAD FACTOR CONSTRAINT ON STAGING CONDITIONS

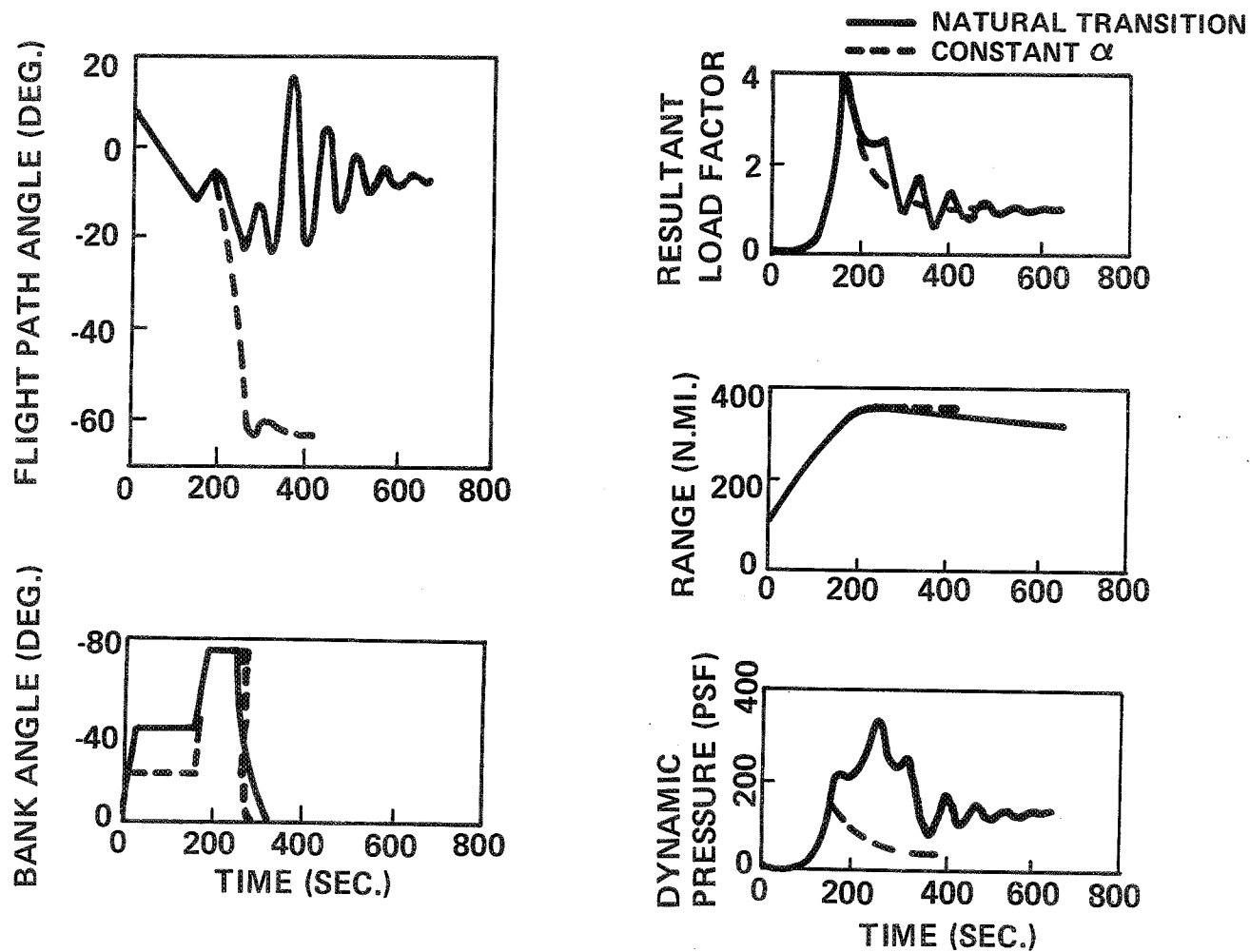


### COMPARISON OF ENTRY MODES

Two modes of booster entry are presented. This comparison contrasts the "natural pitch transition" type of entry with the "constant angle of attack" type. The initial bank angle was adjusted in both cases to give a maximum load factor of 4.0 g's. The trajectories are quite similar until the maximum load factor point at  $t = 160$  seconds is passed. The constant angle of attack case decelerates more rapidly after this time due to its lower  $L/D$ , and reaches a termination altitude at  $t = 415$  sec. The natural pitch transition case terminates at  $t = 655$  seconds. The flight path angles are widely divergent after  $t = 200$  sec. The constant angle of attack case reaches a value of  $-63^\circ$  at termination. The natural pitch transition case, after some oscillation, damps out to a value of  $-7^\circ$ . This large difference is due to the large difference in subsonic  $L/D$ .

The natural pitch transition case exhibits a flyback range about 35 n. mi. less than that for the constant angle of attack case. This is primarily due to subsonic gliding ability with natural pitch transition. The natural pitch transition case encounters a higher dynamic pressure, 335 psf, as opposed to 150 psf for the constant angle of attack case.

## COMPARISON OF ENTRY MODES



## ENVIRONMENTAL FACTORS

The effects of two environmental factors on entry performance have been considered, i. e., the atmosphere model and winds during entry.

The nominal booster entry trajectory was generated utilizing the U.S. Standard Atmosphere, 1962. A similar trajectory was calculated with atmospheric properties taken from a 30° North Latitude, July Supplemental Atmosphere. Two very similar trajectories resulted; however, some differences were noted. At sea level, the density is lower for the 30° N Atmosphere because the temperature is 29° F hotter. However, at all altitudes above 30,000 ft., the region in which most of the entry takes place, the density for the 30° N Atmosphere is higher. Thus at staging the dynamic pressure is 14.4 psf for the 30° N atmosphere compared to 12.8 psf for the Standard Atmosphere. This is equivalent to staging at a slightly lower altitude which results in a lower load factor, 3.8 g's compared to 4.0, and lower flyback range, 307 n. mi. compared to 311 n. mi.

A booster entry trajectory was generated in which the effect of winds was included. The 95% NASA wind profile for Cape Kennedy was used to establish the wind velocity at each altitude. The wind was assumed to be from the west at all altitudes, thus tending to drift the booster farther from the launch site. A comparison of this trajectory with the still air trajectory reveals that the ground trace is altered but the other parameters are unchanged. The effect of winds on the ground trace results in an increase in the flyback range from 311 n. mi. to 334 n. mi.

## EFFECT OF ATMOSPHERE MODEL ON NOMINAL TRAJECTORY

	1962 STD	30°N JULY
SEA LEVEL TEMPERATURE	59° F	88° F
SEA LEVEL DENSITY	0.00238 slugs/ft. <sup>3</sup>	0.00225 slugs/ft. <sup>3</sup>
STAGING DYNAMIC PRESSURE	12.8 psf	14.4 psf
MAXIMUM RESULTANT LOAD FACTOR	4.0g	3.8g
FLYBACK RANGE — STILL AIR — NASA WIND PROFILE	311 n.mi. 334 n.mi.	307 n.mi.

## SUBSONIC PERFORMANCE

The subsonic performance characteristics of the space shuttle booster are presented, together with the significant trade-offs used to define a baseline configuration. The performance of the nominal booster for cruise, go-around, and landing flight and for ferry mission operation is discussed.

# **SUBSONIC PERFORMANCE**

- 1. FACTORS AFFECTING WING SIZE**
- 2. PERFORMANCE CHARACTERISTICS**

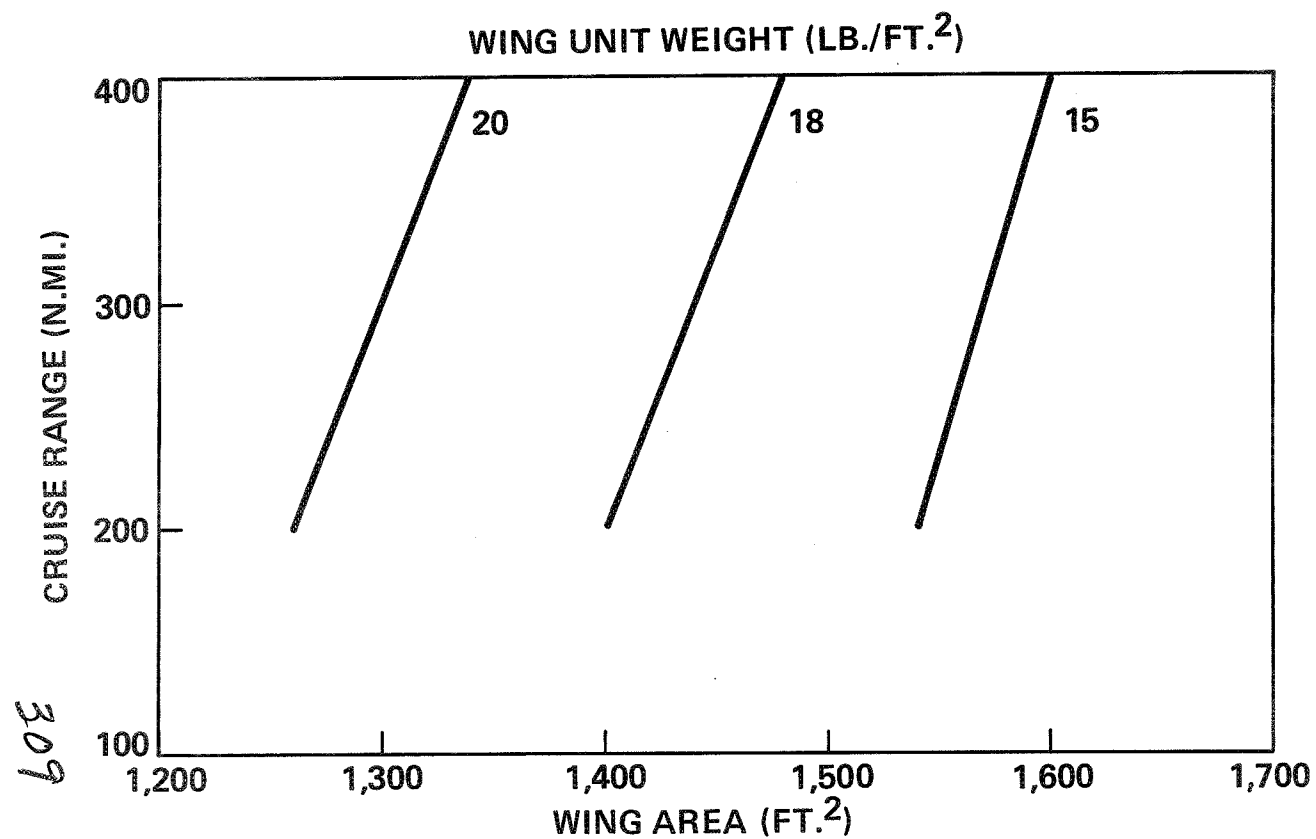
### OPTIMUM CRUISE WING AREA

The effect of wing size on vehicle cruise performance can be determined by trading off wing area with wing unit weight for a constant cruise range. A change in wing area directly affects wing weight and indirectly affects engine weight and cruise fuel by altering the aerodynamic efficiency of the vehicle. The total engine, wing, and fuel weight was determined as a function of wing area for various cruise ranges and wing unit weights. Wing areas from  $800 \text{ ft}^2$  to  $2400 \text{ ft}^2$  were selected together with wing unit weights of  $15 \text{ lb/ft}^2$ ,  $18 \text{ lb/ft}^2$ , and  $20 \text{ lb/ft}^2$  for cruise ranges of 200 n.mi., 300 n.mi. and 400 n.mi. The wing area required to minimize total weight is presented as a function of wing unit weight and cruise range. As shown by the data, the optimum wing area is a stronger function of wing unit weight than of cruise range. As the cruise range is increased and the fuel requirement becomes greater, this trend tends to reverse. For the flyback ranges considered for the shuttle operation, namely 300-350 nautical miles, wing areas from  $1300 \text{ ft}^2$  to  $1600 \text{ ft}^2$  are optimum, depending upon wing unit weight.

The addition of headwinds tends to drive the optimum wing area from the  $1300 \text{ ft}^2$  -  $1600 \text{ ft}^2$  range to higher values. Cruise operation against a headwind increases the fuel requirement for a given range, and thus has the same effect on wing area as an increase in cruise range in still air. Headwind operation requires an additional 7500 lb of fuel, equivalent to an increase in range of approximately 150 nautical miles in still air. This results in an increase in wing area of nearly  $100 \text{ ft}^2$  to optimum values ranging from  $1400 \text{ ft}^2$  to  $1700 \text{ ft}^2$ .



# OPTIMUM CRUISE WING AREA



## EFFECT OF WING SIZE ON LANDING DISTANCE

The determination of wing area when based on vehicle landing performance may show a different result. Landing distance as a function of wing area is presented for the clean configuration. Touchdown is made at a speed of 1.1 times the speed at trimmed power-off  $C_{L_{\max}}$ . Touchdown under actual shuttle operations may be at a speed higher than this

because of gust considerations, handling qualities, and pilot technique. Required field lengths would then increase accordingly. The data is presented for a landing gross weight of 463,750 lb. at sea level, standard day conditions. Braking is made on a dry concrete surface; throttles are at idle power. The field length, based on the Federal Aviation Regulations .6 factor for scheduled stops, exceeds the 10,000 ft requirement for shuttle operations. The addition of a plain, unslotted flap at 45° deflection results in landing distances which satisfactorily meet this requirement. This is primarily due to the lower landing speeds resulting from an increase in  $C_{L_{\max}}$ .

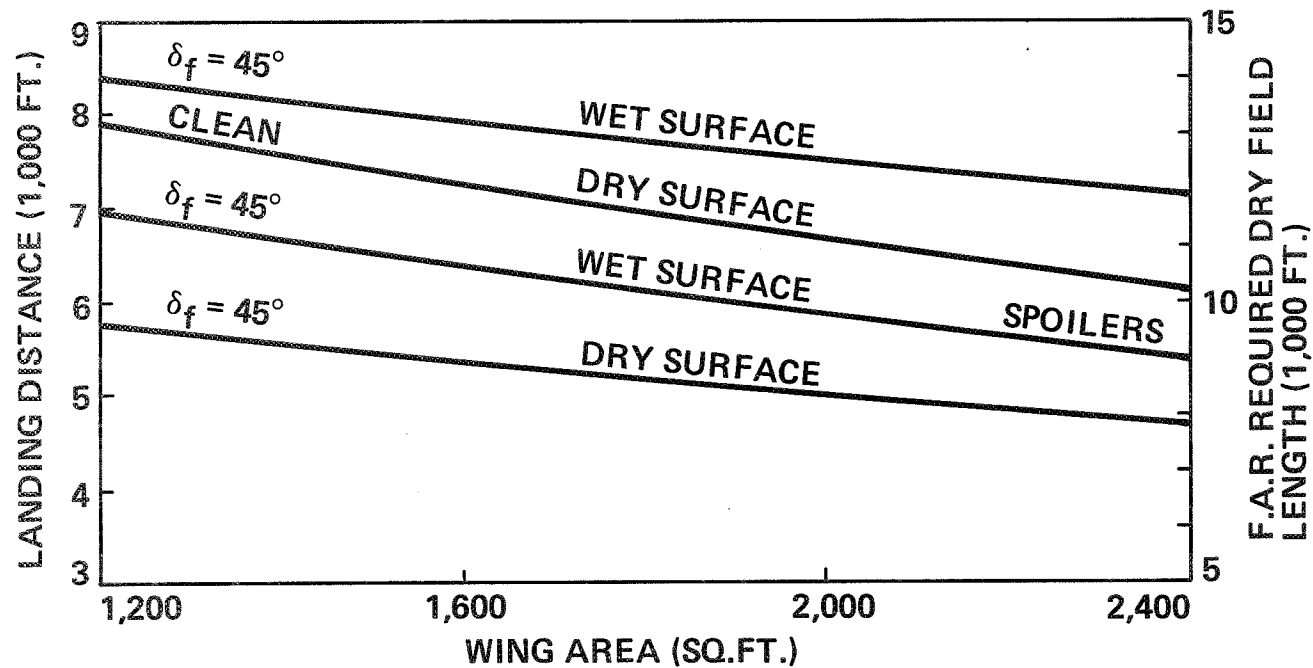
Since shuttle landings will not always be made on dry concrete runways at sea level, standard day conditions, the wing areas selected for optimum cruise performance, 1300 ft<sup>2</sup> to 1700 ft<sup>2</sup>, may not be adequate for the landing requirement. Wet field operation at sea level, standard day conditions increases the landing distance to values from 8,000 ft to 8,500 ft for these cruise wing areas. Federal Aviation Regulations for commercial transport category aircraft state that the demonstrated wet landing distance cannot be less than the required dry field length. Operation of the shuttle vehicle under these ground rules increases the demonstrated landing distance for wet field operation to values from 8,700 ft to 9,500 ft. If the wet runway landing distance is not demonstrated, it is then defined to be 115% of the required dry field length according to the same Federal Aviation Regulations. This increases the wet runway distances to values exceeding 10,000 ft. The addition of wing spoilers can reduce this distance as shown such that operation into a 10,000 ft field can be performed with a greater margin of safety. However, when the added penalty of hot day and/or altitude conditions is imposed on the landing operation, other braking devices such as thrust reversers or drag chutes may have to be considered for safe operation if the wing size is to remain near the optimum cruise value. But the degraded cruise performance resulting from the added weight penalty of these devices must be compared with that of the larger wing area required without them before the usefulness of such devices can be established.

# EFFECT OF WING SIZE ON LANDING DISTANCE

BRAKING COEFFICIENT = 0.34 (DRY) & 0.17 (WET)

GROSS WEIGHT = 463,750 LB.

SEA LEVEL & STANDARD DAY



## CRUISE PERFORMANCE

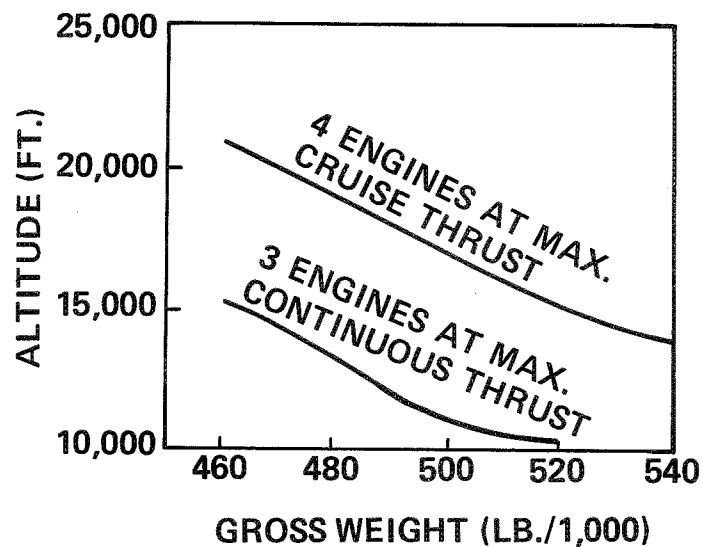
The optimum cruise altitude, defined as the altitude for maximum range, is the highest altitude at which the velocity for  $(L/D)_{\max}$  is equal to the maximum velocity of the vehicle at the maximum cruise thrust power setting in still air. Cruise specific range was determined at this condition for a vehicle with a wing area of  $2000 \text{ ft}^2$  using hydrogen burning turbofan powerplants with average cruise SFC's of  $.192 \text{ lb/hr/lb}$ . Specific range is defined as the velocity divided by the required fuel flow, or the distance traveled for each pound of fuel burned. Cruise performance with one engine inoperative at maximum cruise power lowers the cruise ceiling since the available thrust at the velocity for  $(L/D)_{\max}$  is decreased. A corresponding degradation in specific range also results because of the decreased cruise velocity at the lower altitude. Some of this performance loss can be made up by operating at the maximum continuous power setting with one engine inoperative. Operation at this higher power setting increases the cruise ceiling, and results in higher cruise velocities which improve specific range.

As the vehicle burns fuel and decreases in weight, the thrust required at  $(L/D)_{\max}$  decreases, resulting in a higher cruise altitude. This decrease in required thrust and higher altitude result in decreased engine fuel flows and improved specific range. Thus as the vehicle uses fuel its cruise performance continually improves as it seeks a higher altitude. A plot of cruise ceiling versus cruise gross weight is presented for both four-engine maximum cruise and three-engine maximum continuous power settings. Cruise range versus required cruise fuel for both conditions is also shown.

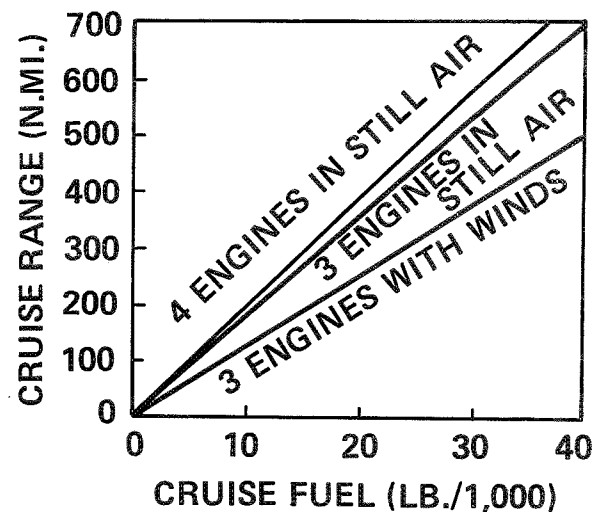
The effect of headwinds on the cruise performance of the vehicle results in a significant change in the optimum cruise altitude and a further degradation in cruise performance. The NASA Eastern Test Range 95 Percentile wind profile was used to determine this effect. The cruise ceiling no longer represents the optimum cruise altitude with winds because the large headwind values at these altitudes result in decreased ground velocities which degrade specific range. The smaller headwinds near sea level tend to drive the optimum cruise altitude to low altitudes where engine fuel flows are high. The result is degraded cruise performance at all altitudes, but decreasing in severity as the altitude decreases. A comparison of the three-engine cruise data with winds with the still air data reveals the degradation in specific range. For an average cruise gross weight of  $480,000 \text{ lb}$  the optimum cruise conditions change from an altitude of  $13,250 \text{ ft}$  at maximum continuous thrust, where the specific range is  $.01753 \text{ n. mi./lb}$ , to sea level at the partial power setting for a maximum specific range of  $.01268 \text{ n. mi./lb}$ . If cruise operation with winds is maintained at the cruise ceiling, the specific range is reduced to  $.01172 \text{ n. mi./lb}$ , a decrease of  $7.5\%$  from the optimum value. The performance penalty on cruise range and fuel is presented. For a flyback range of  $325 \text{ n. mi.}$ , typical for the space shuttle operation, the required cruise fuel increases  $7,500 \text{ lb}$  because of headwinds.

## CRUISE PERFORMANCE

### CRUISE CEILING



### CRUISE RANGE VS. FUEL

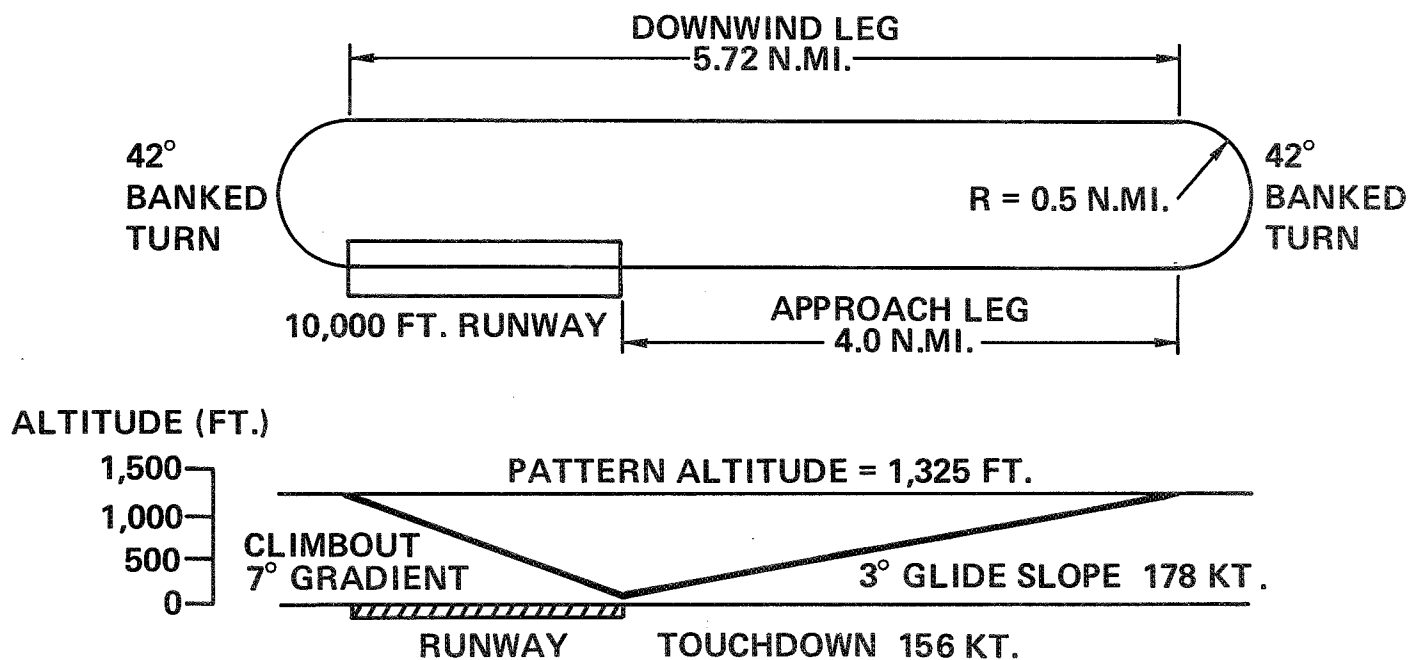


## GO-AROUND PERFORMANCE

Space shuttle go-around performance is based on four-engine operation at maximum continuous power under sea level, standard day conditions. The go-around maneuver consists of a 3-degree approach on the glide slope with flaps at  $45^\circ$  at a speed of 1.25 times the speed at trimmed power-off  $C_{L_{max}}$ . The wave-off is initiated at the 50 ft obstacle.

Throttles are advanced to maximum continuous power, flaps to  $25^\circ$ , gear retracted, and a climb to pattern altitude is made. A 42-degree banked turn is initiated to the downwind leg, and another 42-degree banked turn is made at the end of the downwind leg to intercept the glide slope 4 nautical miles out from the 50 ft obstacle. The entire maneuver is made at a constant velocity of  $1.25 V_{stall}$ . Aerodynamic data for the approach and go-around maneuver is based on a wing area of  $2000 \text{ ft}^2$ . Go-around performance is presented for an estimated approach gross weight of 464,850 lb and a speed of 178 knots.

# 



## LANDING PERFORMANCE

The landing performance is based on a touchdown speed of 1.1 times the speed at trimmed power-off  $C_{L_{max}}$  in the landing configuration. A vehicle angle-of-attack of zero degrees is assumed during the ground roll with the flaps in the 45 degree position. Throttles are maintained at idle power. Both wet and dry concrete runway field lengths are presented with and without spoilers for standard day, sea level operation. The spoilers are activated at touchdown for the duration of the ground roll. No time delays are used for nose wheel contact, pilot reaction, or for brake and spoiler activation. Flare distance from 50 ft to touchdown is considered a constant 955 ft for a 3-degree glide slope. Landing distance is presented as a function of gross weight; the data includes the Federal Aviation Regulations .6 factor for scheduled stops.

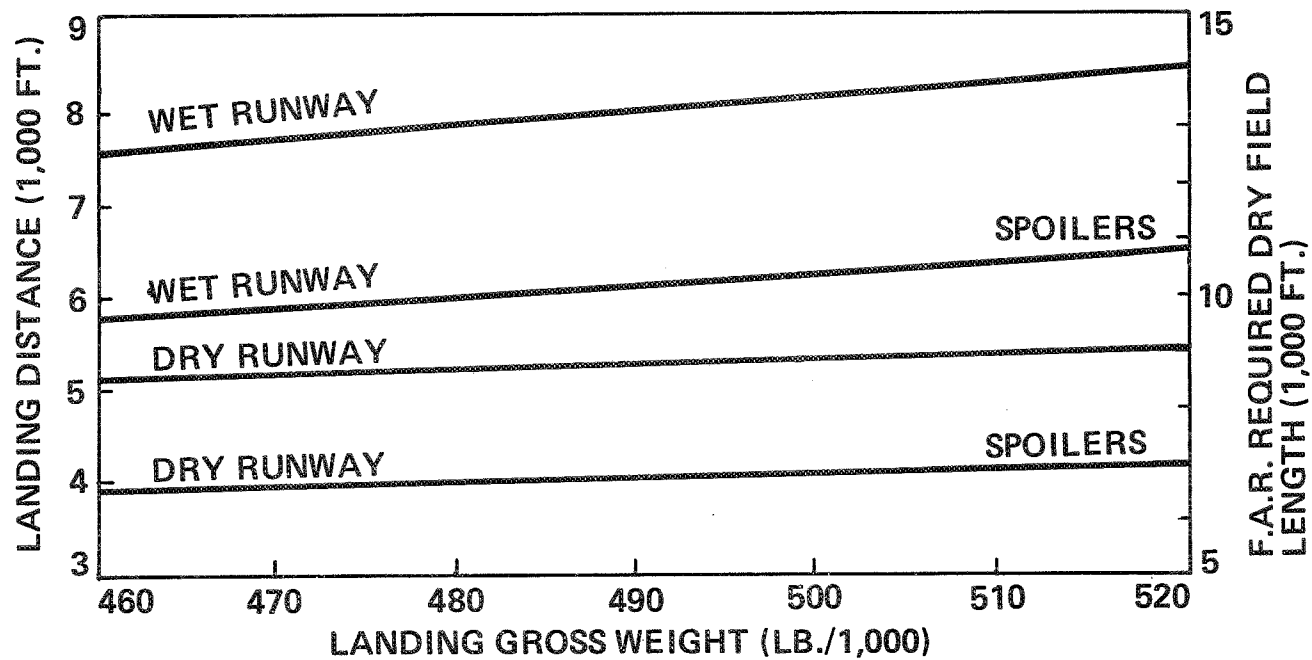


# LANDING PERFORMANCE

BRAKING COEFFICIENT = 0.34 (DRY) & 0.17 (WET)

SEA LEVEL & STANDARD DAY

WING AREA = 2,000 FT.<sup>2</sup>



## FERRY PERFORMANCE

Vehicle ferry range is based on the maximum gross weight capable of being taken out of a 10,000 ft field under sea level, standard day conditions and four-engine operation. Speed at the obstacle is assumed to be 1.2 times the speed for power-off  $C_{L_{\max}}$  in the take-off configuration with the flaps at 25 degrees. No winds are considered for the ferry mission. A minimum fuel climb is made at maximum continuous power to optimum cruise altitude, where the velocity for  $(L/D)_{\max}$  is equal to the maximum velocity of the vehicle. The climb schedule for minimum fuel is that velocity at which the fuel flow divided by the rate of climb ( $W_f/R_c$ ) is a minimum at each altitude. This is approximately the velocity for  $(L/D)_{\max}$ . Descent is made at idle power at  $(L/D)_{\max}$  from the end-of-cruise altitude.

The distance and fuel for each segment of the ferry mission is presented. Total mission range is determined to be 1462 nautical miles, with a fuel requirement of 83,251 lb.

If the take-off requirement is based on the balanced field concept, i.e., the critical engine is made inoperative during the ground roll and the remaining distance to take-off is equal to the distance required to decelerate and stop the vehicle, the take-off gross weight is reduced by approximately 50,000 pounds. This results in a reduction of approximately 900 nautical miles in ferry range, and seriously impairs ferry mission capability.

## FERRY MISSION SUMMARY

FLIGHT CONDITION	DISTANCE (N.MI.)	FUEL (LB.)
TAKEOFF	—	407
CLIMB	48	4,325
CRUISE	1,390	77,157
DESCEND	24	260
GO-AROUND	—	1,102
LAND	—	—
	<u>1,462</u>	<u>83,251</u>

## SUMMARY AND CONCLUSIONS

Optimization of the return performance of the space shuttle booster can result in significant reductions in booster inert weight and increased system payload. The important factors that determine return performance have been indicated.

Several observations and/or conclusions relating to the booster entry phase of the return mission may be listed:

1. A nominal entry trajectory, with a 4.0 g load factor constraint, has been presented which established a flyback range of 311 n. mi.
2. The effect of staging conditions on booster flyback range, for a 4.0 g load factor constraint, has been established.
3. A comparison of the "natural pitch transition" and "constant angle of attack" entry modes was made. From the staging point until the maximum load point, the trajectories are virtually the same. Two advantages of natural pitch transition are that it has 35 n. mi. less flyback range and it terminates at a small negative flight path angle. An advantage of the constant angle of attack mode is that it encounters a peak dynamic pressure of about half that for natural pitch transition.
4. Changes in booster entry performance due to changing the atmosphere model from the 1962 Standard Atmosphere to the 30 degree North Latitude July Supplemental Atmosphere are small.
5. Westerly winds during entry increase booster flyback range. For the 95% NASA wind profile an increase in flyback range of 23 n. mi. was noted.

From analysis of the subsonic performance capabilities of the space shuttle booster, the following conclusions may be stated:

1. Sizing the wing for optimum cruise performance may result in wing areas too small for safe landing operations in accordance with Federal Aviation Regulations under adverse weather conditions. When wet runways together with hot day and/or altitude conditions are imposed on the shuttle operations, the use of other decelerating devices such as thrust reversers or drag chutes may have to be employed if larger wing areas are not considered.
2. The ground rules used for the ferry mission include take-off with all engines operating at sea level standard day conditions. If take-off capability must be demonstrated on three engines, with a critical engine failure during the ground roll, the gross weight of the vehicle must be severely reduced to maintain the 10,000 ft field length requirement. This reduction in take-off gross weight reduces the ferry mission by approximately 900 nautical miles. A further imposing of hot day and/or altitude conditions on the take-off requirement will eliminate the ferry mission from space shuttle operations if the 10,000 ft field length restriction is to be maintained.

# **SUMMARY & CONCLUSIONS**

## **1. ENTRY PHASE**

- a. FLYBACK RANGE ESTABLISHED**
- b. EFFECT OF STAGING CONDITIONS, LOAD FACTOR**
- c. TWO MODES OF BOOSTER ENTRY COMPARED**
- d. EFFECT OF CHANGE IN ATMOSPHERE**
- e. EFFECT OF WINDS ON FLYBACK RANGE**

## **2. SUBSONIC PHASE**

- a. ALL-WEATHER LANDING OPERATION INTO 10,000 FT. RUNWAYS MAY REQUIRE LARGER WING AREAS AND/OR DECELERATING DEVICES**
- b. FERRY MISSION CAPABILITY SERIOUSLY RESTRICTED BY 10,000 FT. FIELD LENGTH REQUIREMENT**



# PROVIDING SAFE LANDING AT HIGH APPROACH SPEEDS FOR SPACE SHUTTLE

by Robert J. Pruin

The Boeing Company  
Seattle, Washington

## INTRODUCTION

A desired system characteristic of Space Shuttle is to land on a runway no longer than 10,000 feet and provide landing characteristics comparable to operational land-based aircraft. Trade studies indicate appreciable payload performance improvement with the decrease in inert weight that could be realized if it were possible to use high approach speeds.

A preliminary study of the feasibility of space shuttle landing at high approach speeds is presented here. The approach used consists of three steps:

- 1) Examine the factors contributing to landing characteristics and define a quantitative model of operational margins in field length. Federal Aviation Regulations that govern commercial airliners are used as a starting point.
- 2) Identify hardware and operational technique changes that would allow approach speed to be increased without increasing required runway length or degrading landing characteristics.
- 3) Evaluate quantitatively the increase in approach speed that could reasonably be achieved and identify those areas that appear promising for further study.

This study is concerned only with landing distance and does not include consideration of associated aspects such as stability and control, handling qualities, etc.

### HIGH APPROACH SPEED PROVIDES PERFORMANCE GAIN

Improvement in launch vehicle performance is available from both booster and orbiter if high approach speeds can be used. The performance gain is the result of inert weight reduction that can be obtained if approach speed is increased. At a fixed launch weight, inert weight saved on the orbiter converts directly (pound-for-pound) to payload; while the booster requires 5 to 6 pounds of inert weight reduction for each pound of payload improvement.

Typical booster trade study results are shown for a 3-1/2 million pound launch weight. As booster wing area is reduced, the landing approach speed increases. The booster inert weight decreases with reduced wing area until approach speed reaches 200 to 230 knots. At this point, the decrease in wing weight is matched by increases in flyback fuel, flyback engine weight, and increased unit area thermal protection system weight. The flyback fuel and engine weight increase because subsonic lift-to-drag ratio decreases with reduced wing area. Thermal protection system weight per square foot increases because of higher temperatures during booster reentry.

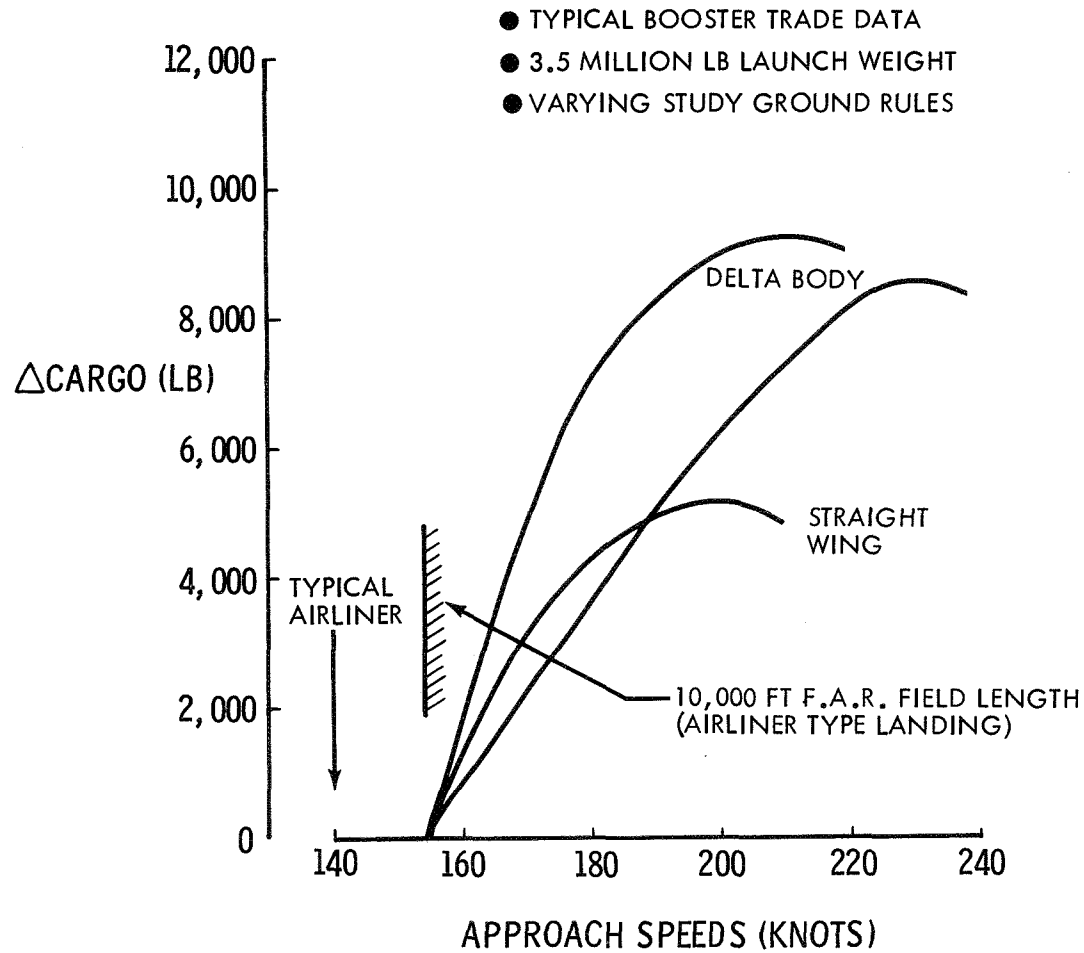
Payload improvement is shown for delta-body and wing-tail configurations. The increment in payload weight is a substantial fraction of typical design payloads for space shuttle.

Similar results can be shown for the orbiter. Also of interest for the orbiter is use of unpowered landings which require high approach speed for energy management. Elimination of the airbreathing engines on the orbiter would provide a payload increase on the order of 12,000 pounds.

These trade study results are typical. They are presented here to illustrate why the use of high approach speeds is of interest for space shuttle.



## HIGH APPROACH SPEED PROVIDES PERFORMANCE GAIN



## LANDING PROFILE

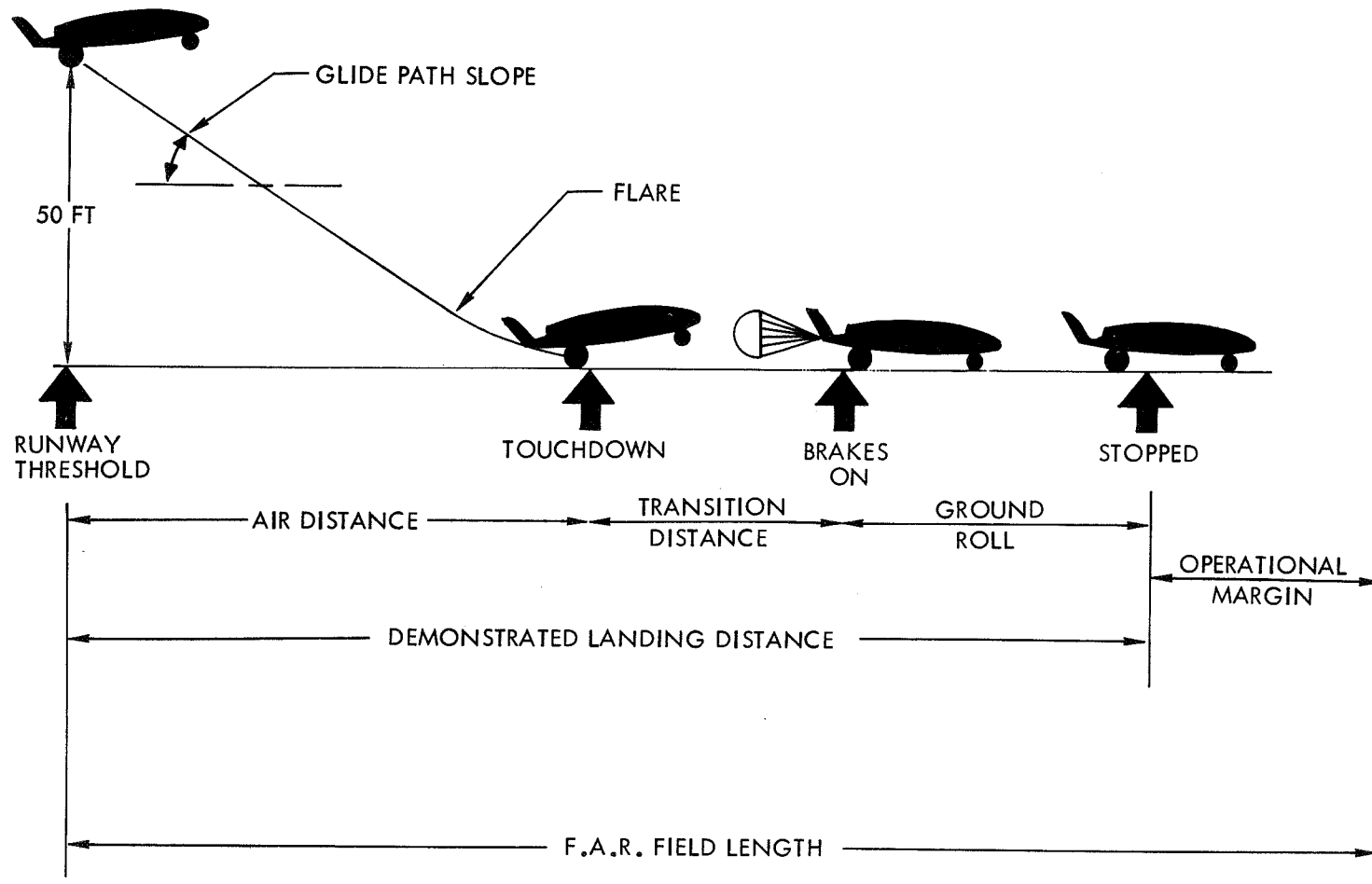
The field length required for landing consists of two parts: (1) the runway actually used during landing, and (2) an operational margin that is added to the "demonstrated" landing distance.

The "demonstrated" landing distance consists of three parts: (1) the air distance from 50-feet over the runway threshold to the point of touchdown with the main gear; (2) the transition distance during which the vehicle rotates down to place the nose gear on the runway, spoilers are actuated and brakes are applied; and (3) the ground roll distance to a complete stop. If the configuration uses a landing parachute, the chute is assumed to be deployed at the end of the transition distance.

The air distance is dependent upon the glide slope angle and the flare load factor. Flare load factor is the ratio of aerodynamic lift to vehicle weight used to bring the flight path from the glide slope angle to nearly tangent to the runway. The transition distance is proportional to the product of approach speed and the time required for transition. Transition time is primarily a function of the vehicle attitude at touchdown, the higher the touchdown attitude, the longer the transition time. The runway used for ground roll depends upon the deceleration obtained from the brakes, the aerodynamic drag, and thrust reversers.

The operational margin is added to account for variations in all the parameters including pilot technique and atmospheric conditions. Federal Aviation Regulations for commercial airliners provide for a field length margin of 67% on dry concrete. This field length is increased by 15% for all weather operation. The required field length for all weather operation then becomes 1.917 times the actual landing distance.

## LANDING PROFILE



### LANDING SPACE SHUTTLE LIKE AN AIRLINER

Landing field length is shown for a typical shuttle configuration for approach speeds from 140 to 240 knots. The field length is calculated with commercial airliner landing characteristics and Federal Aviation Regulation (F.A.R.) operational margins.

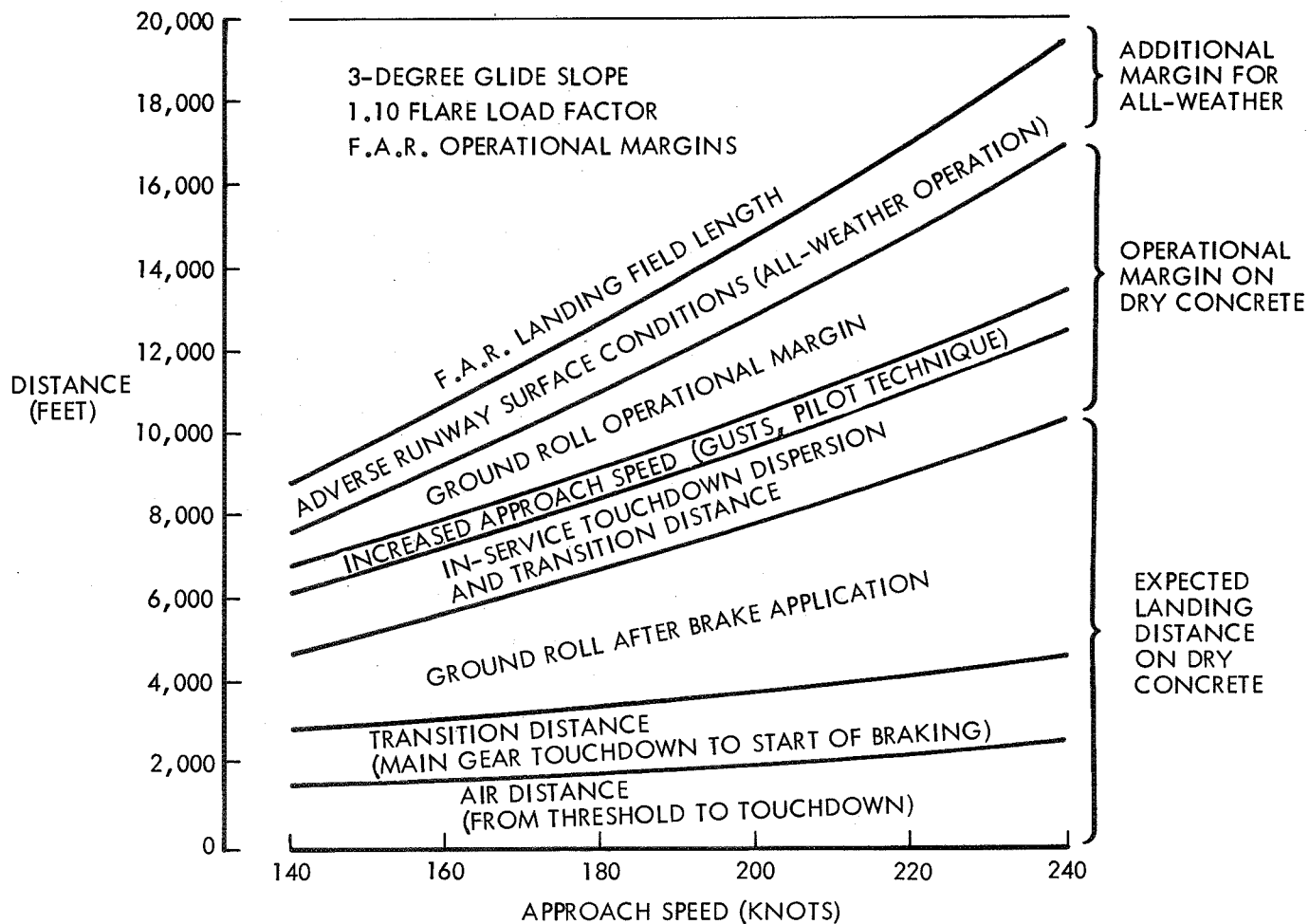
The expected landing distance is broken down into its three components. The air distance is for a three degree glide slope and a 1.1 flare load factor. The transition distance is based upon a transition time of six seconds which accompanies a high attitude (above 12 degrees) at touchdown that is typical for tailless configurations. This transition time is appreciably larger than that for a typical airliner. The calculated ground roll distance assumes main gear braking only.

The F.A.R. margin for dry concrete is divided into three basic components. This breakdown is subject to judgment and interpretation, but is felt to be representative of what would result from a more extensive study. Inservice touchdown dispersion accounts for the variation in the point along the runway where the vehicle settles on the main gear. The distance for transition also varies in operation and is combined with touchdown dispersion as one component. Touchdown speed can be increased by raising approach airspeed to account for wind and gusts. Approach airspeed is typically increased by reported gusts and 1/2 the steady wind. During descent to touchdown the wind decreases by the gradient associated with altitude and touchdown speed is increased in the absence of gust. Also, pilot technique variation may include carrying approximately 5 knots of increased approach speed.

This landing field length composition represents a starting point at which it is felt the shuttle would have landing characteristics similar to a commercial airliner. However, maximum approach speed would be limited to 154 knots in order to meet a 10,000 ft. field length constraint.

The next step, then, is to examine the individual components in an attempt to increase approach speed while holding field length constant without degrading landing characteristics.

# LANDING SPACE SHUTTLE LIKE AN AIRLINER



### OBTAINING HIGH APPROACH SPEEDS WITH EQUIVALENT SAFETY

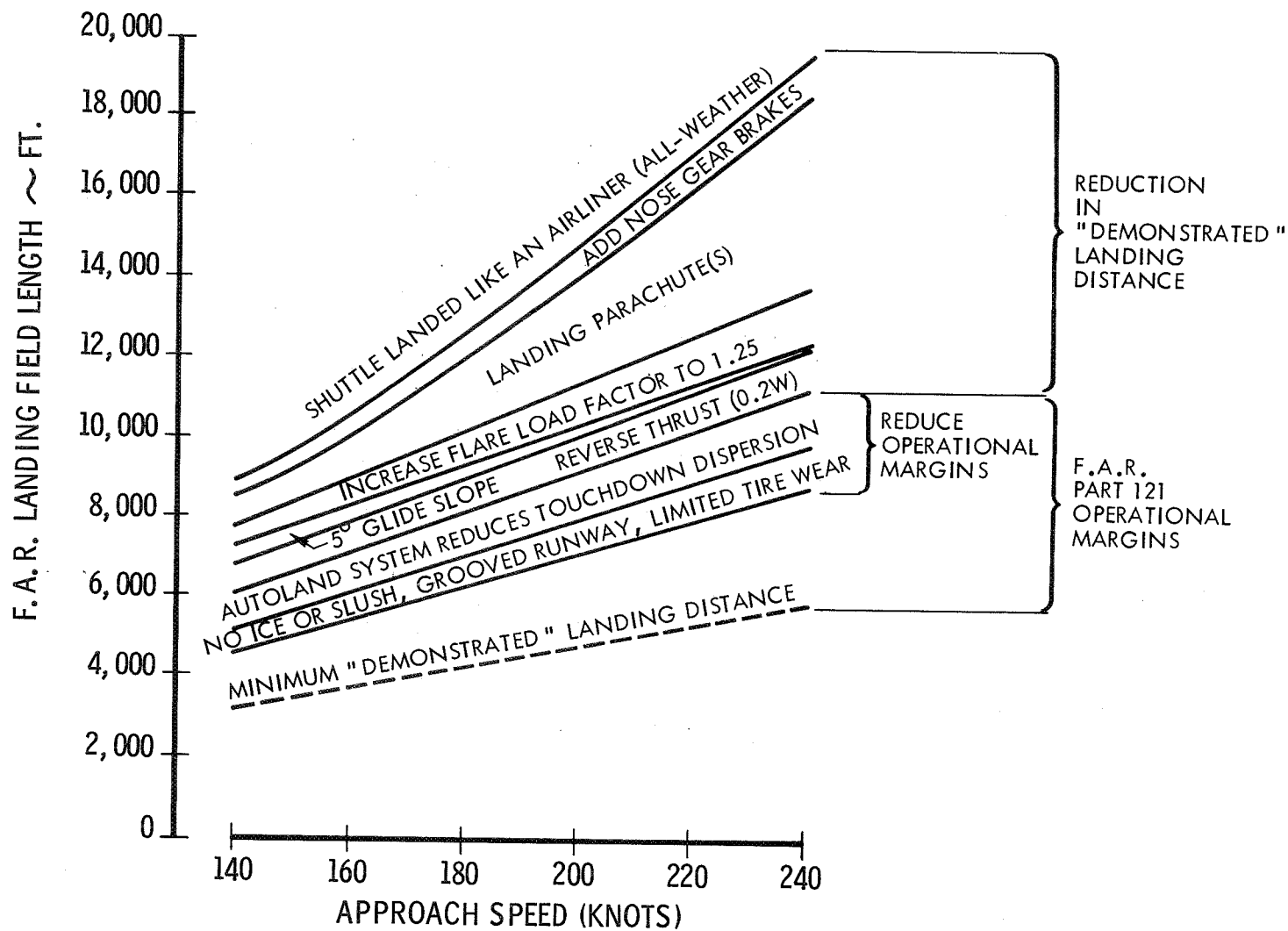
Reducing "demonstrated" landing distance is the first area where improved landing performance is sought. A reduction in "demonstrated" landing distance provides a decrease in required landing field length of 1.917 times the "demonstrated" reduction since the field length includes the operational margin allowance.

Adding nose gear brakes provides a decrease in ground roll distance. Use of landing parachutes provides a large increase in drag force during ground roll and since drag force is proportional to the square of velocity, the chute provides a larger increment as approach speed is increased. Increasing the flare load factor from 1.1 to 1.25 reduces the distance from threshold to touchdown. A flare load factor of 1.25 is above normal airline operational practice, however, during certification Boeing airliners have exceeded 1.3 and are generally about 1.16 to 1.20. The air distance can also be decreased by using a steeper glide slope. Either of these latter two changes requires designing landing gear for increased sink rate at touchdown.

The ground roll distance can also be reduced by use of thrust reversers. In commercial airliner certification thrust reversers are not used for demonstrated landing distance but are held as part of the operational margin. Procedures do exist, however, for certification with use of thrust reversers and the question of equivalent safety here rests with the reliability of the engine and the reverser. Simultaneous use of thrust reversers and parachute could result in reduced effectiveness of the parachute. The amount of reduction would be configuration dependent.

Two potential areas in the operational margin that could be reduced while retaining equivalent safety are the touchdown dispersion and the allowance for adverse runway surface conditions. Touchdown dispersion is expected to be reduced as shown by use of an autoland system. An autoland system provides automatic landing, removing the man from the control loop. Autoland systems are certified and available on present jetliners. The margin for adverse runway surface conditions could be reduced by restricting landings to fields where ice and slush would not be encountered. Limiting allowable tire tread wear would eliminate the need for any margin presently included for worn tires on wet concrete.

# OBTAINING HIGH APPROACH SPEEDS WITH EQUIVALENT SAFETY



POTENTIAL APPROACH SPEED INCREASE

FOR A 10,000 FEET FIELD LENGTH

This preliminary study indicates the possibility of using approach speeds exceeding 220 knots with a 10,000 foot field length. Landing parachutes and an automatic landing system are the prime requirements for accomplishing this.

The landing parachute provides the required deceleration during ground roll independent of runway surface conditions. The automatic landing system will provide control over touchdown dispersion and allows the use of increased flare load factors. Use of the higher flare load factor will require landing gear to be designed for sink rates on the order of 10-14 feet per second.

Approach speed can be increased to 217 knots by decreasing the "demonstrated" landing distance. The parachute provides the largest increment. The parachute as used here in combination with full braking provides an average deceleration of .9g and a corresponding maximum deceleration of 1.2g's for an approach speed of 205 knots. These deceleration levels are considered reasonable for the flight crew but would probably require aft facing passenger seats. The required parachute drag assumed here for a booster landing weight of 500,000 pounds would require two 50 ft. diameter chutes.

The approach speed could be increased to 243 knots by reducing the operational margin associated with touchdown dispersion and to 264 knots by also eliminating the margin associated with icy runways and worn tires on wet concrete.



POTENTIAL APPROACH SPEED INCREASE WHILE  
HOLDING 10,000 FEET FIELD LENGTH

	<u>MAXIMUM APPROACH SPEED - KNOTS</u>
<u>LANDING WITH COMMERCIAL AIRLINER TECHNIQUE</u>	154
<u>REDUCTION IN "DEMONSTRATED" LANDING DISTANCE</u>	
Add Nose Gear Brakes	159
And, Use Landing Parachute(s)	178
And, Increase Flare Load Factor to 1.25	195
And, Increase Approach Glide Slope from 3 to 5 deg.	200
And, "Certify Using Thrust Reversers	217
<u>REDUCTION OF OPERATIONAL MARGINS WITH EQUIVALENT SAFETY</u>	
Autoland System	243
And, No Ice or Slush, Limit Tire Tread Wear, Grooved Runway Surface	264

#### STATUS OF RECOMMENDED LANDING SYSTEM

The landing system presently recommended for space shuttle consists basically of using: (1) automatic landing system, (2) best brakes available, and (3) landing parachutes.

Nose gear brakes would be used along with the most advanced anti-skid system presently used on jetliners. The landing parachutes would be sized to bring the ground-roll deceleration near the limits imposed by human factors. The flare load factor would be as near 1.25 as the aerodynamics of a particular configuration would allow. Use of the higher flare load factor is possible only with the automatic landing system.

Also recommended is that full advantage be derived from the presence of the autoland system to reduce the operational margin allowed for inservice touchdown dispersion. Allowable tire tread wear should be limited, together with appropriate landing site restriction to eliminate operational margin associated with ice and slush on runway surface. The combination of these factors could allow use of approach speeds high enough to be limited by such factors as maximum speed for wheels and tires. This speed is estimated to be about 225 knots, which corresponds to an approach speed of approximately 237 knots.

This landing system should allow use of approach speeds high enough to achieve maximum launch vehicle performance. Also, a cost effectiveness optimum could occur at a slightly lower approach speed.

STATUS OF RECOMMENDED SHUTTLE LANDING SYSTEM

- IN ORDER OF PRIORITY
- 10,000 FT. FIELD LENGTH

MAXIMUM APPROACH SPEED - KNOTS

WITH COMMERCIAL AIRLINER PROCEDURE 154

HARDWARE AND LANDING TECHNIQUE CHANGES

USE ADVANCED BRAKING SYSTEM 159

AND, USE LANDING PARACHUTES 178

AND, INCREASE FLARE LOAD FACTOR TO 1.25 195

REDUCE OPERATIONAL MARGIN REQUIREMENTS  
WITH NEW SYSTEMS

AUTOLAND (FAIL OPERATIVE) 220

AND, EXCLUDE ICE OR SLUSH, LIMIT TIRE  
WEAR, GROOVE RUNWAYS 242

## RECOMMENDATIONS FOR FURTHER STUDY

### FURTHER ANALYSIS OF OPERATIONAL MARGINS

Assessment of Composition (Definition of Components)

Means for Reduction with Equivalent Safety

### DEMONSTRATED LANDING DISTANCE FACTORS

#### Brakes

Possible improvement in braking coefficient

Energy absorption considerations

Weight and cost

#### Parachutes

Configuration applicability

Requirement for redundancy

Operation behind blunt base

Environmental protection

Qualification considerations

#### Flare Load Factor and Glide Slope

Pilot skill requirements and pilot acceptability

Effect upon maximum rate-of-sink (gear design requirements)

#### Thrust Reversers

Reliability, cost, weight

Applicability to particular configuration

### SYSTEM COST EFFECTIVENESS CONSIDERATIONS

Determine Most Cost Effective Approach Speed

Review of Landing Field Length Limit



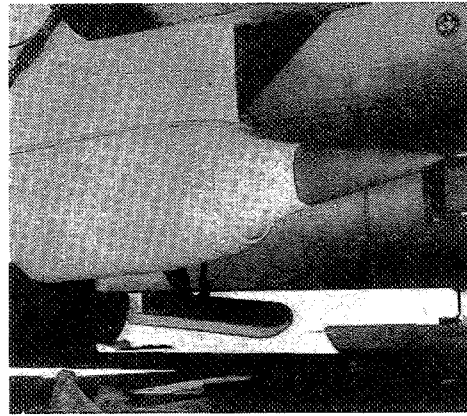
# SHOCK INTERFERENCE HEATING AND THE SPACE SHUTTLE

by Barry E. Edney

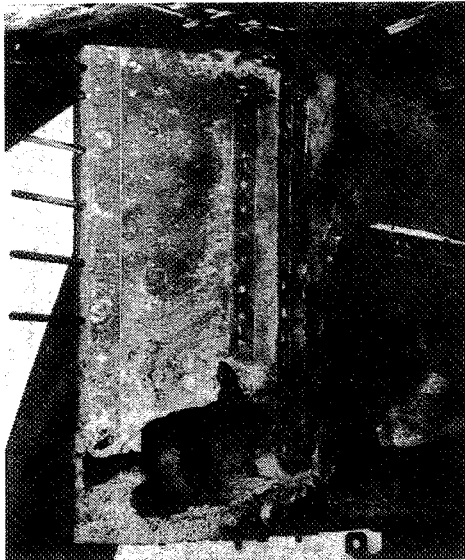
Bell Aerospace Company  
Buffalo, New York

IN OCTOBER 1967, THE NASA X-15A-2 RESEARCH AIRCRAFT SUFFERED SEVERE STRUCTURAL DAMAGE TO ITS VENTRAL FIN DURING A  $M=6.7$  FLIGHT (1). THE VENTRAL FIN, WHICH SUPPORTED A BOILER PLATE RAMJET TEST MODEL WAS BURNED COMPLETELY THROUGH IN SEVERAL PLACES AND THE MODEL TORE LOOSE PREMATURELY. THE UPPER PRE-FLIGHT PHOTOGRAPH SHOWS THE BOILER PLATE MODEL MOUNTED ON THE VENTRAL FIN. BOTH ARE COVERED IN A THICK LAYER OF ABLATIVE MATERIAL. IN ADDITION TO THE HOLES IN THE VENTRAL, THERE WAS ALSO STRUCTURAL DAMAGE TO THE FUSELAGE (EVIDENT IN THE LOWER PHOTOGRAPHS) CAUSED BY THE FIN BOW SHOCK/FUSELAGE, BOUNDARY-LAYER INTERACTION, AND TO THE BOILER PLATE TEST MODEL. INCREASED HEATING WAS ALSO EVIDENT ON THE WING LEADING EDGES, AS A RESULT OF THE FUSELAGE BOW SHOCK WAVE IMPINGING ON THE WINGS.

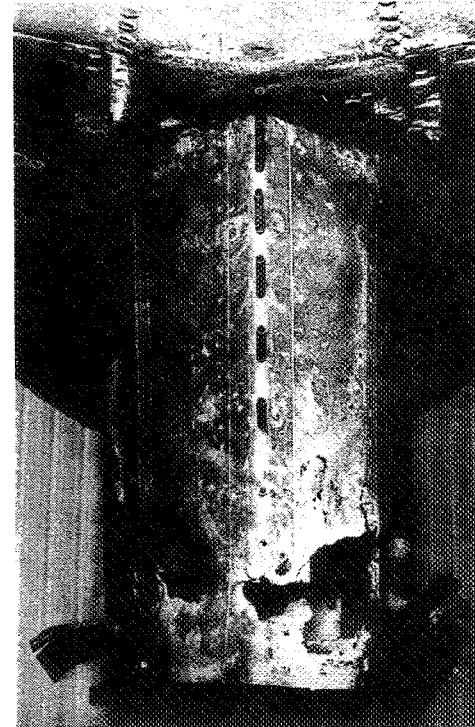
## SHOCK INTERFERENCE



RAMJET MOUNTED ON X-15A FIN

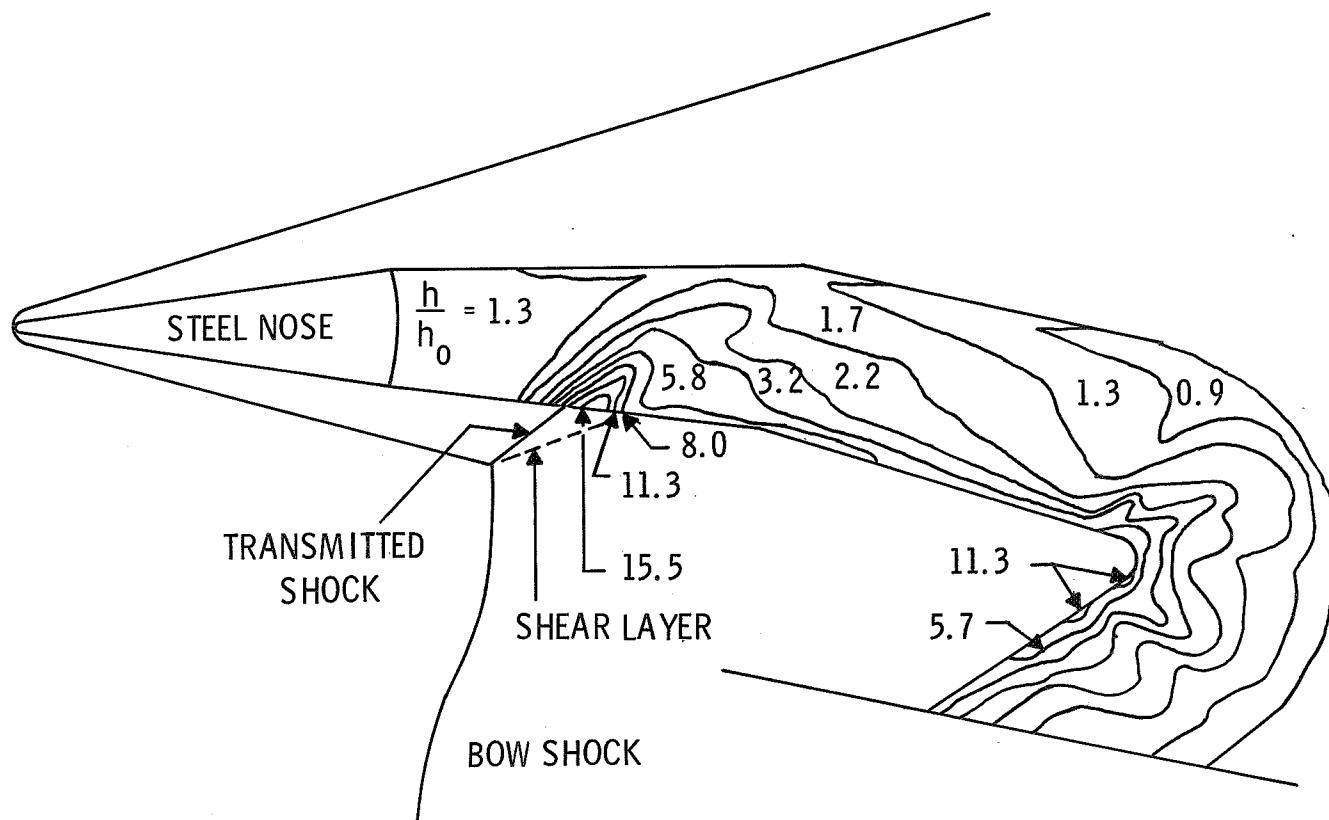


FIN DAMAGE DUE TO SHOCK IMPINGEMENT



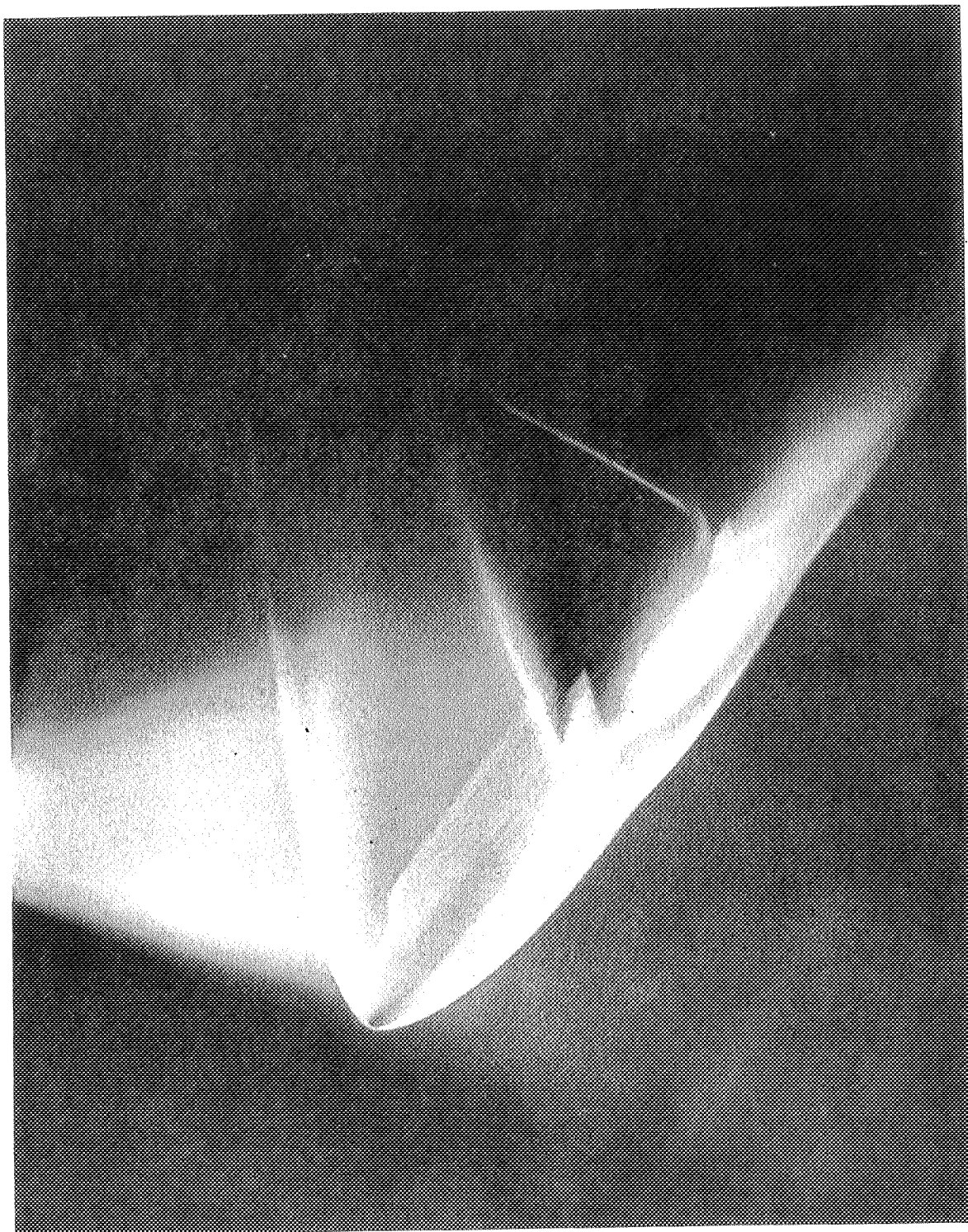
IN GENERAL PROBLEMS WITH SHOCK INTERFERENCE HEATING DID NOT ARISE DURING THE APOLLO PROGRAM. ONE EXCEPTION WAS AN ANTENNA DESIGNED TO EXTEND BEYOND THE IONIZED SHOCK LAYER DURING REENTRY. UNFORTUNATELY, THE INTERACTION BETWEEN THE ANTENNA SHOCK WAVE AND THE DETACHED SHOCK WAVE AHEAD OF THE CAPSULE LED TO A SEVERE HEATING PROBLEM, WHICH WOULD ALMOST CERTAINLY HAVE DESTROYED THE ANTENNA. THE ACCOMPANYING FIGURE SHOWS THE HEATING RATES MEASURED IN THE LRC M=8 FACILITY. THE LOCATIONS OF THE TRANSMITTED SHOCK WAVE AND THE SHEAR LAYER, WHICH IMPINGE ON THE ANTENNA AND WHICH RESULT IN LOCATION AMPLICATION OF THE HEAT TRANSFER RATE IN EXCESS OF 15, WERE PREDICTED THEORETICALLY. THIS IS AN EXAMPLE OF TYPE III INTERFERENCE WHICH WILL BE DESCRIBED LATER.



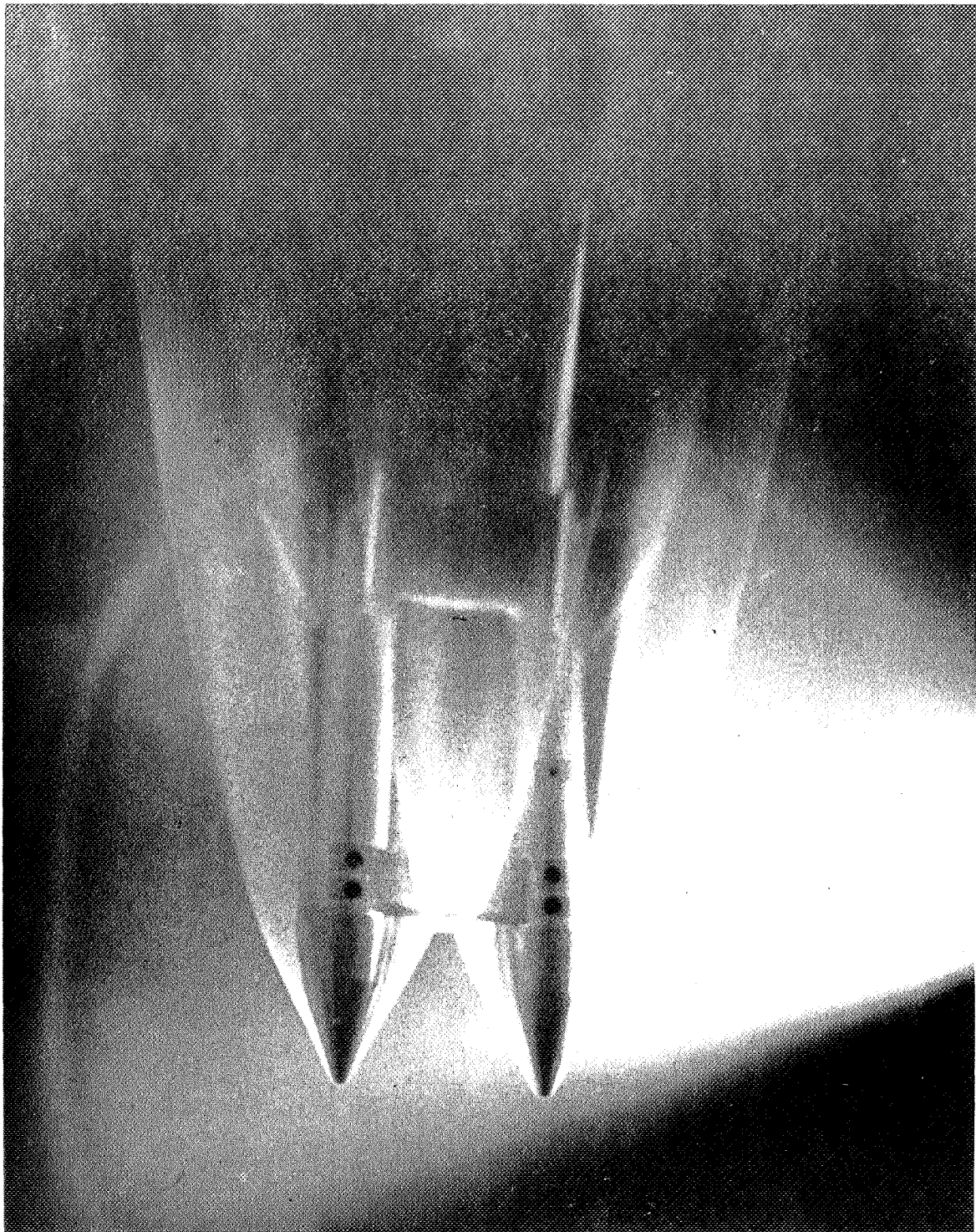


TYPE III INTERFERENCE HEATING ON APOLLO ANTENNA,  $M_\infty = 8$

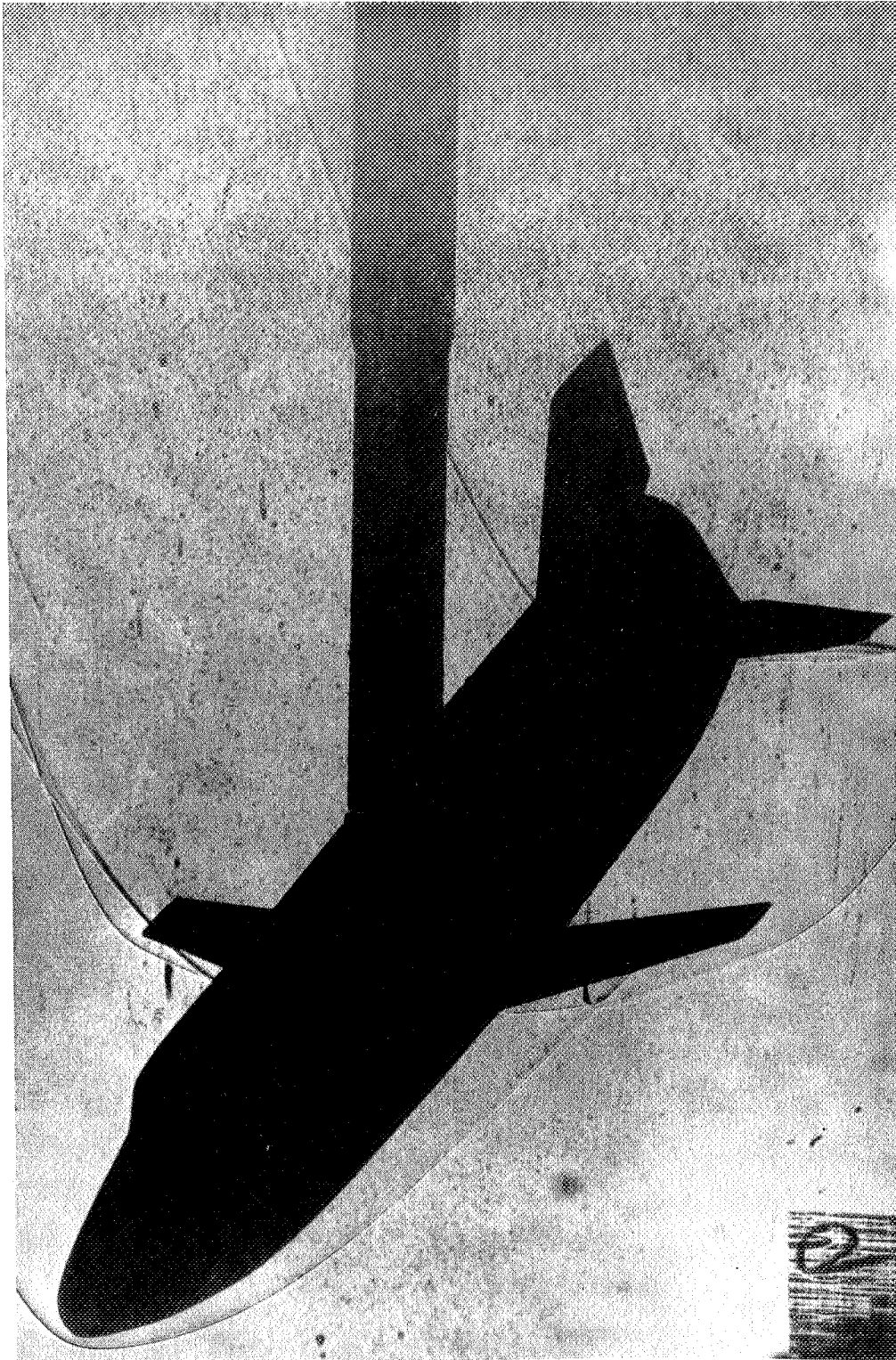
THE STRAIGHT-WING ORBITER CONFIGURATIONS SUFFER FROM SHOCK INTERFERENCE PROBLEMS AT ANGLES OF ATTACK LESS THEN  $60^\circ$ . IT SHOULD BE NOTED, HOWEVER, THAT THIS IS AN OFF-DESIGN CONDITION FOR THE SHORT CROSS-RANGE MISSION. THE ACCOMPANYING PHOTOGRAPH OF THE MSC ORBITER TAKEN BY ARRINGTON VIVIDLY ILLUSTRATES THE FUSELAGE SHOCK WAVE IMPINGING ON THE WINGS OF THE VEHICLE. THIS PHOTOGRAPH WAS TAKEN IN THE NASA LRC M-20 HELIUM TUNNEL USING AN ELECTRON BEAM VIZUALIZATION TECHNIQUE.  $\alpha = 20^\circ$ .



SHOCK INTERFERENCE HEATING IS NOT CONFINED TO THE ORBITER. THIS PHOTOGRAPH OF THE MARTIN BOOSTER SHOWS COMPLEX INTERACTIONS ON THE CROSS MEMBERS JOINING THE TWO FUSELAGES. THIS IS AN EXAMPLE OF TYPE IV INTERFERENCE WHICH WILL BE DISCUSSED LATER. NASA LRC M=20 HELIUM TUNNEL.



THIS OBLIQUE SCHLIEREN PHOTOGRAPH OF THE MSC ORBITER AT 50° ANGLE OF ATTACK  
TAKEN BY SEEGMILLER SHOWS AN EXAMPLE OF TYPE V INTERFERENCE ON THE PORT  
WING. NOTE THE TWO DISTURBANCES ORIGINATING AT THE IMPINGEMENT POINT AND  
CROSSING THE WING. NASA AMES 3-1/2 FT HYPERSONIC TUNNEL, M=7.4.



IN THIS PHOTOGRAPH OF THE OIL FLOW PATTERN ON THE UPPER SURFACE OF THE MSC ORBITER AT  $\alpha = 50^\circ$ , WE SEE QUITE CLEARLY THE TWO REGIONS OF HIGH SHEAR AND CONSEQUENTLY HIGH HEAT TRANSFER. THE PICTURE IS FURTHER COMPLICATED BY BACK FLOW AROUND THE TRAILING EDGE.





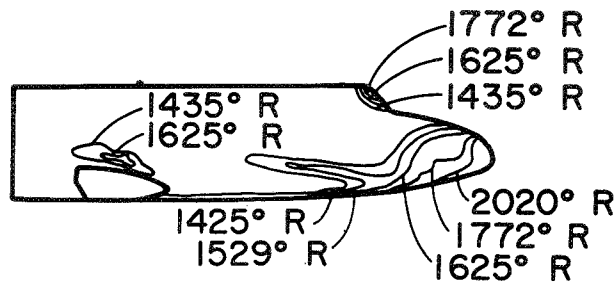
THE CORRESPONDING OIL FLOW PATTERN ON THE LOWER SURFACE INDICATES STRONG EVIDENCE OF SHOCK/BOUNDARY - LAYER AND/OR VORTEX ACTION. ANALYSIS OF THESE COMPLICATED THREE-DIMENSIONAL FLOW FIELDS ARE PRESENTLY BEYOND THE STATE-OF-THE-ART.



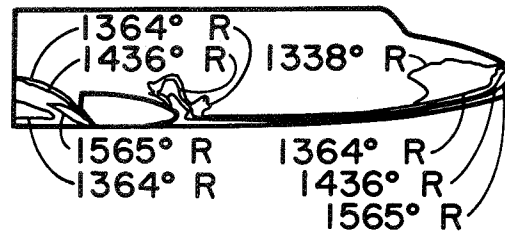
THESE TEST DATA FOR THE MSC ORBITER CONFIGURATION, OBTAINED BY HENDERSON AT AL, CLEARLY SHOW THAT THE INTERFERENCE HEATING AT THE WING FUSELAGE JUNCTION MAY EXCEED THE NOSE HEATING UNDER CONDITIONS. WHETHER THIS IS ATTRIBUTABLE TO A SHOCK BOUNDARY LAYER INTERACTION OR VORTICES GENERATED AT THE WING ROOT HAS NOT YET BEEN ESTABLISHED.

MSC ORBITER EQUILIBRIUM SKIN TEMPERATURE ON SIDE PANEL,  
VARIOUS CONSTANT  $\alpha$  ENTRY TRAJECTORIES

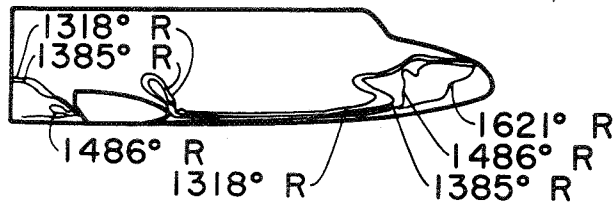
353



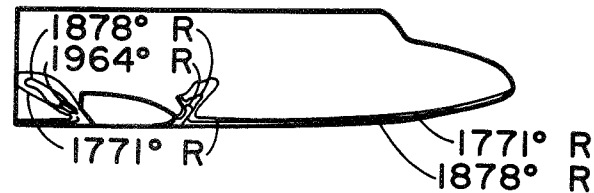
$\alpha = 20^\circ$



$\alpha = 60^\circ$



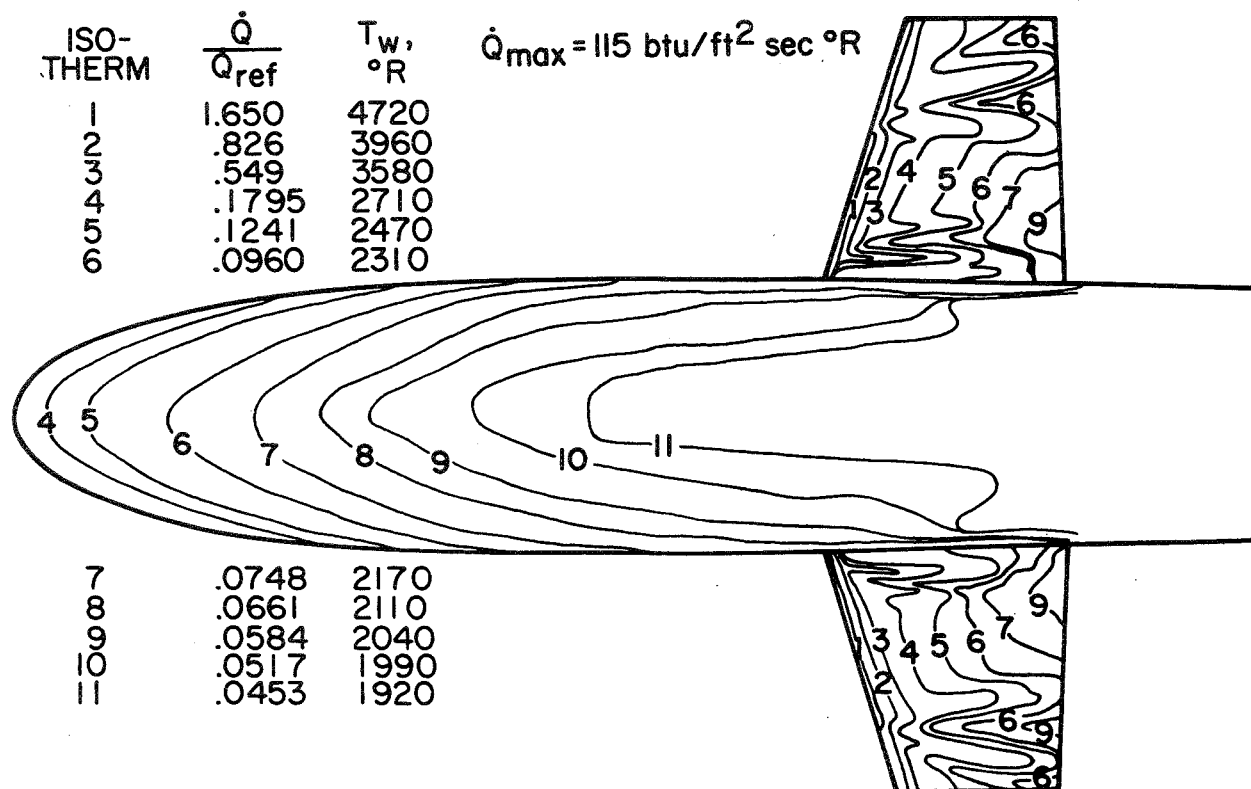
$\alpha = 40^\circ$



$\alpha = 80^\circ$

THESE TEST DATA OBTAINED IN THE NASA LRC M=8 VARIABLE DENSITY TUNNEL, SHOW QUITE CLEARLY THE EFFECTS OF THE FUSELAGE SHOCK WAVE IMPINGING ON THE WING AT  $\alpha = 20^\circ$ . THE INCREASED HEATING NEAR THE WING ROOT POSSIBLY RESULTS FROM BOUNDARY LAYER SEPARATION. SOMEWHAT LOWER HEATING RATES HAVE BEEN MEASURED IN HELIUM, UNDER SIMILAR CONDITIONS WHICH LENDS SUPPORT TO THE HYPOTHESIS THAT REAL GAS (i.e.  $\gamma$ ) EFFECTS MAY BE SIGNIFICANT.

MSC ORBITER MAXIMUM HEAT TRANSFER AND EQUILIBRIUM SKIN TEMPERATURE,  
CONSTANT  $\alpha = 20^\circ$  ENTRY TRAJECTORY, LRC M = 8 VDT

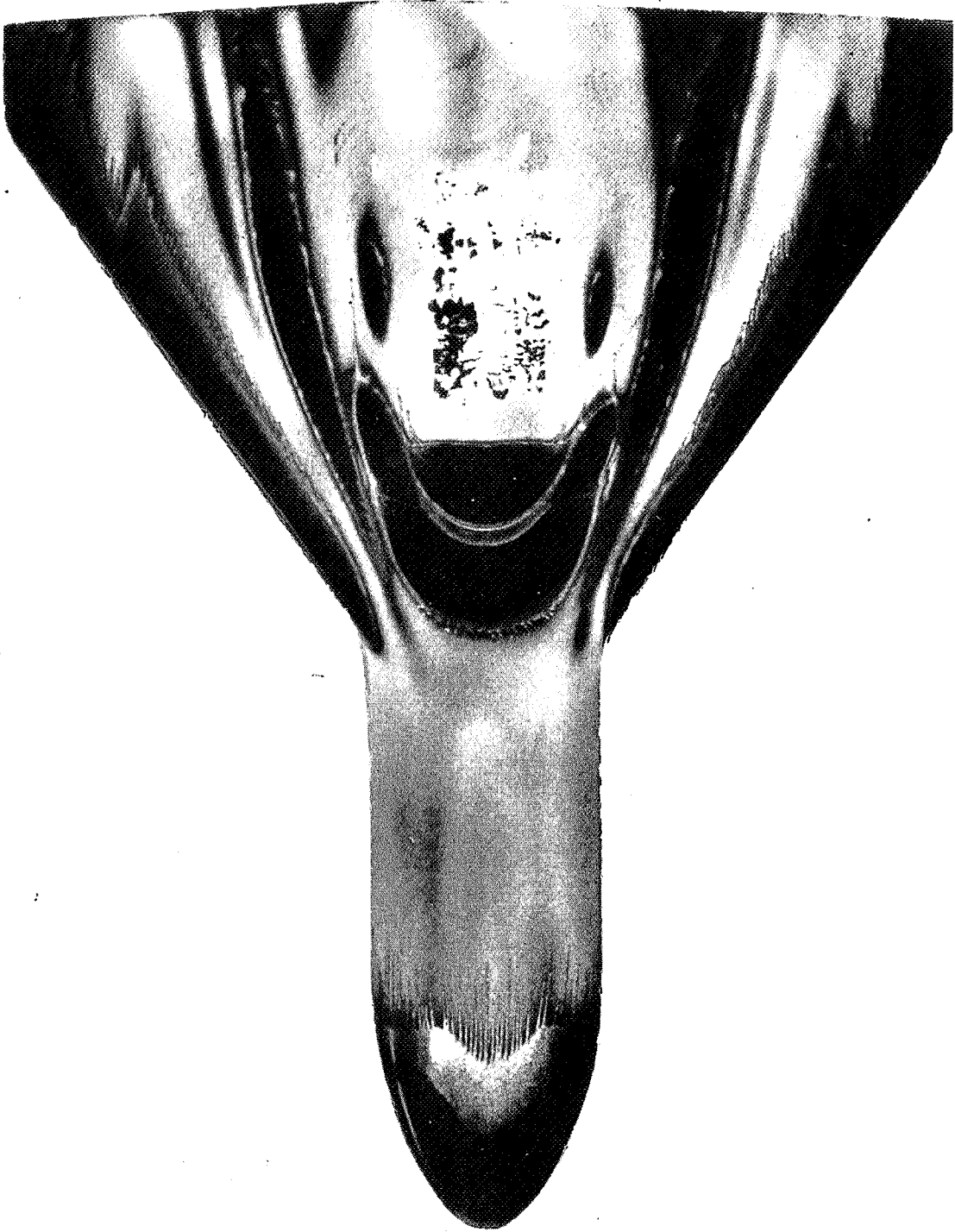


THESE HEAT TRANSFER DATA FOR THE MARTIN BOOSTER CONFIRM THE HIGH INTERFERENCE HEATING ON THE CROSS MEMBERS, SUGGESTED BY THE ELECTRON BEAM VISUALIZATION PHOTOGRAPHS. NOTE, TOO, THE SHOCK/BOUNDARY LAYER INTERACTIONS AT THE FIN/FUSELAGE JUNCTIONS. THERE IS ALSO EVIDENCE OF SHOCK INTERFERENCE HEATING OUTBOARD ON THE LOWER SURFACE OF ONE OF THE FINS.



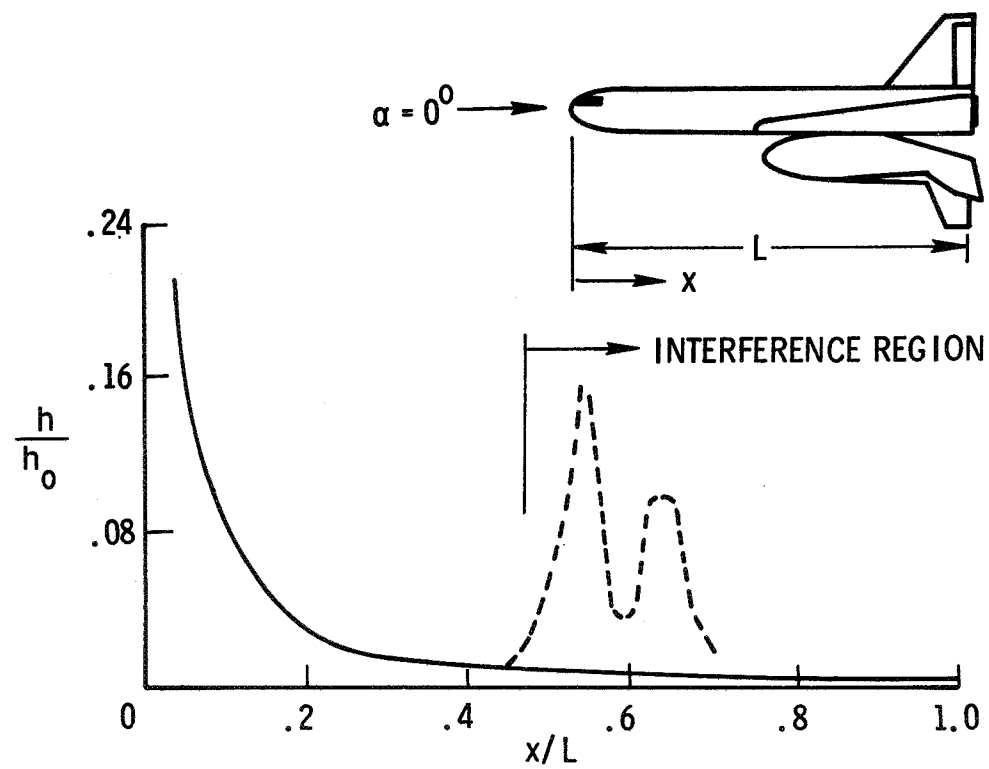


PROBABLY THE MOST SEVERE SHOCK INTERFERENCE HEATING PROBLEMS WILL ARISE AS A RESULT OF MATING THE BOOSTER AND ORBITER DURING THE ASCENT STAGE. THIS PHASE CHANGE PAINT, HEAT TRANSFER TEST, CONDUCTED BY D. CRAWFORD AT NASA LRC, SHOWS THE INTERFERENCE HEATING ON THE MCDONNELL-DOUGLAS BOOSTER WHEN MATED WITH THE HL10 ORBITER. THE LOCATION AND SEVERITY OF THE HOT SPOTS ARE A STRONG FUNCTION OF THE GEOMETRY OF THE BOOSTER AND ORBITER, THEIR RELATIVE POSITIONS, STAGING ALTITUDE AND VELOCITY.

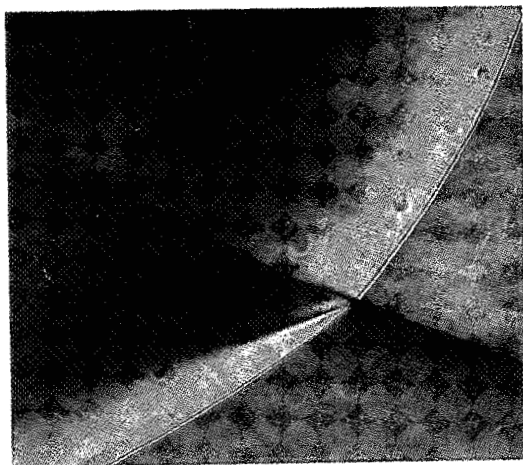


THIS FIGURE SHOWS THE CENTER LINE HEAT TRANSFER DISTRIBUTIONS ON THE BOOSTER. IF THE ORBITER IS MOUNTED FURTHER FORWARD THE ABSOLUTE HEAT TRANSFER RATES AND RESULTING SKIN TEMPERATURES WOULD BE CONSIDERABLY HIGHER AND MAY EXCEED THE CORRESPONDING VALUES AT THE NOSE.

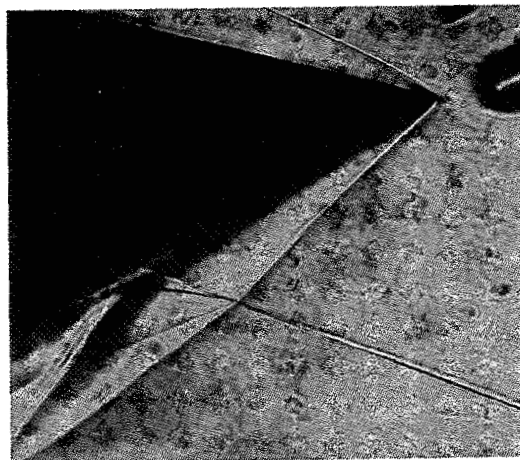
MDAC HL-10 LAUNCH CONFIGURATION INTERFERENCE HEATING ON MDAC BOOSTER,  
LRC,  $M = 10$ , CFHT



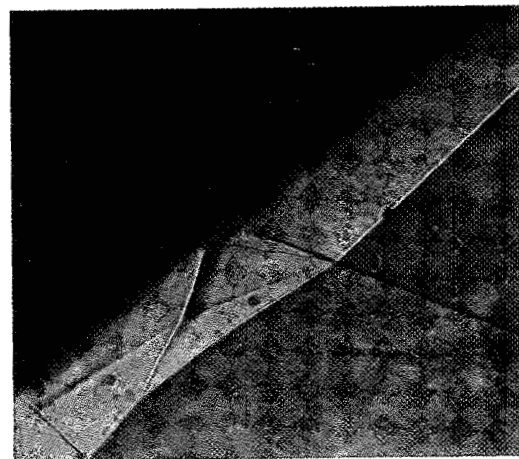
THE TYPE OF INTERFERENCE PATTERN SET UP AND HENCE THE LOCATION OF THE HOT SPOTS AND THE MAGNITUDE OF THE HEATING CAN BE PREDICTED GIVEN THE STRENGTHS OF THE TWO IMPINGING SHOCK WAVES. SIX TYPES OF INTERFERENCE HAVE BEEN IDENTIFIED. THE TEXTBOOK TYPE I INTERFERENCE OCCURS WHEN TWO WEAK OBLIQUE SHOCKS OF OPPOSITE FAMILIES INTERSECT, AS SHOWN IN THE ACCOMPANYING FIGURE. NOTE THAT THE TRANSMITTED SHOCK WAVE, PR, MAY GIVE USE TO BOUNDARY LAYER TRANSITION AND/OR SEPARATION WITH AN ATTENDANT INCREASE IN BOTH PRESSURE AND HEAT TRANSFER.



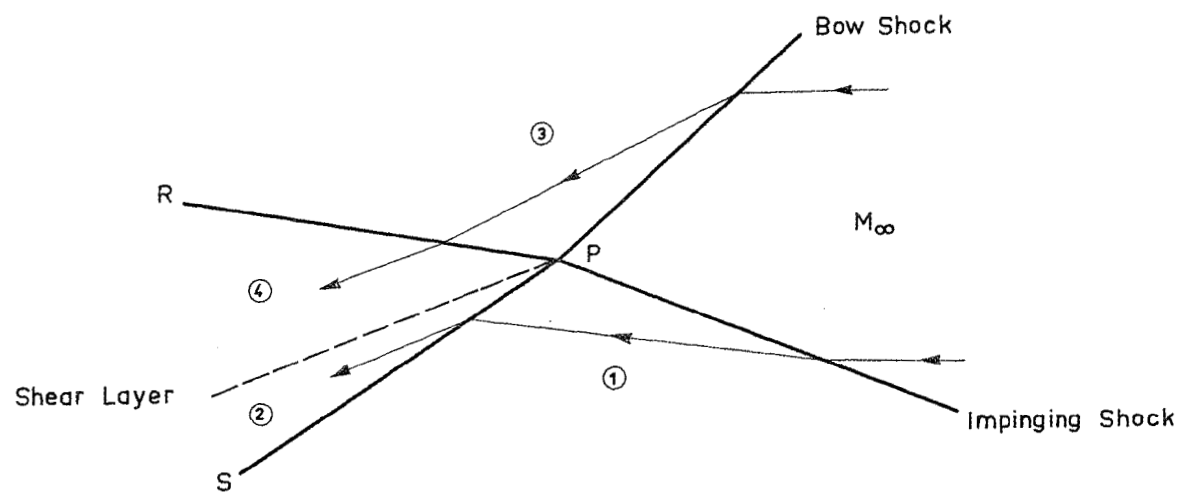
(a) CYLINDER//PLATE L.E.



(b) WEDGE



(c) SWEEP CYLINDER

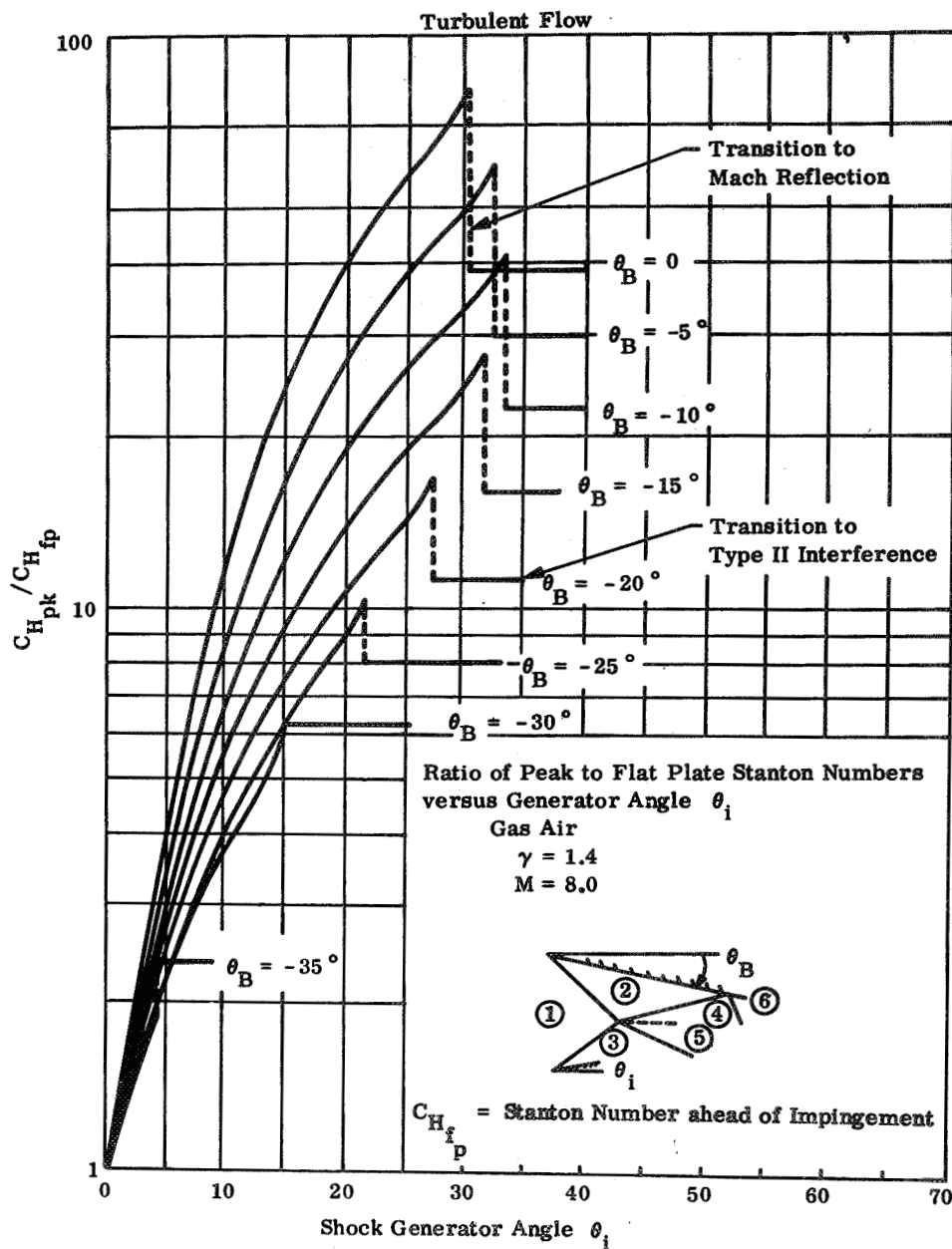


Type I interference.  $M = 4.6$ ,  $\xi = 10^\circ$ .

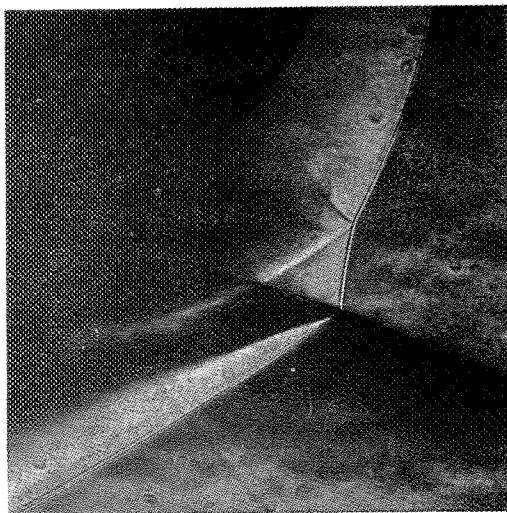
THIS FIGURE SHOWS THE HEAT TRANSFER AMPLIFICATION FACTOR,  $C_{HPEAK}/C_{Hfp}$ , AS A FUNCTION OF THE SHOCK GENERATOR ANGLE  $\theta_i$  WITH  $\theta_B$  AS A PARAMETER. NOTE THE SUDDEN REDUCTION IN THE AMPLIFICATION WHEN A MACH STEM REFLECTION OCCURS; THE TRANSITION TO TYPE II INTERFERENCE IS ALSO INDICATED.



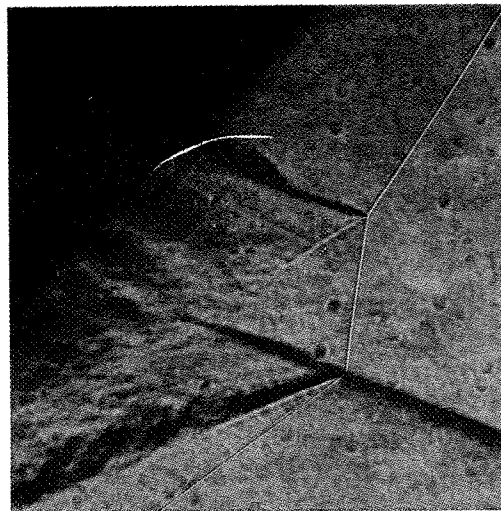
# RATIO OF PEAK TO FLAT PLATE STANTON NUMBERS VERSUS GENERATOR ANGLE



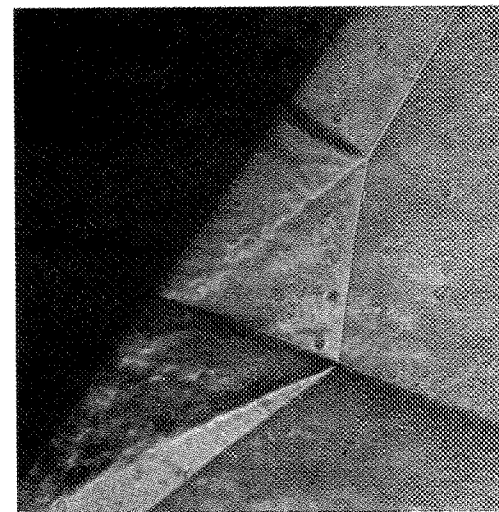
AS THE STRENGTH OF THE BOW SHOCK WAVE OR THE IMPINGING SHOCK WAVE INCREASES A POINT IS REACHED WHERE A TYPE I PATTERN IS NO LONGER POSSIBLE. THIS MARKS THE ONSET OF TYPE II INTERFERENCE, WHICH IS CHARACTERIZED BY THE SUBSONIC PATCH QP. ELSEWHERE THE FLOW IS SUPERSONIC. THE TRANSMITTED SHOCK WAVE QR AGAIN LEADS TO A SHOCK/BOUNDARY LAYER INTERACTION WITH AN INCREASE IN PRESSURE, HEAT TRANSFER ETC AS IN THE CASE OF TYPE I INTERFERENCE.



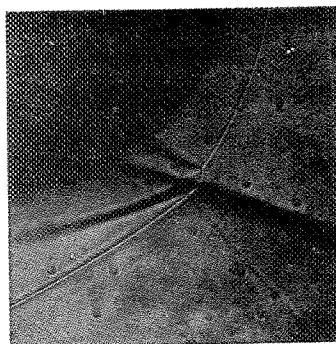
(d) CYLINDER//PLATE L.E.



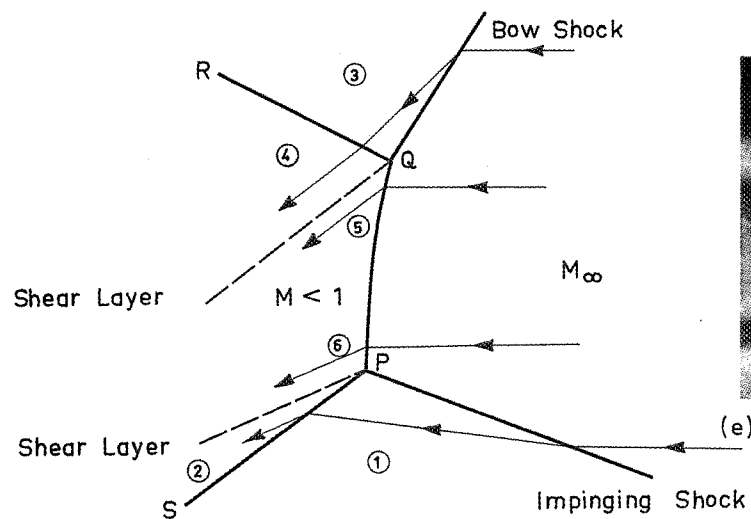
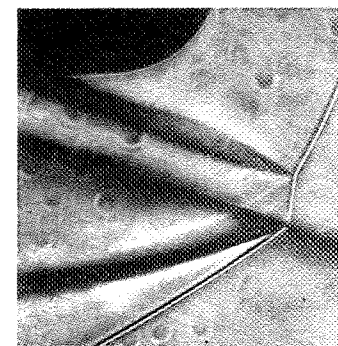
(b) WEDGE



(c) SWEEP CYLINDER

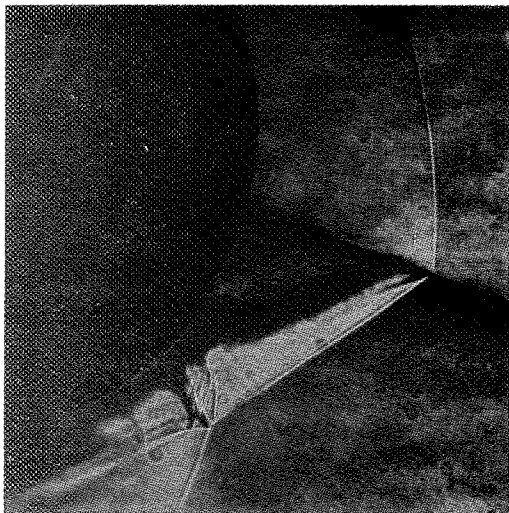


(d) HEMISPHERE

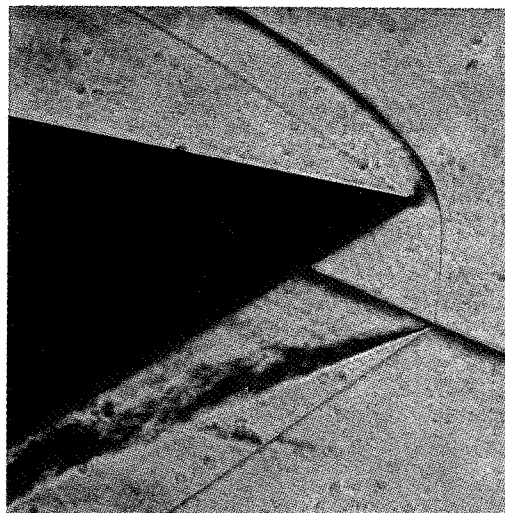
Type II interference,  $M = 4.6$ ,  $\xi = 10^\circ$ .

(e) FLAT FACED CYLINDER

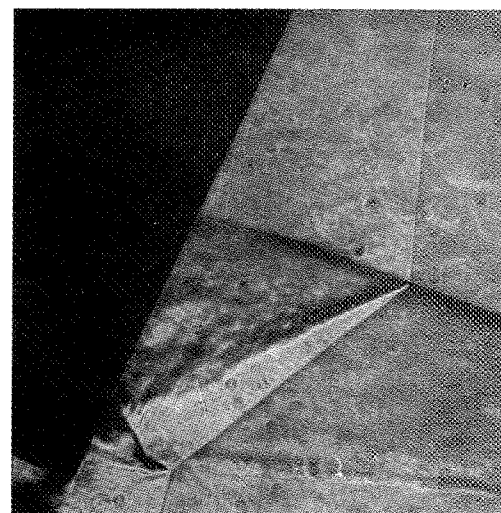
WHEN THE FLOW BEHIND THE BOW SHOCK WAVE IS SUBSONIC WE HAVE EITHER TYPE III OR TYPE IV INTERFERENCE. IN REGION 2 THE FLOW IS STILL SUPERSONIC AND IF THE INCLINATION OF THE FLOW IN REGION 2 RELATIVE TO THE BODY SURFACE IS SUFFICIENTLY SMALL, THE FLOW IS DEFLECTED THROUGH AN OBLIQUE, ATTACHED SHOCK WAVE RQ. THIS IS TYPE III INTERFERENCE. THE ATTACHMENT OF THE FREE SHEAR LAYER PR IS ANALOGOUS TO THE REATTACHMENT OF A SEPARATED BOUNDARY LAYER BEHIND A BACKWARD FACING STEP IN A SUPERSONIC FLOW. THE PRESSURE RISE AT R IS EASILY CALCULATED. THERE IS ALSO A LARGE INCREASE IN THE HEAT TRANSFER RATE AT R, RESULTING FROM THE DRASTIC THINNING OF THE BOUNDARY LAYER. METHODS TO PREDICT THIS HEATING ARE PRESENTLY BEING DEVELOPED.



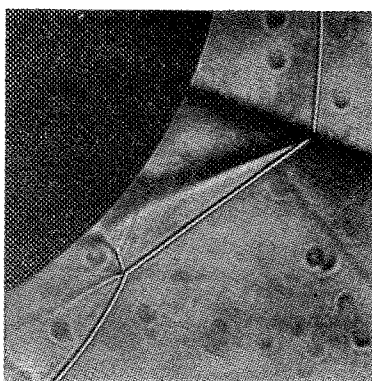
(a) CYLINDER // PLATE L.E.



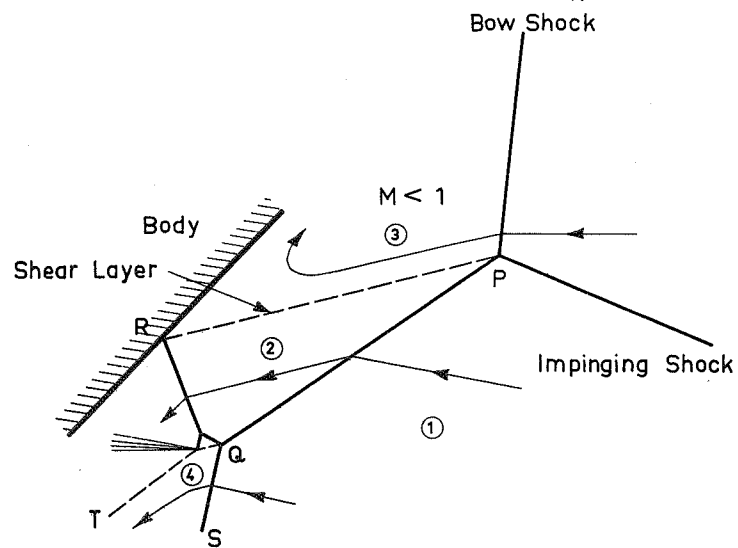
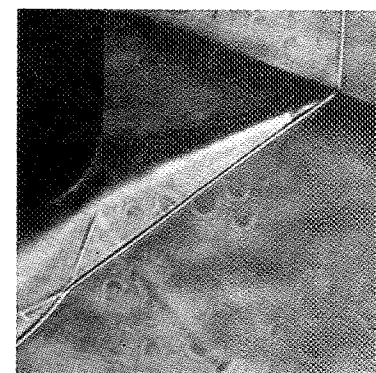
(b) WEDGE



(c) SWEPT CYLINDER

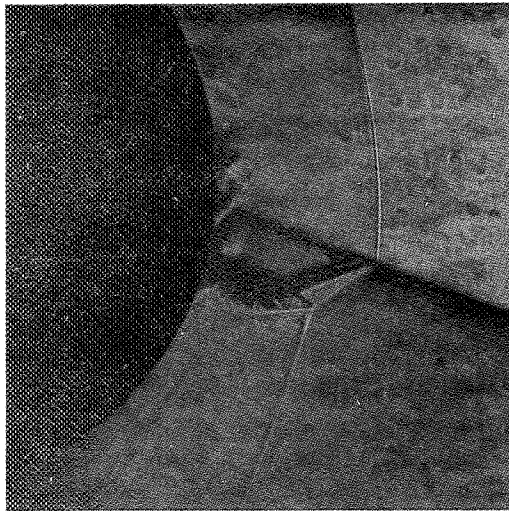


(d) HEMISPHERE

Type III interference.  $M = 4.6$ ,  $\xi = 10$ .

(e) FLAT FACED CYLINDER

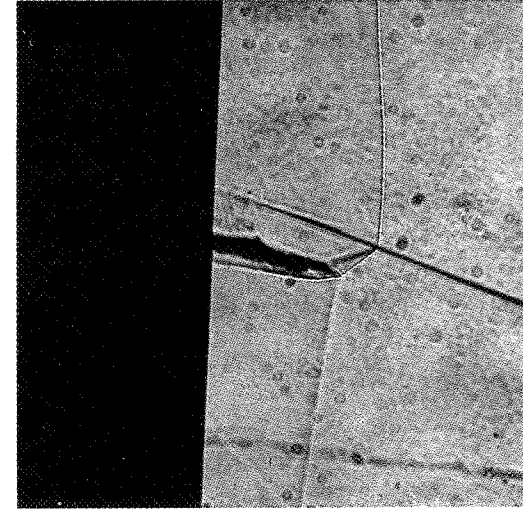
THIS FIGURE SHOWS TYPE IV INTERFERENCE, WHICH IS CHARACTERIZED BY A CURVED, SUPERSONIC JET EMBEDDED IN A SUPERSONIC FLOW FIELD. IT IS SET UP WHEN THE FLOW INCLINATION IS REGION 2 RELATIVE TO THE BODY SURFACE IS TOO LARGE FOR THE FLOW TO BE DEFLECTED THROUGH AN ATTACHED SHOCK WAVE. THE PRESSURE RECOVERY IN THE JET MAY BE MANY TIMES THAT IN REGIONS 3 AND 4. THE COMBINATION OF HIGH PRESSURE RECOVERY AND A NARROW JET, WITH LARGE VELOCITY GRADIENTS AT THE STAGNATION POINT, RESULT IN EXTREMELY HIGH HEAT TRANSFER RATES. TYPE IV INTERFERENCE IS THE MOST SEVERE TYPE OF INTERFERENCE.



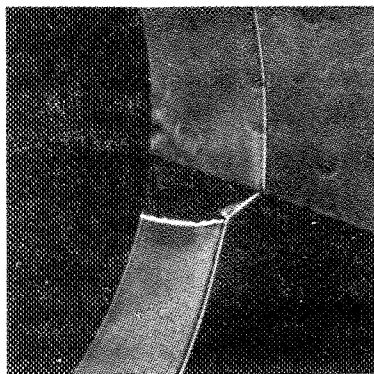
(d) CYLINDER // PLATE L.E.



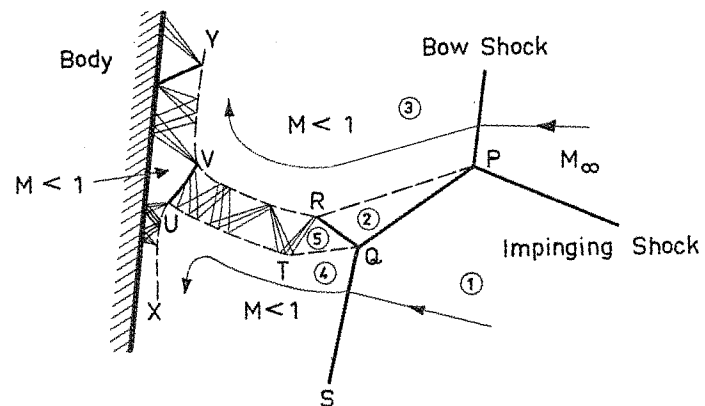
(b) WEDGE



(c) SWEEP CYLINDER



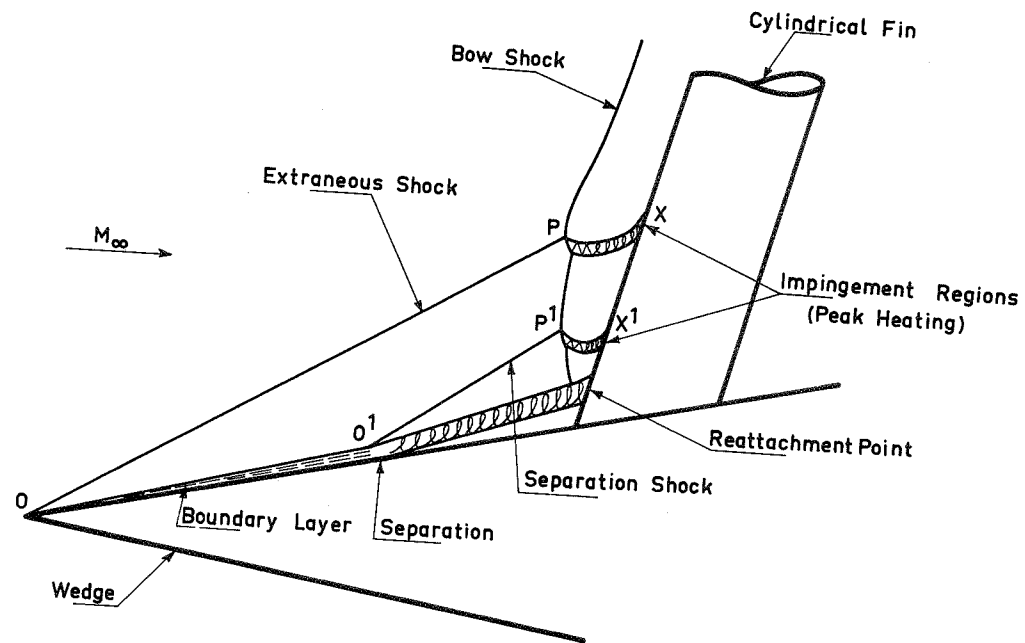
(d) HEMISPHERE

Type IV interference,  $M = 4.6$ ,  $\xi = 10^\circ$ 

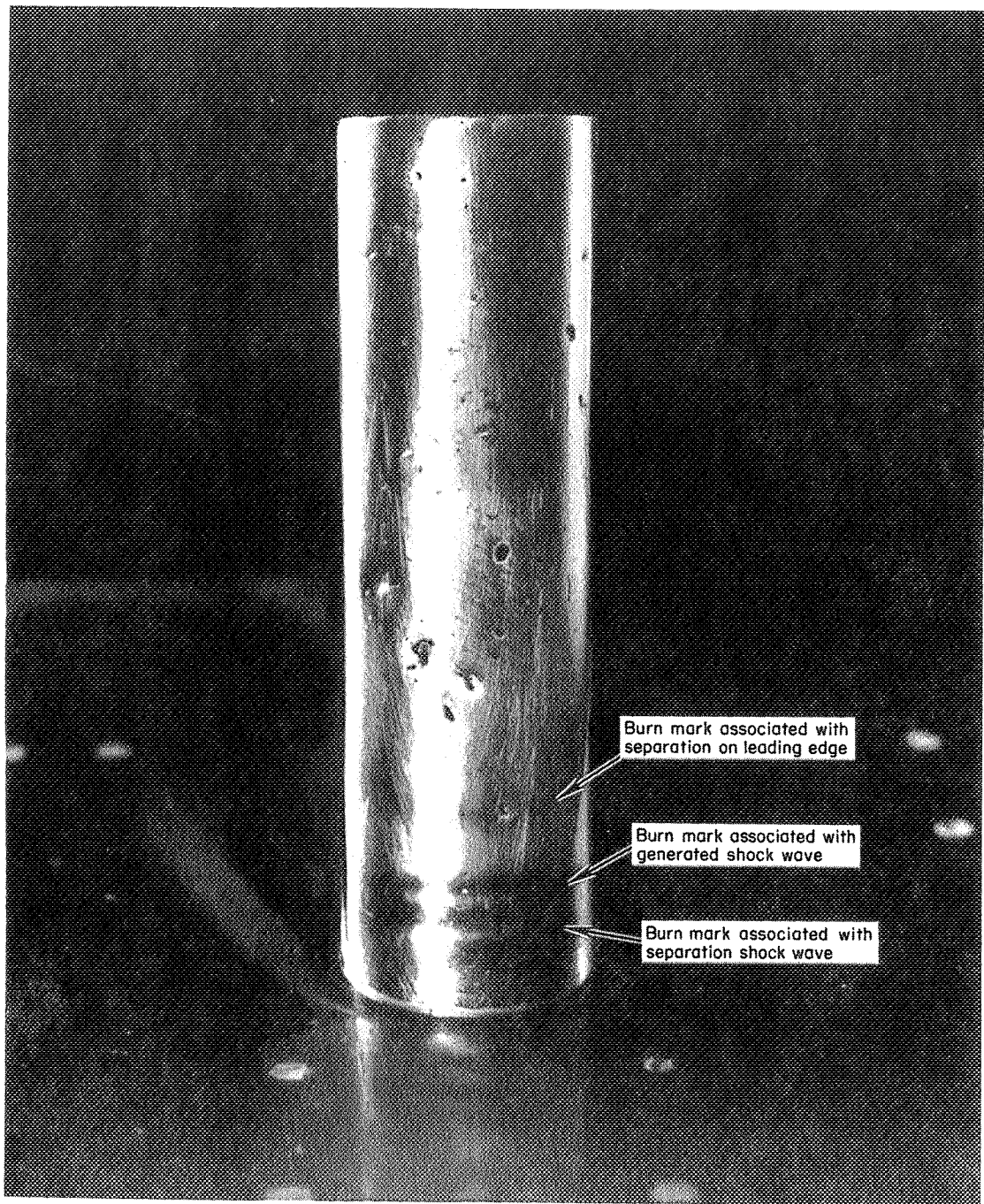
(e) FLAT FACED CYLINDER

THE FIGURE SHOWS HOW BOUNDARY LAYER SEPARATION AHEAD OF A BLUNT FIN, TYPICAL OF EARLIER EXPERIMENTS CAN GIVE RISE TO SEVERAL HOT SPOTS ALONG THE LEADING EDGE. IN THIS CASE TWO TYPE IV INTERFERENCE REGIONS EXIST.



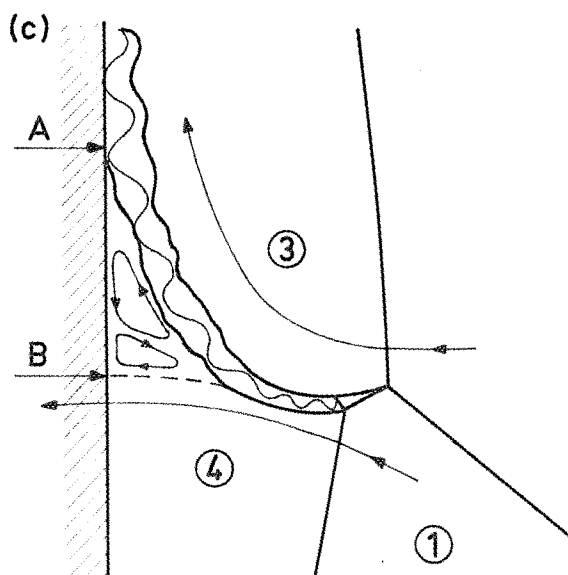
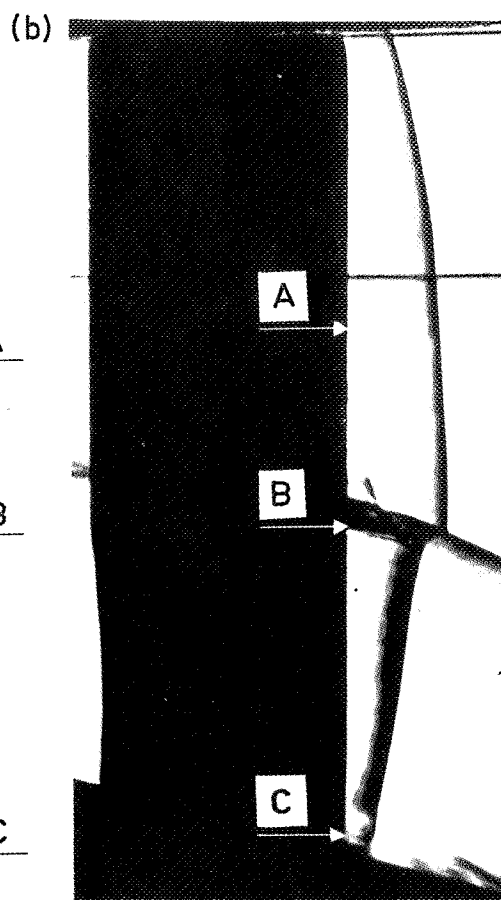
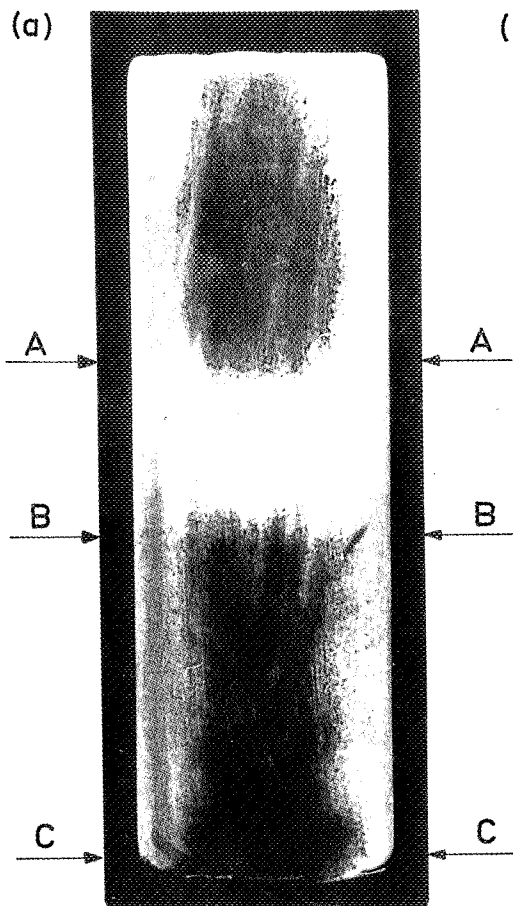


THIS PHOTOGRAPH BY HIERS AND LOUBSKY VIVIDLY ILLUSTRATES THE EFFECT OF SHOCK IMPINGEMENT ON A BLUNT LEADING EDGE. IN SPITE OF THE SHORT DURATION OF THE TEST ( $\sim 5$  MSEC) IN THE NASA AMES COMBUSTION DRIVEN SHOCK TUNNEL, THE METAL HAS BEEN 'BLUED' IN SEVERAL PLACES. NOTE ALSO THE HEATING ON THE FLATPLATE SHOCK GENERATOR CAUSED BY THE DETACHED FIN SHOCK.



UNDER CERTAIN CONDITIONS THE SUPERSONIC JET MAY BE DEFLECTED UPWARDS TO THE POINT WHERE IT ONLY JUST GRAZES THE FIN LEADING EDGE. VISCOUS FORCES ALSO REDUCE THE IMPACT PRESSURE OF THE JET. IN SUCH CASES THERE MAY BE A REDUCTION IN THE STAGNATION POINT HEATING AS SHOWN IN THE ACCOMPANYING FIGURE, WHICH SHOWS THE RESULTS OF HEAT TRANSFER TESTS USING A TEMPERATURE SENSITIVE PAINT.

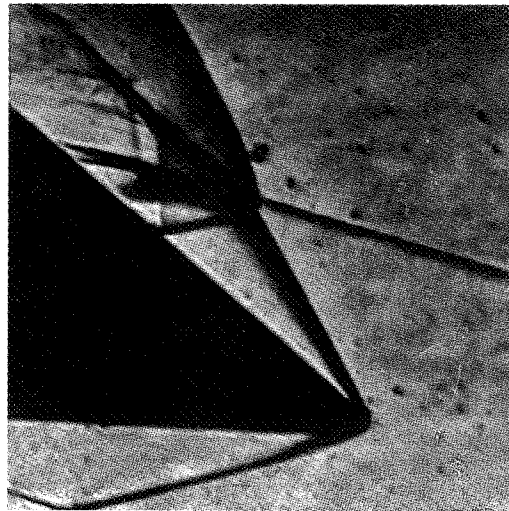
WHETHER WE HAVE A STRONG INTERACTION AS SHOWN IN FIGURE 19 OR A WEAK INTERACTION AS SHOWN IN FIGURE 20 IS THOUGHT TO DEPEND ON THE RATIO OF THE LEADING EDGE RADIUS TO THE DISTANCE BC. FOR SMALL VALUES THE INTERACTION IS WEAK FOR LARGE VALUES IT IS STRONG. FURTHER WORK TO RESOLVE THIS PROBLEM IS NEEDED.



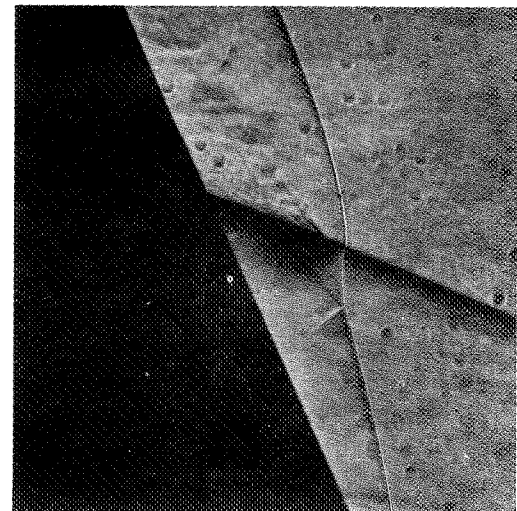
THIS SHOWS TYPE V INTERFERENCE. IT IS SIMILAR TO TYPE II INTERFERENCE EXCEPT THAT THERE IS A THIN SUPERSONIC JET ORIGINATING AT P RATHER THAN A SIMPLE SHEAR LAYER.



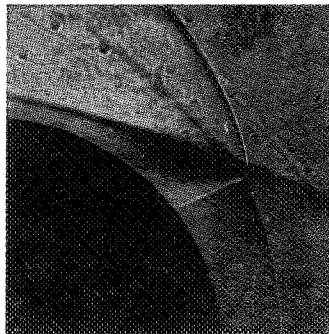
(d) CYLINDER // PLATE L.E.



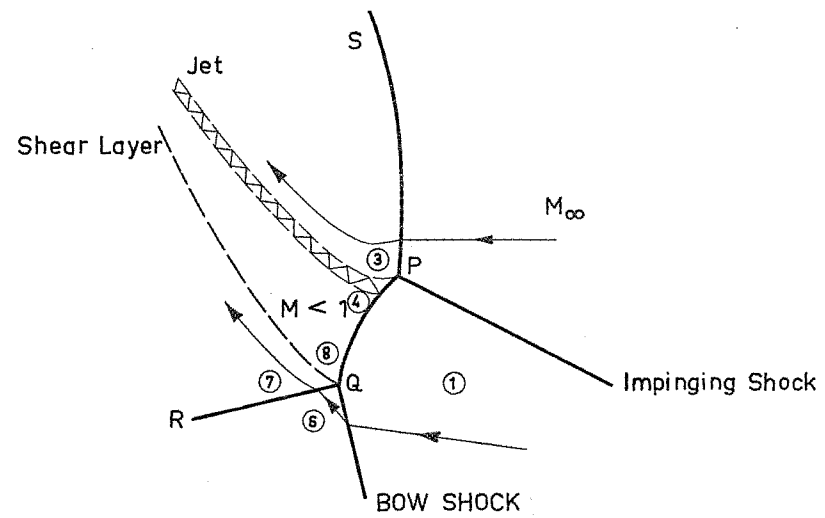
(b) WEDGE



(c) SWEPT CYLINDER



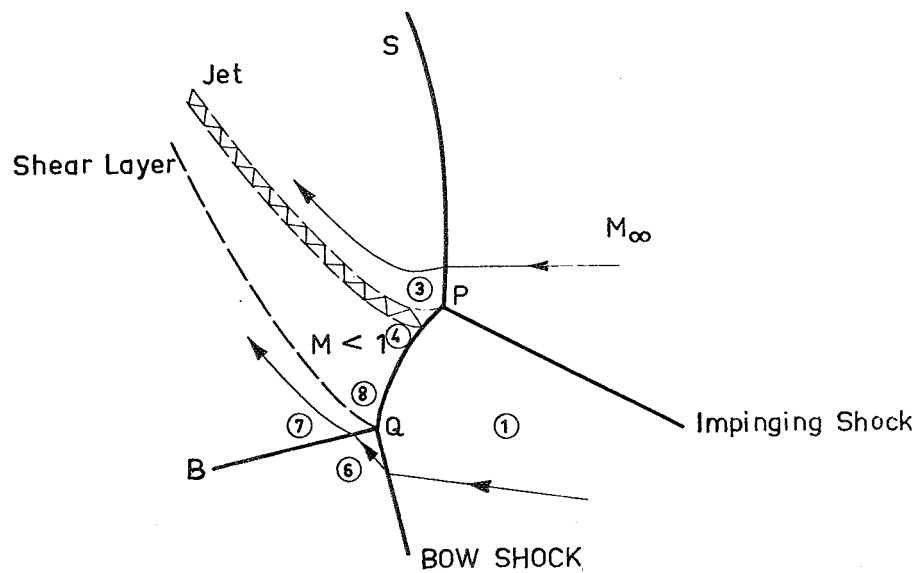
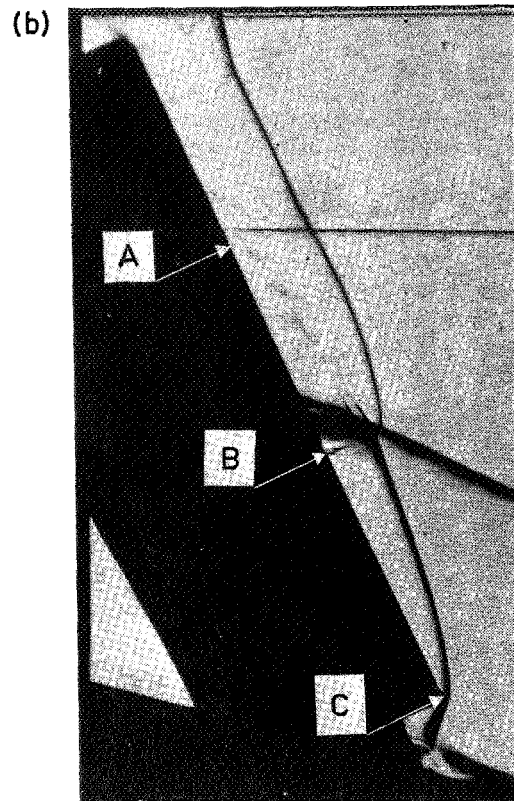
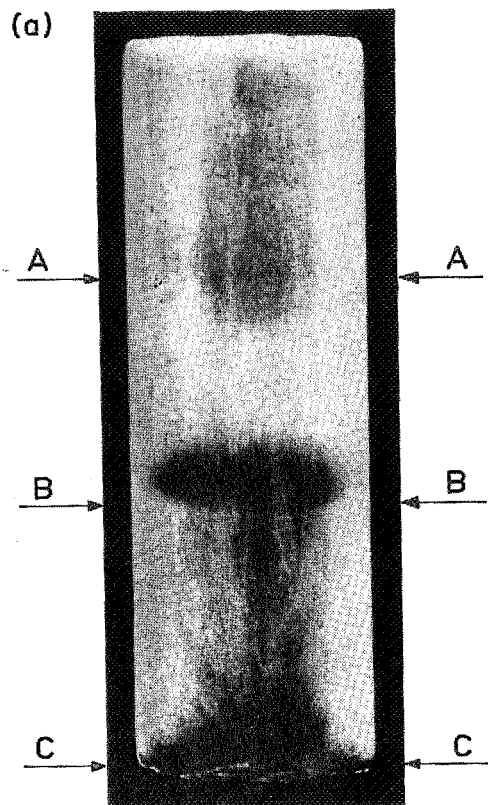
(d) HEMISPHERE



Type V interference.  $M \approx 4.6$ ,  $\xi = 10^\circ$ .

TYPE V INTERFERENCE MAY RESULT IN SEVERAL HOT SPOTS ALONG THE LEADING EDGE AS SHOWN IN THE ACCOMPANYING FIGURE. THE HEATING CAUSED BY THE TRANSMITTED SHOCK WAVE QB AND THE MERGING SHEAR LAYER AND JET IMPINGING ON THE FIN AT A ARE CLEARLY DETECTABLE.

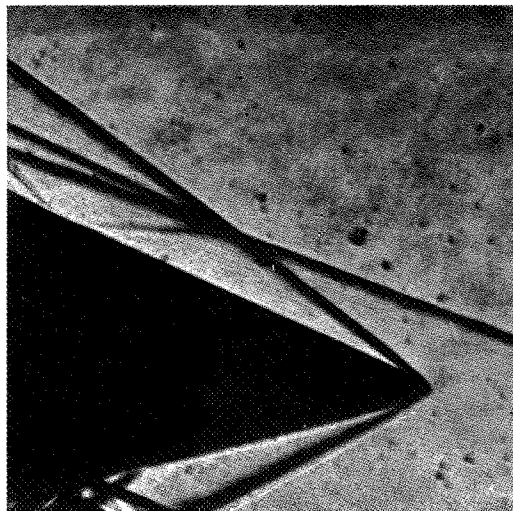




TYPE VI INTERFERENCE OCCURS WHEN WEAK, OBLIQUE SHOCKS OF THE SAME FAMILY INTERSECT. THE TRANSMITTED EXPANSION ORIGINATING AT P CAUSES NO PROBLEMS, SINCE IT RESULTS IN A FAVORABLE PRESSURE GRADIENT. THE SHEAR LAYER RARELY IMPINGES ON THE BODY AND THEREFORE CANNOT EFFECT THE HEAT TRANSFER.



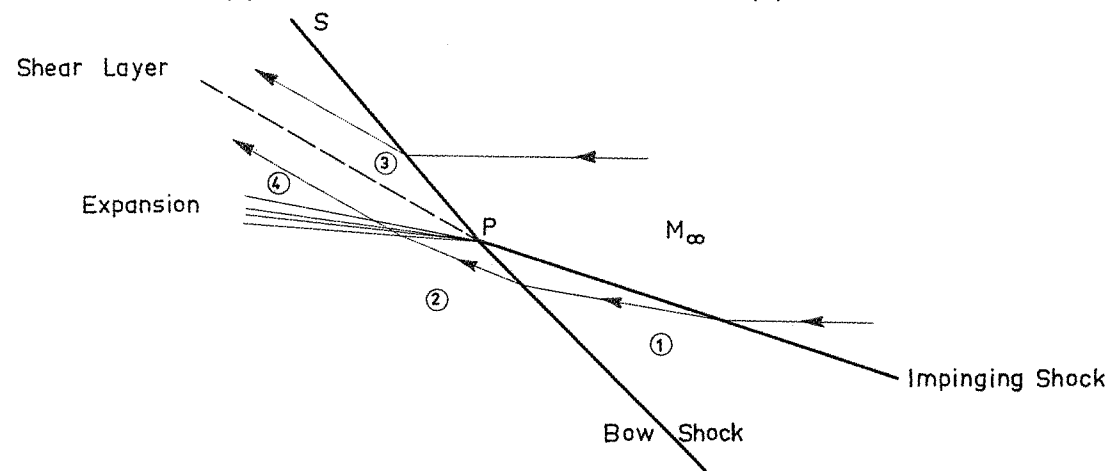
(a) CYLINDER // PLATE L.E.



(b) WEDGE



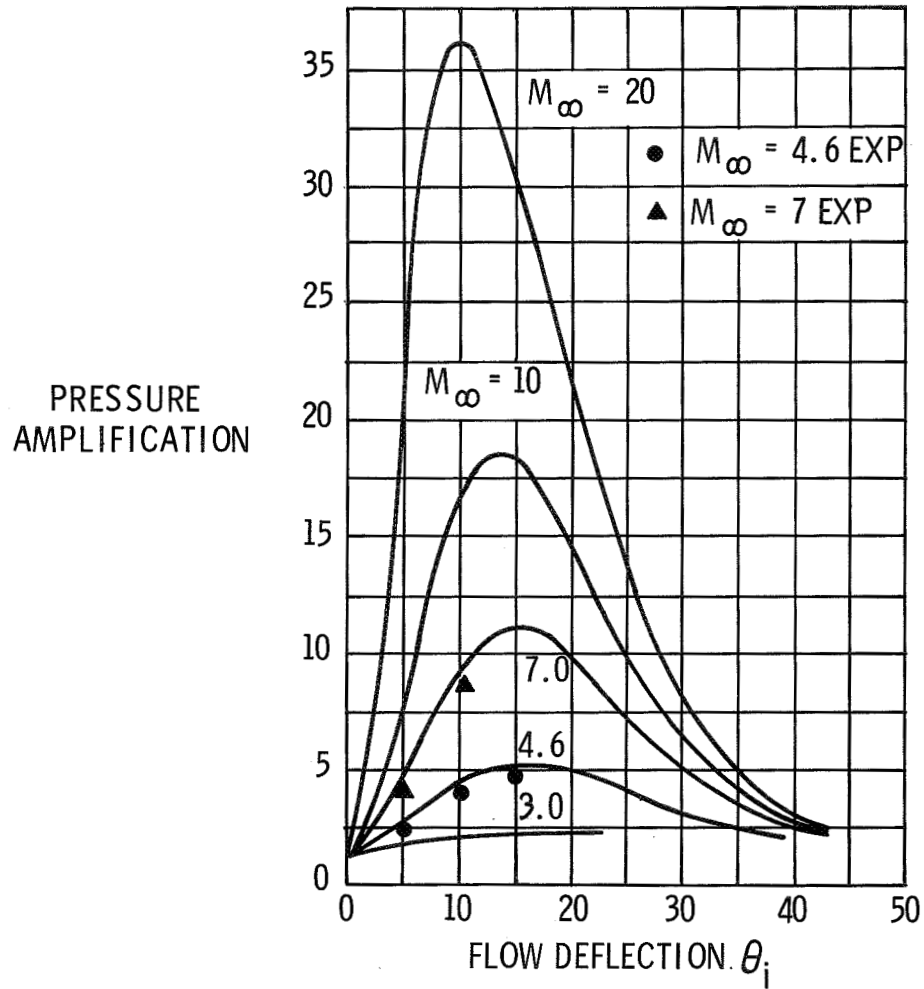
(c) SWEPT CYLINDER



Type VI interference,  $M = 4.6$ ,  $\xi = 10^\circ$ .

IN THIS FIGURE WE SHOW THE PRESSURE AMPLIFICATION (I.E., THE PEAK PRESSURE NORMALIZED WITH RESPECT TO THE STAGNATION POINT PRESSURE IN THE ABSENCE OF THE SHOCK) AS A FUNCTION OF THE FLOW DEFLECTION  $\Theta_1$  THROUGH THE IMPINGING SHOCK WAVE. NOTE THAT THE PRESSURE AMPLIFICATION INCREASES MONOTONICALLY WITH INCREASING MACH NUMBER AND IS A MAXIMUM FOR  $\Theta_1$  BETWEEN 10 AND 15° DEPENDING ON  $M_\infty$ . THE AGREEMENT WITH EXPERIMENT AT  $M=4.6$  AND 7 IS EXCELLENT.

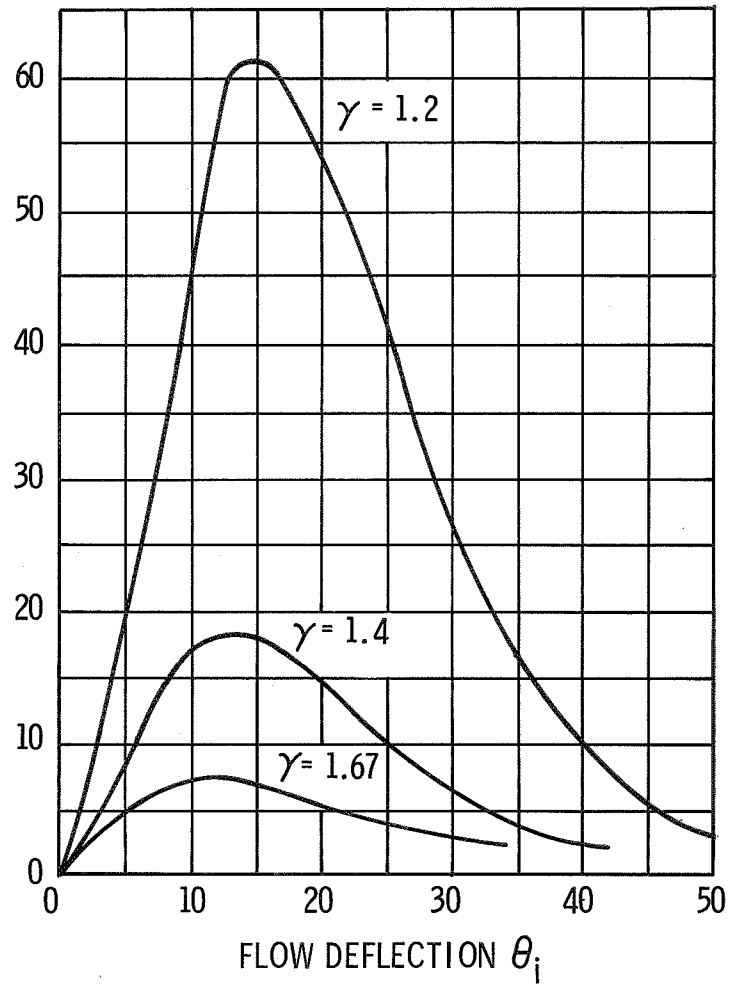
PRESSURE AMPLIFICATION FOR TYPE IV INTERFERENCE AS A  
FUNCTION OF  $\theta_i$  FOR VARIOUS FREE-STREAM MACH NUMBERS  $\gamma = 1.4$



IN THIS FIGURE WE SHOW THE EFFECT OF VARYING  $\gamma$  FOR A CONSTANT  $M_\infty = 10$ . THERE IS ALMOST AN ORDER OF MAGNITUDE DIFFERENCE IN THE AMPLIFICATION IN HELIUM ( $\gamma = 1.67$ ) AND AIR AT HIGH ALTITUDE ( $\gamma = 1.2$ ). EXPERIMENTS ARE PRESENTLY BEING CONDUCTED TO CHECK THESE PREDICTIONS. THESE CALCULATIONS SUGGEST THAT REAL GAS EFFECTS MAY BE APPRECIABLE AND A CORRECTION FACTOR MUST BE APPLIED TO DATA OBTAINED IN HELIUM OR LOW ENTHALPY AIR FACILITIES.

PRESSURE AMPLIFICATION FOR TYPE IV INTERFERENCE  
AS A FUNCTION OF  $\theta_i$  FOR VARIOUS  $\gamma$ .  $M_\infty = 10$ .

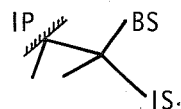
PRESSURE  
AMPLIFICATION



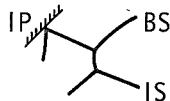
KNOWING THE CONDITIONS FOR A GIVEN TYPE OF INTERFERENCE PATTERN TO OCCUR, WE CAN MAKE AN EDUCATED GUESS AS TO THE LOCATION OF HOT SPOTS ON THE VEHICLE, THE TYPE OF INTERFERENCE AT THAT POINT AND THE MAGNITUDE OF THE HEATING. THE ACCOMPANYING FIGURE ILLUSTRATES THIS APPROACH.



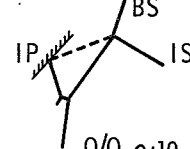
## SHOCK INTERFERENCE PATTERNS

TYPE I  
INTERFERENCE

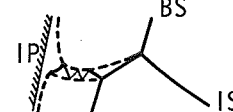
$$Q/Q_0 \sim 10$$

TYPE II  
INTERFERENCE

$$Q/Q_0 \sim 5$$

TYPE III  
INTERFERENCE

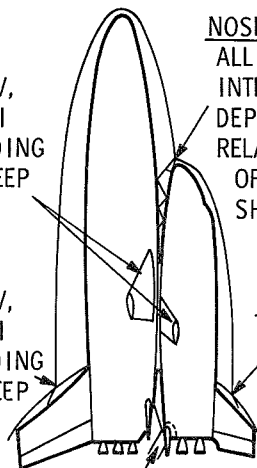
$$Q/Q_0 \sim 10$$

TYPE IV  
INTERFERENCE

$$Q/Q_0 \sim 20$$

WINGS:  
TYPE IV,  
V OR VI  
DEPENDING  
ON SWEEP

FIN:  
TYPE IV,  
V OR VI  
DEPENDING  
ON SWEEP

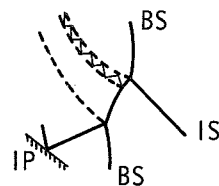


NOSE:

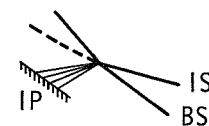
ALL TYPES OF  
INTERFERENCE  
DEPENDING ON  
RELATIVE LOCATION  
OF STAGES (TYPE III  
SHOWN HERE)

FIN:  
TYPE IV, V OR  
VI DEPENDING  
ON SWEEP

BETWEEN STAGES:  
TYPE I OR II

TYPE V  
INTERFERENCE

$$Q/Q_0 \sim 5$$

TYPE VI  
INTERFERENCE

$$Q/Q_0 \sim 1$$

# INTERFERENCE AND RADIATION BLOCKAGE EFFECTS ON SURFACE TEMPERATURES OF COMPOSITE FLIGHT VEHICLES

Alfred C. Thomas

The Boeing Company  
Seattle, Washington

## SUMMARY

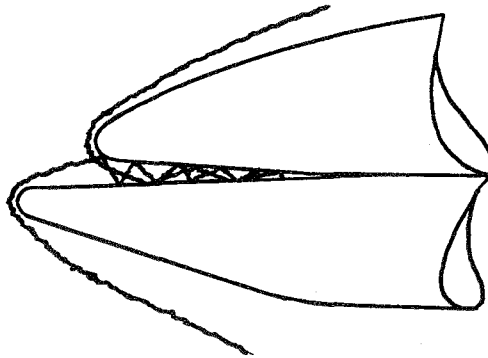
An analysis is presented that exposes a potential critical thermal protection system (TPS) problem for composite flight vehicles (CFV). The problem is caused by flow field interference and radiation blockage in the gap between a combined booster and orbiter vehicle during boost. Data shown here indicate that CFV TPS surface panels in the gap may exceed Rene' 41 design limit temperatures of 1600°F for about 60 seconds during boost and at some point in the gap may reach temperatures in excess of 2200°F. This is significant because reusable booster vehicle TPS panels are designed for conditions corresponding to booster flyback (not boost) and do not generally require high temperature capability.

## INTRODUCTION

Two stage space shuttle transportation systems consist of an orbiter vehicle, a booster vehicle, and a composite flight vehicle. The composite flight vehicle is formed by combining the orbiter and booster into one vehicle for the launch phase of the mission. Twelve different arrangements of booster and orbiter vehicles or CFV are presented in Reference 1. All but one are combined in a parallel arrangement, the exception being the ordinary end to end arrangement. Vehicle combinations of wing to wing, wing to back, and back to back are shown in that study.

A predominant feature of the parallel arrangement is the gap that exists between the two vehicles due to forebody geometry if the vehicles are not "nested" together. Pressure, heating and temperature distributions along the surfaces forming the gap, which is convergent axially and divergent radially, will be quite different during boost from what they would be without the gap because of flow field interference and radiation blockage.

Consider the wing to wing CFV arrangement illustrated in Figure 1. Shock waves will develop over the forebodies during the supersonic and hypersonic portions of boost. These shock waves will close on the two bodies as the Mach number increases. At some condition, the shock wave created by the protruding vehicle may impinge upon the lower portion of the second vehicle nose cap. Multiple and plane shocks similar to those found in supersonic inlets will form at that time. The shock system in the gap may be similar to that illustrated here:



Computer programs such as that described in Reference 2 can be used to predict flow field parameters including local pressures for a multiple shock system in a three-dimensional axisymmetric or two-dimensional supersonic inlet. On the other hand, data presented in Reference 3 indicate that surface pressures in the region of shock impingement can not be predicted with any certainty for parallel staged blunt delta wings. As such, while pressure at any location in the gap can be defined as the product

$$\frac{P}{P_{\infty}} = \prod_{n=1} \frac{P_{n+1}}{P_n} \quad (1)$$

(where n is representative of the number of oblique shocks the flow crosses

as it travels along the surface), analytic techniques have not as yet been developed to define the flow field resulting from the complex interactions present there.

The two-body flow interference affects aerodynamic heating. Data and analysis for two and three dimensional interactions shown in References 4 and 5 indicate sharp increases in heating rates in proximity of plane shocks. As a result, heating rate increases are expected in the gap which are essentially due to sharp increases in static pressure as the flow is shocked down in the simultaneously divergent-convergent channel formed by the two vehicles. Heating rate increases in the gap cannot be predicted analytically with confidence, however, and test results are required.

Since the surface temperature of a reusable shuttle vehicle is dependent upon radiation as a significant cooling mode, the special problem of radiation blockage must be considered in the gap region. Aerodynamic heating and simultaneous radiative blockage coupled with interference effects on heating have been investigated for a gap. An analysis is presented in Reference 6 for a gap which indicates temperatures higher than expected for the level of aerodynamic heating encountered if radiation to space is inhibited.

The purpose of this paper is to present data and analysis that will indicate if a potential TPS problem exists for the booster vehicle portion of a CFV during the boost phase. Results of a test to obtain heating rate data in a CFV gap at  $M_\infty = 8$  are presented. Data derived from this test are applied along a typical boost trajectory to establish booster vehicle CFV surface temperatures in the gap with and without radiation blockage. Surface temperature histories are presented.

#### Model, Test and Data Reduction Description

Phase-change thermal paint heat transfer data have been used to provide the basis for the analyses presented here. A teflon model of a composite flight vehicle composed of booster and orbiter configurations described in Figures 2 and 3 was tested in the Lockheed California Company-30 inch hypersonic wind tunnel and the Arnold Center Tunnel B-50 inch hypersonic wind tunnel. Tests were conducted at  $M_\infty = 8$  for Reynolds numbers between  $0.5$  and  $2.0 \times 10^6$  per foot.

Data, shown in this analysis for  $\alpha = 0^\circ$  and  $\pm 5^\circ$ , were obtained using 16 MM motion picture cameras that photographed the models in plan and side views while the models were in the tunnel test section. Heat transfer data were evaluated from the isotherm melt lines shown on the films using the method and assumptions described in Reference 7.

## Data Presentation

Representative data in the nose region of a booster, an orbiter, and a composite flight vehicle are presented for the vehicle geometries illustrated in Figures 1-3.

Booster and orbiter thermal paint data obtained with the lower surfaces of the models essentially normal to the camera used to record the progression of the paint melt lines are shown in Figures 4 and 5 for  $\alpha = 0^\circ$ . Isotherms shown along the lower surfaces have been reduced to heat transfer coefficient ratios ( $h/h_o$ ) assuming a constant value of the recovery factor. Centerline values of  $h/h_o$  are presented on the same two figures in a more conventional manner in order to clearly illustrate the distribution of heating along the lower surface centerline. Spanwise data shown on these two figures indicate that heating rates increase with distance normal to the centerline at centerline  $X/L$  distance ratios greater than about .05.

Booster lower surface data in the nose region could also be obtained using model side view pictures because of lower surface curvature. These data are presented for both the booster and composite flight vehicle in Figures 6 through 9. Due to the curvature in the booster lower surface and the lack of any other visual evidence, it is extremely difficult to pinpoint exactly where the isotherms shown are located on the lower surface. Examination of the data indicated, however, that good comparisons of heating to the booster alone and to the CFV can be obtained by examining pictures taken by the same camera for models at the same attitude in the tunnel. This technique is applied here. Data for  $\alpha = 0^\circ$  and  $\alpha = -5^\circ$  are shown on these four figures. Booster alone data are presented on Figures 6 and 8, along with the isotherm distribution on the side of the body. These data are relatively uniform and are distributed in the same manner as the data shown in planform pictures along the centerline.

Orbiter effects on booster heating at  $\alpha = 0^\circ$  are shown in Figure 7. These data indicate that at this angle of attack, very little, if any, increase in heating occurs on the booster lower surface. This is not the case for the CFV at  $\alpha = -5^\circ$  (booster nose down). A large disturbance of the flow field in the gap is indicated by the heating rate distribution on the booster surface as shown on Figure 9. Heating along the surface continues to increase with distance, after an initial and normal decrease in heating rates near the nose cap. The flow field indicated by these data is characteristic of that known to exist in a supersonic inlet or diffuser that has a series of multiple shocks down its length. Peak heating rates on the booster surface that are equivalent to those in proximity of the nose cap are present at an

X/L of approximately 0.29. These booster data are the most severe obtained on the CFV during the test. They are used to determine the interference effect on aerodynamic heating in the analysis that follows.

#### Analysis of Interference Effects on Aerodynamic Heating

The objective of this analysis is to determine, within the limits and applicability of the available heat transfer data, the maximum increase in heating rates that can be expected on the booster surface when it is in proximity of the orbiter during boost. One approach is to examine and compare data on the booster surface for the case of the booster alone and for the booster and orbiter joined. Another approach is to calculate a heating rate distribution for the booster alone and compare it to CFV data. The latter approach is taken here because tests of the booster alone did not result in data at locations on the booster corresponding to surfaces in the gap of the CFV.

Prediction of the booster heating distribution on the lower surface is complicated by the lack of any flow field or pressure information. As a result, different flow field assumptions were made and used with the laminar  $\text{RhoMu}$  heating rate prediction method (Reference 8) until the data were correlated. Data-theory comparisons are presented for the booster and orbiter in Figures 10 and 11. At  $\alpha = -5^\circ$ , normal shock expansion theory was combined with sharp unyawed cone theory to establish an inviscid pressure distribution. This method assumes that all of the gas at the surface has passed through a normal shock, stagnates at the nose cap stagnation point, and then expands isentropically to conditions that would exist on a sharp unyawed cone. Nose bluntness effects on local pressures downstream of the nose cap were determined along the centerline using correlations based on a blast wave analogy. The induced pressure component of the local pressure is computed using the following expression from Reference 9.

$$C_{p_N} = \frac{0.060 \left( \frac{M_\infty}{X/D} \right)^2 (C_{D_N})^{1/2} - 0.45}{1/2 \gamma M_\infty^2} \quad (2)$$

where  $C_{D_N}$ , the nose cap drag coefficient, has been assumed equal to 0.9.

At  $\alpha = 0^\circ$ , a modified oblique shock theory assumption was necessary to obtain the data correlation shown in Figure 10. This method assumes that the booster shock is attached at  $X/L = 0$  and the pressure coefficient at  $X/L = 0$  is 0.5 of 1% higher than the pressure coefficient at the nose cap

shoulder (including induced pressure effects). This assumption results in a finite velocity at  $X/L = 0$  and reduces the downstream effect of the initial entropy gain on the local velocity distribution as the gas is allowed to expand isentropically along the centerline.

At  $\alpha = 5^\circ$ , the technique described for  $\alpha = 0^\circ$  was used to obtain the pressure distribution along the centerline. To obtain a reasonable data-theory correlation, it was necessary to account for the pressure gradient normal to the centerline (crossflow pressure gradient) on streamline divergence along the centerline. This gradient is accounted for by evaluating the streamline divergence parameter  $f$  in RhoMu theory. Reference 10 defines  $f$  for an axisymmetric body as

$$\frac{1}{f} \frac{\partial f}{\partial x} = \frac{1}{2r} \left[ -\frac{\partial r}{\partial x} + \sqrt{\left(\frac{\partial r}{\partial x}\right)^2 - \frac{4}{\rho_e U_e^2} \frac{\partial^2 P_e}{\partial \theta^2}} \right] \quad (3)$$

where  $r$  is local body radius,  $\rho_e$  is density,  $U_e$  is velocity and  $P_e$  is pressure along the streamline, and  $\theta$  is the angle measured from the windward generator.

Orbiter heating rate data-theory correlations are presented on Figure 11 for  $\alpha = 0^\circ, +5^\circ$ . Lower surface centerline heating was estimated using delta wing theory as described in Reference 11. Local pressures were determined using the sharp body technique described for the booster with isentropic expansion from  $X/L = 0$  to sharp delta wing values. These data indicate that the flow on the orbiter at  $\alpha = 0^\circ$  is expanding at a much faster rate than estimated by this method. More extensive analysis is required to infer flow field properties for this vehicle at  $\alpha = 0^\circ$  than is necessary to complete the objectives of the analysis presented in this paper.

Heating rate distributions on the adjacent surfaces of the two vehicles which form the CFV are shown as a function of the booster non-dimensional distance ratio in Figure 12. A negative value of  $X/L$  indicates that the orbiter nose protrudes in front of the booster nose as shown by the illustration on the figure. These data indicate that the peaks and valleys occur at different values of  $X/L$  on the two vehicles. This difference depends directly on the oblique shock system that exists between the two vehicles.

Empirical heating rate distributions along the bottom of the booster and orbiter vehicles similar to those presented in Figures 10 and 11 (which were obtained using a plan view camera) were determined using a side view camera and extended to applicable values of  $X/L$  using theoretical parameters in order to provide a basis for comparison. Booster heating rate ratios shown in Figure 12 have been ratioed to the theoretical values and are presented

as a function of  $X/L$  in Figure 13 for  $\alpha = -5^\circ$  (booster nose down). Interference effects are intensified as the gap size converges axially.

In the course of the data analysis, it was determined that peak heating rates caused the paint to melt faster than the film technique used could record the recession. The peaks can be inferred, however. Straight line extrapolation of the data shown on Figure 13 indicate that peaks occur at  $X/L$  of approximately .035, .12, .17, and .29. In between the peaks lower heating rates were measured. These data indicate also that heating peaks are increasing with distance along the surface until  $X/L = .29$ . Evidently a normal shock occurs at about this location which causes the flow to go subsonic. Heating rates due to interference are expected to be sharply decreased in subsonic flow.

In order to determine an upper limit, the worst case obtained experimentally has been analyzed. An envelope of the extrapolated peak interference heating rates, neglecting the valleys indicated by the data, was drawn and is presented as Figure 14. For this vehicle, the maximum increase in the heating rates due to interference is 9.6 times the undisturbed value. It is interesting to note that this increase agrees quite well with the maximum increase due to interference shown in Reference 12 for a combined booster-orbiter of quite a different design. That maximum increase is indicated along the ordinate of Figure 14 for comparison purposes.

#### Radiation Blockage Effects on Surface Temperature

No interference data are available for this configuration at Mach numbers lower than eight. The approach used here to estimate transient surface temperatures during boost is to use the maximum increase measured at the test Mach number as a multiplier on the undisturbed convective heat transfer coefficients at the lower Mach numbers. Theoretical calculations are used to determine undisturbed heating rate values as a function of time from launch.

Transient temperature at most locations on the booster TPS surface can be estimated using the heat balance relationship:

$$\rho c \ell \frac{dT}{dt} = B h (T_{AW} - T) - \sigma \epsilon T^4 \quad (4)$$

where  $\rho$  and  $c$  are TPS material density and specific heat,  $\ell$  is the TPS



gauge,  $\epsilon$  is the TPS emissivity,  $\sigma$  is the Stefan-Boltzman constant,  $h$  is the undisturbed heat transfer coefficient,  $B$  is the multiplier due to interference effects,  $T_{AW}$  is the driving function (recovery temperature),  $t$  represents time and  $T$  is the local TPS surface temperature. This relationship implicitly assumes free radiation to space. However, in the gap that exists on most composite flight vehicles, free radiation to space from the surfaces in proximity of each other cannot occur. Instead, at each element of the surface a portion of the radiant energy is transmitted to space and a portion is directed at surface elements of the attached vehicle.

As a result, an effective radiation interchange exists between the booster and the orbiter and the radiation term in Equation (2) must be expressed as

$$(\dot{q}_R)_{NET} = \sigma F_{1-2} F_\epsilon (T_1^4 - T_2^4) \quad (5)$$

where  $F_{1-2}$  is a geometric view factor which relates how well any particular radiating surface element "sees" an element of a second radiating surface,  $F_\epsilon$  is an emissivity factor that accounts for the departure of the TPS surface from a black body, and  $T_1$  and  $T_2$  are the temperatures of the surface elements involved in the interchange. This equation implies that surface temperatures will be higher in the gap. The effects of reradiation in the gap can be determined by defining a blockage multiplier  $F$  that accounts for  $F_{1-2}$ ,  $F_\epsilon$  and surface temperature differences, and allows equation (2) to be rewritten

$$\rho c \ell \frac{dT}{dt} = Bh (T_{AW} - T) - \sigma F T^4. \quad (6)$$

Now  $F$  will change for each specific CFV arrangement, vehicle contour and surface material. In order to demonstrate the effects of  $F$  on CFV transient temperatures, calculations have been made along the boost trajectory shown in Figure 15 and the results are presented here for values of  $F = 0, .25, .5, .75$  and  $1.0$ . Temperature results are presented in Figure 16 as a function of time from launch for a Rene' 41 TPS surface, .022 inches thick, having  $\epsilon = 0.8$ .

The analysis shows that there is a 1000°F difference indicated between uninhibited radiation to free space ( $F = 1$ ) and no radiation capability at all ( $F = 0$ ). Booster TPS lower surface panels reach Rene' 41 limit design temp-

temperatures during boost if 50% of the radiation from the booster is blocked. This analysis also indicates that at some locations along the centerline, TPS surfaces may reach temperatures in excess of 2200°F.

Actual TPS temperature histories in the gap are very trajectory history dependent. Calculations have been performed along the three trajectories presented in Figure 15 for  $F = 0$  to show the effect of the trajectory history on gap temperatures. The temperature histories are presented in Figure 17. There is a 860°F difference indicated between the most and least severe trajectories at staging. This indicates that radiation blockage effects on surface temperatures must be evaluated along specific design trajectories.

### Conclusions

Parallel staged composite flight vehicle gap heating during boost presents a potential booster vehicle design problem. TPS skin panels in the gap are affected by increases in heating rates due to flow field interference and higher than ordinary increases in temperature due to radiation blockage.

This analysis indicates that gap TPS temperatures are very dependent upon the CFV trajectory history and that booster TPS surface panels having the greatest temperature capability should face the orbiter in any CFV configuration in order to lower booster vehicle total TPS skin panel weight.

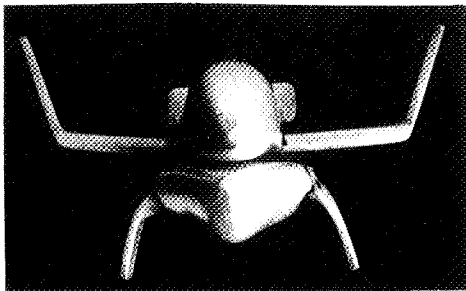
Predictions of the increases in heating due to interference in the CFV gap will be made with confidence only after additional analytic and experimental studies are completed that further define the complex flow field and pressure field that exists there. The effects of radiation blockage on particular combinations of booster and orbiter vehicle TPS surface temperatures require detailed thermal analysis along specific design trajectories to insure adequate protection during boost.

# LIST OF SYMBOLS

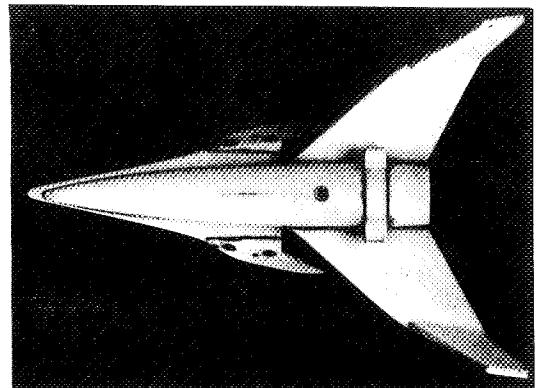
B	Interference effect multiplier, dimensionless.
c	Specific heat, BTU/lb <sub>m</sub> °R
C <sub>D</sub>	Drag coefficient, dimensionless
C <sub>p</sub>	Pressure coefficient, dimensionless
D	Nose cap diameter, inches.
F	Reradiation blockage multiplier, dimensionless.
F <sub>1-2</sub>	Geometric view factor, dimensionless.
F <sub>e</sub>	Emissivity factor, dimensionless.
f	Divergence parameter, Equation 3, inches.
h	Heat transfer coefficient, BTU/ft <sup>2</sup> -sec-°R
L	Total length, inches.
ℓ	Thickness, ft.
M	Mach number, dimensionless
P	Pressure, psia
r	Radius, inches.
T	Surface Temperature, °R
t	Time, sec.
u, v	Velocity normal to and parallel to centerline, fps
X, x	Axial distance, inches.
y	Distance normal to centerline, inches.
α	Angle of attack, degrees.
Y	Ratio of specific heat, dimensionless.
ε	Emissivity, dimensionless.
π	Product of n terms ( $\frac{P_2}{P_1} \times \frac{P_3}{P_2} \times \dots \times \frac{P_{n+1}}{P_n}$ ), dimensionless
ρ	Density, lb <sub>m</sub> /ft <sup>3</sup>
σ	Stefan-Boltzman constant, BTU/-ft <sup>2</sup> -sec-°R <sup>4</sup>
θ	Angle measured from windward generator, degrees.

## SUBSCRIPTS

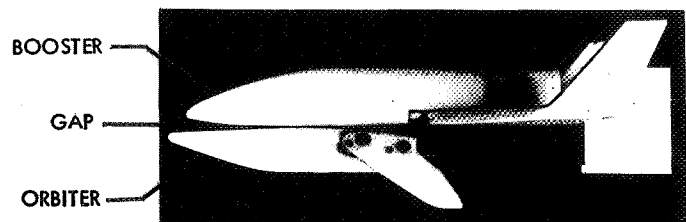
AW	Adiabatic Wall
e	Boundary layer edge
N	Nose
n	Number of oblique shocks
o	Stagnation conditions
∞	Free stream



FRONT VIEW



PLAN VIEW

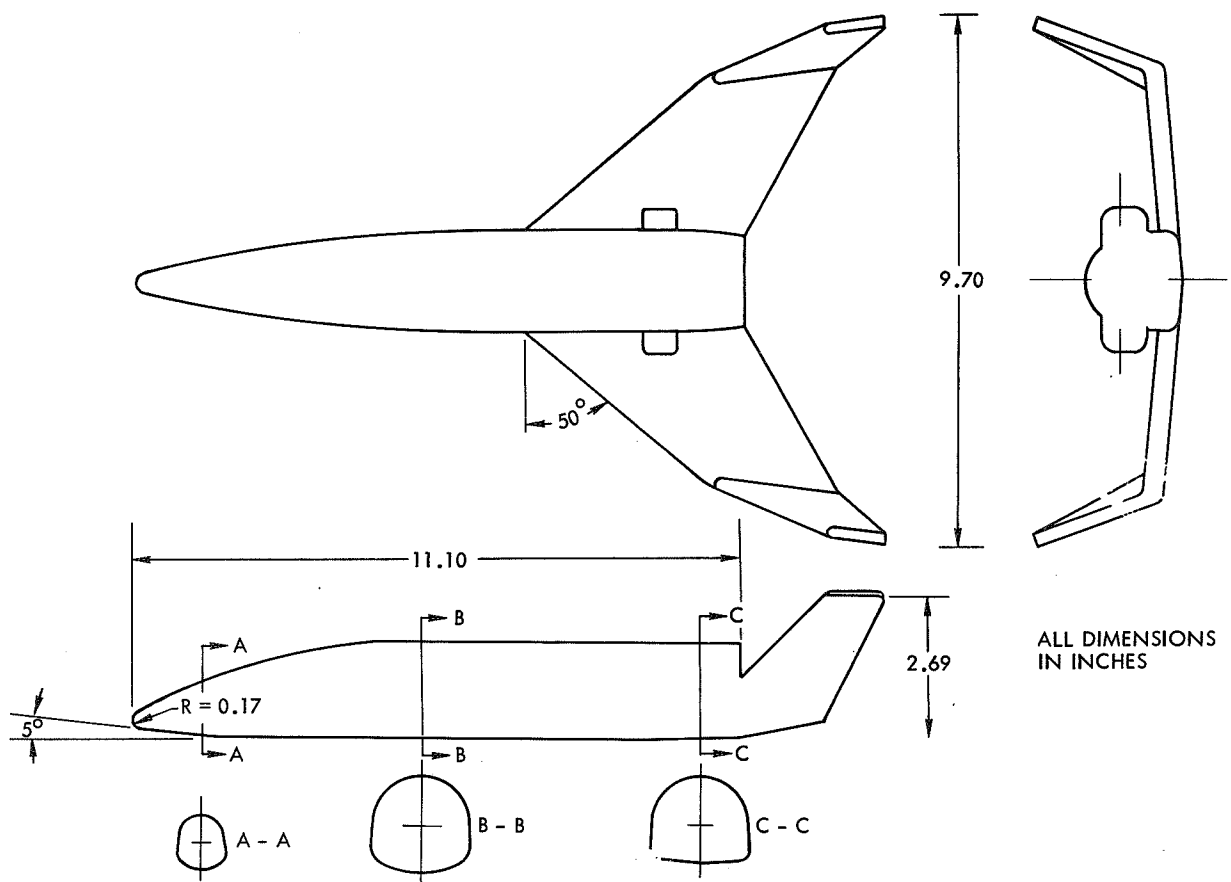


SIDE VIEW

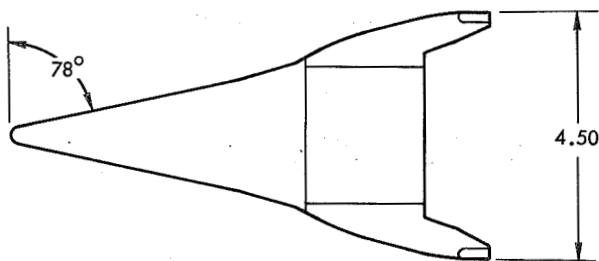
COMPOSITE FLIGHT VEHICLE (CFV)  
FIGURE 1

## REFERENCES

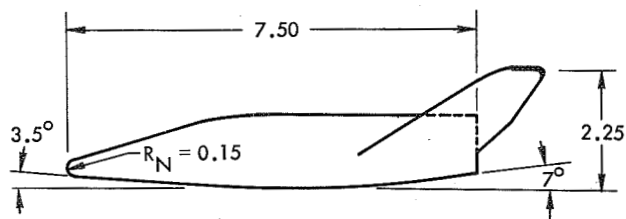
1. McDonnell Douglas Corporation: "Integral Launch and Reentry Vehicle System," Volume 1, Book 1, "Configuration Design and Subsystems," NASA-CR-66864, November, 1969.
2. Sorensen, V.L.: "Computer Program for Calculating Flow Field in Supersonic Inlets," NASA TND 2897, 1965.
3. Jenson, R., Dahlem III, V., Schnabel, C.W.: "Hypersonic Aerodynamic Interference Analysis of Parallel Staged Blunt Delta Wings," AFFDL-TR-68-116, Air Force Flight Dynamics Laboratory, November, 1968.
4. Gulbran, C.E., Redecker, E., Miller, D.S., and Stack, S.L.: "Heating in Regions of Interfering Flow Fields - Part I: Two and Three Dimensional Laminar Interactions at Mach 8," AFFDL-TR-65-49, Part I, Air Force Flight Dynamics Laboratory, July, 1965.
5. Neumann, R.D. and Burke, G.L., "The Influence of Shock Wave Boundary Layer Effects on the Design of Hypersonic Aircraft," AFFDL-TR-68-152, Air Force Flight Dynamics Laboratory, March 1969.
6. Brogren, E.W. and Cheng, H., "Gap Heating Testing," D2-81317-1, The Boeing Company, October 1965.
7. Jones, R.A., and Hunt, J.L., "Use of Fusible Temperature Indicators for Obtaining Quantitative Aerodynamic Heat Transfer Data," NASA TR R-230, February, 1966.
8. Savage, R.T., Jaek, C.L., and Mitchell, J.R.; "Investigation of Turbulent Heat Transfer at Hypersonic Speeds - Volume III: The Laminar-Turbulent  $\rho, \mu$ , Momentum Integral and Turbulent Nonsimilar Boundary Layer Computer Programs," AFFDL-TR-67-144, Air Force Flight Dynamics Laboratory, December, 1967.
9. Van Hise, V., "Analytic Study of Induced Pressure on Long Bodies of Revolution with Varying Nose Bluntness at Hypersonic Speeds," NASA TR R-78, 1961.
10. Savage, R.T. and Jaek, C.L.; "Investigation of Turbulent Heat Transfer at Hypersonic Speeds - Volume I: Analytic Methods," AFFDL-TR-67-144, Air Force Flight Dynamics Laboratory, December, 1967.
11. Thomas, A.C., Perlbachs, A., and Nagel, A.L., "Advanced Reentry Systems Heat Transfer Manual for Hypersonic Flight," AFFDL-TR-65-195, Air Force Flight Dynamics Laboratory, October, 1966.
12. Forsythe, C.G., "Supporting Report No. R.O.T. IV-2, Experimental Heat Transfer Distributions (Lockheed Parallel Development Program)," LR-18584, Lockheed-California Company, January, 1965.



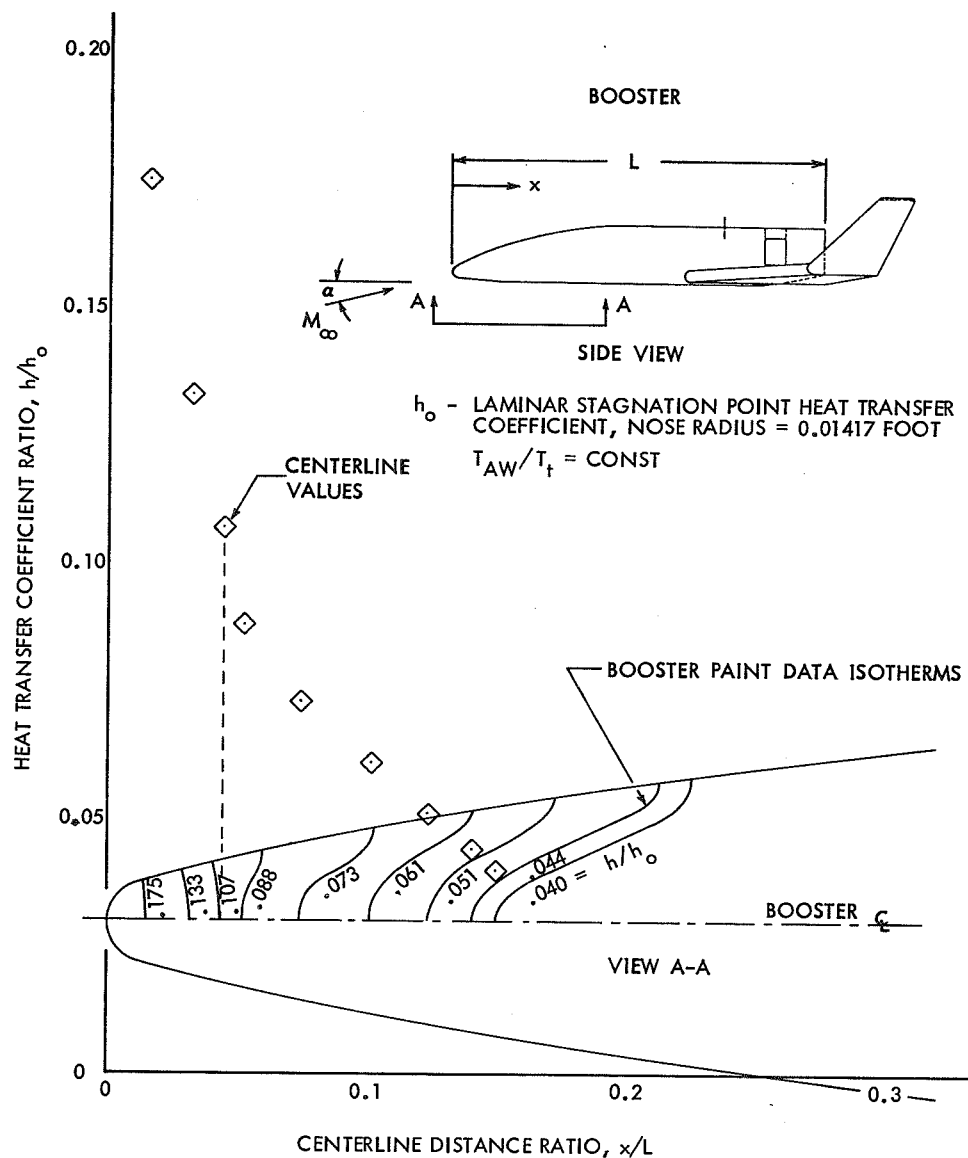
BOOSTER WIND TUNNEL MODEL  
FIGURE 2



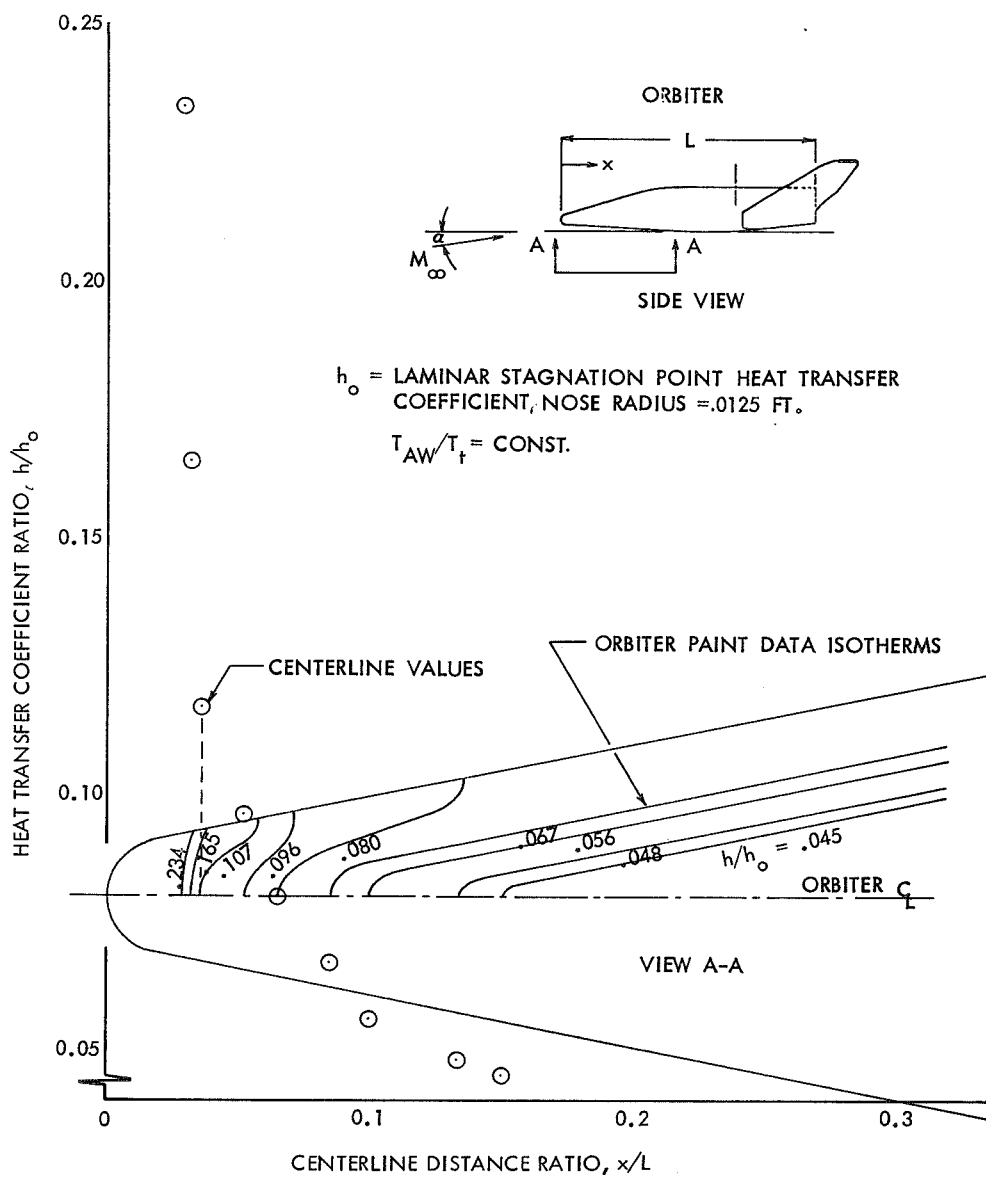
ALL DIMENSIONS  
IN INCHES



ORBITER WIND TUNNEL MODEL  
FIGURE 3







ORBITER HEATING RATE---ISOTHERM CENTERLINE DISTRIBUTION  $\alpha = 0^\circ$   
FIGURE 5

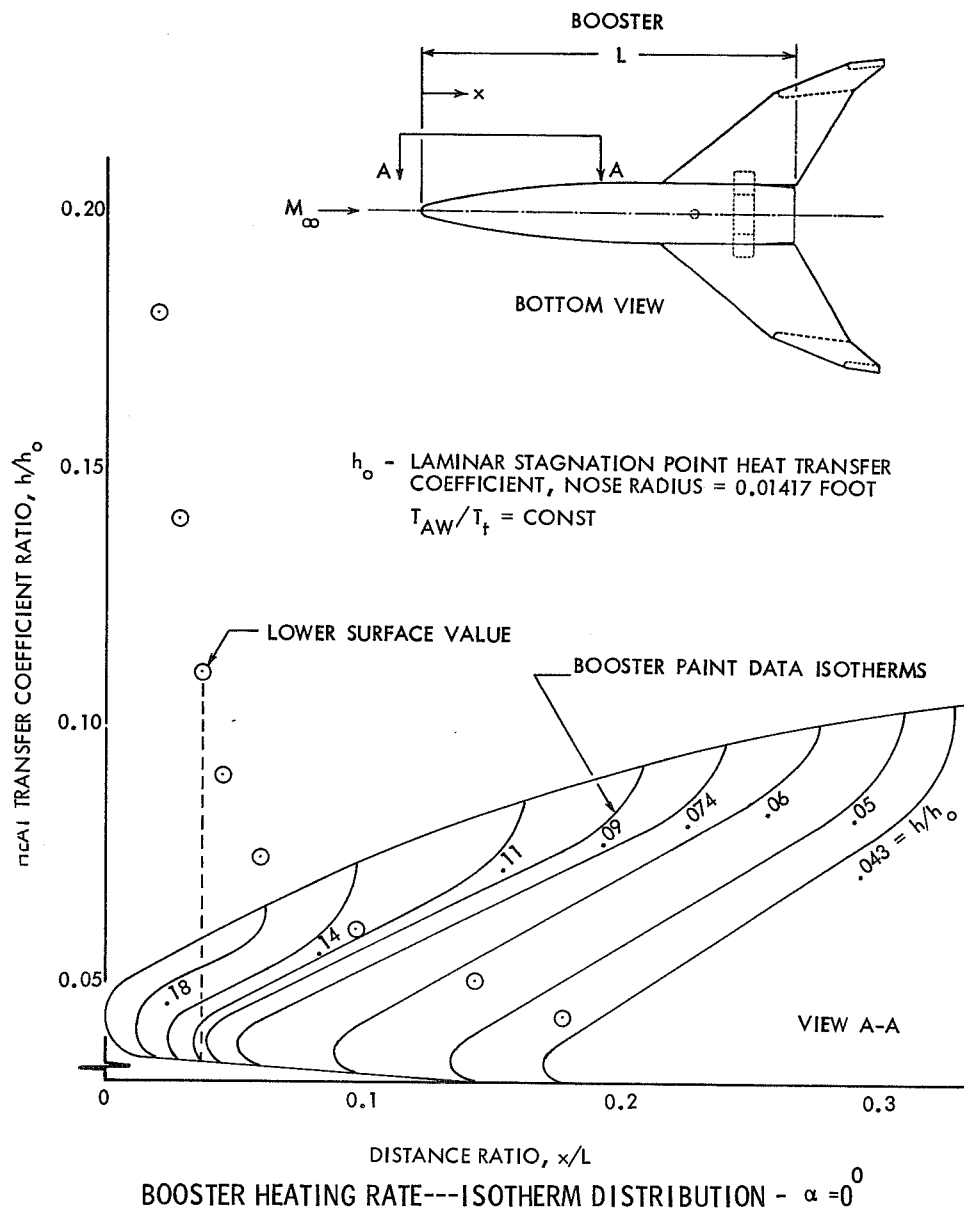
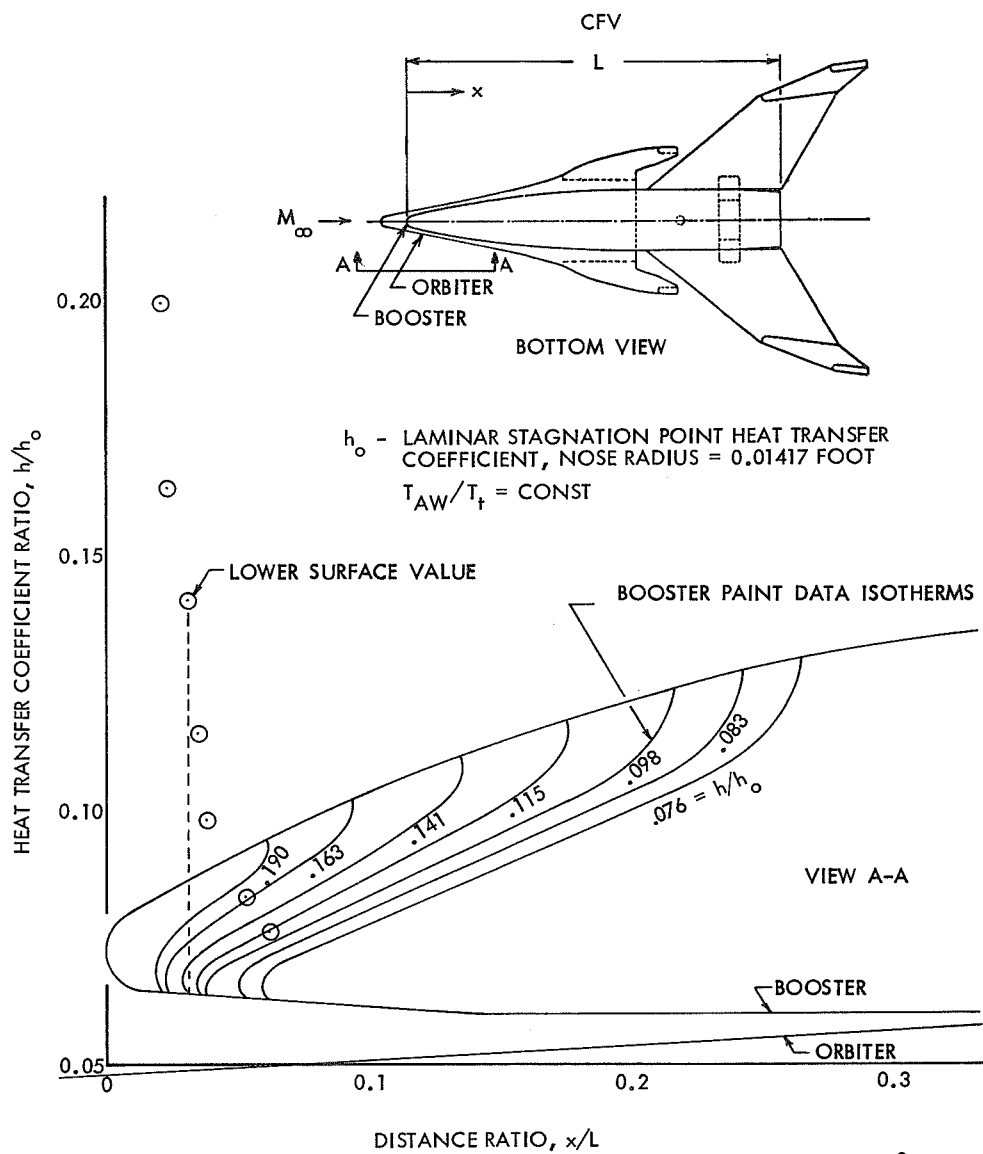
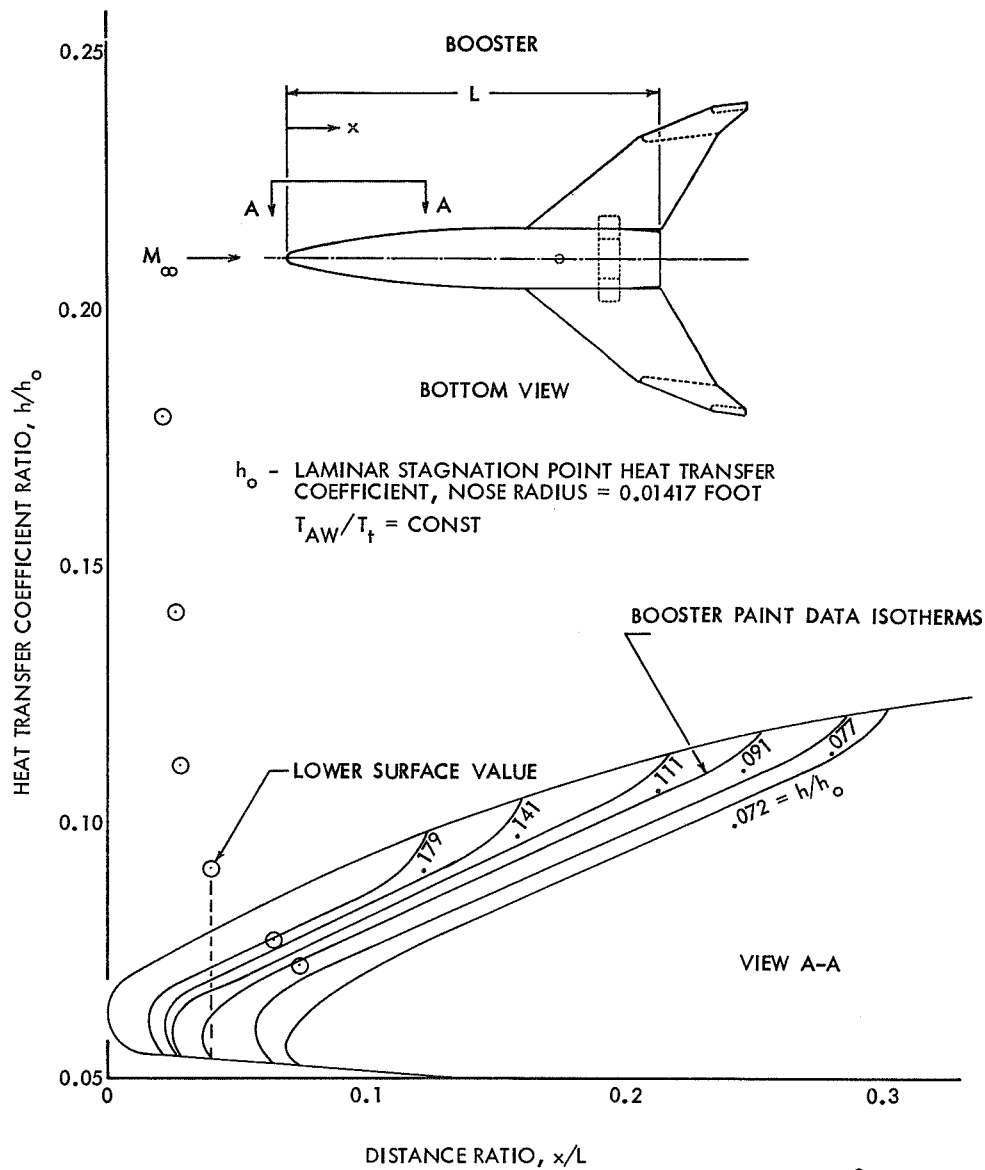


FIGURE 6



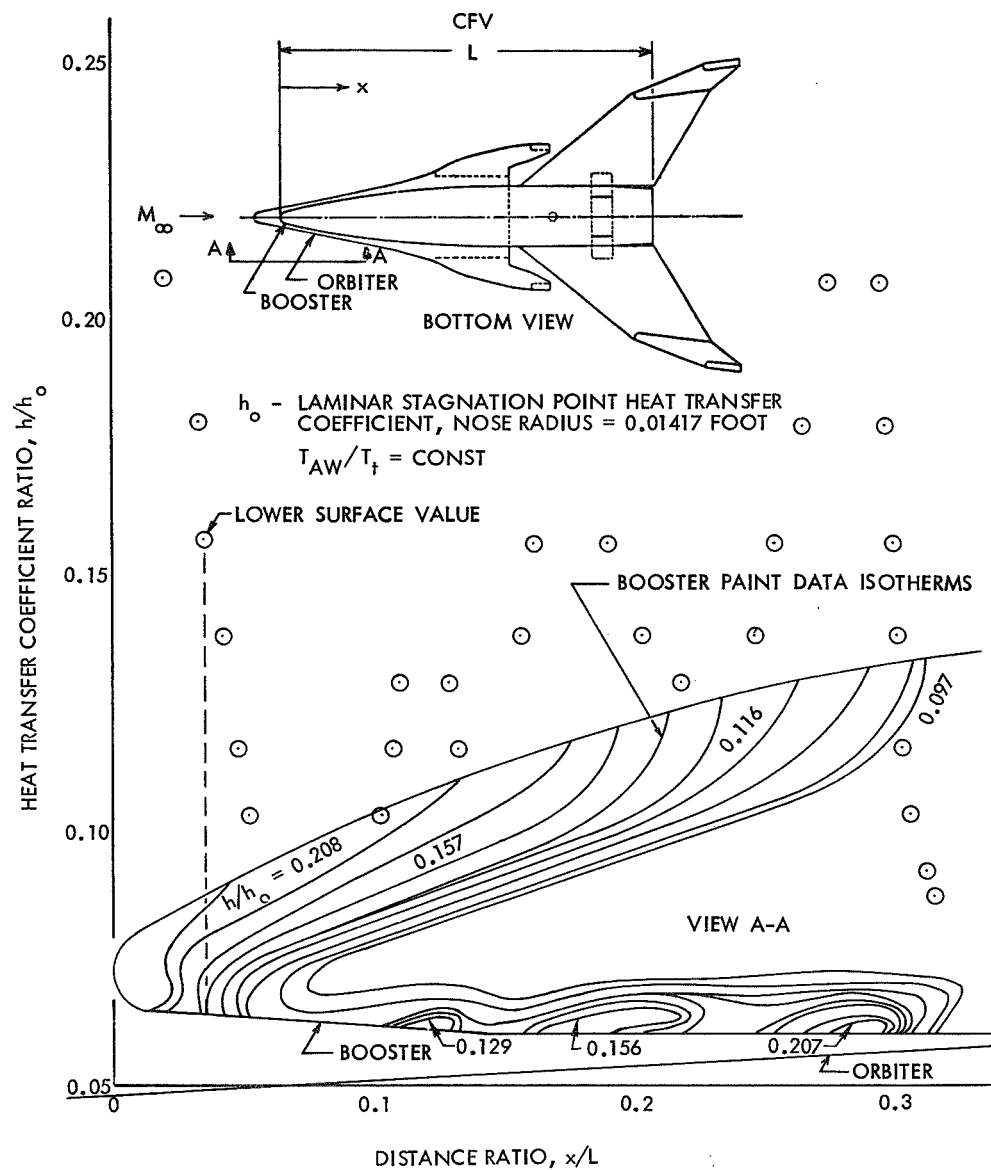
ORBITER EFFECT ON BOOSTER HEATING RATE DISTRIBUTION -  $\alpha = 0^\circ$

FIGURE 7



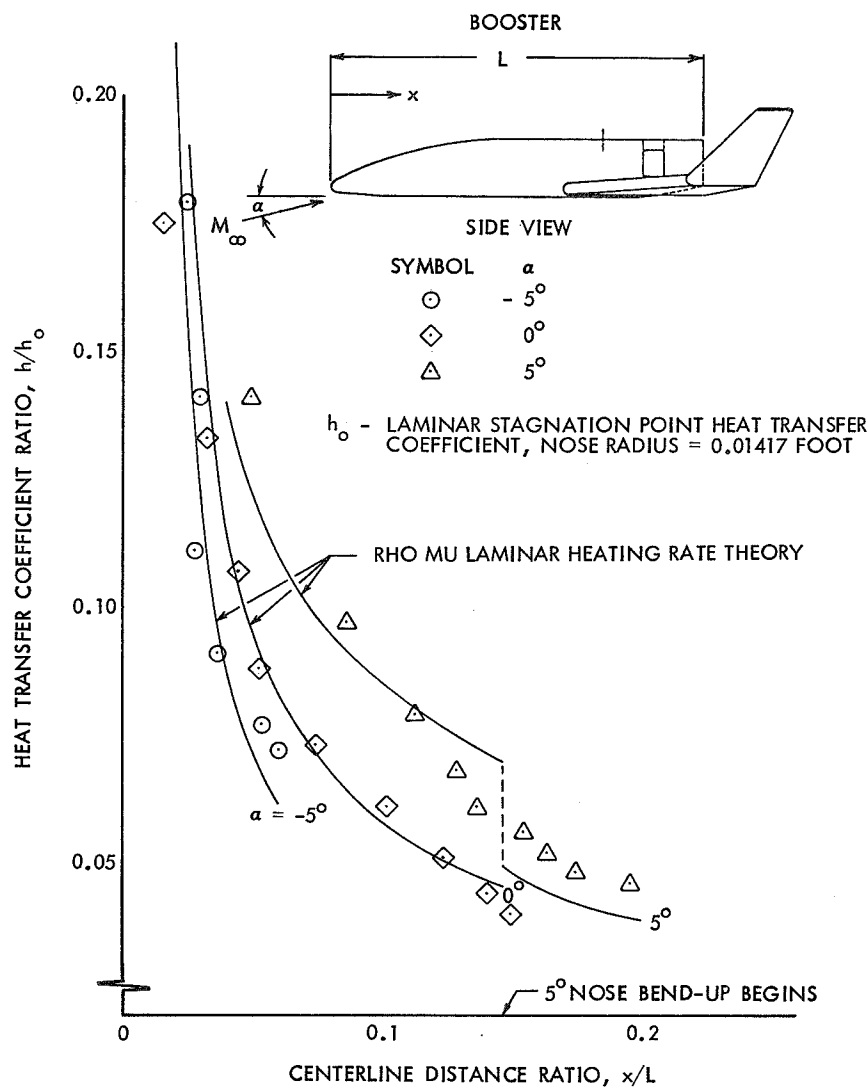
BOOSTER HEATING RATE---ISOTHERM DISTRIBUTION -  $\alpha = -5^\circ$

FIGURE 8



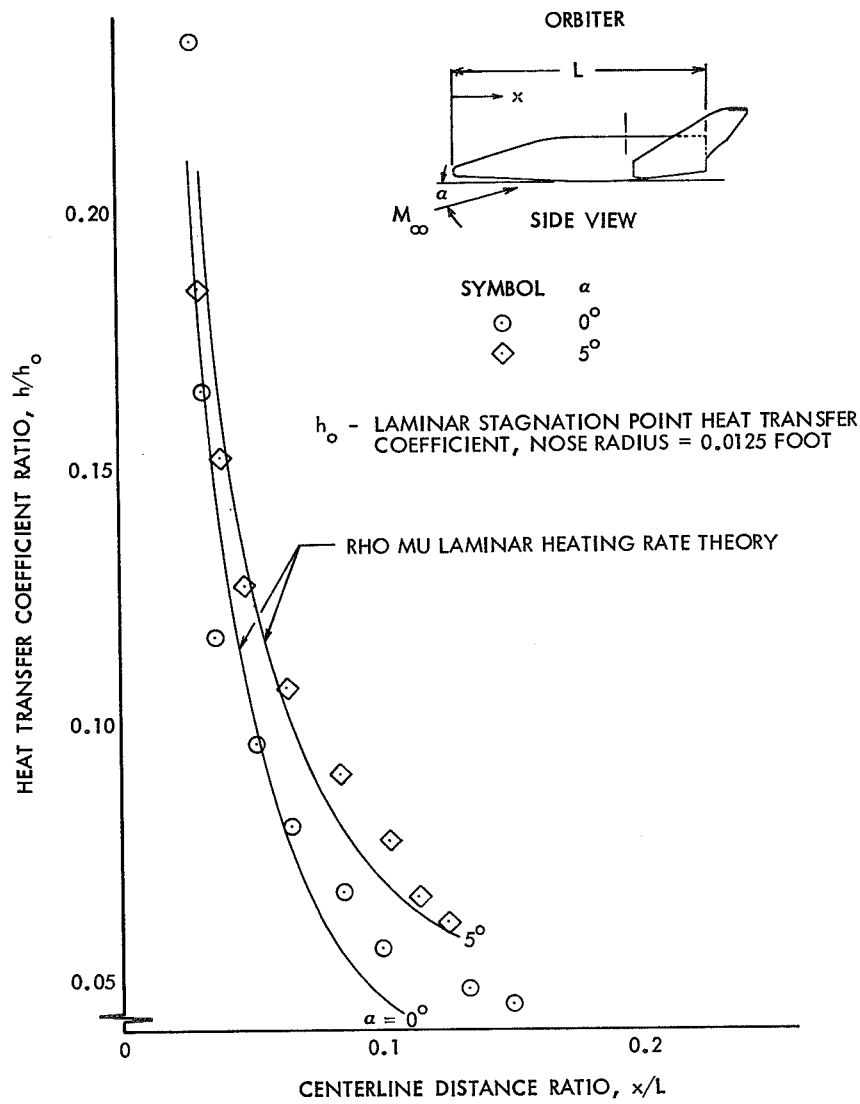
ORBITER EFFECT ON BOOSTER HEATING RATE DISTRIBUTION  $-\alpha = -5^\circ$

FIGURE 9



BOOSTER, DATA-THEORY COMPARISON

FIGURE 10



ORBITER, DATA-THEORY COMPARISON

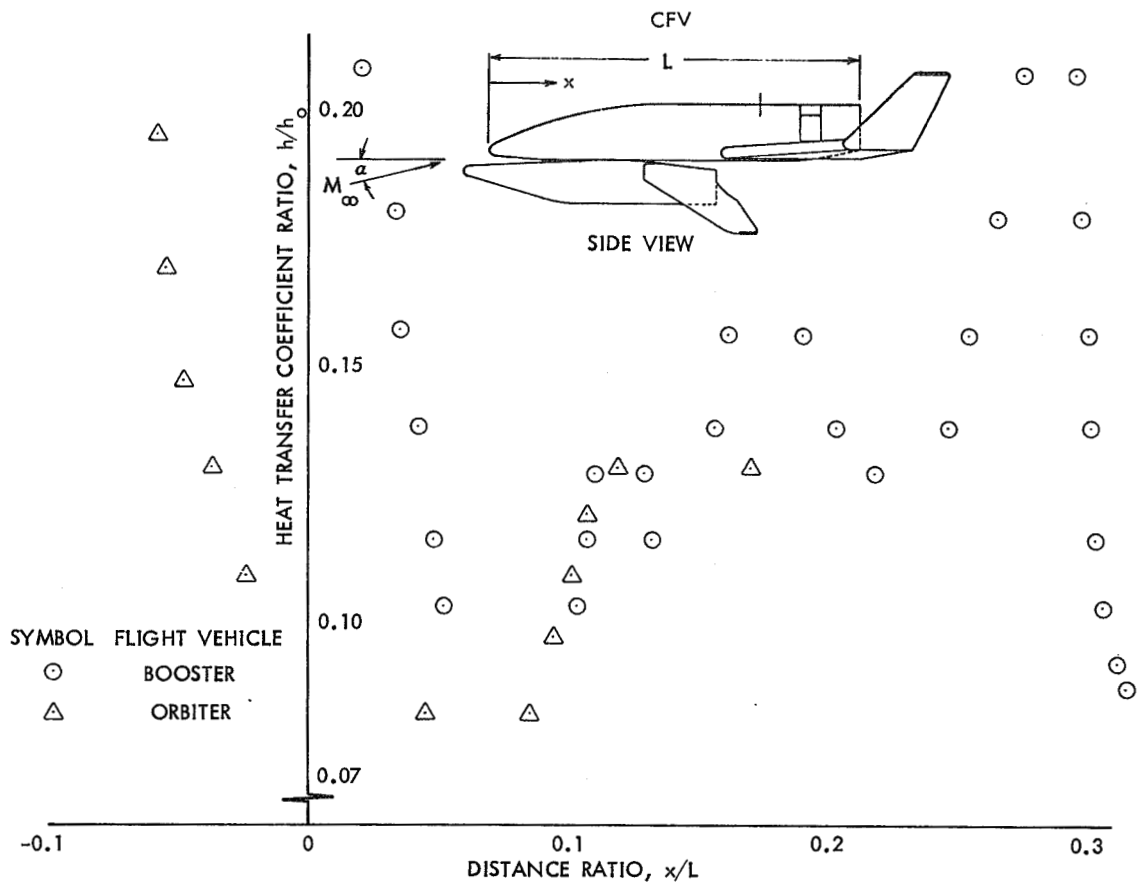
FIGURE 11

BOOSTER

$h_o$  - LAMINAR STAGNATION POINT HEAT TRANSFER  
COEFFICIENT, NOSE RADIUS = 0.01417 FOOT

ORBITER

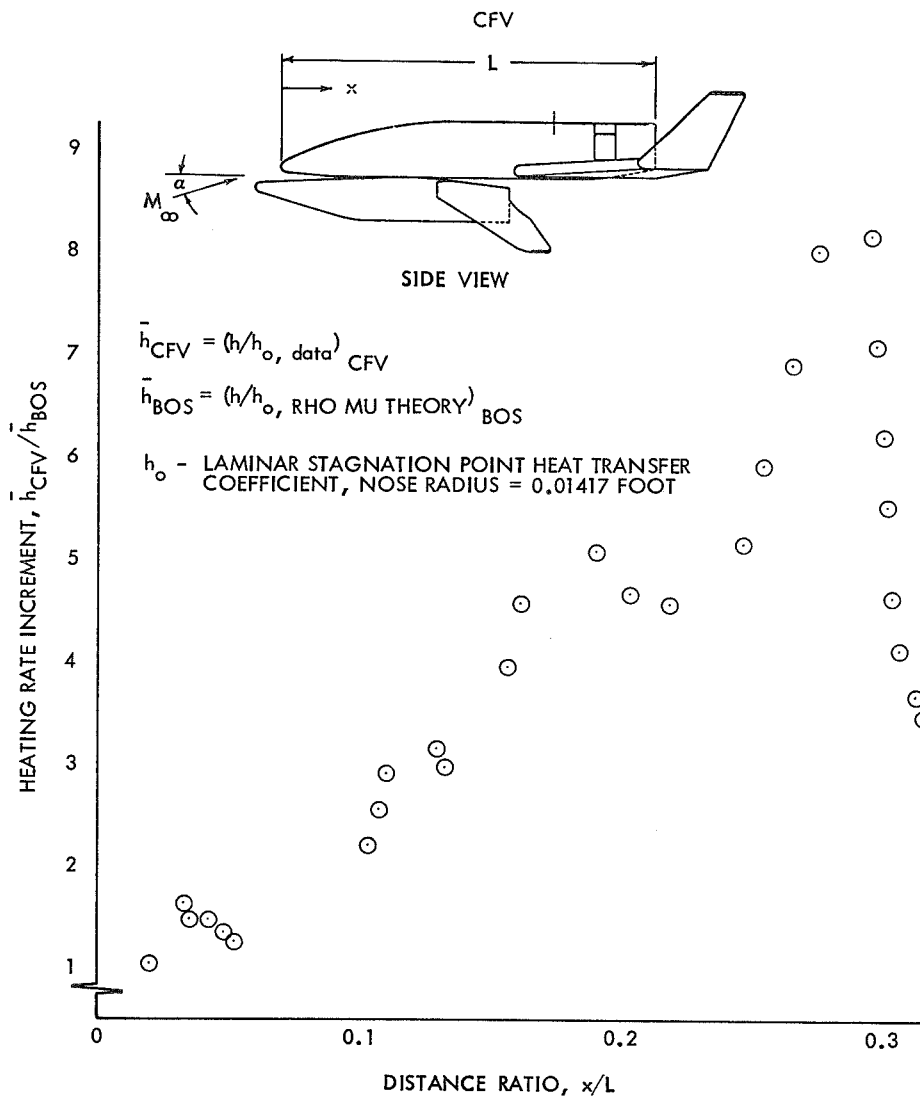
$h_o$  - LAMINAR STAGNATION POINT HEAT TRANSFER  
COEFFICIENT, NOSE RADIUS = 0.0125 FOOT



CFV LOWER SURFACE HEAT TRANSFER DISTRIBUTION -  $\alpha = -5^\circ$

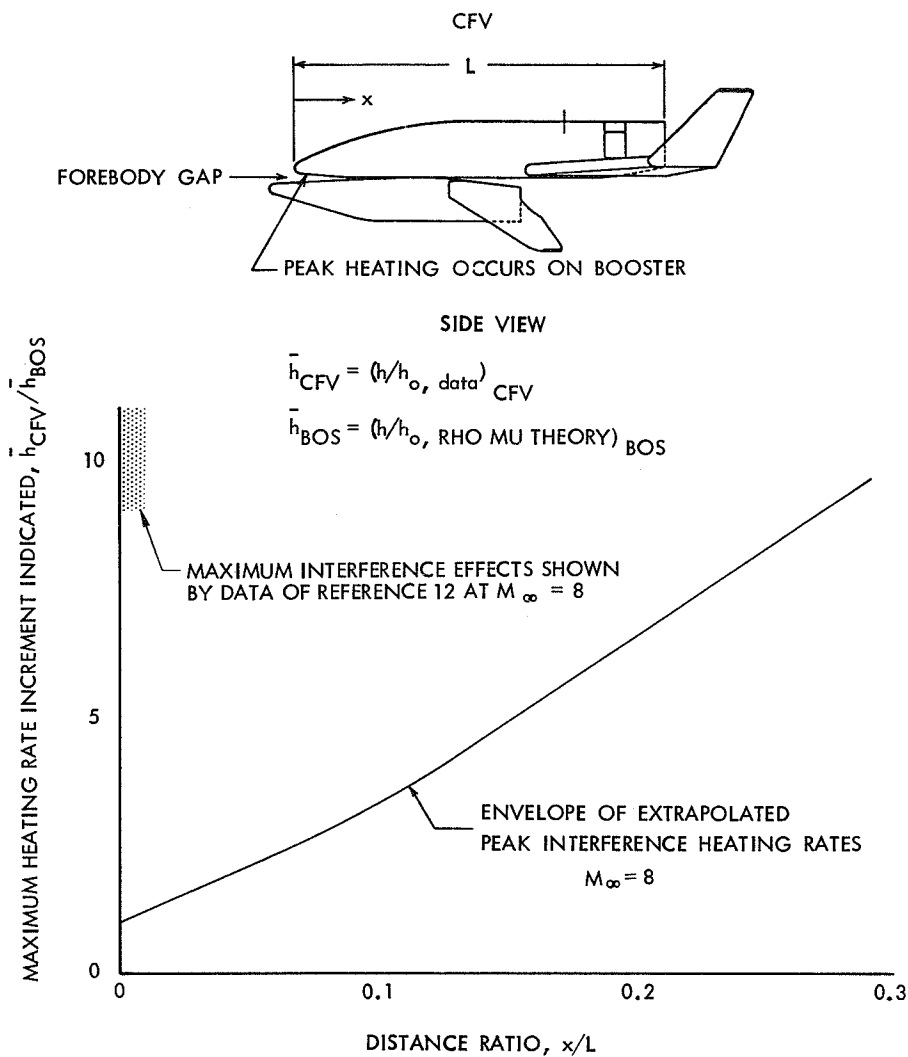
FIGURE 12



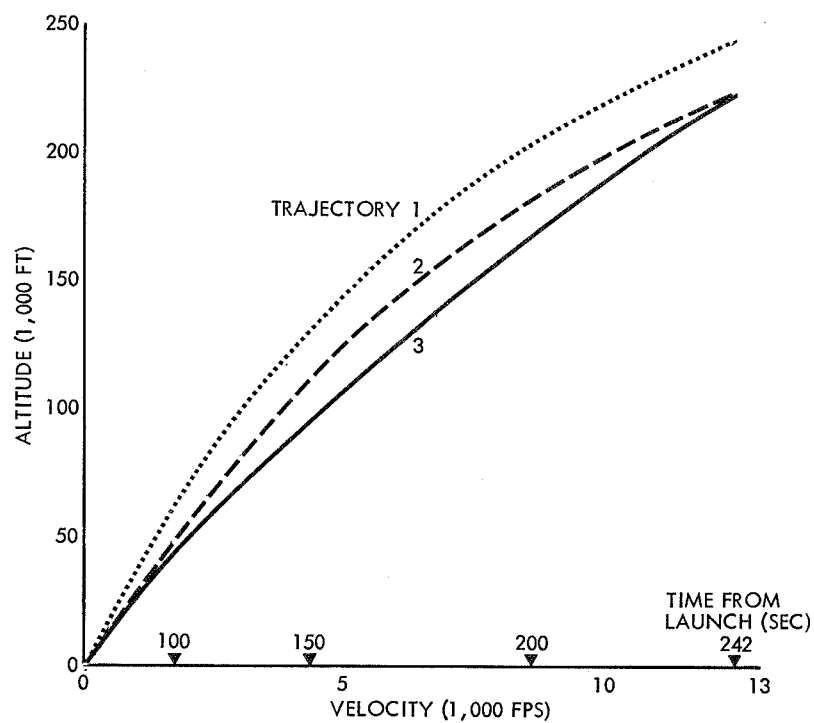


ORBITER EFFECT ON BOOSTER HEATING RATES -  $\alpha = -5^0$

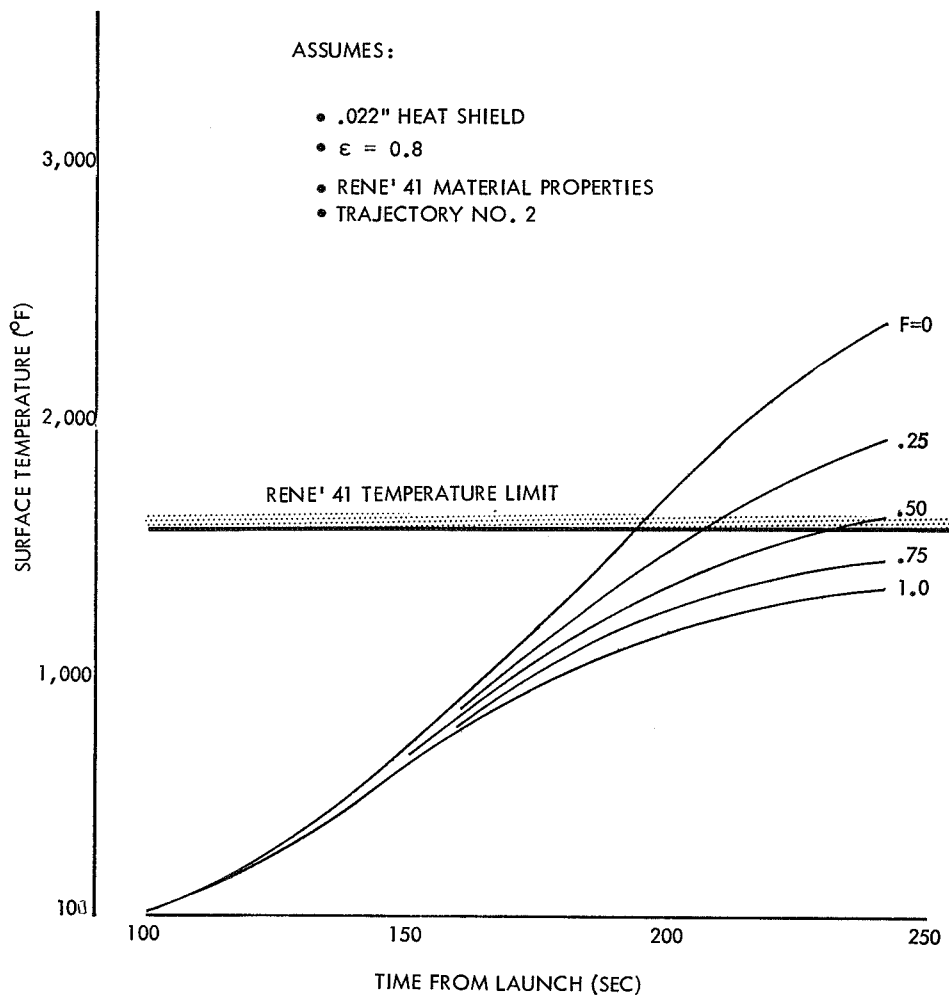
FIGURE 13



CFV FOREBODY GAP PEAK INTERFERENCE HEATING ON BOOSTER  
FIGURE 14

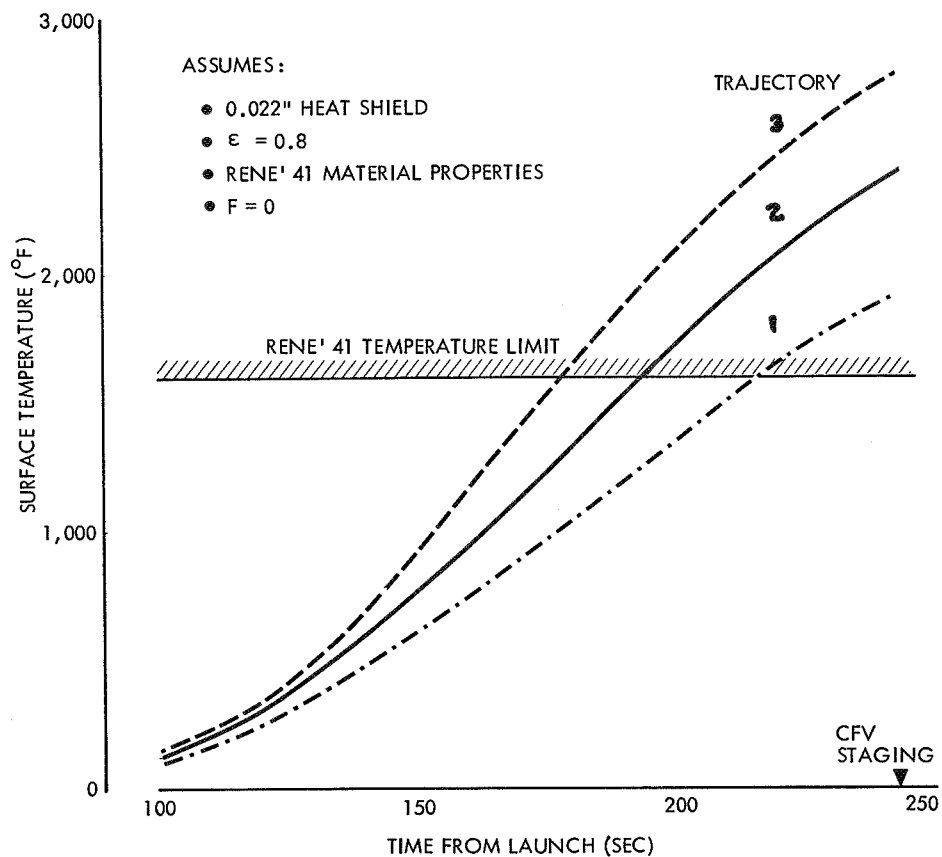


POSSIBLE CFV BOOST TRAJECTORIES  
FIGURE 15



RADIATION BLOCKAGE EFFECTS ON BOOSTER GAP TEMPERATURES

FIGURE 16



TRAJECTORY HISTORY EFFECTS ON BOOSTER GAP TEMPERATURES  
FIGURE 17

TRANSITIONAL AND TURBULENT HEAT TRANSFER CORRELATIONS  
FOR A LIFTING ENTRY VEHICLE AT MACH 10

by C. H. Young, D. C. Reda, and A. M. Roberge

General Dynamics/Convair  
San Diego, California

INTRODUCTION

The necessity for accurate prediction of aerodynamic heat transfer to Space Shuttle vehicles needs little elaboration. Many recent papers have discussed the influence of aerothermodynamic predictions on thermal protection system sizing and material selection. It has generally been concluded that two topics, boundary layer transition and turbulent heat transfer, are of paramount importance to Space Shuttle design. At present we must rely heavily on wind tunnel data for information about these flow phenomena. To obtain such data a series of tests was conducted in Tunnel C of the AEDC von Karman Gas Dynamics Facility. A lifting entry vehicle of relatively simple geometry was used.

Applicability of the results of these tests to Space Shuttle will be discussed. Particular attention will be given to Reynolds number and angle of attack effects on transition and turbulent flow on the vehicle lower surface centerline. Correlations with existing heat transfer prediction techniques will be shown for selected portions of the data. Results concerning onset of transition and a possible mechanism for observed transition behavior will be presented. Length of the transition zone and heat transfer variation through the transitional region will be described.

## **MAJOR AREAS OF DISCUSSION**

- APPLICATION TO SPACE SHUTTLE
- REYNOLDS NUMBER/ANGLE OF ATTACK EFFECTS
- COMPARISON WITH PREDICTION TECHNIQUES
- TRANSITION ONSET
- TRANSITION ZONE EXTENT

## COMPARISON OF BOOSTER TRAJECTORY WITH TUNNEL CONDITIONS

A typical booster ascent and entry trajectory is presented in terms of freestream Mach number and freestream Reynolds number based on total vehicle length. The maximum Mach number reached is approximately 9.8. The trajectory shown has angle of attack modulation during entry from 60° to about 45° throughout the significant heating portion of flight.

Wind tunnel conditions for the present test series were:

Mach number,  $M_{\infty} = 10$

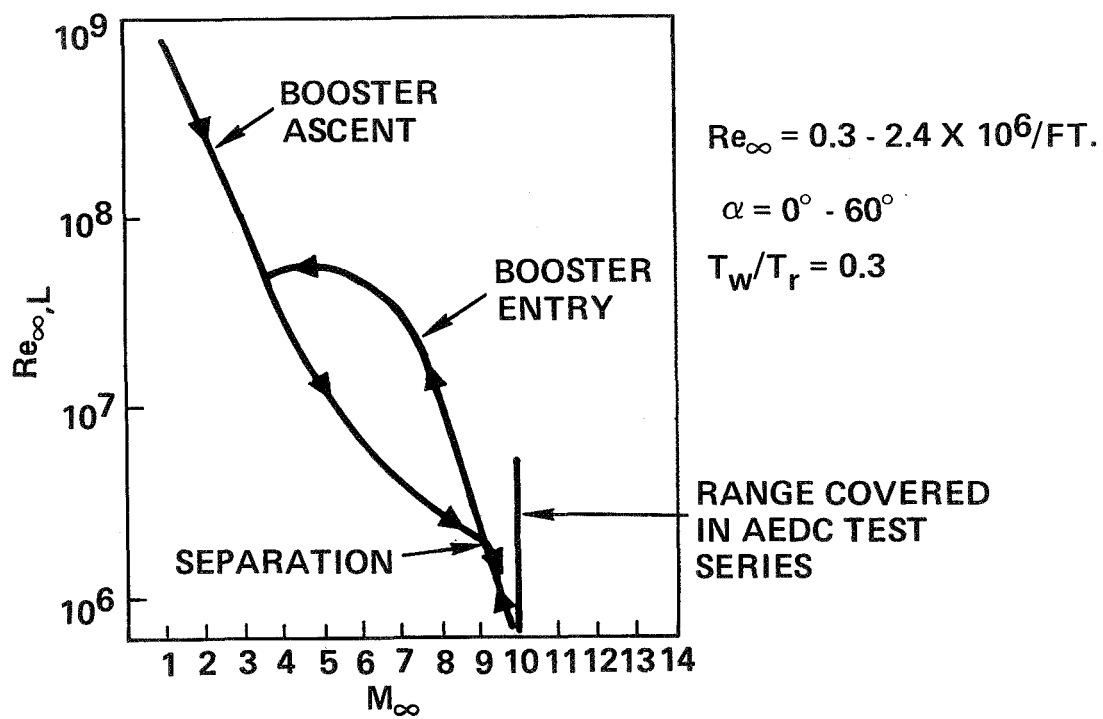
Angle of Attack,  $\alpha = 0^{\circ}$  to  $60^{\circ}$

Freestream Unit Reynolds Number,  $Re_{\infty} = 0.3$  million to 2.4 million/ft

These values result in a Reynolds number range based on total model length of approximately 0.65 million to 5.2 million. The wall to recovery temperature ratio was approximately 0.3. Therefore, the significant tunnel parameters of Mach number and Reynolds number closely approximated values to be experienced over a major portion of the booster ascent and entry.



## COMPARISON OF BOOSTER TRAJECTORY WITH TUNNEL CONDITIONS



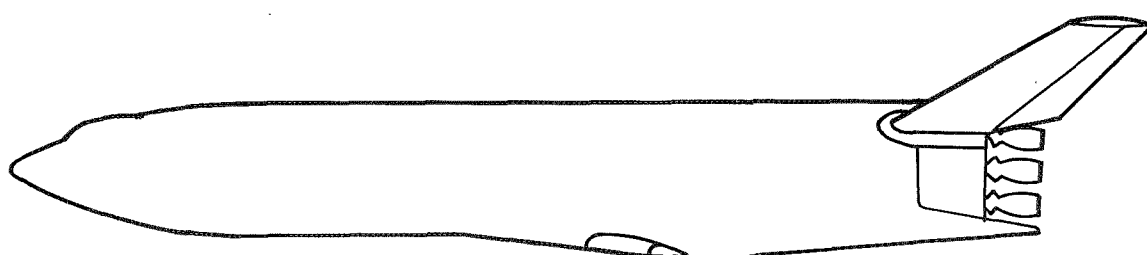
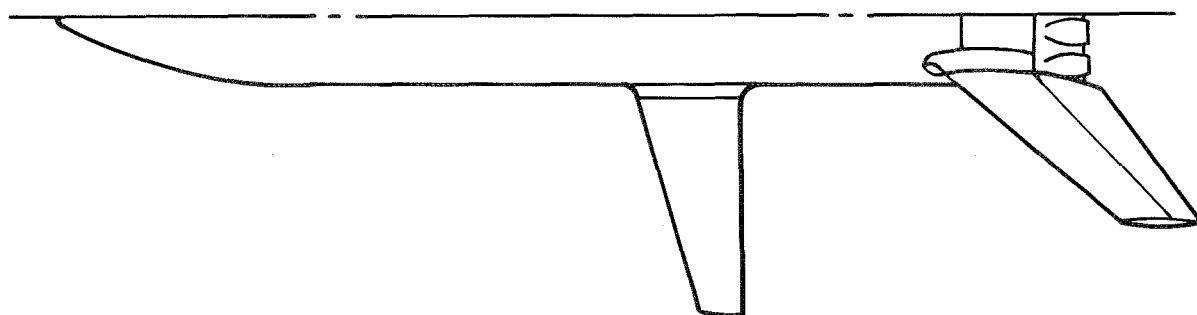
## CONVAIR STRAIGHT-WING BOOSTER

A straight wing booster configuration currently under study at Convair is shown.

Principal features of interest to this discussion are:

1. Blunted nose region
2. Cylindrical forward fuselage
3. Contour variation (cylindrical to flat) forward of the wings
4. Angular changes or "breaks" in lower surface contour
5. Majority of fuselage lower surface is away from wing interference regions

## CONVAIR STRAIGHT-WING BOOSTER



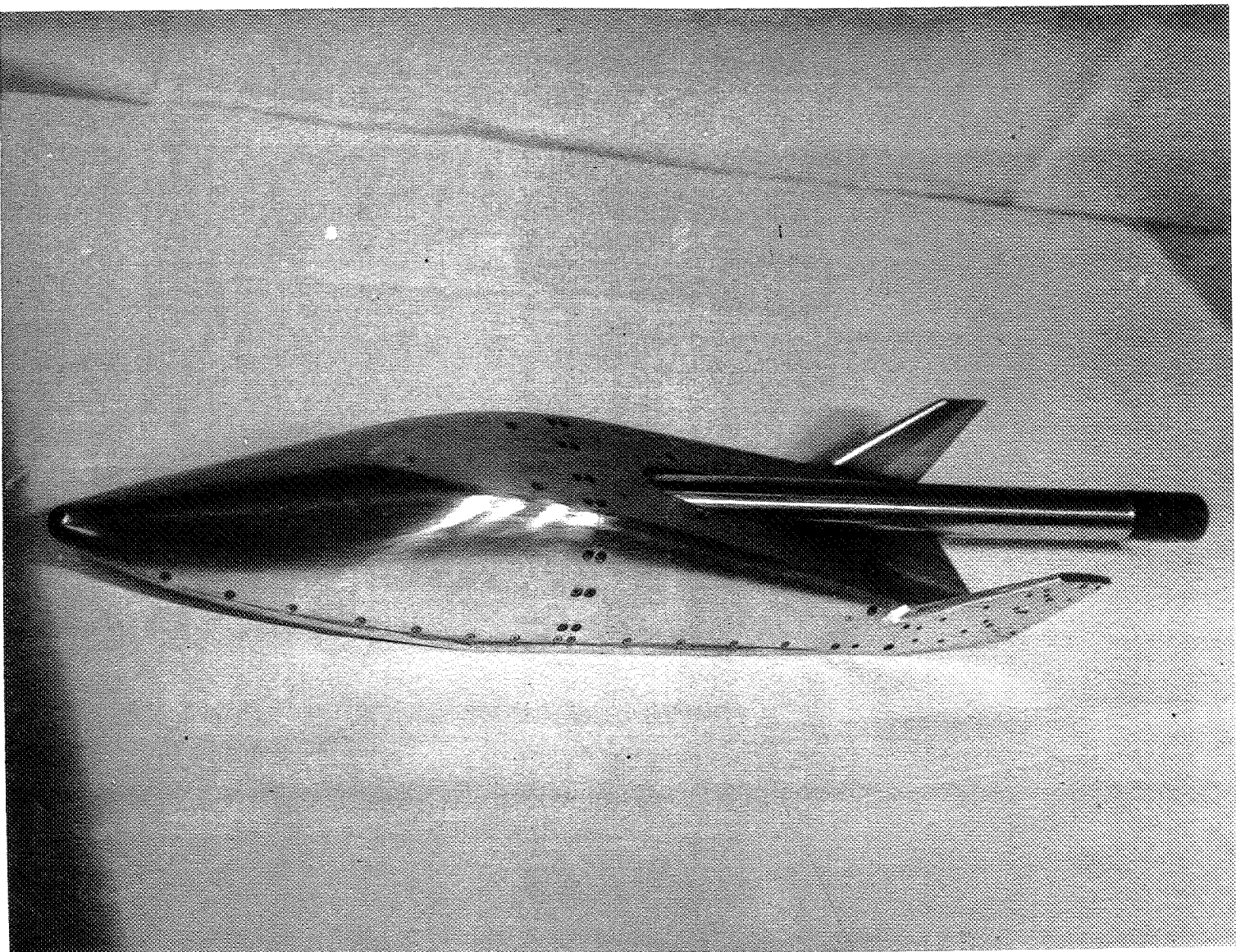
## WIND TUNNEL MODEL

A thin-skin stainless steel heat transfer model approximately 26 inches long was used for this test series. Data were obtained from transient response of thermocouples attached to the model skin. Only lower surface centerline heat transfer data and correlations will be discussed in the present paper.

Characteristics of the model geometry pertinent to this discussion are:

1. A blunt hemispherical nose having a radius of approximately 0.47 inches.
2. A flat lower surface with an angular change of  $6.75^\circ$  at 40% of the vehicle total length.
3. The aft ramp of the lower surface is parallel to the vehicle centerline.
4. The forward ramp (inclined at  $6.75^\circ$  to the vehicle centerline) has a delta planform.
5. The aft ramp sides are nearly parallel to the vehicle lower surface centerline.

In subsequent discussion the angular change in the lower surface is referred to as the "break." It should be observed that the true angle between the front ramp and the freestream velocity vector is  $6.75^\circ$  greater than the vehicle angle of attack. All reported angles of attack are referenced to the vehicle centerline.



## CENTERLINE HEATING VARIATION WITH $\alpha$

Lower surface centerline heat transfer data are shown for the 2.4 million freestream unit Reynolds number runs at angles of attack from 5° to 60°. Data trends seen here are representative of those at other Reynolds numbers. Data are presented in two groups, (1) 5° to 35°, and (2) 40° to 60°, because of differences in heat transfer behavior in these two regimes. Laminar, transitional and turbulent regions were determined through inspection of heat transfer and shadowgraph data, and through correlation with various prediction techniques. Significant features of data are discussed.

### Angles of Attack From 5° to 35° (Data Points Removed For Clarity):

1. Laminar heating increases uniformly with increasing angle of attack.
2. Turbulent heating increases uniformly with increasing angle of attack.
3. Transition location moves forward with increasing angle of attack.
4. Length of the transition zone decreases with increasing angle of attack.

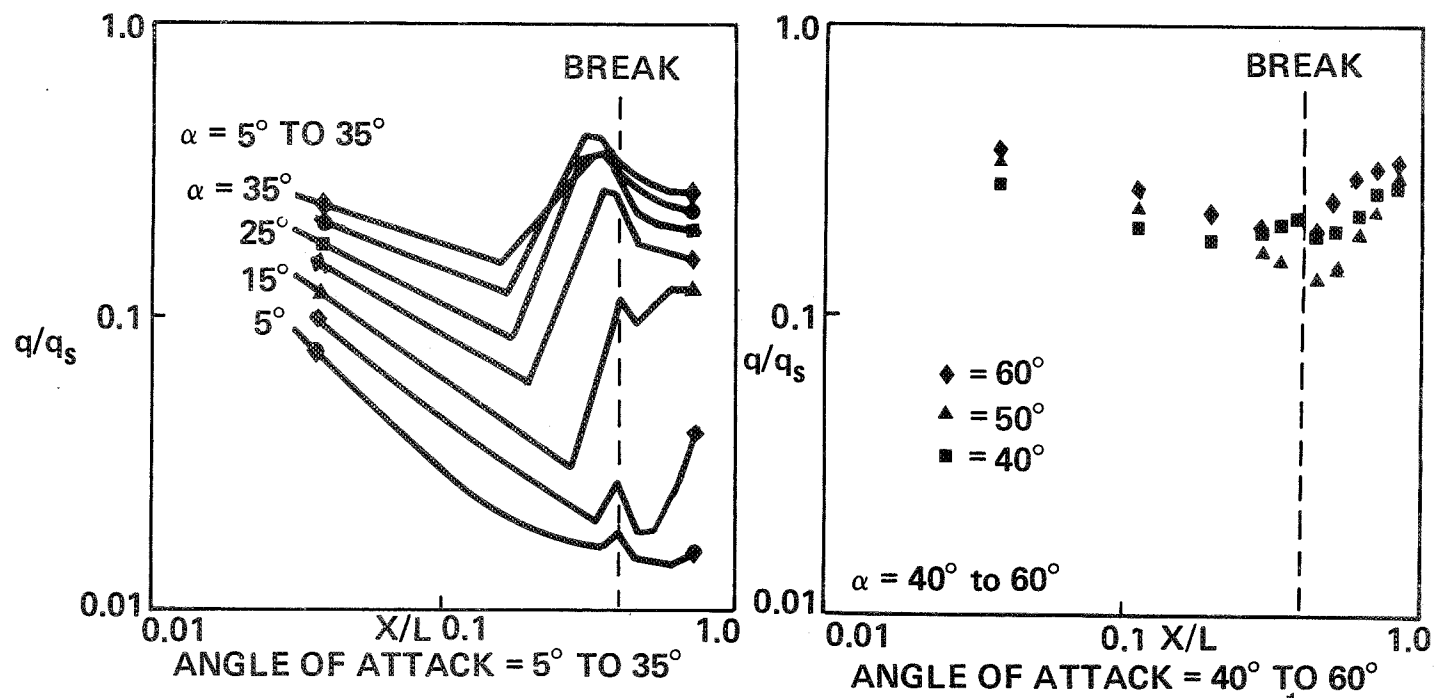
### Angles of Attack From 40° to 60°:

1. The heat transfer distributions change markedly.
2. Transition location moves back suddenly.
3. Length of transition zone increases; 50° data does not appear to reach turbulent level while 45° and 55° data (not shown) reach the same final level as 60° data.

# CENTERLINE HEATING VARIATIONS WITH $\alpha$

$$Re_{\infty} = 2.4 \times 10^6 / FT.$$

$$M_{\infty} = 10$$



## CENTERLINE HEATING VARIATION WITH $Re_\infty$

Two selected angles of attack, typical of the two regimes shown on the previous slide, are presented:  $20^\circ$  for low angle of attack regime and  $60^\circ$  for high angle of attack regime.

### $20^\circ$ Angle of Attack

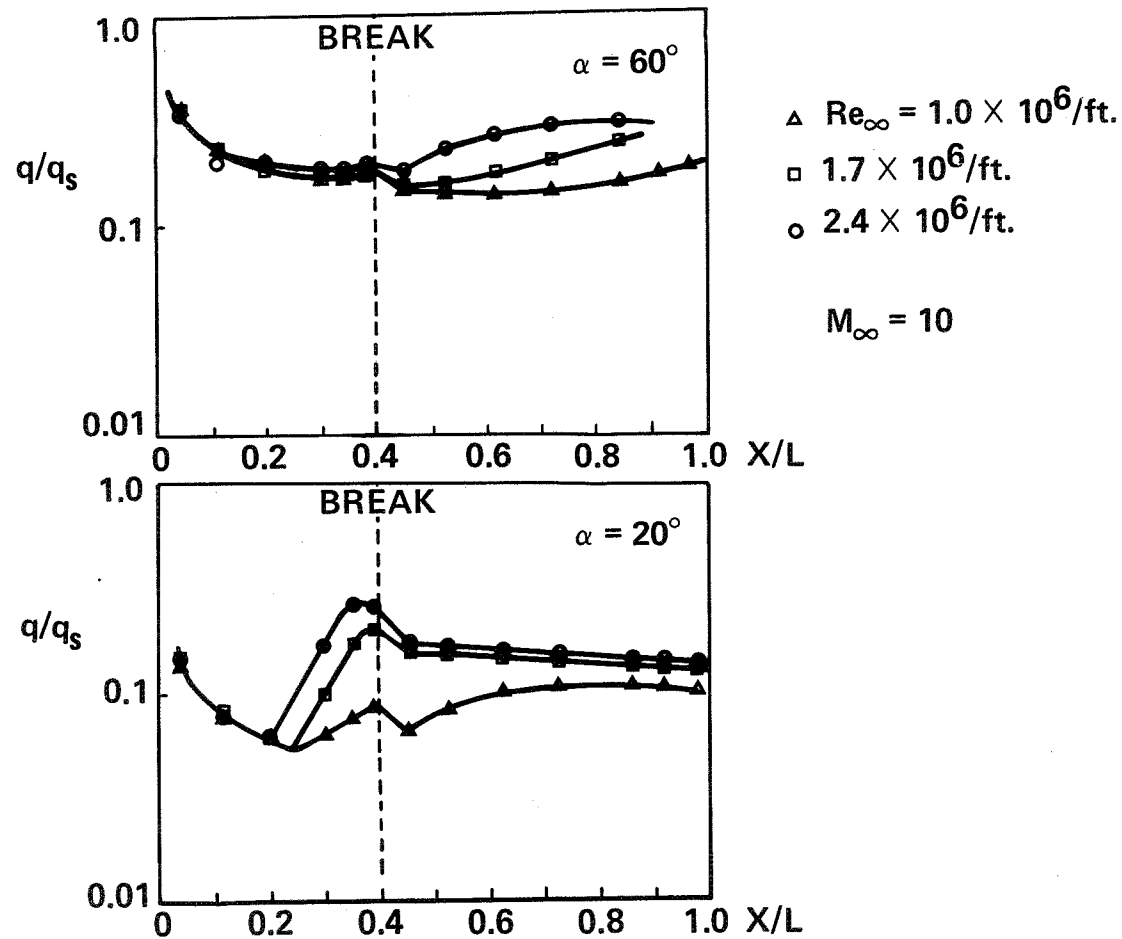
1. Transition occurs on the front ramp for all Reynolds numbers shown.
2. Transition location does not move forward appreciably with increasing Reynolds number.
3. Length of transition zone decreases with increasing Reynolds number.
4. Final turbulent level increases with increasing Reynolds number.

### $60^\circ$ Angle of Attack

1. Laminar flow exists over most of vehicle at a freestream unit Reynolds number of  $1.0 \times 10^6/\text{ft}$ .
2. Location of the start of transition is farther back on the vehicle and the length of the transition zone is longer than at  $\alpha = 20^\circ$ .



# CENTERLINE HEATING VARIATION WITH $Re_\infty$



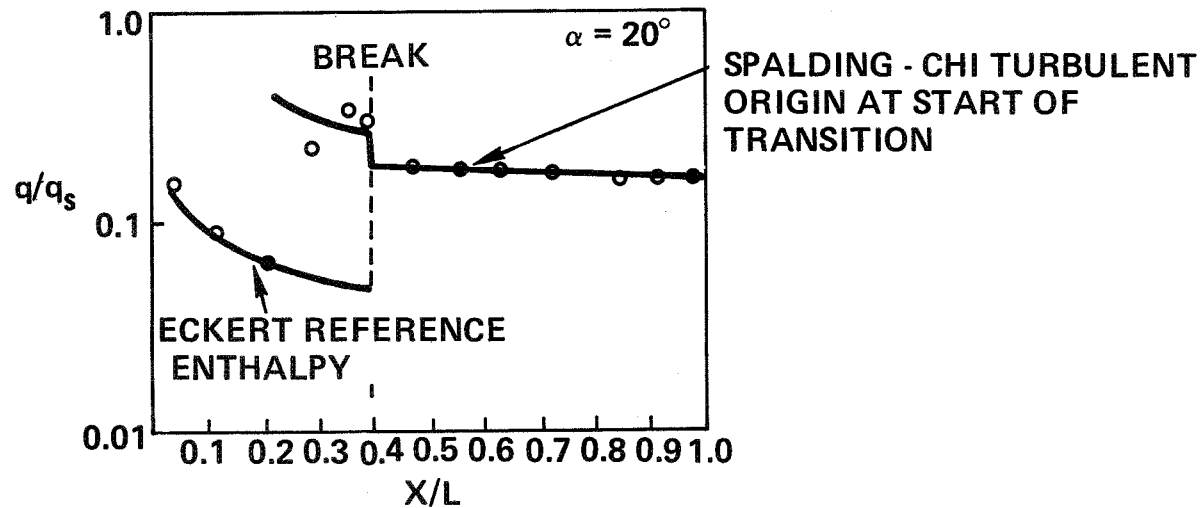
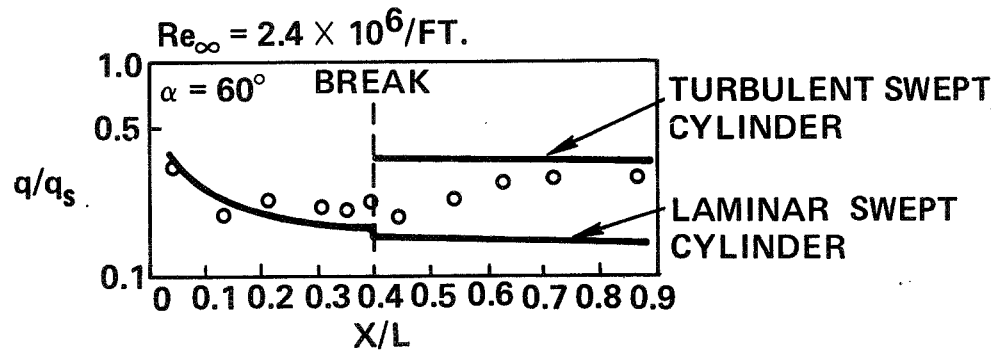
## HEAT TRANSFER CORRELATION

Laminar and turbulent heat transfer correlations are shown for angles of attack of  $20^\circ$  and  $60^\circ$ ; these again are representative of the low and high angle of attack regimes, respectively. Only the maximum freestream unit Reynolds number correlations are shown but the results are comparable for other Reynolds number data.

At  $20^\circ$  angle of attack the laminar data were correlated best using the Eckert reference enthalpy method with flow field properties determined by normal shock expansion to modified Newtonian pressure. A number of turbulent heating methods were used in the data correlations. Spalding-Chi with a boundary layer origin at the start of transition yielded the best fit of the data at  $35^\circ$  angle of attack and below. Flow field properties were obtained from a tangent wedge solution for the front ramp with a Prandtl-Meyer expansion to the aft ramp angle. Reasons for the use of a high entropy flow field for the laminar region and a low entropy flow field in the turbulent region will be discussed on a later slide.

Data for  $60^\circ$  angle of attack were correlated most successfully using swept cylinder theories. Laminar swept cylinder values were obtained by modifying spherical stagnation point heating for two-dimensionality and sweepback. Turbulent rates were obtained from the method of Beckwith and Gallagher. Both laminar and turbulent heat transfer rates were corrected for the variation in stagnation line velocity gradient caused by a non-cylindrical cross section. The form of this correction was taken from previous work by Bertram, Feller and Dunavant.

# HEAT TRANSFER CORRELATION



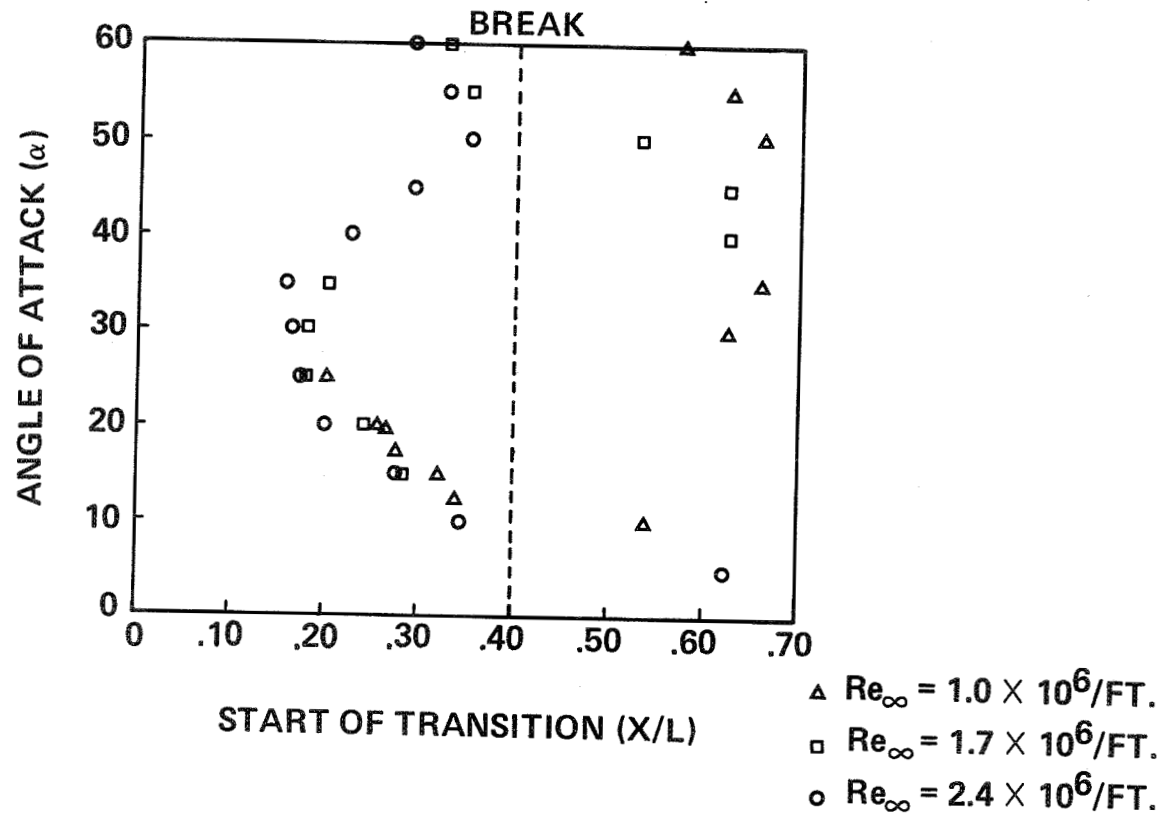
## VARIATION OF TRANSITION LOCATION WITH $\alpha$

The location of the start of transition on the vehicle lower surface centerline was found to be a strong function of angle of attack. Shown are the X/L locations of transition for free stream unit Reynolds numbers of  $1.0 \times 10^6/\text{ft.}$ ,  $1.7 \times 10^6/\text{ft.}$  and  $2.4 \times 10^6/\text{ft.}$  At an angle of attack of  $0^\circ$ , transition did not occur for any of the Reynolds numbers tested. As the angle of attack increased, transition started on the aft ramp and then progressed forward to the front ramp. Surprisingly, the location of the start of transition on the front ramp seemed almost independent of freestream unit Reynolds number for angles of attack from  $10^\circ$  through  $35^\circ$ . In this range, transition occurred at a fixed location for a given angle of attack. Shadowgraphs shown in the following slide suggest a reason for this behavior.

Above  $35^\circ$  the location of the start of transition ceased its forward progression and rapidly moved aft. At the lower Reynolds numbers, transition retreated to the aft ramp and, at  $40^\circ$  and  $45^\circ$  degrees, did not occur at all for a Reynolds number of one million per foot. Further increases in angle of attack, above  $50^\circ$ , resulted in a resumption of the forward progression of transition.

These trends, observed above  $35^\circ$  angle of attack, were felt to be associated with changes in flow field characteristics, i.e., high angle of attack flows, with subsonic boundary layer edge velocities, as opposed to low angle of attack flows, with supersonic boundary layer edge velocities.

# VARIATION OF TRANSITION LOCATION WITH $\alpha$



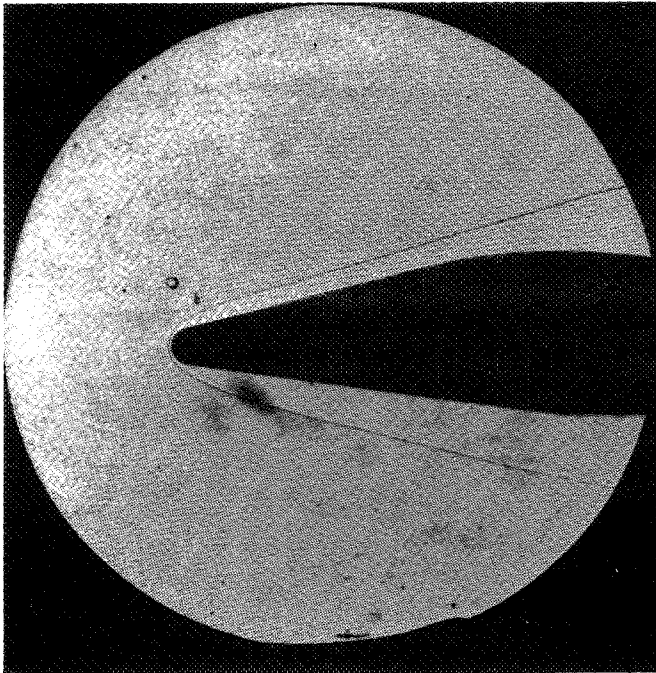
## ANGLE OF ATTACK EFFECT ON SHOCK LAYER

Two shadowgraphs are shown to illustrate the features of importance. At  $0^\circ$  angle of attack, the shock layer is seen to be free of disturbances. An inflection point can be seen in the shock shape but it is well away from the nose and appears to have no influence on the body. Bluntness effects dominate the flow. Increases in angle of attack, however, have a profound effect on the flow field. For  $15^\circ$  angle of attack (a true local body angle of  $21.75^\circ$  on the front ramp) the shock inflection point has moved much nearer the nose of the vehicle. This inflection point represents a minimum shock angle relative to the freestream velocity. Through this minimum shock angle passes a streamline of maximum total pressure and maximum unit Reynolds number.

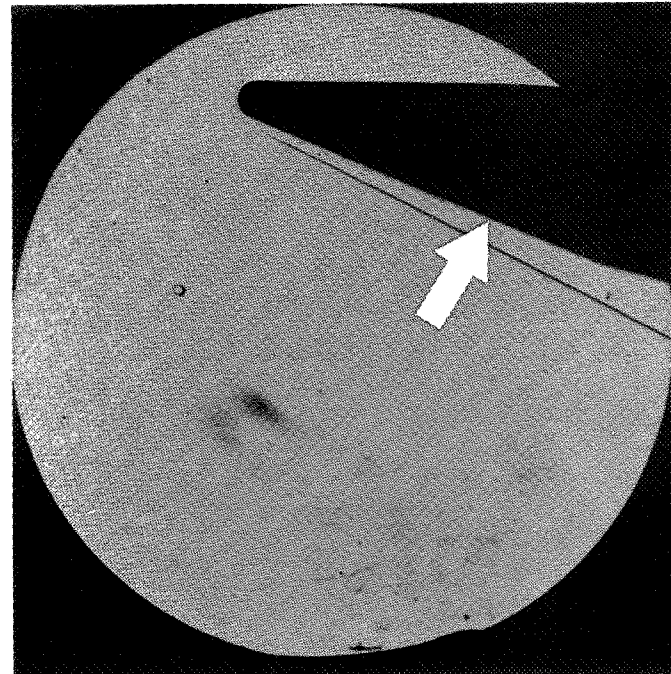
This streamline is the demarcation between the high entropy (rotational flow) blunt nose region and the low entropy (irrotational flow) oblique shock region. It appears on the shadowgraphs as a white line, emanating from the shock inflection point.

The intersection of this line with the boundary layer closely coincided with transition onset, as determined from heat transfer measurements, over the angle of attack range  $15^\circ$  to  $30^\circ$ . It was concluded that laminar flow existed in the high entropy region, but as soon as "entropy swallowing" occurred, the resulting Reynolds number jump at the boundary layer edge caused transition. Since the shape of the shock wave is predominantly influenced by Mach number and body shape, the location of transition appears to be determined by these parameters once some threshold value of Reynolds number is exceeded. The location of transition indicated by heat transfer data is shown by the white arrow on the  $15^\circ$  angle of attack shadowgraph.

## ANGLE OF ATTACK EFFECT ON SHOCK LAYER



$\alpha = 0^\circ$



$\alpha = 15^\circ$

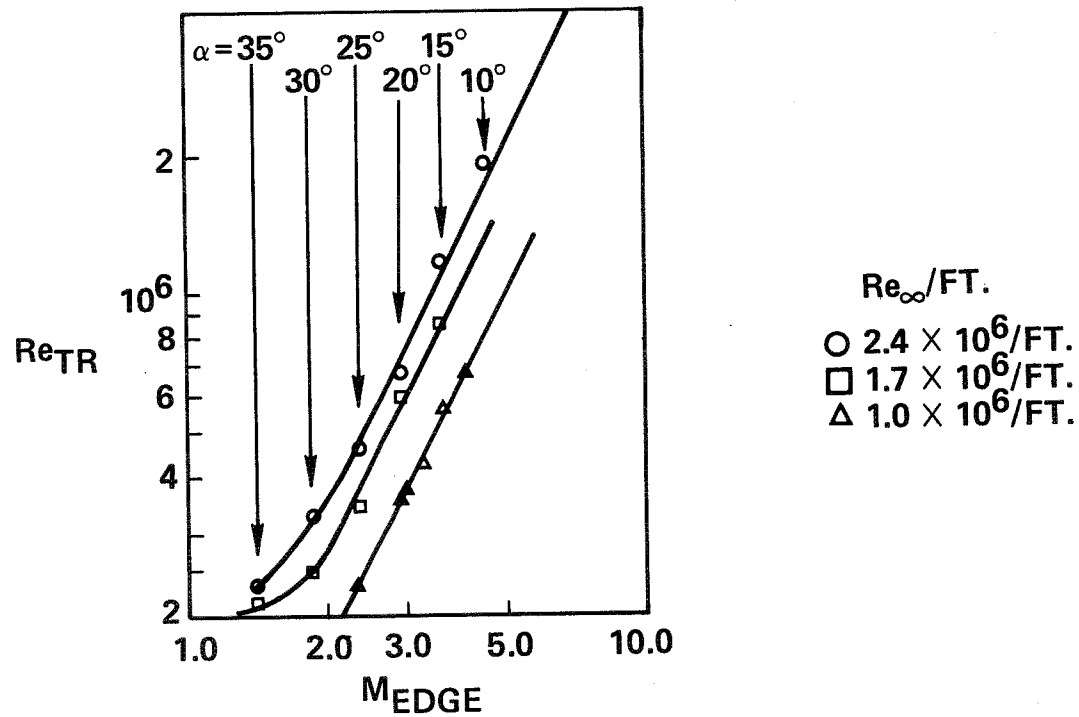
UNIT REYNOLDS NO. AND EDGE MACH NO.  
EFFECT ON  $Re_{TR}$

Transition Reynolds number was shown to be a strong function of boundary layer edge Mach number and, therefore, of vehicle angle of attack. A strong freestream unit Reynolds number effect was indicated, but this apparent result must be tempered by the conclusions of the previous two slides.

Transition Reynolds numbers were calculated from boundary layer edge properties as determined by oblique shock relations and run lengths from the stagnation point.



# UNIT REYNOLDS NO. & EDGE MACH NO. EFFECT ON $Re_{TR}$

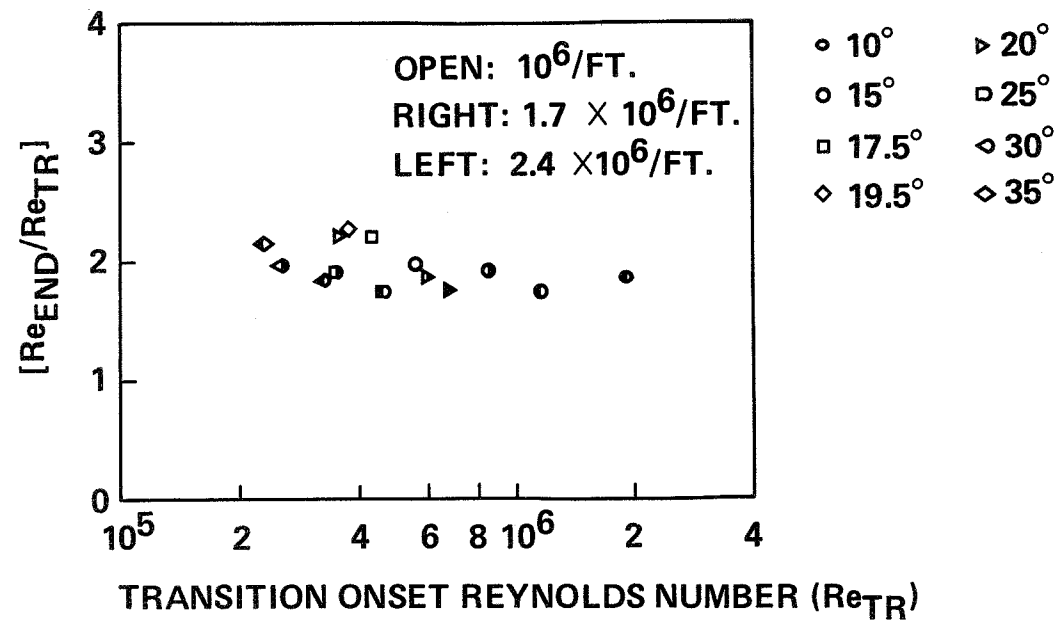


## VARIATION OF TRANSITION ZONE LENGTH WITH $Re_{TR}$

Length of the transition zone can be characterized by the ratio of the Reynolds number of the end of transition to the Reynolds number at the start of transition. Values of this ratio near two were found. A general decrease in the value of this ratio with increasing transition Reynolds number was also found, i.e., the transition zone became shorter as the transition Reynolds number increased.

An even stronger effect was exerted by the freestream unit Reynolds number. For a given angle of attack, a significant decrease in transition zone length with increasing unit Reynolds number was observed. For example, at  $20^\circ$  angle of attack, the transition length ratio was approximately 2.2 for a unit Reynolds number of  $1.0 \times 10^6/\text{ft.}$ , 1.85 for a unit Reynolds number of  $1.7 \times 10^6/\text{ft.}$  and 1.75 for a unit Reynolds number of  $2.4 \times 10^6/\text{ft.}$  Similar trends can be seen for the other angles of attack.

# VARIATION OF TRANSITION ZONE LENGTH WITH $Re_{TR}$



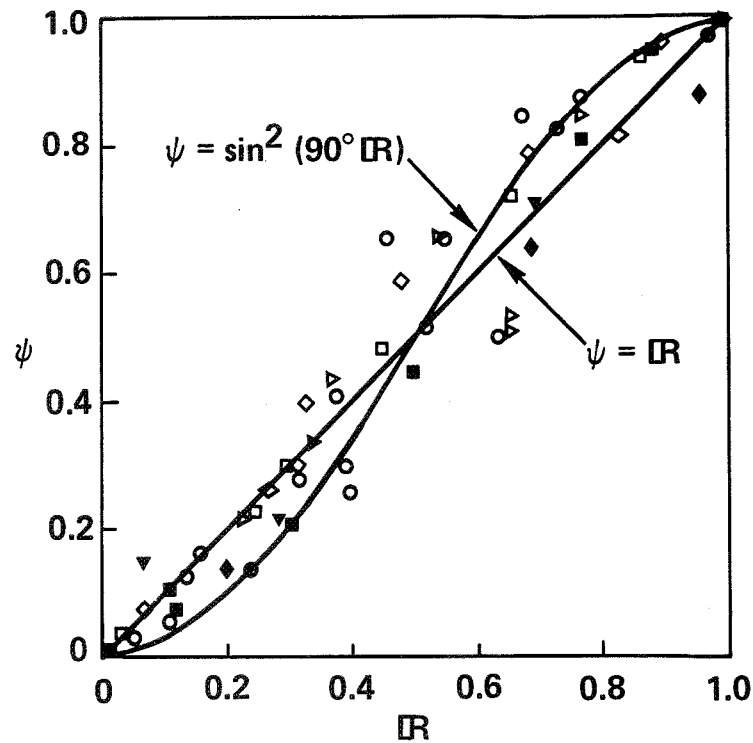
## TRANSITION ZONE HEAT TRANSFER CORRELATION

A correlation of heat transfer in the transition zone as a function of Reynolds number was obtained. Shown is a Stanton number parameter,  $\Psi$ , (which has a value of zero for laminar flow and a value of 1.0 for turbulent flow) plotted against a Reynolds number parameter,  $R$  (which is zero at the start of transition and 1.0 at the end of transition). Two proposed models for heat transfer variation through the transition region are shown on the figure: (1) a linear variation of  $\Psi$  with  $R$ , and (2) a  $\sin^2$  variation.

Neither model was found superior in comparison to the present data.

# TRANSITION ZONE HEAT TRANSFER CORRELATION

$Re_{\infty}/FT. = 1.0 \times 10^6 \text{ TO } 2.4 \times 10^6$



- $10^\circ$
- $15^\circ$
- $17.5^\circ$
- ◇  $19.5^\circ$
- ▷  $20^\circ$
- ◆  $25^\circ$
- ▼  $30^\circ$
- ◇  $35^\circ$

$$\psi = \frac{St_X - St_{LAM}}{St_{TURB} - St_{LAM}}$$

$$IR = \frac{Re_X - Re_{TR}}{Re_{END} - Re_{TR}}$$

## CONCLUSIONS

Several conclusions can be drawn concerning application of the present experimental results to Space Shuttle vehicle design:

1. Wind tunnel results indicate that turbulent flow can occur throughout the angle of attack range for the highest Reynolds numbers tested. Since the Space Shuttle booster will operate at Reynolds numbers based on vehicle length above those tested here, turbulent flow must be expected during booster entry.
2. Existing heat transfer prediction methods correlated quite well with wind tunnel data. For booster entry, tunnel conditions simulated the entry conditions of Mach number and Reynolds number reasonably well; enthalpy levels were not duplicated. Available prediction methods are quite satisfactory for preliminary design calculations.
3. Finite transition zones have been observed throughout the angle of attack range tested. General validity of a transition zone length approximately equal to the onset length has been verified, but important trends with unit Reynolds number have been observed.
4. Transition onset appears to be highly dependent on vehicle geometry, edge Mach number and angle of attack. Great caution should be exercised in extrapolating low angle of attack transitional results to higher angles of attack.

## **CONCLUSIONS**

- **TURBULENT FLOW DURING SPACE SHUTTLE BOOSTER ENTRY IS HIGHLY PROBABLE**
- **EXISTING HEAT TRANSFER PREDICTION TECHNIQUES ARE ACCEPTABLE FOR PRE-LIMINARY DESIGN ESTIMATES**
- **FINITE TRANSITION ZONE CONCEPT IS VALID FOR ANGLES OF ATTACK TESTED**
- **TRANSITION ONSET APPEARS TO BE HIGHLY DEPENDENT ON VEHICLE GEOMETRY AND ANGLE OF ATTACK**





BOUNDARY LAYER TRANSITION ON LIFTING ENTRY VEHICLE  
CONFIGURATIONS AT HIGH ANGLE-OF-ATTACK

by R. V. Masek

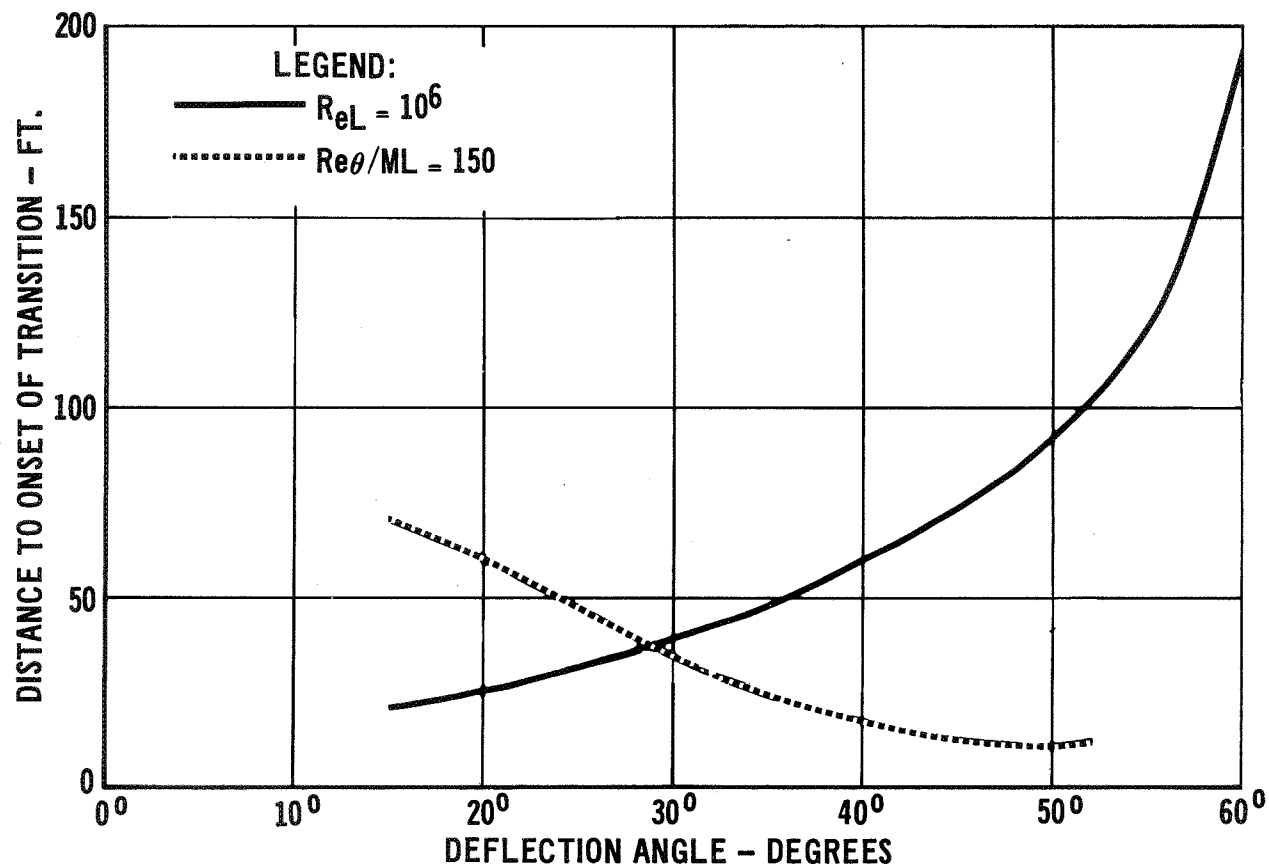
McDonnell Douglas Corporation  
St. Louis, Missouri

SUMMARY

Methods of correlating boundary layer transition on the centerline of highly swept configurations at angles of attack between  $15^\circ$  and  $60^\circ$  have been investigated. The correlating parameters included local Reynolds number at transition onset, angle of attack, local Mach number, local Reynolds number per foot and local Reynolds number based on momentum thickness. It was found necessary to account for streamline divergence in formulating the momentum thickness for the high angle-of-attack data in order to achieve reasonable correlation of the data. The best correlation was achieved utilizing the parameter  $Re_0/M_L (Re_x)^{-2}$ , a form which has also successfully correlated flight and ground test slender cone data at zero degrees angle of attack. The resulting scatter of data around a mean curve fit corresponds to an uncertainty in transition distance of a factor of 4. The scatter of the same data using local Reynolds number at transition as the correlating parameter corresponds to an uncertainty of a factor of 20 in the transition distance. The data at angles of attack greater than thirty degrees are not extensive, and additional experimentation should be conducted to validate use of zero degree angle of attack slender body correlation parameters at high angles-of-attack. This work was conducted as a part of Independent Research and Development at McDonnell Douglas Astronautics Company - Eastern Division.

A number of criteria for predicting the location of boundary layer transition were utilized in the Phase A studies. A comparison of the effect of these criteria for the distance to transition onset are shown here. Note that at the high angles-of-attack the predicted transition location on the vehicle centerline differs by an order of magnitude. This comparison is based on equilibrium glide ( $W/S = 30$ ) at a free stream velocity of 17,000 ft/second. If a transition Reynolds number of  $10^6$  were used the entire vehicle would be laminar @  $60^\circ$  angle of attack whereas use of  $Re_{\theta}/M_L = 150$  would result in a considerable region of turbulent flow. In order to better establish which criterion is most applicable, existing high angle of attack transition data on  $\Delta$  and lifting reentry vehicle configurations were correlated using various parameters.

## UNCERTAINTY IN TRANSITION LOCATION



I have chosen to group the factors which affect the transition Reynolds number into two categories:

- (1) Those factors which are primarily the sources of initial disturbances in the boundary layer and
- (2) The parameters which cause the boundary layer to dampen or amplify the disturbances.

The disturbance sources may occur at the wall e.g., surface roughness, mass injection, vibration; in the inviscid flowfield, e.g., bluntness induced vorticity, shock impingements, interacting flowfields; and in the free stream, e.g., free stream turbulence.

Boundary layer parameters which have been shown through theory and test to dampen or amplify such disturbances are:

Boundary layer edge Mach number.

Unit Reynolds number.

Boundary layer cooling.

Boundary layer edge gradient.

For a fixed set of disturbance sources, one might expect that the transition Reynolds number could be correlated in terms of those parameters which produce amplification or dampening of the disturbances.

# PARAMETERS AFFECTING BOUNDARY LAYER TRANSITION

## POTENTIAL DISTURBANCE SOURCES

- SURFACE ROUGHNESS
- NOSE OR LEADING EDGE BLUNTNES
- SWEEP ANGLE AND ANGLE OF ATTACK
- SHOCK INTERACTIONS
- MASS ADDITION
- VIBRATION

## AMPLITUDE MODIFIERS

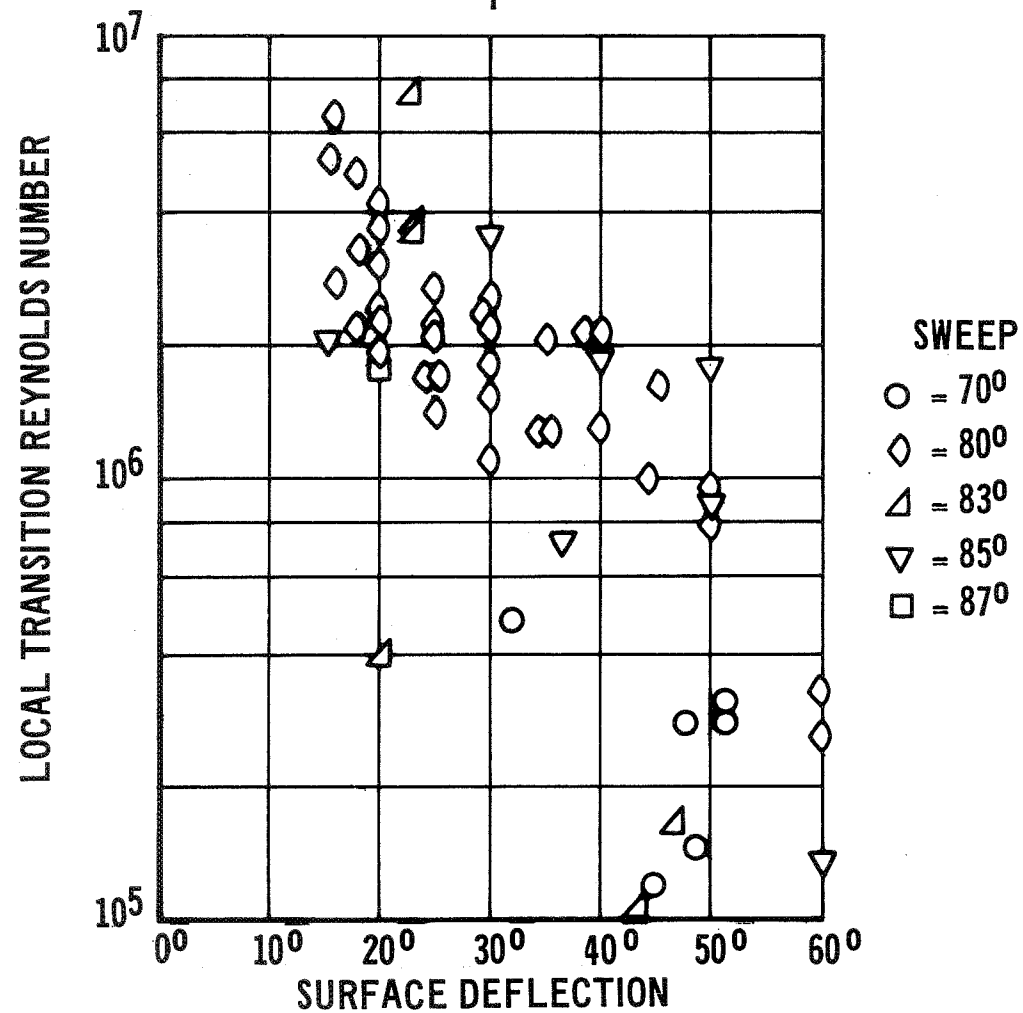
- MACH NUMBER
- UNIT REYNOLDS NUMBER
- BOUNDARY LAYER COOLING
- PRESSURE GRADIENT

Approximately 60 transition data points have been compiled for angles of attack (surface deflections) greater than  $15^\circ$ . The configurations were highly swept lifting geometries or delta wings. The data were obtained at hypersonic free stream Mach number (i.e.  $M_\infty$ )  $> 5$ . If the local Reynolds number number at transition onset is plotted as a function of angle-of-attack, the transition Reynolds number is shown to continually decrease. Considerable scatter of the data is shown. This scatter corresponds to a transition distance variation of a factor of 20. Note that a transition Reynolds number of  $10^6$  is not conservative. In fact, at  $60^\circ$  angle of attack, transition Reynolds numbers  $\approx 10^5$  have been measured. This reduction in transition Reynolds number with increased angle-of-attack does not necessarily mean that the transition distance at a given free stream condition is reduced by increasing angle-of-attack. For example, data taken on a  $\Delta$  configuration by the AFFDL for a range of angles-of-attack have indicated that the transition location moved aft as angle-of-attack was increased from 0 to  $40^\circ$  angle of attack and then moved forward as the angle-of-attack was further increased to  $60^\circ$ .

A consistent set of symbols is used in this and the following curves designed to identify significant differences in geometry. Included in the figure are data recently obtained by NASA Langley on an MSC orbiter configuration and NASA Ames on an  $10^\circ$  included angle pyramid shape.

## CORRELATION OF DELTA WING TRANSITION DATA

### $Re_T$ vs $\delta$



Another approach to correlate the data considered the parameters shown here. The variation of transition Reynolds number with Mach number, a parameter with a well known influence on boundary layer stability.

The scatter is essentially the same as in the previous curve. The transition Reynolds number increases with local Mach number over the entire Mach number range. This is not the typical "J" curve seen in some of the flat plate and slender cone data which indicated that the transition Reynolds number shows a decrease with local Mach number at Mach numbers below 3 - 4 and an increase with Mach numbers above  $M = 4$ .

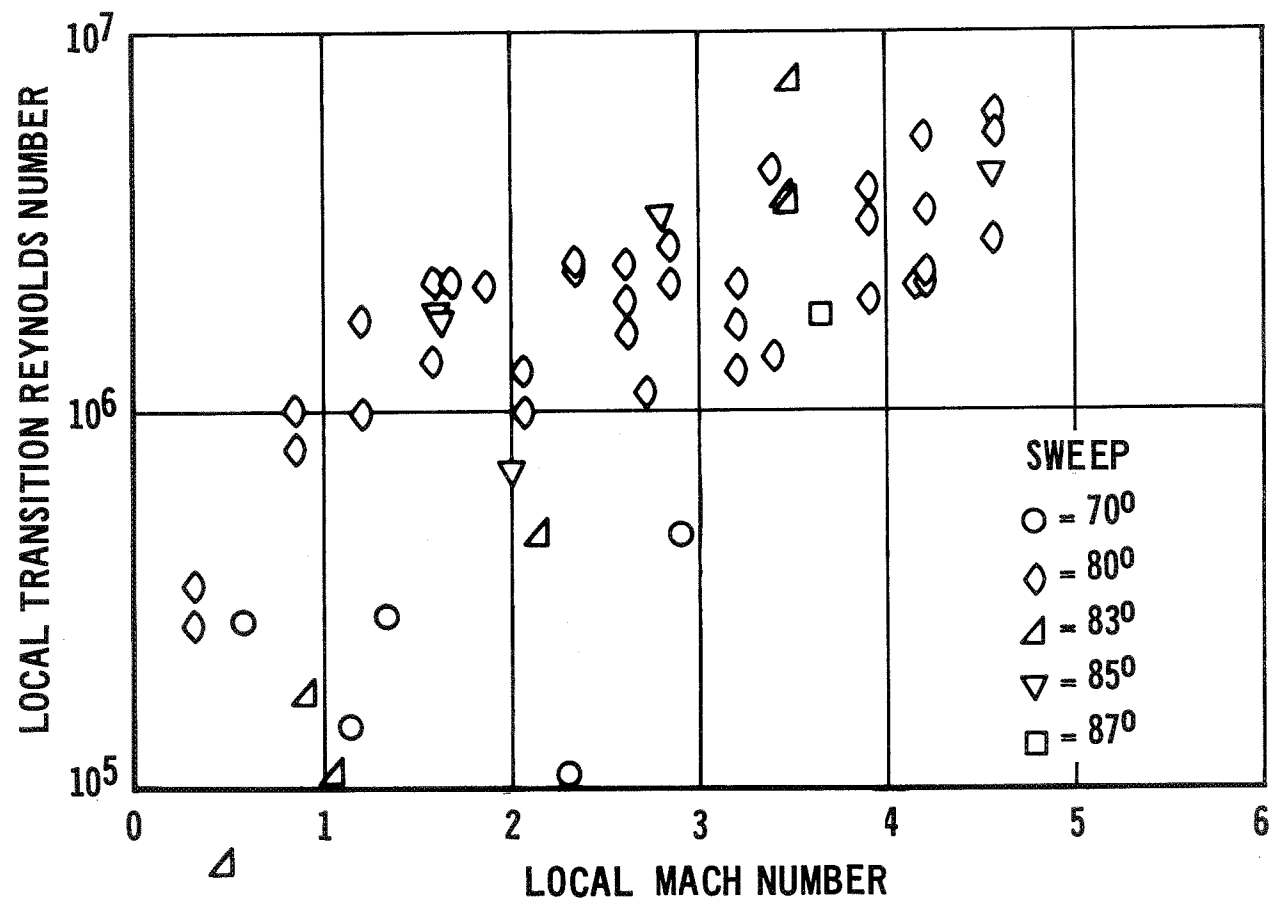
This difference in characteristic may be due to the fact that the local Mach numbers were varied by changing angle-of-attack rather than free stream Mach number and all data were obtained at hypersonic free stream conditions.

A similar characteristic is present in high angle-of-attack cone data as in these delta wing data.



# CORRELATION OF DELTA WING TRANSITION DATA

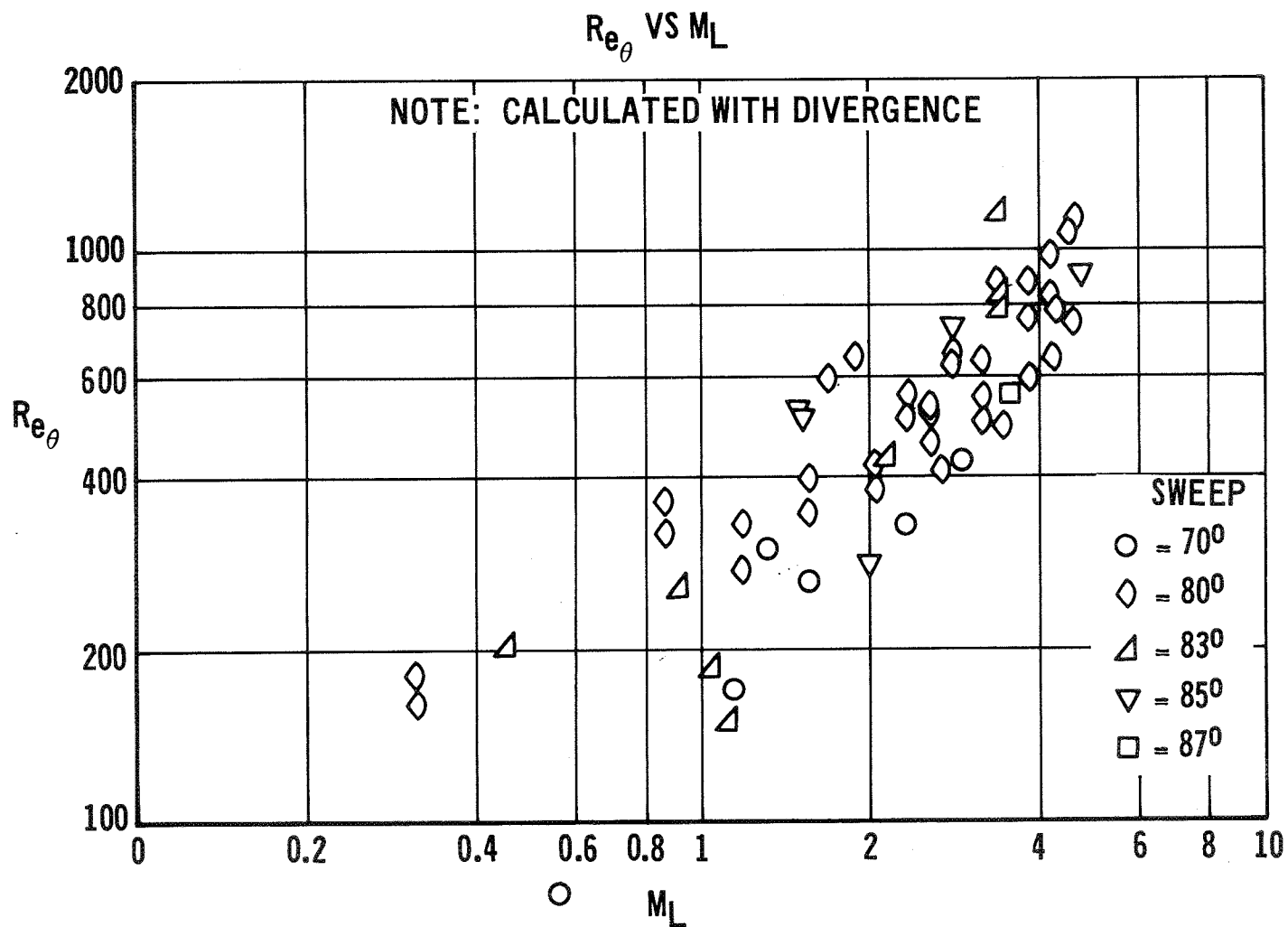
$Re_L$  VS  $M_L$



Since considerable three-dimensionality is present in the flow around the configurations it was suspected that the data scatter could be reduced if the momentum thickness were used as characteristic dimension in the Reynolds number rather than the surface distance to transition. The result is shown. The momentum thickness was computed for a wedge and an approximate correction for flow divergence applied: The correction utilized the centerline velocity gradient correlation derived by Bertram et. al (NASA TMX-316) based on the blunt disc analog, to define the streamline divergence and resulting momentum thickness. Note that the variation of transition Reynolds number based on momentum thickness is essentially linear with Mach number  $Re_{\theta} \sim M_L$ . This suggests the parameter  $Re_{\theta}/M_L$  as correlating parameter.

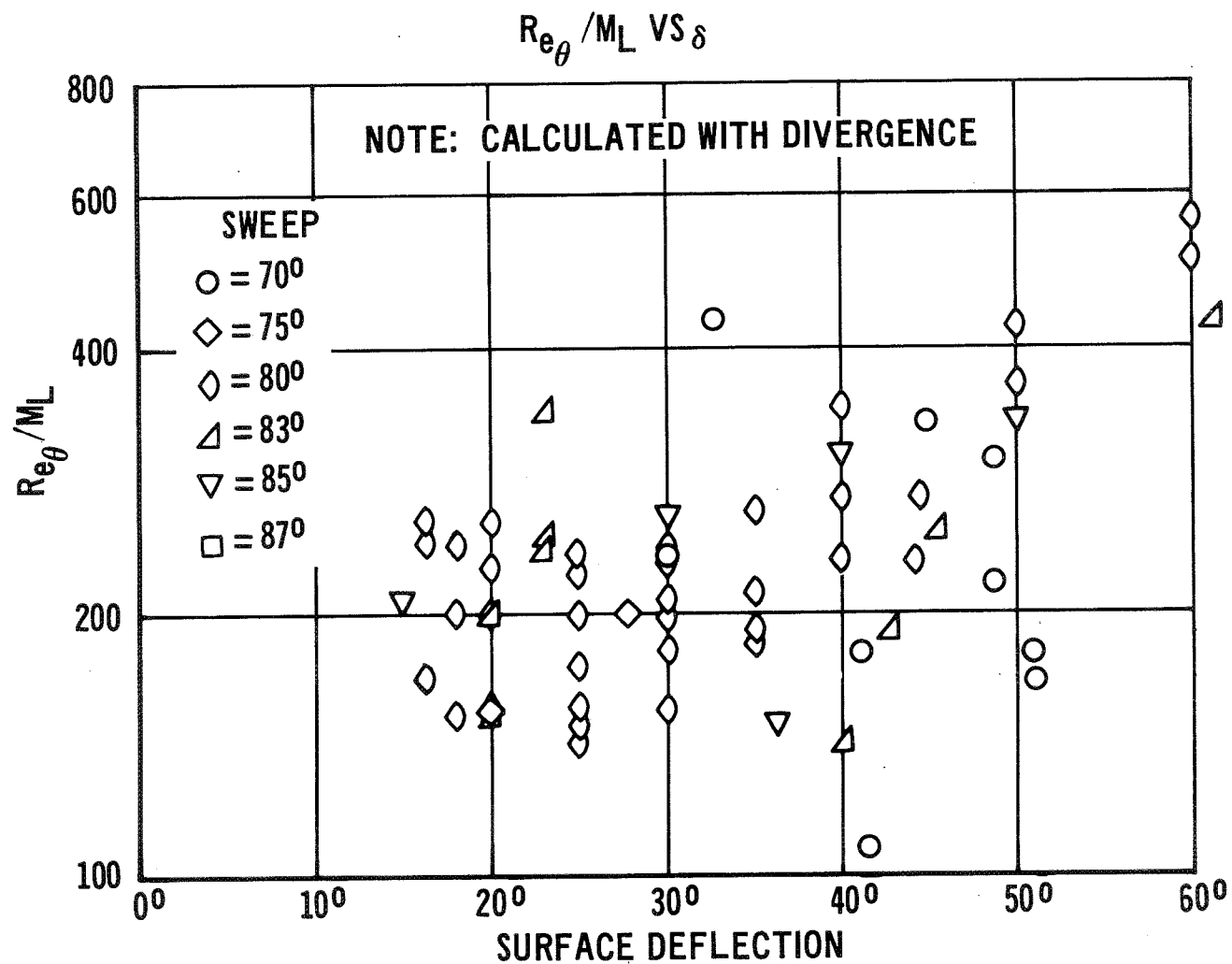
Because of the limited resources available for this study the momentum thickness for some of the data were calculated using incompressible relations. This effect is expected to reduce the momentum thickness less than twenty percent and is unlikely to affect the conclusions of this study, but probably does affect the data scatter.

# CORRELATION OF DELTA WING TRANSITION DATA



Such a correlating parameter,  $R_{eo}/M_L$ , is used in this plot. It was anticipated that this parameter may be independent of angle-of-attack. The scatter shown in the figure corresponds to a transition distance variation of approximately 10. However, the majority of the data are above a value of  $R_{eo}/M_L = 150$ , a value used in some of our Phase A studies, and no consistent trend with angle-of-attack is noted.

# CORRELATION OF DELTA WING TRANSITION DATA

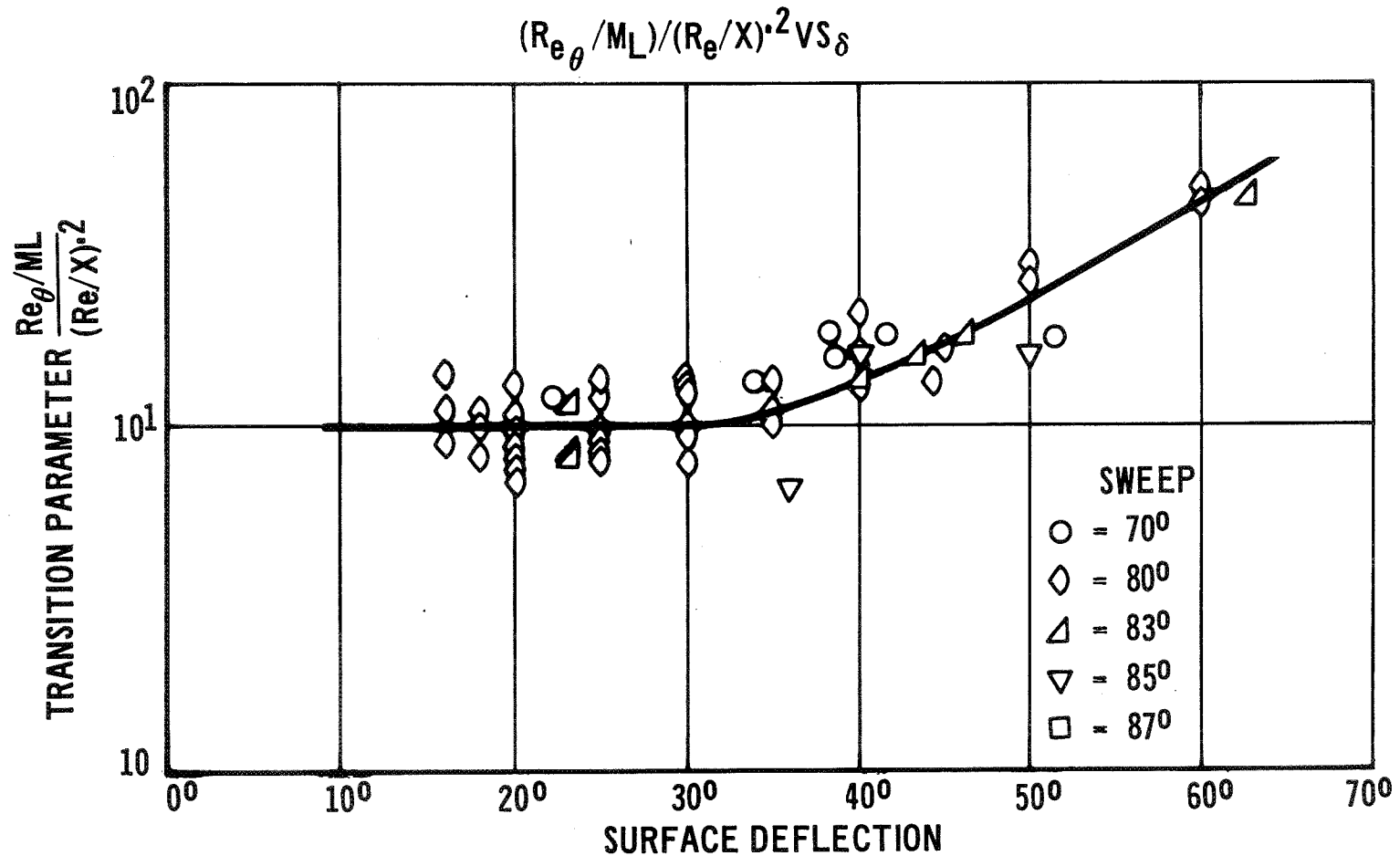


Earlier correlation of slender cone data had indicated an effect of unit Reynolds number, i.e. Reynolds number per foot, on the transition Reynolds number. In wind tunnels this has been often ascribed to tunnel boundary layer noise. The effect, however, has also been seen in free flight data. The transition Reynolds number has been shown to be directly proportional to the unit Reynolds number to a power:  $Re_{et} \sim (Re/x)^n$  where  $n \approx .4$ . The corresponding variation in momentum thickness Reynolds number at transition would vary with unit Reynolds number to the .2 power. This criterion is shown to have a value of approximately 10 at angles-of-attack below  $35^\circ$ , rising to 60 at  $60^\circ$  angle-of-attack.

The scatter around the data fit is less than any other correlation attempt, and the resulting variation in transition distance is less than a factor of 4.

Note the recent data obtained at Langley. The Ames data have not been included since the parameters necessary to calculate the momentum thickness were not available.

# CORRELATION OF DELTA WING TRANSITION DATA



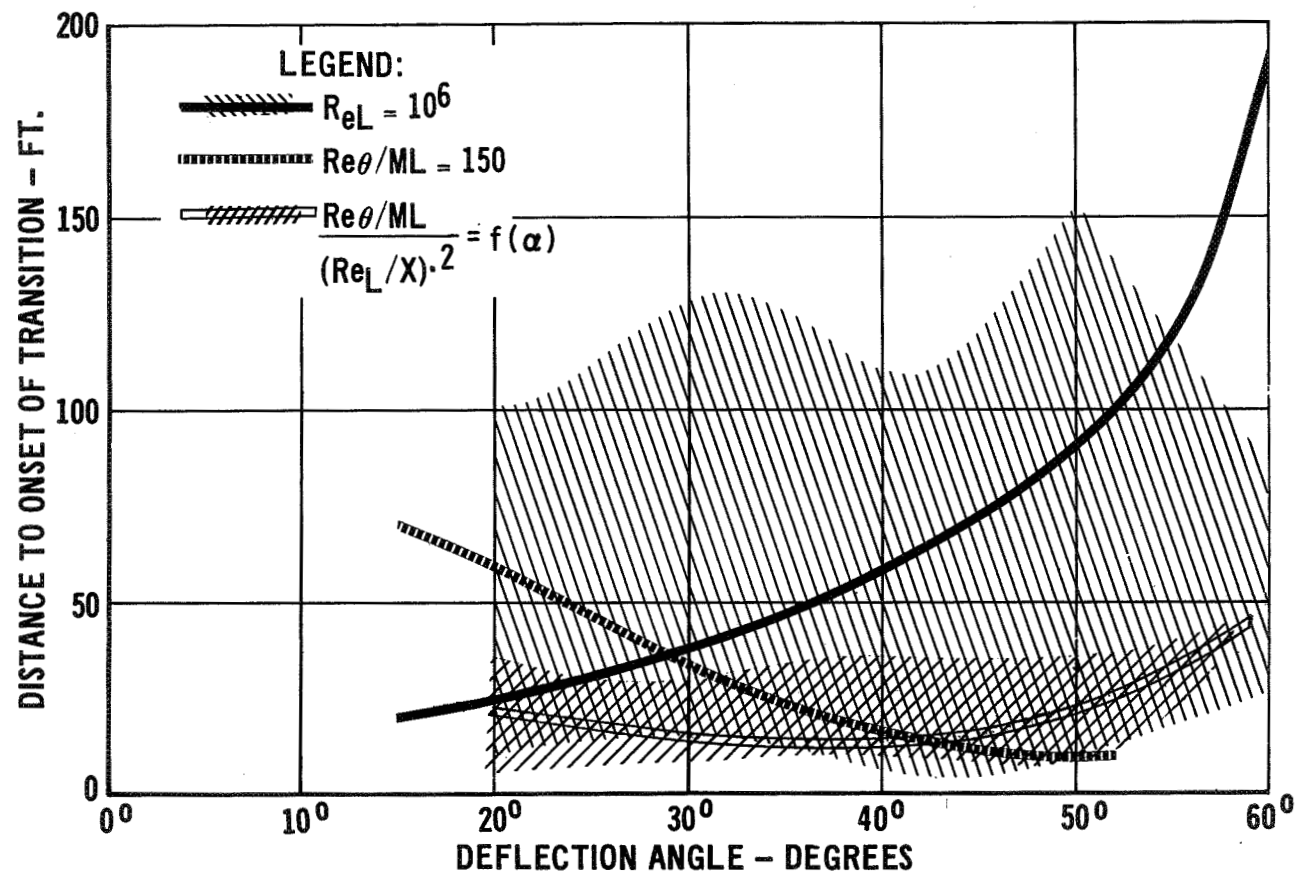
NOTE:  $\theta$  CALCULATED WITH DIVERGENCE

The impact of these correlations for typical shuttle flight conditions is shown. This overlay shows the variations in transition distance resulting from the local Reynolds number and more complex  $R_{e0}/M_L (Re/x)^{.2}$  correlating approaches and the scatter about the best fits.

It is obvious that transition is likely to occur on the vehicle at all angles-of-attack below  $60^\circ$  but that considerable uncertainty remains.



# UNCERTAINTY IN TRANSITION LOCATION



### CONCLUDING REMARKS

A number of pertinent conclusions were derived in this search and correlation of high angle-of-attack boundary layer transition data on lifting entry vehicle configurations:

1. Very high angle-of-attack data are few in number (less than 10 points for  $\delta \geq 50^\circ$ ).
2. Centerline transition data at  $\delta > 50^\circ$  occurred at local Reynolds numbers less than 500,000.
3. Best correlation resulted with the use of a correlating parameter,  $Re_\theta/M_L(Re/x)^{.2}$ , derived in correlations of slender cone transition data.

It is recommended that (1) more extensive data be obtained at very high angle-of-attack for the candidate Shuttle configurations to define both the centerline, spanwise and upper body transition locations (2) the streamline patterns on the configurations be defined through oil flow experiments and theoretical 3-D flow field studies and (3) tests be conducted to evaluate effect of shock impingements due to wing and control surfaces on the transition Reynolds number.

Prior to the availability of such data, configuration and mission comparisons should incorporate the effects of the 3-dimensionality of the flow field, local Mach number, angle-of-attack and unit Reynolds number on the transition locations. Less sophisticated approaches do not provide the correct sensitivities to configuration and mission variables, e.g., TPS weight penalties for cross-range, and the effect of area loading ( $W/S$ ) on peak temperature.

# TURBULENT HEATING ON SPACE SHUTTLE ORBITERS DURING REENTRY

H. Harris Hamilton

NASA Langley Research Center  
Hampton, Virginia

## INTRODUCTION

463

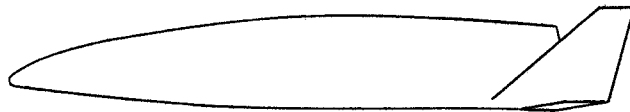
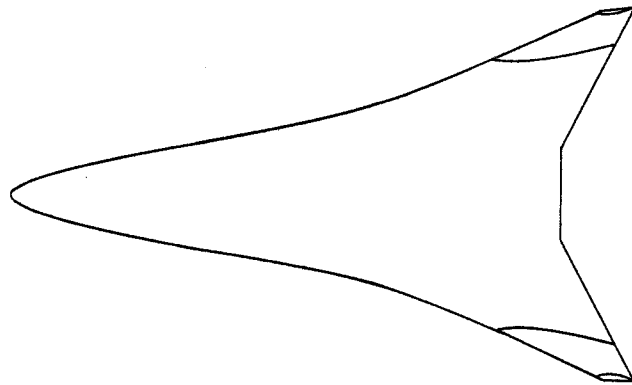
The feasibility of the fully reusable space shuttle concept depends heavily on the development of a nonablating thermal protection system that can be used over many flights without extensive refurbishment. This requires a sound definition of the environment to which the system will be subjected, particularly in the area of aerodynamic heating. The bottom surface of the space shuttle orbiter will have approximately 40 percent of the total surface area and portions of it will be subjected to high heating rates during entry that will raise the surface temperature beyond the upper limit for state-of-the-art metallic heat shield. Thus, the lower surface is the region that will present the greatest challenge in developing a thermal protection system that will meet the necessary requirement of low refurbishment cost. The problem will be further complicated because the highest heating rates over portions of the lower surface may occur when the flow is turbulent. Thus, in the design of any space shuttle orbiter, very careful consideration must be given to turbulent heating.

The results of a study of turbulent reentry heating on the lower surface centerline of two space shuttle orbiter configurations will be presented. The purpose here is to show some of the problems that arise when the flow is turbulent as well as to point out some of the uncertainties that exist in computing turbulent heating.

The two configurations used in the study were a delta wing orbiter (left) and a straight wing orbiter (right). These configurations were chosen because they represent two broad classes of orbiters presently being considered for the space shuttle.

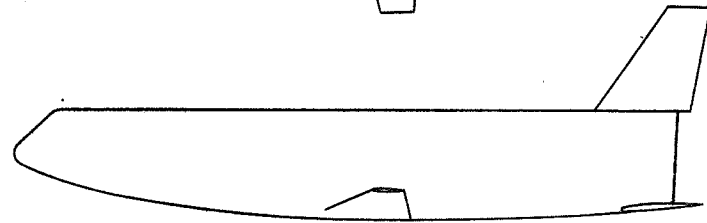
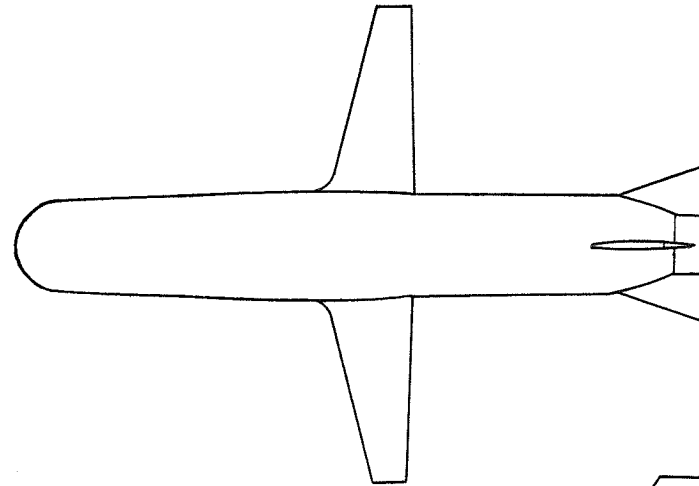
## CONFIGURATIONS

DELTA WING ORBITER



160 ft

STRAIGHT WING ORBITER



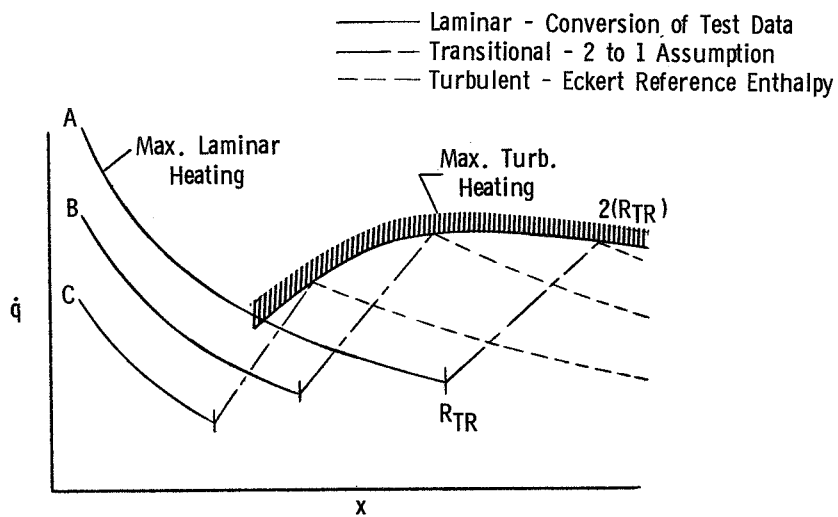
200 ft

Typical distributions of heating on bottom surface of orbiter are shown in upper part of figure. The distribution labeled "A" might correspond to point during entry where maximum laminar heating occurs. Laminar heating rates were obtained by converting wind-tunnel data to flight conditions. Gradual transition was assumed with fully turbulent flow beginning at twice the specified transition Reynolds number ( $R_{TR}$ ). Turbulent heating was computed by Eckert reference enthalpy method with the virtual origin at the start of transition. By computing heating distributions ("B" and "C") at other times during entry, the envelope of maximum turbulent heating was defined. In the discussion that follows, the equilibrium wall temperatures for maximum turbulent heating will be compared to those for maximum laminar heating.

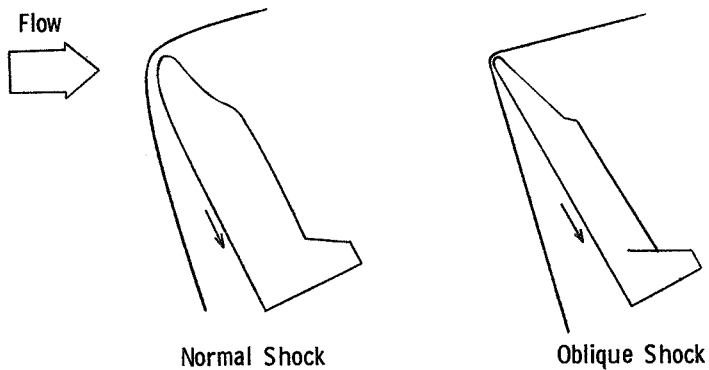
Two methods were used to compute boundary-layer edge flow properties. In the first method ("normal shock" method) the flow was assumed to have expanded isentropically from stagnation conditions behind a normal shock to the local Newtonian pressure. In the second method ("oblique shock" method) the flow was assumed to have passed through an oblique shock of sufficient strength to raise the pressure to the local Newtonian pressure. Which is the better method to compute flow properties depends largely on body bluntness and angle of attack. However, at present, there is no clear line of demarcation between the two methods in many applications.

The effect of transition Reynolds number will be illustrated by comparing results for assumed transition Reynolds numbers of  $1/4$  million and 1 million. These values were selected because they are in the range where transition is expected to occur in flight and because of the 4 to 1 change in magnitude.

## METHOD OF COMPUTING TURBULENT HEATING



## BOUNDARY LAYER EDGE PROPERTIES

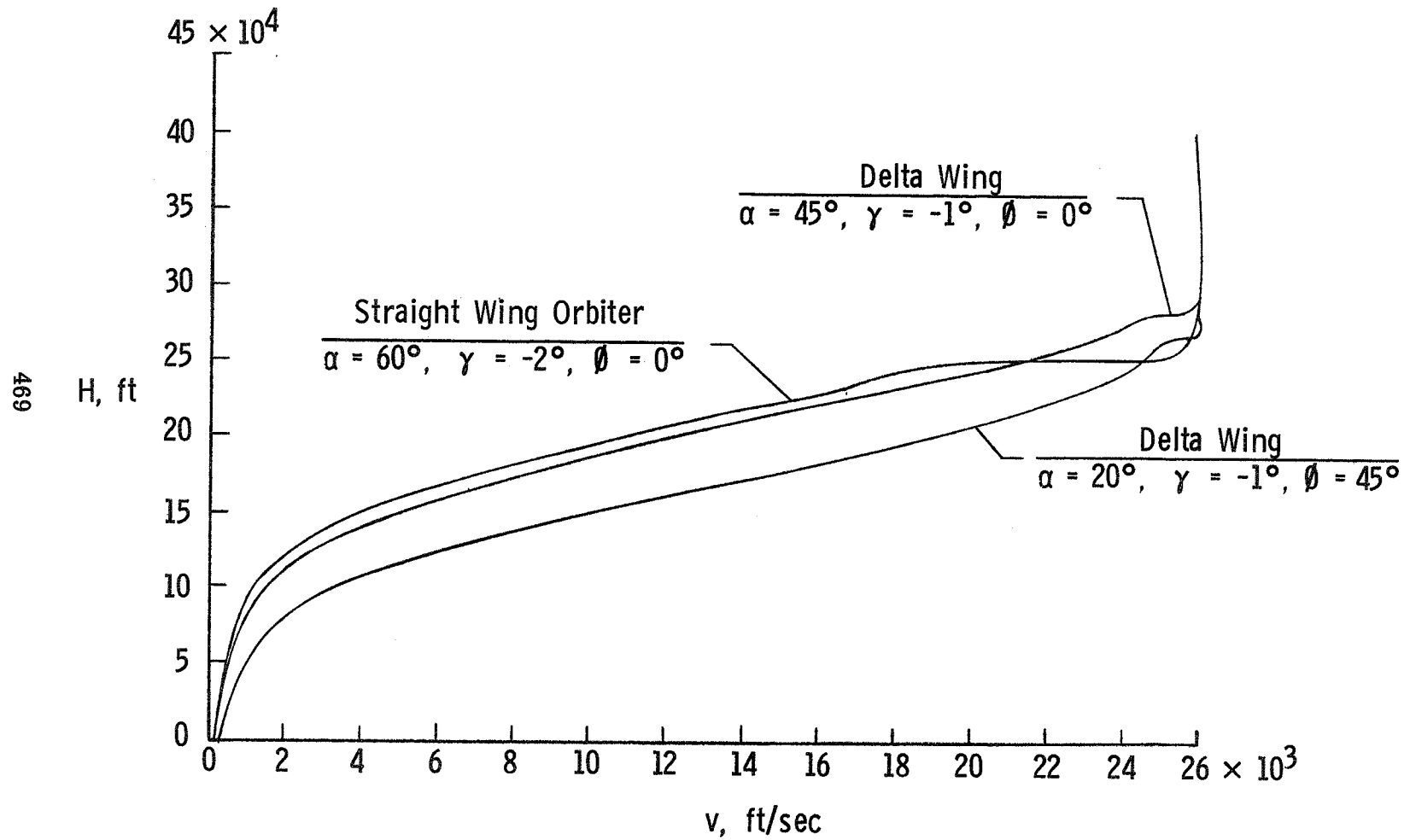


Transition Reynolds Numbers  $0.25 \times 10^6$   
 $1.0 \times 10^6$

The velocity-altitude entry trajectories are shown in this figure. The entry conditions are representative of these classes of orbiters but are not optimum. The straight wing orbiter entered at high angle of attack ( $\alpha = 60^\circ$ ) on a low cross-range trajectory. Two modes of entry were considered for the delta wing orbiter. The first was a high angle of attack ( $\alpha = 45^\circ$ ), low cross-range entry; the second was a low angle of attack ( $\alpha = 20^\circ$ ), high cross-range entry. Note that the impact of turbulent heating on the straight wing and delta wing orbiters should not be compared directly because of the differences in entry angle and angle of attack.

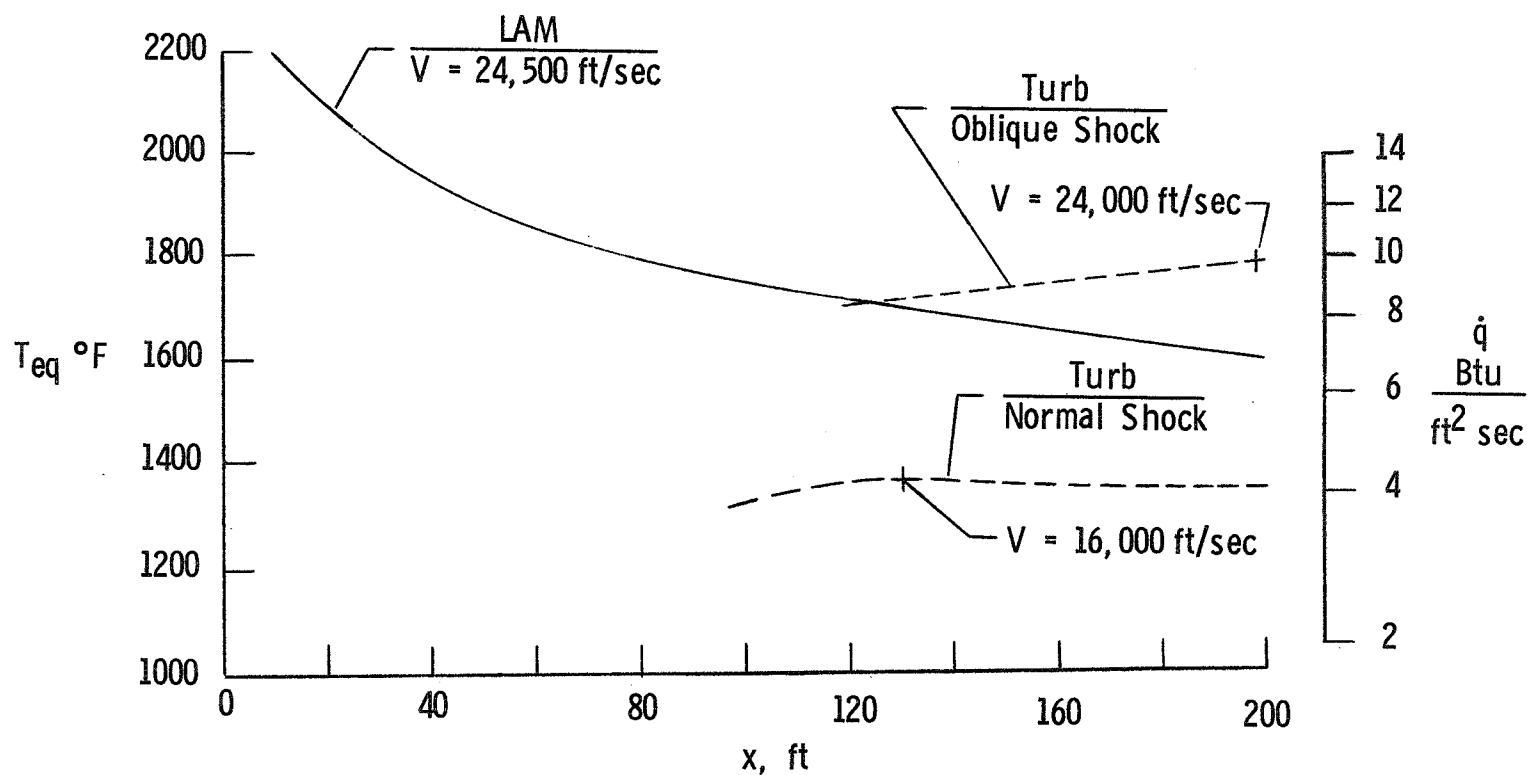


# ENTRY TRAJECTORIES



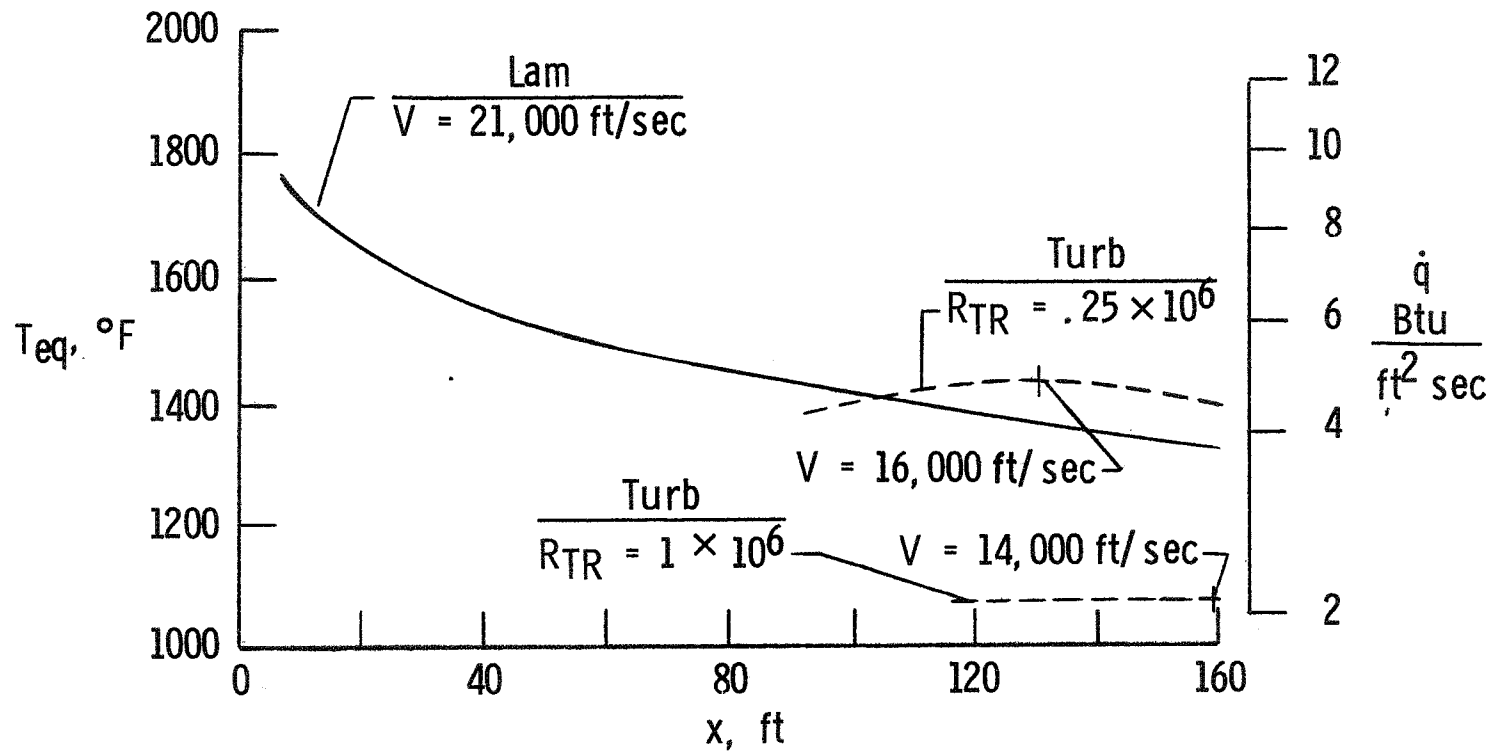
This figure shows maximum centerline equilibrium wall temperatures on the straight wing orbiter at  $\alpha = 60^\circ$ . The assumed transition Reynolds number was 1/4 million and the emissivity was 0.8. Equilibrium wall temperatures for maximum laminar heating (which occurred at  $v = 24,500$  ft/sec) vary from approximately  $2200^\circ$  F near the nose to  $1600^\circ$  F near the trailing edge. The maximum turbulent equilibrium wall temperatures computed using oblique shock edge properties exceed the maximum laminar wall temperatures over the rearward portion of the bottom surface centerline and the highest wall temperature is approximately  $1800^\circ$  F (which occurred at a velocity of  $24,000$  ft/sec). When normal shock edge properties are used, the maximum turbulent wall temperatures are lower than the maximum laminar wall temperatures. The assumed transition Reynolds number is reached much earlier in the trajectory, and the maximum turbulent wall temperatures are much higher for the oblique shock case.

MAXIMUM CENTERLINE EQUILIBRIUM WALL TEMPERATURE  
 STRAIGHT WING ORBITER,  $\alpha = 60^\circ$ ,  $R_{TR} = .25 \times 10^6$ ,  $\epsilon = .8$



This figure shows the effect of transition Reynolds number on the maximum centerline wall temperatures for the delta wing orbiter at  $\alpha = 45^\circ$ . Boundary-layer edge properties were computed using the normal shock method. For a transition Reynolds number of  $1/4$  million, the maximum wall temperatures for turbulent flow exceed the maximum wall temperatures for laminar flow over the rearward portion of the bottom surface centerline; and the highest wall temperature is approximately  $1450^\circ$  F (which occurred at  $v = 16,000$  ft/sec). For a transition Reynolds number of 1 million, the maximum turbulent wall temperatures are lower than the maximum laminar wall temperatures. Note that the highest turbulent heating rate occurs at a much lower velocity than maximum laminar heating.

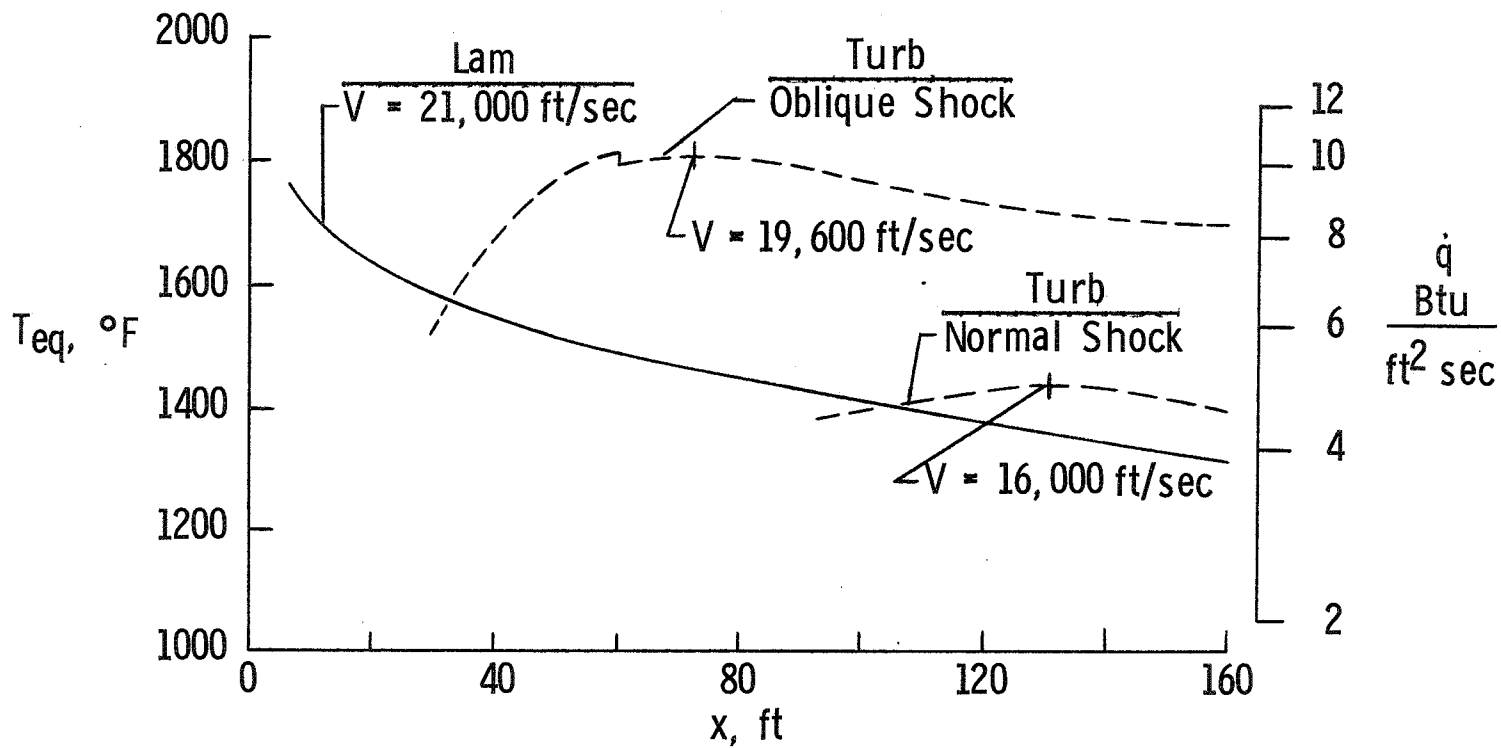
EFFECT OF TRANSITION REYNOLDS NUMBER ON  
 MAXIMUM WALL TEMPERATURE  
 DELTA WING ORBITER,  $\alpha = 45^\circ$ ,  
 NORMAL SHOCK EDGE PROPERTIES,  $\varepsilon = 0.8$



This figure shows the effect of boundary-layer edge properties on the maximum centerline wall temperatures for the delta wing orbiter at  $\alpha = 45^\circ$  (same orbiter and entry conditions as in fig. 5). The transition Reynolds number is  $1/4$  million. The maximum turbulent wall temperatures for the oblique shock case are significantly higher than either the maximum laminar wall temperatures or the maximum turbulent wall temperatures for the normal shock case. Note for the first time the step in the turbulent wall temperature distribution at  $X = 60$  ft which was caused by the higher forward ramp angle on the bottom surface of the delta wing orbiter. Because of the higher wall temperatures obtained, using oblique shock edge properties could have an impact on thermal protection system design.

# EFFECT OF BOUNDARY LAYER EDGE PROPERTIES ON MAXIMUM WALL TEMPERATURE

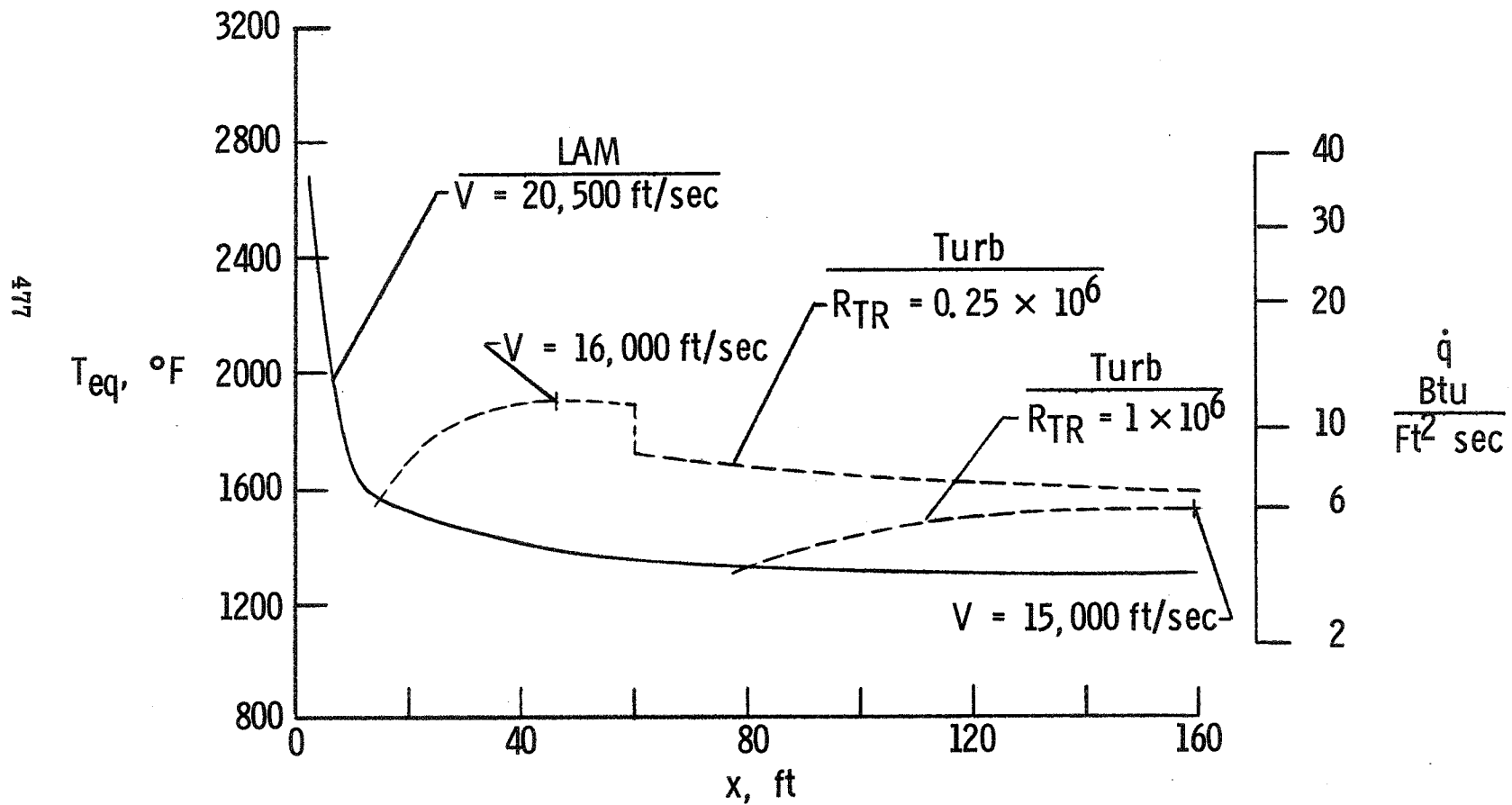
DELTA WING ORBITER,  $\alpha = 45^\circ$ ,  $R_{TR} = .25 \times 10^6$ ,  $\epsilon = .8$



This figure shows the effect of transition Reynolds number on the maximum centerline wall temperatures for the delta wing orbiter at  $\alpha = 20^\circ$ . Here, the delta wing orbiter entered at lower angle of attack and has larger cross-range capability than at the higher angle of attack (figs. 5 and 6). Note first that entering at the lower angle of attack reduces the maximum laminar wall temperatures over much of the lower surface. The maximum turbulent wall temperatures were computed using normal shock edge properties. For a transition Reynolds number of 1 million, the maximum turbulent wall temperatures exceed the maximum laminar wall temperatures over the rearward portion of the bottom surface centerline, but the highest wall temperature is less than  $1600^\circ$  F. For a transition Reynolds number of  $1/4$  million, the maximum turbulent wall temperatures are higher than the maximum laminar wall temperatures over most of the bottom surface centerline and the highest wall temperature reaches approximately  $1900^\circ$  F.



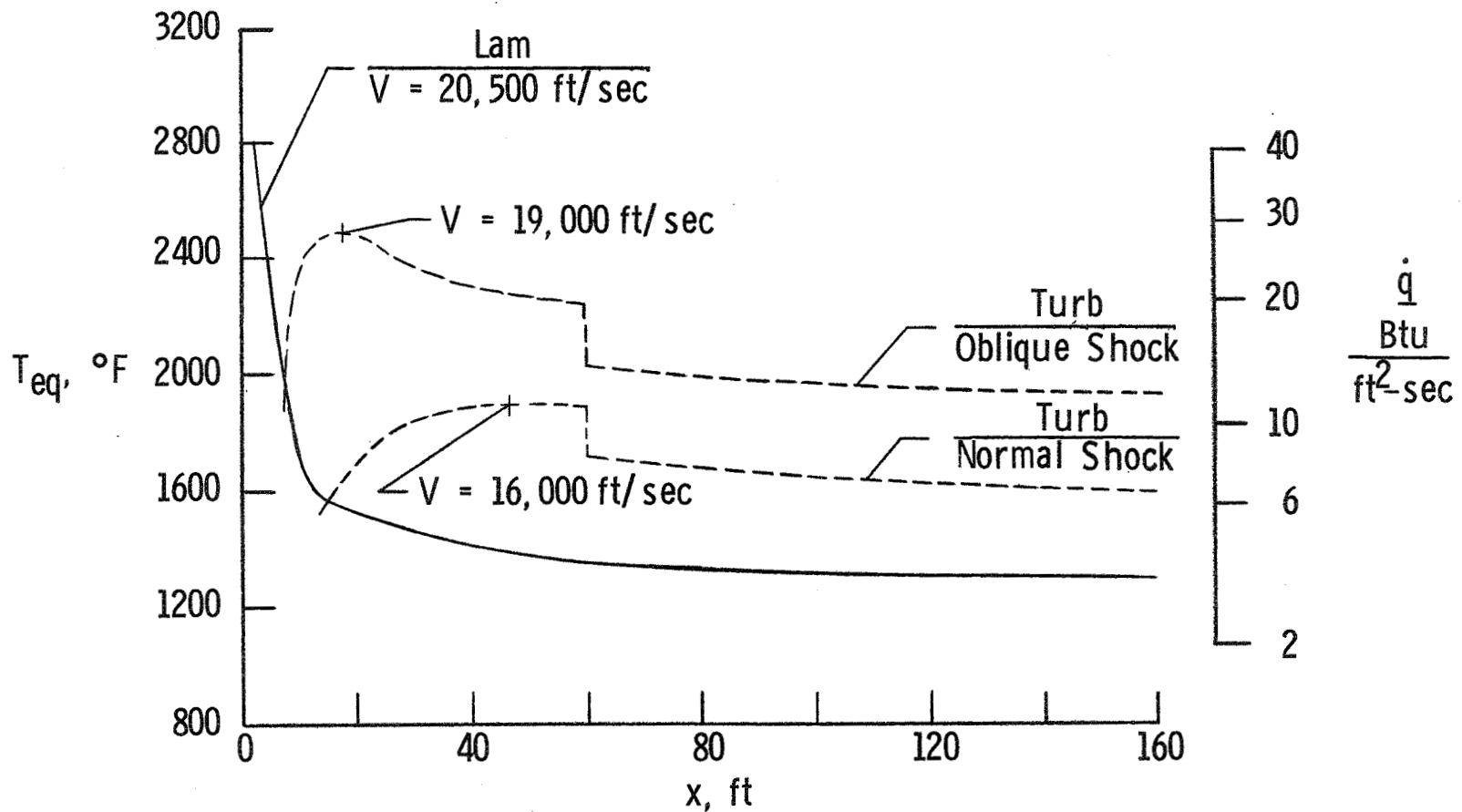
EFFECT OF TRANSITION REYNOLDS NUMBER  
ON MAXIMUM WALL TEMPERATURE  
DELTA WING ORBITER,  $\alpha = 20^\circ$  NORMAL SHOCK  
EDGE PROPERTIES,  $\varepsilon = 0.8$



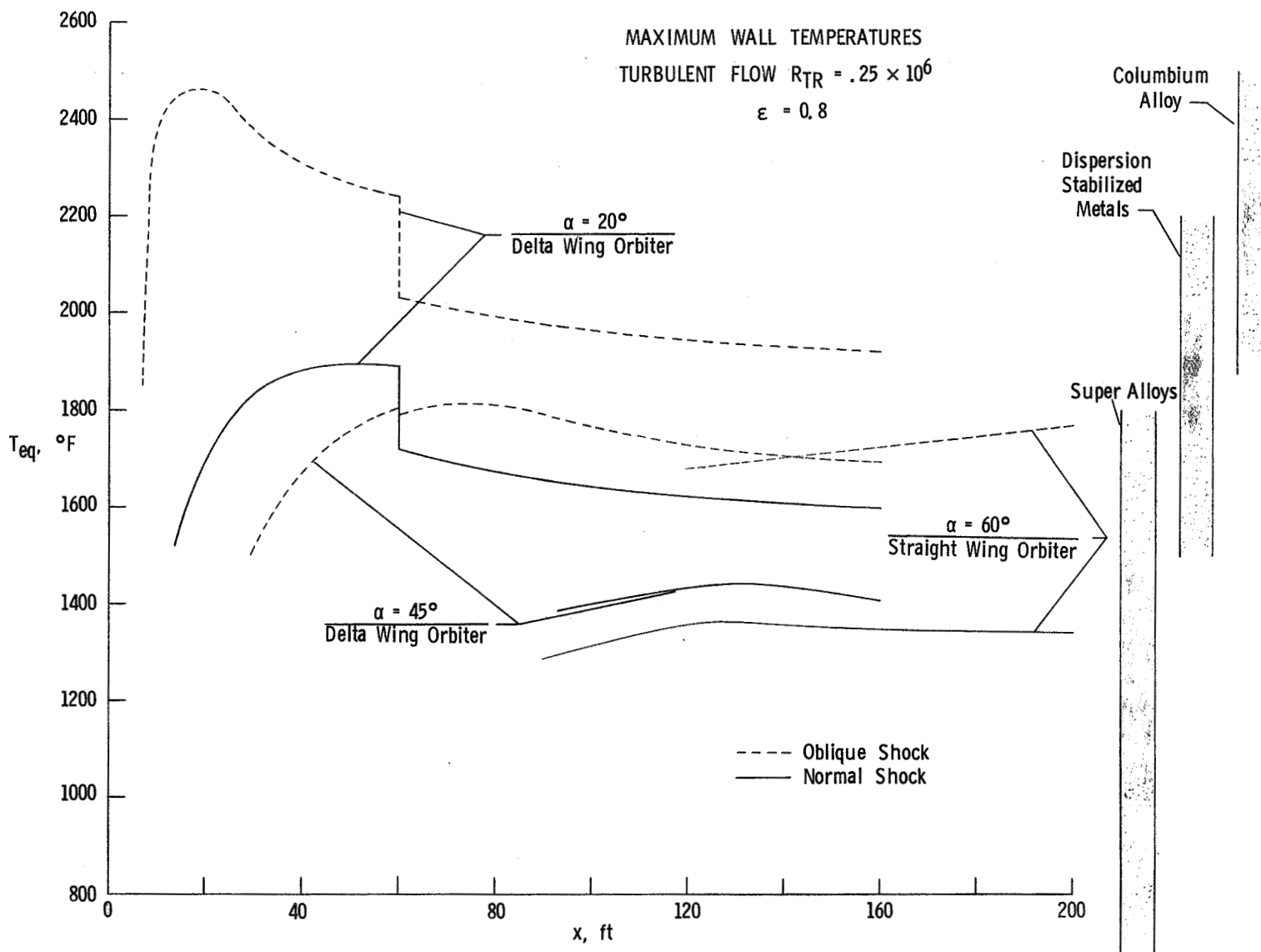
This figure shows the effect of boundary-layer edge properties on the maximum centerline wall temperatures for the delta wing orbiter at  $\alpha = 20^\circ$  (same orbiter and entry conditions as in fig. 7). The assumed transition Reynolds number was 1/4 million. The maximum turbulent wall temperatures computed using oblique shock edge properties exceed  $1900^\circ$  F over almost the entire bottom surface centerline and rise to approximately  $2500^\circ$  F near  $X = 20$  ft. Note that using oblique shock edge properties to compute turbulent heating will have a large impact on thermal protection system design.

# EFFECT OF BOUNDARY LAYER EDGE PROPERTIES ON MAXIMUM WALL TEMPERATURE

DELTA WING ORBITER,  $\alpha = 20^\circ$ ,  $R_{TR} = .25 \times 10^6$ ,  $\epsilon = 0.8$



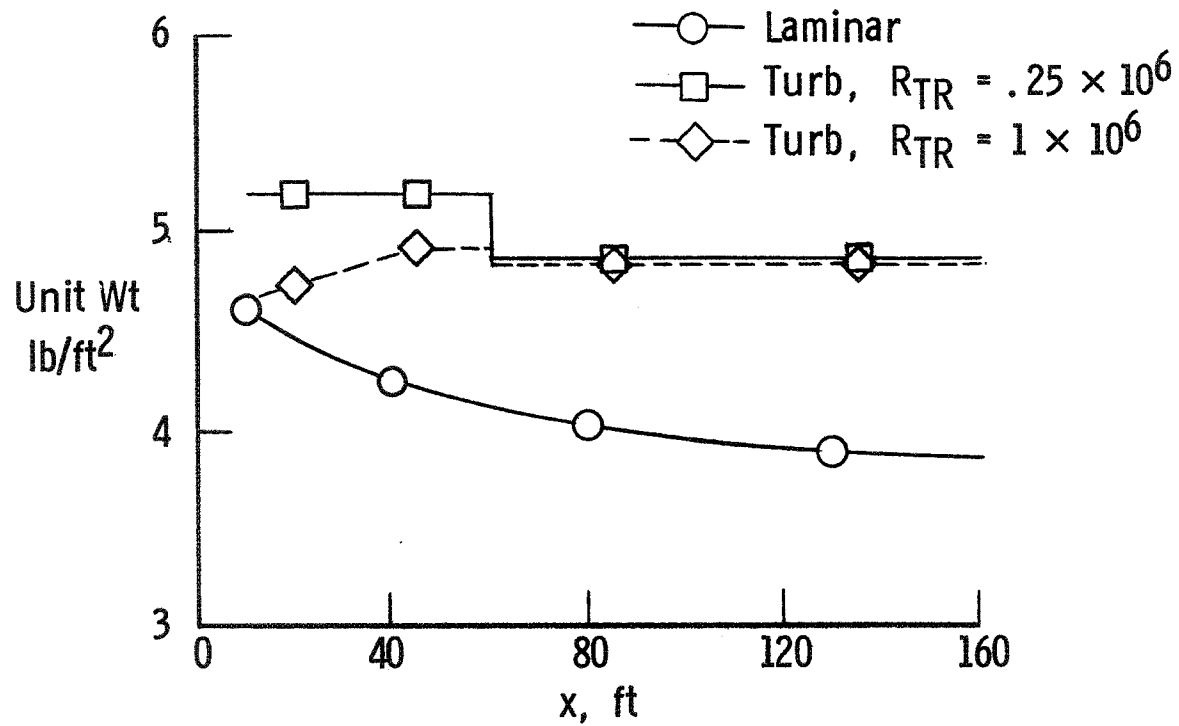
This figure summarizes the maximum centerline wall temperatures shown on the previous figures for turbulent flow with a transition Reynolds number of  $1/4$  million. The approximate useful ranges for several classes of metallic heat-shield materials are shown on the right of the figure. Several points are to be noted. First, for a given orbiter and entry mode using oblique shock edge properties (dashed lines) instead of normal shock edge properties (solid lines) produces higher wall temperatures. Second, the maximum centerline wall temperatures on the straight wing orbiter and the delta wing orbiter at  $\alpha = 45^\circ$  fall within the range where super-alloy heat-shield materials could probably be employed. It is interesting to note that the wall temperatures for these two orbiters are approximately the same but, as pointed out earlier, they should not be compared directly because of differences in the entry angle and angle of attack. Next, for a given method of computing boundary-layer edge properties, the wall temperatures on the delta wing orbiter at the lower angle of attack are higher than the wall temperatures for the same orbiter at the higher angle of attack. This is opposite to the effect of  $\alpha$  that was noted earlier for laminar flow. In fact, for the oblique shock case, the centerline wall temperatures always exceed the upper limit for super alloys and even exceed the upper limit for dispersion stabilized metals over a portion of the bottom surface centerline. The turbulent heating was more severe on the delta wing orbiter at  $\alpha = 20^\circ$  because it penetrated deeper into the atmosphere during entry.



This figure shows an estimate of the effect of turbulent heating on the bottom surface centerline TPS unit weight for the delta wing orbiter at  $\alpha = 20^\circ$ . Turbulent heating rates were based on oblique shock edge properties. This was the most severe case of turbulent heating that was encountered. The unit weights were obtained from a one-dimensional transient heat transfer calculation for a metallic heat shield backed by insulation (with a density of  $8.25 \text{ lb/ft}^3$ ) and a back surface heat sink. The unit weights of the heat-shield material were taken as  $1.3 \text{ lb/ft}^2$  for areas where the maximum wall temperature was less than  $1800^\circ \text{ F}$  and  $1.7 \text{ lb/ft}^2$  for areas where the maximum wall temperature was above  $1800^\circ \text{ F}$ . The system was required to maintain the back surface temperature below  $200^\circ \text{ F}$  with no cooling (probably a severe requirement).

For a transition Reynolds number of  $1/4$  million, the increase in centerline TPS unit weight varies from approximately  $1/2 \text{ lb/ft}^2$  at the forward point of the turbulent heating zone to approximately  $1 \text{ lb/ft}^2$  at the trailing edge. For a transition Reynolds number of 1 million, the TPS unit weights were decreased over the forward portion of the bottom surface centerline (compared to the  $1/4$  million transition Reynolds number) but was affected very little over the rearward portion. This was because transition occurred so early in the trajectory that there was little difference in the total heat load on the rearward portion of the lower surface centerline for each transition Reynolds number.

EFFECT OF TURBULENT FLOW ON  
 CENTERLINE TPS UNIT WEIGHT  
 DELTA WING ORBITER,  $\alpha = 20^\circ$   
 OBLIQUE SHOCK,  $\varepsilon = .8$



#### SUMMARY

It has been shown that turbulent heating can have a large impact on thermal protection system design both in the choice of the heat-shield materials and in the system unit weight. Additional work is needed to define more clearly (1) the proper criteria to be used for boundary-layer transition, and (2) the most appropriate method for computing boundary-layer edge flow properties for entry vehicles of the space shuttle class.



A COMPARISON OF SIMPLE TURBULENT HEATING ESTIMATES AND BOUNDARY LAYER TRANSITION CRITERIA  
WITH APPLICATION TO LARGE, LIFTING ENTRY VEHICLES

Blaine E. Pearce

The Aerospace Corporation  
El Segundo, California

INTRODUCTION

The feasibility of a reusable heat shield for the bottom (windward surface) of the Space Shuttle is essentially determined by the maximum surface temperature attained during entry. Preliminary analyses have shown that outside the relatively small areas near the stagnation point and leading edges, peak heating to a large fraction of this surface can occur when the boundary layer is turbulent. Predictions of the heat transfer in fully turbulent flow and the concomitant prediction of the onset and extent of transition from laminar to turbulent flow are therefore important elements in the design of the Space Shuttle.

This paper presents some results concerning the heat transfer predictions in fully turbulent flow and the effects of boundary layer transition criteria on the heating predictions for the windward surface of a large, lifting entry vehicle. The work is a summary of that done in support of the Air Force-sponsored Space Transportation System study contracts.

The conditions for which the boundary layer on the windward surface is turbulent will be specified at the outset in order to restrict the discussion to the range of local Mach number and, more importantly, the ratios of the wall to adiabatic wall enthalpy expected to occur near peak turbulent heating. Predictions for heating rates in turbulent flow used in the initial studies will then be examined along with the appropriate form of Reynolds analogy factor. The various predictions are then compared with experimental data for heat transfer to a flat surface with uniform boundary layer edge conditions in order to select in a rational manner that method which gives the most accurate estimates of the heating.

The effect of boundary layer transition is examined by comparing the predictions from different specifications for the onset of transition. In this case, no recommendation is made concerning the most appropriate criterion, but rather the consequences of using the different criteria are examined.

The effects of both the different heat transfer prediction methods and the different transition onset criteria are examined by means of the calculations for peak temperatures on the windward centerline for a specific configuration consisting of a flat, delta wing.

It is important that the conditions for which the heat transfer predictions are to be made be carefully defined in order to assure that any comparison with experimental data is applicable to the Space Shuttle. The boundary layer edge Mach number and the ratio of wall to adiabatic wall enthalpy which occur at peak turbulent heating are summarized here. These conditions occur along an equilibrium glide trajectory for a vehicle with a planform loading of 50 lbs/ft<sup>2</sup>.

These results show that the boundary layer edge Mach numbers of interest vary from about 8 down to nearly unity, and the wall to adiabatic wall enthalpy ratio for a radiatively cooled heat shield is of the order of 0.1. It is for these conditions that the most accurate prediction method is needed.

TABLE I  
*SUMMARY OF BOUNDARY LAYER EDGE CONDITIONS FOR  
 PEAK HEATING IN FULLY TURBULENT FLOW*

ANGLE OF ATTACK, DEG	LOCAL MACH NO., $M_l$	WALL ENTHALPY RATIO $h_w / h_{aw}$	ALTITUDE, kft
10	8.3	0.15	150
20	5.8	0.11	190
30	4.3	0.10	210
40	3.2	0.093	220
50	2.3	0.078	220
60	1.2	0.068	230

CONDITIONS:

1. EQUILIBRIUM GLIDE TRAJECTORY
2. NEWTONIAN LIFT COEFFICIENT
3. OBLIQUE SHOCK SOLUTION

There were four primary predictions methods for turbulent heating used by the contractors in the initial Space Shuttle studies. These were: (1) Eckert's method, (2) the adiabatic wall reference enthalpy method, (3) the reference density-viscosity ( $\rho\mu$ ) product method, and (4) Spalding and Chi's correlation. All make use of transformations which relate the skin friction and Reynolds number in a compressible, turbulent boundary layer to equivalent quantities in a constant property turbulent flow for which the density and transport properties are evaluated at a reference enthalpy. Heat transfer predictions are then obtained by using Reynolds analogy. The transformation factors  $F_c$ ,  $F_R$ , and  $F_{R0}$  (in Spalding and Chi's notation), skin friction laws, and the analogy factors for each method are summarized in this table.

The four methods examined here, with the exception of the  $\rho\mu$ -method, are strictly valid for a flat plate in a uniform flow. The subsequent comparison is with data which approximates the heating to a flat surface in a uniform flow. The comparison therefore seeks to determine the method which correctly accounts only for the fact that the density and transport properties vary through the boundary layer. It is these effects which are the principal source of discrepancy between the predictions.

In addition to the effects of variable properties, the predictions differ in that different skin friction laws and Reynolds analogy factors are used. There can be as much as 15 percent difference due to the skin friction law and as much as 15 percent due to the Reynolds analogy factor. The particular combinations used here are those proposed in the original specification of each method, except for Eckert's method, which was originally proposed with Colburn's equation for the Reynolds analogy factor.

It is known that the boundary layer edge flow on the windward surface of a lifting vehicle is three-dimensional with gradients in both the longitudinal and transverse directions. However, for flat surfaces and far from the bluntness-dominated regions near stagnation points and leading edges, the effects of the initial longitudinal gradients are small, particularly for highly cooled surfaces. In addition, on the centerline, it is believed that cross-flow effects result in only small additions to the heating for a purely two-dimensional flow. The prediction methods examined here are therefore expected to be useful, especially along the centerline.

TABLE 2  
SUMMARY OF BOUNDARY LAYER PREDICTION METHODS

METHOD	$F_c$	$F_R$	$F_{R\theta}$	$h^*$	SKIN FRICTION LAW	REYNOLDS ANALOGY FACTOR
ECKERT	$\rho_1 / \rho^*$	$\frac{\rho^* \mu_1}{\rho_1 \mu^*}$	$\mu_1 / \mu^*$	$1/2 (h_w + h_1) + 0.22 r (h_0 - h_1)$	PRANDTL	VON KARMAN
ADIABATIC WALL	$\rho_1 / \rho^*$	$\frac{\rho^* \mu_1}{\rho_1 \mu^*}$	$\mu_1 / \mu^*$	$h_1 + 0.72 r (h_0 - h_1)$	PRANDTL	COLBURN
SPALDING-CHI	$\left[ \int_0^1 \left( \frac{\rho}{\rho_1} \right)^{1/2} d \left( \frac{u}{u_1} \right) \right]^{-2}$	$\frac{F_{R\theta}}{F_c}$	$\left( \frac{h_w}{h_1} \right)^{-0.702} \left( \frac{h_{aw}}{h_w} \right)^{0.772}$	-----	TABULAR	VON KARMAN
$(\rho\mu)$ - METHOD	$\frac{\rho_1 \mu_0}{\rho^* \mu^*}$	$\frac{\rho^* \mu_1 \mu^*}{\rho_1 \mu_0^2}$	$\mu_1 / \mu_0$	-----	MODIFIED SCHULTZ-GRUNOW	COLBURN

## SKIN FRICTION LAWS :

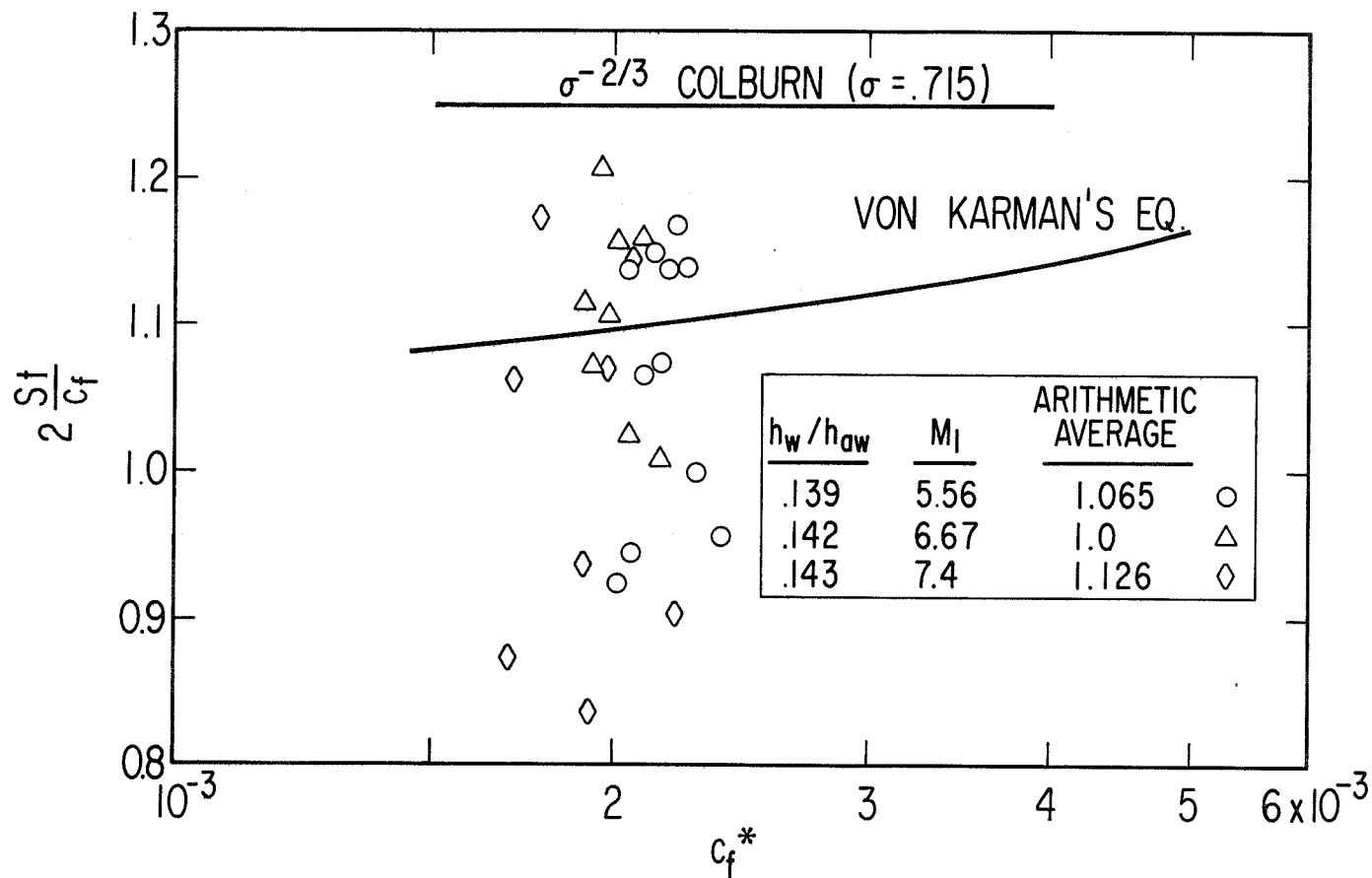
1. PRANDTL  $C_f^* = 0.0592 Re_x^{*-1/5}$
2. MODIFIED  
SCHULTZ-GRUNOW  $C_f^* = \frac{0.37}{[\log_{10} (Re_x^* + 3000)]^{2.584}}$

## REYNOLDS ANALOGY FACTOR :

1. COLBURN  $\frac{2 St}{C_f} = \sigma^{-2/3}$
2. VON KARMAN  $\frac{2 St}{C_f} = \left[ 1 + 5 \sqrt{\frac{C_f^*}{2}} \left( \sigma^{*-1} + \ln \frac{5\sigma + 1}{6} \right) \right]^{-1}$

An essential element in each prediction is the value assigned to the Reynolds analogy factor. For this study the data from Wallace and McLaughlin's <sup>(1)</sup> report was examined and the results are summarized in Figure 1. The arithmetic averages of the data were between 1.0 and 1.13. These values are essentially those predicted by Von Karman's equation for the analogy factor. Colburn's equation is shown to predict too large a value. These results have been verified by a recent, more extensive survey reported by Cary <sup>(2)</sup>.

FIGURE 1  
**REYNOLDS ANALOGY FACTOR**

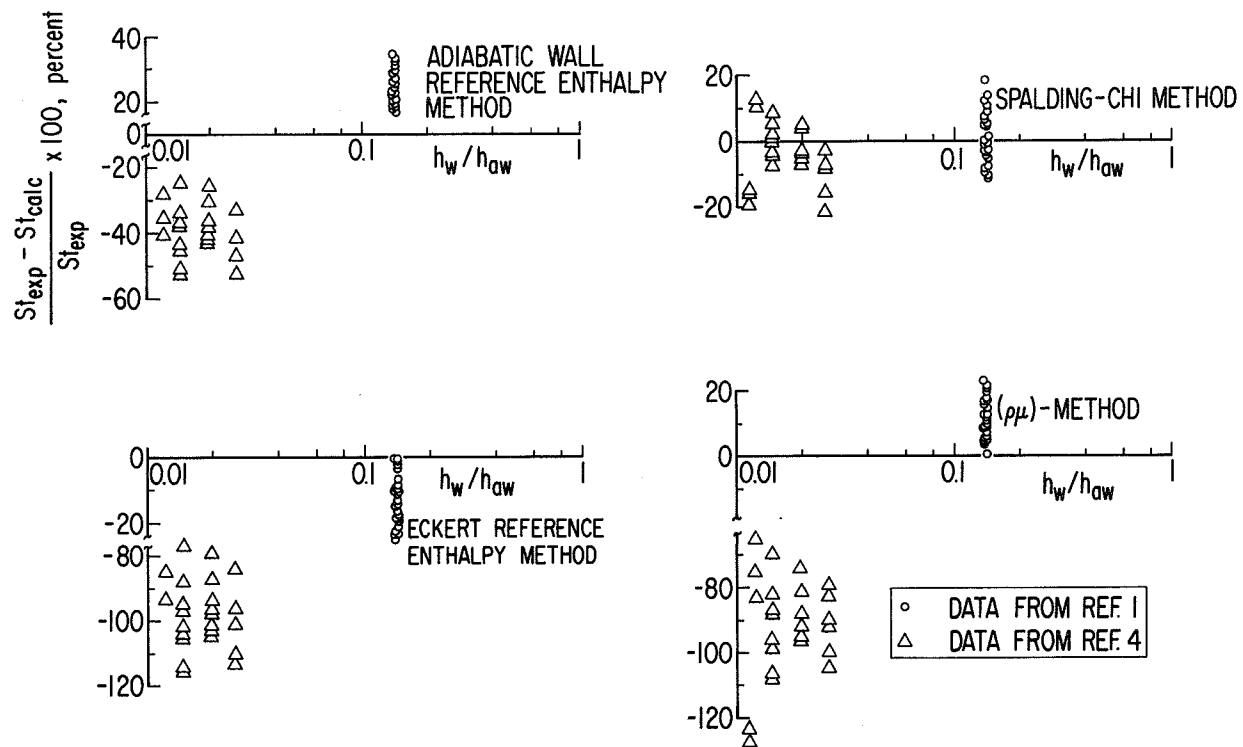


A detailed comparison between predictions from each of the four methods and experimental data for both heat transfer and skin friction has been made by Pearce (3). The results for heat transfer at the lowest wall enthalpy ratios are summarized in Figure 2. The experimental data is from the work by Wallace and McLaughlin (1) and by Hopkins and Nerem (4). The latter experiment approximates the boundary layer on a flat plate by flow in the entrance region to a hollow cylinder in a shock tube. The data are for wall enthalpy ratios even smaller than those applicable to the Space Shuttle and provide an end point to which other data at higher wall enthalpy ratios can be extrapolated.

From this comparison with a limited amount of data it is concluded that Spalding and Chi's correlation with a Reynolds analogy factor given by Karman's equation provides the most uniformly accurate specification of the heat transfer at the cold wall conditions applicable to the radiatively cooled heat shield of the Space Shuttle. In general, the predictions from this method are within  $\pm 20$  percent of the data. At these low wall enthalpy ratios, Spalding and Chi's correlation was also indicated to give the best agreement when compared with skin friction measurements (3). In addition, Von Karman's equation is indicated to be in agreement with the measurements of Reynolds' analogy factor. The combination of these two equations therefore provides a consistent prediction which is indicated to be the most accurate at the low wall enthalpy ratios.



FIGURE 2  
COMPARISON OF HEAT TRANSFER PREDICTIONS WITH EXPERIMENTS



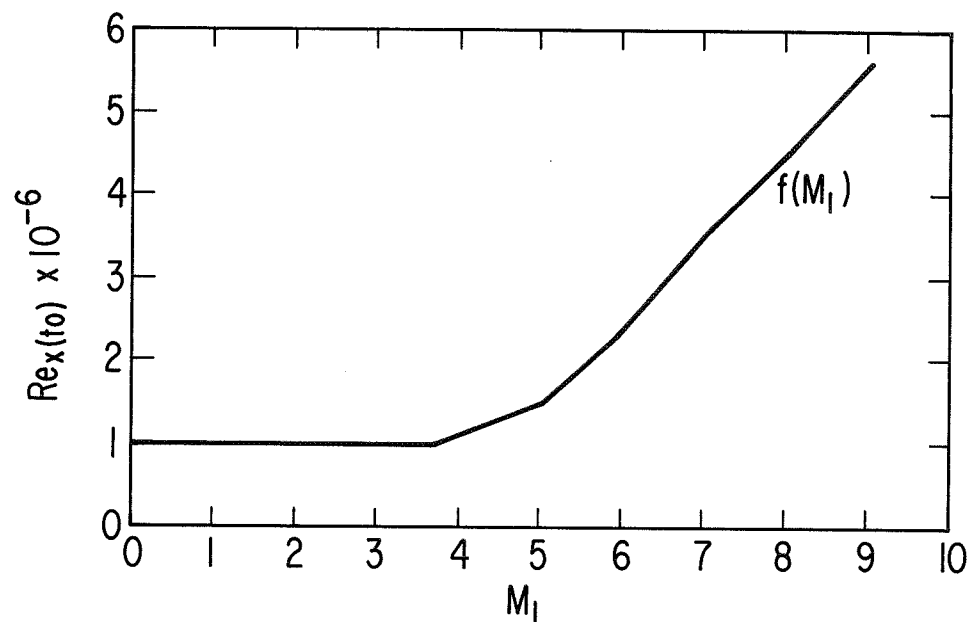
Presented here are the criteria for the onset of transition to turbulent flow. Three criteria will be examined in order to determine their importance on the heating predictions in fully turbulent flow. The first criterion is that of a fixed length Reynolds number and the second is a length Reynolds number that increases with increasing Mach number for Mach numbers greater than about 3.5. The second follows the general trend of increasing transition onset Reynolds number with increasing Mach number measured on cones and flat plates at low incidence. The third criterion is a momentum thickness Reynolds number which is specified by a constant times the local Mach number. For Mach numbers around 1 and 2, this criteria corresponds to the familiar values for the momentum thickness Reynolds number of transition onset used for blunt bodies.

The effect of these criteria on the heating during entry of a lifting vehicle will be examined by means of specific calculations for a particular configuration. This is a flat delta wing with 80-degree sweep and a planform loading of 50 lbs/ft<sup>2</sup>. A Newtonian lift coefficient is used and the trajectories are equilibrium glide. In addition, we assume that the transition is gradual, with fully turbulent flow occurring at a point where the length Reynolds number is twice that at transition onset. The effective origin of the turbulent boundary layer is taken to be at transition onset.

A small correction to the heating which accounts for cross-flow at the centerline has been added which varies from zero at small incidence to at most 13 percent at 50 degrees angle of attack. This correction approximates the transverse velocity gradient at the centerline by the stagnation point velocity gradient on an equivalent circular disk with a radius equal to the local wing semispan and placed normal to a flow with a velocity equal to the component of the free stream velocity normal to the wing. The boundary layer edge conditions are those behind a plane, oblique shock. No cross flow correction has been applied to the transition onset criteria.

The subsequent results of the calculation are given in terms of the peak radiation equilibrium temperature along the centerline of the windward surface as a function of the angle of attack. A surface emissivity of 0.85 is used for all calculations. Since these calculations are valid only for the particular set of parameters used here, the temperature differences and the indicated trends should be emphasized rather than the magnitude of the predicted temperatures.

FIGURE 3  
*BOUNDARY LAYER TRANSITION CRITERIA*

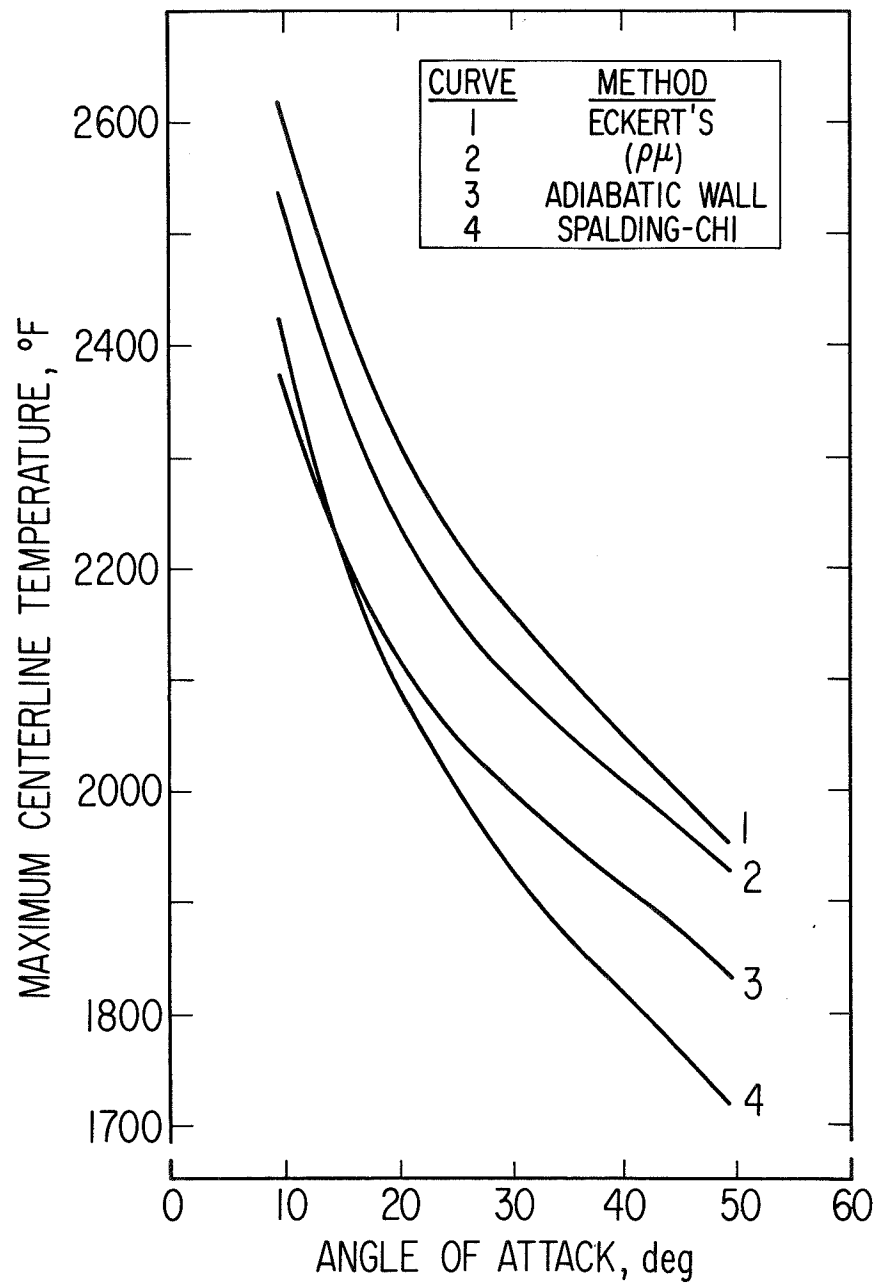


(1)  $Re_{x(t_0)} = 10^6$       (2)  $Re_{x(t_0)} = f(M_1)$       (3)  $Re_{\theta(t_0)} = 150 M_1$

In this figure and those to follow the point where the boundary layer is initially fully turbulent (point of peak turbulent heating) occurs at different positions and altitudes for different angles of attack. For the trajectory and the transition onset criteria used in this paper the location of the point of initially fully turbulent flow varied between 8 and 400 feet (transition onset between 4 and 200 feet) from the apex of the wing for angles of attack between 10 and 60 degrees. Since only heating in fully turbulent flow is considered and the lift coefficient used is independent of the vehicle length, the calculations are independent of total vehicle length. However, it is believed that the proposed vehicles will not exceed 200 feet in length and peak turbulent temperatures are therefore not shown for longer vehicles.

In this first example the results are for the criterion of a fixed onset length Reynolds number. The predominant characteristic is the strong decrease in peak temperature with increasing angle of attack. In addition, these calculations show that the predictions from the different heating methods differ by as much as 200°F between the highest and lowest. Spalding and Chi's correlation, with Von Karman's equation for the Reynolds analogy factor, which was indicated to give the best agreement with experiment, is shown to give the lowest predictions of the peak temperature for angles of attack greater than about 15 degrees.

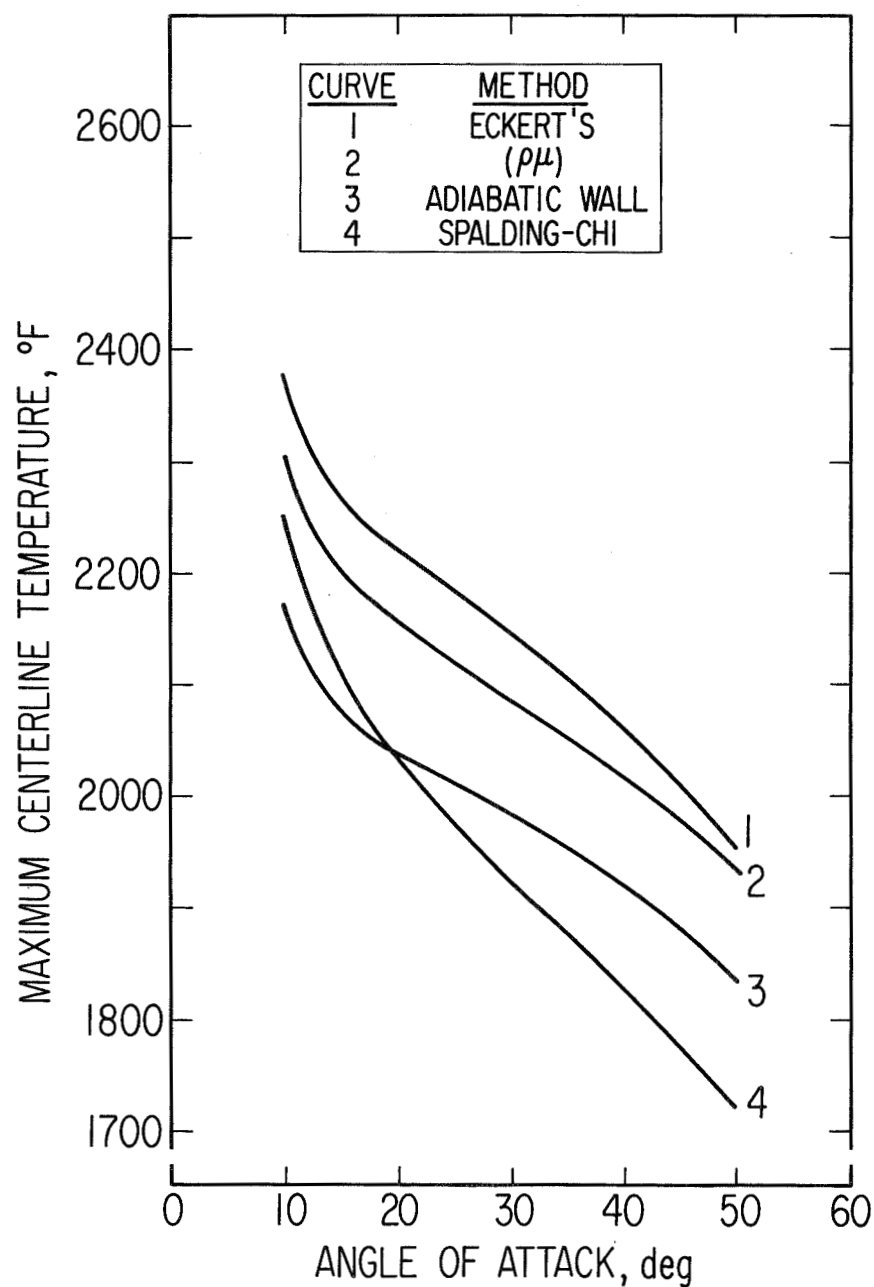
FIGURE 4  
*ONSET CRITERION:  $Re_x(t_0) = 10^6$*



In this example the onset criterion is again a length Reynolds number but in this case a delay in transition at higher Mach numbers is included. The dependence on Mach number is approximately that indicated by wind tunnel experiments on cones and flat plates at low incidence. When applied to the present problem, the transition delay is reflected in lower temperatures at the lower angles of attack. At the higher angles of attack, the transition criterion and the resulting temperature predictions coincide with those for the fixed onset length Reynolds number.

FIGURE 5

*ONSET CRITERION:  $Re_{x(t_0)} = f(M_I)$*



In contrast to the previous two criteria the onset criterion in this case is defined in terms of a momentum thickness Reynolds number. There will be a different dependence of the peak temperature on angle of attack for the reason that the momentum thickness depends on the square root of the length. In addition, the criterion is linearly dependent on the Mach number. The results for this case show a reduced dependence of the peak temperature on the angle of attack. Moreover, the criterion affects the predictions from the different heating methods by different amounts. In this case, all but Spalding and Chi's method show very little dependence of peak temperature on angle of attack beyond about 30 degrees. Also, the highest and lowest temperature predictions differ by as much as 300°F.

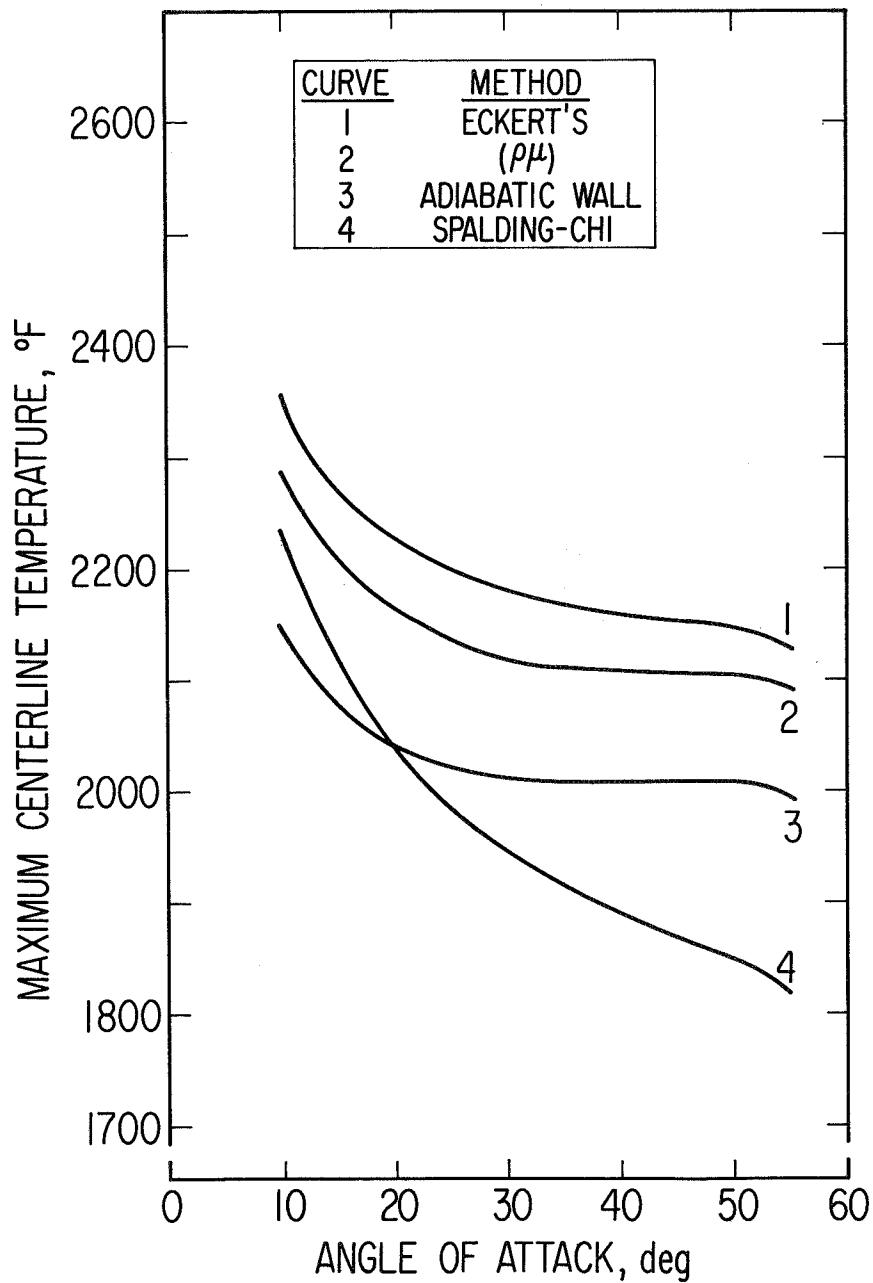
This criterion and that of the fixed length Reynolds number provide the two extremes of the transition onset criteria examined in this paper. The two give different results that lead to different conclusions concerning peak temperatures as a function of angle of attack. For a fixed length Reynolds number criterion the conclusion is that the minimum temperature occurs for the highest angle of attack for all four heating prediction methods. In contrast, for all heating predictions except Spalding and Chi's, the momentum thickness Reynolds number criterion suggests that there is only a small temperature penalty for flying at lower angles of attack, which results in an increased cross-range capability.

In addition, comparing results for the length and momentum thickness Reynolds number criteria shows that the heating predictions depend upon both the heat transfer prediction method and the onset criterion together because the different onset criterion appear to affect the heat transfer predictions by different amounts.

There are other variables which strongly affect the heating predictions but are not examined in this paper. In particular, the lift coefficient can strongly influence the peak temperature dependence on angle of attack. For example, it is possible to completely change the dependence of peak temperatures on angle of attack from a decreasing to an increasing function by using a lift coefficient that is different from that for a completely flat vehicle. Additions of ramps and surface curvature can affect the peak temperature predictions by changing both the magnitude and slope of the lift coefficient curve. Of course, these are changes in the aerodynamics of the vehicle and do not affect transition or the heating predictions when considered independently. They do strongly affect the final prediction of the heating through their influence on the trajectory.



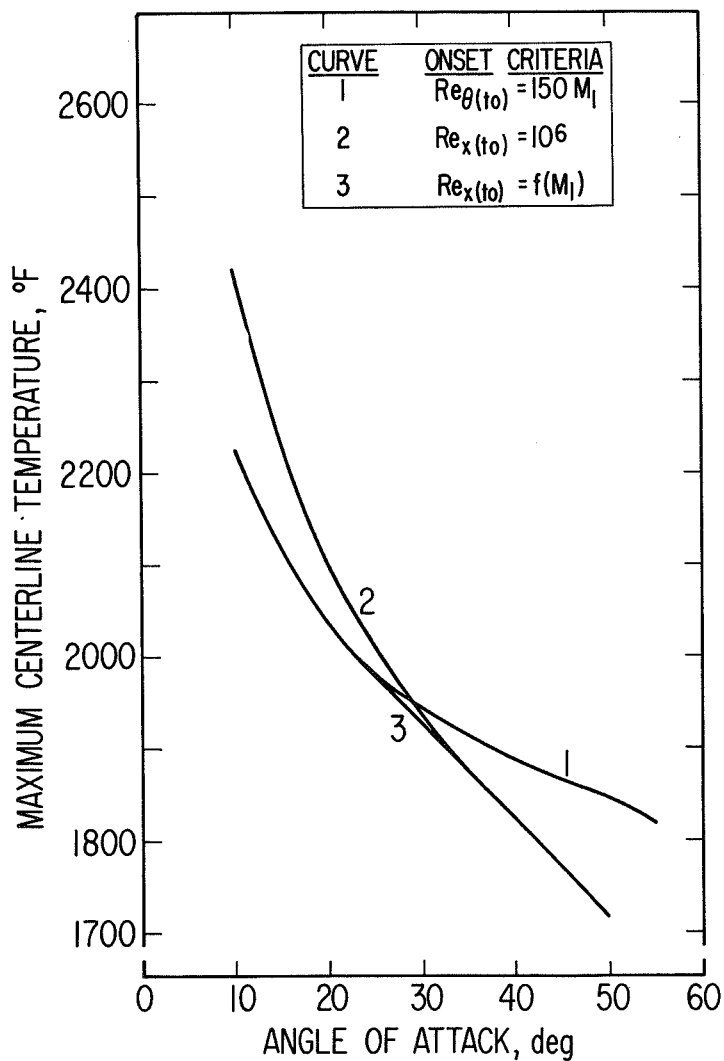
FIGURE 6  
*ONSET CRITERION:  $Re_{\theta(t_0)} = 150 M_1$*



In order to emphasize the predictions from the heating method which is indicated to be the most accurate, the maximum centerline temperatures for each of the three transition onset criteria are summarized in this figure for Spalding and Chi's correlation. The summary also points out the fact that Spalding and Chi's correlation predicts heating which is less sensitive to the particular onset criterion than the other three heat transfer prediction methods.

The sensitivity of the heat transfer predictions from each of the four methods to the transition criteria is determined by the different skin friction laws and, more importantly, by the different  $F_R$  factors, which multiply the Reynolds number in the real flow to obtain the Reynolds number in the equivalent, incompressible flow. For the present set of calculations the  $F_R$  factor for Spalding and Chi's correlation was found to vary in such a manner that it partially offsets the differences in transition Reynolds number predicted by the three onset criteria. This effect was also found in the other three prediction methods, but to a lesser extent. In addition, the Prandtl equation, used with the Eckert and adiabatic wall reference enthalpy methods, and the modified Schultz-Grunow equation used with the  $(\rho\mu)$ -method, are more strongly dependent on Reynolds number than is Spalding and Chi's correlation. The net result is that the predictions from Spalding and Chi's correlation are less sensitive to the transition onset criteria.

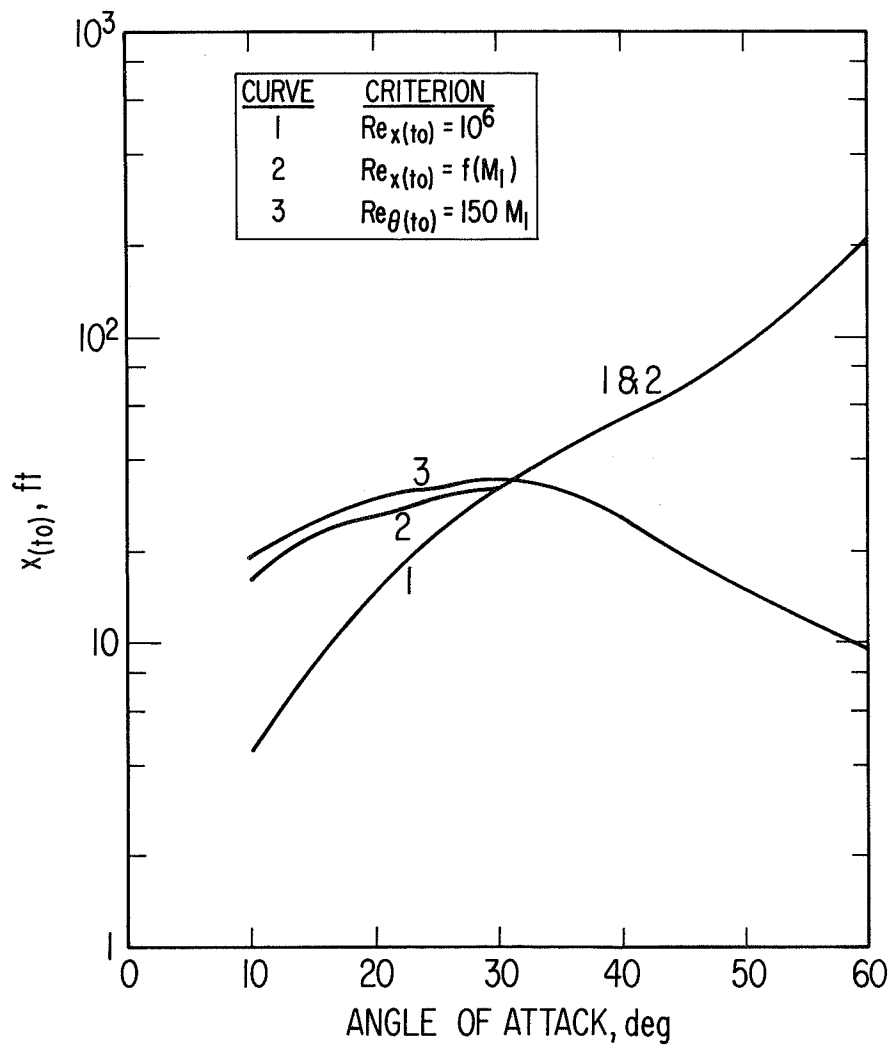
FIGURE 7  
 MAXIMUM CENTERLINE TEMPERATURE FOR ALL ONSET  
 CRITERIA WITH SPALDING AND CHI'S CORRELATION



The location of transition onset affects the magnitude of the heating in fully turbulent flow and also determines where fully turbulent flow will occur on the vehicle. Locations of transition onset are summarized in this figure for the three criteria and indicate widely different results. The differences are due essentially to the different Mach number dependences and to the square root dependence of the momentum thickness on the length.

Although the heating in fully turbulent flow has been shown to be not strongly sensitive to the transition criterion for Spalding and Chi's correlation, the different onset lengths do suggest an important effect of the transition criteria. For short vehicles, say near 100 feet, the momentum thickness Reynolds number criterion predicts that the point where the boundary layer is fully turbulent will occur on the vehicle for any angle of attack. In contrast, the rapid increase in onset length with increasing angle of attack predicted by the length Reynolds number criteria implies that fully turbulent flow will not occur on the short vehicles at the higher angles of attack and peak heating will therefore occur where the boundary layer is transitional, or even laminar.

FIGURE 8  
*TRANSITION ONSET LENGTH*



## CONCLUSIONS

The various heating prediction methods used in preliminary analyses of the Space Shuttle orbital vehicle have been compared with a limited amount of experimental data obtained at test conditions that approximately match the Mach number and wall enthalpy ratios expected for the windward surface of a radiatively cooled heat shield. The conclusion is that Spalding and Chi's correlation with real gas properties and Von Karman's equation for the Reynolds analogy factor gives the most uniformly accurate estimates of the heating in compressible, turbulent flow on a flat plate in a uniform stream.

Specific calculations for a flat delta wing and an equilibrium glide trajectory show that for a particular onset criterion the predictions of the peak temperature in fully turbulent flow along the windward centerline can differ by as much as 300°F among the four heat transfer prediction methods. When both the heat transfer prediction method and onset criteria are varied, the difference can be as great as 450°F.

It is suggested by these calculations that the peak temperature predictions from Spalding and Chi's correlation are less sensitive to the choice of transition onset criteria than the other three heating estimation methods.

The widely different transition onset lengths predicted by the three onset criteria used in the calculations imply that the choice of onset criteria becomes more important as the vehicle length is decreased.

#### REFERENCES FOR HEAT TRANSFER PREDICTION METHODS

1. Eckert, E. R. G., "Survey on Heat Transfer at High Speeds", WADC Technical Report 54-70 (1954)
2. Quinn, R. D., and M. Politz, "Comparison of Measured and Calculated Turbulent Heat Transfer on the X-15 Airplane at Angles of Attack to  $19^{\circ}$ ", NASA TM X-1291 (Confidential).
3. Savage, R. T., and C. L. Jaek, "Investigation of Turbulent Heat Transfer at Hypersonic Speeds", AFFDL-TR-67-144 Vol. 1 (1967).
4. Spalding, D. B., and S. W. Chi, "The Drag of a Compressible Turbulent Boundary Layer on a Smooth Flat Plate with and without Heat Transfer", J. Fluid Mechanics 18 (1) pp. 117-143 (1964)

#### GENERAL REFERENCES

1. Wallace, J. E., and E. J. McLaughlin, "Experimental Investigation of Hypersonic Turbulent Flow and Laminar, See-Side Flow on Flat Plates", AFFDL-TR-66-63, Vol. 1 (1966).
2. Cary, A. M. Jr., "Summary of Available Information on Reynolds Analogy for Zero-Pressure-Gradient, Compressible, Turbulent Boundary Layer Flow", NASA TN D-5560 (1970).
3. Pearce, B. E., "A Comparison of Four Simple Calculation Methods for the Compressible Turbulent Boundary Layer on a Flat Plate", Aerospace Corp. Report No. TOR-0066(5758-02)-3 (1970).
4. Hopkins, R. A., and R. M. Nerem, "An Experimental Investigation of Heat Transfer from a Highly Cooled Turbulent Boundary Layer", AIAA Journal 6 (10) pp. 1912-1918 (1968).





ENTRY MANEUVER/AEROTHERMODYNAMIC INTERACTIONS FOR HIGH CROSS-RANGE  
CANDIDATE ORBITERS

James P. Arrington  
NASA Langley Research Center  
Hampton, Virginia

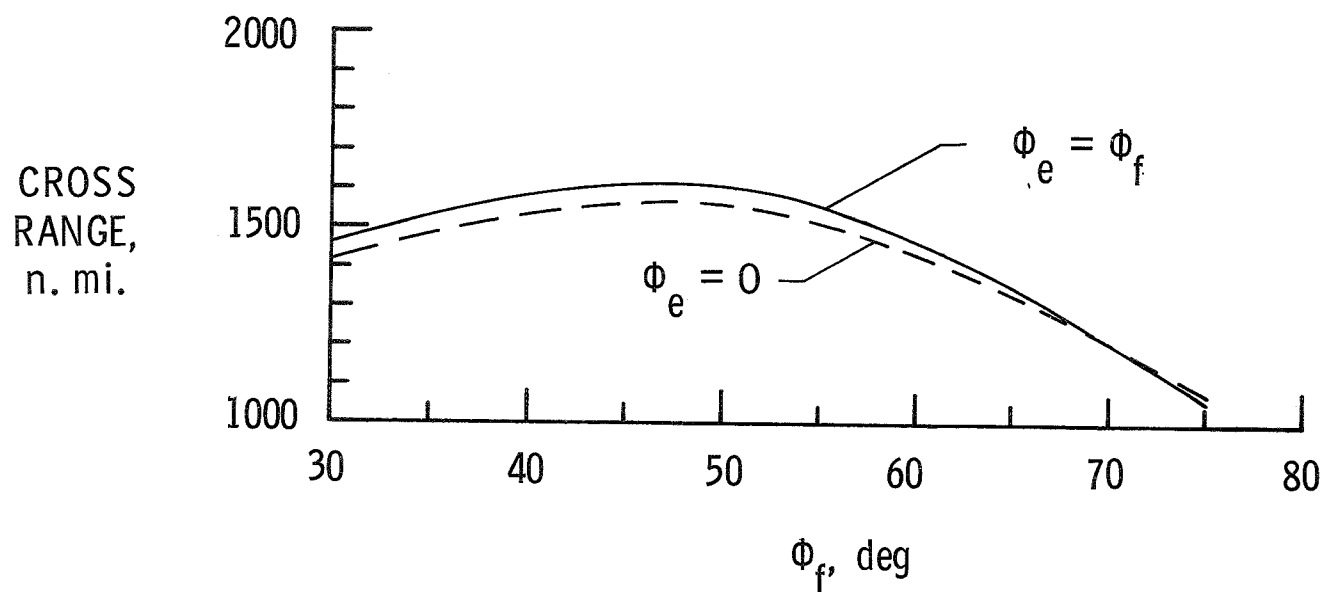
INTRODUCTION

One of several contractor proposals for high cross-range space-shuttle orbiters included an entry mode with pitch modulation. The vehicle attitude was held near  $C_{L,max}$  ( $45^\circ$  angle of attack) from entry down to a Mach number of about 20. At this point, a pitch modulation maneuver was initiated to provide the desired cross range; the pitch maneuver down to  $(L/D)_{max}$  was completed at low hypersonic Mach numbers. An alternate entry mode approach with the orbiter flying at a constant angle of attack can also be utilized to achieve the required cross range. This paper compares the entry heating environment and bottom surface temperature distributions for the constant attitude and variable angle-of-attack entry modes. Hypersonic performance capabilities of  $(L/D)_{max} = 2.0$  and  $2.4$  at reference conditions of Mach 20 at 200,000-feet altitude are assumed. The relaxation in heating environment due to initially operating a high cross-range orbiter as a low cross-range vehicle is also examined. The results of an experimental  $M=10$  laminar heat study provide the basis for the prediction of the maximum equilibrium temperatures expected over the lower surface of the vehicle.

Effect of bank angle on cross range for constant altitude entry maneuver. Atmospheric cross range was achieved by a nominal constant altitude maneuver (bank modulation) with a fixed bank angle from entry to pullout, followed by flight at a fixed bank angle after the constant altitude hold to a heading angle change of  $90^\circ$ . At that point the bank angle was reduced to zero and normal fixed attitude glide flight was initiated. The effect of the initial bank angle at entry,  $\phi_e$ , and the final bank angle after pullout,  $\phi_f$ , on cross range is shown for a fixed attitude mode ( $\alpha = 28^\circ$ ) in figure 1. For the 1500 n. mi. cross-range cases, having the initial and final bank angles the same results in about a 50 n. mi. increase in cross range. The desired cross range of 1500 n. mi. can be reached by selecting the four following bank-angle combinations:  $\phi_e = 0$  and  $\phi_f = 36.5$ ;  $\phi_e = 0$  and  $\phi_f = 56^\circ$ ;  $\phi_e = \phi_f = 33^\circ$ ; and  $\phi_e = \phi_f = 58^\circ$ .

# EFFECT OF BANK ANGLE ON CROSS RANGE FOR CONSTANT ALTITUDE ENTRY MANEUVER

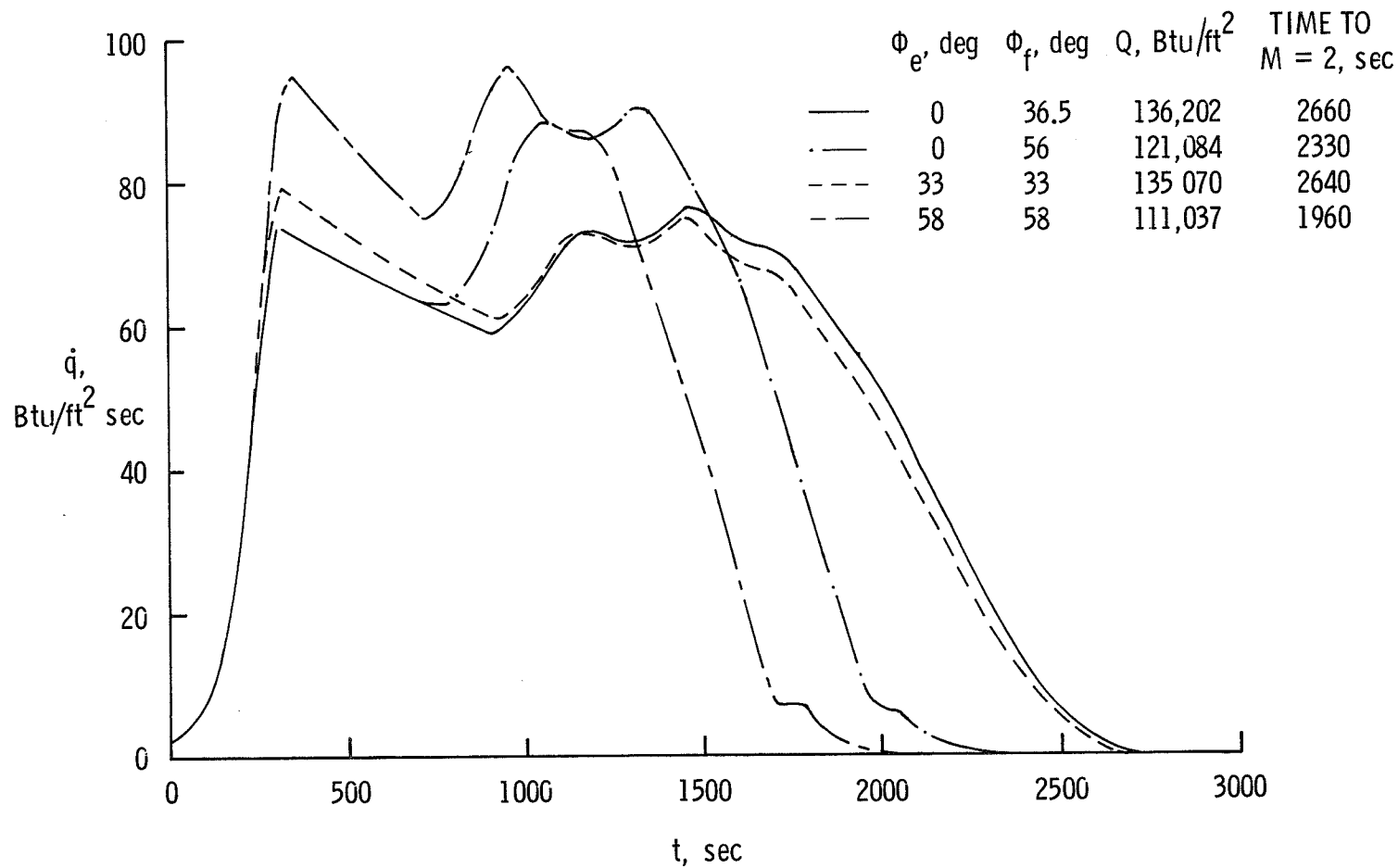
$$\gamma_e = -1.32, L/D = 1.62, W/c_D S = 137 \text{ psf}$$



Stagnation heating rate-time histories for 1500 n. mi. cross range. The stagnation heating rate referenced to a 1-foot radius sphere for the fixed attitude case,  $\alpha = 28^\circ$ , is shown in figure 2 to be dependent upon the magnitude of the bank angle. The lower bank-angle cases resulted in similar heating rate-time histories and remained essentially independent of the initial bank angle. Although the higher bank-angle cases had higher heating rates that were dependent upon the initial bank angle, the total heat load and soak times were less than for the lower bank-angle cases. For the remainder of the study, a compromise bank-angle selection of  $\phi_e = \phi_f = 45^\circ$  was used.

# STAGNATION HEATING RATE-TIME HISTORIES FOR 1500 n. mi. CROSS RANGE

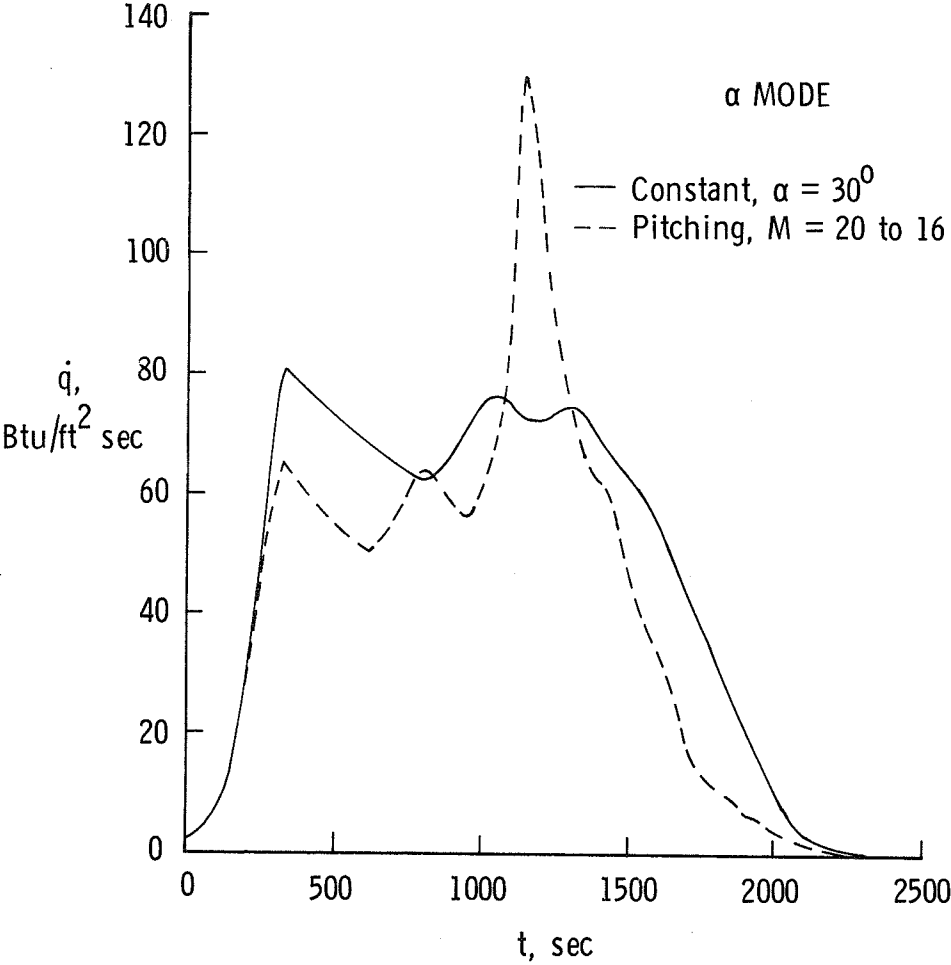
$\gamma_e = -1.32^\circ$ ,  $L/D = 1.62$ ,  $W/C_D S = 137$  psf, 1 ft RAD. SPHERE



Stagnation heating rate-time histories for 1500 n. mi. cross range. The stagnation heating rate-time histories are compared for a moderate performance vehicle ( $L/D_{\max} = 2$  at  $M = 20$ ) operating either at a constant angle of attack or with a pitch modulated entry mode. For the fixed attitude case, the angle of attack is that required to generate the 1500 n. mi. cross range ( $\alpha \approx 30^\circ$ ) with  $\phi_e = \phi_f = 45^\circ$ . For the pitch modulated case, since the pitch modulation was initiated at  $M = 20$ , the modulation to  $(L/D)_{\max}$  must be conducted rather rapidly in order to obtain the desired cross range. The resulting rapid decrease in lift coefficient caused a steep plunge with corresponding increases in the peak stagnation heating rate of better than 60 percent compared to that for the fixed attitude mode. However, the total heat load and the soak time were greater for the fixed attitude case.

STAGNATION HEATING RATE-TIME HISTORIES FOR 1500 n. mi. CROSS RANGE

$(L/D)_{\max} = 2$  AT  $M = 20$ ,  $W/S = 37$  psf, 1 Ft RAD. SPHERE



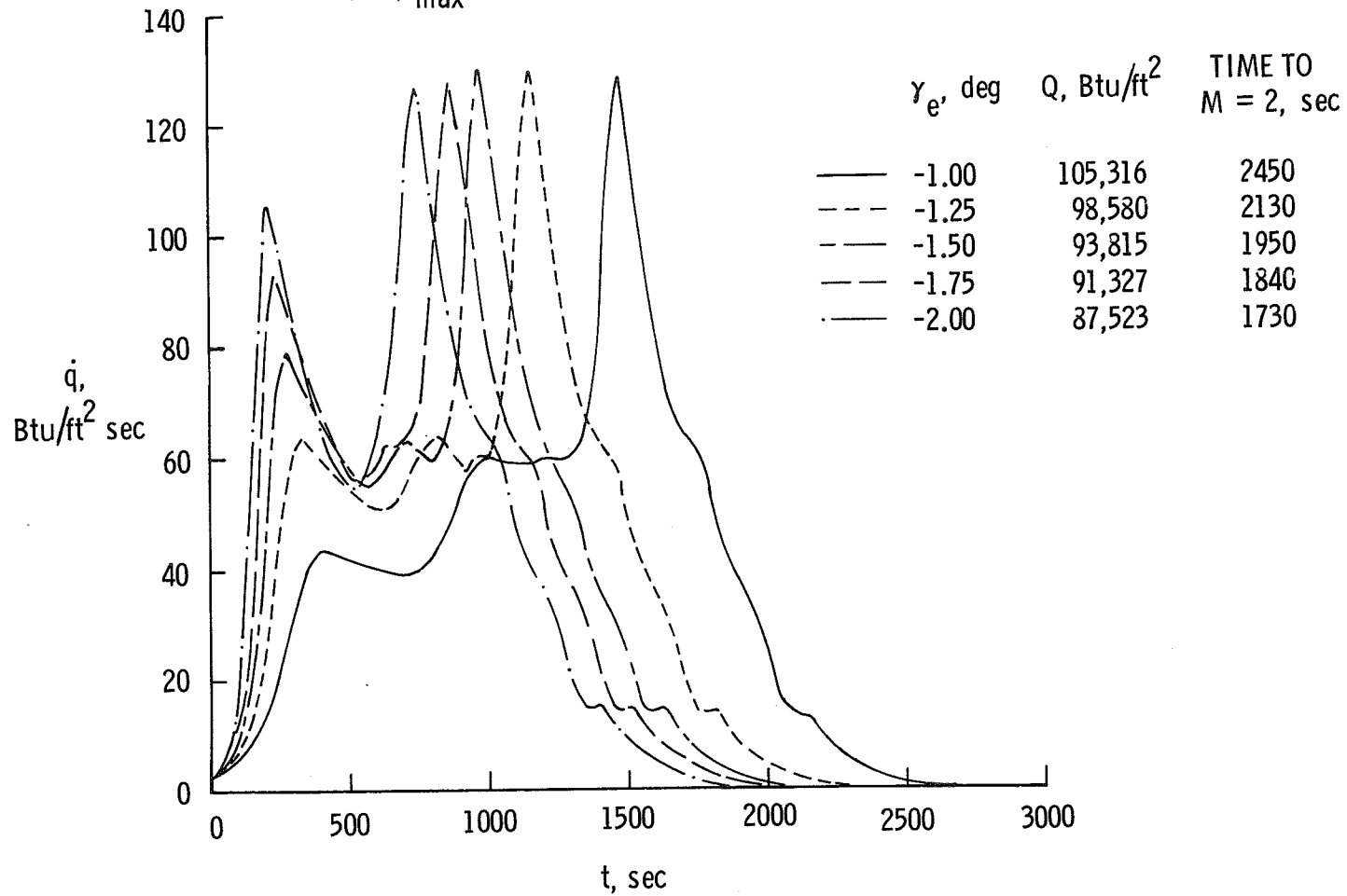
$\alpha$ MODE	$\gamma_e$ , deg	$Q$ , Btu/ft <sup>2</sup>	TIME TO $M = 2$ , sec
— Constant, $\alpha = 30^\circ$	-1.32	112,450	2230
-- Pitching, $M = 20$ to 16	-1.27	98,124	2110

Stagnation heating rate-time histories for 1500 n. mi. cross range with pitch modulation,  $M = 20$  to  $M = 16$ . An analysis of the influence of entry angle on the peak heating rate for the pitch modulated entry mode was conducted. Although the first peak heating rate varies strongly as a function of entry angle, the second peak (occurring near the end of the pitch-modulation maneuver at  $M \approx 16$ ) is shown to be insensitive to entry angle for the range of  $-1^\circ$  to  $-2^\circ$ . Therefore, steeper entry angles can be used to reduce total heat load and soak time with no penalty in peak surface temperature. However, a trade-off analysis of the resulting savings in thermal insulation weight versus the penalty in deorbit propellant requirements must be conducted.



STAGNATION HEATING RATE-TIME HISTORIES FOR 1500 n. mi. CROSS RANGE  
WITH PITCH MODULATION,  $M = 2.0$  TO  $M = 16$

$(L/D)_{\max} = 2$  AT  $M = 20$ ,  $W/S = 37$  psf, 1 ft RAD. SPHERE

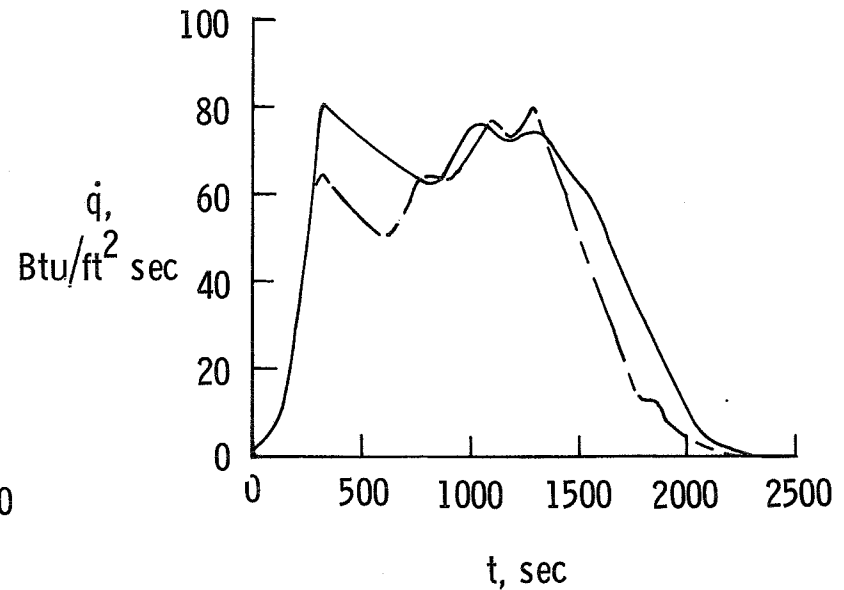
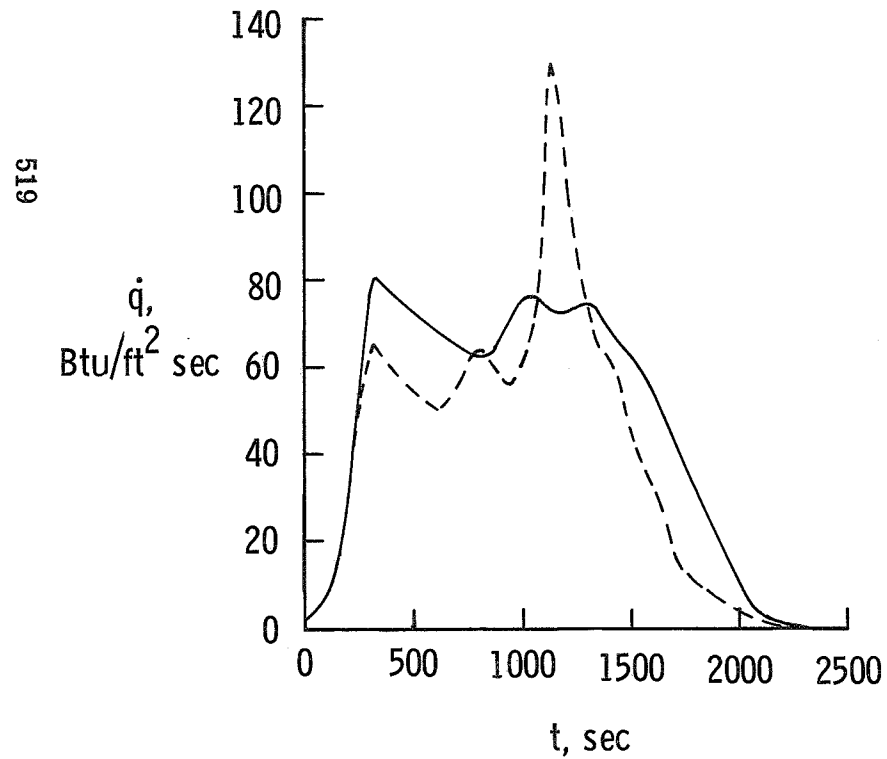


Stagnation heating rate-time histories for 1500 n. mi. cross range. Two pitch modulation entries, one occurring over a longer time than the other, are compared with the constant attitude mode to determine the effects on entry heating. By initiating the pitch modulation earlier in the entry at  $M = 24$ , the 1500 n. mi. cross-range objective can be reached by modulating the pitch over a longer time period resulting in a decrease in the maximum heating rate. In addition, the total heat load is less with about the same soak times compared with the pitch modulation from  $M = 20$  to  $M = 16$  and the constant attitude ( $\alpha \approx 30^\circ$ ) cases. Potential disadvantages may result, however, from varying temperature distributions associated with pitch modulation. Also, the influence of pitch modulation on boundary-layer transition must be determined.

# STAGNATION HEATING RATE-TIME HISTORIES FOR 1500 n. mi. CROSS RANGE

L/D = 2 AT M = 20, W/S = 37 psf, 1 ft RAD. SPHERE

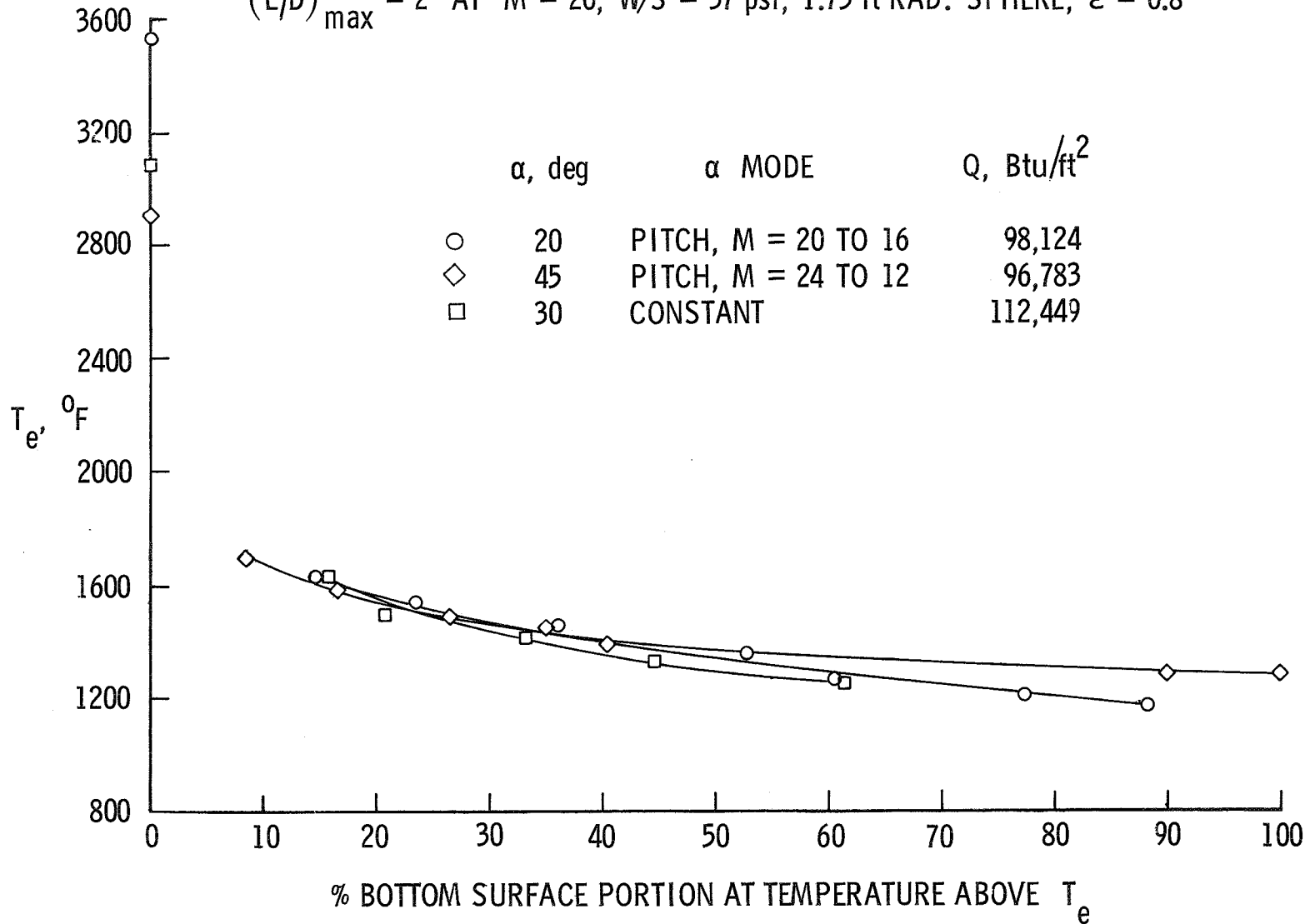
	$\alpha$ MODE	$\gamma_e$ , deg	Q, Btu/ft <sup>2</sup>	TIME TO M = 2, sec
—	CONST 30°	-1.32	112,450	2230
- - -	PITCH, M = 20 TO 16	-1.27	98,124	2110
- · -	PITCH, M = 24 TO 12	-1.27	96,783	2150



Maximum equilibrium temperature for 1500 n. mi. cross range. The maximum stagnation heating rates for the constant attitude and pitch modulated entry modes have been applied to the results of a  $M = 10$  laminar-flow heat study to obtain the maximum radiation equilibrium temperatures expected over the lower surface of a delta wing orbiter. A nose radius of 1.75 feet and an emissivity of 0.8 have been assumed. The figure shows the lowest value of the maximum temperature expected for a portion of the lower surface. For example, at least 20 percent of the bottom surface will have a maximum radiation equilibrium skin temperature of  $1600^{\circ}$  F. Except for the stagnation region, where no data were taken, the temperature levels are within the currently available thermal protection technology. It is of interest to note that for over 90 percent of the lower surface the differences in the temperatures are insignificant regardless of the entry mode.

# MAXIMUM EQUILIBRIUM TEMPERATURE FOR 1500 n. mi. CROSS RANGE

$(L/D)_{\max} = 2$  AT  $M = 20$ ,  $W/S = 37$  psf, 1.75 ft RAD. SPHERE,  $\epsilon = 0.8$

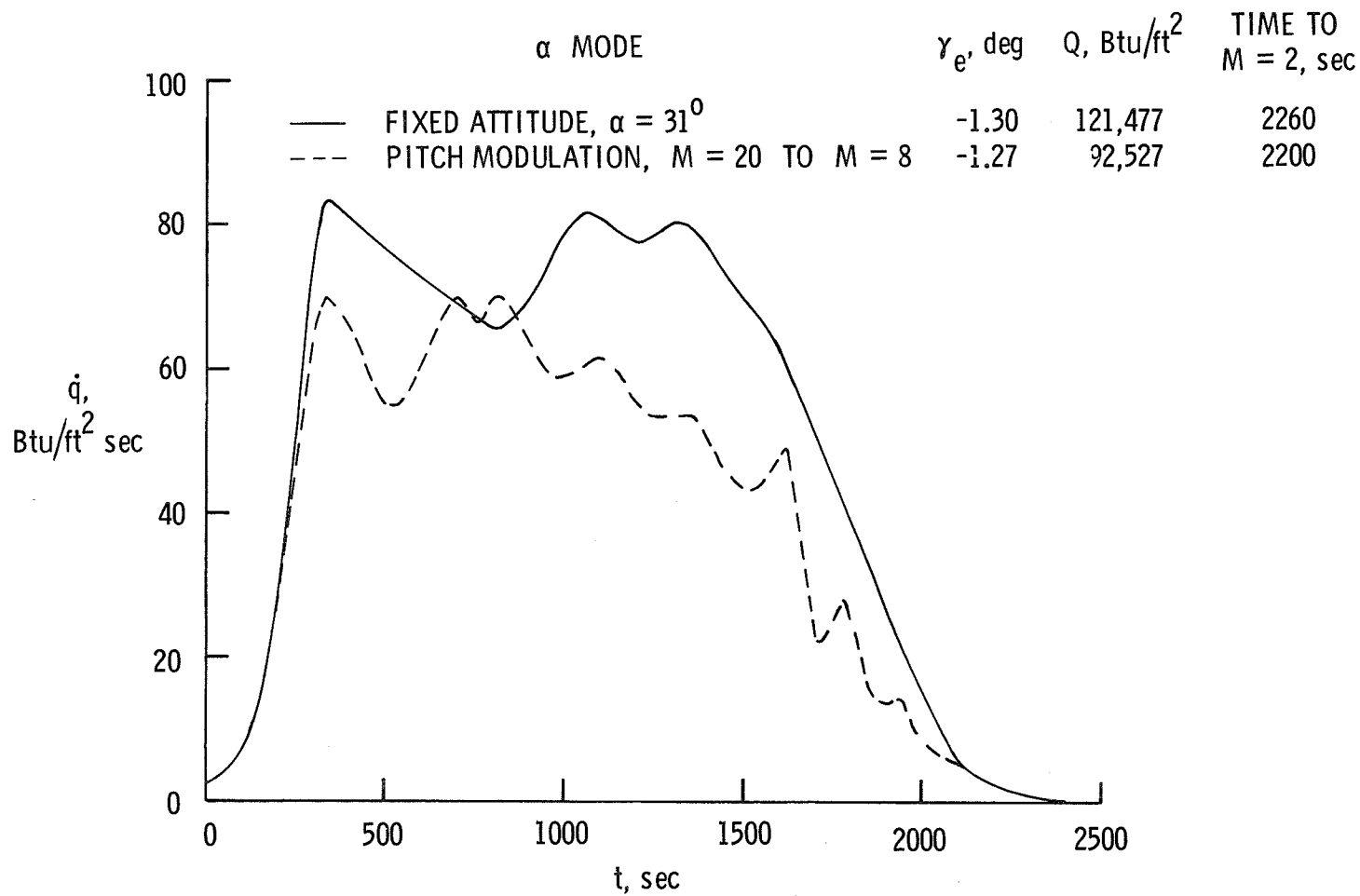


Stagnation heating rate-time histories for 1500 n. mi. cross range. A higher performance vehicle could accomplish the cross-range requirement with a more gradual pitch modulation beginning at  $M = 20$ . To illustrate the effects of such higher performance, figures 7 and 8 compare fixed attitude entry with pitch modulated entry for an orbiter with  $(L/D)_{\max} = 2.4$  at the reference conditions of  $M = 20$  and 200,000 feet altitude. In order to obtain 1500 n. mi. cross range, the modulation occurs over a Mach number range of 20-8 as compared with 20-16 for the previous lower performance vehicle.

The pitch modulation from  $M = 20$  to 8 resulted in lower stagnation heating rates, lower total heat load, and equivalent soak times compared with the fixed attitude case ( $\alpha = 31^\circ$ ). A comparison of the pitch modulation results of figure 5 for the  $(L/D)_{\max} = 2$  orbiter with figure 7 indicates that the lower performance orbiter is competitive for the 1500 n. mi. cross-range constraint if the pitch modulation is initiated early in the flight.

# STAGNATION HEATING RATE-TIME HISTORIES FOR 1500 n. mi. CROSS RANGE

$(L/D)_{max} = 2.4$  AT  $M = 20$ ,  $W/S = 37$  psf, 1 ft RAD. SPHERE

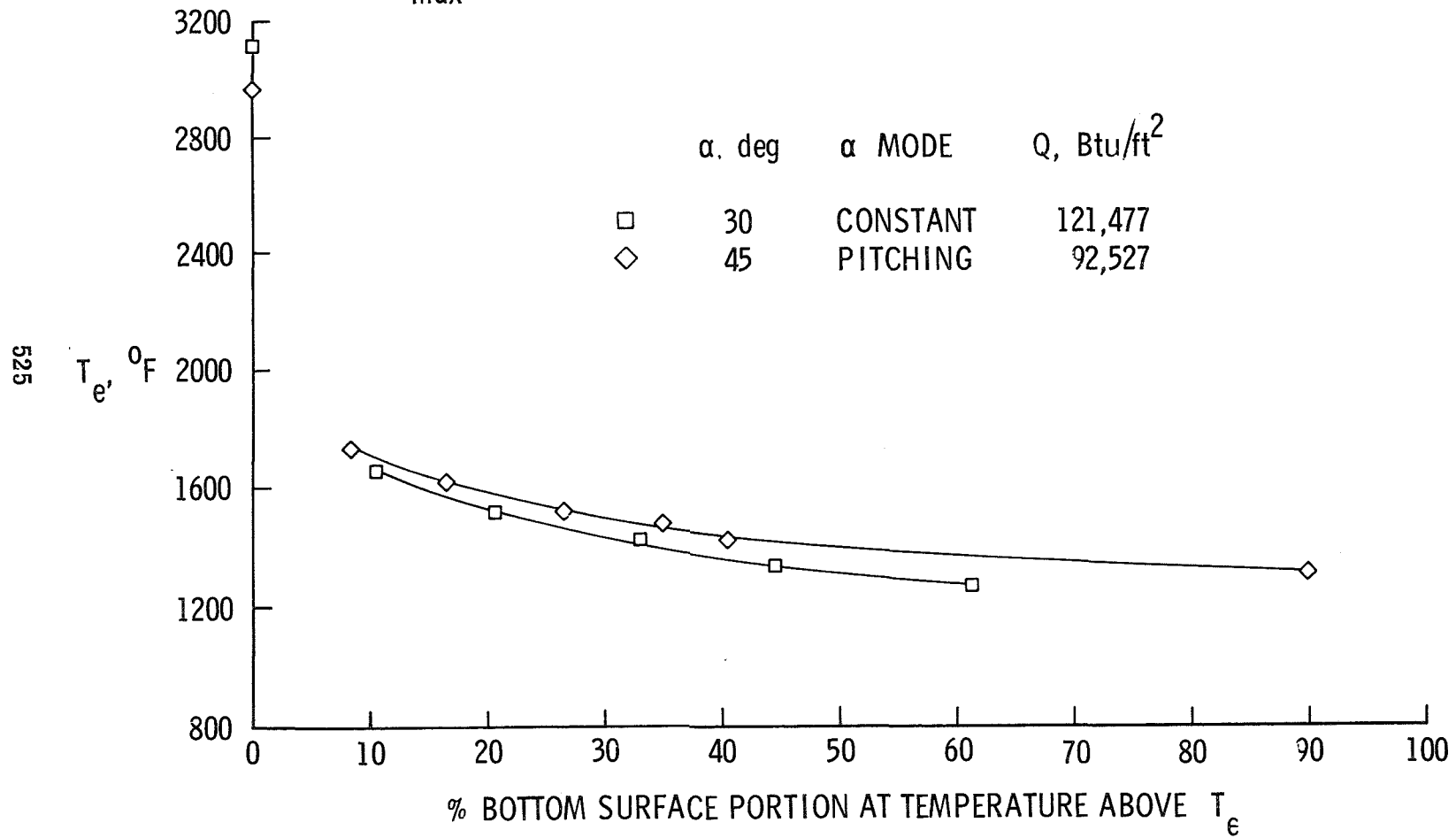


Maximum equilibrium temperature for 1500 n. mi. cross range. The results of the  $M = 10$  experimental heating study discussed earlier were applied to the constant attitude and pitch modulated entry modes to obtain the maximum radiation equilibrium temperatures over the lower surface of the  $(L/D)_{\max} = 2.4$  vehicle with a 1.75-foot nose radius. The maximum temperatures shown in figure 8 are similar to the values for the  $(L/D)_{\max} = 2$  orbiter.



# MAXIMUM EQUILIBRIUM TEMPERATURE FOR 1500 n. mi. CROSS RANGE

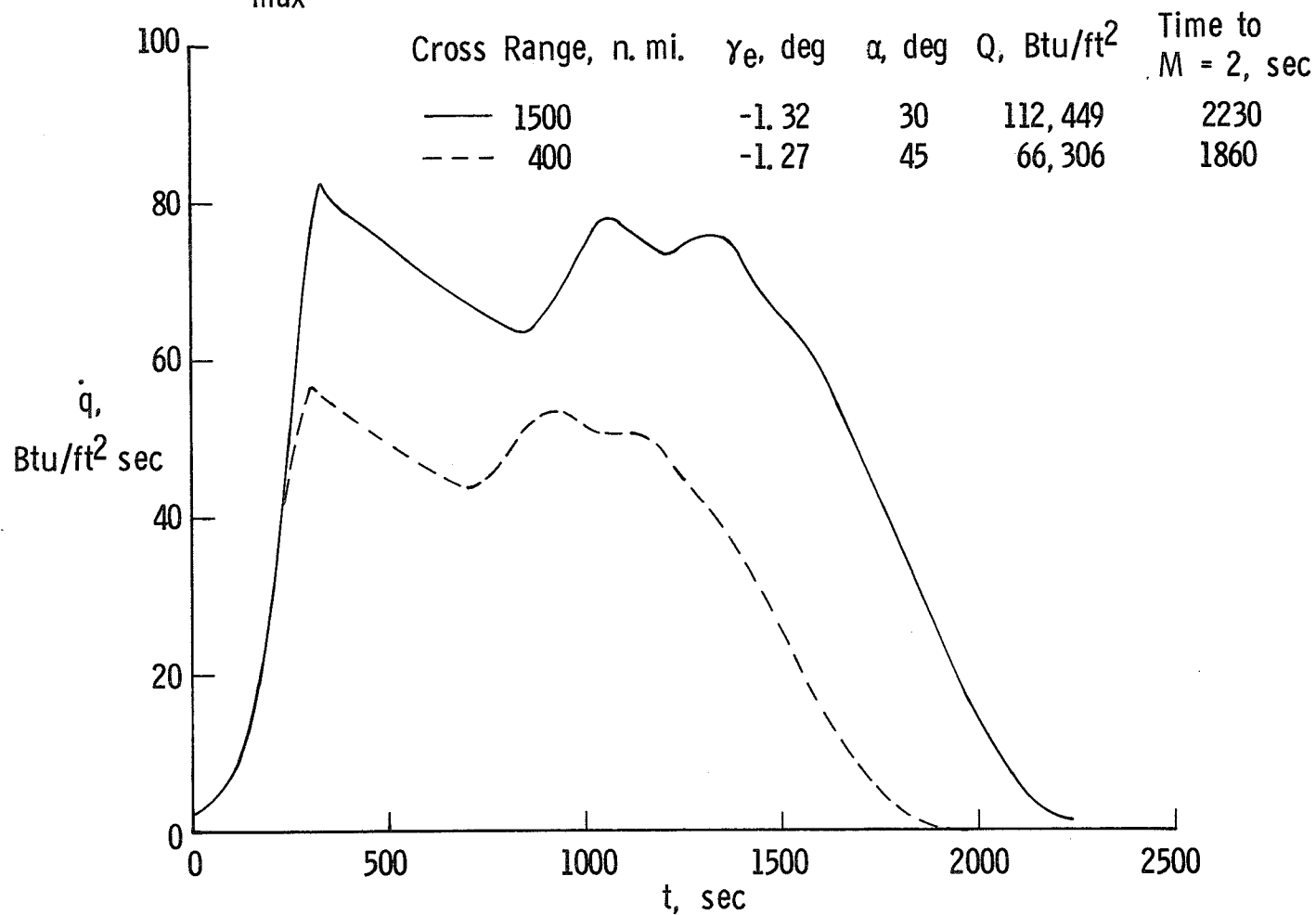
$(L/d)_{\max} = 2.4$  AT  $M = 20$ ,  $W/S = 37$  psf, 1.75 ft RAD. SPHERE,  $\epsilon = 0.8$



Stagnation heating rate-time histories for high and low cross range. Initially operating an orbiter with an atmospheric maneuvering cross-range potential of 1500 n. mi. ( $L/D = 2$  at  $M = 20$ ) as a low cross-range vehicle (400 n. mi.) reduced the stagnation heating rate by about 25 percent for constant attitude entry modes. In addition, the total heat load and the soak time were reduced by 41 percent and 17 percent, respectively.

# STAGNATION HEATING RATE-TIME HISTORIES FOR HIGH AND LOW CROSS RANGE

$(L/D)_{\max} = 2$  AT  $M = 20$ ,  $W/S = 37$  psf, 1 ft RAD. SPHERE

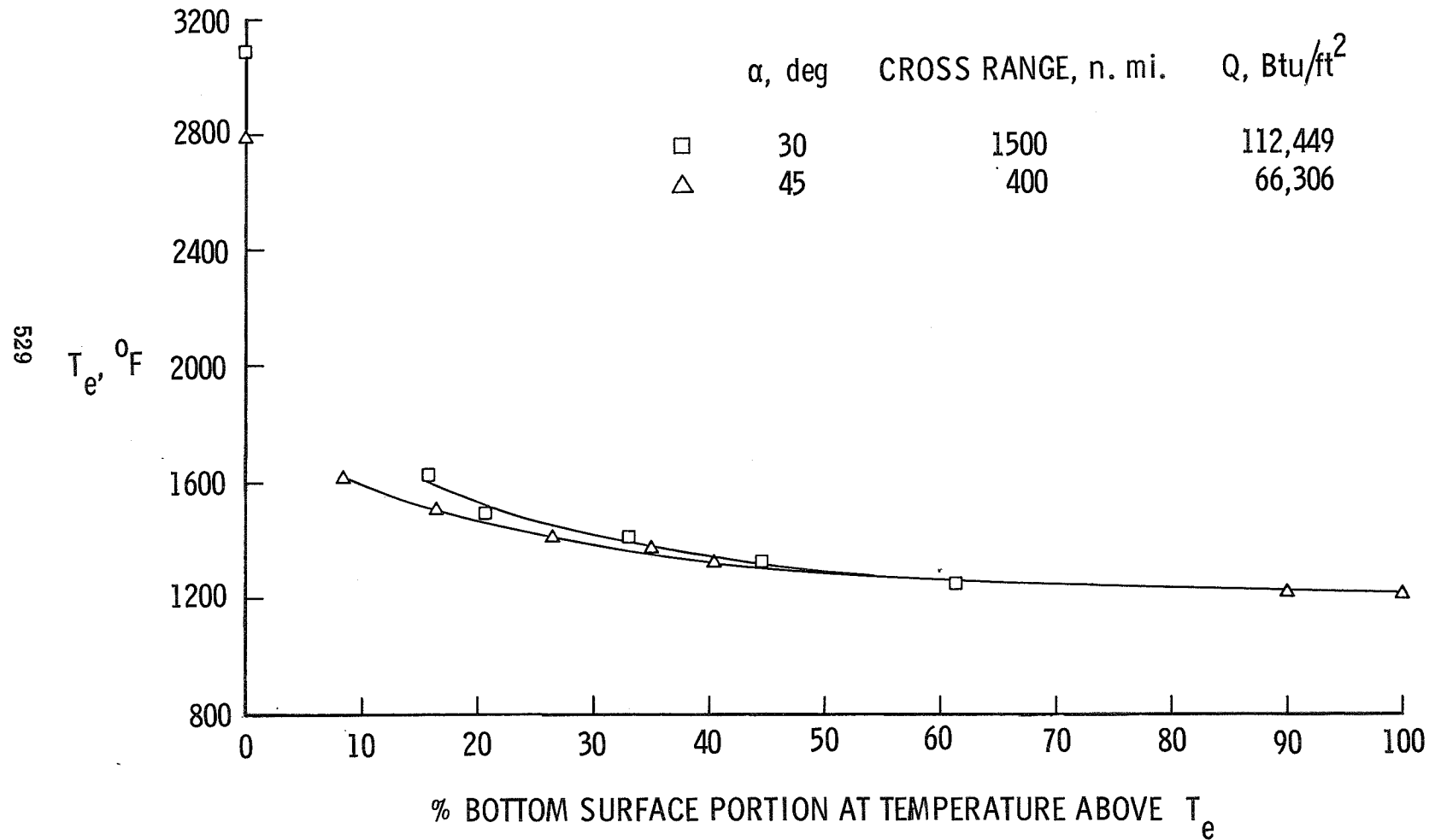


Maximum equilibrium temperature for high and low cross range. The maximum radiation equilibrium temperature for the  $(L/D)_{\max} = 2$  vehicle operating in a 1500 n. mi. cross-range mode ( $\alpha = 30^\circ$ ) and in a 400 n. mi. cross-range mode ( $\alpha = 45^\circ$ ) shown in figure 8 were obtained by applying the Mach 10 heating results discussed previously. As before, the temperatures are based on a vehicle with a 1.75-foot nose radius and an emissivity of 0.8.

Except for the stagnation region where the difference was on the order of  $300^\circ$  F, there was little effect on the lower surface maximum radiation equilibrium temperatures due to the cross-range selection. Therefore, the payload penalty associated with cross-range potential can be estimated with reasonable accuracy by a relatively simple analysis of thermal insulation requirements.

# MAXIMUM EQUILIBRIUM TEMPERATURE FOR HIGH AND LOW CROSS RANGE

$(L/D)_{\max} = 2$  AT  $M = 20$ ,  $W/S = 37$  psf, 1.75 ft RAD. SPHERE,  $\epsilon = 0.8$



#### CONCLUDING REMARKS

An analysis of constant attitude and pitch modulated entry modes has been conducted for space shuttle orbiters capable of 1500 n. mi. cross range. Significant reductions in total heat load and peak heating rates with minor decreases in soak times were demonstrated for the pitch modulated entry mode. For the  $(L/D)_{\max} = 2$  orbiter, a large increase in stagnation heating rate was avoided by initiating the pitch modulation earlier during entry. However, the angle-of-attack mode had very little effect on the maximum radiation equilibrium temperatures over 90 percent of the lower surface of a typical vehicle indicating some flexibility in the choice of entry mode.

By initially operating an orbiter designed for a cross range of 1500 n. mi.  $\left((L/D)_{\max} = 2\right)$  as a low cross-range vehicle, the stagnation heating rate can be reduced by 25 percent, the total heat load by 41 percent, and the soak time by 17 percent. However, except for the stagnation region where the difference was on the order of  $300^{\circ}$  F, there was also little effect on the lower surface maximum radiation equilibrium temperatures due to the cross range. Therefore, the basic difference between high and low cross-range operations of an orbiter with high cross-range potential is the weight of the thermal insulation material required.

The influence of vehicle attitude on boundary-layer transition and the resulting turbulent heating levels should be evaluated prior to the selection of a nominal entry mode.

A MINIMUM HEATING FLIGHT MODE FOR HIGH LATERAL RANGE SPACE  
SHUTTLE ENTRIES INCLUDING THE EFFECTS OF TRANSITION

Jack D. Moote

North American Rockwell  
Downey, California

INTRODUCTION

The Space Shuttle Program requirements for economy and reusability present many problems in the analysis, design, manufacturing, and operations areas. Not the least of these is the definition and production of an entry thermal protection system (TPS). Unlike Apollo and other currently operational entry vehicles, the space shuttle orbiter entry flight profile must be close to the optimum, in terms of the heating environment, if the system is to be producible within the specified time frame. This presentation is directed toward the entry flight profile optimization portion of the overall TPS design and analysis effort.

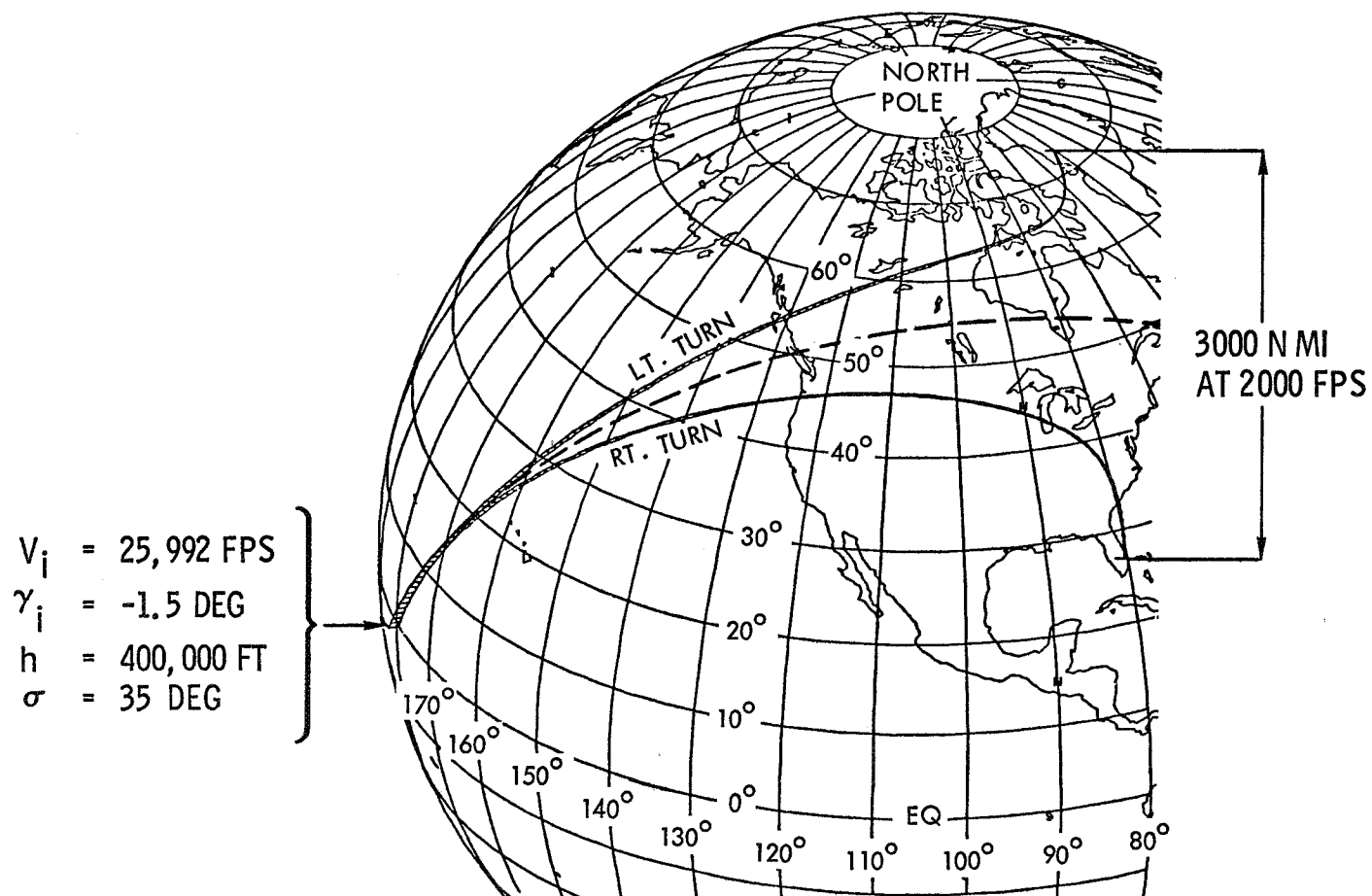
The heating environment experienced during an entry flight depends upon the entry conditions (velocity and flight path angle), the vehicle weight and the aerodynamic characteristics, and the flight mode (angle of attack and bank angle histories). The aerodynamic ranging requirements severely restrict the selection of these parameters, particularly the flight mode. This presentation describes a flight mode optimization study and discusses the aerothermal evaluation of the final trajectory data relative to the selection of boundary layer transition criteria. Entry heating environment improvement by means of reducing weight, improving aerodynamic characteristics or improving entry conditions will not be discussed in this presentation.

### HIGH LATERAL RANGE SPACE SHUTTLE ORBITER ENTRY TRAJECTORIES

The primary purpose of this chart is to show a long range space shuttle entry trajectory in relationship to the earth. The lower trajectory provides for landing at ETR by utilizing the full right turn lateral ranging capability. The entry (400,000 ft) velocity and flight path angle are 25,992 fps and -1.5 degrees, respectively, corresponding to a 435 fps retro from a 270 NM circular orbit. The entry latitude and longitude are  $0^{\circ}$  and  $180^{\circ}$  W, respectively, and the azimuth is  $35^{\circ}$  ( $55^{\circ}$  inclination). The intersection of the entry orbit plane and the earth is shown by the dashed line. The 1500 NM lateral ranging requirement was interpreted to mean a total difference between left and right turns of 3000 NM as shown. It should be noted that the entry orbit groundtrack reaches maximum latitude ( $55^{\circ}$ ) at approximately  $95^{\circ}$  W longitude. Since the landing site is at  $80^{\circ}$  W, this entry is considered to be from the descending node although the entry interface is during the ascending node. The groundtrack which crosses the ETR during the descending node, crosses the equator at  $230^{\circ}$  W longitude (not shown). Comparing this with the  $180^{\circ}$  W for the shown trajectory gives an indication of the increased return flight capabilities provided by the high cross range capabilities.



# HIGH LATERAL RANGE SPACE SHUTTLE ORBITER ENTRY TRAJECTORIES



### ANGLE OF ATTACK AND BANK ANGLE HISTORIES

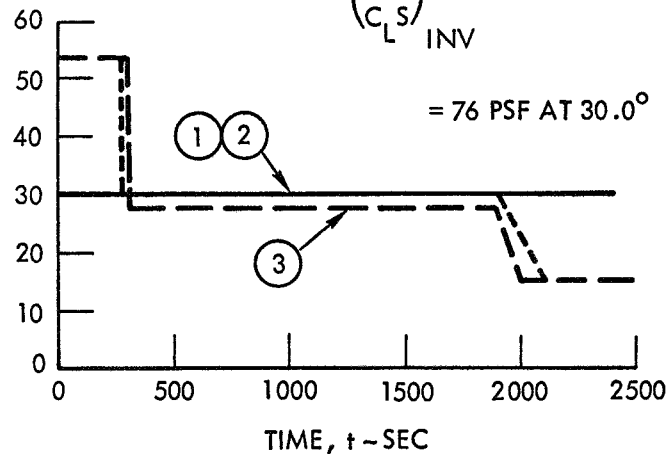
This chart shows the variation with flight time of the two independent (controllable) flight parameters, angle of attack and bank angle. Trajectory (1) utilizes a constant angle of attack flight mode with the bank angle modulated to maintain constant flight path angle,  $\gamma$ , or held constant. The  $\gamma$  values were selected to provide low heating conditions. This trajectory provided less than the required 3000 NM cross range capability and also produced high stagnation heating at pull-up (300 sec). Heating rates are discussed on the next chart. Trajectory (2) incorporates angle of attack changes to reduce pull-up heating and to extend the lateral range. The initial entry lift parameter,  $W/C_L S$ , was reduced from 76 psf to 43 psf by increasing the angle of attack from  $30^\circ$  to  $53.5^\circ$  (max  $C_L$ ). After the high heating conditions had subsided ( $\approx 1900$  sec) the angle of attack was reduced to near maximum L/D to increase the lateral range, however, only 65 NM were realized because of the reduced turning provided shortly after pull-up (note bank angle reduction). Trajectory (3) utilized bank modulation to maintain constant heating rates. The initial entry is made banked to provide increased turning before and after pull-up relative to trajectory (2). After pull-up the bank angle is modulated to maintain the pull-up stagnation heat rate until a pre-selected condition is reached (approximately 1000 sec) at which time the bank angle control is changed to maintain constant turbulent heat rate. The heat rate control is discontinued when the bank angle reaches  $60^\circ$  (1700 sec) and the angle of attack is reduced to maximum L/D after the heat rate decreases. The constant angle of attack after pull-up was reduced to  $27.5^\circ$  to increase the L/D and consequently the lateral ranging (2929 NM).

## ANGLE OF ATTACK AND BANK ANGLE HISTORIES

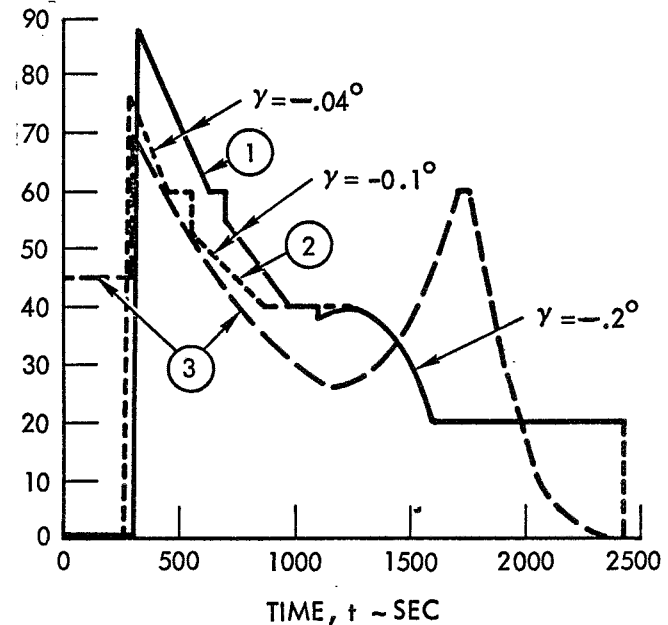
TRAJ	CURVE	*TOTAL CROSS RANGE	DOWN RANGE	FLIGHT MODE
①	SOLID	2800 N MI	6200 N MI	CONST $\alpha$ - BANK MOD
②	DOTTED	2865 N MI	6420 N MI	VAR $\alpha$ - BANK MOD
③	DASHED	2929 N MI	6000 N MI	VAR $\alpha$ - CONST $\dot{q}$

\*LEFT TURN PLUS RIGHT TURN  
MEASURED AT 2000 FPS

ANGLE OF ATTACK,  $\alpha$  - DEG



BANK ANGLE,  $\phi$  - DEG



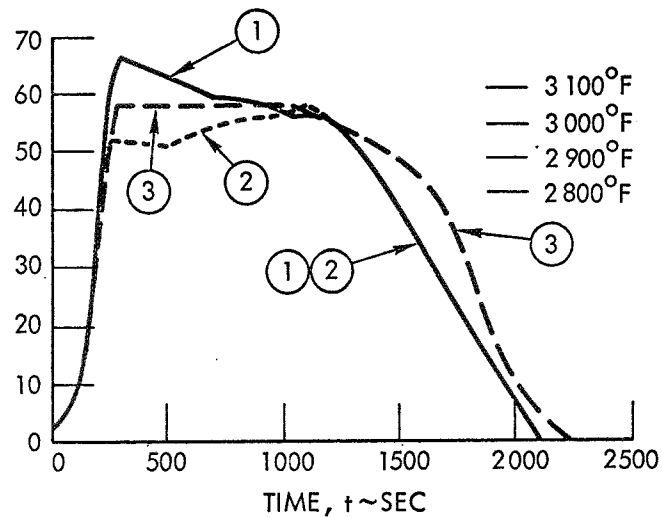
### STAGNATION AND TURBULENT HEAT RATE HISTORIES

The heat rates shown on this chart should be considered indicators rather than absolute numbers and therefore show relative heating environments for the three trajectories discussed on the preceding chart. The stagnation heat rates indicate laminar heating (nose, leading edges, etc.) variations whereas the turbulent heat rates indicate variations after transition to turbulent flow. The early portions of the turbulent curves are therefore not applicable. Transition criteria and their effects on heating are discussed on charts 5, 6, and 7. The curves show that the constant angle of attack trajectory (1) is generally hotter than the other two trajectories. The stagnation heating peak of trajectory (1) was reduced by increasing the initial entry angle of attack (trajectory (2)). The turbulent heating peaks of trajectories (1) and (2) were reduced by decreasing the bank angle schedule during trajectory (3) as required to maintain the value at 1000 sec. The primary message of this chart is that trajectory (3) has lower heating than either of the other two trajectories and yet provides more lateral ranging capability.

# STAGNATION AND TURBULENT HEAT RATE HISTORIES

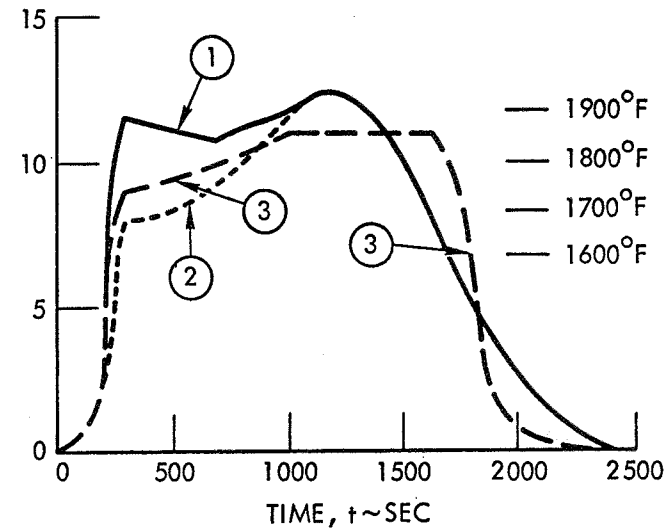
ONE FOOT RADIUS SPHERE

STAGNATION  
HEAT RATE,  $\dot{q}_s$   
~BTU/FT<sup>2</sup> - SEC



UNDERBODY CENTERLINE - X/L = 0.7

TURBULENT  
HEAT RATE,  $\dot{q}_T$   
~BTU/FT<sup>2</sup> - SEC



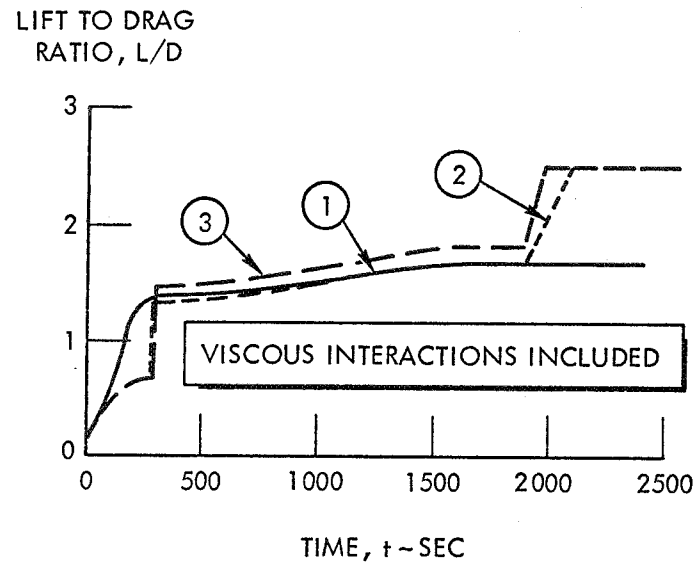
### LIFT TO DRAG RATIO AND LOAD FACTOR HISTORIES

The curves at the top of the charts indicate the available lift to drag ratio as influenced by the angle of attack selection and the viscous interactions. The curve for trajectory (1) is of particular interest because it is at constant angle of attack and therefore shows the considerable influence of the viscous interactions at high altitudes and velocities. However, even though the  $L/D$  appears to be significantly depressed during the initial portion of the flight, the reduction in lateral range due to viscous interactions is only in the order of 10 to 15 percent.

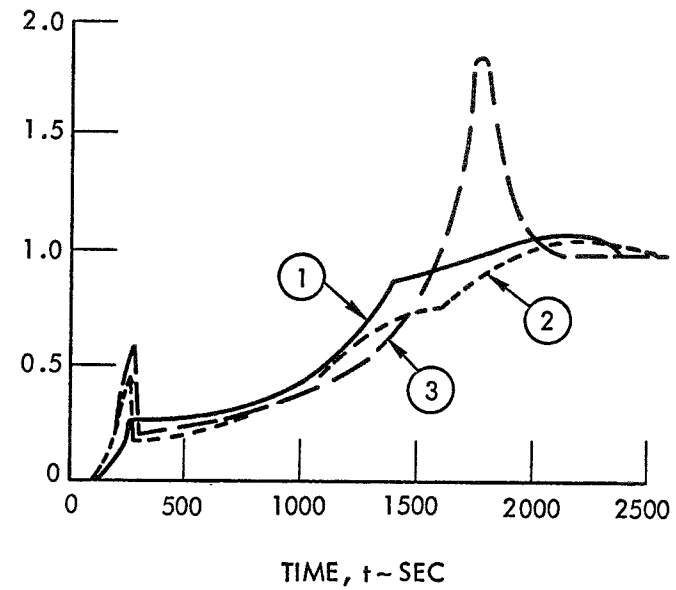
The curves at the bottom of the chart shows the generally low loading conditions corresponding to low heating entry trajectories. The 1.8 g peak indicated for trajectory (3) is due to the increasing bank angle which causes steeper flight path angles and dynamic pressures. This can be reduced by continued flight mode optimization.

## LIFT TO DRAG RATIO AND LOAD FACTOR HISTORIES

539



RESULTANT LOAD FACTOR,  $N \sim G$ 'S



EFFECT OF TRANSITION CRITERIA ON HIGH CROSS RANGE,  
DELTA WING ORBITER MAXIMUM ENTRY TEMPERATURES

The current high cross range flight mode is to enter at  $(C_L)_{\max}$  ( $\alpha = 53.5^\circ$  in this case) to pull-up and then to pitch-down to a lower angle of attack ( $\alpha = 30^\circ$ ) to obtain a major portion of the cross range and then to lower the angle of attack to  $(L/D)_{\max}$  to obtain the remainder of the desired cross range. An advantage of this flight mode from an aerodynamic heating standpoint is that low angles of attack and resultant high local Reynolds numbers are delayed until the higher heating portion of the trajectory is traversed.

The effect of transition criteria on high cross range orbiter entry heating is examined in the accompanying chart. Maximum radiation equilibrium temperatures along the fuselage underbody centerline were computed using Eckert's laminar flat plate reference enthalpy method, modified for cone flow and the Spalding and Chi turbulent flat plate theory, modified for cone flow and real gas effects. A statistically weighted factor ( $3\sigma$ ) of 1.25 obtained from analysis of a variety of turbulent heating data, was applied to the Spalding and Chi theory.

As can be seen, the current transition criteria predict maximum temperatures that are less than  $2350^\circ$  F. Assuming a transition criterion of  $Re_{x_{TR}} = 1.0 \times 10^6 = \text{constant}$  yields a maximum rise in temperature of  $150^\circ$  F with respect to the current criteria. Assuming an extremely conservative criterion of  $Re_{x_{TR}} = 100,000 = \text{constant}$  gave a maximum temperature rise of  $430^\circ$  F. The lower transition criteria precipitates severe changes in TPS material selection, demonstrating the fact that the high cross range designs are very sensitive to transition criteria.

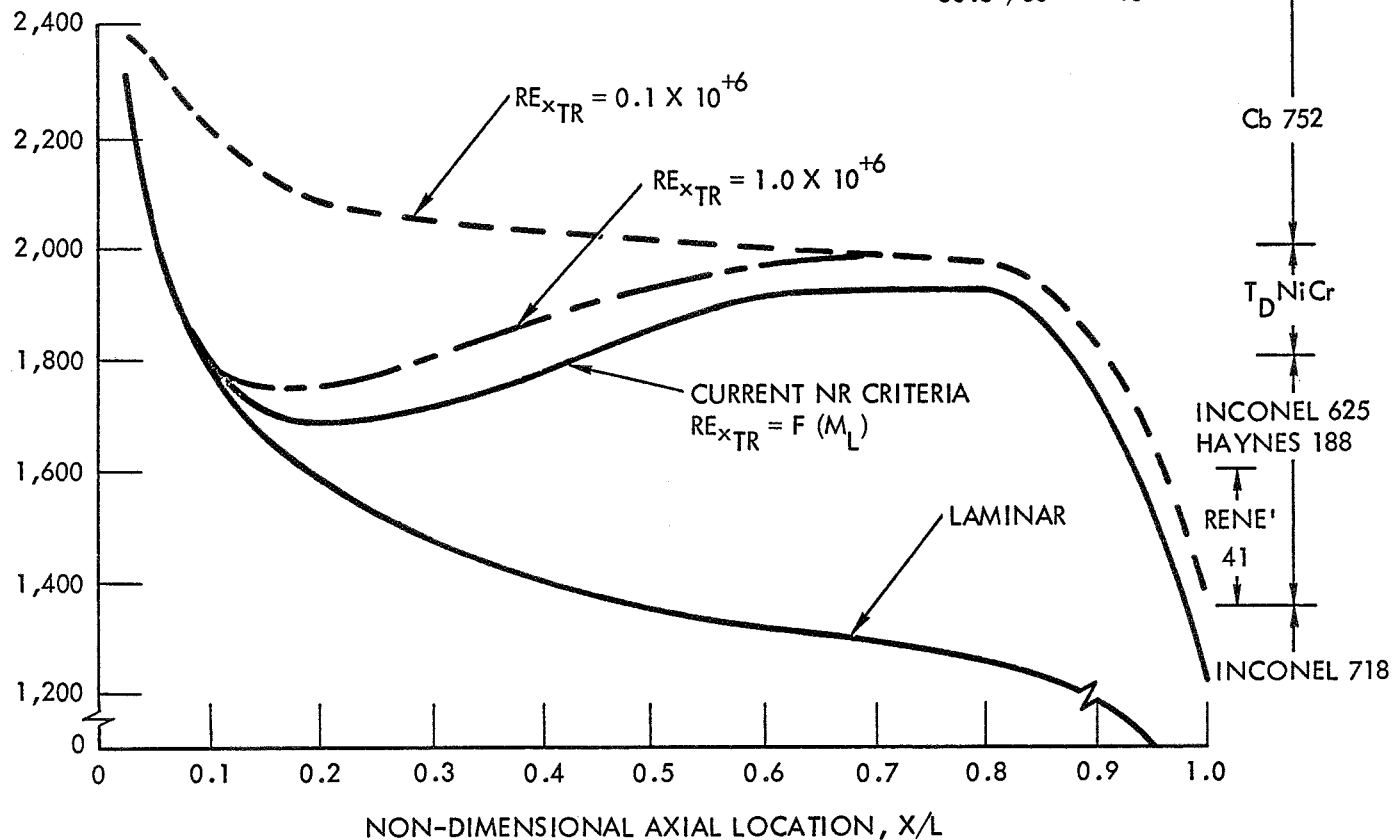


# EFFECT OF TRANSITION CRITERIA ON FUSELAGE UNDERBODY CENTERLINE MAXIMUM ENTRY TEMPERATURES

MAXIMUM RADIATION  
EQUILIBRIUM TEMP (°F)  $\epsilon = 0.8$

HIGH CROSS RANGE, DELTA WING ORBITER

$$\alpha = 53.5^\circ / 30^\circ \rightarrow 15^\circ$$



EFFECT OF TRANSITION CRITERIA ON LOW CROSS RANGE,  
STRAIGHT WING ORBITER MAXIMUM ENTRY TEMPERATURES

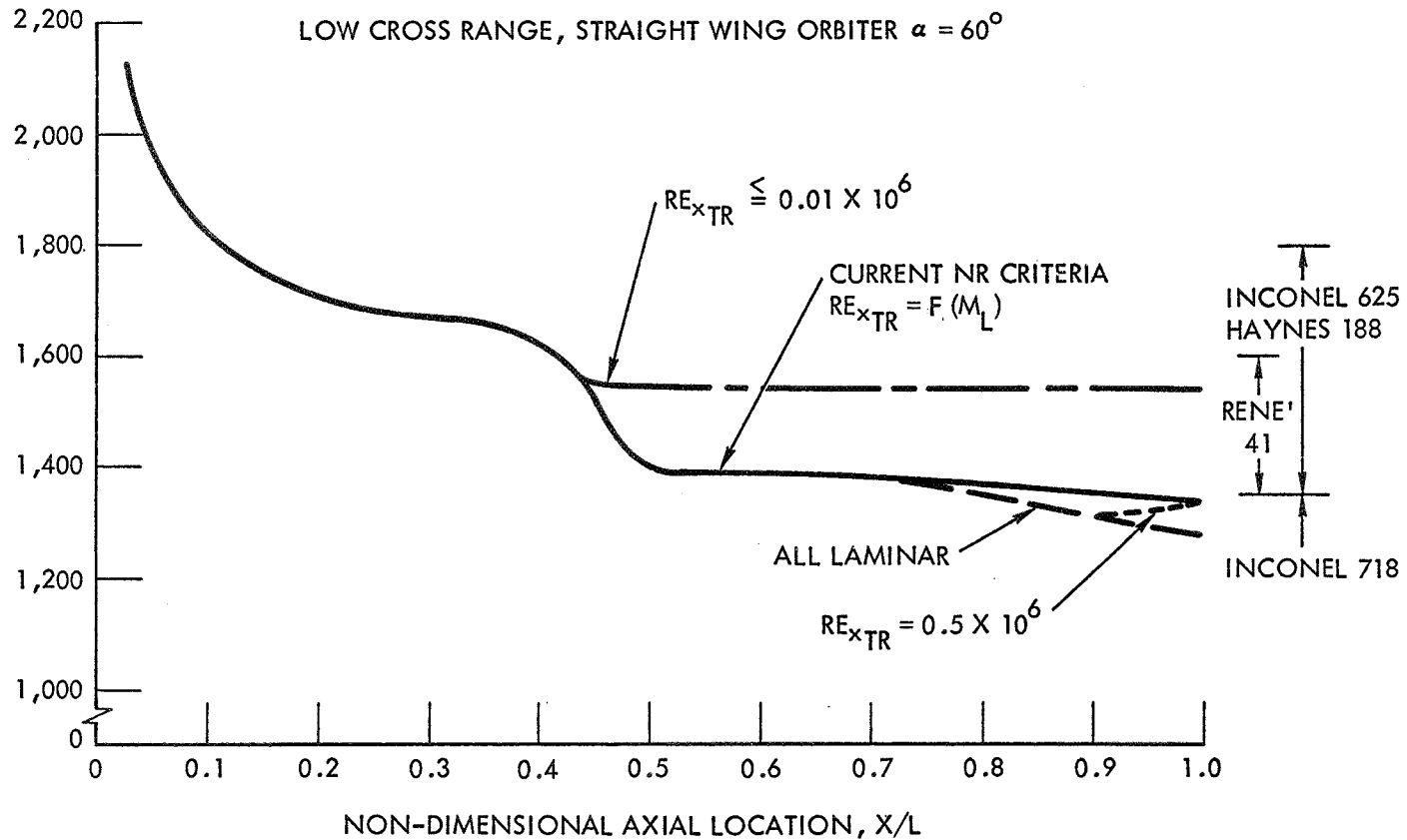
The current low cross range flight mode is to enter at very high angle of attack ( $\alpha = 60^\circ$ ) and maintain this attitude until subsonic Mach numbers are reached. An advantage of this flight mode from an aerodynamic heating standpoint is locally low Reynolds numbers which tend to delay transition to turbulent flow. However, because of the low local Mach numbers, the transition Reynolds numbers tend to be low also.

The effect of transition criteria on low cross range orbiter entry heating is examined in the accompanying chart. Maximum radiation equilibrium temperatures along the fuselage underbody centerline were computed using laminar swept cylinder theory, modified for local velocity gradient, and the Spalding and Chi turbulent flat plate theory, modified for cone flow and real gas effects. These prediction methods gave excellent correlation of wind tunnel data recently obtained on a swept wing orbiter at  $\alpha = 60^\circ$ . A statistically weighted factor ( $3\sigma$ ) of 1.25, obtained from analysis of a variety of turbulent heating data, was applied to the Spalding and Chi theory.

As can be seen, the current transition criteria gave a maximum rise of only  $60^\circ$  F over the pure laminar values. Assuming an extremely conservative transition criterion of  $Re_{x_{TR}} = 10,000 = \text{constant}$  gave a maximum rise of  $260^\circ$  F, however, this  $Re_{x_{TR}}$  criterion did not cause a change in TPS material selection from that corresponding to the current NR criteria. These results indicate that low cross range designs are less sensitive to transition criteria than high cross range designs.

# EFFECT OF TRANSITION CRITERIA ON FUSELAGE UNDERBODY CENTERLINE MAXIMUM ENTRY TEMPERATURES

MAXIMUM RADIATION  
EQUILIBRIUM TEMP ( $^{\circ}\text{F}$ )  $\epsilon = 0.8$



### BOUNDARY LAYER TRANSITION CORRELATIONS

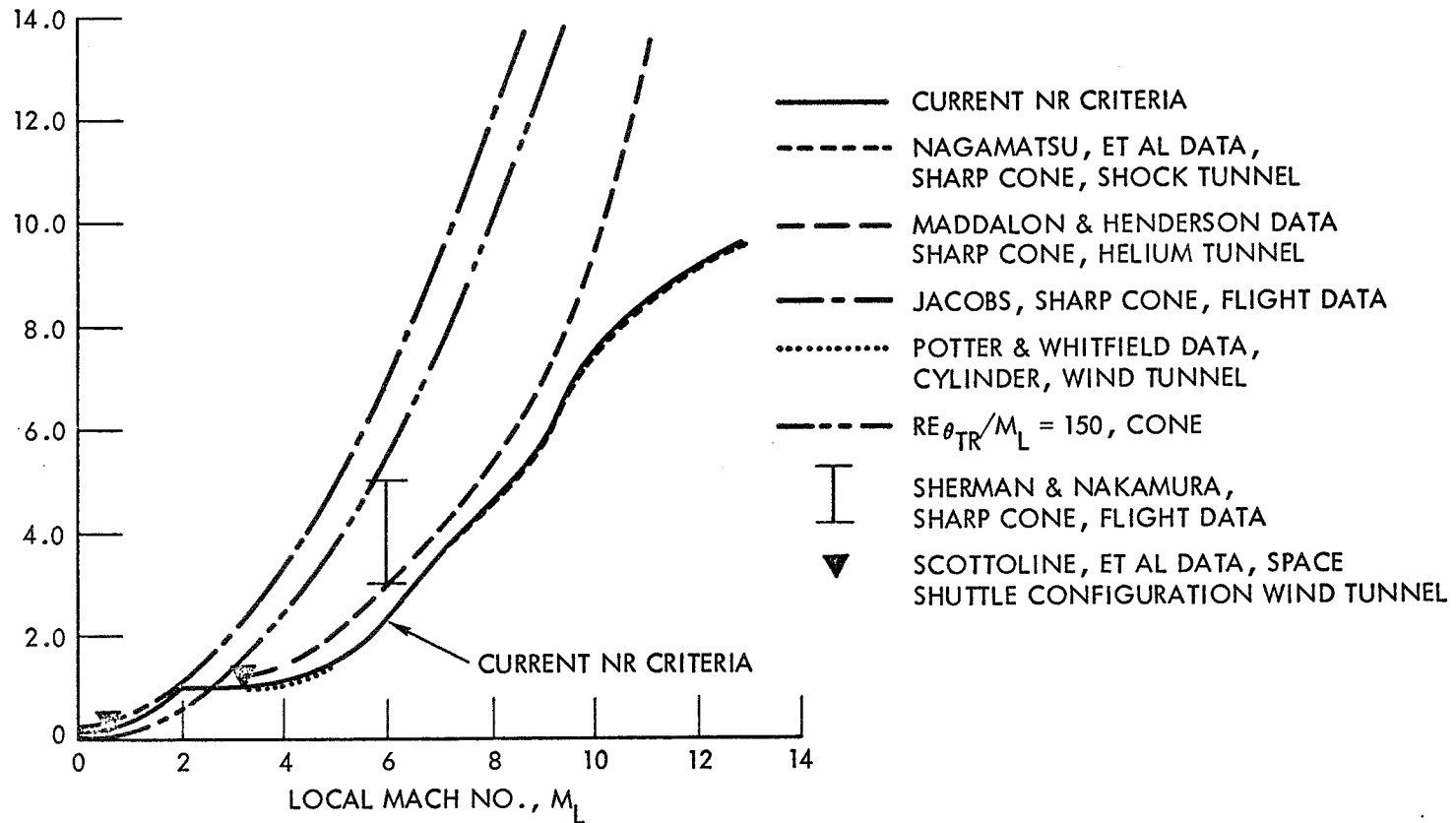
Boundary layer transition has been observed to be affected by many variables. Local Mach number has been shown to have a first order effect on transition. Because of the complicated nature of transition from laminar to turbulent flow, experimental data have been extensively relied upon for the prediction of the onset of transition. However, most experimental data have been obtained on sharp flat plates or sharp cones and are not directly applicable to actual aerodynamic shapes.

The accompanying chart shows examples of sharp cone transition correlations available in the unclassified, open literature. Shown with these correlations are recent transition data obtained by Scottoline, et al, on a swept wing Space Shuttle orbiter configuration at  $\alpha = 60^\circ$  ( $M_L = 0.6$ ) and  $\alpha = 25^\circ$  ( $M_L = 3.2$ ) in the AEDC "B" tunnel at  $M = 8$ . The Jacobs correlation is somewhat optimistic compared to the Shuttle data at  $M = 0.6$  and is considerably more optimistic than the data at  $M = 3.2$ . The criterion of  $Re_{\theta_{TR}}/M_L = 150$  is seen to be more conservative than the low Mach number shuttle data and more optimistic than the higher Mach number data. The correlation of Maddalon and Henderson data with the  $M = 3.2$  data is shown to be good. The current NR criteria are a correlation of data of Nagamatsu, and Potter and Whitfield combined with a modification to the Jacobs correlation. The NR correlation is seen to be slightly conservative compared to the Shuttle data and also to the lower bound of recently reported sharp cone flight data.

As more Shuttle transition data are obtained, the NR design transition criteria will be modified accordingly.

## BOUNDARY LAYER TRANSITION CORRELATIONS

TRANSITION REYNOLDS  
NUMBER  $RE_{x_{TR}} \times 10^{-6}$



## CONCLUSIONS

---

1. A CONSTANT HEAT RATE TYPE FLIGHT MODE PROVIDES MINIMUM HEATING FOR THE 1,500 N MI LATERAL RANGE ENTRY TRAJECTORY
  2. HIGH LATERAL RANGE, MINIMUM HEATING ENTRY TRAJECTORIES CAN BE FLOWN WITH VERY LOW AERODYNAMIC LOADS
  3. MORE INVESTIGATIONS ARE REQUIRED TO OBTAIN MORE APPLICABLE BOUNDARY LAYER TRANSITION CRITERIA FOR HEATING PREDICTIONS
-